IAEA-TECDOC-410

PROPERTIES OF NEUTRON SOURCES

PROCEEDINGS OF AN ADVISORY GROUP MEETING
ON PROPERTIES OF NEUTRON SOURCES
ORGANIZED BY THE
INTERNATIONAL ATOMIC ENERGY AGENCY
AND HELD IN
LENINGRAD, USSR, 9–13 JUNE 1986

A TECHNICAL DOCUMENT ISSUED BY THE
INTERNATIONAL ATOMIC ENERGY AGENCY, VIENNA, 1987

PROPERTIES OF NEUTRON RESOURCES
IAEA, VIENNA, 1987
IAEA–TECDOC–410

Printed by the IAEA in Austria
March 1987

PLEASE BE AWARE THAT
ALL OF THE MISSING PAGES IN THIS DOCUMENT
WERE ORIGINALLY BLANK

FOREWORD

Neutron sources are widely used not only in basic research but also in a large number of applications: bio-medical, bore hole and bulk media assay, neutron radiography, radiation-damage study and others. The development of advanced instrumentation of neutron sources and more detailed information on neutron source characteristics have become increasingly important to meet the demand of research and applications. It was therefore a quite logical evolution to organize a new IAEA Advisory Group Meeting on Properties of Neutron Sources now, six years after the previous meeting (IAEA Consultants' Meeting on Neutron Source Properties, Debrecen, Hungary, 17-21 March 1980). The IAEA Nuclear Data Section, with endorsement by the International Nuclear Data Committee (INDC) at its 14th meeting in October 1984, and in co-operation with the Radium Khlopin Institute, Leningrad as host, held this Advisory Group Meeting during the week 9-13 June 1986 at Leningrad, USSR.

The meeting was attended by 31 non Soviet scientists and 35 Soviet scientists. It covered 14 Agency Member States and three international organizations. Twenty-four invited and 28 contributed papers were presented.

The meeting programme and selection of invited speakers were based on advices received from the organizing committee of this meeting, which comprised the following scientists:

J. W. Boldeman (AAEC, Australia)
S. W. Cierjacks (KFK, FR Germany)
S. S. Kapoor (BARC, India)
S. S. Kovalenko (RKI, USSR)
E. Menapace (ENEA, Italy)
A. Michaudon (ILL, France)
D. Seeliger (TUD, German Dem. Rep.)
N. Shikazono (JAERI, Japan)
A. B. Smith (ANL, USA), Chairman
K. Okamoto (IAEA), Sci. Secretary

During the last two days of the meeting the participants split into the following Workshops:

Group-1: Cf-252 Fission-neutron Spectrum (Chair, J.W. Boldeman)
Group-2: Monoenergetic Neutron Sources (Chair, M. Drosg)
Group-3: White Neutron Sources and Fields (Chair, C.D. Bowman)
Group-4: 14-MeV Neutron Sources and Associated Equipment (Chair, H.K. Vonach)

The proceedings contain the Chairman's (A.B. Smith) texts (Prologue, Introductory Remarks and Summary Comments), all invited talks prepared especially for this meeting and contributed papers as well as the conclusions and recommendations of the Workshops.

This meeting was held approximately one month after the Chernobyl accident. Although it deals with neutron sources, the accident itself was not included in the meeting agenda. The anxiety of the non-Soviet participants at Leningrad was, however, relieved to some extent by the brief report presented at the meeting on the accident affecting the RBMK-1000 nuclear power plant.

This IAEA meeting is expected to be the last to deal with such broad topics and there is no doubt that these proceedings together with the issue of the Supplement of the Debrecen Meeting in 1980 [INDC(NDS)-114] will be the best available sources of information covering neutron source properties in general (except reactor neutron sources).

I wish to thank A.B. Smith for his excellent chairmanship before, during and after the meeting. It is my pleasure also to acknowledge the work carried out by the Organizing Committee, the Chairmen of the Workshops and Sessions. My sincere thanks go to all participants of the meeting for coming to Leningrad and for contributing to the success of the meeting.

As scientific secretary of the meeting, I wish to express my appreciation to the Radium Khlopin Institute for its kind arrangement and assistance in hosting the meeting. I am particularly grateful to N.P. Kocherov, the local organizer, for his devotion to the management of the meeting. I extend my thanks to the staff of the Radium Khlopin Institute for providing their assistance. Last but not least, I would like to acknowledge the kind support of the USSR State Committee on the Utilization of Atomic Energy, Moscow.

Koichi OKAMOTO
Scientific Secretary
of the Meeting

EDITORIAL NOTE

CONTENTS

SESSION III — CALIFORNIUM-252 PROMPT FISSION NEUTRON SPECTRA AND OTHERS

SESSION IV – MONOENERGETIC SOURCES AND FILTERED BEAMS

SESSION V — 14 MEV NEUTRON SOURCES

SESSION VI — SELECTED SPECIAL APPLICATION

SESSION VII — GENERAL INTEREST SESSION

* Combined with presentation in Session I.

PROLOGUE

A.B. Smith

Neutron-source properties have been an essential consideration in the provision of nuclear data for applications and in the fundamental study of the neutron-nucleus interaction. With the rapidly growing emphasis on precise nuclear data and with the increased focus on the more difficult measurement regimes, the importance of the characteristics of the neutron sources has greatly increased. This growing interest includes: intensities, spectral-characterization, and technological applications. Concurrently, maturing applications areas are demanding far better understanding of neutron source properties: for example, as applied to neutron therapy. These demands have stimulated considerable attention to neutron sources in recent years. The needs and the contemporary technological advances have been recognized by the IAEA Nuclear Data Section, which sponsored a comprehensive specialist's meeting dealing with neutron sources and their properties in 1980. That meeting did much to assemble contemporary knowledge and stimulate future work over the subsequent half-decade. It is now proper that the status of neutron sources be re-assessed, with particular attention to recent advances. This meeting was convened by the IAEA for that purpose.

The primary objectives of the present meeting are to:

1) Setforth and summarize the contemporary status of neutron sources for basic and applied research,

2) Establish recommended evaluated neutron-source characteristics for basic and applied utilizations (e.g., intensities, cross sections, angular distributions, etc.),

3) Define conventional and innovative technologies, and recommend procedures for neutron-source applications, and to

4) Identify outstanding problem areas and recommend future endeavors directed toward their solution.

The primary energy scope of the meeting extends from thermal energies to 30 MeV; with, secondarily, extension to other energies where they are directly relevant to important applications. White and monoenergetic (pulsed and steady state) accelerator based sources, pulsed and steady state fission- and fusion-based sources, and sources based upon radioactive decay are discussed. The scope is relevant to neutron-nuclear research and applications, but generally exclusive of condensed matter and/or molecular studies. Particular attention is given to the innovative use of the modest facilites available to workers in many of the IAEA member states.

INTRODUCTORY REMARKS

A.B. Smith

"The outstanding issue in neutron physics is source intensity"

Alexander Langsdorf, 1969

In the beginning it is fitting and proper to reflect on whence we came, where we are and where we may be going. Hopefully, these proceedings will bring a conclusion to a number of neutron-source issues, provide essential understanding for basic and applied endeavors, and give guidance as to future neutron-source efforts.

Neutron sources based upon radioactive decay processes find wide application in basic and applied sciences. Their properties are generally well established and, thus at this meeting we address only the Cf-252 prompt-fission-neutron spectrum which has come to be accepted as the fission-spectrum standard, and is widely used in a number of applications including: detector calibrations, production of standard fields, and, of course, the precise definition of the source term in fission-energy systems. The first experimental measurements were made nearly thirty years ago and since that time increasing refinements have resulted in excellent definition over the energy range 0.5-10.0. (e.g., W. Poenitz and T. Tamura, 1982). Many of the older measurements are suspect due to improper background and dead-time interpretations and only measurements over the last few years are probably reliable. These results generally confirm an average energy of approximately 2.13 MeV, in contradiction to the higher values obtained in some early measurements. Despite this precise new information, discrepancies persist at both low and high neutron energies. The underlying concept of statistical emission from a highly excited post-scission flying fragment was set forth very early (R. Peierls, 1939) and subsequently developed. The recent improvements (e.g., Madland and Nix, 1985) are largely due to a better understanding of the de-excitation of the highly excited fragments and the ability to model such complex processes. The models are primarily dynamic in nature and it is known that static effects (e.g., shell closures) play a part in the fission process (B. Wilkins et al., 1971). Generally, a unification of static and dynamic fission theory is sought. For applications, the physical concepts must be incorporated into comprehensive evaluations. At this meeting we may well have reached the point where a definitive evaluated Cf-252 fission spectrum is a reality. The Cf-252 spectrum should now have the status of the standard integral field, with other standard responses referenced to it.

The implications of the improved understanding of the Cf-252 fission-neutron spectrum on applications is a concern. The new and improved Cf-252 results must be propagated into the common fission processes. It is noted that is not necessarily so. For example, in one prominent

evaluated file, the Pu-239 spectrum has a significantly lower average neutron energy than that of U-235, in contradiction to both microscopic and integral observation.

The physics of the primary monoenergetic neutron sources has been reasonably known for thirty years. One will not go very wrong if he makes reference to the 1958 review of Brolley and Fowler. Since that time the details and exact magnitudes have been much refined but the basic concepts have not changed significantly. The regions of strengths and weaknesses remain the same. There have really been no breakthroughs and none are foreseen. The advances have been essentially technological (particularly including the wide application of fast-pulsed techniques), and the remaining problems are similarly so. These are practical matters, more an art and craft than a science. The practical understanding is distributed over the experience of a wide range of laboratories and generally not available to the uninitiated. It seems that now we should be able to summarize definitively the physical character of these reactions. The technological application is where the remaining questions lie. These should be addressed. They are important details such as: i) the handling of gaseous targets, ii) characterization of target yields and perturbations, iii) exact knowledge of the emission spectra, etc. It is likely that these sources have the most potential for future development with modest resources, but this has not been exploited (L. Cranberg, 1960). Modern accelerator technology is able to produce far more intense monoenergetic ion beams, well beyond the power-handling capability of the targets. Monoenergetic sources have, in principle, some unique characteristics that are too often ignored. They provide control of all the canonical variables, space, time and energy. This is a fundamental advantage in many types of measurements (e.g., determination of activities and life-times, double-differential measurements, etc.). Monoenergetic sources have a wide range of utility and are relatively economical. In many areas they remain the key to successful observations.

Filtered beams at steady-state reactors are a variant of the monoenergetic source, providing not otherwise available intensities at selected lower energies. They have been particularly useful in studies of low-energy capture (R. Chrien, 1983). More recently, the technique has been coupled to pulsed-white-accelerator sources to provide unique capabilities, particularly with respect to the determination of inelastic-scattering cross sections at very low excitation energies. The results are of outstanding applied interest (e.g., excitation of low lying levels in fissile nuclei, (Dabbs et al. 1979 and Kegel et al. 1985)), and of fundamental value (e.g., astrophysical chronometers based upon inelastic excitation of the 10 keV state in Os-187, Macklin et al. 1983). No other techniques appear capable of determining such low energy properties with anywhere near equivalent accuracies. Though limited in range, filtered beams, coupled to accelerator sources, should be further exploited.

Perhaps even more acutely, the 14-MeV source issues are technological rather than fundamental. Certainly, the d(t,alpha)n reaction is well known at the lower energies of primary interest. It is technologically easily possible to make very intense low-energy deuteron beams. The problem is the power-handling capability of the targets, and, at lower intensities, the quantitative characterization of the the emitted spectra. Very high-intensity targets (e.g., yields of 10**12 to 10**13) have been successfully operated but they are not in common use and, if anything, their use is decreasing. With the wide availability of modest 14 MeV sources and the encouragement of the IAEA, it is puzzling that there persist so many discrepancies in 14 MeV neutron data. They must be

associated with other aspects of the measurement systems (e.g., flux monitoring). Whatever the cause, common activation cross sections can disagree by amounts far beyond their respective uncertainties, the ratios of 14-MeV fission cross sections are disturbingly different, etc. 14-MeV sources are increasingly less popular at major institutions where the measurement skill is good. Very soon, major nations will have little, if any, capability to address 14-MeV neutron properties.

In recent times, low-energy neutron research has relied very heavily upon powerful conventional electron accelerators (e.g., at AERE, ORNL and CBNM). They have been outstandingly productive in neutron-resonance research. However, as was pointed out by Leiss twenty years ago, their potential appears to be approaching a practical limit. Recent improvements have been in the area of very short pulses (illustrated by the buncher at GELINA), giving superior resolution, rather than in simple intensity. Like all pulsed white sources, they must compromise time to obtain energy definition, thus they are not suitable for a number of types of experiments (e.g., studies of secondary neutron emission, activities etc.). They are troubled by large gamma-ray flashes and the facilities are large and costly to build and run.

Faced with limitations in the above electron facilities, the future of pulsed white sources may well be in positive-ion accelerators with energies up to approximately 1 BeV, using light-particle or spallation reactions for neutron production. Once fragmentary knowledge of spallation reactions is now much improved, making possible far better estimates of potential capability. This closes a circle as the first pulsed white sources were of that type (e.g., Dunning et al. 1940). It is not clear whether very high currents and relatively low energies or the converse is the more desirable and both concepts will be addressed at this meeting. Two entirely dedicated spallation-source high-energy facilities appear to be operational or essentially so (IPNS and Rutherford). A third is operating in a parasitic mode (LAMPF). The former are dedicated to condensed matter studies. In principle one should be able to combine condensed matter and fast-neutron source requirements at the same facility, but in practice the two types of endeavor seem mutually exclusive. One faces the same old argument, should one optimize capability for a single objective, or compromise performance for utility? LAMPF is unusual in that it addresses both areas well, abetted by a unique storage ring providing very high intensities and short pulses. Energy ranges accessible with a spallation source are very large. The problem of high-energy particle and meson contamination of the neutron beam remains and and the facilities are extremely costly. The later fact has led to the demise of several excellent concepts (e.g., SNQ). Perhaps costs can be reduced by innovative facility concepts (e.g., superconducting devices), but that is not clear at present.

The characterization of accelerator-based fast-neutron fields leaves much to be desired. It is surprising that, after many years of inquiry, uncertainties persist, particularly at relatively low energies. Such fields can provide exceptional intensities making possible measurements not otherwise feasible. Moreover, recently developed statistical methods promise success with unfolding techniques, making attractive measurements and energy coverages not accessible with other methods (D. Smith, 1983). Realization of this potential requires a far better knowledge of the respective neutron field, including the angular dependence. The acquisition of such detailed information appears a straightforward technological matter and will be addressed in these proceedings. The

results have wide applications impact, including; the determination of long-lived activities, access to "forbidden" energy domains, and even medical therapy.

Steady-state research reactors are generally thermal and sub-thermal sources of primary interest to condensed-matter studies. Twenty years ago (INS Conf.) the most advanced such systems were citing thermal fluxes of a few times 10**15. It remains so today. A number of facilities planned or operating at that time have been abandoned for reasons of cost, safety, and the emergence of more promising alternate concepts. Recent low-enrichment high-density fuels, motivated by anti-proliferation considerations, may have the potential for increases in intensity (A. Travelli, 1986). However, the power densities involved are impressive and inherent to the concepts. It seems likely that future intensity increases will be considerably less than an order of magnitude.

Repetitively-pulsed reactors have the advantages of high peak pulse with relatively low average power dissipation, thereby mitigating some of the limitations on the steady-state counterpart, and making possible the more effective use of timing techniques. There are engineering problems that have limited their use, and only one major facility is in routine operation (IBR-USSR). We shall learn of its accomplishments and potential. A hybrid system employs an accelerator driver with or without change of reactivity, ultimately going to the "booster" at white-source accelerator facilities (e.g., at AERE Harwell, and ANL IPNS). All of these approaches result in long pulses which limit their usefullness to relatively low energies or to condensed-matter studies. There are a number of operational single-burst reactors, the ultimate being an underground explosion (Diven, 1966). They are generally used for engineering and integral tests and have not made a significant impact on basic or applied research.

Most of this meeting deals with "conventional" source problems. However, innovative sources can be the key to very challenging fundamental investigations. Among these are polarized white and monoenergetic sources, neutrons induced by heavy ions, and cold and ultra-cold neutron sources. These concepts will be briefly addressed in these proceedings.

There is a continuing need for improved and universally accepted energy standards for use at both monoenergetic and white-source facilities. The problems will be considered at this meeting and, hopefully, a list of definitive standards can be agreed upon. The reference points for white-source measurements appear the best defined. Monoenergetic energy-calibration points are not as plentiful nor as well-known, and many of the values in common use date back many decades. Vernier methods are available for making very accurate energy determinations at monoenergetic facilities. Unfortunately, they are not widely used.

This is a neutron source meeting, but we should not forget that the source is only a portion of the measurement system. History shows that advances in the other components of the system may, in fact, have a greater impact at far less cost. For example, in some types of measurements, the advent of the solid-state gamma-ray detector (e.g., GeLi detector) has had a far greater impact than any amount of costly source development. Other examples with similar consequences or potential are:

large liquid scintillators and BGO systems, wide use of fast nucleonics equipment, and, perhaps beyond all else, the impact of the digital computer. One must balance the effort and cost of source development against that of other aspects of the measurement system, and throughout one must always remember that the source is only one of the tools toward the primary objective-- basic or applied physical understanding.

The author is indebted to R. Howerton and D. Smith for their comments and suggestions.

SUMMARY OF WORKSHOP 1

THE Cf-252 FISSION-NEUTRON SPECTRUM

Chairman: J. Boldeman

1. Differential Experimental Data

Results of two new experimental studies (Boettger et al. and Chalupha et al.) were presented at the Meeting. In addition, revision of some of the previous experimental results has been completed and final values released (Blinov et al. (1984), Poenitz and Tamura (1983), and Boldeman et al. (1986)). The following conclusions can be drawn from the main body of post-1979 data sets.

A. The majority of the experimental data are in agreement between 0.2 and 20.0 MeV. Relative to a maxwellian with a temperature of T=1.42 MeV, they show:

   0.2-1.2 MeV a negative deviation with a maximum of -4% at low energies,

   1.2-4.5 MeV a postive deviation of up to +3% with a peak at about 3 MeV, and

   5.0-20.0 MeV a negative deviation, increasing with energy and becoming -20% at 20 MeV.

B. Below 0.2 MeV the data are not in particularly good agreement.

C. Measurements above 20 MeV are very difficult due to the very small emission rate which must be observed in the presence of cosmic-ray background. New experimental results in this high-energy region were presented from a collaborative IRK/PTB time-of-flight study in a deep mine. An integral measurement, using activation techniques sensitive to this high-energy region was presented by Mannhart et al. Their results do not show an excess in the neutron spectrum above 20 MeV compared to a maxwellian with T=1.42 MeV as indicated by the TUD (1982) experiment and partially supported in a separate TUD/PTB experiment (1984,1985). This excess may have been caused by a residual contribution from cosmic-radiation background.

2. Integral Data

The evaluation of integral data presented by Kimura et al. confirms the negative deviation of the Cf-252 spectrum above 5.0 MeV relative to a maxwellian with T=1.42 MeV.

3. Theoretical Calculations

Theoretical models (CEM, GMNM, MNM, HFC) based upon purely statistical approaches considering neutron evaporation from fully-accelerated fragments continue to improve in their capability to reproduce the deviations

of the experimental data from a maxwellian with T=1.42 MeV. An accurate description of the Cf-252 spectrum over the full energy range can only be obtained in the framework of a complex model reflecting the physical characteristics of fission and fragment de-excitation in reasonable detail. The application of specific complex models to other fission processes, as required for practical purposes, is restricted because of the limited knowledge of the necessary fission data. Some theoretical developments with the promise of improving the calculational capability are in progress (e.g., GMNM2).

4. Physics of the Neutron-Emission Process

At present consideration of neutron-emission mechanisms, other than the primary component from the fully accelerated fragments, in the calculation of fission-neutron spectra is not reasonable as the physical characteristics of the so called "scission" neutron emission and the emission during fragment acceleration have not been clearly identified, experimentally or theoretically. As has been emphasized in recent detailed studies of neutron-emission mechanisms (RIL and TUD), an adequate statistical approach to the main component is necessary to avoid non-realistic conclusions. Recent data dealing with the anisotropy of neutron emission from Cf-252 can be reproduced on the basis of pure complex statistical models without the need for special emission mechanisms.

5. Evaluation

The quality of the experimental data has improved to the extent that a comprehensive evaluation of the recent experimental results has been possible. The evaluation presented by Mannhart suggests that the spectrum is now known to high accuracy from 25 keV to 20 MeV.

RECOMMENDATIONS

1. Between 0.2 and 20 MeV recent experimental data are in good agreement and the quality of the data on the shape of the Cf-252 fission-neutron spectrum has now reached a level consistent with the status of a well defined standard spectrum. Further studies between 0.2 and 15 MeV will be of value only if improved techniques are used.

2. Above 20 MeV a positive excess in the spectrum relative to a maxwellian with T=1.42 MeV probably does not exist. All groups making experimental measurements in this higher-energy region are requested to finalize their analyses, including full evaluation of all the experimental uncertainties. This may make possible the extension of the recommendations to spectrum energies above 20 MeV.

3. To improve the precision of the data below 0.2 MeV there may be some value to a new measurement, however this part of the energy spectrum is not as important from the purely data standpoint.

4. Theoretical models continue to improve and groups are encouraged to continue relevant theoretical work. A principle objective should be the extension of the calculations to other fissile systems.

5. The physics of the emission process is not understood satisfactorily. Further experimental and theoretical work in this area is strongly recommended, particularly measurements and calculations bearing upon fragment-neutron angular correlations and associated differential spectra. There may be value in a future consultant's meeting dealing with this topic.

6. The spectrum derived in the evaluation of Mannhart is the recommended shape of the Cf-252 fission-neutron spectrum. This evaluated data should be put in appropriate form for transmission to all data centers. This recommendation is particularly addressed to the INDC/NEANDC Standards Subcommittee for their detailed consideration.

SUMMARY OF WORKSHOP 2

MONOENERGETIC NEUTRON SOURCES

Chairman: M. Drosg

The properties and applications of the following monoenergetic neutron sources have been considered by this working group: $^{3}H(p,n)^{3}He$, $^{1}H(t,n)^{3}He$, $^{2}H(d,n)^{3}He$, $^{3}H(d,n)^{4}He$ (excluding the generation of 14-MeV neutrons), $^{2}H(t,n)^{4}He$, $^{7}Li(p,n)^{7}Be$, $^{9}Be(p,n)^{9}B$, $^{9}Be(alpha,n)^{12}C$, $^{11}B(p,n)^{11}C$, $^{45}Sc(p,n)^{45}Ti$ and $^{51}V(p,n)^{51}Cr$. Also considered were inverse (p,n) and (d,n) reactions.

1. Neutron Generation by Interactions among the Hydrogen Isotopes (p-T, d-D, and d-T)

The absolute differential cross sections are generally known to ± 3% for projectile energies up to about 15 MeV. The $^{2}H(d,n)^{3}He$ angular distributions near 5 MeV are even absolutely known to approximately ± 2%. Therefore, it is recommended that the absolute differential cross sections (complete angular distributions) of the $^{2}H(d,n)^{3}He$ reaction for projectile energies around 5 MeV and the zero-degree cross sections of this reaction between 3 and 15 MeV be applied as neutron-flux standard using a gas target. The application of this standard requires careful consideration of all effects influencing the actual neutron yield. It is important to note that the same precautions must be taken for any worthwhile determinations of these reactions generally.

The following requirements were discussed in some detail:

A. The necessity of determining the zero-degree direction to better than 0.1 degree (systematic angular uncertainties are critical).

B. The necessity of measuring individual angles to 0.1 degrees.

C. The necessity of knowing the mean projectile energy to within at least 0.5% (including effects due to energy loss in foils and gas, foil straggling, etc.).

D. The necessity of making, or at least considering, corrections for: angular straggling, multiple scattering (especially serious in charged-particle work), opening angle, attenuation due to the beam stop, in-scattering from target assembly and air, and background from the back-scattered charged-particle beam.

E. The necessity of knowing the effective areal density of the target isotope, in particular: it's purity, the reduction of gas density in the beam area (beam heating may be a serious problem), and the effective target length (flexing of the entrance foil).

In applications where the shape of the neutron energy distribution is important, it is advisable to simulate the neutron spectrum (or even the

entire experimental arrangement) with a computer (e.g., using Monte-Carlo procedures). The usefulness of the d-d reaction has been increased by the capability of analytically describing the energy spectrum of the break-up neutrons for energies up to approximately 9 MeV.

2. Low-Energy (below 0.1 MeV) Neutron Production

Work on the $^{45}Sc(p,n)^{45}Ti$ reaction, presented at this meeting, demonstrates its usefulness for neutron production between 1 and 36 keV, especially for dosimetry purposes. However, the specific neutron yield is low (10**3 neutrons/sr-microcoul.). The yield data for the $^{51}V(p,n)^{51}Cr$ source show an unresolved discrepancy of about 40%. In many applications, filtered beams from reactors or pulsed white-source accelerators are a better choice than these low-yield (p,n) reactions.

3. Alternate Choices for Higher-Energy Neutrons

At present there seems to be little use for p-Be and alpha-Be reactions as monoenergetic sources. The status of the evaluated $p-^{7}Li$ reaction is not satisfactory so the use of this reaction for efficiency measurements is discouraged, though its usefulness for energy calibrations is acknowledged. Therefore, a determination of the threshold energy at the 10**-4 accuracy level appears desirable. For "monoenergetic" neutron production above 20 MeV this source is suitable. Angular distribution measurements up to 40 MeV appear to have value for efficiency determinations. The $p-^{11}B$ source is competitive with the p-T source (involving Ti-T targets) for energies up to 2.4 MeV (or even to 4.9 MeV as a two-line source). However, difficulties in producing reliable ^{11}B (or natural boron) targets may be a handicap in the application of this reaction.

4. Unusual Sources

Among the inverse (p,n) and (d,n) reactions there are several with outstanding properties. Some require the use of bunched heavy-ion beams at neutron-measurement facilities [e.g., ^{11}B on ^{1}H which could serve as an alternative source to cover the 8-14 MeV "gap," and inverse (d,n) reactions with multiline spectra, which could be developed as calibration sources for efficiency measurements]. Some of these alternate sources have already been used, e.g., ^{7}Li on ^{1}H, t on ^{1}H and t on ^{2}H. Whereas ^{7}Li on ^{1}H and t on ^{2}H are useful in special applications, t on ^{1}H could be the most powerful general-purpose monoenergetic neutron source. However, because of radioactivity concerns, it has been in only limited use until now.

RECOMMENDATIONS

1. The d-D reaction is recommended as a fast neutron-flux standard.

2. A catalogue of all error contributions and corrections relevant to monoenergetic neutron production by two-body reactions using both gas and solid targets is necessary in order to avoid errors in converting neutron production cross sections to neutron yield, or vice versa.

3. The discrepancy in the scale of the integrated $^{51}V(p,n)^{51}Cr$ cross section should be removed.

4. The threshold energy of the $^{7}Li(p,n)^{7}Be$ reaction should be determined to an accuracy of about 10**-4. Use of the inverse reaction in such a measurement increases the sensitivity by a factor of seven.

5. The analytical description of the neutron break-up spectrum of the d-D reaction should be tested in actual applications (e.g., activation analysis).

6. A reproducible procedure for constructing reliable boron targets suitable for neutron production should be established.

7. The development of new monoenergetic sources based on inverse (p,n) and (d,n) reactions is encouraged.

SUMMARY OF WORKSHOP 3

WHITE NEUTRON SOURCES, STANDARD FIELDS AND FILTERED BEAMS*

Chairman: C. Bowman

As neutron-based technology has grown so have the methods for neutron production, and now we are at the threshold of significantly larger source intensities and improved measurement methods. Although further increases in reactor intensities will probably be limited due to the large energy release (about 200 MeV/neutron), the accelerator based sources are not near such a barrier and thus a variety of accelerator concepts for increased intensity are under study. In addition there are institutional advantages in the accelerator concepts (e.g., ease of control, reduced residual activity) and accelerator reliability is approaching that of the reactor. Systems used for pulsed-white-source production can be characterized as follows: i) spallation sources, greater than 200 MeV, ii) electron linacs, 30-150 MeV, iii) ion accelerators, less than 200 MeV, iv) electron linacs, 10-15 MeV, v) pulsed reactors, up to several keV, and vi) electrostatic accelerators, up to 20 MeV. These characterizations are only guidelines as other factors, such as utilization, may be governing. Reactors are well established and filtered beams and standard fields will continue to see substantial use. Engineering advances might also lead to some further increase in reactor intensity.

1. Accelerator-Based Sources

The advantage of the spallation source is the low energy release per emitted neutron (about 25 MeV/neutron), which is an important consideration in target-heat-dissipation and accelerator energy efficiency. The concepts have been proven in high-energy research facilities and demonstrated in condensed-matter neutron research (e.g., at Argonne, Tsukaba, Los Alamos, Rutherford and Gatchina). The spallation source has considerable development potential. Additional advantages are: small gamma-flash, flexibility between pulsed and continuous-mode operation, spectral options extending from cold to very fast neutrons, and the capability for multiple measurement stations. A disadvantage is the presence of a high-energy neutron component which is difficult to shield against. Experience also indicates the presence of high-energy proton and meson backgrounds that are not always easily removed from measurement systems. Though the neutron production process is efficient, power costs can be a concern. The applicability of the spallation source in both steady-state and pulsed modes is outlined in Table 1.

---

*Membership in the working group included:

R. Johnson
C. Coceva
M. Blinov
V. Ya. Golovnya
S. Qaim
K. Boeckhoff
A. Michaudon
N. Shikazono
T. Nakamura
R. Dierckx
V. Luschikov
E. Kozulin
G. Muradyan
C. Bowman, Chairman

Table 1. Comparative Utilization of Pulsed White-neutron Sources.+

Source Category	Type of Utilization: Solid State	Medium Energy Phys.	Nucl. Phys.	Neutrino Phys.	Nucl. Data	Bio-Research	Isotope Production	Act-Analysis	Neut. Radiography	Cancer Therapy	Radiation Damage
Spallation Sources, E_p or d $\gtrsim$ 700 MeV	●	●	●	●	●	●	●	●	●	●	●
Electron Beams 30-150 MeV	●	-	●	-	●	●	●	●	●	-	-
Ion Accelerators < 200 MeV, No Storage Ring	●	-	●	●	●	●	●	●	●	●	●
Electron Beams 10-12 MeV	●	-	●	-	●	●	-	●	●	-	-
Electrostatic Accelerators Thick Targets	-	-	●	-	●	●	-	-	●	-	-
Pulsed Reactor	●	-	●	-	●	●	-	●	●	-	●

+The degree of applicability depends on the details of the method.

Electron linacs continue to be effective as intense pulsed neutron sources. Even though less energy efficient than the spallation source, these devices have proven very successful and should remain so into the future. Short pulses are important and much progress has been made in producing neutron bursts with widths of a nsec or less. While S-band technology is quite mature, it is possible that an order of magnitude increase in intensity can be obtained with L-band technology. The range of applicability is shown in Table 1.

Proton and deuteron accelerators of less than 200 MeV have been productively utilized to provide white sources of neutrons. They are less neutron efficient than the higher-energy spallation source but they have advantages. The pulse width is characteristically approximately one nsec, except for induction linacs which would probably operate in the 10-100 nsec range. The neutron emission is strongly forward peaked, making the source particularly useful for radiation damage and therapy applications, as well as neutron spectroscopy. The duty cycle is high, an advantage for many experiments, and the spectrum harder than that of most electron linacs. A linear induction accelerator with a maximum energy of about 100 MeV could provide a powerful and versatile facility at relatively modest cost, though detailed engineering studies have not provided quantitative definition. These systems can accelerate high currents of both electrons and light ions. In addition, the induction linac can be used as a source of quasi-monoenergetic neutrons and the light ions can be directly employed in neutron studies. This type of device has wide application as outlined in Table 1. The interesting potential of heavy-ion accelerators for the production of intense neutron sources has not been fully explored.

Electron beams of 10-12 MeV using Ta(e,gamma) converters and Be or D (gamma,n) radiators can be used for neutron production, with efficiencies approaching that of a 100 MeV beam. Recent technological advances permit a trade-off between beam current and energy. The high current low-energy option has some significant advantages. The spectrum is free of high-energy components. The shielding requirements are less, reducing cost and space requirements. The accelerators are simple single-section units and induced radioactivities are modest. With present technology, the neutron production is less than that of the 100 MeV facility, but induction-linac technology (cited above) with its promise of 1000 ampere beams may alter this situation. A disadvantage of the concept is the absence of neutrons with energies above about 4 MeV (e.g., as needed for therapy) and less source brightness. The applicability of the concept is outline in Table 1.

A further category is the low-energy electrostatic accelerator which, with thick targets, offers opportunities for specialized work with comparatively high intensity. Optimum utilization of the approach demands solution of the target-power-dissipation problem if the full beam power is to be realized. The method is particularly useful in the keV and low MeV ranges where good results can be obtained with modest facilities and at relatively low costs. Applicability is outlined in Table 1.

2. Pulsed Reactors

High repetition-rate pulsed reactors have a special place among white sources. The pulse width is generally about 200 micro-seconds, which is useful for measurements with thermal neutrons. They also can be driven using low repetition-rate ion or electron bursts, leading to pulse widths

of a few microseconds. This concept provides very intense neutron beams in the low-resonance region with modest experimental energy resolution. Such pulsed reactors are useful, not only for conventional cross section measurements, but also for spectroscopic studies of secondary particles such as resulting from (n,gamma), (n,f), (n,p) and (n,alpha) reactions. An average power of 2 MW has been achieved at such sources resulting in an average neutron production of about 6 X 10**16 n/sec. Applicability is outlined in Table 1.

3. General Considerations

Neutron energy standards are a concern not related to specific white-source types. Accurate energy calibration is a continuing problem in white-source neutron time-of-flight spectroscopy. The resonance standards presented by Coceva at this meeting are recommended for future neutron measurements.

There is a continuing need for new intense neutron sources for basic and applied studies. Large facilities are costly but can be used by scientists from several disciplines and may be operated as multi-national facilities thus distributing the large construction and operating costs. It is recommended that scientists from different disciplines further coordinate their efforts to design and build multi-purpose facilities. Such an interaction is desirable at the earliest conceptual stage, if possible before the design is frozen, so that all the various aspects of the future use of the facility are taken into account. It must be remembered that the construction of a major facility does not imply that all small facilities are no longer of use. They will remain of value for special experiments, preparation of experiments to be carried out at larger facilities, and for training.

4. Filtered Beams and Standard Fields

Calibrated neutron beams and fields include: i) filtered beams, ii) thermal reactor beams, and iii) neutron fields (reactor or accelerator driven). The accuracy and quality of these beams and fields were discussed.

Filtered beams at reactors and, to a lesser extent, accelerators extend over a wide range of energies and have been a useful tool in basic and applied endeavors where high accuracies and intensities are sought. The most widely used filter-beam energies are: i) 2.35 MeV (^{16}O), ii) 144 keV (Si), iii) 55 keV (Si), iv) 24 keV (Fe), v) 2 keV (Sc) and vi) 186 eV ^{238}U). These beams are particularly valuable at energies below 30 keV where other methods are difficult. Neutron spectroscopy is not the general application. Thus the availability of a well defined energy approximately every decade below 200 keV is probably adequate. With this assumption the primary shortcoming is in the 20-50 eV range. This low-energy region is difficult as even the 186 eV (U-238) is subject to background problems. Beam purity is a general concern and attention should be given to alternate material combinations, isotopic filters, etc. At low energies (below 2 keV) improved methods of beam characterization are desirable. The stable nature of reactor-filtered beams is an advantage: e.g., in dosimetry applications. The use of filtered beams at pulsed-white-source accelerators leads to reduced backgrounds in time-of-flight experiments and provides pulsed-monoenergetic sources at selected and otherwise difficult-to-reach energies. In other usage there is an advantage to pulsed filtered beams at small accelerators using thick targets (e.g., ^{7}Li(p,n)), and this capability should be

further examined. The production of intense monoenergetic beams via thermal-neutron de-excitation of isomeric atoms, molecules or nuclei is encouraged.

Energies in the low-keV region are important in dosimetry applications as they contribute to typical neutron fields encountered near nuclear power stations. Below 2 keV a better calibration field would be very helpful. The interaction of neutrons with Cd and ^{10}B implanted in tissue is of diagnostic and therapy interest. Generally, the physics of neutron damage to biological specimens is not clearly understood and it is reasonable to expect filtered beams to help resolve such issues.

The $^{9}Be(d,n)$ specra have found increasing application in recent years as standard fields for the integral testing of evaluated dosimetry data. For dosimetry studies, nuclear-reaction cross sections up to about 50 MeV are needed. Due to the lack of monoenergetic neutron sources beyond 28 MeV, those needs cannot presently be met by means of microscopic differential studies. Nuclear models can provide estimates of these data, but with large uncertainties. Integral measurements using the Be(d,n) field provide a useful check of such calculations. For high threshold reactions (e.g., (n,t) and (n,He-3) reactions) there are no presently satisfactory calculational methods though a considerable body of integral data has been accumulated. An unfolding method has been suggested for the derivation of differential data from these integral measurements. Although the method has limitations, it may have considerable potential that should be explored. Alternative sources for the production of such high-energy neutron fields are the $^{9}Be(p,n)$ and $^{7}Li(d,n)$ reactions. There are continuing efforts to provide a high-energy high-intensity neutron field of about 10**14 n/sec-cm**2 over a volume of 20-100 cm**3 for radiation damage studies, particularly associated with the damage in the region of the first wall of fusion-power systems. Diagnostic instruments to evaluate the microscopic basis of materials changes using neutron techniques have also been considered. Diagnostic spectrometers have used moderated source neutrons in the thermal and cold ranges for small-angle neutron scattering and diffraction studies on irradiated samples.

Calibrated thermal beams from reactors provide a further energy range for instrument calibrations and (n,gamma) work. Standard neutron fields play an important role in nuclear power development. They are frequently derived by placing a ^{235}U fission source in a cavity within a reactor thermal column. Appropriate use of moderators and/or absorbers tailors the cavity spectrum to the particular need. The cavity-field geometries are simple, the spectra calculated to accuracies of about 5%, intensities are about 10**9 n/sec-cm**2, and the spectra verified by benchmark measurements. The alternative accelerator-based white-source fields are accurate and can be tailored to special applications. The use of calibrated neutron fields should be improved by the implementation of a variety of complimentary approaches.

SUMMARY OF WORKSHOP 4

14 MeV NEUTRON SOURCES AND ASSOCIATED EQUIPMENT

Chairman: H. Vonach

1. Very Intense Sources (Source Strength Greater than 10**14 n/sec)

A research program was described by J. C. Davis illustrating the present high-intensity capability and suggesting the potential feasibility of d-t sources with neutron outputs of 3-4 X 10**14 n/sec. Such neutron sources would be extremely useful for fusion-reactor materials and radiation-damage studies. Furthermore, the proposed development of tritium targets having reduced deuterium accumulations and correspondingly longer half lives would be very beneficial at the many other less intense neutron generators. Therefore, it is highly recommended that a target development program of the nature described be implemented in the near future.

2. Intense Sources (Source Strengths of 10**12-5 X 10**13)

A large portion of the contributions to this meeting in the 14-MeV field has been devoted to reports of forthcoming new intense neutron generators. Such new sources will become operational in the near future in Bratislava (CSR), Dresden (DDR), and Debrecen (Hungary), and the existing Octavian facility in Osaka (Japan) will be upgraded for extremely high intensities in nsec pulsed operation.

The new nsec high-intensity generators will make possible large progress in both the measurement of differential neutron data for fusion power programs and corresponding integral experiments. The intense steady-state facilities can also be expected to make substantial contributions to fusion-reactor neutronics and other interesting fields such as the determination of cross sections for very rare reactions, activation analysis, and neutron radiography (as previously cited in the recommendations of the 1980 meeting).

Concerning the technical problems of the above cited facilities, the design and operation of the required rotating target systems and the reliable supply of the corresponding tritiated materials is still somewhat difficult. As in 1980, it is recommended that the relevant laboratories closely cooperate in the resolution of the technical questions associated with target technologies, with the object of a degree of standardization that might help to establish a reliable supplier of suitable targets at a reasonable cost. The considerations of Dr. Pivarc concerning optimum design (presented at this meeting) could probably serve as a good starting point for such collaboration.

3. Conventional Neutron Generators (Source Strength 10**10 - 10**11 n/sec)

Conventional neutron generators still have important applications: e.g., in basic nuclear physics, nuclear data for fusion, activation analysis, development of neutron spectrometers for d-t fusion diagnostics, and in neutron metrology. Conventional neutron generators can probably provide

one of the cleanest and best characterized fast-neutron fields for calibration of fast-neutron flux monitors and will be needed for this purpose into the foreseeable future.

Standard neutron generators equipped with nsec pulsing capability can be used to carry out almost all measurements of differential neutron-nuclear data for fusion-reactor design in the 14 MeV energy region.

It is regretable that the number of operating neutron generators in the developed countries has drastically decreased in the last decade, and there is danger that the necessary expertise in this field maybe lost. It is therefore recommended that the few existing installations continue in operation. Eventually a part of the relevant work may be performed by neutron generators given by the IAEA to various developing countries. However, most of the needed measurements require the skills of very well trained and experienced scientists. Considerable further transfer of experience and technology will be necessary if the facilities in the developing countries are to become fully productive. The IAEA is a good vehicle for such transfer.

Concerning technical problems, it has to be pointed out that many of the neutron-generator laboratories in the developing countries, which were equipped by the IAEA with commercially-produced neutron generators, have severe repair and maintenance problems as the commercial suppliers have largely (or completely) lost their interest in the field over the past few years due to a falling demand for machines and components. This technological problem could be addressed by the IAEA as a part of its technology transfer programs.

SUMMARY COMMENTS AND PERSONAL REFLECTIONS

A.B. Smith

Following on the wealth of technical information presented during the past few days, and the excellent summaries of the skilled workshop chairman, it is appropriate to confine these remarks to some personal reflections on the Meeting.

A major topic was the Cf-252 prompt-fission-neutron spectrum. Unlike the situation of fifteen years ago (IAEA Specialist's Meeting, 1971), this spectrum is now accepted as the fission-spectrum standard. Other fission spectra should be referenced to it, it should be increasingly used as a standard integral field of a purity not generally available from neutron-induced fission, and it should be more widely applied as a calibration reference for neutron-detection systems. This spectrum now appears known to 2% or better from 0.2-12+ MeV, making it probably the best known of any continuum neutron spectrum. That accuracy and energy scope is now probably sufficient for applications purposes. The remaining issues are ones of fundamental physical understanding rather than of applied use. A rigorous numerical evaluation of the experimental results was presented. It is important that this evaluation be thoroughly documented and widely disseminated as soon as possible. Only then can it be subjected to the detailed tests and examinations that are essential for its final endorsement for general use. The physical interpretations of the Cf-252 spectrum are notable for the quantitative use of sophisticated statistical nuclear models. They are particularly useful for extrapolation and interpolation. The trend seems to be toward a unification of dynamic and static models. These are interesting and challenging investigations, but their difficulty should not be underestimated. They involve the interpretation of processes far from the line of beta stability, including highly excited nuclei, with all the uncertainties of statistical level properties, model parameters, etc. Such quantitative interpretations have not been mastered in much simplier cases involving neutron scattering from stable targets, and predictions of capture in fission products are known to vary widely. These uncertainties should not discourage theoretical study, but one should remain cautious of the calculational result without detailed experimental test. Considerable effort has been devoted to the high-energy (12+ MeV) portion of the Cf-252 spectrum. The region is of little applications note, but of fundamental interest. It is increasingly apparent that the initial reports of neutron abundance at very high energies were premature. Carefully controlled measurements show little, if any, deviation from an extrapolation from the lower-energy region. Measurements directed toward pre-scission emission, emission anisotropy, the low-energy portion of the spectrum, etc. are encouraged as these are areas of fundamental physical interest. Their resolution will have not appreciable effect on the application of the spectrum. Perhaps now of most importance is the application of the new-found information to the precise determination of the "primary" (e.g., U-235, U-238 and Pu-239) and transplutonium fission spectra so as to provide internally consistent evaluated fission-spectra for nuclear-energy development.

A triad of accelerator-based pulsed-white-neutron sources were discussed. The workhorse during the past several decades has unquestionably been the electron linac. Its success is partly due to the emphasis that has been given to steady improvements in performance, particularly with respect to timing and increasing energies. There appears to be a near-term potential for continuing improvements, and I expect this type of source to remain the major tool for resonance-neutron studies for the remainder of my professional career. The long term potential is not so clear, and there are wide classes of important experiments that are generally physically forbidden to the white-source method. An alternate, and as yet unproven concept, is the induction linac. Its potential is in the very high intensities, the ability to handle electrons or ions, and in expandability. The limitations are in burst duration (probably no better that 10 or more nsec), which restrict the measurement regime to relatively low energies. At this point an induction linac facility for neutron work is a concept. Detailed engineering designs should be pursued so as to make possible quantitative cost and performance estimates. Spallation sources, operating in the 500-1000 MeV energy range with very short pulse durations, are particularly attractive white-neutron sources due to intensity, time resolution, wide energy range, and the overall efficiency of converting energy to neutron yield. Only one such facility (WNR-LAMPF) appears to be coming on-line in the foreseeable future. A few preliminary experiments at that facility (without the storage ring) have given encouraging results, but the potential remains to be fully proven. There is little gamma-ray flash but there is a high-energy particle contamination. These high-energy spallation-sources are massive and costly, and for that reason proposals have not generally faired well. It seems clear that such massive facilities cannot be supported by neutron work alone. Thus, the neutron studies must be in concert with fundamental physics endeavors which provide a major portion of the support. Lower-energy spallation sources (generally including ion beams on thick targets, e.g., as demonstrated at the KFK cyclotron) have been projected to have considerable potential at modest facility cost. However, it was pointed out that the knowledge of the requisite lower-energy nuclear reactions on thick targets is very fragmentary and is a limitation to design predictions. This is odd as the measurements are known not to be particularly difficult. Better basic reaction information is needed for assessment of the potential of low-energy spallation facilities and the same information will be very useful in neutron therapy work where, apparently, the future energy regime will extend upward from 60-100 MeV.

Monoenergetic neutron sources have fundamental physical advantages due to their ability to control both the time and energy of the neutron emission. These advantages are the key to success in a wide range of important measurements. The primary sources are the hydrogen-induced reactions, either on hydrogen targets or light elements (e.g., Li-7). They are generally well known, particularly the d(d,n) reaction which is even a standard near 5 MeV. All of them, at some energy, become non-monenergetic, with usually a continuum breakup component. The latter for the important d(d,n) reaction was particularly effectively addressed at this Meeting. There are in the literature a number of evaluations of these reactions. It would be desirable if these were updated to a definitive contemporary statement. The source problems are largely technological, involving the detailed application of the reaction (such as target configuration, gas-cell windows, etc.), not in the physical reactions themselves, and that technology has been far from fully exploited. There are secondary (p,n) reactions that have special usage; one, V(p,n), was defined at the Meeting. Another, B-11(p,n), may be a promising alternative to the Li-7(p,n) reaction if the technology of target fabrication can be suitably

mastered. Inverse reactions (e.g., H(Li,n), H(t,n), etc.) have potential for increased range of monoenergetic performance and/or high intensities in local regions. Again technological concerns limit their application (e.g., the use of tritium beams, high incident energies, heavy-ion capability, etc.), and it is unlikely that they will come into wide usage.

To be most effective, material-damage studies (for fusion-energy development) require NVT in the range 10**18-20. That intensity is not available with conventional sources and special concepts (e.g., FMIT) have been abandoned. In the foreseeable future, alternate methods of damage study (e.g., charged-particle equivalence) must be resorted to.

Considerable improvement has been achieved in the characterization of contiuum fields, such as those from the Be(d,n) and Li(d,n) reactions, including the detailed specification of covariance information. They provide access to the "forbidden" energy ranges (e.g., 10-14 MeV) and can be used to obtain much needed integral information. With newly developed unfolding techniques, the latter has promise of providing long sought differential information. In addition, these sources are suitable for certain integral benchmark tests, or the mockup of engineering environments such as fusion blankets. These continuum fields maybe one of the more promising near-term advances in source applications.

Filtered beams provide valuable intensities at selected lower energies for basic and applied studies and for bio-medical applications. Coupled with the pulsed white source, they also provide intense pulsed "monoenergetic" sources that have proven very useful in special applications. Variants of these filtered beams will continue to be very useful, but in a limited scope.

14-MeV sources are a special case of the monoenergetic source, set aside by the properties of the (d,t) reaction. At the high intensities they are the only operating sources for many radiation-damage studies, and some types of integral measurements associated with fusion-energy development. The intensities can probably be increased by a factor of approximately x 10 by upgrading current technology, but already the cost of operation is limiting. As a consequence, some of the most powerful such facilities are being shut down and soon 14-MeV high-intensity capability will be confined to Japan and Eastern Europe. At modest 14-MeV intensities there are a number of applied data problems that can be effectively addressed. That was recognized in the IAEA CRP program of 14-MeV studies. The measurement problems are generally technological: the mastery of various aspects of the source and the detection methods. The latter are generally governing and the reason why large discrepancies persist in the 14-MeV data area despite decades of study. The measurement capability is very often not well developed at those institutions operating 14-MeV generators. Where there is measurement capability there is little or no interest in 14-MeV data. The technological development of 14-MeV capabilities, by adapting major accelerators to 14-MeV measurements, where broad measurement programs are routine is desirable (steps toward this end have been taken in Japan).

Energy standards were only briefly discussed. This does not alleviate their importance. For white sources, a new scale was proposed. It should be carefully reviewed and, if judged suitable, made an international standard. The coverage is good to 1.0 MeV, but weak at higher energies. There is far less guidance in the area of energy standards for monoenergetic sources. Commonly used thresholds, (p,gamma) points,

etc. are too often based upon very old data, not always easy to apply, and not conveniently summarized for reference. Updating is warranted, including new measurements, compilations and evaluations.

Relatively little attention was given to uncertainties, covariances, etc. (e.g., discussed largely in the context of the Cf-252 spectrum, field specifications and integral responses). Many aspects of neutron sources are essentially standard quantities, and far more care must be given to uncertainty specification. Perhaps the most glaring illustration of the shortcoming is the paucity of properly defined Cf-252 results suitable for rigorous evaluation (only about 400 data points were used in the above-cited evaluation).

There are some trends at major neutron facilities. The future probably implies broad programs with both basic and applied relevance. Such facilities increasingly transcend specific programs or even laboratories, and wide applicability is essential to obtain the requisite support. The concept of joint programs should be introduced at the conceptual planning stage. The major facilities are properly complimented by smaller and local facilities that remain an essential part of the measurement "mix". This duality will probably be the way of the future. Over-riding all aspects of the facility, is the availability of skilled personnel with breadth of interest and youth. In this critical aspect there appears to be considerable variation from region to region. Finally, one should always remember that the source is only one part of the measurement system and often not the major component. Other facets may be far less costly and have greater impact on achieving the overall research objective (e.g., consider the impact of the GeLi detectors, fast nucleonic equipment, and the digital computer). One should always remember the objective--achieving basic and/or applied understanding as effectively as possible.

Many of the above views were cited in my introductory remarks. The Meeting did not change their importance.

SESSION I

WHITE NEUTRON SOURCES, PRIMARILY PULSED

MULTI-PARTICLE ACCELERATOR FOR NEUTRON AND HIGH-LET RADIATION RESEARCH

R.G. JOHNSON
National Bureau of Standards,
Gaithersburg, Maryland,
United States of America

Abstract

The staff of the Center for Radiation Research of the National Bureau of Standards (NBS) has recently analyzed the neutron and high-LET radiation research program at NBS. From this study it was recommended that a full design study of a linear induction accelerator as a possible replacement for the present electron linac be performed. This paper is an updated report on the preliminary study on which that recommendation was based.

Recent technological advances have significantly improved the practicality of induction linacs for moderate-energy high-current accelerator applications. Of primary significance is the development of magnetic pulse compression techniques and the related development of iron-based metallic glasses.

The target parameters of the preliminary design were chosen with many considerations in mind and represent in most cases only modest requests of the technology. The accelerator was designed to accelerate up to 250 A of electrons to 100 MeV with a pulse structure of 100-ns maximum length at repetition rates up to 1000 Hz. Because of the versatility of induction linacs, protons and other light ions can also be accelerated with currents limited only by space charge effects. The design includes provision for accelerating protons and deuterons at maximum currents of 2.5 A and 1.2 A, respectively.

This accelerator would be a powerful and versatile tool for neutron and high-LET radiation research. Both continuous and quasi-monochromatic beams of neutrons would be available and the light ions could be used directly.

1. Introduction

In 1982 the staff of the Center for Radiation Research of NBS completed a comprehensive evaluation of research and measurement opportunities involving neutron and other high-LET (linear energy transfer) radiations. One of the principal recommendations of this analysis was to perform a full design study including cost estimates of a linear induction accelerator. Such an accelerator would not only replace the present 20-year old 140-MeV electron linac as an improved neutron source but would considerably enhance capabilities for research in several other areas. This paper is based on the preliminary study on which the recommendation was made.

The linear induction accelerator principle has been the subject of intense development over the last few years. The technology which has been and continues to be developed for these machines is impressive. These accelerators should be considered for any application where a modest-energy high-current source is required.[1] Especially significant in the present application is the development of magnetic pulse compression techniques which can provide high-voltage, high-current pulses at high repetition rates.[2] A related development is the availability of iron-based metallic glasses. The present design relies heavily on these recent developments and is at, but probably not beyond the state-of-the-art.

The principle of linear induction acceleration by magnetic induction is illustrated schematically in Figure 1. A beam of charged particles passes through a toroidal core of ferromagnetic material at the same time that a change in flux in the core is produced by a voltage pulse applied to a driving loop. A voltage appears across a gap in a second loop during the flux change. The particles that thread the core during the pulse are accelerated in the field across the gap in the second loop. In order to increase the accelerating voltage for the same drive voltage the induction cores can be stacked radially or longitudinally or both.

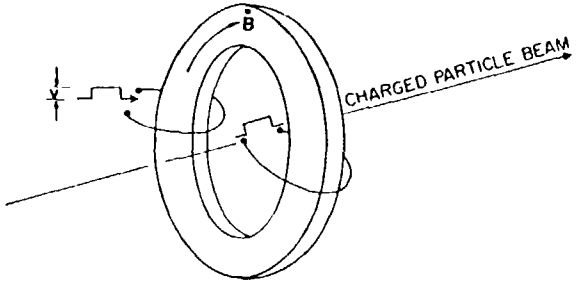

Figure 1. The principle of induction acceleration.

2. Design Parameters

Selection of design parameters for an induction linac is a difficult and somewhat arbitrary process. From the neutron and high-LET radiation research study it was clear that for the broadest applicability both intense beams of electrons and light ions with energies of at least 100 MeV are required. Although an induction linac can be designed to accelerate multi-kiloamperes of electrons, other conflicting requirements lead to the choice of a smaller current. First, the capital cost and operating cost of the accelerator increase with increased current demands. Second, the beam handling and neutron target design become more difficult at higher currents. On the other hand neutron production scales directly as power. An electron current of 250 A is a compromise for these conflicting requirements. However, this current will provide an order of magnitude increase in neutron production over the best rf electron linac currently used in neutron research.

For protons and other light ions the primary limitation in current is space charge effects. Consequently, a maximum proton current of 2.5 A and a maximum deuteron current of 1.2 A were selected. Other ion species can be accelerated with currents limited by the beam transport system.

Since a major use of the accelerator is neutron time-of-flight measurements, the pulse characteristics are important. A maximum pulse length of 100 ns and a maximum repetition rate of 1000 Hz were selected for the design. For work at higher neutron energies, shorter pulse lengths are desirable. Methods to achieve pulse compression with peak current multiplication will be discussed in a later section.

The basic design parameters of the accelerator are shown in Table 1 with the Lawrence Livermore National Laboratory (LLNL) Advanced Test Accelerator (ATA)[3] parameters shown for comparison. The ATA machine has met its design parameters.

Table 1. Induction linac design parameters.

Accelerator	NBS (Preliminary design)	ATA (LLNL)
Max energy (MeV)	100	50
Peak electron current (A)	250	10,000
Peak H^+ current (A)	2.5	--
Peak D^+ current (A)	1.2	--
Pulse length (ns)	10-100	50
Repetition rate (Hz)	100-1000	5[a]
Duty cycle	2×10^{-5}	2.5×10^{-7}

a) Repetition rate of 1000 Hz for a proposed upgrade.

3. Accelerator Design

It should be emphasized that the study presented here is a conceptual design. In a full engineering study considerable refinement and possible changes in design should be expected. The purpose in the present study is to identify the critical elements of the accelerator and to develop possible solutions which will meet the design goals. The solutions selected are at but not beyond the state-of-the-art.

a. Induction modules

The versatility of a linear induction accelerator is primarily due to the fact that it consists of a number of individual modules which are independently controlled. Consequently, the design of these modules is critical to the performance of the accelerator. One of the recent technological developments which is important in this context is the development of iron-based metallic glass. Specifically, Metglas alloy 2605CO is used as the core material for the induction modules. This material can maintain a flux swing (ΔB) of over 3 T and has a resistivity (ρ) of 130 $\mu\Omega$·cm.

The equations[4] which govern the design of the induction modules are those for the product of voltage (V) and time before saturation (τ)

$$V\tau = \Delta B A S \frac{2}{1 + \sqrt{b/a}} \qquad (1)$$

and the current at saturation (i_τ)

$$i_\tau = V \frac{\pi}{2} \frac{a}{AS} \frac{d^2}{\rho} \left(\frac{1 + \sqrt{b/a}}{2}\right) \qquad (2)$$

where a and b are the inner and outer radius of the core, A is the cross section area of the core, S is the packing fraction of the magnetic material, and d is the thickness of the metal foil.

Induction modules were designed to sustain a 450-kV pulse for 125 ns. The design is shown in Figure 2. The cores are wound with 5-cm wide 13-μm thick Metglas 2605CO with a 2.5-μm thick interlaminar insulation. This module has a 10-cm diameter beam aperture and its overall length is 37 cm. At saturation the current is 240 A. With a compensation circuit to provide pulse shaping, a module would draw 300 A during the pulse plus a beam loading of up to 250 A. The average power in each module at full pulse length and repetition rate is 25 kW.

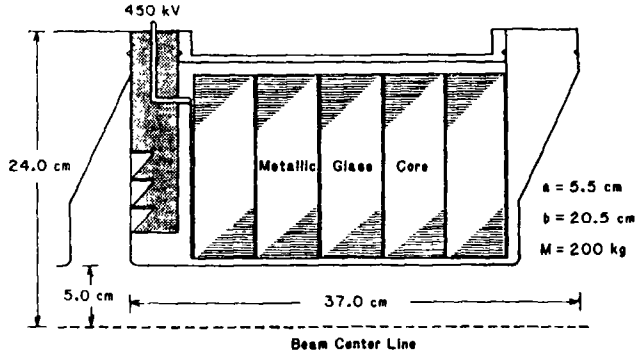

Figure 2. Half section of a 450-kV induction module.

b. Pulse Forming Network

One of the major problems in the design of a linear induction accelerator is in providing a high-voltage, high-current, fast-rising pulse to the induction modules. The development of the magnetic pulse compression

technique at LLNL[5] has provided one solution to this problem. The magnetic pulse compression drive which has been developed for ATA can produce 80-ns wide pulses at 450 kV and 25 kA. These drivers have been demonstrated to operate at repetition rates of 1000 Hz.

In Figure 3 a schematic diagram of the pulse forming network which would drive an induction module of the accelerator is shown. In concept it is exactly the same as that proposed for the ATA upgrade. However, the current requirements for the present design are a factor of 45 smaller so the scale of the device can be reduced. In fact since magnetic core volume and capacitor volume scale linearly with energy an order of magnitude reduction in scale can be expected.

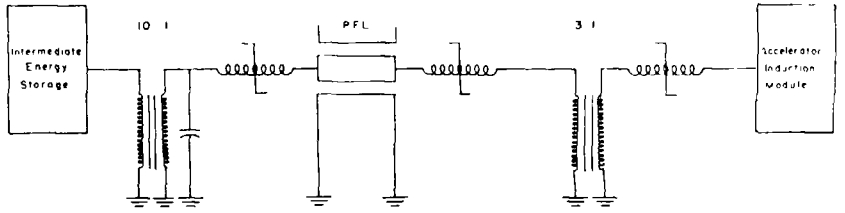

Figure 3. Pulse forming network using magnetic pulse compression.

The magnetic pulse compression is a passive technique so it requires an initial pulse to operate. This pulse is generated by conventional techniques at lower voltage, ~ 25 kV. The voltage of the pulse is then increased by a 10:1 pulse transformer. The magnetic driver contains two stages of compression. The pulse output is transported to the accelerator where a 3:1 pulse transformer and pulse sharpener feed the accelerator induction module.

Since both positive and negative charges are to be accelerated, voltage reversibility needs to be considered in more detail. Compensation circuits also need to be designed into the system.

c. Injectors

Several electron sources developed for other accelerators could be adapted for the present design. A scaled down version of the ATA plasma-board injector[6] or the thermionic gun used on the PHERMEX accelerator at Los Alamos National Laboratory (LANL)[7] appear to be suitable. The latter gun directly meets the present requirements. At a 450-kV extraction voltage this gun will deliver over 300 A with a beam radius of less than 3 cm and an emittance of about 0.01 π cm•rad.

For the light ion injector the multicusp ion source developed at Lawrence Berkeley Laboratory (LBL)[8] has been demonstrated to provide the necessary current density at the extraction grid. Again with 450-kV extraction using a dual-gap system this source can supply at least 2.5 A of protons into a beam of less than 3-cm radius and an emittance of 0.04 π cm•rad. Recent developments in pulsed plasma sources for heavy ion fusion[9] may provide an ion source with several important advantages. The new method uses a biased grid to remove electrons from the flowing plasma which effectively decouples the optics of the ions in the high voltage gap from the plasma source. Using this method, bright, uniform, low emittance ion beams have been obtained. Other advantages which may be realized for the present application are high efficiency ion production and simple control of ion species.

The extraction voltage for both the electron or ion injector would be provided by a modified induction module. A possible configuration for an injector (in this case for electrons) is shown in Figure 4. It is based on the PHERMEX design slightly reduced in size and is shown to set the scale of the design. The cathode and anode diameters are 8.0 cm and 5.0 cm, respectively. After extraction either light ions or electrons would enter a low-energy acceleration system consisting of six induction modules modified to

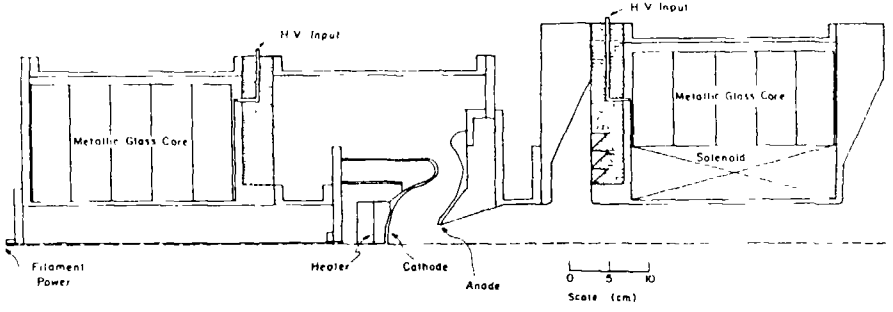

Figure 4. Electron injector (half section) for the induction linac.

accept a solenoid. These modules have a 7-cm larger inner radius and a 4-cm larger outer radius. The solenoids can provide nearly continuous focusing for the acceleration which brings the beam to over 3 MeV. In the worst case these solenoids need to produce a 5.0-kG field and would require 10 kW to do so.

d. Beam Transport

Both continuous focusing using solenoids inside the acceleration modules[3] and periodic focusing[10] have been used for induction linacs. For the present design, a periodic focusing system has been chosen because it uses less power itself and allows for smaller induction modules which use less power. A focusing system of either quadrupole doublets or short solenoids spaced every 2.0 m (after each fourth accelerating module) can provide the necessary beam transport. For example, at the low energy end of the accelerator quadrupoles with a pole-tip field of 1.3 kG focus a 1.2-A O^+ beam within an envelope with a 16% growth from waist to maximum radius. In this case the zero current phase advance and beam loaded phase advance per period are 60° and 38°, respectively--well within suggested stability limits.[11] For this focusing system (and for the injector acceleration system) the beam currents are less than half the estimated maximum currents allowed.[12]

The accelerator would require 220 induction modules and 55 quadrupole doublets. The total length of the accelerator is estimated to be 120 m.

4. Neutron Production

Before discussing the neutron production rate in detail, an additional feature of the accelerator needs to be discussed. As mentioned above, for work at higher energies pulse lengths shorter than 100 ns are desirable. For the acceleration of light ions compression of the pulse can be accomplished by appropriate shaping of the acceleration pulses. It will be assumed that provision for a factor of 10 pulse compression has been incorporated in the design of the accelerator. An increase in the peak ion current by the same factor will be obtained. The technique of ion pulse compression is being developed at LBL.[13]

For a white neutron source a number of parameters influence the energy resolution and intensity for a particular experiment including pulse width, flight path, and overlap of neutrons from one pulse to the next. To simplify the comparison of this design with other white sources only two cases are considered--low energy (eV range) and high energy (MeV range). In each case the present design is compared to typical but fictitious sources based on a rf electron linac and on a high energy proton accelerator. The comparison for low energy neutrons is made in Table 2.

Table 2. Comparison of white neutron sources at low energies (eV range).

Accelerator	Energy (MeV)	Peak Current (A)	Repetition Rate (Hz)	Pulse Length (ns)	Power (kW)	Average Neutron Strength (10^{13} n/s)
RF Electron Linac	100	1	100	2000	20	4
Induction Linac (e)	100	250	100	100	250	50
Proton Spallation	800	15	50	200	120	940

Even though electrons are not as efficient as light ions in producing neutrons, the electron currents in the induction linac are so much higher that electrons will produce the highest neutron source strength. The neutron production of the induction linac exceeds that of the rf linac by an order of magnitude. In addition, for higher energies (keV range) where the repetition rate can be increased, the neutron production of the induction linac increases directly as the repetition rate. Clearly the high energy proton spallation sources which have been designed for condensed matter research have the highest source strength for this energy region.

In the high energy region the mode of the induction linac is switched to a light ion accelerator for several reasons. First of all, it avoids problems with gamma flash. Secondly, the neutron spectrum induced by light ions is in general harder than that produced by electrons on a heavy metal target.

Finally, the pulse compression technique can be applied. The best projectile and target are, however, still open to question. Protons on a heavy target produce about four times the number of neutrons as protons on a thick lithium target.[14] However, in the latter case the spectrum will be harder and more forward peaked. For comparison of neutron sources, a proton beam and a heavy metal target are assumed.

The neutron source strengths for the high energy region are compared in Table 3. Here the induction linac has the highest neutron production. However, for some measurements the longer pulse length may reduce the effective strength.

Nearly monoenergetic neutron beams can be produced with the thin target $^{7}Li(p,n)$ reaction[15] for energies above about 25 MeV. The neutron spectrum shows a sharp peak at the proton energy and a small tail extending to lower energies. For a 1.0-MeV thick target the proton beam from the induction linac would produce a 4×10^{11} n/sr•s neutron beam at 0°.

Finally, the direct light ion beam from the induction linac will be useful in high-LET radiation studies. Applications in radiation biology, chemistry, dosimetry, and physics are foreseen. An example of such research is pulse radiolysis with light ions. For this research short high current pulses of light ions with energies above 30 MeV are required.

Table 3 Comparison of white neutron sources at high energies (MeV range)

Accelerator	Energy (MeV)	Peak Current (A)	Repetition Rate (Hz)	Pulse Length (ns)	Power (kW)	Average Neutron Strength (10^{13} n/s)
RF Electron Linac	100	100	1000	1	10	2
Induction Linac (p)	100	25	1000	10	25	78
Proton Spallation	800	0.24	50000	0.2	2	15

5. Conclusions

The linear induction accelerator, as discussed above, would provide a powerful and versatile tool for neutron and high-LET radiation research. This conceptual design fully justifies the call for a complete engineering and cost study.

As a neutron source the induction linac produces at least an order of magnitude more neutrons than the latest rf electron linac and in several areas is competitive with the high energy proton spallation sources. In addition, the induction linac can be used as a source of quasi-monoenergetic neutrons and the light ion beams can be used directly.

References

1 J. F. Leiss, "Induction Linear Accelerators and Their Applications," IEEE Trans. Nucl. Sci. NS-26, 3870 (1979).

2. D. L. Birx et al., "Technology of Magnetically Driven Accelerators," IEEE Trans. Nucl. Sci. NS-32, 2743 (1985).

3. R. J. Briggs, "High Current Electron Linacs (Advanced Test Accelerator/Experimental Test Accelerator)," 1984 Linear Accelerator Conference, ed, N. Angert (GSI, Darmstadt, 1984) 507.

4. J. E. Leiss, N. J. Norris, and M. A. Wilson, "The Design and Performance of a Long-Pulse High-Current Linear Induction Accelerator at the National Bureau of Standards," Particle Accelerators 10, 223 (1980); and references therein.

5. D. L. Birx et al., "The Application of Magnetic Switches as Pulse Sources for Induction Linacs," IEEE Trans. Nucl. Sci. NS-30, 2763 (1983).

6. C. H. Jackson et al , "The Advanced Test Accelerator (ATA) Injector," IEEE Trans. Nucl. Sci. NS-30, 2725 (1983)

7. I. A. Builta et al., "PHERMEX Electron Gun Development," IEEE Trans. Nucl. Sci. NS-30, 2728 (1983).

8. K. W Ehlers and K. N. Leung, "Characteristic of the Berkeley Multicusp Ion Source," Rev. Sci. Instrum. 50, 1353 (1979)

9. H. L. Rutkowski et al., "Ion Source Development for the Los Alamos Heavy Ion Fusion Injector," IEEE Trans. Nucl Sci. NS-32, 1742 (1985).

10. A. N. Anatsky et al, "Design of 30-MeV High-Current Linear Induction Electron Accelerator-Injector for NEP-2 Pulsed Reactor," IEEE Trans. Nucl. Sci. NS-18, 625 (1971).
11. I. Hofmann et al., "Stability of the Kapchinskij-Vladimirskij (K-V) Distribution in Long Periodic Transport Systems," Particle Accelerators 13, 145 (1983).
12. M. Reiser, "Periodic Focusing of Intense Beams," Particle Accelerators 8, 167 (1978).
13. C. H. Kim et al., "Synthesis of MBE-4 Accelerating Waveforms," IEEE Trans. Nucl. Sci. NS-32, 3190 (1985).
14. K. T. Jones et al., "Measured and Calculated Neutron Yields for 100 MeV Protons on Thick Targets of Pb and Li," International Collaboration on Advanced Neutron Sources, ICANS IV (1982).
15. C. J. Batty et al., "Intermediate Energy Neutron Sources," Nucl. Instrum. and Meth. 68, 273 (1969).

ELECTRON LINAC BASED PULSED WHITE NEUTRON SOURCES FOR HIGH RESOLUTION NEUTRON TIME OF FLIGHT SPECTROSCOPY — STATUS AND PERSPECTIVES*

K H. BOCKHOFF
Central Bureau for Nuclear Measurements,
Joint Research Centre,
Commission of the European Communities,
Geel

Abstract

With r.f linacs nowadays intense, subnanosecond bursts of neutrons can be produced which allow neutron time of flight measurements in a range covering in favourable cases 11 decades of neutron energy (1 meV - 100 MeV).

The number of neutrons contained in such short bursts is larger than the corresponding numbers generated with the short burst spallation source at LAMPF** and with the Karlsruhe cyclotron. The considerably larger average neutron intensities at the latter two accelerators are due to the much higher pulse repetition frequencies. This advantage is cancelled if pulse overlap conditions require a reduction of the p r.f. down to the level at which electron linacs operate. Taking this into account the contemporary linac equipped with a subnanosecond pulsing facility like GELINA continues to offer the best intensity/resolution performance for neutron time of flight spectroscopy between 10 keV and a few MeV

At very low (meV range) and at high (> some ten MeV) neutron energies the LAMPF neutron sources occupy with distinction the first rank while in the low MeV range the KFK cyclotron is clearly superior to electron linacs and competitive with the LAMPF short burst satellite source.

Plans or thoughts to replace some electron linacs by more powerful accelerators have existed for several years. So far none of them has had the chance of realization Instead of going the way of completely new and very expensive concepts which carry a non-negligible technological risk, for the field of applied neutron nuclear data the following two approaches are suggested:

* This is a combined paper of two presentations given by the author (at Sessions I and VII)

** Los Alamos Meson Physics Facility.

a) Case of dominant interest in neutron data for fission reactors:
Exploitation of the L-band linac to the same level as it is done for S-band linacs, including post acceleration pulse compression. This and a slight increase of the p.r.f. could bring a factor of 10 in intensity compared to contemporary electron linac driven sources. Development requirements are modest. No new infrastructure would be needed.

b) Case of dominant interest in neutron data for fusion reactors.
Use of a KFK cyclotron type source. With 70 MeV deuterons on uranium a hundred times more neutrons would be available at 14 MeV than with contemporary electron linac driven sources. No development would be required. There is however development potential for still higher neutron intensities. The γ-flash effect associated with electron linacs would be avoided.

---

1. Introduction

The interest in differential neutron data for energy applications moved within the past 40 years from thermal/epithermal to resonance data in the eV/keV range and from there now to data in the low MeV range. It therewith followed the general trend of technological developments from thermal to fast fission reactors and from here - in a projection into the future - anticipated the development of terrestrial fusion power sources. In parallel, but largely independent, suitable neutron spectrometers for the measurement of these data were developed which could cope with most of the data requirements.

The thermal reactor neutron beam sources equipped with mechanical choppers or crystal spectrometers, which were the only facilities to measure thermal neutron cross section data at the beginning of the "Nuclear Age" were superseded by electron linac based pulsed white neutron sources. The potential of these facilities for differential neutron data measurements soon proved to be largely superior to that of the first generation of neutron spectrometers, mainly due to their possibility to produce much shorter neutron bursts than the mechanical choppers, an essential requisite for high resolution neutron time of flight spectroscopy. With this property and with the progressive shortening of electron beam pulses from fractions of microseconds down to fractions of nanoseconds, last but not least also with the continuous increase of peak beam power intensities the linac based neutron time of flight spectrometers became not only matchless instruments for the measurement of neutron data in the resonance neutron energy range but also entered into a serious competition with Van de Graaff accelerator and cyclotron based sources, which before governed the upper keV and low MeV neutron energy range.

With contemporary electron linac based pulsed white neutron sources it is now possible to measure e.g. high resolution neutron transmission data in an energy range extending from one meV up to 100 MeV, covering thus 11 decades of neutron energy. The intense bremsstrahlung-flash associated with the neutron production process in high Z electron linac targets may present serious problems in some experiments. Generally it does not give rise to difficulties, since it can be attenuated to tolerable levels by suitable shielding measures.

The relative neutron intensity deficiency in the MeV range as compared to other possible source options, the interest in neutron data for fusion and the exploitation saturation of contemporary electron linac based white neutron sources give rise to plans or thoughts to replace the existing linacs by a new generation of more powerful neutron source drivers for high resolution neutron spectroscopy.

A considerable amount of information shown or used in this paper can be found in ref.(1).

2. Contemporary electron linac based neutron time of flight spectrometers

2.1. Traveling wave r.f. electron linear accelerators - a reminder

Fig.1 gives a schematic functional view of such an accelerator. Electromagnetic (E.M.) waves produced in pulses by klystrons at a power level of 20 to 30 MW are injected into an accelerator section which consists of linear arrays of resonating cavities. The dimensions of the cavities, in particular the diameter of the coupling holes which serve also as a passage for the electron beam are designed in such a manner that the phase velocity of the selected wave mode is adapted to the local velocity of the

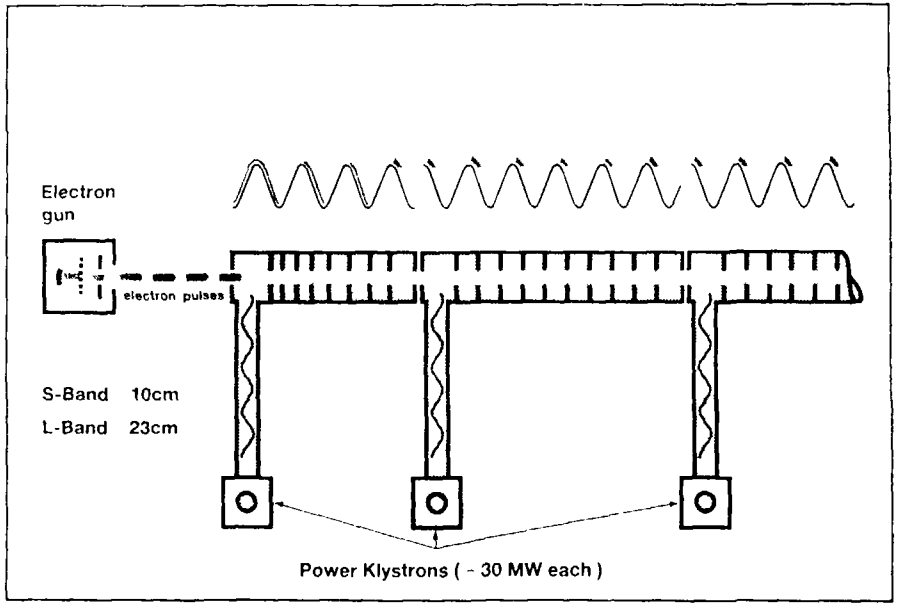

Fig 1 Electron Linear Accelerator

electrons. When this velocity approaches the speed of light, the cavity structure must not vary any longer. This is practically the case for electron energies larger than some MeV. The electron pulses are generated by a triode gun. Part of the electrons are lost since they meet the E.M. wave at the front end of the accelerator in a decelerating phase or in a phase-instable position. To increase the phase acceptance a pre-buncher is applied. In clever designs phase acceptances up to 70% of the injected beam have been achieved. The original pulse is chopped into a train of micropulses (bunches) which have widths of about 10 ps The repetition rate depends on the microwave frequency of the accelerator (~3 GHz for S-band, ~ 1.3 GHz for L-band linacs). So in an S-band linac the time interval between successive micropulses is 333 ps. The electrons of each bunch undergo phase oscillations in the early stage of acceleration before they "condense" around a working phase which is normally chosen close to the top of the wave in order to achieve maximum energy. In classical linacs the electron energy gain is of the order of 10 MeV/m. The lengths of the micropulse trains forming a (macro-)pulse can be adjusted between some nanoseconds and several microseconds The pulse repetition rates (p.r f.) can be varied between single shot and values of the order of 1000 Hz (JAERI Linac: 600 Hz, Harwell Linac: 2000 Hz).

2.2. Electron pulse compression

Resolution and spectral intensity are the essential parameters of each spectrometer - so also of a neutron time of flight spectrometer. There is a never ending quest for improving both quantities. In the case of the electron linac based t.o f. spectrometer both quantities can be dramatically ameliorated simultaneously by a practical lossless compression of the electron (macro-)pulses. Two approaches are possible: pre- or post-acceleration pulse compression. The first one was tried at the Oak Ridge electron linac (ORELA)[2], the latter one was realized at the Geel electron linac (GELINA)[3]. It is briefly reviewed below

Fig. 2 illustrates the method.

For electron pulse widths, which are much smaller than the so-called filling time Γ_f of an accelerator section (time required to fill that section with E.M. energy - for GELINA T_f = 1.1 μs), the energy gain of the accelerated electrons is exclusively won from the E M. energy stored in the cavities of the section. The first micro-pulse in the train of all those forming a (macro-) pulse sees the maximum acceleration field, the next one gets a little bit less acceleration since a (small) part of the stored energy was consumed by the forerunner. So the energy of the micro-pulses in the train is successively and monotonically reduced from the beginning to the end of the pulse. This intrinsic feature of time-energy relationship along the (macro)-pulse can be used for pulse compression:

If one injects such a pulse into a magnet system, which is designed to allow the beam electrons a 360° turn in the magnetic field before they leave the system in the original direction, then one gets the

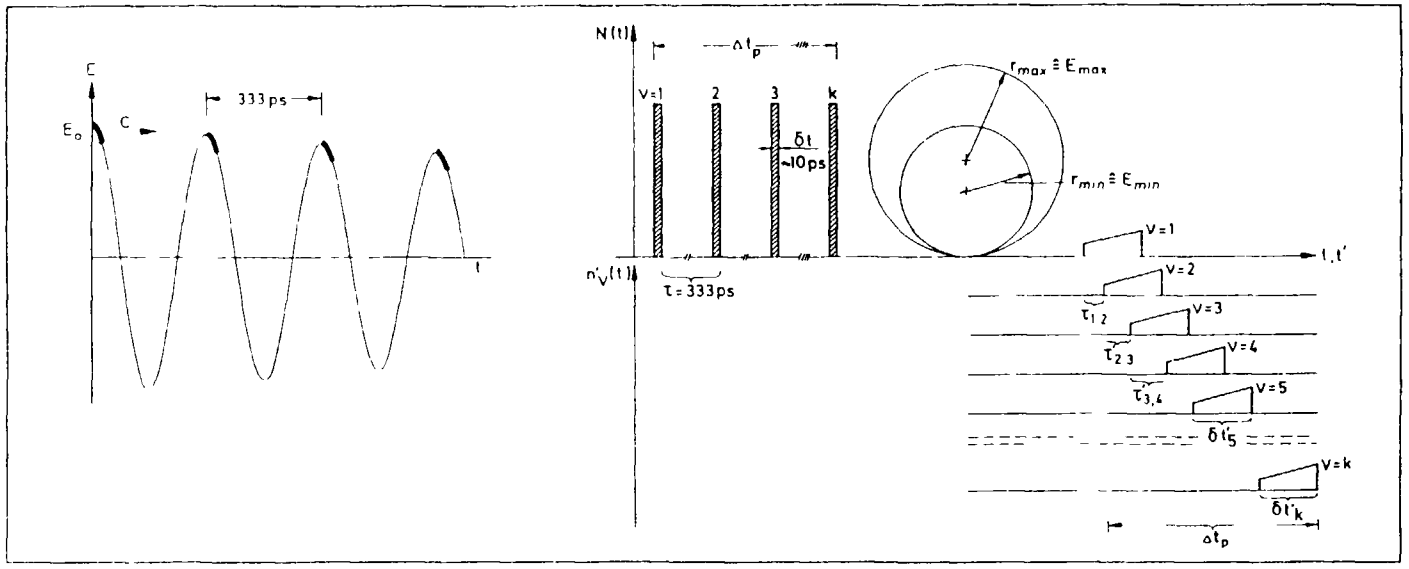

Fig 2 Post acceleration electron pulse compression at GELINA

The train of micropulses (width ~ 10 ps, spacing 333 ps) forming a (macro-)pulse of e g 10 ns width enters a magnet system from which the electrons leave after a 360° turn The exclusive use of stored E M energy available in the cavities of the Linac implies a monotonous decrease of the electron energies from bunch to bunch and therewith a corresponding length decrease of the electron trajectories within the magnet system Leading and trailing edge of the pulse come closer together The individual micropulses are somewhat stretched in time due to their energy spectrum One can find a magnetic induction B such that the transformed micropulses are stacked one on each other at the same time when leaving the magnet Pulse widths of 0 67 ns have been observed for such micropulse stacks They correspond to real pulse widths of 0 6 ns

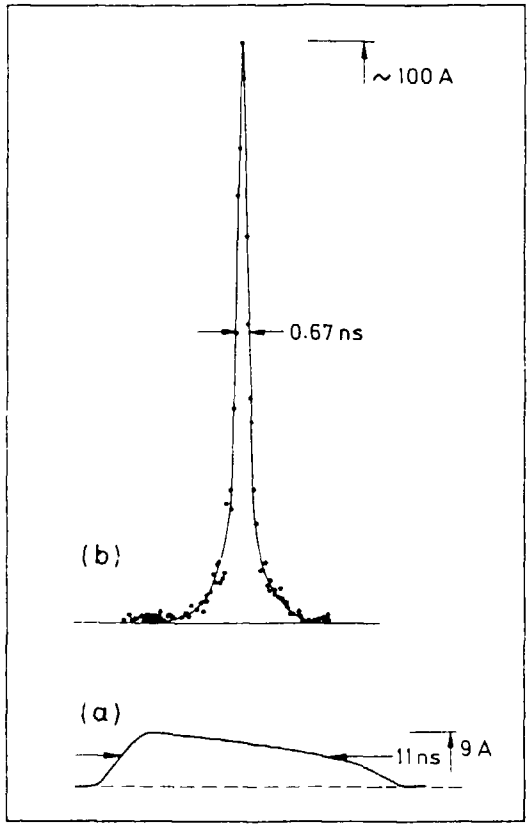

Fig. 3.

Inititial (a) and compressed (b) pulses measured at GELINA with a plastic scintillator by means of the γ flash

first micro-pulse (having the highest energy) moving on the largest trajectory and the last micro-pulse (with the least energy) moving on the smallest one. Since all the electrons after acceleration have speeds close to c, a compressed pulse appears at the exit of the magnet system. It contains practically the same number of electrons as the entrance pulse. This means that the pulse height is increased in the same rate as the pulse width is shortened. **Fig. 3** shows a result measured via the γ-flash by means of a plastic scintillator[3]. Pulses with an average width of 0.6 ns have been so obtained. Recently a pulse compression magnet has been proposed and patented in which the electrons can perform a double turn [4]. This allows a reduction of the diameter of the magnet.

2.3. Linac targets

The accelerated electrons impinge on a thick high Z target (uranium or tantalum), generate there an intense bremsstrahlung-flash which subsequently produces in the same target body photo-neutrons and in an U-target to a lesser amount also fission neutrons. Above about 30 MeV electron energy the neutron production rate is nearly proportional to the electron beam power [5]. From a thick natural uranium target about 6 neutrons are emitted per 100 electrons of 100 MeV. Use of enriched uranium increases the rate by only ~10% [6]. The corresponding neutron production rate of tantalum is about 60% of that of natural uranium. Both water and mercury cooling is in use. Power density in the targets may reach several tens of kW/cm^3. Mercury cooling is preferred if neutron moderation is to be avoided. (Moderators can be placed independently if required.)

Fig. 4a illustrates the design of some targets in use or provided for use at contemporary electron linacs. At the Harwell electron linac (HELIOS) a special booster target [7] is still available as a supplement to the high power fast target. This uses the neutron multiplication of a small subcritical ^{235}U assembly to enhance the neutron output by a factor of 10 with respect to the conventional target. The application of the fission chain reaction is unavoidably coupled with a broadening of the neutron burst width In this case the burst width is 120 ns which limits the use of the booster source to t.o.f. measurements in the thermal/epithermal neutron energy range.

Besides the existing stationary and rotary mercury cooled natural uranium targets also a heterogeneous U-Be target [8] will be in use at GELINA which should enhance the neutron yield above 10 MeV by a factor two to three Calculated neutron yields for such a target are shown in **Fig. 4b**.

2.4. Neutron spectra/moderators

Below a few MeV the original neutron spectrum, produced by an electron bombarded uranium or tantalum target, is similar to that of a fission neutron spectrum. It extends however to higher energies. Even at 100 MeV a small but still useful neutron intensity has been observed [9]. To enhance the spectral intensities at eV/keV neutron energies moderators consisting of polyethylene or water are placed as close as possible to the targets. Polyethylene can only be used at relativily low electron beam power levels. It exhibits radiation damage resulting in deformation, cracks and gradual neutron spectrum hardening. The "life time" of such a moderator is about 4 kW (beam power) weeks. The optimization of the dimensions of the GELINA polyethylene moderator was based on Monte Carlo calculations [10] which also yielded energy dependent distribution functions of the moderation times (resp. distances) and their averages as well as the spectrum of the escaping neutrons. At GELINA this moderator is now replaced by beryllium canned water moderators situated above and below the rotary target. Beryllium is used instead of stainless steel to avoid resonance structured neutron beam intensities. Neutron spectra obtained at GELINA with and without polyethylene moderator are shown for higher neutron energies in **Fig.5a**[11] and with moderator for thermal/epithermal energies in **Fig.5b**[12].

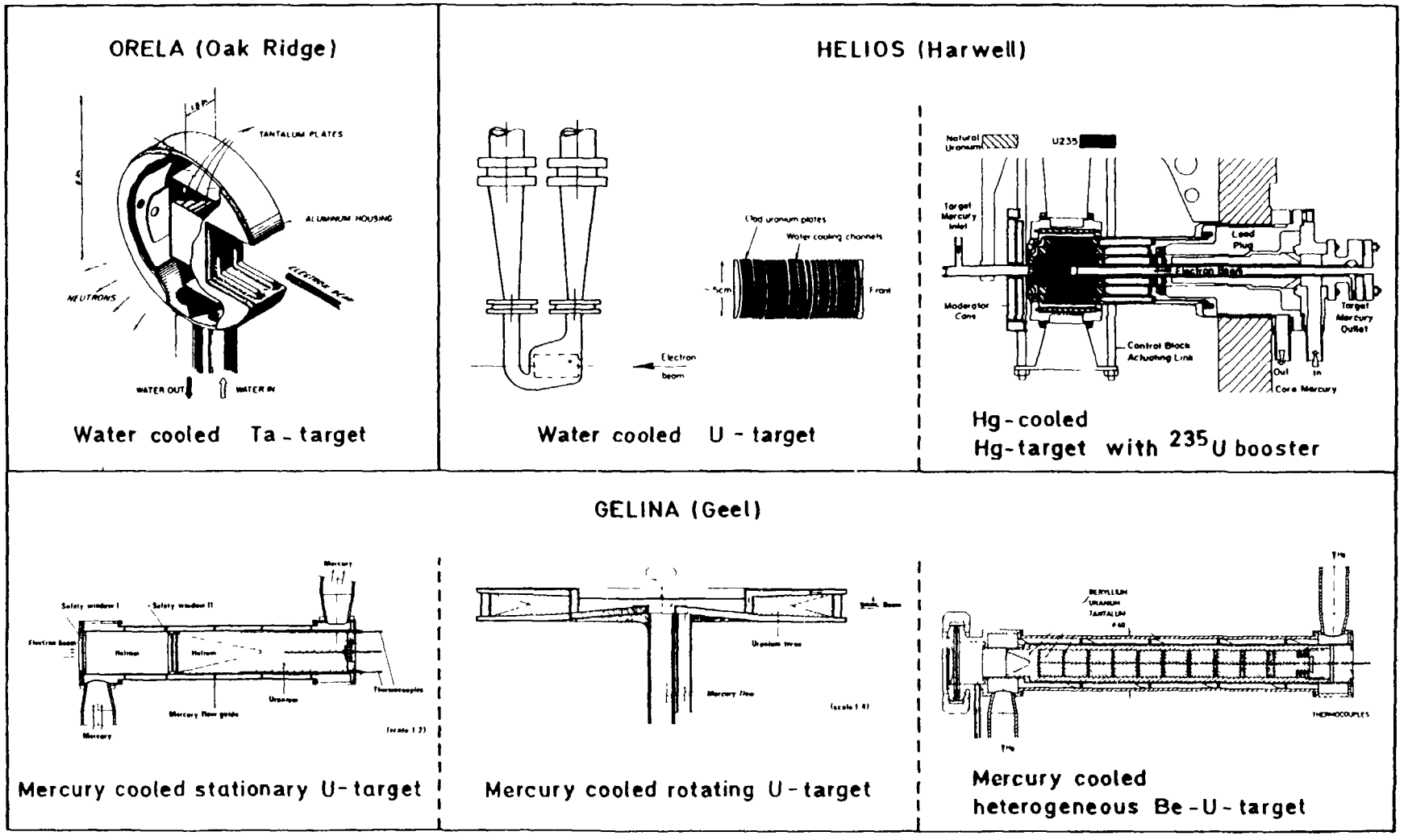

Fig. 4a. Neutron producing targets at some contemporary electron linacs

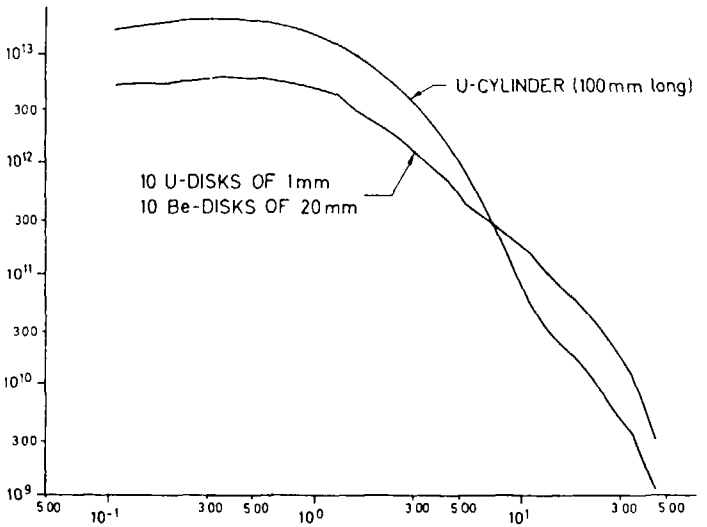

Fig. 4b. Calculated neutron yields of a uranium and a heterogeneous uranium-beryllium target

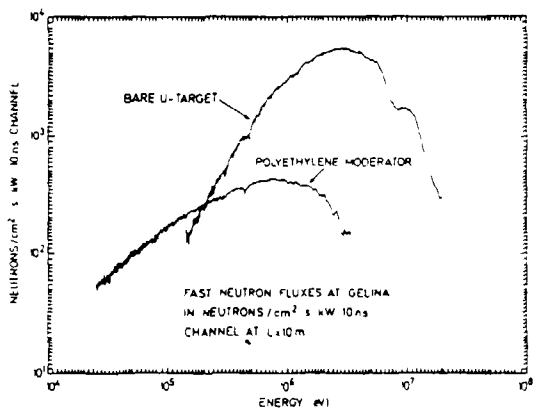

Fig.5a Polyethylene moderator. keV/MeV range

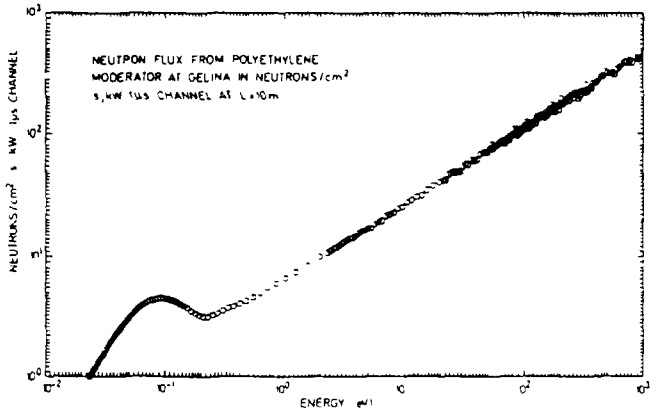

Fig.5b Polyethylene moderator meV/eV range

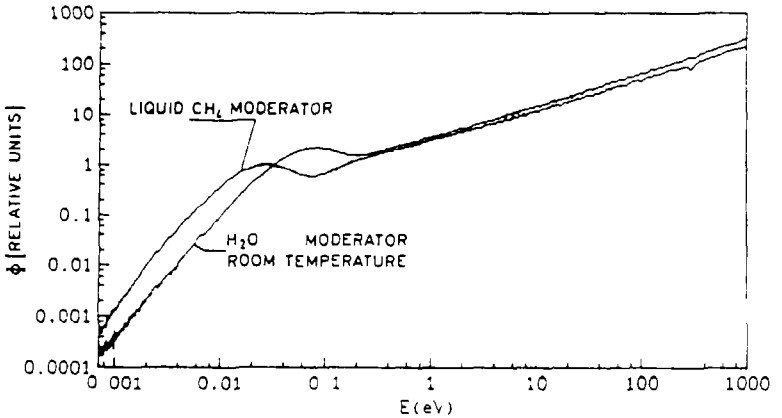

Fig.5c Liquid CH_4 moderator (-164°C). meV/eV range

Fig's 5. Neutron spectra at GELINA

To enhance the neutron intensities at subthermal energies a liquid methane moderator has been installed at GELINA which operates at -164°C. **Fig.6** shows the construction and **Fig.5c** the neutron spectrum obtained with this moderator[13] in perspective with the spectrum available at ambient temperatures with a water moderator. A spectrum enhancement factor of up to five can be achieved by the CH_4 moderator below 25 meV.

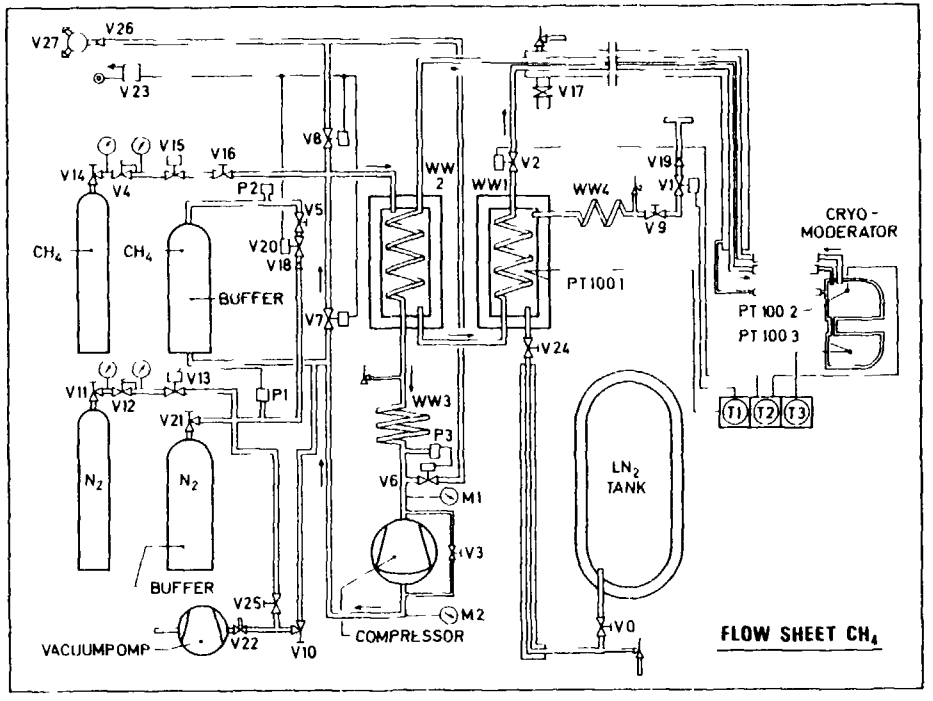

Fig. 6. Liquid methane moderator

2.5. Neutron time of flight facilities

The neutron emission from the electron linac targets described above is nearly isotropic This allows the installation of many flightpaths, which to a good fraction can be operated simultaneously (annual average at Geel . ~5 of 12 installed) The stronger foreward peaked γ-flash favours flightpath installations around the direction vertical to the electron beam axis. **Figure 7** gives examples of lay-outs of some major neutron time of flight facilities around electron linacs

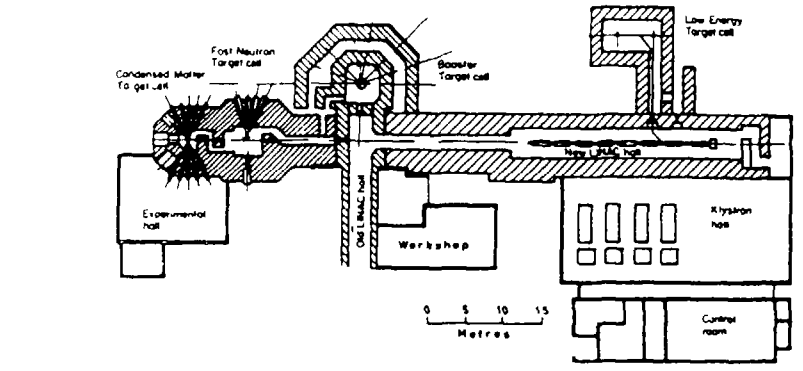

HARWELL

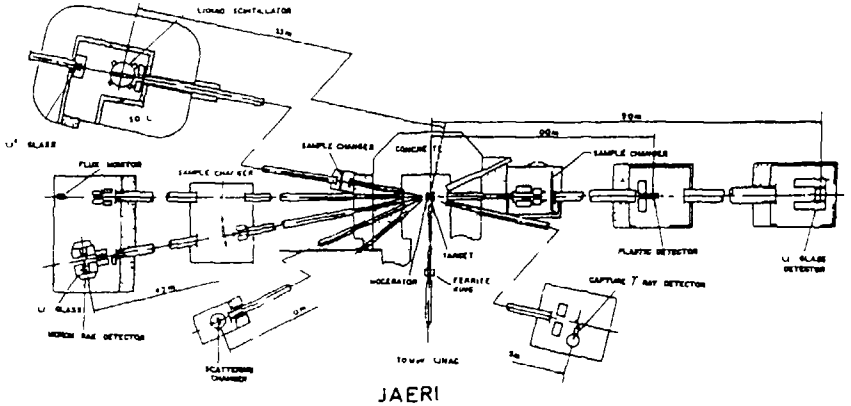

JAERI

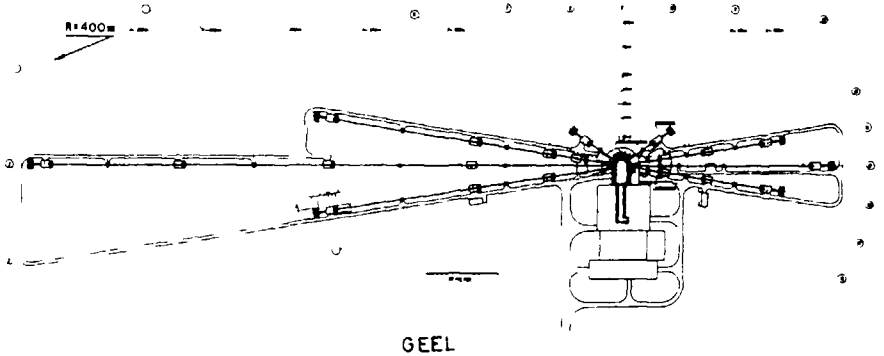

GEEL

Fig. 7. Some linac based neutron time of flight facilities

2.6. Intensity/resolution considerations pertaining to pulse compression

For any given spectrometer spectral intensity and resolution are normally anti-correlated: The better the resolution, the smaller the spectral intensity and vice-versa. In the case of pulse compression both the neutron pulse intensity and the resolution become better at the same time ! We investigate here the improvement of neutron intensities for a given total energy uncertainty, when pulse compression is applied:

If I(E) denotes the number of neutrons per cm^2, keV and second arriving at a distance L from a pulsed source, which emits S(E) neutrons per keV and second isotropically and if ΔE is the total neutron energy uncertainty produced by the flightpath length uncertainty ΔL and the flight time uncertainty Δt, with

$$\Delta L^2 = \Sigma \Delta L_i^2 \quad ; \Delta t^2 = \Sigma \Delta t_i^2$$

then one may express I(E) by S(E) and these uncertainties:

① $$I(E) = S(E).\Delta E^2/16\pi E^2 \ (\Delta L^2 + E\Delta t^2/72,3^2)$$

(E is measured in MeV, L in meter and t in ns).

Comparing now two t o f. spectrometers with equal energy resolution ΔE, the same source strength S(E) and the same ΔL one obtains for the intensity ratio

② $$V(E) = \frac{I_1(E)}{I_2(E)} = \frac{\Delta L^2 + E.\Delta t_2^2/72,3^2}{\Delta L^2 + E.\Delta t_1^2/72,3^2}$$

$$\rightarrow \left(\frac{\Delta t_2}{\Delta t_1}\right)^2 \quad \text{for } \Delta L^2 \ll E.\Delta t^2/72,3^2$$

This is the case of pulse compression if we denote with index 1 intensity and time uncertainty after and with index 2 before compression.

One has to make here the following remarks:

- the shortest routinely available, intensity optimized pulse width at GELINA without pulse compression is 4 ns and the corresponding peak current 10 A To assess the real improvement one has to compare the spectrometer operated with these parameters and that one available now with pulse compression (starting pulse width: 10 ns, peak current· 10 A).
- the other time and length uncertainties must be taken into account. This strongly reduces the advantage factor for most of the experimental situations But what is left is still considerable.

Fig. 8 displays ratios **V(E)** of the neutron intensities of the old (4 ns) spectrometer to those of the new one (10 ns → 0.6 ns compression) for a target without moderator (negligible moderation time) The ratios are calculated for the respective cases of target and detector contributions to the flight length uncertainties of 1 cm each (upper curve) and 2 cm each (lower curve). The parameters for the Δt_1 contributions quoted in the plot correspond to the realistic case of a performed transmission experiment. The plot demonstrates·

- the considerable improvement in neutron intensities for a given neutron energy uncertainty ΔE achievable by pulse compression
- the importance of flightpath uncertainties (target and detector thicknesses) even at MeV neutron energies.

It is legitimate to ask whether the burst width of 0 6 ns measured at GELINA via the γ-flash corresponds to the real neutron burst width. The rather massive rotary uranium target may in fact enlarge somewhat the original burst. There is however an indirect proof that such an effect cannot be substantial: High resolution transmission measurements have been carried out on the resonances of ^{16}O at 3438 6 keV and 3441.63 keV at the KFK cyclotron [14] with $\Delta E/E = 2.6 \cdot 10^{-4}$ and at GELINA [15] with $\Delta E/E = 1.9\ 10^{-4}$ both using pulse width of 0.7 ns and the longest flightpaths (resp. 200 and 400 m). The result is shown in **Fig.9**. The observed resonance widths seem to correspond to the resp. calculated energy resolutions which do not consider a possible burst broadening by the targets.

$(\Delta t_{burst})_1$	= 0.6 ns	$(\Delta t_{burst})_2$	= 4 ns
$(\Delta t_{ch})_1$	= 0.15 ns	$(\Delta t_{ch})_2$	= 2 ns
P_1	= 10 kW	P_2	= 4 kW

Δt_{det} = 0.26 ns

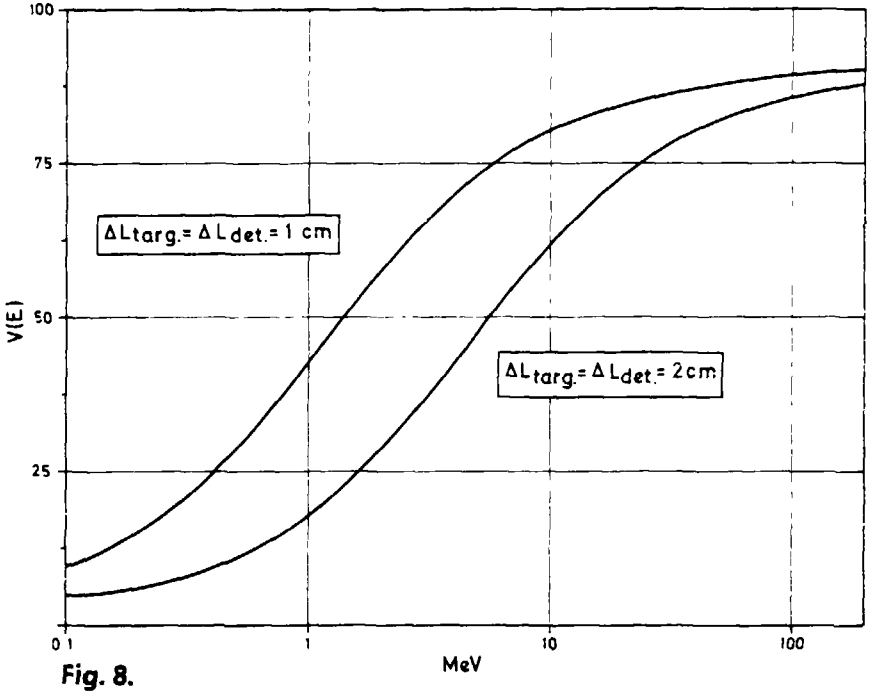

Fig. 8.

Ratios of the neutron intensities of the old (4 ns burst width) to the new (0.6 burst width) GELINA neutron time of flight spectrometer for equal energy resolution ΔE. The ratios are calculated for the respective cases of target and detector thicknesses of 1 cm each (upper curve) and 2 cm each (lower curve). The parameters for the Δt_i contributions quoted in the plot correspond to the case of a performed experiment

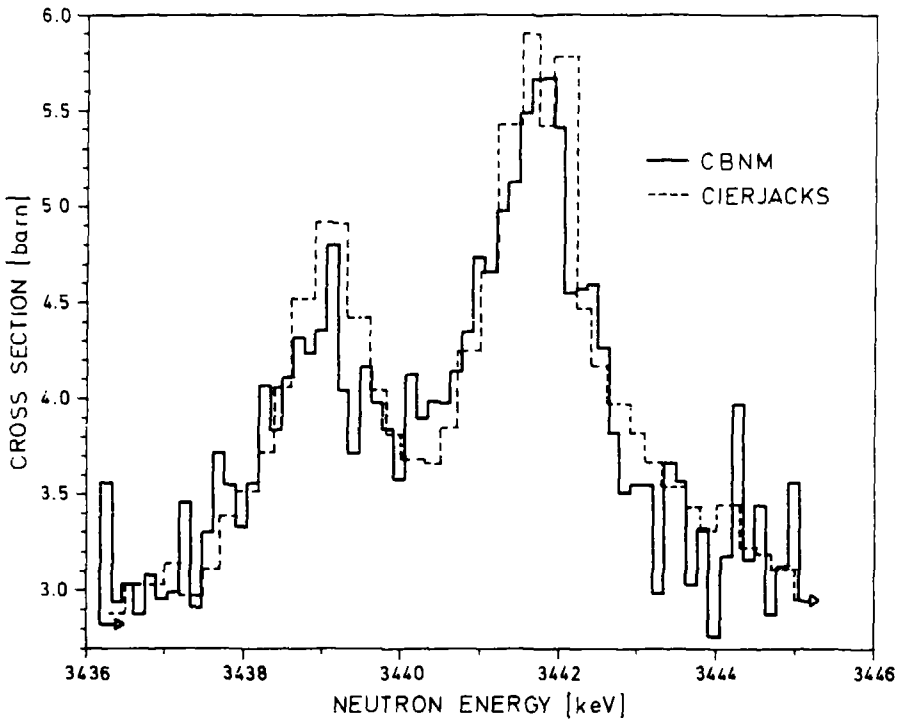

Fig. 9.

High resolution transmission data on the resonances of ^{16}O at 3438.6 keV and 3441.63 keV

- *full line :* GELINA with $\Delta E/E = 1.9\ 10^{-4}$
- dotted line : KFK cyclotron with $\Delta E/E = 2.6\ 10^{-4}$

both using burst widths of 0.7 ns and the longest flightpaths (GELINA: 400 m, KFK: 190 m)

2.7. The different types of contemporary accelerator based neutron time of flight spectrometers in perspective.

2.7.1. Intensity intercomparisons

Table I displays updated and selected information contained in table V.6 of Cierjacks' monograph [1].

In the Fig's 10 a,b,c and d spectral intensities are plotted with reference to different interesting quantities and for different source reactions used or considered for use in the past and nowadays.

Fig.10a shows the thick target neutron yields per incident particle, keV, sr and second as a function of neutron energy. It demonstrates the efficiency of neutron production by the spallation process and the relative merits of d-U, d-Be(Li) reactions for producing MeV neutrons (fusion interest).

Fig.10b surveys the thick target neutron yield per shortest bucket of incident particles, keV, sr and second as a function of neutron energy.

Electron linacs of the kind considered here operate with maximum pulse repetition frequencies (p.r.f.'s) of 600 Hz (JAERI) to 2000 Hz (Harwell) The other considered sources have much higher p r.f.'s . In t.o.f. neutron spectroscopy the p.r.f. has to be limited to avoid overlap of neutrons from successive bursts. For all those experiments in which due to overlap conditions the p.r.f. needs to be reduced down to the 1000 Hz level the sources should be compared on the base of neutron yields per burst (anisotropy effects not considered). Such situations are frequently found (depending on flightpath length, samples, detectors, etc.) when the interesting neutron energy range extends (e.g. from 1 MeV) down to the low keV or eV range. These are the cases where electron linacs have the highest application potential as compared to other accelerator types.

TABLE I Accelerator Based Pulsed White Neutron Sources
(updated and selected information. Source: table V.6 of ref.1)

Source	Particle	Target	Particle Energy [MeV]	Peak Pulse current [A]	Minimum Pulse Width [ns]	Maximum p r f [Hz]	Flight Path Lengths [m]	Neutron Production Rate in Pulse [n/s]	Best Nominal Resolution [ns/m]
GELINA a)	e	U	120	> 100	0 6	900	8 - 400	6 x 10^{19}	0 0015
HELIOS a)	e^-	U	94	6	5	2000	4 - 400	2 2 x 10^{18}	0 01
JAERI a)	e^-	Ta	120	6	10	600	15 - 190	1 4 x 10^{18}	0 05
KURCHATOV a)	e^-	U	60		50	900	10 - 300	2 9 x 10^{17}	0 16
LI+ERMORE a)	e	Ta	115	10	5	1440	7 - 250	2 3 x 10^{18}	0 02
WBS a)	e^-	Ta	120	4	5	720	20 - 200	~1 x 10^{18}	0 025
ORLA a)	e^-	Ta	140	5	3	1000	10 - 200	4 x 10^{18}	0 01
HARWELL a)	e^-	Ta	80		10	720	10 - 250	1 6 x 10^{17}	0 04
KFK SKALE b)	d	U	50	1 5	0 8	20000 (200000)	12 - 200	2 2 x 10^{18}*	0 004
KFK FZJ c)	p	U	800	0 25 "	0 2 "	58000	40 -(250)	5 x 10^{19}**	0 005

a) linear accelerators, b) cyclotron, c) short burst sattelite source

* 0-degree diff. yield x 4π

** 35 neutrons/proton (800 MeV)

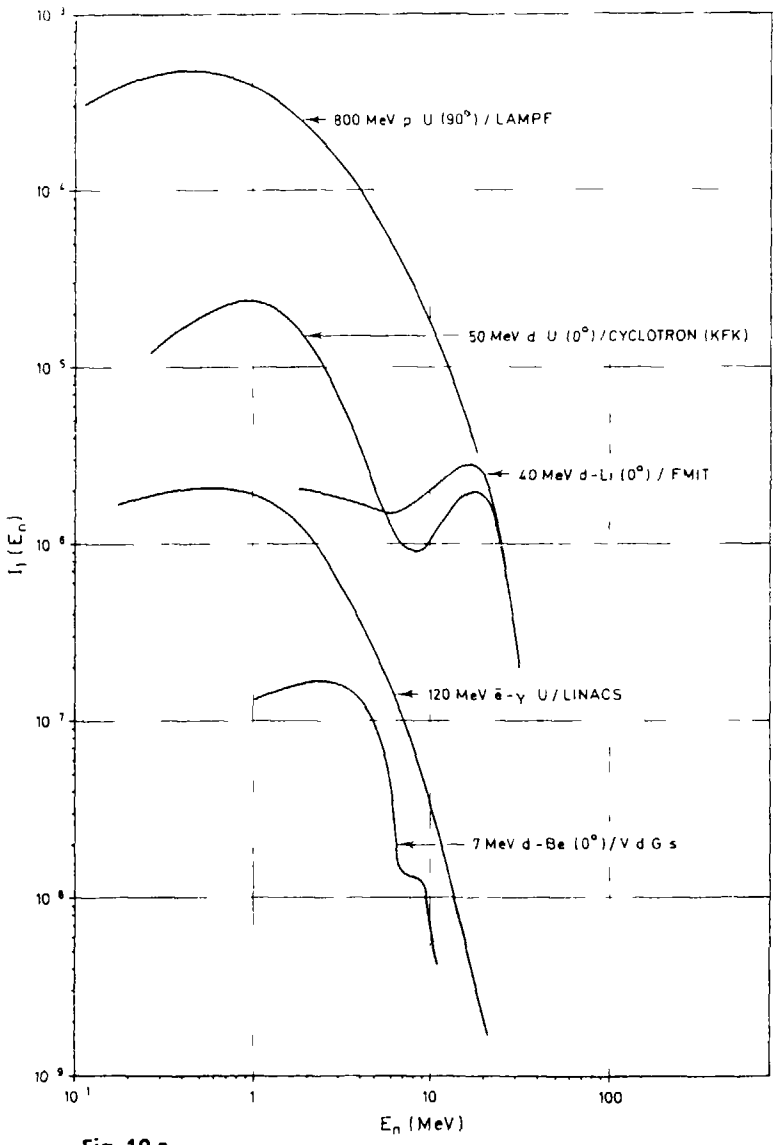

Fig. 10 a.

Thick target neutron yields per incident particle, keV, sr, for different nuclear reactions used or considered for use.

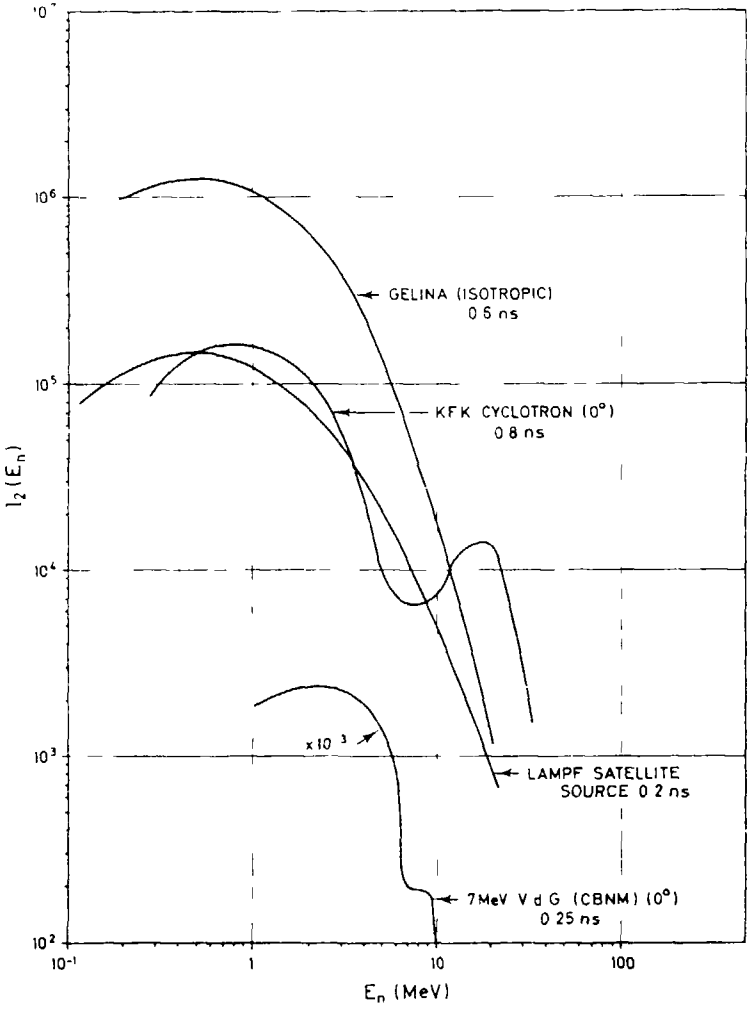

Fig. 10 b.

Thick target neutron yields per shortest pulse of incident particles, keV, sr, s

Table II gives the total number of neutrons per (shortest) burst for the different considered thick sources. It demonstrates that r.f. electron linacs produce the largest number of electrons per burst and that LAMPF and the KFK cyclotron gain their higher average neutron intensities at the shortest bursts only via the higher pulse repetition frequencies!

Table II

	p.r.f. (Hz)	Δt_{min} (ns)	part-icles/ target	particles per pulse	total number of neutrons per burst
GELINA	900	0.6	e-/U	$6 \cdot 10^{11}$	$3.6 \cdot 10^{10}$ (5)
LAMPF	58000	0.2	p/U	$3 \cdot 10^{8}$	$1.0 \cdot 10^{10}$ (23)
KFK cyclotron	$2 \cdot 10^{4}$ ($2 \cdot 10^{5}$)	0.8	d/U	$7.2 \cdot 10^{9}$	$1.8 \cdot 10^{9}$ (1)
FMIT-type*	$8 \cdot 10^{7}$	1.0	d/Li	$7.5 \cdot 10^{9}$	$3.7 \cdot 10^{8}$ (23)
7 MV V.d.G	$6.25 \cdot 10^{5}$	0.25	d/Be	$1.4 \cdot 10^{7}$	(19)

Fig. 10c presents the average number of neutrons per keV, sr and second obtained with the p.r.f.'s in Table II. No account is given to p.r.f. reduction due to overlap conditions which can be effective below about one MeV.

Fig. 10d shows the average neutron intensity per keV, sr and second for equal "instrumental resolution" R, where $R = \Delta t_b \, L$
(Δt_b : burst width in ns and L : flight path length in m.)
The value of R has been chosen equal to 0.0015 ns/m, the minimum value obtained so far at existing t.o.f. spectrometers (GELINA). It has become customary to compare t.o.f. spectrometers on the base of such a source relevant quantity, neglecting the influence of the uncertainty components other than the burst widths which normally also contribute to the energy resolution. This leads to a too idealistic picture in particular for those spectrometers using

* Fusion Material Irradiation Test Facility, (35 MeV deuterons on Li)

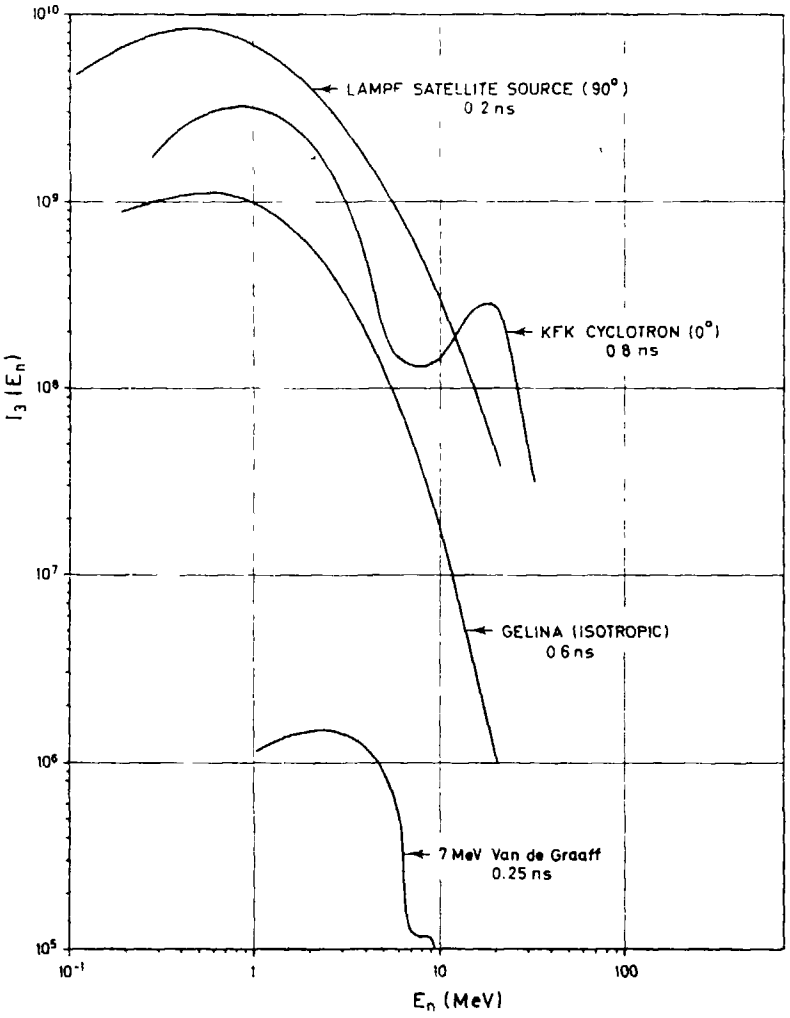

Fig. 10 c

Thick target average neutron yields per keV, sr, s for shortest pulse widths and maximum pulse repetition rates. (Table II)

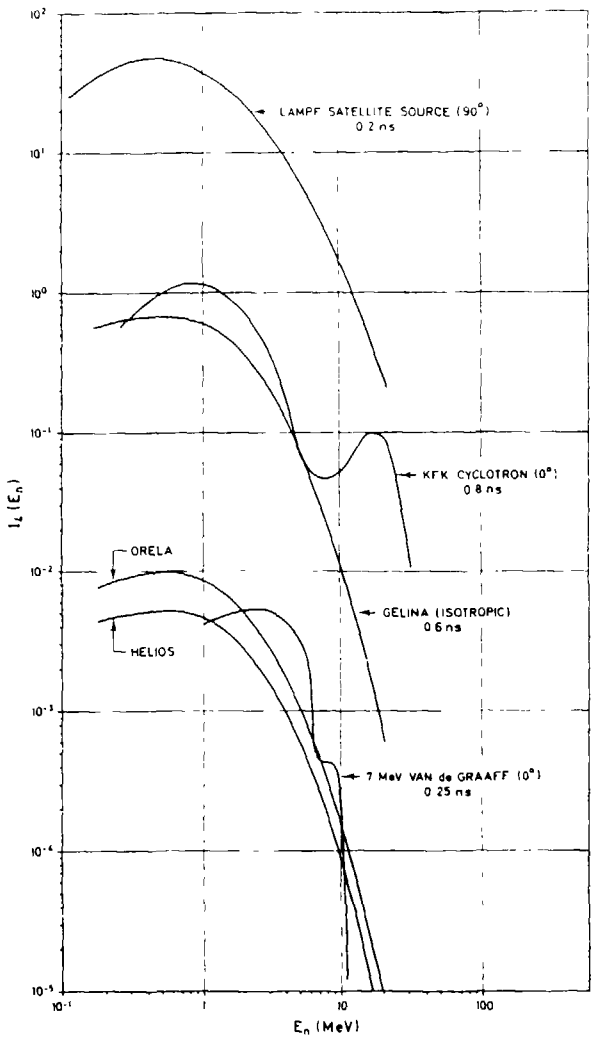

Fig. 10 d.

Thick target average neutron yields per keV, cm², s and for an "instrumental resolution" $R = \Delta t_{pulse}/L$ = 0.0015 ns/m.

The used pulse widths are given in Table II.

ultra-short burst widths (~ 0.2 ns). Here the weight of the other time and length uncertainty components to the energy resolution will in most experimental situations dominate the contribution from the burst width. This becomes evident from

$$(\Delta E/E)^2 = 4/L^2\ (\Delta L^2 + E/72{,}3^2\ \Delta t^2) \qquad (3)$$

which relates the different uncertainty components (L in meters, E in MeV and Δt in ns).

In **Fig. 11** the neutron energy E is plotted against Δt for the case where the length uncertainty contribution to ΔE equals that of the time contribution: $72.3^2\ \Delta L^2 = E\Delta t^2$

One can see that e.g. for Δt = 0.2 ns (total time uncertainty) and for a ΔL = 1 cm (total length uncertainty) the contribution of ΔL to ΔE is dominant even up to neutron energies of 13 MeV.

Instead of comparing spectrometers on the base of $R = \Delta t_b/L$ one finds sometimes also comparisons made with a fixed ΔE as a reference. Since ΔE depends on experimental conditions which differ from case to case and moreover on the neutron energy also such an approach is only of limited value.

One may better construct realistic reference model experiments designed for best possible $\Delta E(E)$ functions and use these functions as references for intensity comparisons.

It can be shown that in the case of transmission experiments performed with the same detector and the same electronics at our different t.o.f. spectrometers and with the experimental parameters used for the high resolution transmission experiments at the KFK cyclotron as the reference case (with only the flightpath length extended from 190m to 400m), the neutron intensity curves shown in Fig. 10d for the ultra-short burst width spectrometer of LAMPF and the 7 MV Van de Graaff would have to be tracked downward by a factor of up to 2.5, while the curves for the other spectrometers would stay almost unchanged.

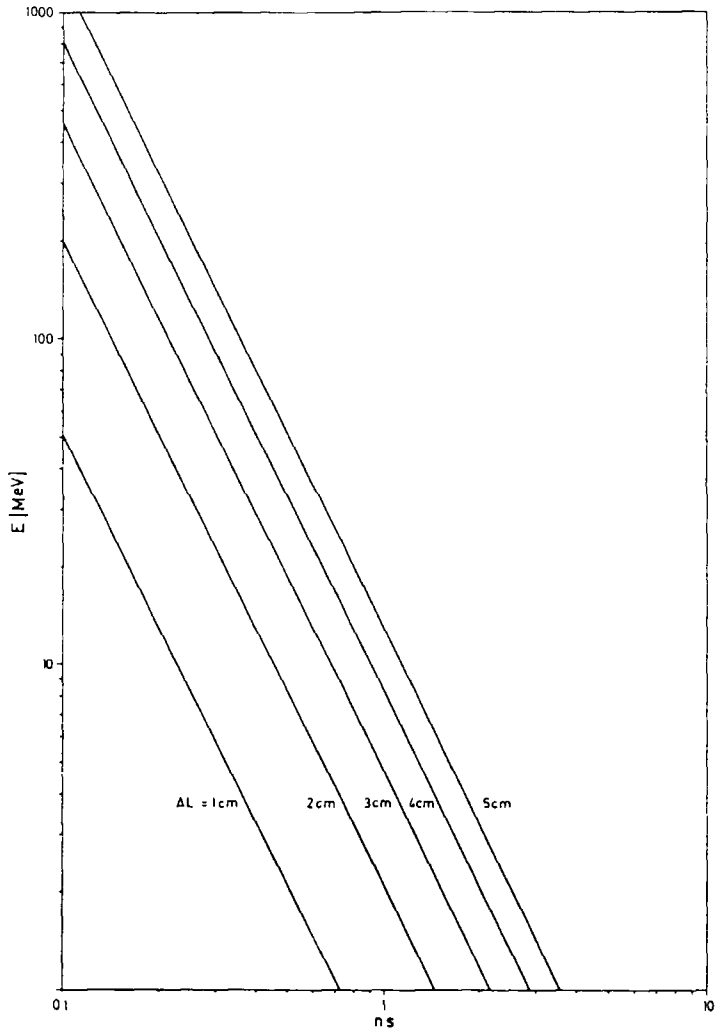

Fig. 11.

Neutron energies at which the contribution of the flight length uncertainty ΔL to the energy uncertainty ΔE becomes equal to the corresponding contribution from the time uncertainty Δt

$E_{MeV} = 0\,523\ \Delta L^2_{cm}/\Delta t^2_{ns}$

2.7.2. General Intercomparison

- **LAMPF subnanosecond beam pulse and proton storage ring facilities (28)**

  The subnanosecond satellite neutron source at LAMPF opens new dimensions in neutron time of flight spectroscopy, in particular at higher neutron energies. It has just become operational. Pulse widths shorter than 0.2 ns are available from the microstructure of a chopped ^-H beam which is accelerated simultaneously with the main ^+H beam and then magnetically separated from it. At 58000 Hz pulse repetition frequency this beam produces average neutron intensities in a W or U target which are superior to those of all other competing high resolution neutron t.o.f. spectrometers. With this neutron source experiments will be carried out in the 3-500 MeV range. At lower neutron energies, however, where t.o.f. overlap considerations limit the neutron burst rate to values below ~ 1000 Hz the r.f. linac based neutron sources are comparable or superior in intensity, depending on the direction of the neutron flightpath used at this LAMPF source. It has to be emphasized here that the spectral intensities presented in Fig.'s 10 b,c,d for that source were derived from data calculated for an observation angle of 90° with respect to the incident proton beam. In the foreward direction the intensities could be higher by a factor of up to 10. Information on spectral neutron intensities at foreward angles was not available for consideration in an intercomparison.

  Remarks :

  - Burst widths as short as 0.2 ns are only useful when all other time and length uncertainties contributing to the energy uncertainty can be made comparatively small. This is achievable at neutron energies above some 10 MeV where the ΔL contribution usually becomes relatively small.

  - There is up to now only one evacuated neutron flightpath available. This has a length of only 40 m. The (geographically)

maximum possible flightpath length is about 250 m. (At the electron linac based neutron t o f. spectrometers ORELA, HELIOS, JAERI and GELINA in total more than 40 evacuated neutron flightpaths are installed.)

Complementary to the subnanosecond pulse facility there is now also a beam available from the proton storage ring which delivers pulses of 0.27 μs width at a rate of 12 Hz on a tungsten target. This neutron source with its unprecedented high average neutron intensities of 1 10^{16} n/s will be mainly used in solid state physics applications (meV/sub-meV range). In the field of nuclear data measurements it could compete favourably with r.f electron linac based neutron sources up to about 10 keV.

Generally it may be said, therefore, that the r.f. electron linac sources are de facto superior to the LAMPF sources in the neutron energy range from 10 keV to some MeV.

- **50 MeV cyclotron at the Kernforschungszentrum Karlsruhe[1]**
(d-U source)

The Fig 's 10 demonstrate the excellent potential of such a source in particular for the measurement of nuclear data which could be of interest for future fusion reactors. At 14 MeV the 0° neutron yield per keV, steradian and second is a factor 50 larger than the corresponding 90° (isotropic) yield of GELINA and even a factor two higher than the 90° yield of the LAMPF subnanosecond source! With 0 8 ns pulse width the spectrometer also has an optimal short neutron burst capability The KFK facility has for a long time been the neutron spectrometer with the best resolution/intensity performance. It is not used any longer in a neutron data program.
Limiting remarks:
- Below 1 MeV the neutron intensities drop down quickly. Moreover the pulse repetition rates need to be reduced to avoid overlap of neutrons from successive bursts. (Fig. 10b)
- The number of possible neutron flightpaths is limited (about 3) due to the use of an internal target.

- **Electron linacs (r.f. type)**

The application potential of fast pulsed neutron sources based on this category of accelerators has its centre of gravity in the eV/keV neutron energy range where medium and heavy weight nuclei show resolvable cross section resonance structure. The enormous amount of cross section data available nowadays in this energy range has almost exclusively been determined by means of electron linacs. High quality neutron data measurements at very low neutron energies (meV range) are also possible (24a,b,c) with these linac neutron sources. In general this range is however the domain of high flux reactors (e.g. ILL) or spallation sources (e.g. LAMPF proton storage ring).
Also the MeV range is accessible with linac based neutron sources and programs to measure fusion relevant neutron data with them exist. In special (transmission) cases the energy range may even be extended up to about 100 MeV. Spallation sources like LAMPF, furthermore the KFK cyclotron facility and sources based on the d-Be or d-Li reaction offer however more favourable neutron spectra. Moreover the γ-flash may be a handicap in some linac experiments with MeV neutrons

The favourable position of GELINA with respect to ORELA and HELIOS (Fig. 10d) is entirely due to the pulse compression system, which in principle - after the installation of more powerful electron guns could also be applied at those L-band accelerators.

- **Van de Graaff accelerators**

Post acceleration pulse compressors now installed at several Van de Graaff's [26] allow pulse widths of 0.2 ns or even less. With the white neutron spectrum from a thick Be-target bombarded with deuterons such facilities are suited for high resolution neutron time of flight measurements in the low MeV range. Since both the

number of deuterons in the short pulses (Table II) and the number of neutrons per deuteron (Fig 10a) are comparatively small, a high pulse repetition rate is required to obtain reasonable neutron intensities (625000 Hz in the case of an experiment with the Geel 7 MV Van de Graaff) Fig 10d shows that between 1 and 10 MeV the intensities at best possible resolution are on a competitive level with ORELA and HELIOS, not however with GELINA. Below 1 MeV the neutron intensities become too low and p.r.f. limitations due to overlap conditions would reduce the available intensities still further.

The remarks concerning the use of ultra-short neutron burst widths which were made in the case of LAMPF hold also here. Usually only one neutron flightpath is installed or considered for installation.

3. Electron linacs and beyond

3.1. General Aspects

The incentives to replace the actual electron r.f.linac based neutron sources by a new generation of more powerful sources can be derived from the following arguments:

- electron linac based neutron sources have existed for several decades. Their exploitation has reached saturation levels. Experiments with higher degrees of sophistication (differentiation), on very radioactive materials or on samples available only in nano- and microgram quantities require a sensible increase in neutron intensities, maintaining the short pulse capacity which is available now.
- the growing interest in neutron data for fusion reactors Electron linac based sources suffer from relative neutron deficiencies in the MeV range.

General desiderata for a new accelerator based neutron source which serves the field of nuclear data for energy applications could be:

- *minimum* accelerator pulse width: < 1 ns
- average neutron intensity improvement factor pertaining to existing linac sources
  - * $E_n \leq 5$ MeV (main fission energy interest): > 10
  - * ~ 5 MeV $< E_n <$ 18 MeV (main fusion energy interest) > 100

3.2. Existing studies for electron linac replacements

3.2.1. ORELA replacement study[27]

Two conceptual design studies have been made by the Accelerator Technology Division of LANL on behalf of ORNL

a) Large Proton Linac (tantalum target)

Design goal was a 200 MeV machine capable of accelerating $5 \cdot 10^{11}$ protons per micropulse at a rate of 1000 Hz. The LANL proposal consisted of a 200 keV duopigatron multi-aperture ion source, followed by a beam chopper, a 40 MHz RFQ (acceleration from 0.2 to 5 MeV), an 80 MHz drift tube linac (acceleration from 5 to 40 MeV) and a 160 MHz drift tube linac (acceleration from 40 to 200 MeV). The calculated intensity was 3×10^{11} protons/micropulse (1 3 neutrons/proton). This means that a peak current of 2A and 200 keV would be required at the entrance of the RFQ. Pulse widths of one microsecond would be provided for long pulse mode operation. They would consist of trains of 40 micropulses. In the short pulse mode the accelerator would deliver 1 ns pulses of 200 MeV starting from 25 ns pulses of 200 keV. The total r f. power consumption would be 7.7 MW and the costs of the total facility including research was estimated to be possibly in excess of 100 million US$ (1981) **Fig. 12a** shows a block scheme of this proposal The total length of the accelerator is more than 120 m.

b) Linac Ring Compressor (LIRIC)

The second study aimed at a source which was expected to be less expensive than the first project. It concerned a system comprising a 250 MeV H^- linear accelerator of the PIGMI (Pion

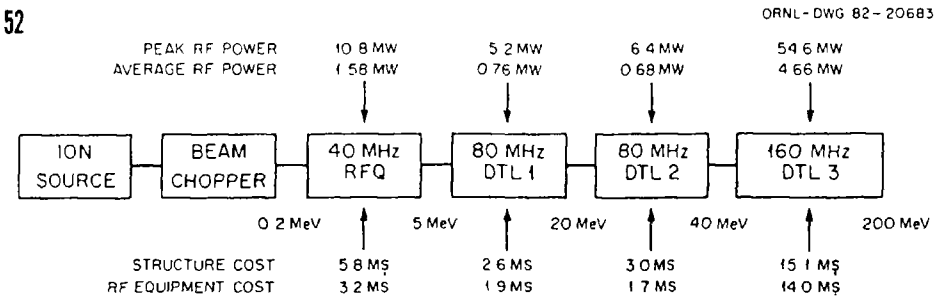

Fig. 12a

Block diagram for the large proton linac with peak rf power requirements, average rf power requirements at 100 pps, structure costs, and rf equipment cost for each accelerator section The total average rf power requirement is 7 7 MW and the total linac manufacturing cost is $ 47M (1981) The average rf power cost would be proportional to the repetition rate

Generator for Medical Irradiations) type and an accumulator ring which is filled 833 times/second with 6 circulating pulses of 6 ns. It comprised furthermore an extraction line on which these pulses are compressed to 1 ns. Each of the bunches is expected to contain $6x10^{10}$ protons. At 250 MeV about 2.3 neutrons are generated per proton. The pulse repetition rate on target is 5000 Hz. Total equipment cost was expected to be 43 million US$ (1984). **Fig. 12b** shows the design of that facility.

3.2.2. Replacement plans for the NBS electron linac[28]

Induction linear accelerators are capable of accelerating kiloamperes of electrons and amperes of protons at the comparatively low voltage gradient of about 0.25 MeV per meter (for comparison: r.f. traveling wave electron linacs: 10 MeV/m). The Livermore ATA induction linac is designed for 10 kA, 50 MeV, 5 Hz, 50 ns electron pulses[29].

NBS has published a preliminary conceptual design study for a 100 MeV induction linac which aims at accelerating 250 A electrons, 2.5 A protons and 1.2 A deuterons with pulse lengths up to 100 ns and repetition rates up to 1000 Hz. The accelerator would be used for neutron and high-LET research. No information on minimum pulse

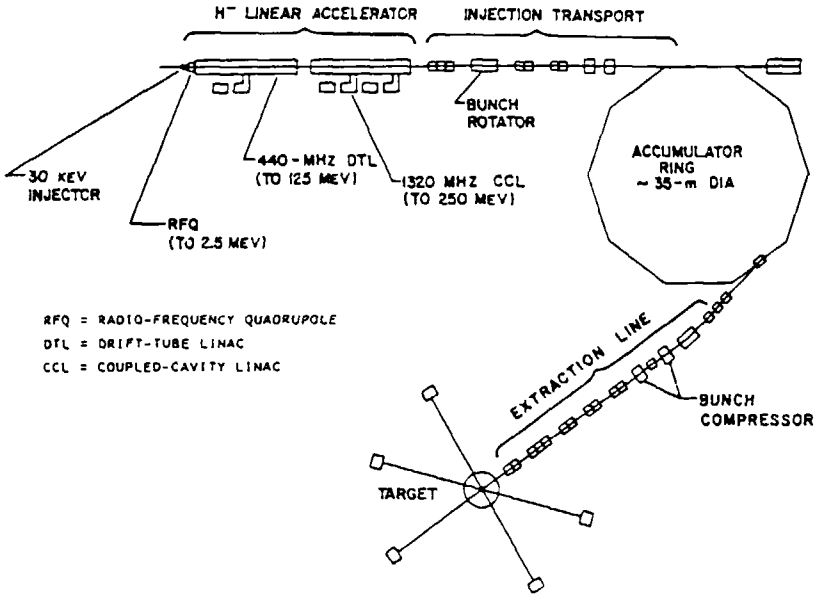

Fig. 12b.

Conceptual design for a 250-MeV Linac-Ring-Compressor (LIRIC) neutron source In the short pulse mode, macropulses are overlayed 30 times in the ring forming 6 ns-wide pulses each containing 6×10^{10} protons These protons are compressed to be 1 ns wide at the target by the 70-m-long compressor line The PIGMI would fill the ring 833 times per second with six circulating pulses giving an on-target repetion rate of 5000 pps

widths is given. The relatively low electrical field strengths in induction linacs and the desired very high peak currents do not allow electron burst widths of 1 ns or below as available at other accelerators. The minimum achievable electron burst width would probably be not smaller 10 ns. The expected high peak currents cannot compensate this deficiency. Induction linacs can therefore not compete in performance with r.f. linacs as bases for high resolution neutron time of flight spectrometers, this in particular not if the latter ones are equipped with post-acceleration pulse compression. Nevertheless they can be powerful neutron sources in applications which do not require highest neutron energy resolution.

3.3. The development potential of r.f. electron linacs - a qualitative assessment -

- S-band linacs ($\lambda \approx 10$ cm)

  The development potential of non-superconducting S-band linacs with respect to a further increase in the number of accelerated electrons in a pulse is exhausted. At GELINA pulses of 100 nC (10A, 10 ns) are accelerated. These utilize ~ 50% of the stored energy which has as a consequence that the electron energy spectra become very broad. This broadening is however fully and very usefully exploited for pulse compression. The average beam intensity may be increased noticeably only via an increase of the pulse repetition frequency. A p.r.f. of 2000 to 3000 Hz may be technically possible at the present peak power rating of GELINA. It would require substantial modifications of the existing modulators and accelerator sections.

  A superconducting S-band linac would allow acceleration of larger quantities of electrons in a bucket due to the possibility of storing in principle more E.M. energy. More important would be that the p.r.f. could be substantially increased. It is difficult to assess which overall improvement factor could be achieved for the average beam intensity. A factor of 10 does not appear utopian. The technology of superconducting S-band linacs is however not advanced enough at present to consider this possibility seriously for a new generation of intense pulsed white neutron sources. Moreover the relative deficiency of neutrons at MeV energies of interest to fusion persists.

- L-band linacs ($\lambda \approx 23$ cm)

  The energy stored in the cavities of a r.f. linac scales as the square of the used wavelengths. L-band linacs can therefore accommodate a factor of five more stored energy than S-band linacs. Consequently in short pulse mode also the maximum number of accelerable charges could be a factor of five larger. Together with a possible increase of the p.r.f. by a factor of two over the present level there may be potential for an overall gain factor of 10 in average beam power and therewith source strength as compared to the existing S-band linac sources. The increase in the number of electrons per bucket implies the construction of new more powerful electron guns which is mainly a matter of up-scaling of geometrical dimensions. Pulse compression at L-band linacs with the method realized at GELINA is principally possible. It requires just that up-scaling of intensities by λ^2 in order to use up the stored E.M. energy at the same rate as in an S-band linac.
  Such an approach would be the cheapest way to improve neutron intensities of an existing linac facility by a factor of about 10 since it would not require a new infrastructure (building, flightpaths, etc.) and could lend on existing technologies.
  Going superconducting with such an L-band accelerator could bring another factor of 10 using the same arguments as before in the case of S-band accelerators. The limiting statements made there, hold however also here.

3.4. Concluding remarks pertaining to possible advanced accelerator based pulsed white neutron sources.

The ultimate choice would depend on :

- the predominant research interest
- the level of funding possibilities

If the interest is mainly in neutron data for fission reactors (eV/keV range), then the cheapest way to achieve a factor of about 10 more neutrons than available with contemporary electron linacs, maintaining sub-nanosecond pulsing capability, would be to exploit the possibilities of L-band linacs to the same level as it is done for S-band linacs and to increase the pulse repetition rate slightly.Existing infrastructure (buildings, flightpaths) could be used.
Any further increase of beam intensities on this line would require superconducting accelerator structures.

If the interest is mainly in neutron data for fusion applications then the obvious solution is to use the d-U, d-Be or d-Li reaction with deuteron energies of 50 MeV or higher. With a cyclotron facility like that of KF Karlsruhe one would obtain 50 times more 14 MeV neutrons than with the most powerful contemporary linacs. With 70 MeV deuterons the relative gain would be more than 100. Also sub-nanosecond pulses would be available and no developmental work would be required. The investments would be substantially lower than for any other possible accelerator based source with the same intensity/pulsing characteristics. There would be probably even an inherent potential for a further increase of the neutron source strength. Without external beam the number of neutron flight paths would be limited to about three.

The **interests of basic physics** with neutrons are at present more concentrated at very low neutron energies (solid state physics) and at intermediate neutron energies. Here the spallation sources of the Los Alamos and Rutherford type or an advanced type like the envisaged (but abandonned) Julich SNQ project seem to be the most appropriate choice.
Satellite use of such a big source for applied neutron data of (mainly) fission and fusion interest is generally more expensive and inconvenient than the installation and use of the dedicated fast pulsed neutron sources quoted above. There is at present no need and justification for a spallation source which predominantly serves the neutron data field.

Acknowledgements
Discussions with Mr. J M. Salome were helpful and are gratefully acknowledged. Thanks are also due to Dr H. Weigmann for critically reading the manuscript.

REFERENCES

(1) NEANDC monograph series "Neutron Physics and Nuclear Data in Science and Technology, Volume 2: Neutron Sources for Basic Physics and Applications" (Editor S. Cierjacks), 1983

(2) Calculations pertaining to the design of a prebuncher for a 150 MeV electron linear acelerator
R.G. Alsmiller, F.S. Alsmiller, J. Barish, T.A. Lewis
Oak Ridge Report ORNL/TM-5419, 1977

(3) A new pulse compression system for intense relativistic electron beams
D. Tronc, J.M. Salomé, K.H. Bockhoff
Nucl. Instr. Meth. Vol. p.228 (1985)

(4) New optical configurations making use of circular faces between magnetic sectors
D. Tronc
Nucl. Instr. Meth. Vol. A240 (1985) 216-220

(5) see ref (1) p. 91 and p. 92

(6) Neutron producing targets at GELINA
J.M. Salomé, R. Cools
Nucl. Instr. Meth Vol. p. 179 (1981)

(7) see ref. (1) p. 110

(8) H. Weigmann, J.M. Salomé, R. Cools: unpublished

(9) F. Poortmans, private communication

(10) Monte Carlo calculations for the moderator of the pulsed neutron target of the Geel Linac
A. Bignami, C. Coceva, R. Simonini
Euratom Report EUR 5157e

(11) F Corvi, private communication and ref. (5)

(12) C. Wagemans, private communication

(13) C. Wagemans, private communication

(14) High precision time of flight measurements of neutron resonance energies in carbon and oxygen between 3 and 30 MeV
S. Cierjacks, F Hinterberger, G. Schmalz, D. Erbe, P. v. Rossen, B. Lengers
Nucl. Instr. Meth. 169 (1980)

(15) The production and measurement of ultra-short intense relativistic electron and neutron bursts
K.H. Bockhoff, F Poortmans, J.M Salomé
Procedings of the International Conference on Nuclear Data and Applied Science,; Santa Fe, USA, 1985, to be published

(16) in Fig. 10a: Calculated data for WNR target.
Private communication

(17) in Fig. 10a: ref. (1), p. 96

(18) in Fig. 10a: ref. (1), p. 96

(19) in Fig. 10a: F. Corvi, private communication

(20) in Fig. 10a: Thick-target $^{9}Be(d,n)^{10}B$ neutron spectrum at E_d= 7 MeV
A. Crametz, H.-H.Knitter, D.L. Smith
Proceedings of the International Conference on Nuclear Data for Science and Technology, Antwerp 1982
D. Reidel Publishing Company

(21) in Fig. 10d: scaled from GELINA data (ref 10) with target yield ratio and beam power ratio

(22) in Fig. 10d: scaled from GELINA data (ref. 10) with beam power ratio

(23) C. Bowman, LANL, private communication

(24) The WNR/PSR Facility - Neutron physics capabilities from sub-thermal to 800 MeV
P.W. Lisowski, S.A. Wender, G.F. Auchampaugh
Proceedings of the International Conference on Nuclear Data and Applied Science, Santa Fe, USA, 1985 to be published

(25a,b,c,) Measurements at subthermal energies at GELINA of
a) $^{235}U(\eta)$ H. Weigmann et al.
b) $^{235}U(n,f)$ C. Wagemans et al.
c) $^{238}U(n,\gamma)$ F. Corvi et al.
private communications

(26) Post-acceleration bunching system for a CN-type Van de Graaff accelerator
A. Crametz, S. de Jonge, H. Liskien, F. Jaeschke, H. Ingwersen
Nucl. Instr. Meth. A242 (1986)

(27) A preliminary study of possible ORELA replacement options
D.K. Olsen, J.A. Martin, D.J. Horen
ORNL/TM-8669-report

(28) Spallation sources for neutron nuclear physics
C.D. Bowman
IAEA Advisory Group Meeting on Properties of Neutron Sources,
Leningrad, June 9-13, 1986

(29) High current electron linacs
1984 Linac Accelerator Conference, ed. N. Angert,
Darmstadt 1984

NEUTRON ENERGY STANDARDS FOR WHITE NEUTRON SOURCES

C COCEVA
Divisione Fisica,
Centro di Calcolo del ENEA,
Bologna, Italy

Abstract

Some new experimental results and calculations bearing on calibration energies for neutron spectrometers are examined, and their influence on values and errors of the 1982 INDC/NEANDC Standard List is discussed. On this basis, a revised list is presented, to be considered as a draft proposed for the next updated issue of the INDC/NEANDC nuclear standards file.

Critical aspects of the absolute determination of resonance energies by neutron time-of-flight are discussed and some recommendations are given for the correct use of the data and for future work in this field.

1. INTRODUCTION

People having to do with neutron induced reactions often meet some difficulty in referring the results of measurements to a common energy scale. As a consequence, there is a general requirement for a set of standard neutron energies, easily reproducible on currently used neutron spectrometers.

The first paper [1] explicitly responding to such a need appeared in 1973. It provides a list of 89 energies corresponding to peaks of "prominent, sharp, isolated neutron resonances in readily available isotopes", deduced from time-of-flight measurements, mainly performed at the Nevis synchrocyclotron of Columbia University, New York. The selected energies range from 4.2 eV (^{181}Ta) up to 0.76 MeV (^{40}Ca). Most of the quoted relative errors are around 10^{-3}, the smallest ones being $\simeq 3\times10^{-4}$.

A standard set is obviously worthy as much as it is generally accepted on a worldwide basis. For this reason the problem had to be taken up by internationally acknowledged bodies. In fact, in 1981 INDC and NEANDC decided to publish periodically a joint standard file of neutron data including the item "Neutron Energy Standards".

In the frame of the work promoted by these committees, G.D. James reviewed the experimental data [2] and eventually published a list [3] of neutron energies in the "1982 INDC/NEANDC Nuclear Standards File". A more recent review was presented by G.D. James [4] at the 1984 Advisory Group Meeting on "Nuclear Standard Reference Data".

To my knowledge, outside this international frame, there are two lists which were presented in the United States as "Standard Neutron Energies" an evaluation [5] published in FNDF-300 (October 1979) and a table [6] appeared in an appendix of the last edition of "Neutron Cross-Sections" volumes (1984). However, these tables have no official character, in fact CSFWG has not recommended any specific value

The 1982 INDC/NEANDC table represents a substantial improvement over the first Columbia data. The new list includes 40 resonance energies, ranging from 0.65 eV (^{191}Ir) up to 12.1 MeV (^{12}C) Quoted errors are an order of magnitude smaller than in ref. [1].

Nine resonances are common to both tables it is interesting to note that for five of them the new values are outside the confidence limits quoted in the first table [1] From this we argue that experimentalists may not always be fully aware of systematic errors affecting their measurements In the following we shall have to consider this possibility if we want to establish a set of "enduring" standard values.

Having issued their basic table, the two Nuclear Data Committees have taken the task upon themselves of reviewing the data from time to time, and bringing their joint file up to date The present paper is based on the work performed to do such a task.

In the following, the consequences of new information now available are examined, and a revised table of standard energies is presented. Some aspects of neutron energy measurements are then discussed. From this, indications are drawn on the correct use of standard values and on future work which could improve the data quality.

2. REVISION OF THE 1982 TABLE

In revising the 1982 data, all of which are from time-of-flight measurements, we make use of new information on the following items

- Moderation time of source neutrons at ORELA
- Length of neutron flight-paths at ORELA
- ^{16}O and ^{12}C resonance energies above 3 MeV
- Velocity-to-energy conversion constant for neutrons.

The above points are discussed separately in the following four sub-sections

2.1. Moderation distance of source neutrons

The main body of data used in the compilation of the INDC/NEANDC table comes from time-of-flight measurements [7] carried out at ORELA (Oak Ridge Electron Linear Accelerator) on a flight-path 150 m long. In this work, systematic errors, which are generally much larger than statistical ones, are mainly due to uncertainty in the moderation time, i.e the average delay from generation of a neutron to its escape from the moderator. This time interval is equivalently given as "moderation distance" by multiplying it by the final velocity of the neutron. In the work of Olsen et al. this distance was assumed to be 16 mm, independent of neutron energy, with an evaluated error of ±10 mm.

James [2], for the Harwell synchrocyclotron, assumed a moderation distance equal to three times the neutron mean free-path at the escape energy, this is equivalent to consider the moderator as an infinite non-absorbing hydrogenous medium [8].

The effect of the finite dimensions of the moderator and of absorptions was first studied by Michaudon [9] by Monte Carlo method

The problem of the determination of the moderation-distance distribution, taking into account the detailed geometry and composition of the target-moderator assembly, was then tackled by Bignami et al. [10] in 1974 and later (1983) solved for the specific case of ORELA [11]. This work shows that the value of the average moderation distance is 21 mm at low energies and increases with energy, according to an empirical formula given in ref. [11] For example, for the ^{32}S resonance at 112 keV, the effective flight-path length should be 26 mm longer than assumed in ref. [7].

By using these results, all ORELA data can be corrected and the corresponding part of the systematic error greatly reduced. Likewise, a similar correction can be applied to the ^{32}S data of ref. [12], which were also used in evaluating the standard energies.

2.2. Flight-path length

Generally, in time-of-flight measurements each detector station is provided with a suitable benchmark, placed in a stable position, whose distance from the neutron producing target is accurately measured once for all. Then, for each experiment the much shorter distance from detector to benchmark may be determined in a relatively less accurate way.

The mentioned neutron resonance data obtained at ORELA [7] relied upon distance measurements between the neutron target and a fiducial line in the 150 m station, taken with a surveying tape when the station was being built. The reported uncertainty of such a length determination is ± 4 mm.

Subsequently, the distances on the (No. 6) flight-path were measured again using a new equipment based on a Laser interferometer [13]. The results could be compared with earlier measurements, also performed with a steel tape, but not with those used to obtain the "standard" data of ref. [7]. The new value, having an uncertainty of 1.5 mm, was found to be 17 mm higher than the old one.

Even if one trusts the new determinations, there is no reason to apply a correction to Olsen's data [7] since the length difference refers to another benchmark. However, the comparison of the results obtained with surveying tapes and with Laser teaches us that at least one of the two sets of measurements is affected by a systematic error which the experimenters were unaware of. Also for the 200 m station on flight-path No. 1, used to obtain the ^{32}S data [12], a difference of 25 mm was found, much larger than the alleged errors. Until we know the origin of the discrepancy, we can only conclude that the length measurement which we are concerned with may have a systematic error of the order of 17 mm.

2.3. Karlsruhe data

High resolution transmission experiments on Carbon and Oxigen were performed at the Karlsruhe isochronous cyclotron [14], providing a new set of calibration points above 3 MeV with a relative accuracy one order of magnitude better than the other standard values. This was achieved by exploiting the exceptional resolution (5.5 ps/m) of the Karlsruhe time-of-flight apparatus and by careful evaluation of all components of time and length measurements. Here, an advantage with respect to lower neutron energies is that source neutrons need no moderation.

Errors in absolute time calibration are negligible, while the absolute length of the flight-path was determined with an accuracy $\Delta L/L = 4.6$ ppm (parts per million). The time-of-flight corresponding to the peak of narrow resonances could be determined with a minimum uncertainty of about 25 ps.

Thus, calibration energies with relative errors as low as 12 ppm could be established.

The published paper [14] reports two tables of peak energies (notice not resonance energies). The first one lists resonances having their width Γ narrower than 10^{-3} E and relative errors $\Delta E/E$ between 12 and 20 ppm. The second table shows resonances which, having larger Γ values, are more suitable as energy standards for neutron spectrometers with a not very high resolution, here the relative energy errors range from 40 to 99 ppm.

2.4. Velocity to energy conversion

In time-of-flight spectrometers, measured neutron velocities are converted to energy by the usual formula

$$E = M_n \left[(1-\beta^2)^{-\frac{1}{2}} - 1\right] \qquad (1)$$

or, more conveniently up to ~ 6 MeV, by its approximated expression

$$E = \frac{1}{2} M_n \beta^2 \left[1 + \frac{3}{4}\beta^2 + \frac{5}{8}\beta^4\right] \qquad (2)$$

In (1) and (2) M_n is the neutron mass expressed in energy units, and β is the neutron velocity expressed in c units.

While the adopted value of the light speed c was practically constant in the last years, this is not true for the neutron mass M_n used in deducing resonance energies.

Table 1 shows the M_n values given by the successive evaluations and the values used in some neutron time-of-flight works, the corresponding deviations are referred to the "1983 evaluation" [18]. We see that M_n values used at Harwell [2] and Oak Ridge [7], which are apparently based on a 1969 evaluation [15], are lower than the currently available "best value" by an amount comparable with the attainable neutron energy uncertainties. In updating the standard energy values it is therefore worthwhile to correct the data of refs. [2] and [7] for the respective mass difference. Unfortunately this is not possible for the other data used in the compilation of the 1982 table since no information is available on the M_n values employed by the different authors.

Table 1

Adopted Neutron Mass

	Reference	Mass (MeV)	Deviation (ppm)
1969 evaluation	15	939.553	- 21.1
1971 evaluation	16	939.576	3.3
1977 evaluation	17	939.573	0.5
James (1977)	2	939.553	- 21.
Olsen et al. (1978)	7	939.551	- 23.
Cierjacks et al. (1980)	14	939.573	0.5
Mughabghab (1984)	6	939.551	- 23.
1983 evaluation	18	939.5726	-

3. THE NEW INDC/NEANDC TABLE OF STANDARD ENERGIES

Table 2 represents a draft of the new INDC/NEANDC list of standard energies. It is only a provisional one since it has not yet been endorsed by these committees.

In order to ease the use of such a table, most of the standard resonances are shown in figs. 1 through 9, where they are labelled with a full dot. These figures reproduce, from the JEF-1 evaluated library, the total neutron cross-section of ^{238}U, Pb, Fe, O and C in the energy intervals containing standard resonances. One sees that also with Pb and Fe it is not necessary to use enriched isotopes to isolate calibration resonances.

The table incorporates the new information available since the compilation of the "1982 file", outlined in the preceding section.

For U resonances the reported data are based on three sets of measurements performed at Oak Ridge [7], Harwell [2] and Geel [19], the last two covering only part of the resonances. A comparison among these three sets of data showed the existence of systematic differences in the energy scales, Harwell's values being lower and Geel's higher than Oak Ridge values. So, rather than taking an average for the resonances having more than a single energy determination, it was preferred to take an average of the energy scales and then apply a normalization factor to the Oak Ridge data, actually this led to an upward correction of 44 ppm.

Two more corrections were applied to the Oak Ridge data:

a) the effective length of the flight-path was increased according to the calculated value of the moderation distance, as explained in 2.1,
b) in the time-to-energy conversion the 1983 standard neutron mass [18] was adopted, instead of the mass used in ref. [7], with a corresponding energy increase of 23 ppm.

The systematic part of the errors given by Olsen et al. [7] might have been strongly reduced on account of the accurate determination [11] of the moderation distance, were not for the doubt raised by the new length measurements [13]. However, such a remarkable uncertainty of about 240 ppm, could be somewhat reduced taking in due account the results obtained at Harwell [2] and Geel [19] for the same ^{238}U resonances.

At low energy the two Ir values [20] were originally calibrated on the U resonance energies as given in ref. [2], in table 2 also these data were corrected according to the new energy scale.

The same normalization procedure was applied:

a) to the data of ref. [12] on ^{32}S, making use of the three ^{32}S values given both in ref. [7] and in ref. [12],
b) to the ^{56}Fe value given in ref. [3] for the resonance at 266.8 keV, making use of the other Harwell synchrocyclotron data overlapping those from Oak Ridge.

Thus, including the energies of Pb, Al and Na resonances simultaneously measured [7] with U, we should have a consistent set of reference data from 0.6 eV to 819 keV.

Table 2

Peak values of neutron resonances. Laboratory system.

Target		Energy (eV)	Error (eV)	Target		Energy (keV)	Error (keV)
Ir 191		0.6529	0.0005	U 238		4.5134	0.0011
Ir 193		1.298	0.001	U 238		5.6520	0.0014
U 238	*	6.673	0.002	Al 27		5.9050	0.0017
U 238	*	10.237	0.004	S 32		30.388	0.013
U 238	*	20.867	0.005	Na 23		53.21	0.04
U 238	*	36.676	0.008	Pb 206	*	71.22	0.04
U 238	*	66.024	0.014	S 32		97.55	0.06
U 238	*	80.740	0.018	S 32		112.23	0.07
U 238	*	145.65	0.03	Fe 56	*	266.80	0.13
U 238	*	189.67	0.04	S 32		412.5	0.2
U 238	*	311.32	0.08	S 32		818.8	0.4
U 238	*	397.65	0.09	O 16	*	1652.1	0.6
U 238	*	463.22	0.11	C 12	*	2078.6	0.5
U 238	*	620.06	0.15	O 16	*	3211.68	0.04
U 238	*	708.39	0.17	O 16	*	3438.60	0.06
U 238	*	905.2	0.2	O 16	*	3441.63	0.04
U 238	*	1420.0	0.3	O 16	*	4594.83	0.07
U 238	*	1474.1	0.3	C 12	*	4937.07	0.07
U 238	*	2489.7	0.6	O 16	*	5369.51	0.11
U 238	*	2672.8	0.6	O 16	*	6076.19	0.11
Pb 206	*	3358.2	0.9	C 12	*	6296.82	0.39
U 238	*	3458.9	0.8	C 12	*	12087.	9.

(*) Resonances shown in Figs. 1 through 9.

Above this energy the resonances of ^{16}O and ^{12}C selected as energy standards are shown in figs. 8 and 9. Unfortunately, the measured values do not have any link with the data below 1 MeV.

For the first two of these resonances, at 1.65 and 2.08 MeV, the values of table 2 are averages of results obtained at Geel [21] and Karlsruhe [22], and at Geel [21], Karlsruhe [22] and Harwell [2], respectively.

The other reference points from 3.2 to 6.3 MeV are taken from ref. [14] (see 2.3 above). It should be noted that in fig. 8 the peak at 3.44 MeV corresponds to a closely spaced doublet which may be used to check the energy resolution. Above 10 MeV the only available calibration point is given by a broad peak in the cross-section of ^{12}C; the corresponding value given in table 2 is an unpublished result obtained at Karlsruhe, already reported in ref. [4].

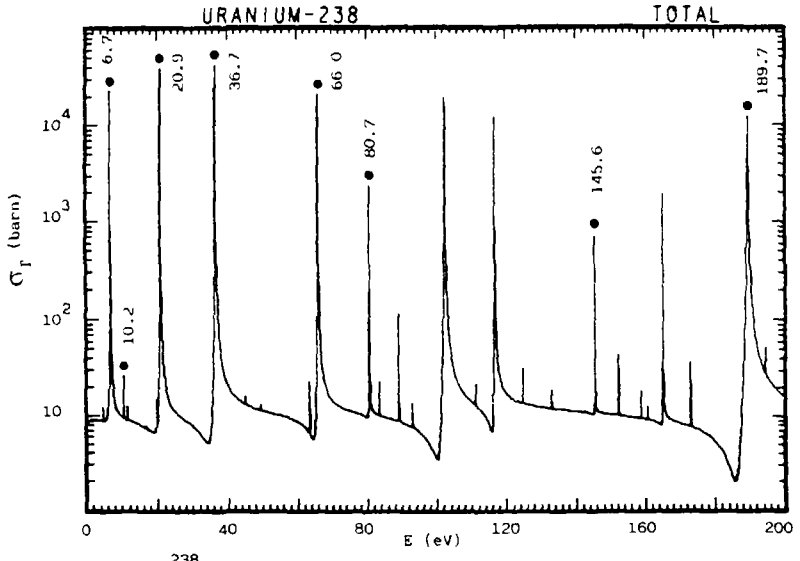

Fig. 1. ^{238}U total cross-section below 200 eV, with eight resonances selected as energy standards. Notice the logarithmic scale

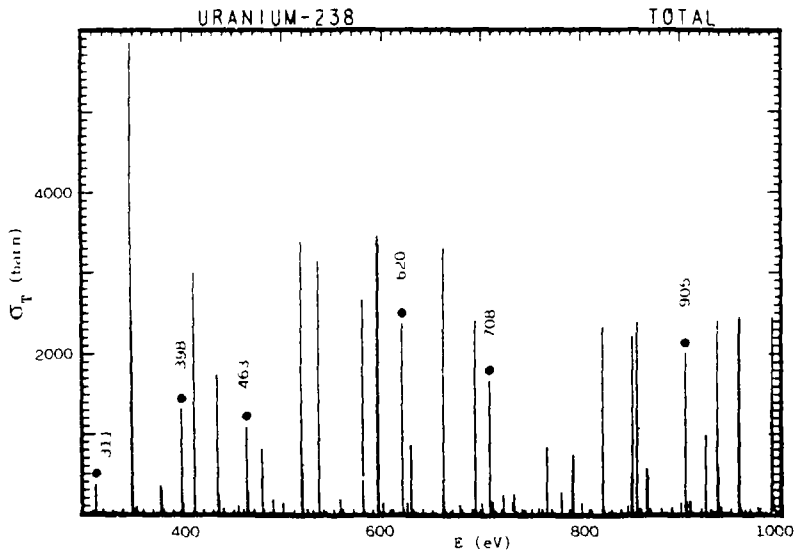

Fig. 2. ^{238}U total cross-section in the range 300–1000 eV, with six resonances selected as energy standards.

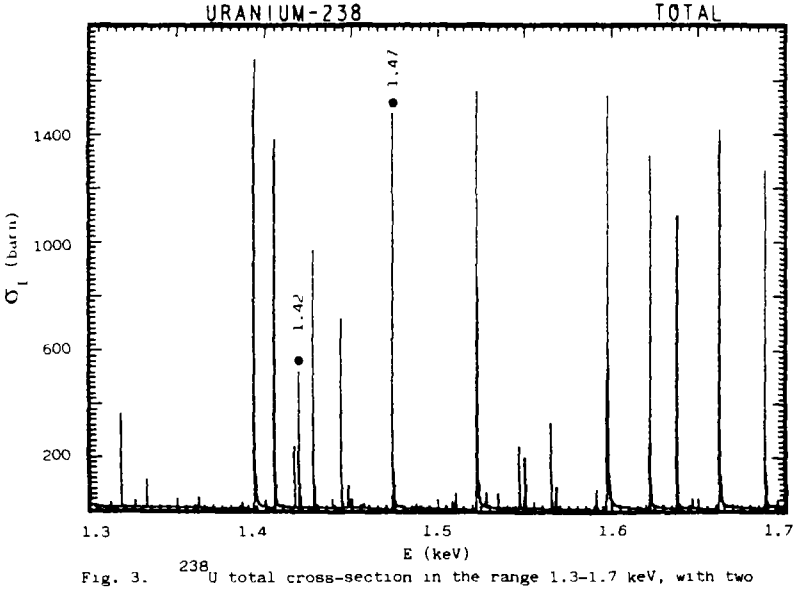

Fig. 3. ^{238}U total cross-section in the range 1.3–1.7 keV, with two resonances selected as energy standards.

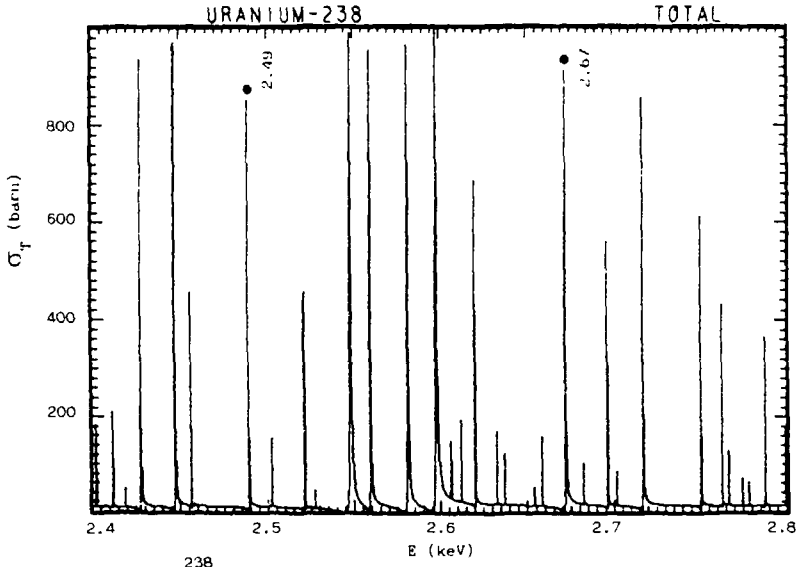

Fig. 4. ^{238}U total cross-section in the range 2.4-2.8 keV, with two resonances selected as energy standards.

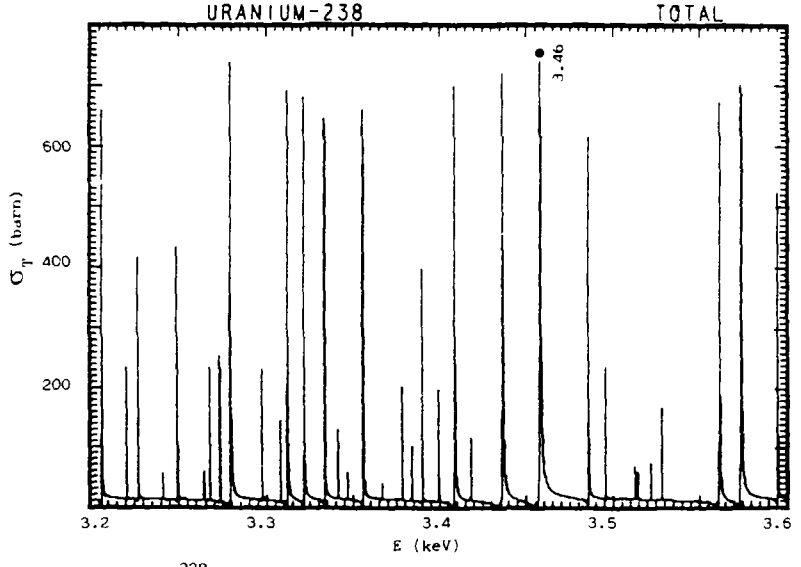

Fig. 5. ^{238}U total cross-section in the range 3.2-3.6 keV, with one resonance selected as energy standard.

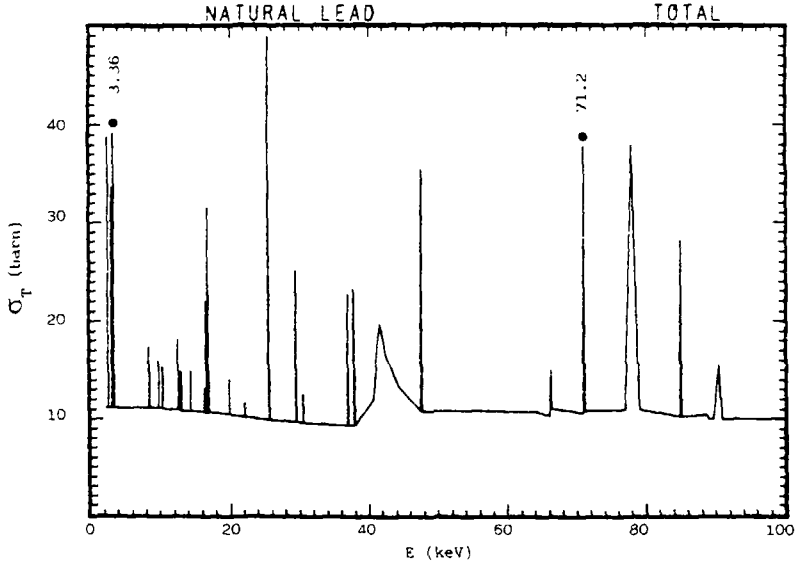

Fig. 6. Natural Lead total cross-section below 100 keV, with two ^{206}Pb resonances selected as energy standards.

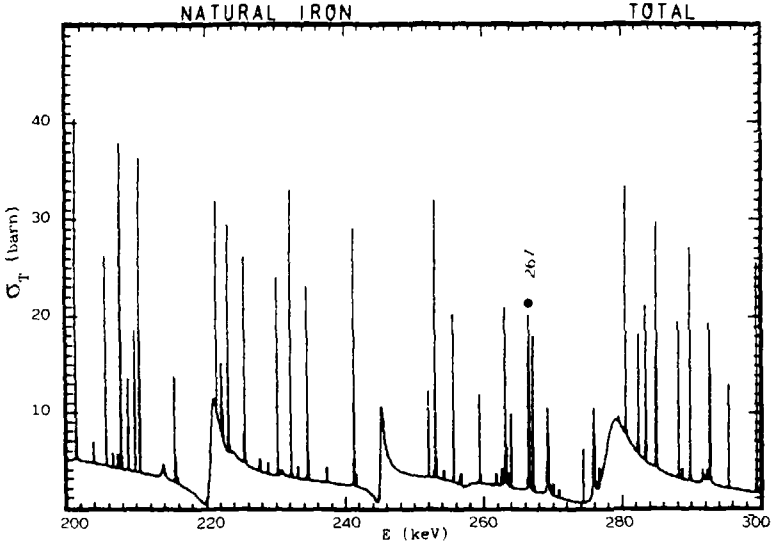

Fig. 7. Natural Iron total cross-section in the range 200-300 keV, with one ^{56}Fe resonance selected as energy standard.

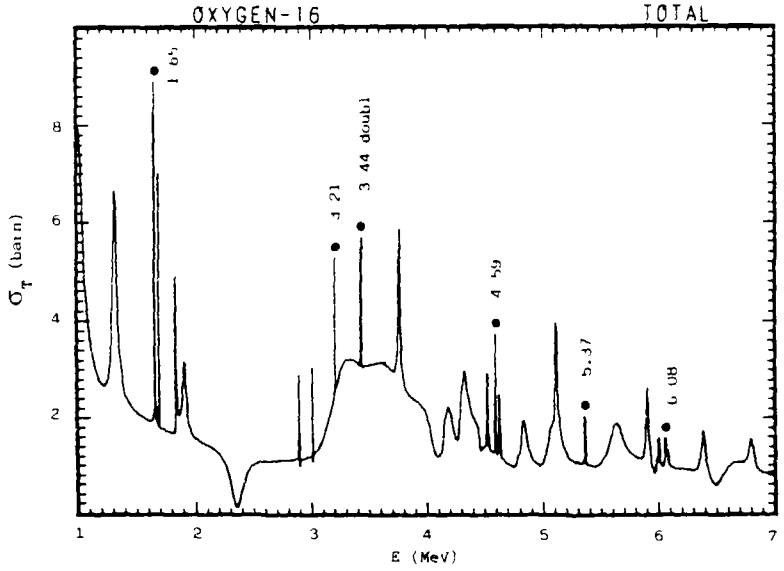

Fig. 8 ^{16}O total cross-section in the range 1-7 MeV, with seven resonances selected as energy standards. Notice the doublet at 3.44 MeV

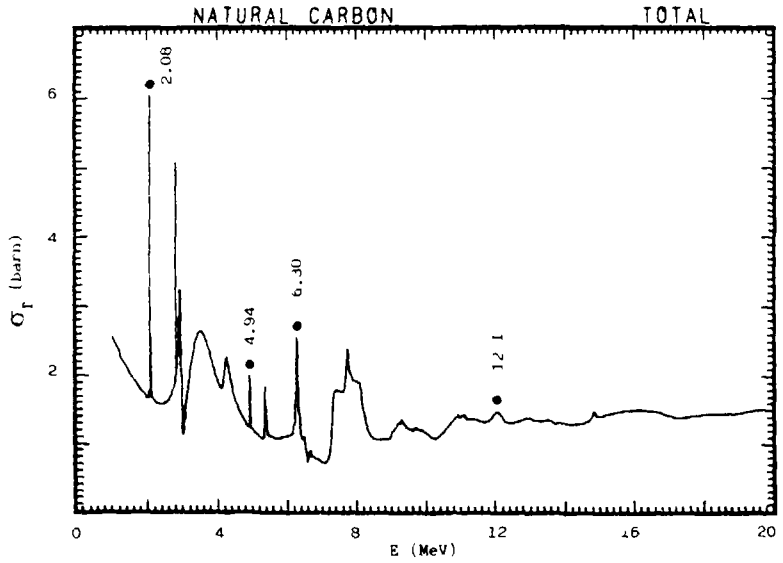

Fig 9. Natural Carbon total cross-section below 20 MeV, with four resonances selected as energy standards.

4. PROBLEMS IN PRECISE ENERGY MEASUREMENTS

An excellent review of the main difficulties and of the necessary precautions in establishing precise calibration energies is found in James' paper [2] at the 1977 Symposium on neutron standards

Here I summarize the main points with some comments.

4.1. Length measurements

The discrepant results obtained at ORELA with different measuring apparatuses prove James' right when, following Youden [23], he asserts that systematic errors should be experimentally assessed by repeating the measurement under significantly different conditions.

With modern instruments [2,13,14] it should be possible to perform length measurements with an error not larger than 2 ppm, which is entirely adequate to our purposes To this end the experience gained at CERN in this kind of precision measurements [24] could be of help.

4.2. Start time

The source-neutron start time is generally determined by measuring the time of arrival of the "gamma flash" with the same detector used for neutrons, on the assumption that gamma-ray emission is coincident with the reaction that generates neutrons.

This time may mainly be altered by two effects

a) dead time of the time-to-digital conversion system,

b) different response time of the timing discriminator for neutrons and for gamma rays.

The first difficulty is easily avoided by partially absorbing the gamma rays in order to have much less than one detection per burst. As far as the second is concerned, the time difference should be evaluated case by case according to the particular detector. Anyway, it may be advisable to use ARC (Amplitude and Risetime Compensated) rather than CF (Constant Fraction) discriminators, the former being in principle less sensitive to the shape of the detector pulse.

4.3. Stop time

The works of D. James [2] and S. Cierjacks et al. [14] have demonstrated the usefulness of using cumulative probability plots for a direct determination of the peak position of a symmetric resonance. These authors obtained an accuracy of one tenth of a timing channel.

More generally, from examination of the above work [14] and of the statistical errors quoted by Olsen *et al.* [7], it can be deduced as a thumb's rule that the time-of-flight corresponding to a narrow resonance peak can be determined with an accuracy of about one fortieth of the resolution width (fwhm). For pulsed accelerator sources having a hydrogenous moderator similar to ORELA, this is equivalent to a contributed energy uncertainty approximately given by $\Delta E/E = 10^{-3}/L$, where L is the flight distance in m.

The error in peak position due to counting statistics is usually calculated by the computer code used in fitting the data. Alternatively, the Monte Carlo procedure described by James [2] can be applied.

4.4. Moderation and detection distances

When source neutrons need to be slowed down, "moderation distance" is the length travelled by a neutron during the time interval from its generation to its escape from the moderator; this length is calculated, as explained in 2.1, for the escape velocity of the neutron. Likewise, detection distance is the length corresponding to the time interval from neutron entrance into the detector to the interaction giving rise to a detection pulse. These two energy dependent lengths must be added to the nominal flight path, which is the distance from the output face of the moderator to the input face of the detector.

Of course, at each energy the sum of these distances has a statistical distribution, which generally forms the major part of the resolution function. In order to determine the effective flight distance corresponding to a peak in the time-of-flight spectrum, in first approximation one may use either the most probable value or the mean of such a distribution. The first quantity should be used when the resolution is wider than the resonance, the second in the opposite case.

4.5. Resolution function

When we think of evaluating a reference point of a peak (be it, for instance, its maximum) with an accuracy of one tenth of a timing channel [2,14], we easily understand how the shape of the peak in the neighbourhood of its maximum must be precisely known. As a consequence, any uncertainty in the shape of a peak is translated into an uncertainty of the above mentioned reference point.

So, for high precision energy measurements we must consider that the measured time-of-flight spectrum is the convolution of transmission with the resolution function and that the flight-time of a reference point in the cross-section can in principle be obtained only through a fitting procedure which requires a detailed knowledge of the resolution function. This is particularly true for the asymmetric shape of the resolution characteristic of spectrometers based on moderated neutrons. Examples of resolution function calculation are given in ref. [25] for two experiments performed at Oak Ridge and Geel.

It must be stressed that when the resolution is evaluated by Monte Carlo simulation, like in ref. [25], all experimental details must be taken into account. For example, in the above mentioned work [25] we found that neglecting the effect of backscattered neutrons from the light guide behind the glass detector resulted in a shift of 250 ppm for the best fitted energy of an isolated p-wave resonance of ^{91}Zr at 3.16 keV.

Moreover, in a transmission measurement, the shape of an asymmetric resonance generally depends on sample thickness. To reduce this effect, the sample should be thin for the resonance under consideration. Ideally, all calibration resonances should be nearly symmetric.

4.6. The $\Delta L/\Delta t$ method

An elegant method was devised by James [2], which avoids the difficult evaluation of moderation and detection distances and which is not affected by a different response time between gamma-rays and neutrons. It consists in measuring the same transmission spectrum at two different distances along the same flight-path with the same detector. The only length which matters is the distance between the two detector positions.

A limitation to the applicability of this method is that the resonance under examination should be well resolved even in the time-of-flight spectrum taken at the short-distance station.

Moreover, this method requires, for each calibration point, a double number of start- and stop-time determinations with respect to the direct method. If we add that the flight-path length is necessarily shorter, we see that the $\Delta L/\Delta t$ method implies a substantially higher relative timing uncertainty.

It should also be observed that the ratio of the resolution to the resonance width is strongly different at the two flight distances; this means that the shape of the same peak is different in the two spectra, which brings with it an uncertainty, so as we have seen before. In this case we are back again with the unpleasant task of evaluating the resolution function.

In spite of the above drawbacks, the idea of obtaining a result based only on directly measured quantities is so attractive as to pay for planning an *ad hoc* experiment in which the resolution function should be as nearly symmetric as possible. This would allow to check, by an independent method, at least some points of the neutron energy scale.

5. CONCLUSIONS

This paper reports on possible improvements of the INDC/NEANDC table of standard neutron energies.

Below 1 MeV no new precision measurements were performed, however, old data could be corrected making use of the results of a Monte Carlo simulation of the neutron moderation process. This shows that, in principle, better accuracies than presently available can be achieved, by almost one order of magnitude. However, this might be obtained only by new experiments. In fact, in this energy range a comparison of energy scales resulting from the data obtained at Harwell, Geel and Oak Ridge disclosed the presence of systematic errors. The true difficulty is hinted also by new measurements of flight-distances carried out at Oak Ridge. We are thus led to the same conclusions reached by James in his 1977 review: for a decisive progress new measurements should be planned in such a way as to uncover possible systematic error.

The present revision succeeds in obtaining a self-consistent set of calibration points from 0.6 eV to 1 MeV, but no firm link could be established with data above 1 MeV. Future work should aim at getting round this difficulty.

A remedy for the lack of useful standard data above 1 MeV was found by introducing the results of a high precision measurement on Oxigen and Carbon carried out at Karlsruhe. These data show much smaller errors than all others; however, in this case too it is desirable to measure again the same resonances with a different experimental apparatus in order to bring out systematic errors, if any.

Besides the proposed new table of standard energies, this report provides a set of cross-section plots which might be of help in choosing the most suitable resonances for calibration purposes and the right sample thickness.

Low energy data were also corrected by employing an updated value of the neutron mass. Concerning this, it is desirable that all neutron time-of-flight experimenters consistently use a common value of the velocity-to-energy conversion constant. The presently recommended value is

$$\frac{1}{2} M_n/c^2 \quad 5227.077\ \mathrm{MeV/(m/ns)^2}$$

which corresponds to the 1983 evaluation of atomic masses.

In my opinion the $\Delta L/\Delta t$ method deserves to be applied, since it avoids measurement or evaluations of certain critical quantities such as target position (which is always in an active area), and moderation and detection distances.

For high precision work, a Monte Carlo simulation of the experimental conditions is suggested in order to evaluate the shape of the resolution function. For a realistic estimate of the error, such a function should be varied within its uncertainty limits to check the corresponding energy variation in the least square fit of experimental data.

ACKNOWLEDGEMENTS

It is a pleasure to acknowledge the interesting suggestions and information kindly provided by G.D. James, S. Cierjacks, D.K. Olsen, P. Young, A.B. Smith, A. Carlson, K.H. Bockhoff and G.C. Panini.

REFERENCES

|1| S. Wynchank et al., Nucl. Sci. and Eng. 51 (1973) 119

|2| G.D. James, Neutron Standards and Applications, National Bureau of Standards Special Publication 493 (1977) 319

|3| G.D. James, International Atomic Energy Agency Technical Report No. 227 (1983) 65

|4| G.D. James, Neutron Standard Reference Data, International Nuclear Energy Agency, Vienna, IAEA-TECDOC-335 (1985) 376

|5| F.C. Perey, Standard Reference and Other Important Nuclear Data, BNL-NCS-51123, ENDF-300, Section A: Measurement Standards, IX (1979)

|6| S.F. Mughabghab, Neutron Cross Sections, Academic Press (1984), Vol. 1, Part B, Appendix B

|7| D.K. Olsen et al., Nucl. Sci. and Eng. 66 (1978) 141

|8| H.J. Groenewold, H. Groendijk, Physica 13 (1947) 141

|9| A. Michaudon, Journ. of Nucl. Energy, Parts A-B, 17 (1963) 165

|10| A. Bignami, C. Coceva, R. Simonini, Euratom Report EUR 5157e (1974)

|11| C. Coceva, R. Simonini, D.K. Olsen, Nucl. Instr. Meth., 211 (1983) 459
See also D.C. Larson, N.M. Larson, J.A. Harvey, Oak Ridge Report ORNL/TM-8880 (1984)

|12| J. Halperin, C.H. Johnson, R.R. Winters, R.L. Macklin, Phys. Rev. C21 (1980) 545

|13| D.C. Larson et al., Oak Ridge National Laboratory Report ORNL/TM-9097 (1985)

|14| S. Cierjacks et al., Nucl. Instr. Meth. 169 (1980) 185

|15| B.N. Taylor, W.H. Parker, D.N. Langenberg, Revs. Mod. Phys. 41(1969)375

|16| A.H. Wapstra, N.B. Gove, Nuclear Data Tables 9 (1971) 267

|17| A.H. Wapstra, K. Bos, Atomic Data and Nuclear Data Tables 19(1977)177

|18| A.H. Wapstra, G. Audi, Nucl. Phys. A432 (1985) 1
See also F.R. Cohen, A.H. Wapstra, Nucl. Instr. Meth. 211 (1983) 153

|19| K.H. Bockhoff, F. Corvi, A. Dufrasne, Euratom Report NEANDC(E)172 'U', Vol. III (1976) 15. Data reported also in ref. |7|

|20| P. Fischer, U. Harz, H.G. Priesmeyer, Atomkernenergie 42 (1983) 203

|21| F. Poortmans, Unpublished data reported in ref. |4|

|22| S. Cierjacks, private communication on measurements performed at Karlsruhe in 1968 and 1972

|23| W.J. Youden, Technometrics 14 (1972) 1

|24| J. Gervaise, CERN Report (1981) CERN-SPS/SU/81-1

|25| C. Coceva, F. Giacobbe, M. Magnani, Nucl. Sci. and Eng. 91 (1985) 209

NEUTRON EMISSION IN THE HEAVY ION REACTIONS AT THE ENERGIES BELOW 20 MeV/A

M.V BLINOV, S.S. KOVALENKO, E.M. KOZULIN
V.G. Khlopin Radium Institute,
Leningrad, Union of Soviet Socialist Republics

Abstract

The yields, the energy spectra and the angular distributions of neutrons at heavy ions interaction with different nuclei are considered in the report. The mechanism of such interactions is discussed.

1. Introduction

The interest to the use of heavy ions in nuclear physics has sharply grown in the recent years. The number of the acting and being constructed heavy ion accelerators has essentially increased. Both the energy of the ions and the intensity of the beams increase. In the heavy ions investigations many problems of nucleus-nuclear interactions are studied, for instance such as the ion kinetic energy dissipation, the behaviour of different collective degrees of freedom of the system (the distribution of the mass, charge, angular momentum, the deformation of the fragments).

A broad use of heavy-ion beams on accelerators determines the expedience of studying these reactions (with different ions and nuclei of the targets) from the practical point of view as neutron sources (determination of the intensities, spectra and angular distributions of the neutrons). This is necessary for using such a neutron source for the purposes of sample activation, making a shielding, determination of background conditions of the experiments, dosimetry and the problems of designing different detectors and devices on the beams. It is worth mentioning that if the characteristics of neutron sources based on the interaction of light ions with nuclei have been studied carefully enough, a different picture is observed for heavy ions: there are quite few works. Neutron sources based on heavy ions accelerators have not been sofar discussed at the IAEA Meetings on neutron sources.

In the present report we shall consider first the neutron emission from thick targets, then the results of the studies of the cross-sections, energy and angular distributions of the neutrons from thin targets, the results of theoretical investigations and the mechanism of neutron emission.

2. Emission from thick targets

There is no information in literature on any systematic studies of neutron emission from thick targets for different masses and energies of the ions, different target nuclei. There are only some works on individual problems.

In reference /1/ the authors analysed different experimental data on the neutron yields for a number of heavy ions. The total number of the neutrons per one incident ion for the energy 10 MeV/A was found to be $\sim 10^{-3}$n/ion which is less than for light ions /2/. Neutron yield at bombardment of thick Be and Li targets by protons and deutrons of the energy 10 MeV is equal $\sim 10^{-2}$ n/ion and of the energy 100 MeV - $\sim 10^{-1}$ n/ion. Neutron yields at interaction of the ions (C, N, O, Ne)(6-16 MeV/A) with thick targets of iron, nickel and copper were determined in reference /3/ for the angle 90° in relation to the direction of the ion beam (Fig. 1). In reference /4/ the ions of Ar, Kr, Xe, Pb and U (5-10 MeV/A) were used for determination of neutron yields in the straight direction ($\pm$30°). In the same work the angular distribution of neutrons was determined in the reaction $^{238}U + ^{238}U$ (9 MeV/A) for the angles interval 0-90°. The angular distribution of neutrons for the ions of C, O, Ne, Ar (7-9 MeV/A) and different nuclei targets was studied in the work /5/ by means of neptunium foils in combination with solid-state detectors (Fig. 2). We have carried out measurements of the energy spectra of the neutrons (interval 5-30 MeV) for different emission angles with a beam of ^{12}C ions (9 MeV/A) and thick targets of

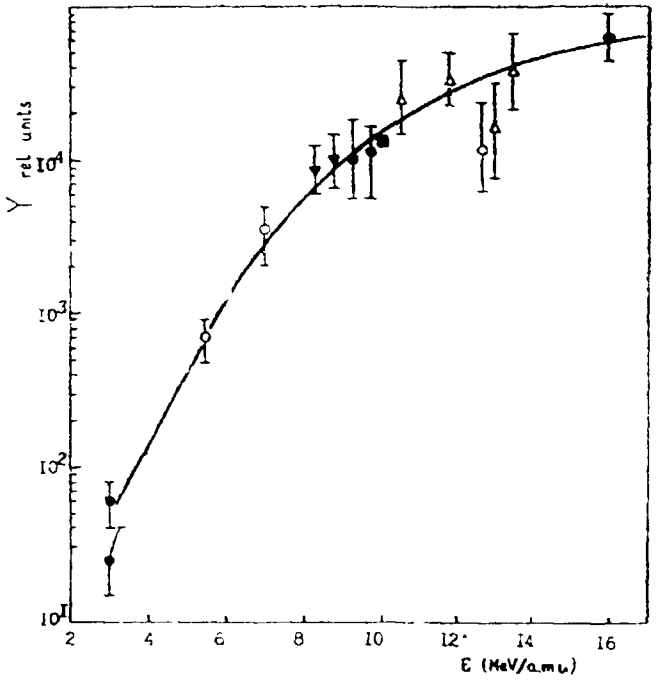

Relative neutron yield Y (per an incident ion), depending on the ion energy /3/.
• - ^{12}C, Δ - ^{14}N, o - ^{16}O, ▽ - ^{20}Ne, ▪ - ^{4}He

Fig. 1.

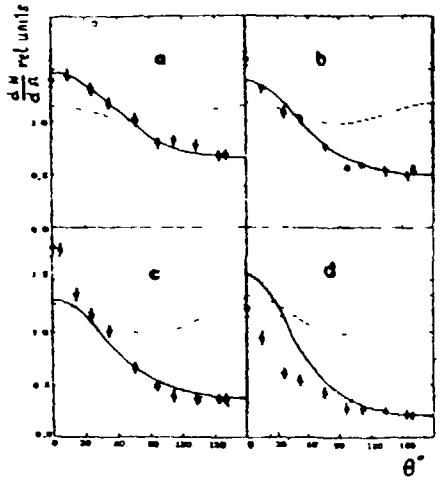

Angular distributions of the neutrons emitted at heavy ion interaction with a thick target of ^{nat}Ag /5/:
a - ions of ^{12}C (81 MeV); b - ^{16}O (135 MeV),
c - ^{22}Ne (175 MeV); d - ^{40}Ar (295 MeV).
Points - experiment, continuous line - calculation for l. s.; dotted line - c.m.s.

Fig. 2.

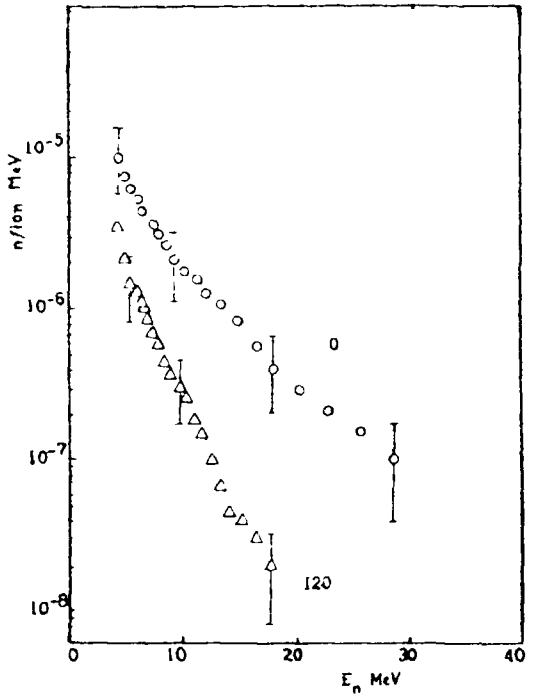

Absolute yield of different energy neutrons for two angles of emission (0 and 120°) at bombardment of ^{12}C ions (105 MeV) of a thick iron target /6/.

Fig. 3.

^{12}C, ^{27}Al, ^{56}Fe, ^{118}Sn, ^{181}Ta /6/. The spectrum of the neutrons in the reaction $^{12}C + ^{56}Fe$ is shown in Fig. 3. In the figure two components of the spectrum are seen - the soft (up to 10 MeV) and the hard (E 10 MeV) ones. Fig. 4 shows the change of the neutron yield for different targets for the neutron energy 7 MeV (angle 0°) (l. s.) in our work. In ref. /7/ total neutron yields from ^{12}C, ^{14}N and ^{20}Ne (10 MeV/A) bombardment of thick targets of various elements were measured by an activation method (Fig. 5).

In reference /1/ the authors propose a simple semiempirical parametrization of the neutron yield on the characteristics of the ion (Z, A and W - the atomic number, the mass number, the energy/nucleon). Besides the authors made an assumption about the insensibility of the yield to the substance of the target, although the experimental data /6, 7/ demonstrate some dependence on the mass of the nucleons target (Fig. 5). The neutron yield was obtained as:

$$Y(W, Z) = C(Z)W^{\beta(Z)},$$

where $C = \frac{1{,}95 \cdot 10^{-4}}{Z^{2{,}75}} \exp(-0{,}475 \log Z^2)$;

$\beta(Z) = 1{,}22\ Z.$

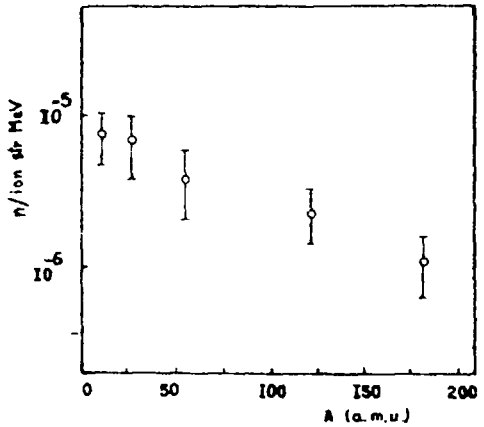

Fig. 4. Absolute yield of neutrons with energy 7 MeV at the angle 0° (l.s.) in dependence on the mass of the target nucleus /6/.

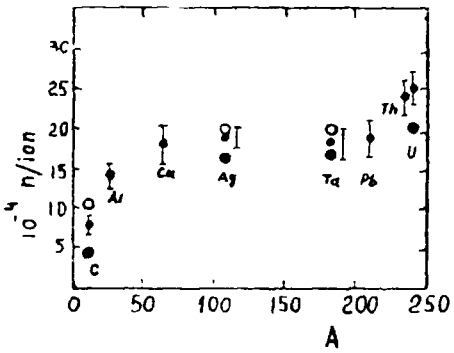

Fig. 5

Fig. 5. Absolute yield of neutrons in dependence on the mass of the target nucleus /7/.
Ions: • - ^{12}C, ○ - ^{14}N, ● - ^{20}Ne (10 MeV/A).

The authors of the work report that by their ovaluation the formula predicts the neutron yield with the precision to the factor 2 and can be applied for ion energies lower 20 MeV/A. The calculations of the neutron yields for the beams of C, Ne and very heavy ions are shown in Fig. 6. The Figure shows, that the neutron yield sharply increases with the increase of energy per nucleon W, especially for ions A > 12. For the angular distribution of the neutrons an empirical formula was used, which had been applied for the fitting of the data.

$$f(\theta) = \frac{1}{4\pi} \frac{1}{\ln \frac{1+\gamma}{\gamma}} \frac{1}{\gamma + \sin \theta/2}.$$

Thus the available information gives some knowledge on the characteristic of the neutrons formed at the bombardment of thick targets with beams of different ions. However these data are not yet complete and precise enough. A further accumulation of experimental information on the yields, spectra and angular distributions

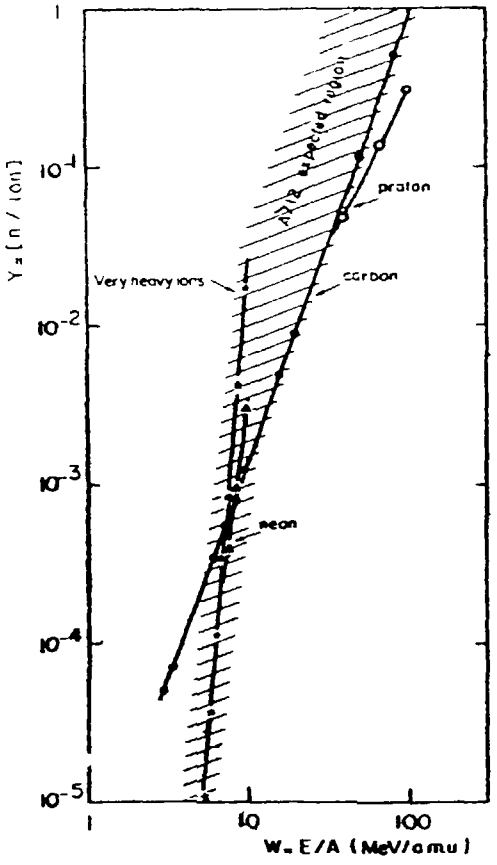

Fig. 6. Results of the calculation by the semiempiric formula of the yield of neutrons (per an incident ion) in dependence on the ion's energy E_1 (MeV/A) /1/.

of the neutrons is desirable for practical purposes.

For prediction of the characteristics of the neutron sources based on heavy ion accelerators it would be very useful also to study the mechanism of the interaction, of the neutron emission and the construction of the corresponding theoretical models. It is worth mentioning that the interaction of heavy ions with nuclei is quite a complicated process (fusion, deep inelastic and quasi-elastic processes, fission, direct interactions) in which different reaction channels are displayed. Therefore it is desirable to carry out investigations for individual reaction channels side by side with the inclusive measurements.

3. Experimental and theoretical studies of neutron emission characteristics

One of the first works devoted to the study of the energy and angular distributions of the neutrons arising in thin targets was work /8/, where the interaction of ^{16}O ions with the nuclei of Al, Ni, Cu, Au was studied. The angular distributions of the neutrons ($E_n < 8$ MeV) had a symmetric (in relation to 90°) angular distribution in the system of the center of mass, and the energy spectra in the measured neutron energy range 1-10 MeV were well described by a one-component Maxwellian distribution. Further on the results were published of a number of inclusive and exclusive measurements of the characteristics of the neutrons arising in thin targets of different substances at the bombardment with different ions. Neutron energy spectra up to 20-30 MeV and more were measured in those works /9-28/. In reference /9/ where the inclusive measurements of the neutron emission in the reaction $^{53}Cr + ^{12}C$ (53 MeV) were carried out, the energy and angular distributions were well explained within the limits of the statistical model. In Fig. 7 there is the obtained experimental neutron energy spectrum and its approximation within the limits of the evaporation model. It should be noted that at studying this reaction the ion energy per a nucleon over the Coulomb barrier was rather small. In further studies with the increase of the ion energy ($E \gtrsim 7$-20 MeV/nucleon) a nonequilibrium component was found in the hard part of the spectrum (over 10-15 MeV) both in the inclusive and in the correlation measurements. If the temperature paremeter T is used to characterize the hardness of the spectrum, then for the high-energy part of the spectrum this parameter several times exceeds the T for the evaporation part of the spectrum. Thus, for instance, in reference /10/, where the

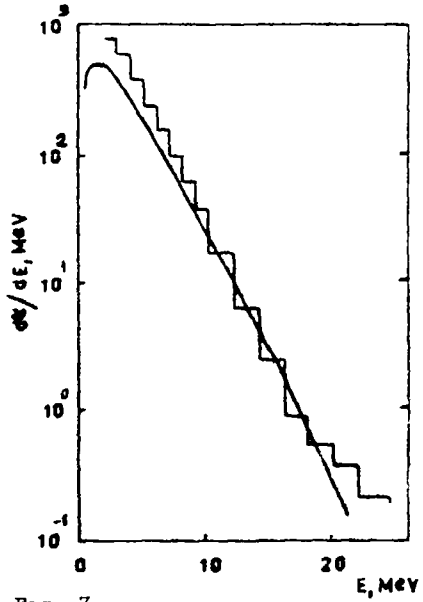

Fig. 7.

Energy spectrum of neutrons from the reaction ^{12}C (53.5 MeV) + ^{53}Cr: histogram - the experimental data; curved line - evaporation calculation by the programme "Overlaid Alice".

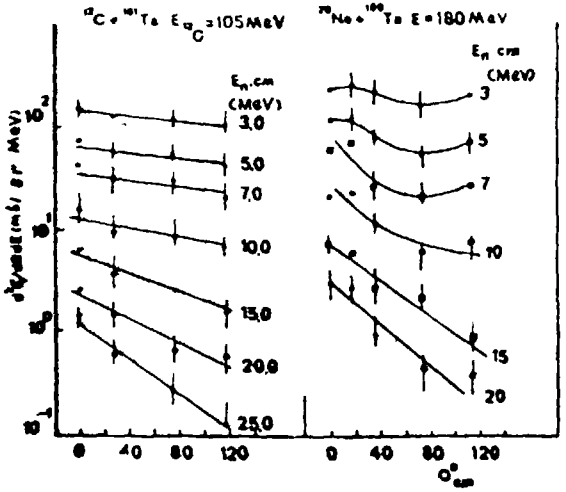

Fig. 8.

Differential angular distributions of the neutrons of different energies from the reactions: ^{12}C + ^{181}Ta (left) and ^{20}Ne + ^{181}Ta (right) /6/.

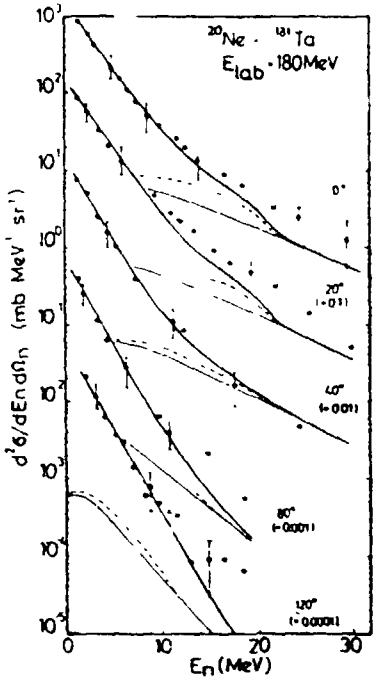

Fig. 9.

inclusive measurements of the neutron emission were carried out, it was shown in the reaction ^{181}Ta + ^{20}Ne (178 MeV) that in the neutron energy spectrum there is a hard component (T = 4,5 MeV) which has an anisotropic angular distribution in relation to 90° in the system of the center of mass (Fig. 8). Using a supposition of only the evaporation mechanism of the neutron emission the hard component failed to be explained in the reaction in question. Fig. 9 shows double differential cross-sections of the neutron emission of this reaction (^{181}Ta + ^{20}Ne). In all the works the value of the temperature parameter of the soft part of the spectrum was obtained by means of a simple fitting of the spectra of the kind $n(E) \sim \sqrt{E}\exp(-E/T)$ to the experimental data, with the parameter T

Double-differential cross-sections of the neutron emission from the inclusive measurements in the reaction ^{20}Ne (180 MeV) + ^{181}Ta. Experimental points from reference /52/.

Thin continuous line - the calculation in the TMPN model of the contribution into the preequilibrium neutron emission from the HZ.

Dotted line - the calculation in the TMPN model of the contribution into the preequilibrium emission from the PEP process.

Thick continuous line - the result of the summary evaluation of the evaporation and the preequilibrium component in the TMPN model.

being within the range 1,5-2,5 MeV. Let's notice that for obtaining the "true" temperature parameter of the soft component one should know the behaviour of the hard component of the spectrum within the energy range less 10-15 MeV, especially in the cases when the intensity of the hard component is high enough. As one can see from reference /11/ the temperature parameter of the soft part of the spectrum can change from 1,6 to 2,4 MeV for one and the same group of the experimental data in dependence on the way of accounting the contribution of the hard component.

In reference /12/ the temperature of the equilibrium heated nuclei was determined on the base of the neutron spectra and also from the data on the measurement of the compound nuclei lifetime by means of the shadow effect and on the study of the X-ray radiation of the compound atom vacancies. In the present work a systematics for the dependence of the neutron's kinetic energy on the excitation energy of the radiating nucleus (Fig. 10) has been worked out on the base of these literature data.

Calculations by the statistical theory using programs of the Grogi-2, Julian, Overlaid Alice type enable to evaluate the cross-sections and the energy spectrum associated with the equilibrium neutron emission. Usually the programs take into account the decay of both the excited nucleus and the daughter nuclei by the five possible channels (n, p, α, γ, f) which compete with each other. The calculations are also carried out accounting for the angular momentum on each stage of the evaporation cascade. The greatest difficulties of the calculation are connected with an inexact knowledge of the partial cross-sections of the processes which are accompanied with neutron emission, with the behaviour of the levels density at high excitation energies and great angular momenta, and also with the increase of the contribution of the pre-equilibrium neutron emission with the increase of the ion energy. Thus, theoretical calculations cannot claim to predict accurately enough the energy spectrum of the equilibrium neutron emission in the reactions with heavy ions. Although a satisfactory agreement of the calculations with the experimental data was noticed in a number of works, but this is mainly due to the fitting of the

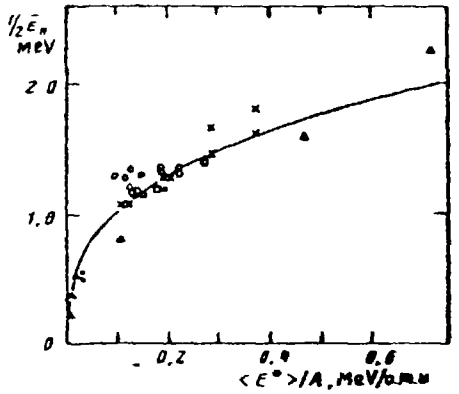

Fig. 10. Systematics of the average neutron energy (or temperature $\varepsilon/2 = T$) in dependence on the ratio of the average thermal energy of the emitting nuclei excitation $E^*>$ to the mass number A /12/.

Points:
- analysis of the excitation function ($H^1, \gamma n$) of the reaction for compound nuclei of erbium;
- determined by the γ-ray continuous spectra,
- analysis of the time of duration of the $^{235,238}U$ (n,f) fission reaction /12/;
- from the results of references /10, 16/;
- from the results of reference /17/.

calculations to the results of the experiment by variation of the free parameters present in the programs.

Experimental studies of the neutron emission in coincidence with definite channels of the reaction show that the hard component is present both at the de-excitation of the compound nucleus and of the fragments formed in the reactions of deep inelastic transfers. In the inclusive measurements the relative contribution of these processes to the full cross-section of the reaction can change essentially in dependence on the ion energy and on the combination of the interacting nuclei. In the case of exclusive measurements these diffeculties are partly passed over, but for

obtaining a summary neutron spectrum the measurements of the energy and angular neutron spectra are necessary for all the channels of the reaction. In the exclusive experiments carried out in the recent years /20-28/ main attention was payed to the study of the harder part of the spectrum, because a new effect associated with the preequilibrium neutron emission had been found in this field.

The first indication of the the presence of the nonequilibrium component in the neutron spectra was obtained in works /13, 14/ where the decay of one and the same compound nucleus was studied in the reactions $^{158}Gd(^{12}C, Xn)^{170-X}Yb$, $^{150}Nd(^{20}Ne, Xn)^{170-X}Yb$ at the ion energies 152 and 175 MeV respectively. The authors evaluated that the contribution of the preequilibrium neutron emission is 16 % in the reaction $^{12}C + ^{158}Gd$ and marked that the effects of the preequilibrium emission (in the neutron energy spectrum below 10 MeV) in the reaction $^{20}Ne + ^{150}Nd$ are manifested much weaker. In work /15/ the nonequilibrium neutron emission was studied in the reaction $^{154}Gd + ^{16}O$ (158 MeV) in coincidence with the compound nuclei from the complete fusion channel. The contribution of the nonequilibrium neutron emission characterized by the temperature parameter 5-6 MeV was obtained for all the measured angles (20, 70, 100, 151 °). In works /17-21/ using ion beams with A > 40 a. m. u. the hard component in the neutron energy spectra practically was not observed (except work /16/). Thus, in work /17/ the neutron emission was studied in the reaction $^{165}Ho + ^{55}Fe$ (476 MeV) in coincidence with different fragments. Statistical analysis of the energy and angular distributions of the neutrons coinciding with the fragments of the compound nucleus fission showed that the measured neutron distribution was well explained by the evaporation of the neutrons from fully accelerated fragments in a mutual Coulomb field. The evaluations of the preequilibrium neutron emission make a contribution not more than 5 % in this reaction. In the reactions $^{197}Au + ^{63}Cu$ (400 MeV), $^{166}Er + ^{86}Kr$ (602 MeV), $^{197}Au + ^{132}Xe$ (1 GeV), where the neutron emission in coincidence with different fragments was studied, the energy and angular neutron distributions were also well enough described by the evaporation from the accelerated fragments. In addition to that one should notice that

in all the enumerated reactions the ion energy was not high ($\frac{E-V_c}{A} \leq 4$ MeV/nucleon). Besides, even if the nonequilibrium component were present in these reactions, its contribution would be relatively small and therefore it was very difficult to detect this component against the great background of the evaporation neutrons.

When investigating the neutron emission in the reactions of deeply inelastic transfers (DET) a preequilibrium neutron emission was discovered in works /21-28/. Thus, in reference /22/ which deals with the study of the energy and angular neutron distributions in coincidence with a light fragment the obtained results couldn't be explained only by evaporation from the fully accelerated fragments. A harder energy spectrum corresponded to the nonequilibrium emission; the spectrum had the temperature parameter 2,5-3 MeV which is much more than T = 1 MeV for the evaporation component. In the reaction $^{158}Gd + ^{12}C$ (192 MeV) /23/ the contribution of the preequilibrium neutron emission into the given reaction channel was about 9 %, and in the reaction $^{20}Ne + ^{150}Nd$ it was much less. The fact that the preequilibrium emission was discovered in coincidence with a light ion-like fragment could point out that the nonequilibrium contribution was connected with an incident ion. Nevertheless it should be noted that, as shown in references /6, 24, 25/, in the reactions $^{157,158}Gd + ^{12,13}C$ (150 MeV), $^{114,124}Sn + ^{12}C$ (105 MeV), $^{58,64}Ni + ^{16}O$ (96 MeV) where the preequilibrium neutron emission was studied in dependence on the binding energy both in the heavy ion and in the target nucleus, it was shown that the target nucleus is the main source of fast neutrons.

In a number of works /26, 27/ the analysis of the preequilibrium neutron emission contribution was carried out at measuring the energy and angular distributions of the neutrons in the channel of the complete fusion reactions. In work /26/ the neutron emission was studied in the reaction $^{20}Ne + ^{165}Ho$ at the incident ion energies 11, 15, 20 MeV/nucleon and in the reaction $^{12}C + ^{165}Ho$ /27/ at the energy 25 MeV/nucleon. Neutron energy spectra measured in coincidence with a compound nucleus are shown in Fig. 11 and 12. For all the energies at the front angles there are two components corresponding to neutron evaporation from a compound

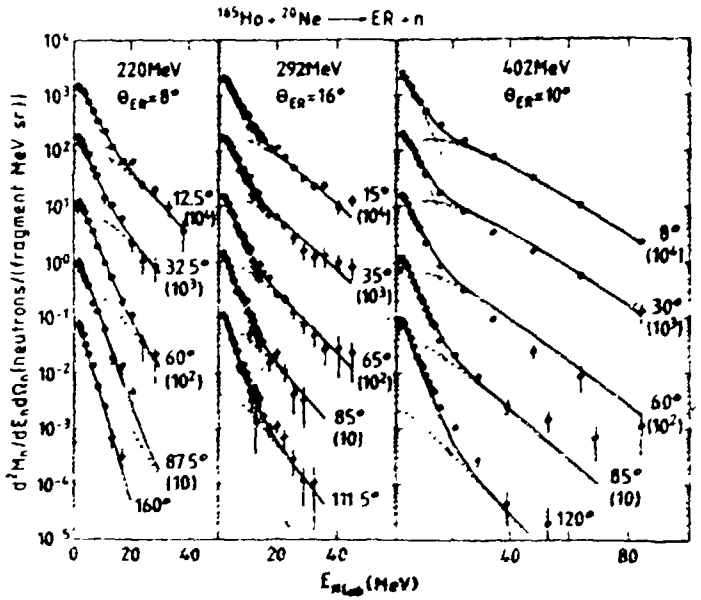

Fig. 11. Double-differential cross-sections of neutrons in coincidence with the compound nucleus from the reaction $^{165}Ho + ^{20}Ne$ (220, 292 and 402 MeV) /26/.
..... - contribution of the evaporation component;
----- - contribution of the preequilibrium component;
_____ - summary evaluation of the two processes (evaporation and preequilibrium neutron emission).

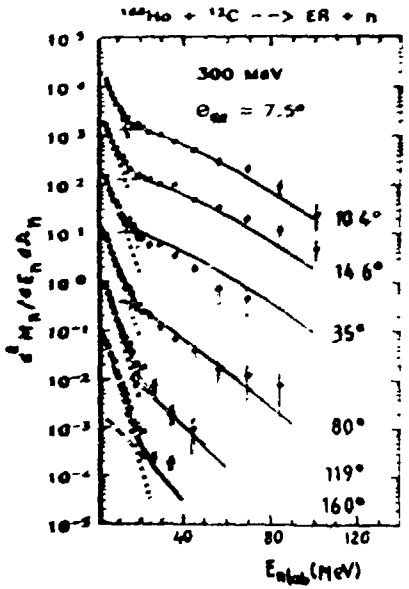

Fig. 12. Double-differential cross-section of neutrons from the reaction $^{165}Ho + ^{12}C$ (300 MeV) in coincidence with the registration of the compound nucleus at the angle 7.5° to the beam.
Experimental points from reference /27/:
..... - result of evaluation of the evaporation contribution, and
----- - of the preequilibrium neutron emission;
_____ - sum of the two processes.

nucleus and to the nonequilibrium emission. It is seen from Fig. 11 that the contribution of the nonequilibrium neutron emission increases with the energy increase and presents a considerable share at the ion energy 20 MeV/nucleon. Using the source parametrization for the description of the neutron spectra, the authors determine a possible velocity of the source emitting nonequilibrium neutrons and also obtain the full multiplicity and the temperature of the nonequilibrium neutrons. It was obtained in works /26, 27/, that in the reaction $^{165}Ho + ^{20}Ne$ and $^{165}Ho + ^{12}C$ from 85 to 95 % of all the neutrons are emitted due to evaporation from the compound nucleus and the excited fragments, and from 5 to 15 %, due to the nonequilibrium processes. In work /28/ a dependence of the nonequilibrium neutron emission multiplicity on the energy of an ion per nucleon over the Coulomb barrier was obtained at an analogous source parametrization. The obtained data are presented in Fig. 13. Thus, for central collisions the yield of the nonequilibrium component, the average neutron energy and the parameter T of the nonequilibrium component temperature increase with the energy increase. The dependence of T on the ion energy E is shown in Fig. 14.

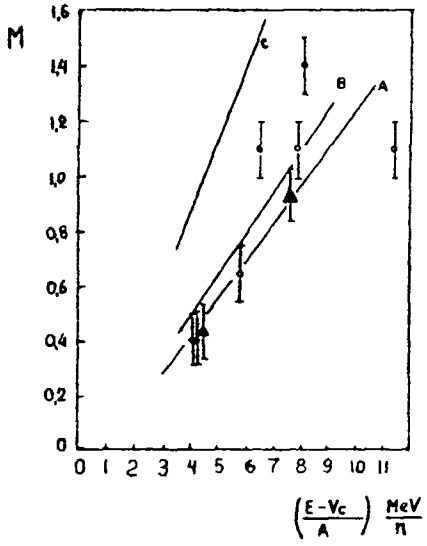

Fig. 13. Multiplicity of the nonequilibrium neutron emission M as a function of energy per nucleon over the Coulombian barrier.
o - ^{12}C, • - ^{13}C, Δ - ^{20}Ne.

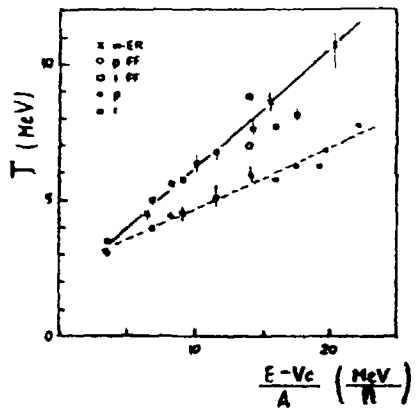

Fig. 14. Dependence of the temperature parameter (T) on the ion energy per nucleon over the Coulombian barrier.
x - corresponds to the neutron measurements in coincidence with the compound nucleus;
o □ - inclusive and exclusive data for protons: the continuous and the dotted lines pass through the exclusive (n) and the inclusive (p) data, respectively.

Despite the fact that there exists quite a great number of models (about 20) /29-50/ used for interpretation of the preequilibrium particle emission, at present there's not a single model explaining the totality of the experimental information. Theoretical models must describe in particular such main characteristics of the nonequilibrium particle emission as the shape of the energy spectrum, the type of the angular distribution, the dependence of the emission cross-section $_{nn}$ on the ion energy, on the mass, the charge of the target nucleus and the ion, and also the multiplicity of the nonequilibrium particle emission and its dependence on the analogic parameters. The most often used models are the exciton, the hybrid models, different modifications of the hot spot models, the prompt emission particle (PEP) models, the direct reaction model (break-up, break-up - fusion, fragmentation, knock-out), the models of incomplete fusion, the source models, etc. They differ greatly by their physical picture. Nevertheless almost all the models may be classed, if considered from the point of view of the residual two-particle nucleon-nucleon interaction and the average field for a one-particle nucleon motion inside the system. Two possible extreme cases may be considered. The first case is different modifications of the "hot source" models /29-33/ where the dominating part of the two-particle collisions is nonevidently supposed. In these models the short length of the free range and the small relaxation time can lead to the formation of the excited zone emitting particles statistically. In these models the parametrization used for description of the preequilibrium particle emission enables to obtain a good agreement

with the experimental data obtained both in the inclusive /6, 9, 10/ and the exclusive measurements /11, 12-24/. However, the success of these models has only a formal character, because they give no physical interpretation of the source development dynamics. Another extreme case is represented by the models offering the mechanism of prompt emission particle (PEP) /38-44/, in which the part of the two-particle nucleon-nucleon collisions is reduced to the formation of the average field where the nucleons move quasi-freely. The most consistent realization of the PEP physical picture are the quantum-mechanical one-particle models /44-46/, and also the self-consistent time-dependent Hartree-Fock method (TDHF) /47, 48/. All these models give too great anisotropy in the angular distributions of the preequilibrium particles /50/. Besides, within the TDHF framework it is obtained that the yield of the fast particles greatly depends on the nucleon binding energy in the incident ion /51/, which evidently contradicts to the experiment /11/.

In the two-step model of the preequilibrium nucleon emission (TMPN) /50, 51/ an attempt has been made to unite different concepts concerning the mechanism of the fast particle emission for applying the positive aspects of these models and for their further development. The initial point of the suggested dynamic model is the trajectory calculation of the average field evolution for the given system in dependence on the impact parameter /49, 50/. Classical equations of the collective parameters motion are solved in it: the distances between the centers of two nuclei, the radius and the curvature of the neck. In the TMPN model two stages of the fast preequilibrium particles emission are supposed. At the first stage of the reaction, when the colliding nuclei are not yet strongly overlapped spatially (before the formation of the neck between the interacting nuclei), the emission of the preequilibrium particles is calculated like the PEP models. The main supposition of these models is that at each instant of time the pulse distribution of the nucleons in the system is a superposition of two nonperturbed Fermi-spheres shifted in relation to each other. On the second stage after the formation of the neck and disappearance of the one-particle potential barrier between the nuclei, this supposition may seem not quite just, therefore on the second stage of the interaction the preequilibrium particles emission in the TMPN is supposed from the hot zone (NZ), expanding at a speed of sound in the radial direction and having a strongly anisotropic velocities particles distribution. In Fig. 9 and 15 the results of the calculations by the TMPN model are shown for the reactions $^{165}Ho + ^{20}Ne$ (11 and 20 MeV/A) /26/ and $^{181}Ta + ^{20}Ne$ (9 MeV/A) /52/. For both reactions carried out at different ion energies there's a good agreement with the experiment. It should be noted that the relative contribution into the nonequilibrium neutron emission from the HZ increases with the incident ion energy increase and with the decrease of the impact parameter ( ) for two interacting nuclei. At tangential collisions in the TMPN model the

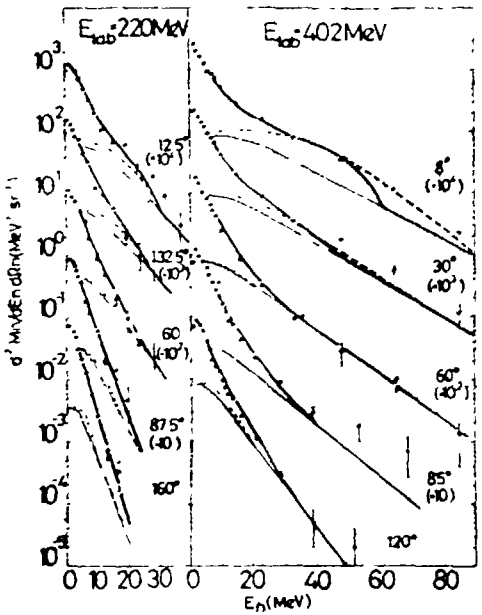

Fig. 15. Double-differential cross-sections of the neutron emission from the reaction $^{165}Ho + ^{20}Ne$. Experimental points from reference /26/. All the designations the same as in Fig. 9.

preequilibrium neutron emission takes place on the first stage only, i. e. the hot zone isn't formed. It should be stressed that within the framework of the given physical interpretation the process of the preequilibrium neutron emission (at the ion energy 10-20 MeV/nucleon) proceeds not at separated impact parameters, but for the whole range of the "l" values. In addition to that the correlation of the preequilibrium neutrons yields from the two processes changes, depending on the impact parameter and the mass of the interacting nuclei. Using the possibilities of the given model /50, 51/ one can predict the regularities of the change of the preequilibrium neutron emission characteristics, depending on the mass of the target nucleons, the mass and energy of the ion, the binding energy of the neutron in the nucleus.

4. Conclusion

At interaction of heavy ion beams with different targets of accelerators (energy less 20 MeV/nucleon) there arises an emission of neutrons, the spectrum of which covers a wide energy range. The properties of the neutron sources based on heavy ion accelerators must be studied for different scientific and practical purposes.

In a number of experimental works the emission of neutrons from various targets was determined in some reactions with heavy ions. The neutron yield at the ion energy $\sim$ 10 MeV was $\sim 10^{-3}$ neutrons/ion and it increases steeply with the ion energy increase. It was also determined that the main part of the neutrons was in the energy range less 10 MeV. The yields and the spectra of neutrons of this low-energy range have been little studied yet in experimental works. Therfore there is no consistent systematics of the emission characteristics. Theoretical calculations cannot yet predict the necessary data for this range accurately enough.

In some works it was found that at the ion energy 2-3 MeV/A over the Coulomb barrier a nonequilibrium neutron emission appeared, characterized by a high temperature parameter ($\sim$ 5 MeV). The probability of the nonequilibrium emission considerably increases with the increase of the ion's energy and reaches 10-15 % at 20 MeV/nucleon. Taking into account the fact that high-energy neutrons are emitted in this case, there is a necessity in further study of this component. However the experimental data are mainly connected with the investigation of the some reaction channels and not the total neutron spectra, which are necessary for predicting the characteristics of neutron sources based on heavy ion accelerators.

The available informations on the properties of neutron sources on heavy ion beams concerns mainly ion energies less 10 MeV/A, therefore it is expedient to carry out investigations in the range of higher ion energies too.

The autors express acknowledgement to A. S. Veshchikov for his aid in drawing up the report.

References

1. Clapier P., Zaidins C. - Preprint I.P.N. France. IPNC-6301.
2. Johnsen S. - Preprint NBSIR. 1977. 77-1279.
3. Ohnesorge et al. - Health Physics, 1980, 1, 39, p. 633.
4. Festag J. - Dose rates during experiments with heavy ions: 5-th Intern. Congress IRPA. Jerusalem, 1980.
5. Ilinov A. S. et al. - Nucl. Phys. 1972, 16, p. 465 (Rus).
6. Blinov M. V. et al. - Neutron Physics. Moscow. 1984, Vol. 3, p. 357 (Rus).
7. Habbard E. et al. - Phys. Rev., 1960, vol. 118, N 2, p. 507.
8. Broek H. W. - Phys. Rev., 1961, vol. 124, N 1, p. 233.
9. Bochkarev O. V. et al.-Proc. Acad. of Sci. USSR. Phys. Ser. 1979, vol. 43, p. 2192 (Rus).
10. Blinov M. V. et al. - Intern. Symposium on synthesis and preparation of new elements (Abstracts). Dubna, JINR, 1980, p. 64. D 7-80-556 (Rus).
11. Gavron A. et al. - Phys. Rev. C, 1981, vol. 24, N 5, p. 2048.
12. Karamjan S. A. - Nucl. Phys. 1984, 40, p. 347 (Rus).
13. Sarantites D. G. - Phys. Rev. C, 1978, vol. 18, N 2, p. 774.
14. Westberg L. - Phys. Rev. C, 1978, vol. 18, N 2, p. 796.
15. Young K. G. - Phys. Rev. C, 1981, vol. 23, N 6, p. 2479.
16. Tserruya I. et al. - Phys. Rev. C, 1982, vol. 26, N 6, p. 2509.
17. Hilcher D. et al. - Phys. Rev. C, 1979, vol. 20, p. 576.

18. Schoröder W. U., Huizeuga I. R. - Annual Rev. Nucl., 1977, vol. 27, p. 465.
19. Tamain B. et al. - Nucl. Phys., 1979, vol. 330, p. 253.
20. Eyal Y. et al. - Phys. Rev. Lett., 1978, vol. 41, N 9, p. 625.
21. Gould C. R. et al. - Z. Phys. A, 1980, vol. 294, p. 323.
22. Gavron A. et al. - Phys. Rev. Lett., 1981, vol. 46, N 1, p. 8.
23. Petitt G. A. et al. - Phys. Rev. C, 1985, vol. 32, N 5, p. 1572.
24. Gavron A. et al. - Phys. Rev. C, 1981, vol. 24, p. 2048.
25. Gemmeke H. et al. - Phys. Rev. Lett., 1980, vol. 97B, p. 213.
26. Holub E. et al. - Phys. Rev., 1983, vol. 28, N 1, p. 252.
27. Holub E. et al. - Phys. Rev., 1986, vol. 33, N 1, p. 143.
28. Gavron A. et al. - Phys. Rev., 1983, vol. 27, N 1, p. 450.
29. Weiner R., Westström M. - Nucl. Phys., 1977, vol. A286, p. 282.
30. Gottschalk P. A., Westström M. - Nucl. Phys., 1979, vol. A314, p. 232.
31. Garpman S. I. A. et al. - Phys. Lett., 1980, vol. 90B, p. 53.
32. Karvinen A. O. T. et al. - Nucl. Phys., 1981, vol. A367, p. 122.
33. Yashida S. - Z. Phys., 1982, A308, p. 133.
34. Nijta K. - Z. Phys., 1984, A 316, p. 309.
35. Machner H. et al. - Phys. Rev. C, 1985, vol. 31, p. 443.
36. Blann M. - Phys. Rev. C, 1981, vol. 31, p. 205; 1985, vol. 31, p. 1245.
37. Holub E. et al. - Phys. Rev., 1986, vol. 33, N 1, p. 143.
38. Bondorf J. P. et al. - Nucl. Phys., 1980, vol. A333, p. 285.
39. Sebille F., Removd B. - Z. Phys., 1983, A310, p. 99.
40. Tricoire H. - Z. Phys., 1983, A312, p. 221.
41. Pavies K. T. R. et al. - Ann. Phys. (N. Y.), 1984, 156, p. 68.
42. Leray S. et al. - Z. Phys., 1985, A320, p. 382.
43. Möhring K. et al. - Nucl. Phys., 1985, vol. A440, p. 89.
44. Cassing W. - Nucl. Phys., 1985, vol. A438, p. 253.
45. Umar A. S. et al. - Phys. Rev. C, 1984, vol. 30, p. 1934.
46. Jolos R. V., Ivanova S. P. - JINR, E-4-85-647, Dubna, 1985.
47. Devi K. R. S. et al. - Phys. Rev. C, 1981, vol. 24, p. 2521.
48. Dhar A. K. et al. - Phys. Rev. C, 1982, vol. 25, p. 1482.
49. Bertsch G. F. - Preprint MSUCL-385, Michigan, 1982.
50. Biederman M. et al. - JINR E7-84-415, Dubna, 1984.
51. Mädler P. - JINR E-7-85-575, Dubna, 1985.
52. Kozulin E. M. et al. - JINR P 7-85-34, 1985 (Rus).

EFFICIENCY OF PULSED SOURCES OF NEUTRONS FROM THE POINT OF VIEW OF SPECTROMETRIC STUDIES

G.V. MURADYAN
I V. Kurchatov Institute of Atomic Energy,
Moscow, Union of Soviet Socialist Republics

Abstract

Efficiency of studies performed by using the time-of-flight method is considered. A high rate of recording neutron-matter interaction is important for and characteristic of these studies. Some criteria for selection and optimization of pulsed sources and neutron spectrometers for the studies of this type have been deduced. Concrete sources are considered as well as possibilities of raising their efficiency.

Possibilities of the time-of-flight spectrometric studies are limited mostly by parameters of pulsed sources of neutrons. These parameters are constantly improved, new more intensive sources allowing us to perform finer experiments are built. As a rule, a lot of experiments require long-term measurements and it is still impossible to carry out some experiments since they require too much time of measurement. In this connection the problem of raising the efficiency of studies by optimizing the source and the set-up as a whole becomes of great importance. Here the efficiency means the value reverse of the measurement time required to obtain a preset accuracy. At a conventional approach the efficiency is divided into two factors, i.e. the efficiency of an experimental set-up and that of a source. The latter is characterized by a

figure of merit Q /1/ which is the flux magnitude over the flight path length L ensuring the preset energy resolution:

$$Q = \frac{A}{\delta t^2} \qquad (1)$$

Here A is the source intensity, δt is the duration of neutron flashes. Note that the violation of conditions underlying the conclusion (1) results in breaking the agreement between the figure of merit and efficiency. For example, eq. (1) does not yield efficiency in the presence of a background uncorrelated with the source intensity /2/.

In the present work we consider the efficiency of a rather wide and promising category of investigations. A high rate of recording the interaction of neutrons with a sample is important for and characteristic of such investigations. Among them is the measurement of small departures of neutron cross sections depending, for example, on the energy, polarization and other factors, or merely the measurement of neutron cross sections with a high accuracy. For the above-mentioned category of investigations the efficiency is determined by the measuring capacity of the recording equipment and the parameters of the neutron source. The dependence on the latter is not reduced to the expression (1). Moreover, it may turn out that out of two sources the one with a smaller figure of merit is more efficient.

The fact that on modern sources the measuring capacity of the equipment becomes significant can be seen from the following estimates. At the energy of neutrons of 10 eV and at a rather high resolution of $\sim 0.3\%$ the pulse intensity of neutrons on a sample having the area of ~ 100 cm^2 may reach $\sim 10^9 s^{-1}$. Whereas, at a dead time of the recording system of $\theta \sim 10$ us and the level of miscount $\beta \sim 0.05$ the allowable load amounts to $\sim 10^4 s^{-1}$. That is five orders less than the neutron intensity.

Let us proceed to a quantitative consideration of efficiency at a limited measuring capacity of the recording equipment. It is obvious that in this case the efficiency is proportional to a mean rate of recording events in a unit interval of energies (V):

$$V = \frac{\nu}{\nu_0} \frac{W \cdot S(E)}{L^2} \qquad (2)$$

Here S(E) is the density of the neutron flux over a flight path length of 1 m at the maximum frequency of flashes ν_0, $W = p \cdot s$ where p is the probability of the fact that a neutron will induce a recorded event in a sample, s is the sample area. It is assumed that the source intensity is proportional to the flash frequency ν. For the pulse load we have

$$J \equiv \frac{V}{\nu} \frac{dE}{dt} = \frac{W \cdot S(E) \cdot E^{3/2}}{L^2 \nu_0 a} \qquad (3)$$

where $a = 36.1 \cdot 10^{-6}$; L is expressed in meters. If the path length (or resolution) is preset, it is possible to ensure the miscount level not higher than β by choosing W in compliance with the condition of $J \leq \frac{2\beta}{\theta} \cdot 10^6 \equiv J_0$. From that condition and formula (3) we find the maximum allowed value of W:

$$W_0 = \frac{aL^3 \nu_0 J_0}{S(E) \cdot E^{3/2}} \qquad (4)$$

Note that if WS changes considerably in the energy range corresponding to the variation of the time of flight by the value θ, one should perform the respective averaging. For the sake of simplicity, we shall consider the case when the above-mentioned changes are negligible.

From eqs (3) and (4) we find the maximum mean rate of recording:

$$V_o = \frac{L \quad aJ_o}{E^{3/2}} \tag{5}$$

In a more general case when $W \leq W_o$ we have

$$V = V_o \frac{W}{W_o} \tag{5}$$

The character of the V dependence on the flight path length for the case of $W = W_o$ (i.e. for $V = V_o$) is presented in fig. 1 (solid curve). At small L the V_o value grows with the increase of L. Beginning from the path length $L = L^*$ corresponding to the equality of the recyclic frequency (ν_r) to the maximum frequency of the source the count rate does not change. That is due to the fact that for $L > L^*$ the frequency $\nu = \nu_r \sim \frac{1}{L}$ which results in the independence of V_o from L. At that V_o does not depend on the source parameters. Thus, in the absence of limitation on the W value (for example, on the quantity of matter of the sample under investigation) the maximum achievable count rate is the same for all sources and does not depend on resolution.

If under the experiment conditions the W value is limited, there exists such a path length L_o above which the inequality $W \geq W_o$ fails to hold. Then it will be impossible to fulfill the equality $W = W_o$ by decreasing W and, according to eq. (6), V will start dropping (broken curves in fig. 1). The greater is the preset value of W, the longer will be the path length at which the above will take place. At $L_o < L$ we have

$$L_o = \sqrt[3]{\frac{WSE^{3/2}}{\nu_o a}} \tag{7}$$

The respective mean maximum count rate will amount to

$$V_o = \frac{1}{E} \sqrt[3]{S \cdot W \cdot J_o^2 \cdot \nu_o^2 \cdot a^2} \tag{8}$$

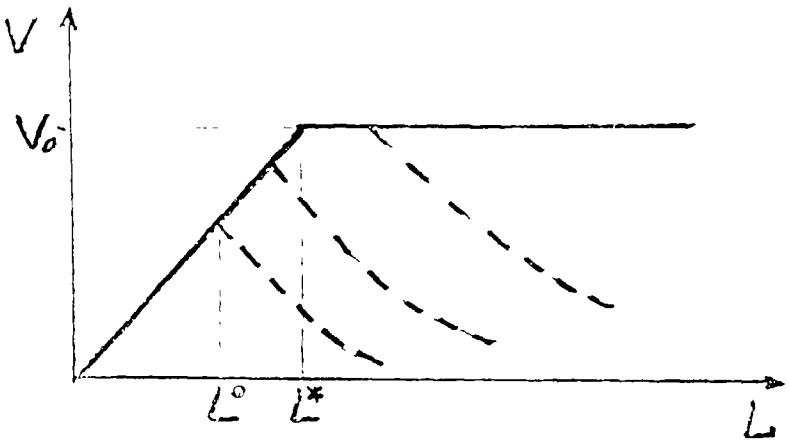

FIG. 1.

It follows from eq. (8) that the source efficiency, from the point of view of achieving maximum rates of recording, is characterized by the value

$$p = \sqrt[3]{A \nu_o^2} \tag{9}$$

where A is the source intensity. As compared with the figure of merit, there arises a considerable dependence on the maximum frequency and the part played by the intensity is far less important. Let us stress that the efficiency estimation according to eq. (9) holds at small W. With the increase of W the difference between the sources gradually disappears.

The dependence of V_o on the energy is rather strong. Thus, for the moderation spectrum $V_o \sim E^{-1.3}$. That suggests the superiority of the lower energy range from the point of view of the particular category of investigations.

Table 1 presents the values of P and $Q = A/\tau^2$ for some sources used in the spectral region of moderated neutrons. The table also gives the relative value of L_o calculated as $\sqrt[3]{A\nu^{-1}}$. The values of A and τ are taken from ref. /3/ (they do not take into account the moderator efficiency). It is clear from the table that the considered sources do not differ by more than 20 times over the parameter P though the difference in quality reaches the order of 7.

For linear accelerators of electrons(linacs)high values of P are achieved at a relatively low intensity A. The path lengths required here are considerably shorter than those of other sources. Creation of short path lengths is quite possible at linacs due to small sizes of the neutron target and the possibility of obtaining a low background at small thicknesses of walls of the protective bunker. Short path lengths are highly suitable for the lower energy range where the resolution is good and the value V_o is relatively high. It is possible to increase somewhat the path length with the increase of A. In particular, it is possible to do so with the help of a booster without decreasing the frequency. Note that in solving problems, which require a high quality, LAE cannot compete with modern proton accelerators.

Table 1

Source	A ($10^{-14}s^{-1}$)	ν_o (s^{-1})	τ (μs)	Q 10^{14}	P 10^5	L_o 10^3
IBR-30/LAE-40 (JINR, Dubna)	7	100	4	0.44	19	19
Linac, GELINA (Belgium)	0.2	900	0.004	$1.2\cdot10^4$	25	2.8
Linac "Pikel" (Moscow)	0.2	900	0.25	3.2	25	2.8
Spectrometer "Gneis" (Leningrad)	1	40	0.01	10^4	5.4	13
LAMPF/LANR with accumulator-buncher PSR (Los Alamos)	15	720	0.001 - 0.2	$1.5\cdot10^7$	90	13
SNS (Great Britain)	300	50	0.4	$1.7\cdot10^3$	42	83

Thus, for the investigations, which require high rates of event counting, the efficiency is characterized by the value $P = \sqrt[3]{A\nu_o^2}$ and by the possibility of realization of the optimal path length. The optimization of set-ups in these parameters increases the number of sources which may be used for a successful performance of the above-mentioned investigations.

References

1. Michaudon A., Special issue "Tailored" Neutron Beams. J. Nucl. Energy 17, No. 4/5 (1963).
2. Muradyan G.V. Methods of measuring neutron cross sections and investigation of parameters of neutron resonances. Doctor Theses. Moscow, 1975 (in Russian).
3. Shabalin V.P. Modern highly intensive pulse neutron sources. Atomnaya Energya 52, No. 2, p. 92 (1982).

80 NEUTRON ENERGY SPECTRA AND YIELDS PRODUCED FROM THICK TARGETS BY LIGHT-MASS HEAVY IONS

T. NAKAMURA, Y UWAMINO
Institute for Nuclear Study,
University of Tokyo,
Tokyo, Japan

Abstract

The measured neutron energy spectra produced from thick targets by light-mass heavy ion beams were analyzed with the phenomenological hybrid model of equilibrium and pre-equilibrium emissions. The neutron energy spectra are fitted to two (in the energy region of incident projectile energy lower than 100 MeV) and three (in the energy region of incident projectile energy higher than 100 MeV) Maxwellian-type components. The lowest energy component corresponds to the evaporation neutrons from a compound nucleus having a nuclear temperature independent to the neutron emission angle and the higher two components to the pre-equilibrium neutron emission having a nuclear temperature depending on the angle.

The total neutron yield was evaluated by surveying several published papers and estimating the neutron yield below a few MeV by fitting some spectra measured above that energy to the Maxwellian distribution.

In order to use for the neutron activation cross section measurement and the induced radioactivity study, a pseudo-monoenergetic neutron beam course in the energy range from 15 to 40 MeV was installed by using the Be(p, n) reaction. The peak neutron energy changes with the proton energy and the beam intensity was relatively high.

---

1. Introduction

As the basic data for various accelerator applications, it is indispensable to get accurate detailed information on secondary neutron production. Much work has been done on secondary neutron production from thick targets bombarded by charged particles, as is summarized in Ref. 1. Neutron production yields have, however, not been systematically investigated as a function of projectile type and energy, and target atomic mass. Recently, a simple empirical formula predicting total neutron yield and its angular distribution has been introduced[2] from the rather dispersed and incomplete experimental data and some theoretical results in the published papers.

But for neutron energy spectra produced from thick targets, our work[3,4] is the only one on their analysis connecting to the mechanism to produce neutrons from nucleon-nucleus and nucleus-nucleus collisions, except for the neutron spectrum analysis on the basis of the Serber model for deuteron stripping[5,6].

The neutron cross sections of energy above 15 MeV are quite insufficient and no evaluated data files exist in the present. Especially for activation cross section and induced radioactivity measurements, we installed a high intensity pseudo-monoenergetic neutron beam course by using the Be(p, n) reaction.

2. Phenomenological Hybrid Analysis of Neutron Energy Spectra

It can be considered that the energy spectrum of neutrons produced by light-mass heavy ion bombardment is composed of the following four components,

1) Evaporation spectrum in the low energy region corresponding to neutron emission from an equilibrium state,

2) Higher energy spectrum coming from pre-equilibrium neutron emission,

3) Knock-on spectrum in the forward direction due to the direct process,

4) Only for ^{3}He and d projectiles, a broad bump in the forward spectrum produced from the breakup reaction of projectiles, (d, np) and (^{3}He, n2p) reactions.

The evaporation cross section in the center of mass (c.m.) system is given by

$$\frac{d^2\sigma}{d\varepsilon d\Omega} = \sigma_{nonel} \frac{K}{4\pi} \frac{\varepsilon}{T^2} \exp\left(-\frac{\varepsilon}{T}\right) \qquad (cm^2 \cdot MeV^{-1} \cdot sr^{-1}), \qquad (1)$$

since the evaporated neutrons are emitted isotropically in the c.m. system, where ε is the neutron energy in the c.m. system, in MeV; Ω is the solid angle in the c.m. system, σ_{nonel} is the nonelastic cross section, K is the total number of evaporated neutrons per nonelastic collision, and T is the nuclear temperature in MeV

The emission angles in the c.m. system and the laboratory (L) system are assigned to be θ and θ, respectively, and the evaporation cross section in the L system is obtained from Eq. (1) as

$$\frac{d^2\sigma}{dEd\theta} = \sigma_{nonel} \frac{K}{2} \frac{\sqrt{E\varepsilon}}{I^2} \exp\left(-\frac{\varepsilon}{I}\right) \sin\theta \qquad (cm^2 \cdot MeV^{-1} \cdot sr^{-1}), \qquad (2)$$

where E is the neutron energy in the L system in MeV.

The relation between E and ε is obvious,

$$\left.\begin{aligned} \varepsilon &= E + E_C - 2\sqrt{EE_C}\cos\theta \ , \\ E_C &= \frac{M_1 M_n}{(M_1 + M_t)^2} E_1 \ , \end{aligned}\right\} \qquad (3)$$

where M_1, M_n, and M_t are atomic masses of the projectile, neutron and target nucleus, respectively, and E_1 is the projectile kinetic energy in the L system.

The evaporation neutron spectrum of the thick target observed in the L system, $\phi(E, \theta)$, is given by

$$\phi(E, \theta) = \int_{E_{th}}^{E_0} N\sigma_{nonel}(E_1) \frac{K\sqrt{E}}{2\pi r^2} \exp\left(-\frac{\varepsilon}{T}\right)\left(\frac{dE_1}{dx}\right)^{-1} dE_1 \ , \qquad (4)$$

$$(\text{MeV}\cdot\text{sr}\cdot\text{projectile})^{-1}$$

where E_0 is the initial kinetic energy of the projectile in MeV, E_{th} is the threshold energy of the neutron-producing reaction in MeV, N is the atomic density of the target in atoms/cm^3, E_1 is the projectile kinetic energy in the target in MeV and dE_1/dx is the stopping power of the projectile in MeV/cm.

When the target atomic mass M_t or the initial kinetic energy of the projectile E_0 is large, ε becomes close to E as can be seen in Eq. (3). Therefore, $\phi(E, \theta)$ in Eq. (4) becomes a function of $E\exp(-E/T)$ and $\phi(E, \theta)/E$ indicates the exponential form $\exp(-E/T)$.

The neutron spectra emitted from the precompound nucleus state can also be expressed in the Maxwellian-type spectrum above the transition energy from equilibrium emission to pre-equilibrium emission. Differently from the evaporation process, however, the nuclear temperature, T', of a precompound nucleus in a pre-equilibrium state is dependent on the neutron emission angle θ. The neutron energy spectrum from the pre-equilibrium emission can be expressed as

$$\phi(E, \theta) = K' \frac{E}{T'^2(\theta)} \exp\left(-\frac{E}{T'(\theta)}\right) \ , \qquad (5)$$

similarly as Eq. (4) The T' value is higher than the nuclear temperature T of a compound nucleus in an equilibrium state and decreases with the emission angle, since the neutron emission from the hotter pre-equilibrium state occurs in a more forward direction

3. Comparison with Experimental Neutron Spectra

In the projectile energy below 100 MeV, among several experimental studies, our experimental data of neutron energy spectra of thick targets of carbon, copper and lead bombarded by 30-MeV proton, 33-MeV deuteron, 65-MeV ^{3}He and 65-MeV alpha particles were selected to use for this phenomenological hybrid analysis, because of their detailed information.

Figures 1 to 3 show the neutron energy spectra divided by energy, $\phi(E, \theta)/E$, of carbon and lead targets from 30-MeV p, 65-MeV α, and 65-MeV ^{3}He, respectively[7]. These figures include the $\phi(E, \theta)/E$ values calculated by Eqs. (4) and (5). The $\phi(E, \theta)$ calculation in Eq. (4) was performed by using $\sigma_{nonel}(E_1)$ given in Ref. (8). As can be seen from Eq. (3), E is strongly dependent on the emission angle, θ, in the L system, so the $\phi(E, \theta)$ value calculated by Eq. (4), the evaporation spectrum, varied with θ in the case of light target nucleus like carbon, but with an increase in the target atomic mass, the change of $\phi(E, \theta)$ with θ became considerably smaller, as can be seen in Figs. 1 to 3. The calculated values of $\phi(E, \theta)$ in Eq. (4) show the good agreement with the experimental results in the lower evaporation spectrum region at all emission angles.

The neutron spectra, $\phi(E, \theta)/E$, are clearly divided into two components in Figs 1 to 3 The higher energy components are well fitted to Eq. (5) corresponding to the pre-equilibrium emission. The values of nuclear temperatures T and T'(θ) best fitted to the measured spectra are shown in Table 1, as a function of θ for all projectiles and targets.

For the alpha projectile shown in Fig. 2, the $\phi(E, \theta)/E$ spectra show a broad bump from their exponential form in the energy region from about 15 to about 45 MeV for all targets. The magnitude of the bump and its most probable energy decrease with increasing emission angle and target atomic number. This shows that the reaction process which leads to the bump spectra is the direct knockout reaction. For ^{3}He incidence, especially on lighter target nuclei, a broad remarkable peak above 10 MeV on the continuum spectra only in the forward direction, 0 and 15 deg, can be seen in Fig. 3. The neutrons in this peak area are produced from the breakup reaction of ^{3}He, (^{3}He, n2p), and the most probable energy of this peak is about 1/3 of the incident ^{3}He kinetic energy.

For the projectile energy above 100 MeV, the experimental neutron spectra from a thick lead target by 590-MeV protons by Cierjacks et al.[9], from a thick uranium by 750-MeV protons by Madey et al.[10], and from carbon and lead by 640- and 710-MeV alpha particles by Cecil et al.[11] were selected for this phe-

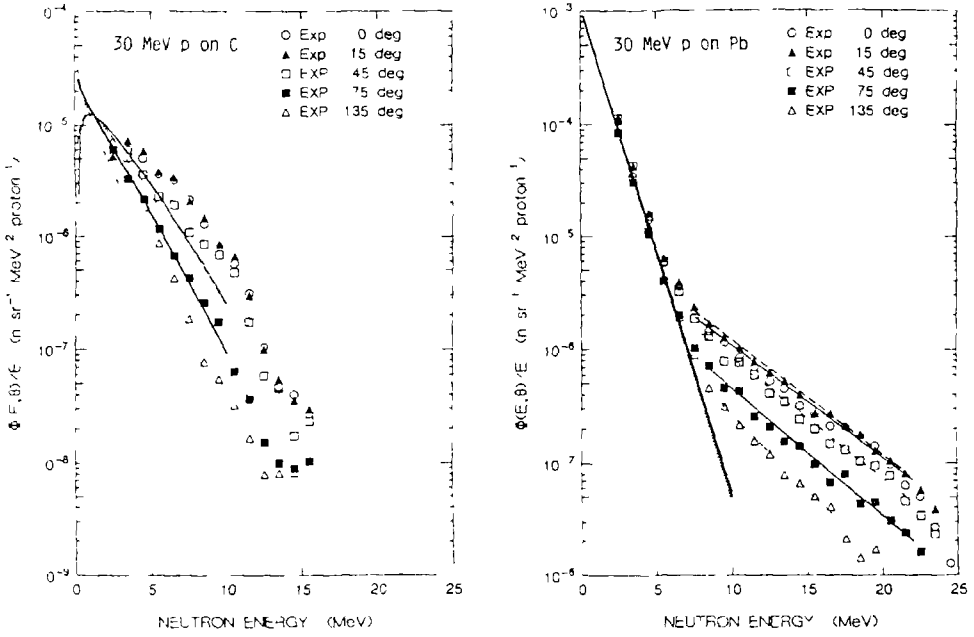

Fig. 1 Analytical fitting of the measured neutron spectra divided by the neutron energy E of $\Phi(E, \theta)/E$ at θ emission angle by 30-MeV proton bombardment to two Maxwellian-type spectra having nuclear temperatures T for evaporation neutrons and $T'(\theta)$ for pre-equilibrium emission.[3)]

(a) Carbon target (b) Lead target

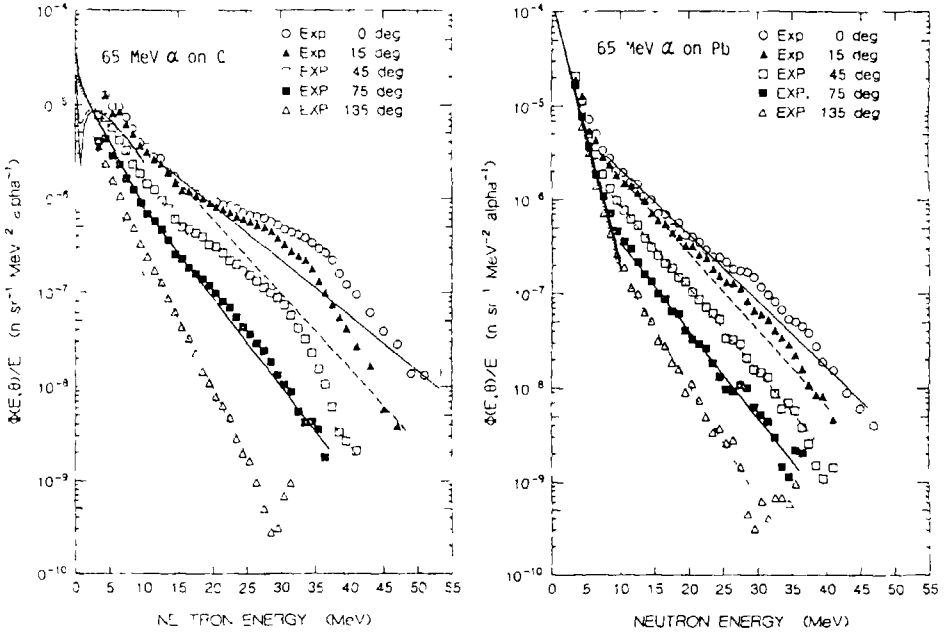

Fig. 2 Analytical fitting of the measured neutron spectra $\Phi(E, \theta)/E$ by 65-MeV alpha ion bombardment to two Maxwellian-type spectra having nuclear temperatures T and $T'(\theta)$ as in Fig. 1.[3)]

(a) Carbon target (b) Lead target

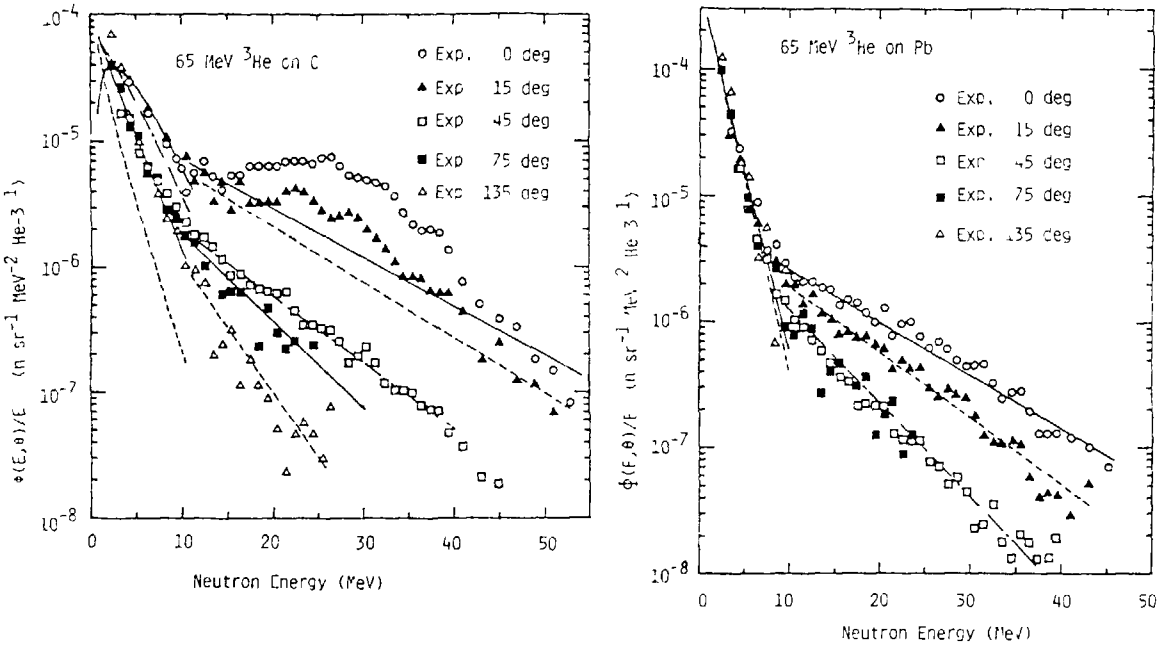

Fig. 3 Analytical fitting of the measured neutron spectra $\Phi(E, \theta)/E$ by 65-MeV ^{3}He ion bombardment to two Maxwellian-type spectra having nuclear temperatures T and T'(θ).[3]

(a) Carbon target (b) Lead target

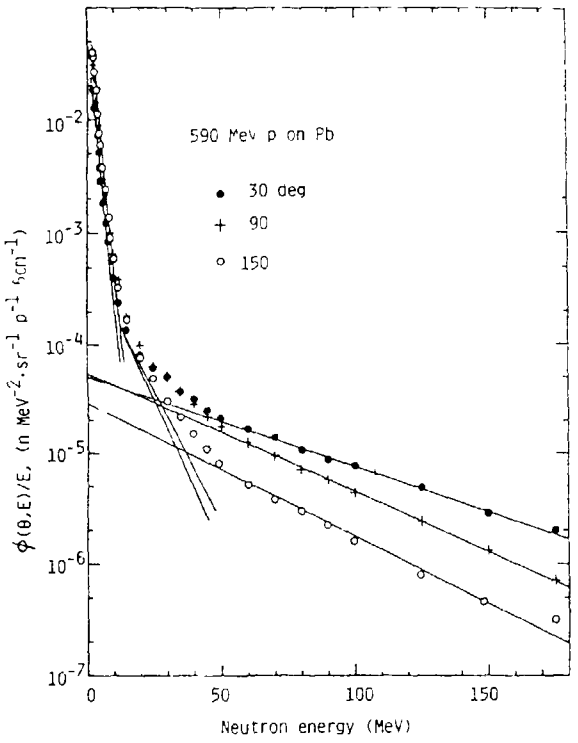

Fig. 4 Analytical fitting of the measured neutron spectra $\Phi(E, \theta)/E$ by 590-MeV proton bombardment on lead target[7], to three Maxwellian-type spectra having nuclear temperatures T, $T'_1(\theta)$ and $T'_2(\theta)$.[3]

nomenological spectrum analysis, because only these data at present give the angular dependent neutron energy spectra down to less than 10 MeV, which is necessary to estimate the nuclear temperature T in the evaporation process. The measured spectra, $\Phi(E, \theta)/E$, by Cierjacks et al. are shown in Fig. 4 and by Cecil et al. in Fig. 5 as examples. As seen in Figs. 4 and 5, the neutron spectra are divided into two exponential components, the evaporation component given by Eq. (4) and the pre-equilibrium component given by Eq. (5). The former has a constant nuclear temperature T independent of the emission angle and the latter has angle-dependent one T'(θ), as well as in the projectile energy below 100 MeV.

For alpha particle incidence shown in Fig. 5, the $\Phi(E, \theta)/E$ spectra also show a broad bump from their exponential form above about 50 MeV for all targets, similarly as in Fig. 2. This bump can be seen in the forward direction of 0 to 45 deg for a projectile energy below 100 MeV (Fig. 2), while clearly seen only

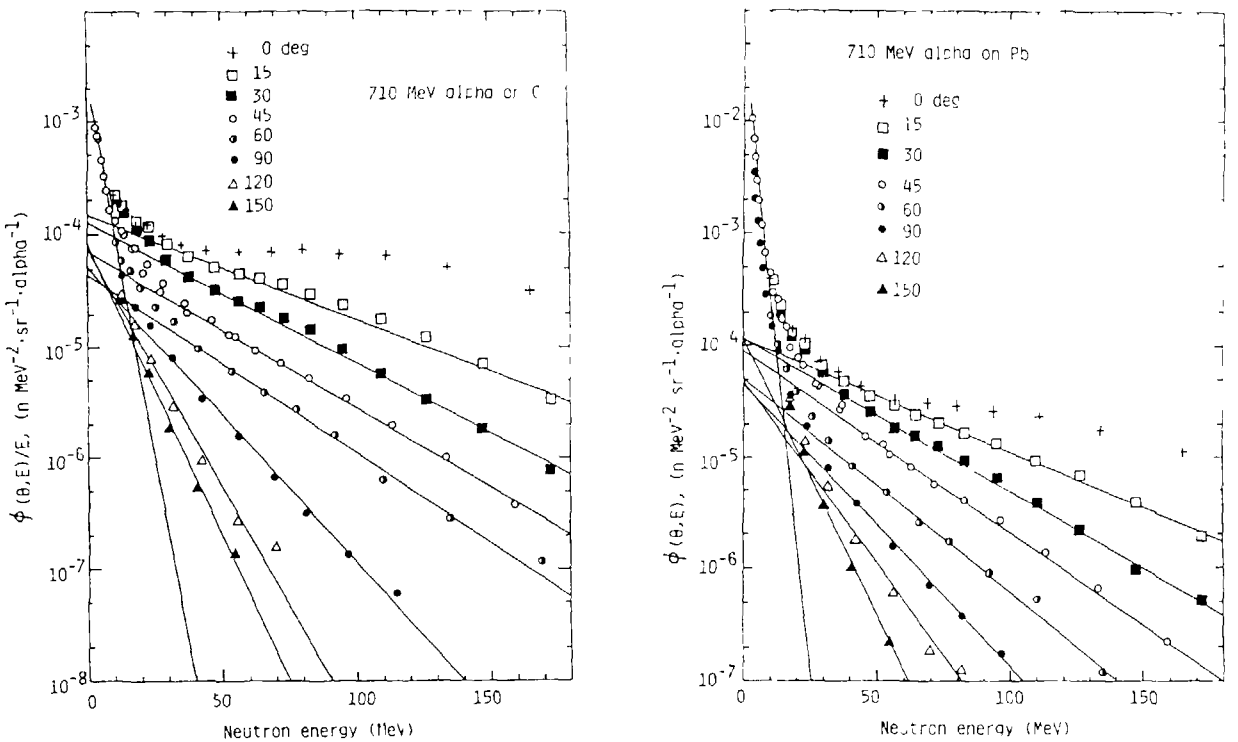

Fig. 5 Analytical fitting of the measured neutron spectra $\Phi(E, \theta)/E$ by 710-MeV alpha ion bombardment[9], to three Maxwellian-type spectra (intermediate component is not shown to avoid the visual complexity) having nuclear temperatures, T, $T'_1(\theta)$ and $T'_2(\theta)$.[3]

(a) Carbon target (b) Lead target

at 0 deg for a projectile energy above 100 MeV (Fig. 5). This may be explained from the fact that the forwardness of neutron emission due to knockout process is much stronger with increasing projectile energy.

One more characteristic feature of the neutron spectra produced for projectile energies in above 100 MeV is that the intermediate third component can be identified. This component may also belong to a kind of pre-equilibrium emission, but its nuclear temperature of Maxwellian-type spectrum is almost independent to the neutron emission angle, differently from that of the highest spectrum component, $T'(\theta)$, in Eq. (5). The evaporation nuclear temperature, T, and two pre-equilibrium nuclear temperatures, $T'(\theta)$, best fitted to the measured spectra in Figs. 4 and 5 and from Ref. (10) are shown in Table 1.

Table 1 Nuclear Temperature T for the Equilibrium State and T' for the Preequilibrium State for Each Projectile-Target Combination

Projectile	Energy E_0 (MeV)	Target	Nuclear Temperature: Equilibrium T (MeV)	Preequilibrium T' (MeV) 0°	15°	30°	45°	60°	75°	90°	120°	135°	150°
p	30	C	1.7	---	---		---		---			---	
		Cu	1.5	4.7	4.6		3.9		3.6			2.6	
		Pb	1.0	4.4	4.3		4.1		3.8			3.3	
d	33	C	2.3	9.3	7.0		5.0		3.9			---	
		Cu	1.5	6.9	5.9		4.3		3.3			2.7	
		Pb	1.1	5.0	4.9		4.3		3.3			3.3	
^{3}He	65	C	2.8	11.2	9.8		8.3		6.3			4.2	
		Cu	2.1	9.8	9.0		6.9		---			---	
		Pb	1.5	10.2	8.2		5.8		---			---	
α	65	C	2.8	7.4	5.5		4.6		4.6			3.0	
		Cu	2.1	7.3	6.8		6.7		5.9			3.5	
		Pb	1.5	6.2	5.4		5.0		4.7			3.6	
p	590	Pb	1.7			$\binom{9}{53}$				$\binom{9}{40}$			$\binom{8}{36}$
p	750	U	1.8				$\binom{---}{38^*}$					$\binom{---}{16^{**}}$	
α	640	Pb	1.5	---	---	---	---	---		---	---		---
α	710	C	3.2	--- ---	$\binom{7}{48}$	$\binom{7}{35}$	$\binom{7}{30}$	$\binom{7}{27}$		$\binom{7}{16}$	$\binom{---}{10}$		$\binom{---}{8}$
		Fe	2.2	--- ---	$\binom{7.5}{48}$	$\binom{7.5}{33}$	$\binom{7.5}{29}$	$\binom{7.5}{25}$		$\binom{7.5}{20}$	$\binom{---}{13}$		$\binom{---}{9}$
		Pb	1.7	--- ---	$\binom{6.5}{43}$	$\binom{6.5}{32}$	$\binom{6.5}{26}$	$\binom{5.5}{23}$		$\binom{5.5}{17}$	$\binom{---}{13}$		$\binom{---}{9}$

* θ = 50° , ** θ = 130°.

The ratio of evaporation component to the pre-equilibrium emission component, as seen in Figs. 2 to 5, becomes larger with lighter projectiles and heavier target nucleus. This reveals that the heavier projectiles and lighter target nucleus produce a larger fraction of high energy neutrons from pre-equilibrium emission and the knockout process, due to a larger momentum transfer from projectile to target nucleus.

Figure 6 shows the nuclear temperature T of the evaporation component of the neutron spectrum as a function of initial projectile energy, E_0. It increases with projectile energy and decreases with increasing target mass number, but does not depend so much on the type of projectile, and approaches a saturated value at about 100 MeV. For T'(θ), the data are too small to discuss their dependence on E_0 and target atomic number.

4. Estimation of Low Energy Neutron Components and Total Neutron Yield

The fast neutron yield, i.e., the number of neutrons of energy higher than E_{cut}, Y^{fast} was obtained from the measured neutron spectra, $\Phi(E, \theta)$, as

$$Y^{fast} = 2\pi \int_0^{\pi} \sin\theta \, d\theta \int_{E_{cut}}^{E_0} \Phi(E, \theta) dE \ , \qquad (6)$$

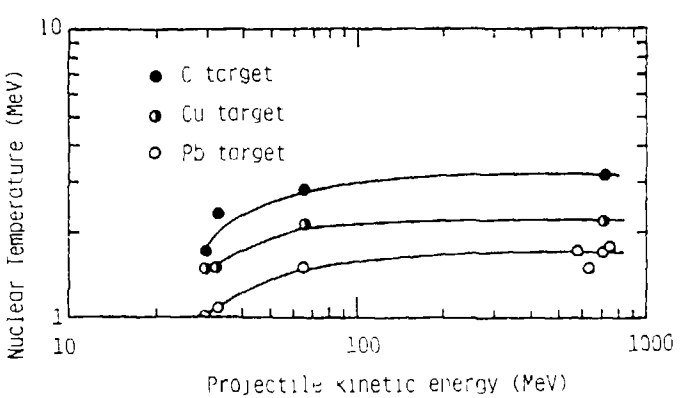

Fig. 6 Dependence of the nuclear temperature T of the compound nucleus in an equilibrium state on the projectile kinetic energy E_0.[3]

since the measured data were often limited to neutron spectra above a few MeV. For practical use, it is necessary to have the total neutron yield, i.e., the number of neutrons produced over the whole energy region, Y^{total}, by estimating the neutrons below that energy E_{cut}. As described before, the neutron spectra in the few MeV region scarcely change with emission angle, excluding neutrons from the carbon target by d, ^{3}He, and α ions, and can be approximated to be a Maxwellian energy distribution given by

$$\Phi(E) = C \frac{E}{T^2} \exp(-E/T) \ . \qquad (7)$$

For the carbon target bombarded by d, ^{3}He and α ions, however, the contribution of neutrons produced by the non-evaporation process could still not be neglected in this low energy region in the forward direction. These non-evaporation neutron components were estimated by subtracting the $\Phi(E)$ value of Eq. (7) from the measured spectra $\Phi(E, \theta)$ for $E_{cut} \leq E \leq 10$ MeV and extrapolating the subtracted results $\Phi^{NE}(E, \theta)$ smoothly into the energy region below E_{cut}. The neutron energy spectra $\Phi'(E, \theta)$ were finally evaluated over the whole energy region as,

$$\Phi'(E, \theta) = \begin{cases} \Phi(E, \theta) \text{ in Figs. 2 and 3}, & \text{for } E_{cut} \leq E \leq E_0 \\ \Phi(E) \text{ of Eq. (7)} + \Phi^{NE}(E, \theta), & \text{for } 0 \leq E \leq E_{cut} \ . \end{cases} \qquad (8)$$

By integrating $\Phi'(E, \theta)$ with energy and angle, the total neutron yield, Y^{total} was obtained as

$$Y^{total} = \int_0^{\pi} \int_0^{E_0} 2\pi \sin\theta \, \Phi'(E, \bar{\theta}) dE d\theta \ . \qquad (9)$$

For p, d, ^{3}He and α ions, the total neutron yields, Y^{total} obtained by Eq. (9), from our experimental results[7] for carbon and copper targets are compared with other experimental results in Fig. 7. Figure 7 also includes the total neutron yields for 710-MeV alpha beams incident on carbon and iron targets which were estimated by Eq. (7) from the neutron angular and energy distributions measured above 3 MeV by Cecil et al.[11]

The total neutron yields increase in the order of p, α, ^{3}He and d projectiles and with the incident projectile energy per nucleon, and so are the largest for deuteron incidence on the carbon target due to a splitting reaction. The values of Y^{total} increase monotonically with the target atomic mass for p, ^{3}He and α projectiles of energy above 10 MeV per nucleon.

The angular distributions of the fast neutron flux integrated over energy for carbon, iron, copper and lead targets,

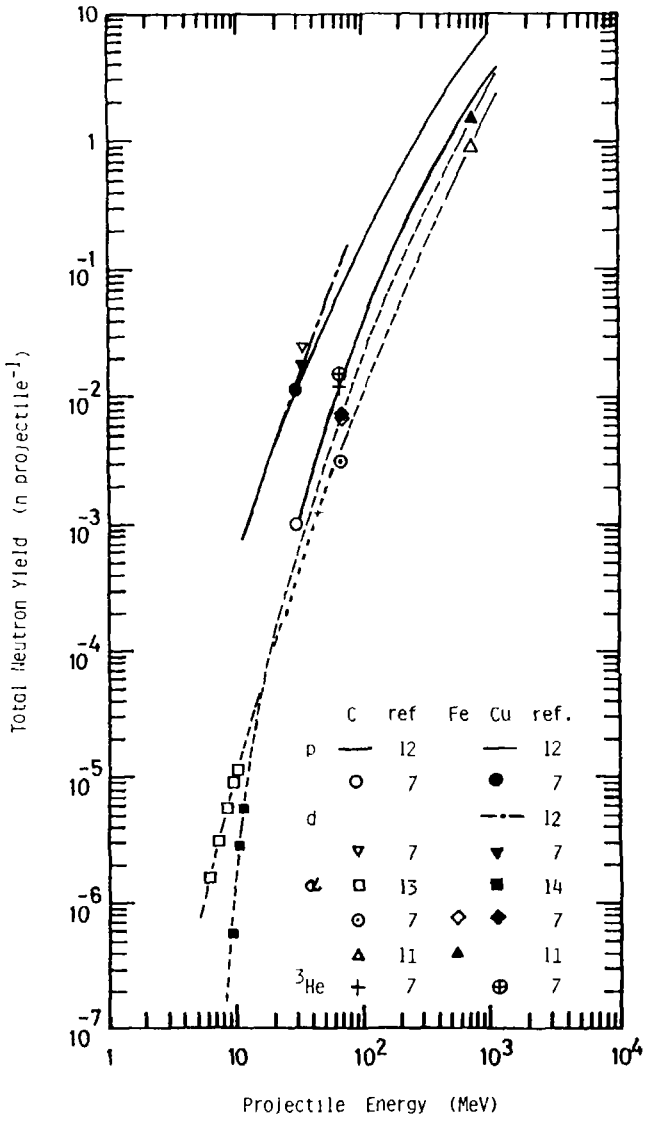

Fig. 7 Total neutron yield data for proton, deuteron, ^{3}He and alpha ions on carbon, iron and copper targets.

$$\phi^{fast}(\theta) = \int_{E_{cut}}^{E} \phi(E, \theta)dE, \qquad (10)$$

are shown in Fig. 8, for E_{cut} of 4 MeV. Figure 8 clearly shows that the fast neutron angular distributions in the backward direction are almost isotropic for all projectile and target combinations, whereas in the forward direction, the forward peaking is stronger in the order of projectile types of p, α, ^{3}He and d, and for lighter target nuclei. This can be explained from the fact that the

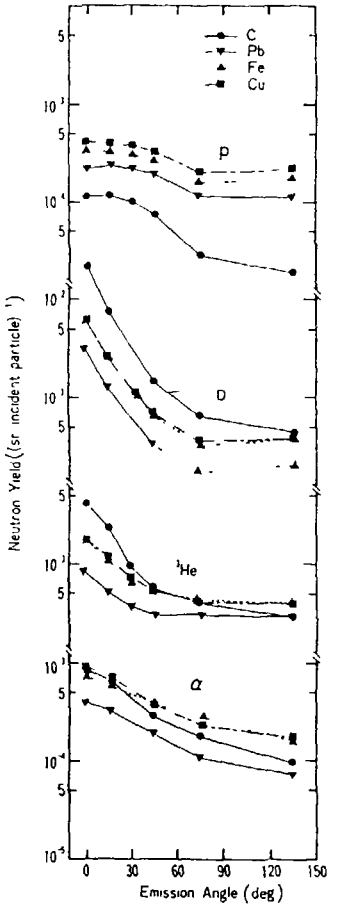

Fig. 8 Angular distributions of fast neutron fluxes integrated above 4 MeV for proton, deuteron, ^{3}He and alpha ion incidence on carbon, iron, copper and lead targets.[7]

splitting reaction of d and ^{3}He projectiles occurs strongly in the forward direction, and that the momentum transfer from a heavier projectile to a lighter target is greater and the velocity of the center of mass is greater in the laboratory system; then based on the kinematics, a nucleon is emitted in the more forward direction from the heavier projectile and the lighter target.

5. High Intensity Pseudo-Monoenergetic Neutron Beam from 15 MeV to 40 MeV

A neutron beam course of pseudo-monoenergy from 15 MeV to 40 MeV was installed by the Be(p, n) reaction, with changing the proton energy up to 40 MeV. The thickness of the beryllium target is selected to be 2 mm for 40 and 35 MeV protons and 1 mm for proton energy lower than 30 MeV, in order to get the neutron yield as much as possible, with keeping the reasonably good energy resolution of the monoenergy peak. The water backing for target cooling is used to stop the proton beam completely, because of low neutron production cross section and high threshold energy of oxygen.

The neutron energy spectra at 0 degree to the proton beam for 40, 35, 30, 25 and 20 MeV proton energies, measured with a NE-213 scintillator, are shown in Fig. 9 as examples, in units of neutron flux density per incident proton. These neutron energy spectra indicate pretty good pseudo-monoenergetic spectra, although they are contaminated with low energy neutron components. For above four proton energies, the peak neutron energies $\bar{E}_n$ and their energy resolutions ΔE_n are listed in Table 2, with the peak and the total (neutron energy above 4 MeV) neutron fluxes. The $\bar{E}_n$ value moves upward with increasing the proton energy and the monoenergetic neutrons in the peak area are about a half of all neutrons produced in the beam course as shown in Table 2.

This pseudo-monoenergetic neutron beam course of variable energy peak between 15 MeV and 40 MeV can be used for induced radioactivity studies of materials, activation analysis of trace elements, activation cross section measurements, study on neutron-rich short-lived nuclei, neutron damage study and so on.

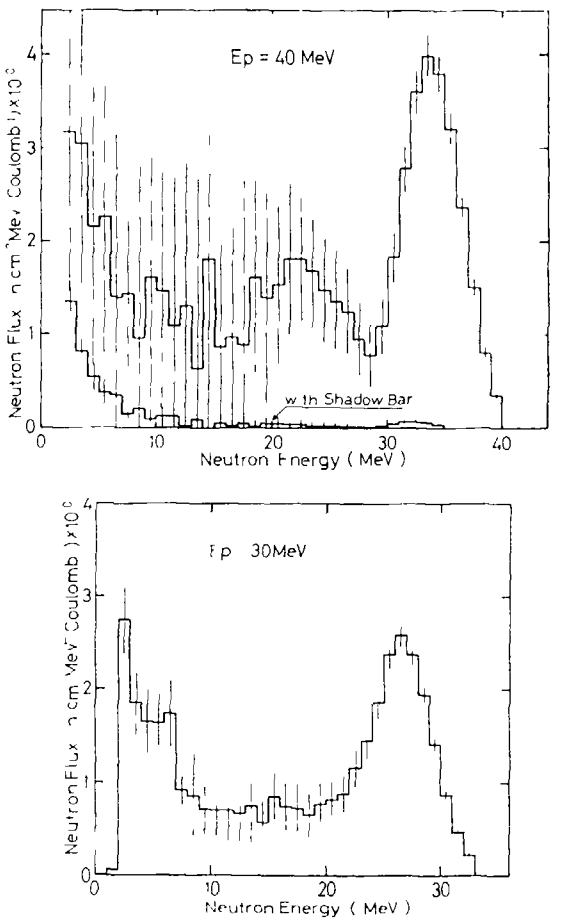

Fig. 9 Measured quasi-monoenergetic neutron energy spectra produced from 1 mm or 2 mm thick beryllium target backed by water bombarded by 30 MeV or 40 MeV proton beam, respectively.

(a) 40 MeV proton (2 mm thick Be)

(b) 30 MeV proton (1 mm thick Be)

Table 2 Characteristics of Pseudo-Monoenergetic Neutron Field

Proton Energy E_p (MeV)	Energy Loss ΔE_p (MeV)	Target Thickness (mm)	Mean Neutron Energy $\bar{E}_n$ (MeV)	Energy Spread ΔE_n (MeV)	Total Flux ($\geq$ 4 MeV) ϕ_t	Peak Flux ϕ_p	Ratio ϕ_p/ϕ_t
40	4.4	2	34.0	± 3.0	1.36 + 16*	5.74 + 15	0.42
35	4.9	2	30.0	± 3.5	1.16 + 16	5.23 + 15	0.45
30	2.8	1	26.5	+ 3.2	5.65 + 15	3.02 + 15	0.53
25	3.2	1	21.0	+ 3.0	4.28 + 15	2.52 + 15	0.59
20	3.9	1	15.5	+ 3.5	3.42 + 15	1.63 + 15	0.48

* 1.36 + 16 means 1.36×10^{16} in units of $n \cdot sr^{-1} \cdot Coulomb^{-1}$.

References

1) T. Nakamura et al., Atomic Data and Nuclear Data Tables, 32 (1985) 471.
2) F. Clapier and C. S. Zaidins, Nucl. Instrum. Methods, 217 (1983) 489.
3) T. Nakamura and Y. Uwamino, Phys. Rev. C, 29 (1984) 1317.
4) T. Nakamura, Nucl. Instrum. Methods, A240 (1985) 207.
5) L. S. August, F. H. Attix, G. H. Herling, P. Shapiro, and R. B. Theus, Phys. Med. Biol., 21 (1976) 931.
6) R. Madey, F. M. Waterman, and A. R. Baldwin, Phys. Rev. C, 14 (1976) 801.
7) K. Shin, M. Fujii, Y. Uwamino, and T. Nakamura, Phys. Rev. C, 29 (1984) 1307.
8) R. G. Alsmiller Jr., M. Leimdoerfer and J. Barish, ORNL-4046 (1967) Oak Ridge National Laboratory.
9) S. Cierjacks, M. T. Rainbow, M. T. Swinhoe, and L. Buth, Proc. IV ICANS Meeting at National Laboratory for High Energy Physics, Tsukuba, Oct. 20-24 (1980).
10) R. Madey and F. M. Waterman, Phys. Rev. C, 8 (1973) 2412.
11) R. A. Cecil et al., Phys. Rev. C, 21 (1980) 2471.
12) L. D. Stephens and A. J. Miller, Proc. 2nd Int. Conf. Accelerator Dosimetry and Experience, Stanford, Calif., Nov. 5-7 (1969), CONF-691101, p459.
13) R. L. Macklin and J. H. Gibbons, Nucl. Sci. Eng., 31 (1968) 343.
14) P. H. Stelson and F. K. McGowan, Phys. Rev., 133 (1964) B911.

SESSION II

FAST NEUTRON FIELDS

Invited Paper

d(Be) NEUTRON FIELDS AND THEIR APPLICATIONS IN NUCLEAR REACTION CROSS-SECTION STUDIES

S.M. QAIM
Institut für Chemie 1 (Nuklearchemie),
Kernforschungsanlage Jülich GmbH,
Jülich, Federal Republic of Germany

Abstract

A short review of some of the properties of d(Be) neutrons is given and the methods of spectrum characterization using various detectors are outlined. Some of the integral tests done using such spectra are discussed. Nuclear reaction cross-section measurements, especially on high-threshold (n,t) and (n,^{3}He) reactions, employing activation and other off-line methods are described. Those studies have contributed significantly to an understanding of the phenomenon of trinucleon emission. A recent effort to determine the excitation function of an (n,t) reaction via irradiations in various neutron fields is discussed.

INTRODUCTION

Fast neutrons produced in the interaction of energetic deuterons (generally from a cyclotron) with Li and Be are of special interest because of high yields and high average neutron energies. Such neutron sources have a great potential for integral data testing, radiation damage studies and biomedical applications. This paper reviews briefly some of the characteristics of the d(Be) neutron fields and describes in more detail their applications in nuclear reaction cross-section studies using activation and other off-line techniques.

The d(Be) and d(Li) neutrons are known to be strongly forward peaked [cf. 1-14]. Time of flight (TOF) studies using various flight lengths and a few selected angles have been performed in several laboratories [cf. 1,3,4,5,7,8,10,13,14]. Some typical neutron yield curves from 40 MeV deuterons on a thick Be target are shown in Fig. 1 [7]. Evidently the intensity of neutrons decreases sharply with the angle of emission. The spectrum around 0° direction is of greater interest since it is of the highest intensity. It consists of a low energy component as well as a bell shaped distribution, centred at $E_n \sim 0.4\ E_d$.

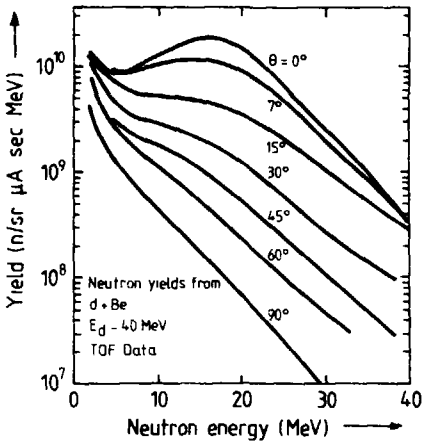

Fig 1 Energy distribution of neutrons emitted at various angles in the interaction of 40 MeV deuterons with a thick Be target [7].

Most of the TOF studies concentrated primarily on the high-energy part of the spectrum, the lower cut off energy of the neutron being 2 MeV or higher. A few measurements [cf. 8,10] on the other hand extended to lower energies and showed that the contribution of neutrons with energies < 2 MeV is rather high. Some recent studies, however, have shown [14] that this contribution is not as high as given earlier [8,10]. The low-energy component falls off almost exponentially with neutron energy. Furthermore, whereas the intensity of the broad peak decreases rapidly with angle, that of the low energy continuum varies very slowly.

The angular distribution of neutrons and the energy dependence of the broad neutron peak show that neutron production at high deuteron energies proceeds via deuteron stripping. The low-energy component is not well understood. It has been postulated [cf. 12] that the neutron unbound states in the target nucleus, excited by direct inelastic scattering reactions, contribute significantly to the production of low-energy neutrons. Other contributing processes are multi-body breakup reactions (which have low thresholds) and evaporation of neutrons from the compound nucleus.

For both the d(Be) and d(Li) neutron sources an increase in the deuteron energy leads to

- enhanced forward-peaked distribution (cf. Fig. 2 [5])

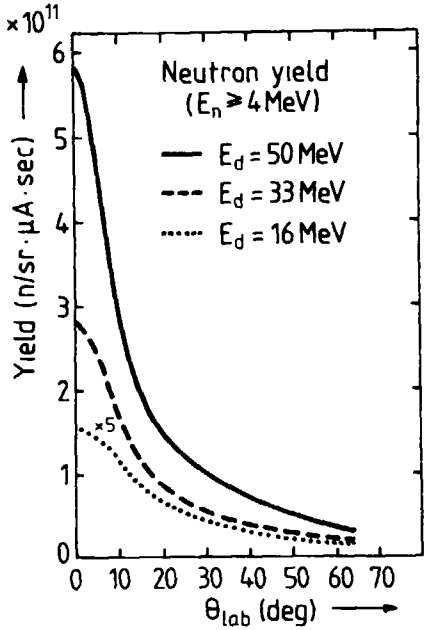

Fig. 2 Angular distribution of neutrons from d(Be) reaction with a thick target at various deuteron energies [5]

- rapid increase in the intensity of neutrons emitted in the 0° direction (cf. Fig. 3A [9])
- increase in the average energy of the neutrons (cf. Fig. 3B [12]).

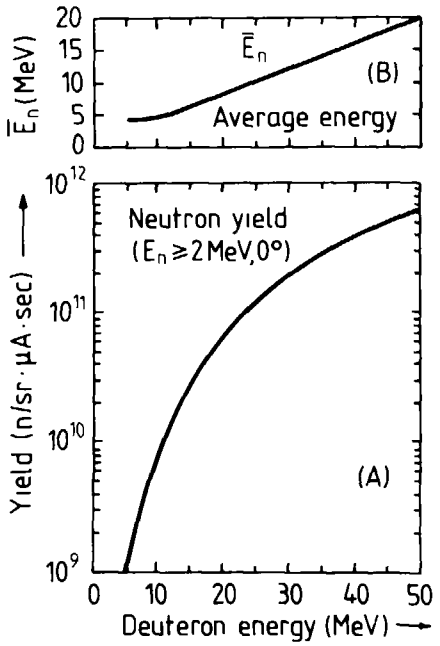

Fig. 3 Thick target neutron yield (A) and average neutron energy (B) as a function of deuteron energy incident on Be [9,12].

Evidently, using energetic deuterons at high beam currents intense neutron fields can be obtained. The major limitation is the strong anisotropy of the source, due to which only small samples can be used for irradiation, mainly in the 0° direction.

CHARACTERIZATION OF NEUTRON SPECTRA

As mentioned above the neutron spectra produced at several incident deuteron energies have been characterized by TOF studies. A pulsed deuteron beam with a width of a few nsec and repetition time of 50 to 100 nsec (e.g. from a cyclotron) falls on a thick Be target and the neutrons produced are detected by an NE 213 scintillator placed at a given angle at the end of a certain flight path. The discrimination between neutrons and γ-rays is easily achieved. There are, however, two major difficulties associated with the TOF method:

a) The detector efficiency determination entails considerable uncertainties since a wide range of neutron energies are involved.

b) The characterization of low-energy neutrons is complicated by pulse overlap, especially in the case of high-frequency accelerators. Due to this difficulty most of the measurements have been done with the neutron detector threshold set above 2 MeV.

Characterization of d(Be) neutron spectra has been done so far for incident deuterons of energies 7,13,14,15,16,18,23,30,33,35,40,50 and 54 MeV (cf. 1,3,4,5,7,8,13,14]. As far as we know no detailed study beyond 54 MeV has been reported.

A more modest method of neutron spectrum characterization (compared to TOF technique) involves activation of several monitor reaction foils and subsequent unfolding of the neutron spectrum using various codes. A set of foils is chosen such that on irradiation with neutrons some 20 nuclear reactions, each with a different threshold, are induced. The nuclear reactions chosen should have well-known excitation functions, covering the entire region of the neutron spectrum. Some of the threshold reactions commonly used are listed in Table I. Cross-section data for several of them are given in dosimetry files; for the others results of individual investigations are available.

The differential neutron flux $\emptyset(E)$ as a function of neutron energy E appears in the activation equation as

$$A_i = \int_{E_{min}}^{E_{max}} \emptyset(E)\ \sigma_i(E)\ dE, \qquad i = 1,2,3.....m,$$

where A_i is the specific saturation activity of i_{th} threshold reaction product (measured generally by γ-ray spectroscopy), and $\sigma_i(E)$ its energy-dependent cross section; E_{min} and E_{max} are the limits of the energy region of the spectrum.

Table I. Some threshold reactions used for neutron spectrum unfolding

Threshold reaction	Maximal response region (MeV)*	Threshold reaction	Maximal response region (MeV)*
$^{115}In(n,n')^{115m}In$	1.5-11.5	$^{48}Ti(n,p)^{48}Sc$	11-26
$^{58}Ni(n,p)^{58}Co$	3.7-15.3	$^{59}Co(n,2n)^{58}Co$	12.6-27.4
$^{54}Fe(n,p)^{54}Mn$	3.7-15.9	$^{89}Y(n,2n)^{88}Y$	13.5-27.5
$^{46}Ti(n,p)^{46}Sc$	6.5-22	$^{45}Sc(n,2n)^{44m}Sc$	14-28
$^{27}Al(n,\alpha)^{24}Na$	9-18	$^{90}Zr(n,2n)^{89}Zr$	14-29
$^{56}Fe(n,p)^{56}Mn$	9-18	$^{59}Co(n,3n)^{57}Co$	21-29
$^{65}Cu(n,p)^{65}Ni$	8.5-25	$^{107}Ag(n,3n)^{105}Ag$	22.5->30
$^{197}Au(n,2n)^{196}Au$	10-20	$^{197}Au(n,3n)^{195}Au$	15->30
$^{93}Nb(n,2n)^{92m}Nb$	11-23.5	$^{89}Y(n,3n)^{87}Y$	>27->30

* $\sigma(E) \geq 0.5\ \sigma_{max}(E)$

Several codes have been used for unfolding neutron spectral distributions [cf. 15-17] from threshold reaction activities. Some of the best known codes are SAND II [cf. 18] and STAY'SL [cf. 19]. Whereas the former is based on iterative methods, the latter uses a more generalized least-squares formalism. A typical unfolded neutron spectrum is shown in Fig. 4 [cf. 20,21] together with the results from TOF measurements. The agreement is quite good. Similar unfolding studies have been performed on neutron spectra produced in the interaction of deuterons of other energies.

The error limits of the unfolded neutron spectrum are generally calculated using a Monte Carlo programme [cf. 22]. A typical case is shown in Fig. 5 [23]. The major errors are those involved in the absolute measurement of radioactivity and the uncertainties associated with the excitation functions of the threshold reactions used. The excitation functions have generally errors of 5 to 10%, but in some cases there is a lack of data in

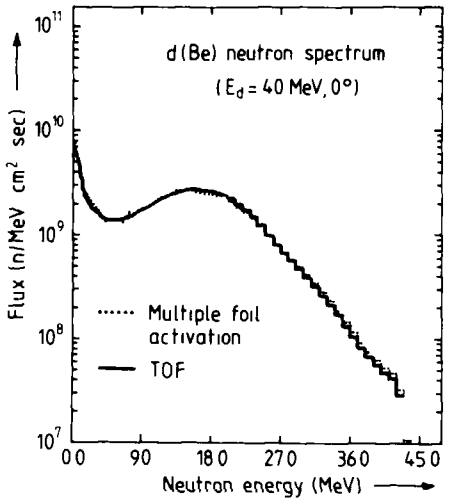

Fig. 4 Neutron spectrum from a d(Be) source at E_d = 40 MeV unfolded at 0° compared to TOF results [21].

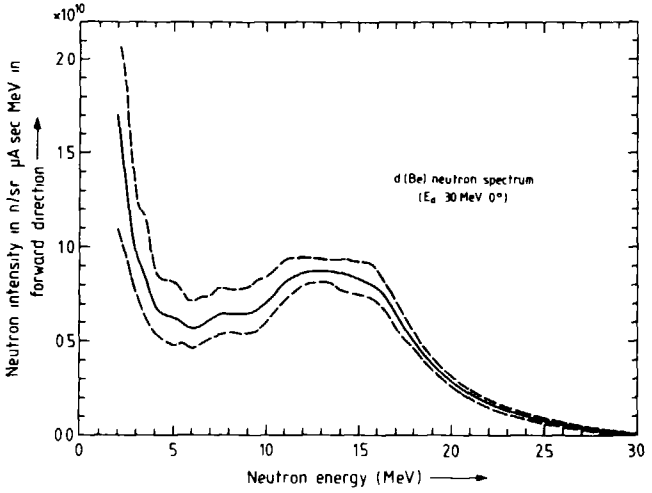

Fig. 5 Unfolded neutron spectrum with error limits [23].

the region of 20 to 30 MeV. Furthermore, beyond 30 MeV there is a serious lack of data. Due to this reason the scope of the multiple foil activation technique is limited up to about 30 MeV.

Fast neutron fields have also been characterized by combining foil activation with helium accumulation passive neutron dosimetry [cf. 24]. In this case mass spectrometric technique was used to determine the accumulated helium. It was possible to discern steep gradients in fluence and spectrum. This type of study is important in irradiations where a knowledge of fluence information is required.

INTEGRAL TESTS

Fast neutron fields calibrated by TOF techniques, especially those produced by 40 and 30 MeV deuterons on a thick Be target, have been used as potential "benchmarks" for integral testing of some dosimetry related reaction cross sections [cf. 21,24-26]. Several foils were irradiated in a well-defined geometry (in the 0° direction) and the radioactivity of each product under investigation was estimated. The activity of the same product was also obtained by calculation using the known excitation function and the neutron flux distribution of the spectrum. Since in several cases no experimental cross sections were known beyond 20 MeV, the information was obtained either by extrapolation of the curves or by nuclear model calculations. A ratio of the measured to calculated activities was then determined and the results for a few cases are given in Table II. Both sets of data agree within about 15%. Taking into account the various uncertainties involved, this agreement appears to be rather good. Presently, efforts are underway to establish some well-defined $^{9}Be(d,n)$ spectra [cf. 13,14,27] which could be used as standard fields for integral testing of evaluated neutron dosimetry cross-section data.

For neutron dosimetric studies nuclear reaction cross sections up to about 50 MeV are needed. However, due to the lack of availability of monoenergetic neutron sources beyond 28 MeV, those needs cannot be met presently by experimental investigations. Nuclear model calculations can yield the required data, though possibly with large uncertainties. Integral measurements using neutron fields, such as the ones described above, could lead to a useful check of those calculations.

Table II. Ratios of measured to calculated activities of some neutron threshold reaction products

Nuclear reaction	Ratio for investigations around 0°	
	40 MeV d(Be) [a]	30 MeV d(Be) [b]
$^{27}Al(n,\alpha)^{24}Na$	1.02	0.92
$^{46}Ti(n,p)^{46}Sc$	1.18	0.86
$^{48}Ti(n,p)^{48}Sc$	0.97	
$^{58}Ni(n,p)^{58}Co$	0.93	
$^{60}Ni(n,p)^{60}Co$	0.97	1.12
$^{93}Nb(n,2n)^{92m}Nb$	0.93	1.00
$^{169}Tm(n,2n)^{168}Tm$	0.91	
$^{197}Au(n,3n)^{195}Au$	0.87	

[a] Ref. [21] [b] Ref. [26]

A second type of integral test incorporates the estimation of a reaction product from the bulk of a material as well as its individual components. Tritium formation cross sections with 30 MeV d(Be) neutrons, for example, were determined [26] for stainless steel as well as its constituents (Cr, Ni, Mn and Fe). The experimentally determined integral value for stainless steel was found to be in agreement with that deduced from the values for various contributing elements. Somewhat similar investigations have been performed on the emission of ^{4}He as well [cf. 24]. A careful measurement of the ratio of $^{63}Cu(n,\alpha)^{60}Co$ cross section to $^{27}Al(n,\alpha)^{24}Na$ cross section was done in a 7 MeV d(Be) neutron

field using a Cu-Al alloy as sample [27]. The ratio was compared with the values derived from evaluated cross sections and the $^{9}Be(d,n)$ spectrum. Similar studies could also be done in the case of elements consisting of several isotopes. Since the thresholds of the various contributing processes are different, the extent of agreement between the integral value and that deduced from the individual components could reflect on the accuracy of the available excitation function and the neutron spectrum.

CROSS-SECTION MEASUREMENTS

Integral cross-section measurements using d(Be) neutrons in the 0^{o} direction have been done on several target nuclides. A typical arrangement for irradiations is given in Fig. 6. The monitor foils are irradiated together with the sample in order to incorporate geometry corrections and to determine neutron flux. The neutron flux is also derived from the charge collected in a Faraday cup. A comparison of the two values gives an indication of the uncertainties involved in flux measurements.

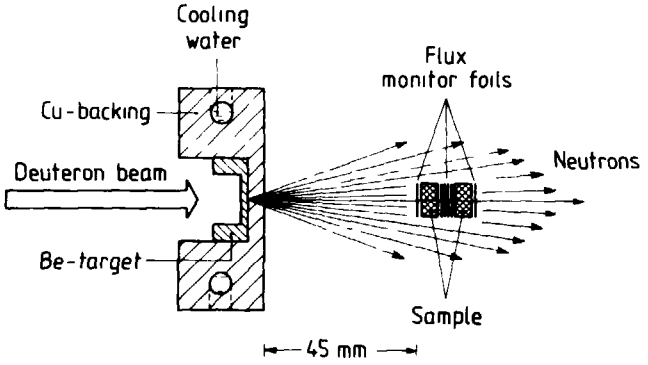

Fig. 6 Typical arrangement for irradiations with d(Be) neutrons [33].

Three off-line techniques, viz. activation, tritium counting and mass spectrometry, have been commonly used for studying the reaction products. With the activation technique the data obtained for (n,xn) and (n,p) reactions are unambiguous, provided mono-isotopic elements or highly enriched isotopes are used as target materials. For the other reactions, however, summed cross sections of various contributing processes are obtained. Tritium counting leads to a useful information on the emission of tritons. Mass spectrometry has been applied to the determination of ^{3}He and ^{4}He particles.

Some cross-section measurements on (n,xn), (n,p), (n,n'p), (n,p2n), (n,α), (n,n'α) and (n,2α) reactions have been performed [cf. 24,26,28-31], especially in connection with radiation damage studies and nuclear model testing. It was found that the (n,n'p) and (n,n'α) reaction cross sections with 30 and 53 MeV d(Be) neutrons are considerably higher than those with 14 MeV neutrons [cf. 26,30,31]. They would therefore contribute appreciably to hydrogen and helium formation, if such a source were to be used for testing fusion reactor materials. The (n,2α) process, on the other hand, is weak even with 53 MeV d(Be) neutrons [30]. From the fundamental point of view, a greater part of the effort, mainly at Julich, has been devoted to the investigation of trinucleon emission reactions (n,t) and (n,^{3}He), for which relatively little information existed. Since the Q-values of those two reactions are highly negative and the cross sections very low, it was found worthwhile to carry out experimental studies with spectral neutrons having intense high energy tails.

The results for the (n,t) reactions investigated by 53 MeV d(Be) neutrons are reproduced in Fig. 7 [28,29]. It is evident that the cross sections for the emission of tritons from the lightest nuclei are quite large, presumably due to direct interactions. The tritium formation cross sections for elements with $Z > 20$ are practically constant. A comparison of the cross sections obtained via tritium counting with those measured via γ-ray spectroscopy of the activation products (Fig. 7 (A) and (B)) reveals that for the light elements, like Ne and Mg, the two types of cross sections are almost identical, suggesting that the activation product is formed exclusively via triton emission. For elements with $A > 40$, on the other hand, tritium emission cross section is much smaller than activation cross section, suggesting thereby that the emission of three particles (1p2n) is more favoured than the emission of a bound tri-nucleon (^{3}H).

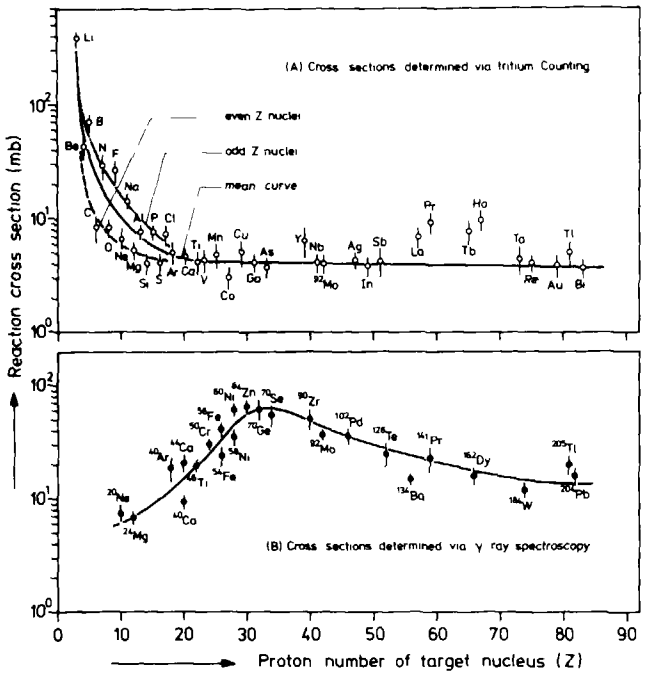

Fig. 7 Cross sections of (n,t) reactions induced by 53 MeV d(Be) neutrons plotted as a function of Z of the target element [28,29].

The results for (n,t) reactions investigated by 30 MeV d(Be) neutrons are given in Fig. 8 [23]. The trend is similar to that with 53 MeV d(Be) breakup neutrons. Apart from the initial decrease the cross section is almost constant over the entire range of Z = 22 to 83. A somewhat similar result is obtained if the cross-section data are plotted against $A^{2/3}$ of the target element. This suggests the occurrence of surface reactions. In Fig. 8 are also shown the results of Hauser-Feshbach calculations on the first chance emission of a triton. The experimental and theoretical data agree within a factor of 2 in the region of Z = 13 to 20, i.e. for nuclei in the (2s,1d) shell. For heavier nuclei, however, triton emission seems to proceed via nonstatistical processes.

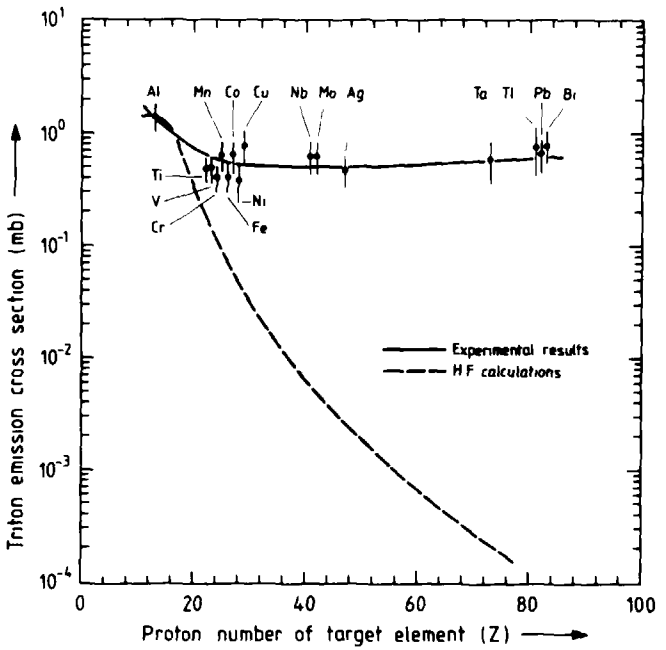

Fig. 8 Systematics of triton emission cross sections with 30 MeV d(Be) neutrons. The results of Hauser-Feshbach calculations are shown as a trend [23].

The results of activation and mass-spectrometric measurements on (n,^{3}He) reactions with 53 MeV d(Be) neutrons are depicted as ^{3}He/^{4}He emission cross-section ratios in Fig. 9 [30,31]. One observes that the ratios obtained using the two techniques agree within 30%. The ratios were also calculated using the Hauser-Feshbach method and the results are given as a general trend in Fig. 9. Apparently, with increasing Z of the target nucleus the contributions of statistical processes decrease much more sharply in the case of ^{3}He-emission than in ^{4}He-emission. However, for a better understanding of the phenomenon of ^{3}He emission, calculations using direct reaction theories are needed.

The foregoing discussion leads to the conclusion that d(Be) neutron fields are of considerable use in integral cross-section

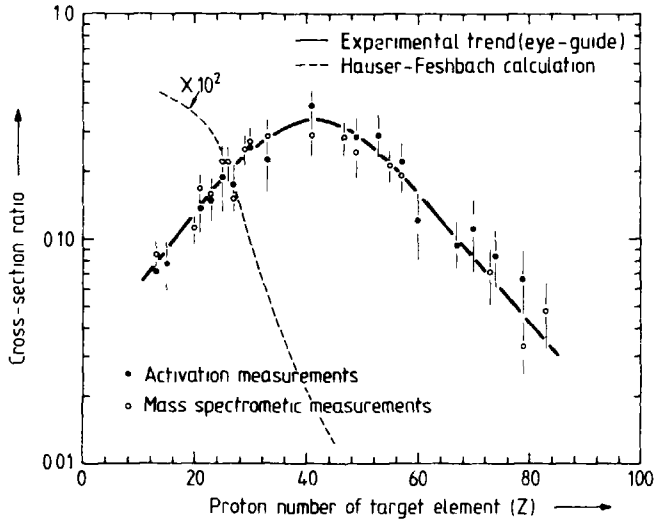

Fig. 9 $^{3}He/^{4}He$ emission cross-section ratios (obtained by activation and mass spectrometry) as a function of Z of the target element. The results of Hauser-Feshbach calculations are also given [30,31].

measurements, especially of high-threshold rare reactions. Such studies have contributed to an understanding of the phenomenon of trinucleon emission from target nuclides in various mass regions.

DIFFERENTIAL DATA FROM INTEGRAL MEASUREMENTS

Due to the lack of monoenergetic neutron sources the determination of excitation functions of neutron induced reactions above 20 MeV is difficult. Therefore, it was thought worthwhile to investigate whether irradiations in different neutron fields, followed by application of mathematical unfolding procedures, could be used to obtain the desired excitation function. A theoretical approach to this goal, illustrated by several hypothetical numerical examples, was developed at Argonne [cf. 32]. The first experimental application of this idea, however, was demonstrated at Julich [cf. 33] in an attempt to determine the excitation function of the (n,t) reaction on aluminum. The aluminum sample and monitor foils were irradiated in the 0^{o} direction with d(Be) neutrons produced at deuteron energies of 17.5, 20.0, 22.5, 25.0, 27.5 and 30.0 MeV. The various neutron spectra were characterized by the multiple foil activation technique and the unfolding code SAND II. From each irradiated Al sample tritium was separated by vacuum extraction and counted in the gas phase. The "excitation function unfolding" was done using the relation mentioned above. Mathematically the problem is the same as in spectrum unfolding, except that $\Phi(E)$ and $\sigma(E)$ are exchanged. For unfolding a least squares code (LSQ-2), very similar to STAY'SL, was used.

The excitation function determined via the unfolding method is given in Fig. 10 [33]. The experimental data points obtained using monoenergetic neutrons up to 19 MeV, as well as the results of Hauser-Feshbach calculations are also shown. The agreement is satisfactory up to ~ 25 MeV, beyond which the slope of the unfolded excitation function becomes too steep.

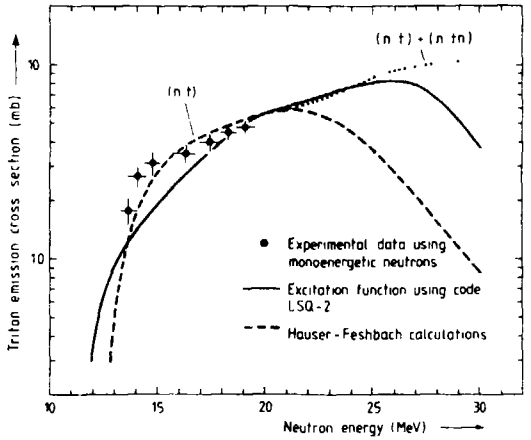

Fig. 10 Excitation function of [(n,t)+(n,tn)] reaction on ^{27}Al obtained via irradiations in diverse neutron fields and unfolding code calculations. The experimental data measured using monoenergetic neutrons up to 19 MeV and the results of Hauser-Feshbach calculations are also shown [33].

The above mentioned study showed that determination of excitation function by application of unfolding codes to activities obtained experimentally in diverse neutron fields is feasible. The method cannot substitute the work with monoenergetic neutrons but can yield useful information in the energy regions not readily accessible by monoenergetic neutrons. For future applications of the reported method, the availability of a greater number of exactly determined monitor excitation functions up to 30 MeV (or more) appears most essential.

Acknowledgements

It is a pleasure to thank Prof. G. Stöcklin for his active support of the Nuclear Data Research Programme at Julich and for stimulating discussions. Acknowledgement is made to Dr. R. Wölfle for help and counsel.

REFERENCES

[1] G.W. Schweimer, Nucl. Phys. A100 (1967) 537
[2] K. Schmidt and H. Münzel, Report KFK-1288 (1970)
[3] V.K. Daruga, E.S. Matusevich and Kh. Narziev, Atomnaya Energia 33 (1972) 934
[4] K.A. Weaver, J.D. Anderson, H.H. Barschall and J.C. Davis, Phys. Med. Biol. 18 (1973) 64
[5] J.P. Meulders, P. Leleux, P.C. Macq and C. Pirart, Phys. Med. Biol. 20 (1975) 235
[6] P. Grand and N.A. Goland, Nucl. Instr. Methods 145 (1977) 49
[7] M.J. Saltmarsh, C.A. Ludemann, C.B. Fulmer and R.C. Styles, Nucl. Instr. Methods 145 (1977) 81
[8] M.A. Lone, C.B. Bigham, J.S. Fraser, H.R. Schneider, T.K. Alexander, A.J. Ferguson and A.B. McDonald, Nucl. Instr. Methods 143 (1977) 331
[9] M.A. Lone, Proc. Symp. Neutron Cross Sections from 10 to 40 MeV, Brookhaven, May 1977, BNL-NCS-50681 (1977) p. 79
[10] M.A. Lone, A.J. Ferguson and B.C. Robertson, Nucl. Instr. Methods 189 (1981) 515
[11] H.H. Barschall, Ann. Rev. Nucl. Science 28 (1978) 207
[12] M.A. Lone and C.B. Bigham, in Neutron Sources for Basic Physics and Applications (S. Cierjacks, ed.), Pergamon Press (1983) p. 133
[13] D.L. Smith, J.W. Meadows and P.T. Guenther, Report ANL/NDM-90 (1985); see also Nucl. Instr. Methods in Phys. Research A241 (1985) 507
[14] G. Dietze, H.J. Brede and D. Schlegel-Bickmann, in Advances in Dosimetry for Fast Neutrons and Heavy Charged Particles for Therapy Applications, IAEA-AG-371/14, Vienna (1984) p. 203
[15] C.A. Oster, Proc. 2nd ASTM-EURATOM Symp. Reactor Dosimetry, Palo Alto, California, 1977, NUREG/CP-0004, 3, 1365, US Nuclear Regulatory Commission (1977)
[16] W.L. Zijp, J.H. Baard and H.J. Nolthenius, ibidem
[17] D.R. Nethaway, R.A. Van Konynenburg, M.W. Guinan and L.R. Greenwood, Proc. Symp. Neutron Cross Sections from 10 to 40 MeV, Brookhaven, May 1977, BNL-NCS-50681 (1977) p. 135
[18] W.N. McElroy, S. Berg, T. Crockett and R.G. Hawkins, Report AFWL-TR-67-41, Vol. 1, Atomics International (1967)
[19] F.G. Perey, Report ORNL/TM-6062 (1977)
[20] L.R. Greenwood, R.R. Heinrich, R.J. Kennerley and R. Mcarzychowski, Nucl. Technology 41 (1978) 109
[21] L.R. Greenwood, R.R. Heinrich, M.J. Saltmarsh and C.B. Fulmer, Nucl. Sci. Engineering 72 (1979) 175
[22] C.A. Oster, W.N. McElroy and J.M. Marr, Report HEDL-TME 73-20 (1973)
[23] R. Wölfle, S. Khatun and S.M. Qaim, Nucl. Phys. A423 (1984) 130
[24] D.W. Kneff, H. Farrar IV, L.R. Greenwood and M.W. Guinan, Proc. Symp. Neutron Cross Sections from 10 to 50 MeV, Brookhaven, May 1980, BNL-NCS-51245 (1980) p. 113
[25] L.R. Greenwood, ibid, p. 75
[26] S.M. Qaim, S. Khatun and R. Wölfle, ibid, p. 539
[27] H. Liskien, D.L. Smith and R. Widera, Proc. Int. Conf. on Nuclear Data for Science and Technology, Antwerp, September 1982, D. Reidel Publishing Company, Dordrecht, Holland (1983) p. 409
[28] S.M. Qaim, R. Wölfle and G. Stöcklin, J. Inorg. Nucl. Chem. 36 (1974) 3639
[29] S.M. Qaim and R. Wölfle, Nucl. Phys. A295 (1978) 150
[30] C.H. Wu, R. Wölfle and S.M. Qaim, Nucl. Phys. A329 (1979) 63
[31] S.M. Qaim, C.H. Wu and R. Wölfle, Nucl. Phys. A410 (1983) 421
[32] D.L. Smith, Report ANL/NDM-77 (1982)
[33] R. Wölfle, S. Sudar and S.M. Qaim, Nucl. Sci. Engineering 91 (1985) 162

INTENSE NEUTRON FIELDS FOR RADIATION DAMAGE STUDIES

R DIERCKX
Joint Research Centre,
Commission of the European Communities,
Ispra

Abstract

Damage, due to radiation by neutrons or charged particles, has to be taken into consideration whenever a material is used as part of a radioactive plant (fission or fusion reactor, accelerator and so on). It is necessary to be able to estimate this damage, especially for future fusion reactors, due to the high investment costs. Therefore, knowledge has to be gained about the damage-producing mechanisms and the correlations between damage and radiation source parameters (energy spectrum, flux and fluence).

Up to now damage studies for fusion applications have been done with fission neutrons, medium-intensity high-energy neutron sources and charged particles. To validate these radiation damage results and make them useful for fusion application, correlations have to be established in radiation environments similar to those of the first wall of a fusion reactor. This can only be done in a fusion reactor itself, or in specially built neutron sources producing or simulating a first wall radiation environment.

The types of possible sources are:

1) 14 MeV sources based on the d-t reaction;
2) d-Li sources which have a broad spectrum, peaking at 14 MeV but with a tail up to 40 MeV,
3) spallation neutron sources which have an evaporation spectrum and a high-energy tail up to 200 - 300 MeV.

Except for the 14 MeV sources, the others are simulations, and the damage results have to be correlated with real fusion spectra.

The characteristics of the neutron sources are discussed and compared, especially in relation to their use for fusion applications.

1. INTRODUCTION

Changes in the physical properties of a material due to neutron irradiation are an important factor in the design of a fusion reactor. Considerable attention is being focused on the radiation damage that will be experienced by the first wall of a magnetically confined fusion reactor In end-of-life irradiations in fission reactors, unexpected microstructural changes have been observed and have been related to mechanical property changes /1/. Microchemical evolution has been shown to be responsible for the acceleration of radiation-induced void growth and creep with fluence. The same should be true for fusion conditions

The complexity of deriving mechanical property changes from the radiation source parameters, material characteristics and physical environment is treated elsewhere /2/. Because of this complexity and the need for technological data, the radiation damage physicist makes use of empirical or semi-empirical correlation functions /3,4/. With these correlations, data obtained in one radiation field can, in principle, be used in other radiation fields. This is very important for fusion materials technology /5,6/.

A fusion reactor in which the materials can be tested has not yet been built and it will be a long time before such facility becomes available. Some projects exist, such as INTOR /7/ and the Fusion Engineering Facility, FEF /8/. Before the real material testing fusion reactors will be realized, an interim solution is the use of the accelerator-based neutron sources /2,9/. Three types of high-intensity high-energy neutron sources are possible

1) 14 MeV sources based on the d-t reaction, such as RTNS II at LLL Livermore, with a flux of 10^{13} n/cm^2, or the projected INS which would have used a blanket to create the non-14 MeV energy part present in the first wall neutron spectrum,
2) d-Li sources which have a broad spectrum, peaking at 14 MeV but with a tail up to 40 MeV. The FMIT project at HEDL is of this type;
3) spallation neutron sources which have an evaporation spectrum and a high-energy tail up to 200 - 300 MeV At JRC-Ispra such a materials test facility, EURAC, is proposed.

Except for the 14 MeV sources, the others are simulations; damage results have to be correlated with real fusion spectra. The question arises, how far do these simulations of fusion reactor radiation environments give valid results and valid correlation functions?

2. RADIATION DAMAGE PARAMETERS

During irradiation the source particles interact with the nuclei of the material and transfer a part of their energy to the nuclei. This interaction process results in primary knock-on atoms (PKA's) and transmutation products. The parameters, dependent on the radiation field, which govern the materials behaviour under irradiation, are:

a) the primary knock-on atom spectrum;

b) formation of gaseous transmutation products (He, H);

c) formation of solid transmutation products.

Apart from this direct effect, the radiation field has an indirect influence on other metallurgical and chemical properties, such as phase stability, precipitation, diffusion, etc.

2.1 The primary knock-on atom spectrum

The projectile (neutron or charged particle) interacts with the target nucleus, displacing atoms and producing primary knock-on atoms with a certain energy distribution /10-13/. In Fig. 1 the PKA spectra for the different sources are compared with those of a real fusion blanket (UWMAK-1). The slope of the PKA spectra above an energy of about 400 keV is the same for all sources except for the fission reactor which has no recoils at high energies. There is a different ratio small energy PKA's to high energy PKA's for every spectrum shown. The high energy PKA's give rise to subcascades /14/. For PKA's above 500 keV, the nature of the subcascades does not change and the number of subcascades per PKA saturates.

The differences between the PKA spectra of the high-energy neutron sources proposed will have a small, or even completely negligible, effect on the resulting radiation damage. However, between fission and high-energy neutron sources, the subcascade formation gives rise to different defect loop-sizes and loop-densities /15/ depending on the diffusion and recombination properties of the material.

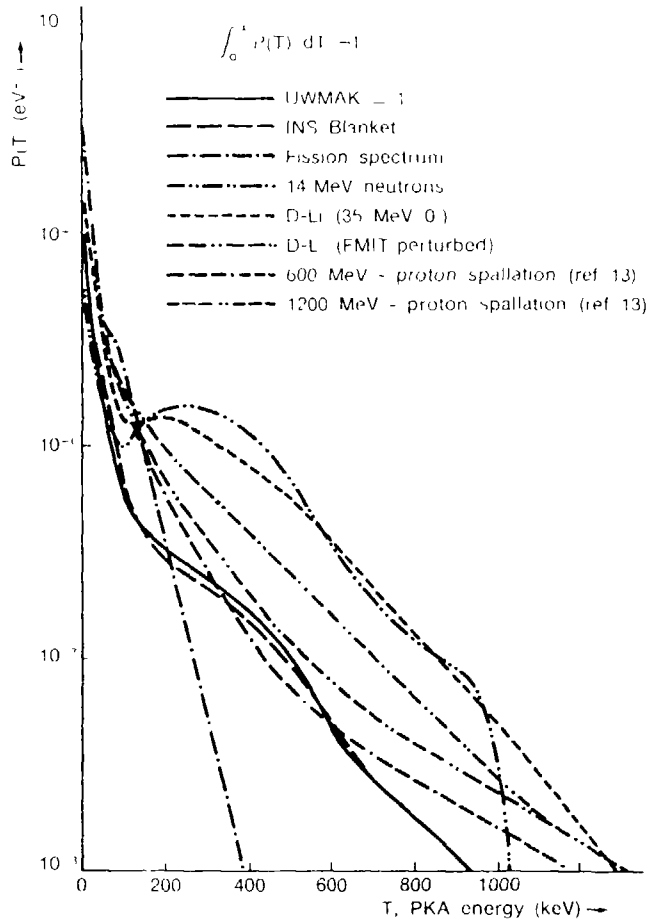

Fig. 1 Normalized primary knock-on atom spectra for iron irradiated in different sources

2.2 Transmutation products

Transmutation products represent a special problem in fusion reactors. The helium production in fusion environments is definitely an important factor. The manner in which helium is formed is found to be very important. The fact that the production of helium occurs at a rate proportional to the damage

production rate seems to be significant. Dual beam experiments at Argonne N.L. (using simultaneous irradiation by self-ions and helium injection) have demonstrated that the damage effects are different to those of pre-injected samples /16,17/.

The high-energy neutrons react with the material atoms according to a series of reactions (n,α), (n,p), (n,nα), (n,np), (n,x), (n,nx), leading to reaction products different from the original material.

The solid transmutation products change the material composition in a different way for different neutron spectra. Some typical examples are: in an ORR (fission reactor) irradiation of pure vanadium, 27% chromium is formed at 100 dpa, but none in a 14 MeV irradiation; at 100 dpa, pure niobium forms 3% zirconium in a 14 MeV irradiation and up to 20% molybdenum in an ORR irradiation. Stainless steel, due to its complex composition, does not change its composition so drastically; nevertheless, it has different compositions depending on the spectrum in which it is irradiated /18/.

Irradiation in a spallation neutron spectrum yields all elements with lower Z /19,13/ in decreasing quantity. In an irradiation of three months and a fluence of $2 \cdot 10^{19}$ n/cm^2 at the beam stop of LAMPF - Los Alamos, the following long-living radioactive transmutation products were measured /20/:

in aluminum	^{22}Na
in iron	^{46}Sc
in titanium	^{42}Ar and ^{46}Sc
in vanadium	^{42}Ar and ^{46}Sc

3. d-t NEUTRON SOURCES

d-t neutron sources with medium intensity /21-23/ exist and are discussed elsewhere at this conference (see section V on 14 MeV neutron sources). The most intense source is the RTNS II (Rotating Target Neutron Source) /24/, which has a flux of 10^{13} n/cm^2.s of 14 MeV neutrons, used for radiation damage studies.

A high-intensity d-t source, INS (Intense Neutron Source), was proposed and studied for several years at LANL, Los Alamos, before being abandoned in favour of FMIT, a d-Li source. Nevertheless, it may be worthwhile to pay attention to this project as it may contain elements for the future development of high-intensity high-energy neutron sources.

The INS facility used a triton beam impinging on a deuterium jet target to produce 14 MeV neutrons. Within the target volume of about 1 cm^3, 10^{15} n/s are produced for a 1 A triton beam /25/. This was originally designed as a supersonic target for a 1 A beam. For a 3 A beam project, a subsonic jet was proposed and tested. By surrounding the 14 MeV point source with a blanket /26/, first wall fusion reactor spectra are obtained.

Preliminary blanket designs were described at a Brookhaven symposium on neutron cross sections from 10 to 40 MeV /27/, and in an LASL report /28/. A typical blanket design and its characteristics are shown in Fig. 2 /29,30/. This standard blanket has a total enclosed volume of 113 cm^3 (of which the effective useable irradiation volume is $\sim$ 75 cm^3) within a contour whose total flux is $2 \cdot 10^{14}$ n/cm^2.s. In this case, the required amount of ^{235}U is 6 kg, and the blanket has a multiplication of $\sim$ 7. By using a primary source strength of $3 \cdot 10^{15}$ n/s, the flux level in the irradiation volume is $2 \cdot 10^{14}$ n/m^2.s. The primary 14 MeV flux, ϕ_{14}, falls off with the square of the radius, whereas the low-energy component, $\phi_{<14}$, is essentially constant within the volume.

The ratio, He production to dpa rate, expected in the tokamak design /31,32/ determines the optimum location for placement of irradiation samples. Fusion reactor first wall spectra are matched from a 1.2 to a 2.8 cm radius from the source, where the dpa rates for iron range from $2 \cdot 10^{-7}$ to $5 \cdot 10^{-7}$ dpa/s (6 to 16 dpa/yr). Inside this volume, the ratio of dpa rate to the helium production rate equals that of the first wall spectrum to ± 20%. The gas target wall in its position nearest to the source will suffer a dpa rate of $1.1 \cdot 10^{-6}$ dpa/s (or 34 dpa/yr). The INS neutron spectrum is a very close match to the calculated first wall spectrum for the tokamak reactor, differing only slightly in the lower keV region. This is due to the nature of the fission blanket, but the differences are not relevant for radiation damage and helium production effects. A preliminary two-dimensional design is shown in Fig. 3.

The other aspects of the INS project (ion source, beam extraction, D_2 jet experiments and beam on target prototype) are fully described together with a complete list of references in the "Intense Neutron Source Facility Progress Reports" of Los Alamos /33/. In 1978 the INS project was abandoned in favour of the d-Li project.

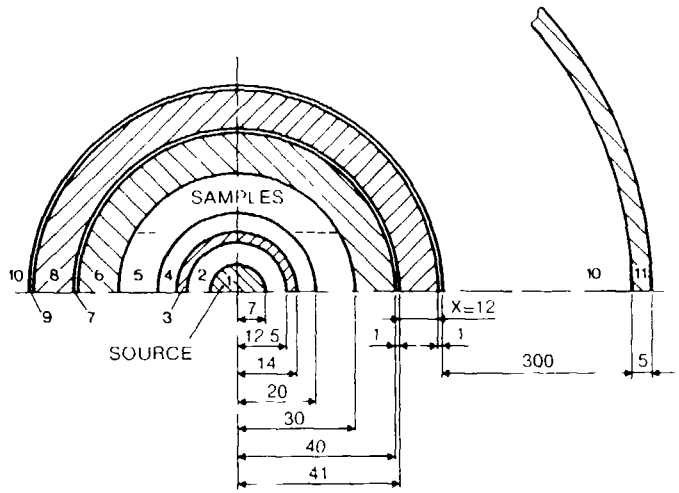

Zone	Material	Outer Diameter (mm)	Thickness (mm)
1	void - source	7.0	7.0
2	void	12.5	5.5
3	Fe	14.0	1.5
4	void	20.0	6.0
5	void (for samples)	30.0	10.0
6	Li	40.0	10.0
7	H_2O	41.0	1.0
8	U^{235}	41.0 + x	x = 12
9	H_2O	42.0 + x	1.0
10	Be	342.0 + x	300.0
11	B_4C	347.0 + x	5.0

Fig. 2 Standard blanket configuration for INS

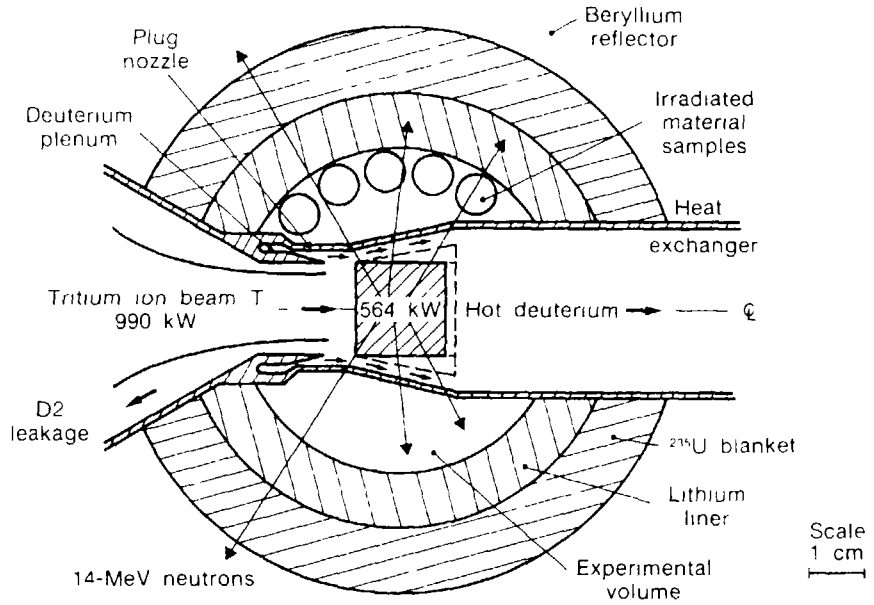

Fig. 3 The supersonic jet target designed for the 3.3-A beam at INS

4. d-Li NEUTRON SOURCES

In this type of sources the neutrons are produced in the stripping reaction of deuterium by lithium. Medium and small intensity d-Be sources /23/ can easily be made available at existing cyclotrons. At these sources, preparative experiments for the high-intensity d-Li source are executed. Neutron yield and neutron energy spectra are measured as functions of the emission angle. They served also for neutron dosimetry development and integral cross-section testing up to 40 MeV neutron energy. Some radiation damage experiments at low fluences are executed at such sources /15/.

Different projects were presented for a high-intensity d-Li neutron source by BNL /34/, by ORNL /35/ and by HEDL /36,37/.

The Fusion Materials Irradiation Test Facility, FMIT, at HEDL is based on a 100 mA, 35 MeV deuteron linear accelerator. The deuteron beam impinges on a liquid lithium target (Fig. 4). The neutrons are stripped from the beam and give rise to a narrow peaked neutron emission.

The neutron spectrum has a broad distribution (up to 40 MeV) with a maximum at about 14 MeV at 0^{o} emission angle (depending on the deuteron energy). The maximum flux is $1.4 \cdot 10^{15}$ n/cm^{2}s or 83 dpa/y in a volume of 10 cc and $5 \cdot 10^{14}$ n/cm^{2}s or 33 dpa/y in a volume of 100 cc /37/. The He to dpa ratio of 10 appm/dpa is about the same as the predicted values for the tokamak /31,32/, INTOR /38/ and UWMAK-I /39/ projects. The flux has steep gradients which make dosimetry of the radiation damage experiments a challenge /40/. The neutron flux in the irradiation positions and the effect of the material inside it have been the object of intense studies /41/. At JRC-Ispra a centrifuge Li target was proposed permitting the use of deuteron beam of a few MW/cm^2 /42/. For that purpose the interaction of a 50 MeV deuterons with lithium was investigated /43/. In 1985 the FMIT project was suspended.

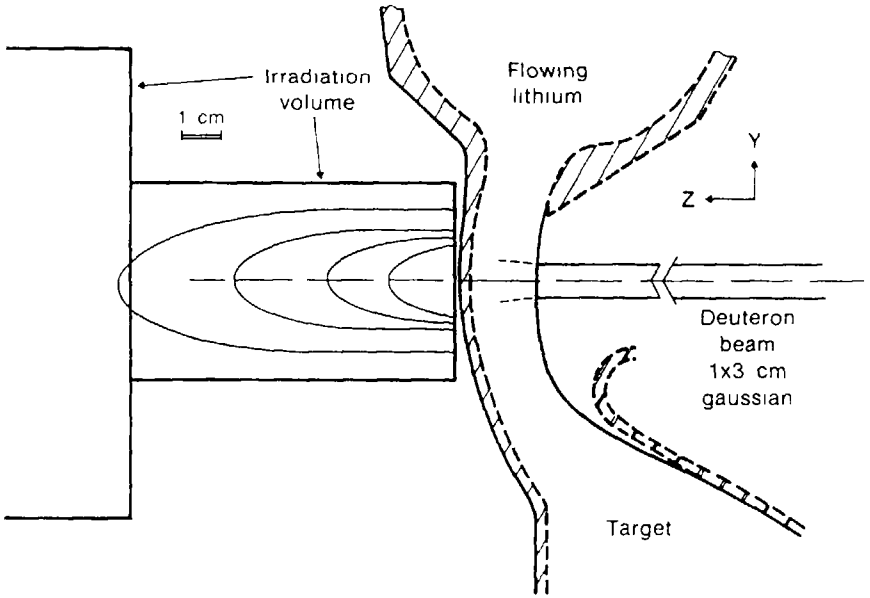

Fig. 4 Beam/target and test module interface for FMIT (ref 37)

5. SPALLATION NEUTRON SOURCES

The use of a spallation neutron source was already proposed in 1974 /44/. Different high-intensity spallation sources have been constructed and are in operation, but only as a source for thermal and cold neutrons for basic physics studies. A few medium-intensity spallation sources are constructed such that radiation experiments are possible.

The new beam stop area /45/ of LAMPF - Los Alamos, permits radiation damage experiments in a maximum flux of $3 \cdot 10^{13}$ n/cm^{2}s for an operation current of 0.5 mA with a proton contamination between 1% and 10%. Calculations and experiments /46/ show that the high-energy tail of the neutron spectrum, unique to spallation radiation damage environments, make significant contributions to displacements and He production rates. The He to dpa ratio is slightly higher than in a physical first wall neutron spectrum. The Intense Pulsed Neutron Source (IPNS) at ANL, although with a lower flux than LAMPF, is also used for radiation damage studies /47/.

At EIR (Switzerland) a study was made to build a spallation neutron source SINQ with a flux (E > 1.0 MeV) of about $2 \cdot 10^{13}$ n/cm^{2}s /46,48/ using a liquid Pb target. It was concluded that it is far more effective to use the direct proton beam than to use the secondary spallation neutrons to produce helium and displacement damage effects.

At JRC-Ispra, an intense neutron spallation source, EURAC /49/, with a flux of about $2 \cdot 10^{16}$ n/cm^{2}s or 320 dpa/y in a volume of 20 cm^3 with a He to dpa ratio between 6 and 13 is proposed. It has a liquid lead spallation neutron target and a ^{235}U booster surrounding the thermal and cold neutron sources. The lead target and the ^{235}U booster are to be optimized in order to get optimal conditions for radiation damage experiments, simulating fusion first wall radiation environments.

6. CONCLUSION

In Table I, the three possible types of high intense neutron sources are compared.

Only the INS blanket gives a real radiation environment of a fusion reactor. It is indeed a hybrid system: driven d-t fusion, uranium boostered. The maximum flux obtainable is lower than for the other two systems, but in the irradiation volume, the flux is nearly constant.

	(INS BLANKET)	d Li (FMIT)	Spallation (LAMPF)	(EURAC)
status	abandoned project studied	suspended project studied	operating	proposal
obtainable fluxes in volume (n/cm² s)	2 10^{14} in 100 cm^3	1 5 10^{5} in 10 cm 5 10^{14} in 100 cm^3	− 3 10 (maximum)	2 10^{16} in 20 cm^3
dpa/y	6 in 100 cm^3	83 in 10 cm^3 39 in 100 cm^3	0 6	320 in 20 cm^3
He/dpa	10 ± 0 2	10	18	6 < < 13
spectrum	exact first wall	broad up to 40 MeV maximum at 14 MeV	evaporation spectrum + tail up to 200 (800) MeV	
PKA spectrum	exact first wall	more high energy recoils and recoils with E > 1MeV		
Trasmutation products	exact first wall	slightly different	largely different	
cross section needs	± known	needed up to 40 MeV not available	needed up to 200 (800 MeV) not available	
dosimetry	feasable	feasable	to be developped	
remarks	—	—	proton contanation	
Technological difficulties	high beam current (3 A) gas target	high current high voltage accelerator (100 mA 50 MeV) liquid Li target	liquid metal (lead) target	

TABLE I : Comparison of different source types

d-Li and spallation neutron sources simulate the fusion radiation environment. Their neutron spectra lead to slightly different PKA spectra which, however, have little or no influence on the damage production, but with creation of different solid transmutation products in different quantities.

The need for cross section data is very severe. Dosimetry for the d-Li spectra is already fairly well developed, but more research and development is necessary for the monitoring of spallation neutron spectra and fluence measurements. The effect of the proton contamination for radiation damage experiments is unknown and has to be studied.

Construction of a spallation neutron source has the advantage of being relatively cheap if the accelerator is built and used for other purposes. d-Li and spallation sources have the potential of making high fluxes and high dpa production per year available, but with steep gradients in the irradiation volume. Special requirements on the metallurgical samples may have to be met.

Radiation damage data obtained in d-Li and spallation neutron sources have to be compared and correlated with data obtained in 14 MeV neutron sources. The scientist has to make sure that they are useful for fusion radiation environments.

REFERENCES

1. F.A. Garner et al., "The microstructural and microchemical origins of irradiation creep in 316 stainless steel", Int. Conf. on Fundamental Mechanisms of Radiation Creep and Growth, Chalk River, 8 - 10 May, 1979.
2. R. Dierckx, "Radiation damage in fission and fusion reactors", IAEA-TECDOC-263, p.11, 1982.
3. R.L. Simons, "Correlation of macroscopic material properties with microscopic nuclear data", IAEA-TECDOC-263, p.241, 1982.
4. R. Gold, E.P. Lippencott, W.N. McElroy and R.L. Simons, "Radiation damage function analysis", in Effects of Radiation on Structural Materials, STP.683, p.380, 1979.
5. D.R. Harries and J.M. Dupouy, "Materials irradiation testing in support of the European fusion programme", in Reactor Dosimetry, Vol.4, p.263, 1984.
6. T.C. Reuther, "Fusion materials research and neutron activation", in Reactor Dosimetry, Vol.4, p.195, 1984.
7. INTOR Phase I report, IAEA, Vienna (1982).

8. H Ida, H. Nakaolima, Y. Kanda and M. Ohta, "Material testing capability of the fusion engineering facility, FEF", J. Nucl. Mat. 133 & 134, p.887, 1985.

9. R. Dierckx, "Neutron sources for the fusion materials radiation damage programme", EUR 6813 EN-FR, Vol.I, p.53 (1980).

10. D. Parkin and A. Goland, "A computational method for the evaluation of radiation effects produced by CTR related neutron spectra", BNL 50434 (1974).

11. A. Goland, "Experimental evaluation of the primary damage process, neutron energy effects", BNL-25807.

12. R. Dierckx and C.R. Emigh, "Characterization for fusion first wall damage studies of using tailored D-T neutron fields", 3rd ASTM Euratom Symposium on Reactor Sodimetry, Ispra, October 1979, EUR 6813, Vol.I, p.230.

13. F. Alchison, W.E. Fischer and M. Pepin, Final report of contract 2007-82-ED-ISP-CH (1985).

14. R. Dierckx, "The importance of the PKA spectram for radiation damage simulation", to be published, 1985.

15. J. Narayan and S.M. Ohr, "The nature of high energy neutron damage in copper and gold", 1st Top. Meet. on Fusion Reactor Materials, Miami Beach, Florida, USA, 1979.

16. F.V. Nolfi Jr., Argonne National Laboratory, private communication.

17. K. Miyahara, N.H. Packan and N. Igata , "The effect of pulse irradiation on void swelling of a "pure" 316 stainless steel", in Effects of Radiation on Materials, STP 782, p.241, 1982.

18. M.W. Guinan, LLL Laboratories, private communications.

19. M. Mattes, G. Prillinger, "Transformation of iron cross sections up to 40 MeV", IKE 6-EUR 10 (1985).

20. R. Dierckx, V. Sangiust, M. Terrani, "Dosimetry in a spallation neutron spectrum", to be published (1985).

21. Proc. of the XIV Int. Symp. on the Interaction of Fast Neutrons with Nuclei, Neutron Generators and Application, November 19-23, 1984, Gaussig (GDR).

22. U. Jahn, E. Paffrath, D. Schmidt, D. Seeliger, "Intensive neutronengeneratoren auf der Basis von der D-T Reaktion", Kernenergie 28 (1985) 11-12, p.433.

23. Proc. of IAEA Consultants'Meeting on Neutron Source Properties, Debrecen, Hungary, 17-21 March 1980, INDC(NDS)-114/GT.

24. D.W. Heikkinen, C.M. Logan, "Recent progress at RTNS II", Nucl. Inst. & Meth., Phys. Res. Sect. B, Vol.B10-11, Vol.2, p.835 (1985).

25. D.D. Armstrong, C.R. Emigh, K.L. Meyer, E.A. Meyer and J.D. Schneider, "A 14 MeV intense neutron source facility", Nucl. Inst. & Meth., 145, p.127 (1977).

26. M.E. Battat, R. Dierckx and C.R. Emigh, "Feasibility study to produce first wall fusion reactor spectra around a 14 MeV neutron point source", Nucl. Techn. 43, p.338 (1979).

27. M. Battat, R. Dierckx and C.R. Emigh, "Neutron spectra characteristics for the intense neutron source, INS", Symp. on Neutron Cross Sections from 10 - 40 MeV, Brookhaven National Laboratory, May 3-5, 1977.

28. "Intense neutron source facility progress report, January 1 - March 31, 1977", LA-6784-PR. Los Alamos Scientific Laboratory (1977).

29. R. Dierckx and C.R. Emigh, "Application of the INS facility as a high-flux benchmark for neutron dosimetry and for radiation damage studies in a D-T fusion spectrum", ASTM/Eurator Symp. on Reactor Dosimetry, Palo Alto, California (USA), October 2-7, 1977.

30. "Intense neutron source facility progress report, April 1 - June 30, 1977", LA-6910-PR, Los Alamos Scientific Laboratory (1977).

31. Don Steiner, "The technological requirements for power by fusion", Nucl. Sci. Eng., 58, 107 (1975).

32. "Fintor 1 - a minimum size tokamak DT experimental reactor", CEC-JRC Euratom, Ispra (1976).

33. - LA-7267-PR and LA-7473-PR, "Intense neutron source facility", progress report for the periods January - March 1978 and April - June 1978.
- A.N. Demuth, Joel Robinson, J.C. Schneider, "DAISY, a data acquisition and IO control system", presented at the CUBE Symposium held at the Los Alamos Scientific Laboratory, October 1978.
- R. Dierckx, C.R. Emigh, D. Parkin, "Correlation of radiation damage results in different neutron spectra", presented at ASTM 9th Int. Symp. on Effects of Radiation on Structural Materials in Richland, Washington, July 10-14, 1978.
- J.C. Hyde, M.C. Cline, G. Hefer, "Gas dynamics studies of an intense neutron source for fusion reactor materials testing", presented at the AIAA 11th Fluid and Plasma Dynamics Conference, in Seattle, Washington, July 10-12, 1978.
- K.L. Meier, "The experimental area and remote handling facilities of the jet target intense neutron source", presented at the 3rd Top. Meet. on the Technology of Controlled Nuclear Fusion, Santa Fe, New Mexico, May 9-11, 1978.
- D.D. Armstrong and C.R. Emigh, "Multi-species beam transport by RMS statistics", Space Charge in Linear Accelerators Workshop Conference Proc., Los Alamos Scientific Laboratory report LA-7265-C, May 1978, p.116.

34. P. Grant, "Accelerator based neutron generator", BNL 20159 (July 1975), BNL 20840 (January 1976), Nucl. Tech. 29, p.327 (June 1976).

35. M.J. Saltmarsh and R.E. Worsham, "INGRID - an intense neutron generator for radiation-induced damage studies in the CTR material program", ORNL-TM-5233, Oak Ridge National Laboratory, Oak Ridge, TN (Jan. 1976).

36. E.W. Pottmeyer Jr., "The fusion materials irradiated test facility at Hanford", HEDL-SA-1734 (Feb. 1979).

37. E.K. Opperman, "FMIT - experimental capabilities and test matrix", HEDL-TME 81-45, UC-20, January 1982.

38. W.M. Stacey Jr. et al., "US contribution to the international tokamak reactor, phase I report", US INTOR report, INTOR 181-1, Georgia Institute of Technology, Atlanta, GA, 1981.

39. G.L. Kulcinski, director, UWMAK-1 a Wisconsin toroidol fusion reactor design, UWFDM-68, Univ. of Wisconsin, March 1974.

40. R. Gold, W. McElroy, J.L. Fuller, E.M. Steen (HEDL) and R. Dierckx (JRC Ispra), "Dosimetry program for the characterization of the FMIT facility", EUR 6813 EN-FR, p.239 (1980).

41. - R.E. Nygren, "Considerations on experiments in FMIT", 8th Symp. on Engineering Problems in Fusion Research, San Francisco, CA, November 13-16, 1979.
- F.M. Mann, F. Schmittroth, L.L. Carter, "Neutron environment in d+Li facilities", Symp. on Neutron Cross Sections from 10 to 50 MeV, BNL-NCS-51245, p.517, Battelle Northwest, Seattle, WA, 1980.
- J. Schiffgens, R.L. Simons, F.M. Mann, L.L. Carter, "Spatial variations of damage parameters in FMIT and their implications", J. of Nucl. Mat. 85-86, p.491, 1979.
- D.L. Johnson, F.M. Mann, J.W. Watson, J. Ullman and W.G. Wyckoff, "Neutron spectra from 35 MeV deuterons on thick lithium for the FMIT facility", 3rd Int. ASTM-Euratom Symp. on Reactor Dosimetry, Ispra (Va), Italy, October 1-5, 1979.
- J.O. Schiffgens, R.L. Simons, F.M. Mann and L.L. Carter, "FMIT damage parameter sensitivity study", Damage Analysis and Fundamental Studies Quarterly Progress Report January - March 1979, DOE/ET-0065/5, May 1979.
- L.L. Carter, "Neutron environment in the fusion materials irradiation test facility", 3rd Int. ASTM-Euratom Symp. on Reactor Dosimetry, Ispra (Va), Italy, October 1-5, 1979.

42. R.F. Palinsky and W. Kley, JRC-Ispra, Italy, private communications.

43. R. Dierckx, W. Kley, A. Verga, E.V. Benton and J. Buschmann, "The stopping of deuterons in lithium", Nucl. Eng. and Design/Fusion 2 (1985) 337-354.

44. Don M. Parkin and Allen N. Goland, "Calculation of radiation effects as a function of incident neutron spectrum", BNL-report, BNL-50434 (1974) and in Radiation Effects, 1976, Vol.28, pp.31-42.

45. - D. Davidson, W.F. Sommer, J.N. Bradbury, D.E. Prael and R.C. Little, "Characterization of the radiation environment at a new proposed irradiation facility at LAMPF", J. Nucl. Mat., Vol.123, 1984, pp.989-994;

Report LA-UR-83-33, Los Alamos National Laboratory, Los Alamos, NM 87545.
- D.R. Davidson, L.R. Greenwood, R.C. Reedy and W.F. Sommer, "Measured radiation environment at the LAMPF irradiation facility", STP 870, p.1199 (1985), Report LA-UR-84-1050, Los Alamos National Laboratory, Los Alamos, NM 87545.
- M.S. Wechsler and W.F. Sommer, "Spallation radiation damage and the radiation damage facility at the LAMPF A-6 target station", J. Nucl. Mat., Vol.123, 1984, p.1078.
- M.S. Wechsler, D.R. Davidson, L.R. Greenwood and W.F. Sommer, "Calculation of displacement and helium production at the LAMPF irradiation facility", in Effects of Radiation on Materials, STP 870, p.1189 (1985), see also: Report LA-UR-84-1124, Los Alamos National Laboratory, Los Alamos, NM 87545.

46. F. Hegedus, W.V. Green, P. Stiller, S. Green, V. Hernberger, U. Steefel, M. Victoria, "The strength of the spallation neutron flux of SINQ for radiation damage fusion technology", EIR Bericht No.579 (Dec. 1985).

47. L.R. Greenhurst and R.K. Smither, "Recent developments in neutron dosimetry and damage calculations for fusion materials irradiations", in Reactor Dosimetry, Vol.I, p.251 (1985).

48. W.E. Fischer, W. Joho, Ch. Tschalar, B. Sigg and H. Rauch, "Studie über eine Kontinuierliche Spallations Neutronenquelle am SIN", Dec. 1978, 200 Dok. int.

49. W. Kley and G.R. Bishop, "EURAC the JRC-Ispra fusion reactor materials test and development facility", EUR 10337 EN (November 1985).

NEUTRON DETECTOR CALIBRATION USING ASSOCIATED PARTICLE METHOD

G MOSCHINI*, L CHENDI, R CHERUBINI, F JIMENEZ**,
R NINO, R POLICRONIADES**, B M STIEVANO, A VARELA**,
G GALEAZZI*, C MANDUCHI*, M T RUSSO MANDUCHI*,
G F SEGATO*
INFN, Laboratori Nazionali di Legnaro,
Legnaro, Padua,
Italy

Abstract

The Associated Particle Technique (A.P.T.) has been used with neutrons from the $D(d,n)^3He$ and $T(d,n)^4He$ reactions to the absolute neutron detection efficiency of an 1.27 x 3.81 cm^2 Stilbene scintillator as function of the light collection threshold and the neutron kinetic energy in the energy range 2-18 MeV
Thin Ti-T and home made deuterated polyethylene targets have been used. The A.P.T. chamber description, the measurements and the comparison with both analytical and Montecarlo (SAN-REMO code) calculations are reported.

1. - INTRODUCTION

The request for reliable nuclear data [1], in particular for neutron cross section measurements from 5 to 14 MeV, is still open, and has nowadays been enhanced with the need of precise fast neutron data for fusion reactor development. Moreover, there is a need for calibrated neutron detectors for making they possible neutron cross section measurement.

* And Dipartimento di Fisica ' Galileo Galilei'', University of Padua, Padua, Italy
** On leave from Instituto Nacional de Investigaciones Nucleares, Mexico, and IAEA Fellows

In order to respond to these needs, at the 7 MV Van de Graaff accelerator of the I.N.F.N. - Laboratori Nazionali di Legnaro (L.N.L.) it was built-up a multipurpose scattering chamber (50 cm inner diameter, 24.2 cm long. See figures 1 and 2) adequate for fast neutron spectroscopy with Associated Particle Technique (A.P.T.) [2], used with thin Ti-T and home made deuterated polyetylene targets (20-350 μgr/cm^2 thick).

As well known [3,4] the A.P.T. with the d-D and d-T reactions provides a simple method for producing monoenergetic neutrons of accurately determined flux in a wide energy range.

In this work we present the tests of the A.P.T. facility, the measurement of the absolute detection efficiency of a Stilbene scintillator (3.81 cm in diameter, 1.27 cm thick) and the comparison with analytical and Montecarlo calculations.

2. - SCATTERING CHAMBER

An overall view of the vacuum chamber, based on a design developed in the L.N.L., is presented in Figure 1.
The basic components, illustrated in the figure, are:

1. External cilindrical body with interchangeable 137° large thin window;
2. Rotating target assembly suitable for self-supporting deuterated polyethylene and thin Tritium-Titanium targets;
3. Charged particle detector table;
4. Beam collimator system;
5. External scattering table with slidding neutron detector mounting;
6. Automatic vacuum system.

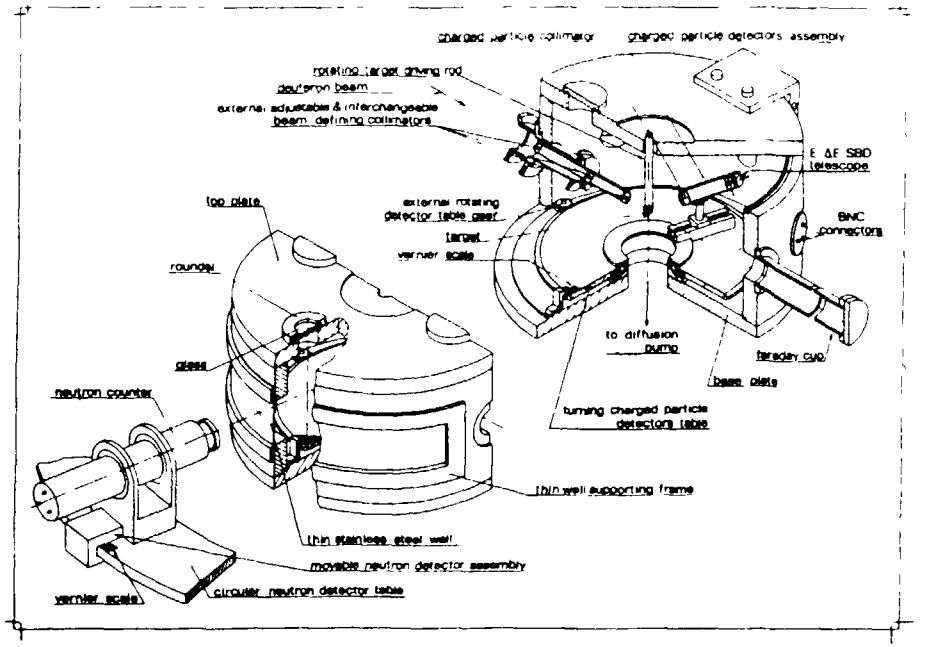

Fig. 1 - Vacuum Scattering Chamber Schematics.

2.1 Rotating Target Assembly

Since polyethylene is a low temperature burning material, a rotating target assembly is a convenient solution to avoid fast deterioration.

Figure 2 shows a schematic drawing of the rotating target assembly, illustrating how a two-dimentional motion (perpendicular to the beam) is achieved with a flexible bellow.

An electric motor (not shown in Fig. 2) transmits (a) a tilting and (b) an up and down movement to the cover flange of the air tight bellow vessel. This then originates a horizontal and up and down movement of the target frame, attached to this flange through a long driving metal rod. A proper choice of the frequencies ω_1 and ω_2, and the amplitudes of each these components of motion, permits a uniform and long lifetime use of the targets.

The movement imposed by our arrangement permits an adjustable rectangular scan of the beam over the target.

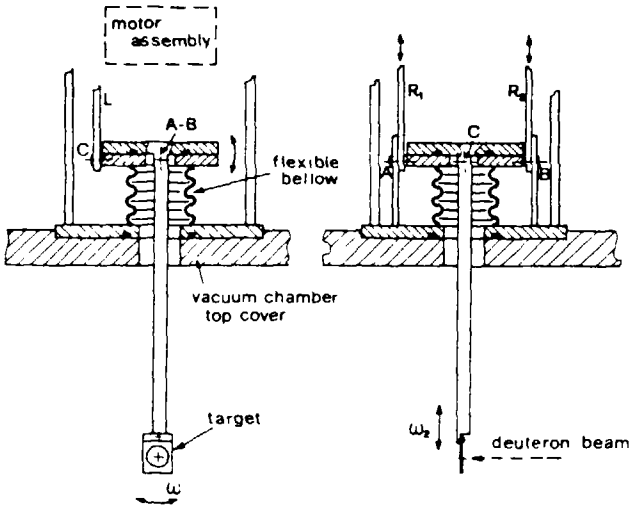

Fig. 2 - Rotating Target Assembly Schematics.

3. - PRELIMINARY TESTS AND PERFORMANCES OF THE A.P.T. SCATTERING CHAMBERS

Once the chamber parts were cleaned and assembled, and the whole apparatus was aligned in the +30° beam line of the Van de Graaff 7 MV CN Accelerator, the vacuum tests reported a final 2 x 10^{-6} Torr pressure normally achieved after 30 minutes.

To study the performance of the A.P.T. facility, preliminary measurements were performed in the neutron energy range 2÷18 MeV using both d-D and d-T reactions.

For a given neutron energy, the neutron profile and the time resolution of the system depend on various kinematical and geometrical parameters concerning the deuteron beam's energy and spot, the targets thickness and composition, and the charged particle's solid angle characteristics.

The following experimental conditions for the tests were set according to the compromise which arises between a good time resolution and a high neutron counting rate.

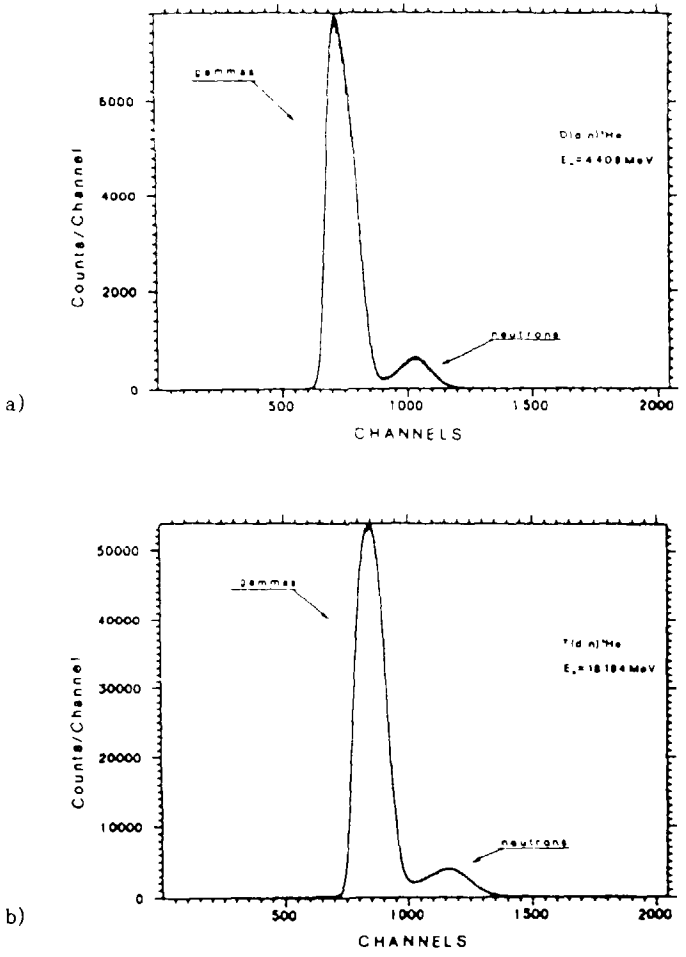

Fig. 3 - Neutron-Gamma Spectra taken with a typical electronic arrangement and the 3.81 cm x 1.27 cm Stilbene detector using a) the $D(d,n)^3He$ reaction for E_d=5.5 MeV, E_n=4.409 MeV and θ_n=80.20°; b) the $T(d,n)^4He$ reaction for E_d=6.0 MeV, E_n=18.194 MeV and θ_n=72.47°. The figures of merit obtained were F_1=1.29 and F_2=1.17, respectively.

In order to obtain a 2 mm diameter deuteron beam spot over the target we used a three circular slit arrangement with the following diameters: 3 mm entrance one, 1.8 mm middle one and 2.5 mm exit one; which ones in proper alignment allows us to obtain 500 nA current on the Faraday cup extension.

The charged particle "ΔE" detector, chosen in agreement with the ^3He (^4He) range, and located at 18 cm from the target, was provided with a pair of limiting circular slits of 1.6 cm (entrance) and 2.2 mm diameters, 3.5 cm apart from each other, in order to have a neutron cone contained in the 3.81 cm diameter (1.27 cm long) Stilbene spectrometer.

Figures 3-a) and 3-b) illustrates the pulse shape discrimination spectra (n-γ) take with a typical electronic arrangement and the Stilbene detector using the $D(d,n)^3He$ reaction for E_d=5.5 MeV , E_n=4.409 MeV and θ_n=80.20° and using the $T(d,n)^4He$ reaction for E_d=6.0 MeV, E_n=18.194 MeV and θ_n=72.47°. The figures of merit obtained were F_1-1.29 and F_2-1.17, respectively.

In Figure 4 a time-of-flight (ToF) spectrum is shown, which illustrates the time correlation between the neutrons and the associated ^3He's, as obtained from the fast Stilbene (stop) pulses using a time-to-amplitude-converter for a $D(d,n)^3He$ reaction with E_d=4.0 MeV, $E(^3He)$=3.154 MeV, E_n=4.115 MeV and θ_n=76.49°. The FWHM was 2 nsec.

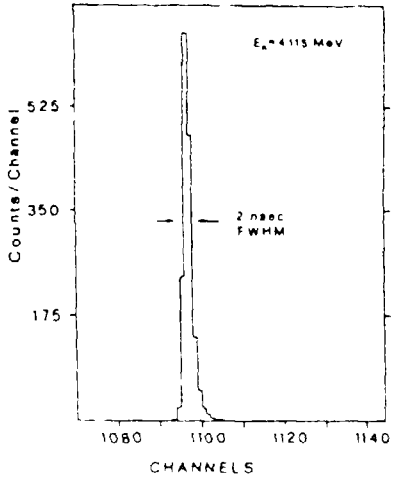

Fig. 4 - Tof Spectrum obtained using the $D(d,n)^3He$ reaction for E_d=4.0 MeV, $E(^3He)$=3.154 MeV, E_n=4.115 MeV and θ_n=76.49°. The FWHM obtained was 2.0 nsec.

Figure 5 shows a vertical and horizontal measurement of the neutron profiles taken from a $D(d,n)^3He$ reaction for E_n=2.41 MeV, (E_d=2.0 MeV). The profiles are taken at a distance of 30.6 cm from the target, and the vertical scales give a relative measure of the ToF to ^3He counts.

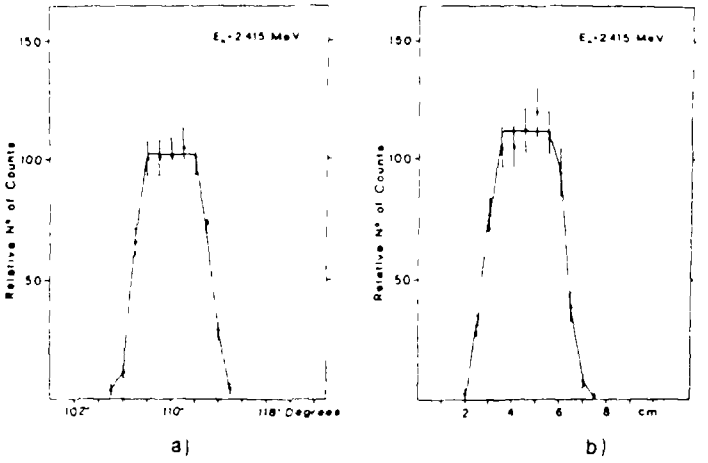

Fig. 5 - a) Horizontal and b) Vertical profiles taken from the $D(d,n)^3He$ reaction for E_n=2.415 MeV (E_d=2.0 MeV) with the detector at 30.6 cm from the target.

Figure 6 shows typical ^3He yields obtained for 119 and 151 μgr/cm^2 deuterated polyethylene home made target, with carbon baking (18 and 19 μgr/cm^2).

4. - CALIBRATION OF A STILBENE SCINTILLATOR IN THE ENERGY RANGE 2-18 MeV WITH THE A.P.T.

The chamber previously described was used by some of us for the measurement of the absolute detection efficiency of the 3.81 x 1.27 cm^2 Stilbene detector as function of the light collection threshold (bias level) and the neutron kinetic energy in the range 2÷18 MeV.

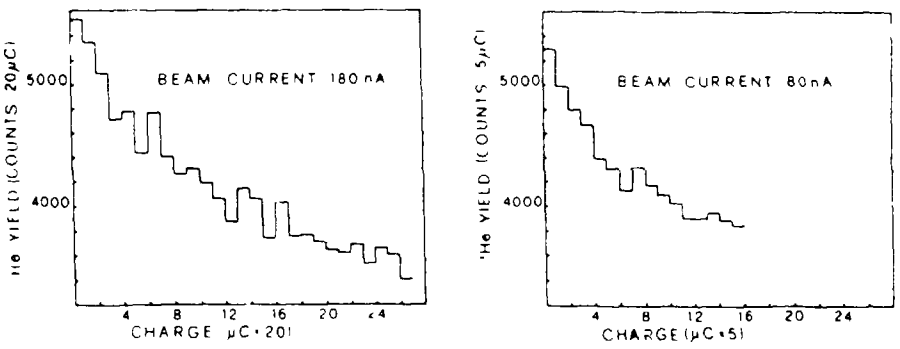

Fig. 6 - Typical ^{3}He yields obtained for 119 and 151 ugr cm^2 deuterated polyethylene home made targets with carbon baking (18 and 19 ugr/cm^2).

For each measurement the energy spectrum of the charged particles, the n-γ spectrum, the He-n time distribution (ToF spectrum) and the neutron energy spectrum were recorded.

The bias level, B, was determined experimentally. For this purpose gamma calibration measurements in term of the electron energy of the Compton edge were performed in an accurate separate experiment (4).

The Figures 7-11 summarize some results of such absolute detection efficiency measurement

Figure 7 shows the electronic used for the Stilbene neutron detection efficiency calibration using the Associated Particle Technique with the d-D and d-T reactions.

The kinematic and geometric conditions chosen for the monoenergetic neutron production in the energy range 2-18 MeV are summarized in Table I. The distances between the target and the SSBD and Stilbene detectors were 13 cm and 30.6 cm, respectively.

For the d-D reaction were used thin home made deuterated polyethylene targets (20÷350 μgr/cm^2). For d-T reaction was used a thin Ti-T target (Nukem, Germany).

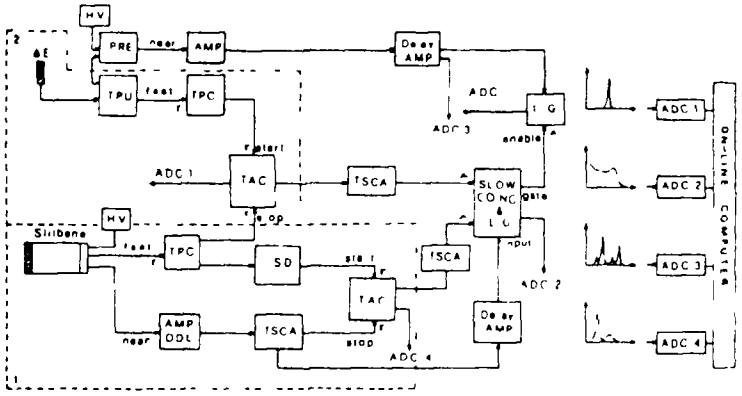

PRE: Preamplifier ORTEC 109A

- TPU Time Pickoff Unit ORTEC 260
- TPC: Time pickoff Control ORTEC 403A
- AMP: Amplifier ORTEC 485

AMP DDL Double Delay Line Amplifier ORTEC 460

Delay AMP Delay Amplifier ORTEC 427A

LSD Logic Shaper and Delay CAMBERRA 2055

TSCA: Timing Single Channel Analyser ORTEC 551

TAC Time To Pulse Height Converter ORTEC 457 e 437A

SLOW COINC & L G : Slow Coincidence and Linear gate ORTEC 409

- L G : Linear Gate ORTEC 426

ADC Analog To Digital Converter

Fig. 7 - Electronics for the Associated Particle Technique used for the absolute detection efficiency of a Stilbene detector in the energy range 2-18 MeV.

In Figure 8 it is shown a typical charged particles energy spectrum obtained with a "Totally Depleted" S.S.B.D. (27.5 μm thick). The spectrum was taken for E_d=5.5 MeV, $E(^3He)$=6.602 MeV, $\theta(^3He)$=50°.

TABLE I

REACTION	Ed(MeV)	En(MeV)	ϑ_n	$E_{^3He}$ (MeV)	$\vartheta_{^3He}$
	2.0	2 4.5	110 00°	2 854	30°
	4.0	3 35	97 08°	4 134	30°
D(d,n ^{3}He	4.0	4 115	76 50°	3 154	40°
	5.5	4 409	80 20°	4 360	35°
	5.5	6 702	49 26°	2 167	50°
	4.0	14 .75	109 50°	7 414	41°
T(d,n)^{4}He	4.0	16 40	80 14°	5 188	62°
	6.0	18 194	72 47°	5.396	62°

Kinematic and geometric conditions for neutron production with the d-D and d-T reactions.

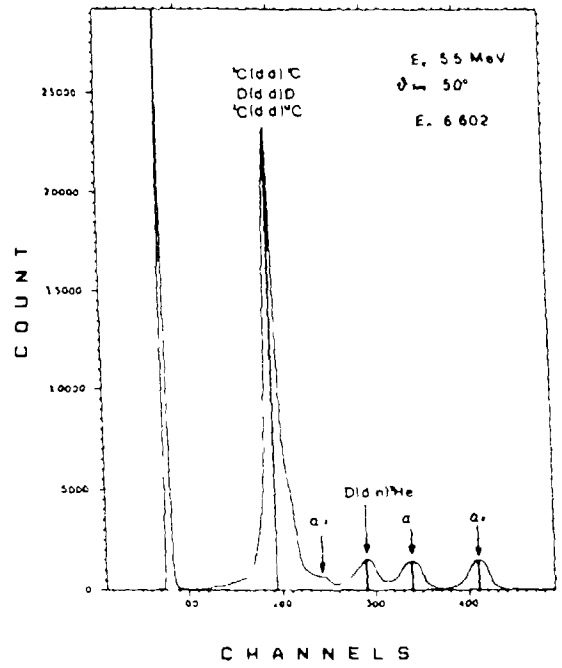

***Fig. 8** - Typical charged particles energy spectrum detected with the "totally depleted" Silicon Surface Barrier detector (27.5 μm thick).*

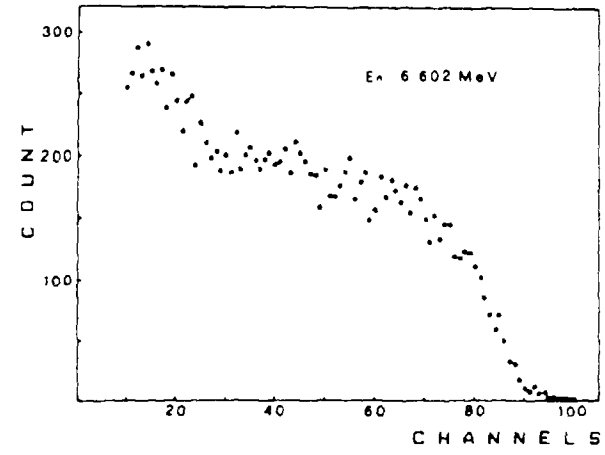

Fig. 9 - Typical linear neutron spectrum.

Figure 9 shows a typical linear neutron spectrum (for E_n=6.602 MeV) obtained with the Stilbene detector.

The experimental response of the Stilbene to electrons and protons is shown in Figure 10. The curves are our data best fits.

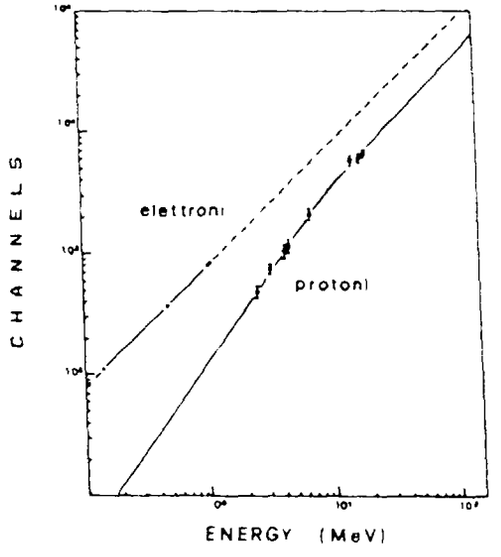

Fig. 10 - *Experimental response of the Stilbene to electrons and protons. The curves are our data best fits.*

The experimental efficiency values obtained in the conditions described above are reported in Table II with an accuracy of about ± 2%.

Our data are compared with the values calculated with both analytical expressions [4,6] and the Montecarlo code SANREMO of Anghinolfi et al. [7]. The computer code, originally written for liquid and plastic organic scintillator, has been modified to be compatible with the characteristics of our Stilbene detector. The main modifications are: (i) physical costant; (ii) use of our experimental proton light response function; (iii) use of alpha and heavy ions light response functions of Nakayama et al. [8], (iv) use of proton light response data of Craun et al. [9].

The experimental and calculated detection efficiencies, for bias level B=124 KeV, are shown in Figure 11

TABLE II

BIAS MeVee	En (MeV)	EFFICIENCY (%)	ERROR %
.08	2.413	10.93	23
	3.135	10.68	22
	4.115	9.84	21
	4.409	9.62	.20
.09	2.415	8.58	18
	3.135	9.28	19
	4.115	8.68	18
	6.602	8.[illegible]	[illegible]
.12	3.135	7.27	15
	4.115	7.49	.15
	4.409	8.22	.17
	6.602	6.61	.14
	14.175	4.[illegible]	19
	16.400	3.56	..4
	18.194	3.46	16
.17	4.115	6.80	14
	4.409	7.54	.16
	6.602	6.46	13
.21	4.[illegible]	5.[illegible]	12
	4.409	7.[illegible]	.15
	6.602	6.[illegible]	17
	14.175	3.[illegible]	15
	16.400	5.41	14
	18.194	3.[illegible]	15

Experimental efficiency values in the neutron energy range 2-18 MeV for a [illegible] Stilbene detector.

The results indicate that the measured efficiencies are reproduced rather well by the computer code calculations and the code could be used for the evaluation of the efficiency of our detector over the energy range 2-20 MeV with an accuracy of about 5-20%. It should be noted that the difference between the experimental and calculated values in the low neutron energy region is mainly due to the uncertainty in the determination of the threshold value affects strongly the efficiency calculations especially in the low energy region.

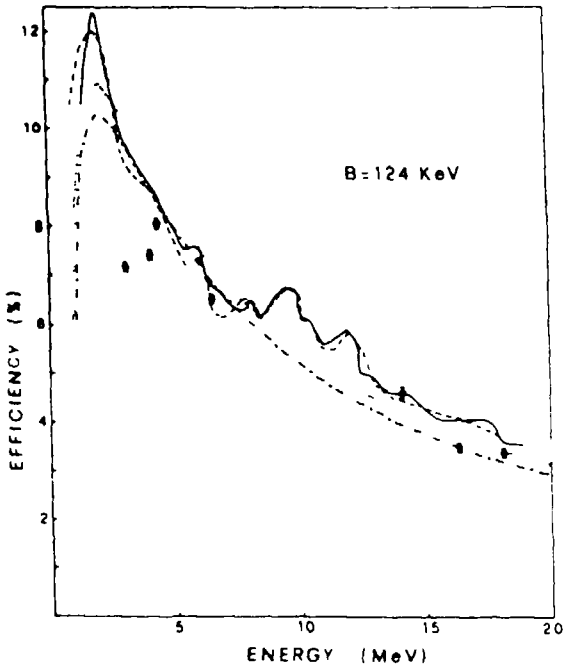

Fig. 11 - Calculated and measured efficiency in energy range 2÷18 MeV with an energy threshold of 124 KeV.
·-·- Drosg Formula (6)
···· J.L Fowler (4)
——— Sanremo Montecarlo Code (7) with our proton light response data
---- Sanremo Montecarlo Code (7) with proton light response of Craun (9).

REFERENCES

(1) CINDA 85, IAEA, Vienna (1985)
WRENDA 83/84, IAEA, Vienna (1983), INDC (SEC) 88/URSF

(2) R. CHERUBINI et al., Report INFN/TC 85/23 (1985)
Laboratori Nazionali di Legnaro (Padova), Italy

(3) H.H. BARSCHALL et al., Rev. Mod. Phys. 24 (1952) 1

(4) J.L. FOWLER et al., Nucl. Instr. and Meth., 175 (1980) 449

(5) R. CHERUBINI et al., to be published

(6) M. DROSG et al., Nucl. Instr. and Meth., 105 (1972) 573

(7) M. ANGHINOLFI et al., Nucl. Instr. and Meth., 165 (1979) 217

(8) K. NAKAYAMA et al., Nucl. Instr. and Meth., 190 (1981) 555

(9) R.L. CRAUN et al., Nucl. Instr. and Meth., 80 (1970) 239

THE DIFFERENTIAL NEUTRON PRODUCTION CROSS-SECTIONS IN THE D(d,np) REACTION

A.B. KAGALENKO, N.V. KORNILOV
Institute of Physics and Power Engineering,
Obninsk, Union of Soviet Socialist Republics

Abstract

The available experimental data on differential neutron production cross-section in break-up reaction have been analysed. It has been established a number of regularities that allowed to estimate the cross-section and neutron spectra at zero degrees for the energy range from a threshold to ~11 MeV in the laboratory sistem. An angular dependence of the neutron spectra has been determined for the initial deuteron energy of ~10 MeV. Neutron yield averaged over the ^{235}U, ^{238}U fission cross-section have been calculated.

The reaction $D(d,n)^3He$ is commonly used as a source of monoenergetic neutrons for energies above 2,5 MeV. But if the incident deuteron energy is above 4,45 MeV the breakup reaction becomes energetically possible and in addition to main neutron group, a low energy component appears. The breakup neutron yield increases rapidly. This fact limits the energy range using the D(d,n) reaction as a neutron source. Therefore, it is worthwhile to make a detailed examination of the D(d,np) reaction. The present experimental works, as a rule, investigated neutron spectra and breakup cross-sections at zero degrees in the laboratory sistem. Although these data are in reasonable agreement and cover a wide range of initial deuteron energies there is no any valid evaluation of the cross-section. Moreover, the regularities of changing spectrum and angular distribution of the neutrons haven't been investigated.

The analysis of available experimental data revealed a number of regularities allowing not only to carry out the evaluation of the cross-section and neutron spectra but probably to stimulate the investigation of a reaction mechanism. In the work we used the previous data on neutron spectra /2/ (E_0 = 5,28 ÷ 7,22 MeV), /3/ (E_0 = 7,93 ÷ 10,94 MeV) and our data (E_0 = 5,89 ÷ 7,44 MeV). The latter data were obtained with using the EGP-10M accelerator and the gas deuterium target by the application of the time-of-flight techniques. The time resolution was ~3 nsec, the path length was ~2 m. The neutron detector efficiency was measured with use of ^{252}Cf prompt fission neutron spectrum and the $D(d,n)^3He$ reaction yield. The neutron spectra at zero degrees were transformed into the centre-of-mass system. Then we'll consider the following notation of the reaction - $m_{o2}(m_{o1},m_1m_2)m_3$:

$$E^* = E - 2\sqrt{E\mathcal{E}_o}\cos\theta + \mathcal{E}_o$$
$$\cos\theta^* = (\sqrt{E}\cos\theta - \sqrt{\mathcal{E}_o})/\sqrt{E^*} \qquad (1)$$
$$\frac{d^2\sigma}{dE^*d\Omega^*} = J\frac{d^2\sigma}{dE\,d\Omega}$$
$$J = (E^*/E)^{1/2}$$

where E^*,θ^*, E,θ - are the energy and the angle of the neutron escape in CMS and LS

J - is the Jacobian of convertion of LS to CMS

$$\mathcal{E}_o = \frac{m_1 m_{o1}}{(m_{o1}+m_{o2})^2}E_o$$

E_o - is the imitial deuteron energy

m_1 - is the neutron mass.

The neutron distribution in CMS is typically cupola-shaped and can be discribed by the average energy $\bar{E}^*$ and the dispersion S. The regularities become most visible if the spectra normalyed to unity should beplotted as a function of $x = (E^* - \bar{E}^*)/S$. The spectra have the same shape ($-2 \le x \le 2$) for a wide range of incident particles energies (Fig.1). The difference is observed on the "tails" of the distribution and appears due to variation of the upper ($\bar{E}^*/S$) and low ($-\bar{E}^*/S$) spectrum limits. Since the distribution is "nearly" simmetric it should be expected that

$$\bar{E}^* = 0.5\,E^*_{max}, \qquad (2)$$

where:

$$E^*_{max} = \frac{m_{o2}}{m_{o1}+m_{o2}}\cdot\frac{m_2+m_3}{m_1+m_2+m_3}(E_o - E_{th}) = 0.1874(E_o - 4.45)$$
$$[E_o] = MeV$$
$$E_{th} = \frac{m_{o1}+m_{o2}}{m_{o2}}Q$$

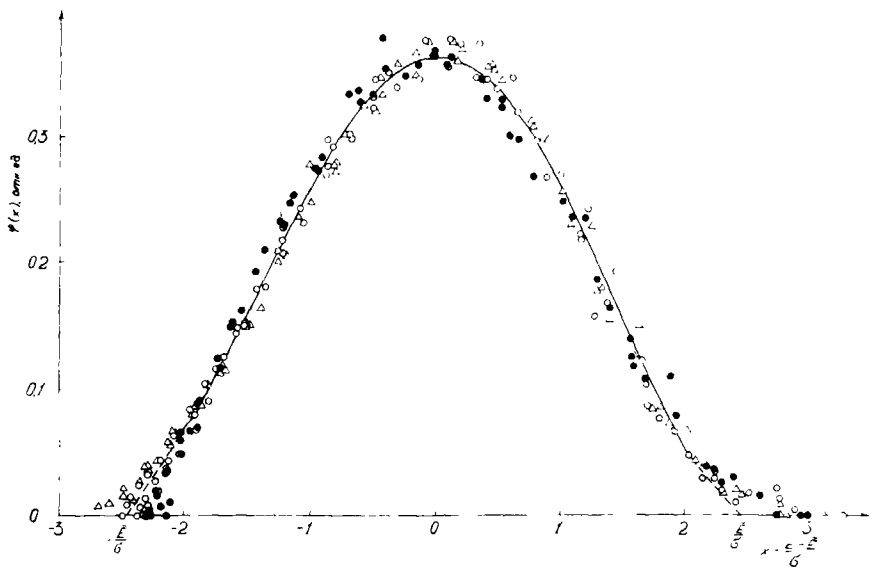

Fig.1. The neutron spectra normalized to unity in CMS. The experimental data for different initial energies are denoted by the following symbols:

(5÷7 MeV) - ●
(7÷9 MeV) - ○
(9÷11 MeV) - △

The solid and dashed lines represent the distribution calculated by the expression 4.

The maximum neutron energy can be easily calculated on the base the laws of energy and momentum conservation. The experimental and calculated by the relation (2) values $\bar{E}^*$ are shown in Fig.2a. The slope of the curve was defined by the least squares method (LSQ) and it agrees with the predicted value within the uncertainty of about 2%. The $S/\bar{E}^*$ ratio was described with a linear function. The parameters of this curve was determined by the LSQ method (Fig.2b)

$$S/\bar{E}^* = 0.541 - 0.0172 \cdot E_0 \qquad (3)$$

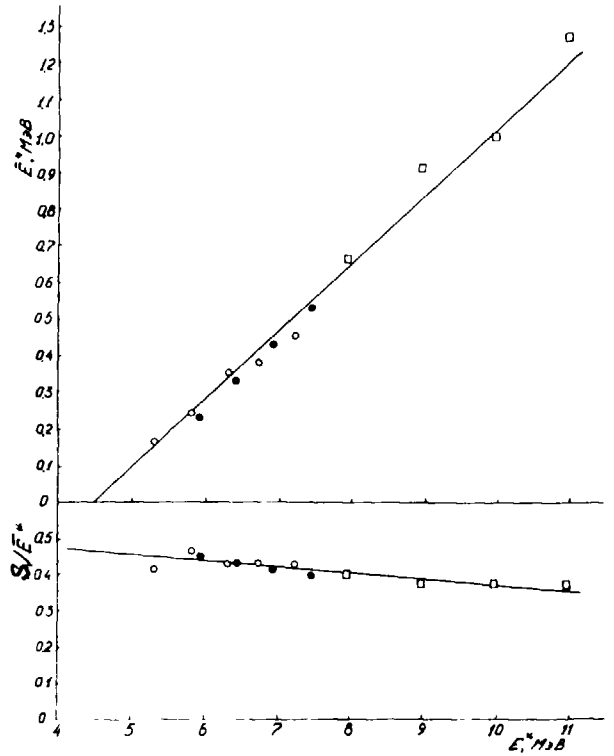

Fig.2. The averaged energy $\bar{E}^*$ and $S/\bar{E}^*$ against the initial deuteron energy. The experimental data are shown by ○ /2/, □ /3/, ● - this work. The solid line represents the calculations by formula 2.

At present there is no successive theory explaining the observed neutron spectra. The spectrum defined in the accessible phase volume theory is described by the expression:

$$(E^*(E^*_{max} - E^*))^{1/2},$$

which doesn't agree with the data shown in Fig.1. The description of the spectrum by the power function using the linear interpolation to the boundary energies is suggested for practice

$$\varphi(E^*) = \begin{cases} 6.926\cdot10^{-2}\cdot(E^*/S + x)/(E^*/S - 2) & -E^*/S < x < -2 \\ 0.3642 + 2.49\cdot10^{-3}\cdot x - 0.1124\cdot x^2 - 1.778\cdot10^{-3}x^3 + \\ + 9.085\cdot10^{-3}\cdot x^4, & -2 \le x \le 2 \\ 5.078\cdot10^{-2}\cdot(E^*/S - x)/(E^*/S - 2) & 2 \le x < E^*/S \end{cases} \quad (4)$$

For the $d\sigma/d\Omega^*$ cross-section estimation in addition to the data mentioned above we used the data /4/, where the cross-section value an and the integration limits are given together. All experimental point are successfully described by the function (Fig.3):

$$\frac{d\sigma}{d\Omega^*} = 7.218\cdot(1 - e^{-0.910\cdot\alpha})\cdot\alpha, \quad (5)$$

where $\alpha = (E_0 - 4.45)^2/E_0$, $\left[\frac{d\sigma}{d\Omega^*}\right] = \frac{mb}{st}$; $[E_0] = MeV$

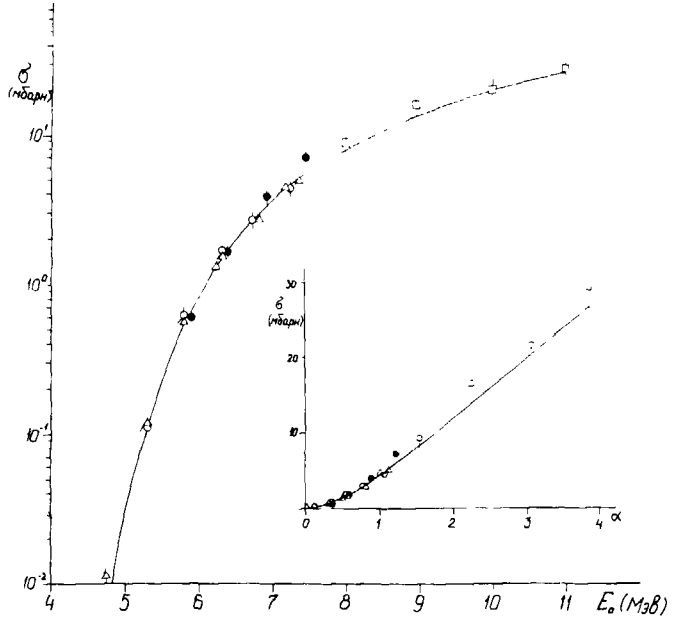

Fig.3. The D(d,np) cross-section at zero degrees in CMS. The dependence 5 is given by the solid line. In the insertion the same values are shown as a function of α. The experimental data of the work /4/ are denoted by triangles. The other symbols are the same as in Fig.2.

The weighted average deviation of the experimental points from the curve is 8%. So, taking into account possible correlations of the data, the uncertainty of the evaluated dependence is (2÷8)%. The expression (5) describes the change of the cross-section by a factor of 200 with high precision. This enables to assume that the function (5) is not only a suitable mathematical model, but the function and its parameters seem to have the specified physical sense.

For example the neutron spectra at zero degrees in the LS for the initial energies of 6 and 10 MeV been calculated by the expressions (1)÷(5) are shown in Fig.4. One should pay attention to the presence of the low-energy component for energy $< E_0$ connected with the neutrons emitted at the angle of 180° in CMS. The behaviour of the spectra in the energy region of $-E^*/S \le x < -2$ is most ambiguous. The experimental data for this energy region are scanty.

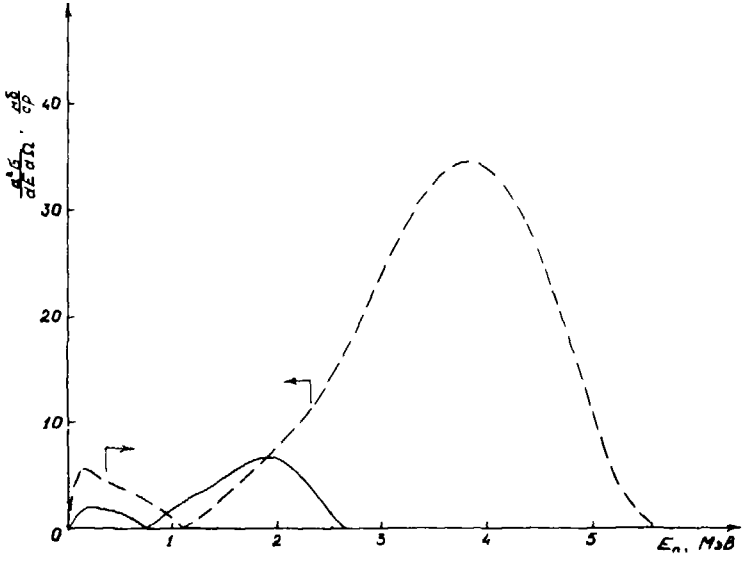

Fig.4. The neutron spectra in LS for the initial energies of 10 MeV - - - - and 6 MeV ———. The regions corresponding to $-E^*/S \le x < -2$ are limited by the arrows.

At $E = \mathcal{E}_0$ the spectra vanished due to using the linear extrapolation. If the neutron spectrum in the energy region in CMS is proportional $\sqrt{E^*}$, the neutron spectrum at $E = \mathcal{E}_0$ in LS doesn't reach zero but in vicinity of $\mathcal{E}_0$ is proportional $\sqrt{E_0}$. The analysis of angular distributions are found difficult because of the experimental data are scanty and also because of the fact that if the angle is not equal to zero the different escape angles in CMS correspond to different neutron energies in LS. We suggested the spectra for different angles could be described by the following expression

$$\frac{d^2\sigma}{dE^* d\Omega^*} = f(E^*\theta^*)\frac{d^2\sigma}{dE^* d\Omega^*}(E^* 0^\circ) \qquad (6)$$

Analysis of the data reported in /3/ for $E_0 \sim 10$ MeV has allowed to make the following conclusions

1. The D(d,np) reaction cross-section is anisotropic in CMS $f(E^*,\theta^*) \neq const$;
2. The degree of anisotropy depends on neutron energy in CMS $f(E^*\theta^*) \neq F(\theta^*)$,

A favourable description of the experimental data (Fig.5,6) is obtained using the function

$$f(E^*,\theta^*) = (1 + \beta E^* \cos^{2n}\theta^*)/(1 + \beta E^*) \qquad (7)$$

if $\beta = 3{,}2$ MeV^{-1}, $2n = 6$.

Within the experimental error the angular distribution can be described for $E_0 = 11{,}75$ MeV /7/ using the same values of parameters. But it is necessary to increase the parameter "b" for lower energies so, $\beta = 5$ MeV^{-1} ($E_0 = 7{,}44$ MeV) and $\beta = 6$ MeV^{-1} ($E_0 = 6{,}31$ MeV /4/) with the same parameter $2n = 6$. This work doesn't consist the successive least squares analysis of angular distributions and, therefore, the mentioned dependence $\beta(E_0)$ is qualitative.

Our general results are summarized in Table 1. In addition to values characterizing the D(d,np) reaction, the background neutron yields are also given for the ^{235}U, ^{238}U fission cross-sections. The fission cross-sections were taken from /5/ and the D(d,n) cross-sections were from /6/.

When employing the results of the work at high energies one should remember that the double deuteron breakup is energetically possible for energies $E_0 \geq 9$ MeV.

Conclusions.

1. The D(d,np) reaction cross-section at zero degrees can be calculated with an accuracy $\leq 8\%$. It'll satisfy the practical needs in many cases and will allow to account the breakup neutrons contribution more reliably.
2. It is necessary to develop the theoretical models to describe the regularities of the behavior of the D(d,np) reaction cross-section and other three-particle reactions.
3. The experimental researches on angular distributions and neutron spectra in the vicinity of $\mathcal{E}_0$ for various initial energies are needed.

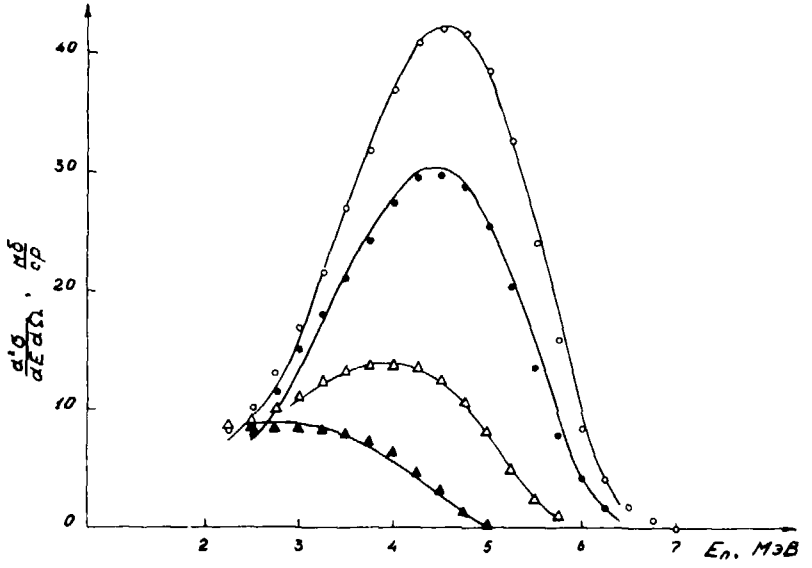

Fig.5. The neutron spectra in LS for the initial energy of 9,94 MeV /3/ at different angles: 0° - O ; 10° - ● ; 20° - Δ , 30° - ▲ . The solid lines represent the calculations by the formula (2)+(7) for the initial energy of 10,17 MeV. The energy increase was made according to the data given in Fig.2.

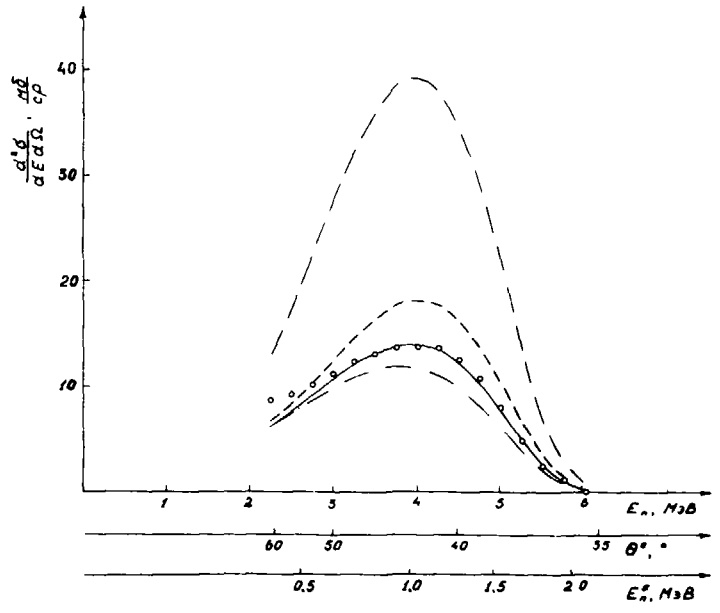

Fig.6. The description of the neutron spectra in LS at the angle of 20° /3/ by the expression (7) with fixed β = 3,2 MeV^{-2} and various values of 2n = 0 - . - . - ; 2n=2 ... ; 2n = 4 ---- 2n = 6 ———; 2n = 8 --..--..--

Table 1.

E_0 MeV	D(d,np)D E_{max} MeV	$\frac{d\sigma\ d,np}{d\Omega}(0°)$ mb/st	D(d,n)^{3}He E_n^o MeV	Y_5, %	Y_8, %
4,5	0,79	0,0004	7,76	0	0
5,0	I,55	0,473	8,24	0,42	0,03
5,5	2,I2	2,97	8,73	2,66	0,85
6.0	2,65	8,37	9,2I	7,4I	3,62
6,5	3,I6	I6,65	9,69	I4,29	8,36
7,0	3,66	27,29	I0,I7	22,52	I4,35
7,5	4,I5	39,58	I0,65	3I,45	2I,32
8,0	4,64	52,87	II,I3	40,30	28,47
8,5	5,I2	66,66	II,60	48,93	35,98
9,0	5,60	80,55	I2,08	56,29	43,34
9,5	6,08	94,35	I2,55	6I,46	50,23
I0,0	6,56	I07,28	I3,03	65,70	56,63
I0,5	7,03	I20,20	I3,50	70,I7	62,23
II,0	7,50	I32,7I	I3,97	74,56	67,I4

where $Y_i = \int_0^{E_{max}} \sigma_{nf}^i(E') \frac{d^2\sigma_{d,np}}{dE'd\Omega}(E_0, 0°, E')dE' \Big/ \frac{d\sigma_{d,n}}{d\Omega}(E_0, 0°)\,\sigma_{nf}^i(E_n^o)$

REFERENCES

1. Drosg H. Proceed. of the IAEA consultant's meeting on neutron source properties, Debrecen, 17-21 March, 1980, INDC(NDS)-114/GT.
2. Meadows J.W., Smith D.L., ANL/NDM-53, 1980.
3. Lefevre H.W., Borchers R.R., Poppe C.H., Phys.Rev., 1962, 128, 3, 1328.
4. Granberg L., Amstrong A.H., Henkel R.L., Phys.Rev., 1956, 104, 6, 1639.
5. Nucl. Data Standards for Nucl.Meas., Technical Reports INDC/NEANDC 227, 1983.
6. Drosg H. Nuclear Science and Engin, 1978, 67, 190.
7. Brolli J., Fowler J. in coll. "Fast Neutron Physics", part 1, Moscow, 1963, p.20.

120 DISTORTIONS OF NEUTRON FLUX AND ENERGY SPECTRUM DURING DEUTERON BOMBARDMENT OF SOLID DEUTERIUM AND TRITIUM TARGETS

V B FUNSTEIN, S V KHLEBNIKOV,
Yu A NEMILOV, Yu A SELITSKIJ
V G Khlopin Radium Institute,
Leningrad, Union of Soviet Socialist Republics

Abstract

The method of (d,p)-reactions is applied for the determination of neutron flux and energy spectrum distortions during deuteron bombardment of solid deuterium-titanium and tritium-titanium targets. The neutron background caused by deuterium accumulation in target backings, carbon build-up, substitution of tritium for deuterium and deuteron or triton break-up is analyzed.

The solid deuterium or tritium containing targets are widely used as sources of monoenergetic neutrons generated in $^{2}H(d, n)^{3}He$ and $^{3}H(d, n)^{4}He$ reactions. These targets are stable when bombarded by high beam currents, convenient and safe under operating conditions. The solid targets consist of Zr or Ti layers impregnated with ^{2}H or ^{3}H and applied to Mo or W backings.

However in the case of targets with the thickness of hydrogen-containing layer less than the range of incident deuteron, the deuterons accumulate continuously inside the target backing, forming so called "drive-in" target. This results in appearance of low-energetic neutron flux component. The distortions of neutron flux value and energy spectrum shape may also occur owing to carbon build-up on the target. At $E_d \geqslant 4$ MeV, an appreciable fraction of the total neutron flux is composed of background neutrons arising from the deuteron or triton break-up in $^{2}H + d$ or $^{3}H + d$ reactions. At $E_d \gtrsim 6$ MeV the background neutrons are produced by interaction between deuterons and construction materials of targets and diaphragms.

In this report a method is described for the determination of neutron flux and spectrum changes during experiment on the basis of proton spectra arising from (d, p) reaction /1/. It is known that the probabilities of $^{2}H(d, n)^{3}He$ and $^{2}H(d, n)^{3}H$ reactions are nearly equal and the differential cross-sections are well examined at $E_d \leqslant 6$ MeV /2/.

This made it possible to obtain from the proton-spectra the data on the changes in neutron flux and spectrum at any emission angle, as well as the information about deuterium distribution profile with the target thickness. The target was located perpendicularly to deuteron beam. The deuteron beam from electrostatic generator was collimated on the target, at mean current density $\sim 80\,\mu A/cm^2$. The targets were cooled by direct water flow or a 1 mm thick brass plate was placed between the circulating water and the target backing. The plate enabled to reduce the heat removal and so the target temperature was raised. The protons generated in (d, p) reactions were registered by Si-detector positioned at the angle 120° to the beam direction. The deuterons scattered by the target material were absorbed by an aluminium foil.

Fig. 1 shows the typical proton spectra for investigated range E_d = 0,7-1,6 MeV measured before and after 20 hours of 1,2 MeV deuteron bombardment of deuterium-titanium target with 0,5 mg/cm^2 thick titanium layer. The target backing was immediately water-cooled. The peak 3 on proton spectra caused by deuteron implantation and subsequent deuterium diffusion in molybdenum backing is clearly defined.

On the basis of experimental proton spectra measured under the different target thermal conditions, the deuterium distribution profiles in the molybdenum backing and the background neutron spectra (Fig. 2) produced by this deuterium at $\theta = 0°$ were calculated. The calculation of neutron flux was controlled by direct measurement of this flux through registration of fission events in ^{238}U target in an ionization chamber (Fig. 3). From Fig. 2 and 3 it is seen that the mean neutron energy and the absolute value of the background neutron flux rise with extended irradiation time and increased target temperature. In a few hours of irradiation, a dynamic equilibrium is reached between the deuterium accumulated in

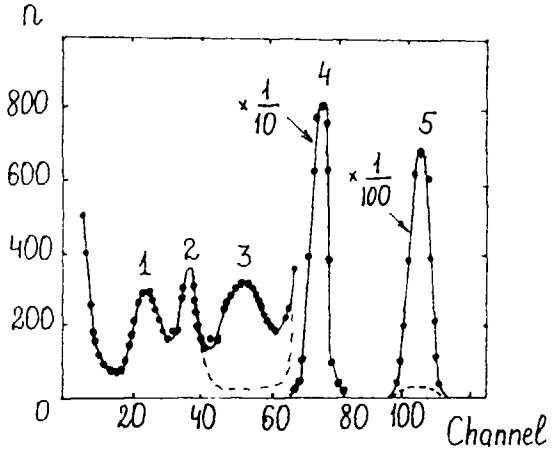

Fig. 1. Spectra of protons generated in deuterium-titanium target at the beginning and after 20 hours of irradiation on immediate water-cooling; n - number of events; the spectrum portions which exhibit any changes at the beginning of irradiation are marked by dashed line. The peaks are conditioned by the following reactions:
1 - $^{16}O(d, p)^{17}O^*$ on the oxidized Mo-backing surface;
2 - $^{16}O(d, p)^{17}O^*$ on the oxide layers of the target surface;
3 - $^{2}H(d, p)^{3}H$ on deuterium implanted in the Mo-backing;
4 - $^{2}H(d, p)^{3}H$ on deuterium in Ti-layer;
5 - $^{12}C(d, p)^{13}C$ on carbon layer of the target surface.

backing and released from it. Background neutron flux at $\Theta \approx 0°$ was found to be 10-13 % of the value of neutron flux produced in deuterium-titanium layer.

The data on deuterium distributions in molybdenum backings within $E_d \approx 0{,}7$-$1{,}6$ MeV permitted to calculate the values of background neutron flux arising by $^{2}H(d, n)^{3}He$ reaction in "drive-in" target at $E_d > 1{,}6$ MeV. The results are presented in Fig. 4 as energy dependence of the ratio between the values of neutron fluxes at 0° generated in "drive-in" target under the saturation conditions and in deuterium-in-titanium layer. The calculations were

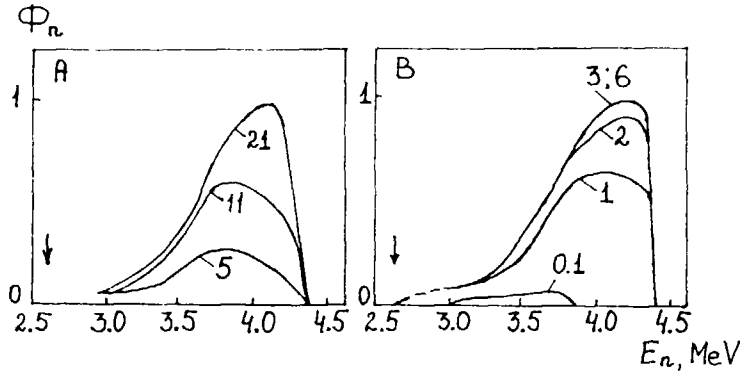

Fig. 2. Spectra of neutrons collinear with the incident beam produced by $^{2}H(d, n)^{3}He$ reaction with deuterium accumulated in Mo-backing.
A - the target with immediate water-cooling;
B - the target with poor cooling. A lower energy edge of neutron spectra is designated by arrow.

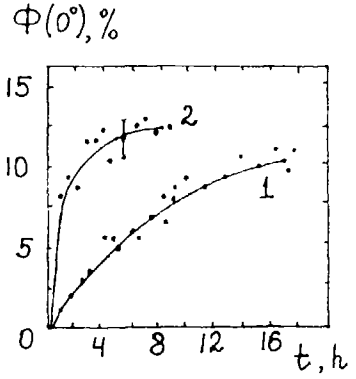

Fig. 3. Density of neutron flux collinear with the incident beam generated by $^{2}H(d, n)^{3}He$ reaction with deuterium accumulated in Mo-backing; 1 - the target with immediate water cooling; 2 - the target with poor cooling; t - irradiation time. The density value of neutron flux generated by deuterium-titanium target with titanium layer thickness 0,5 mg/cm^2 is taken as 100 %.

performed taking into account the constant width of energy spectra of neutron main group ($\Delta E_n/E_n$ = 0,05). As it is shown in Fig. 4, the relative value of neutron background increases gradually with increased deuteron energy and attains 17 % at E_n = 7 MeV for titanium layer thickness 5 mg/cm^2. Lesser values of background neutron fluxes generated from "drive-in" target can be obtained under the incomplete saturation conditions, when moving the beam over the target surface, for example.

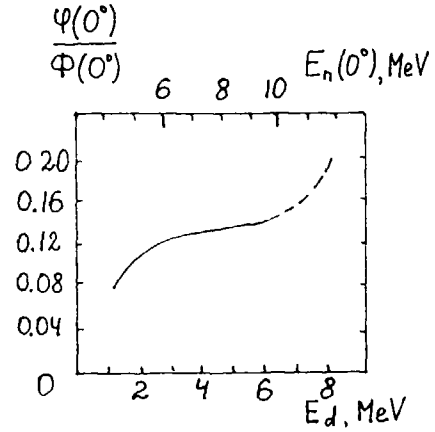

Fig. 4. The ratio of neutron fluxes collinear with the beam produced by ^{2}H(d, n)^{3}He reaction from deuterium accumulated in Mo-target under saturation conditions and from deuterium in titanium layer. The width of energy spectrum of neutrons generated by deuterium in titanium layer, $\Delta E_n/E_n$, is assumed to be equal 0,05.

At E_d > 4,45 MeV an additional source of background neutrons is observed due to ^{2}H + d reactions proceeding with deuteron break-up (at E_d > 8,9 MeV - with break-up both deuterons). In Fig. 5 the characteristics of such neutrons depending on $_d$ are presented, and namely the ratio of neutron fluxes generated in deuteron break-up and ^{2}H(d, n)^{3}He reactions /3/ (curve 2) and the maximum neutron

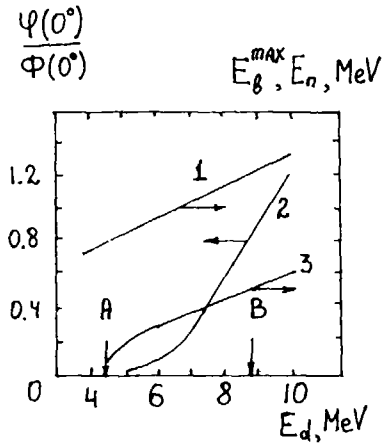

Fig. 5. The flux and energy of neutrons produced by collinear (^{2}H + d) interaction. 1 - the energy of neutrons produced by ^{2}H(d, n)^{3}He reaction; 2 - the ratio of neutron fluxes generated in reactions with deuteron break-up and ^{2}H(d, n)^{3}He reaction /3/; 3 - the maximum energy of neutrons produced by reactions with deuteron break-up. A-B - thresholds of ^{2}H(d, n)p, ^{2}H and ^{2}(d , 2n)2p reactions redpectively.

energy generated in deuteron break-up reaction (curve 3). For comparison the neutron energies for ^{2}H(d, n)^{3}He reaction (curve 1) are given as well.

These data show that at $\Delta E_n/E_n$ = 0,05 and $E_d \lesssim 6$ MeV the neutron background caused by deuteron break-up is less than the back ground arising from the formation of the "drive-in" target. Besides, the background neutron energies generated by deuteron break-up are much below the neutron energies generated by ^{2}H(d, n)^{3}He reaction in titanium layer.

The distortions of neutron flux and energy spectrum shape when deuteron bombardment of solid tritium targets may be governed by different reasons. Within the low E_d values when the thickness of tritium sorbing layer exceeds the deuteron range, the only

possible prosses is tritium substitution for deuterons. At such energies it leads merely to neutron flux decrease. As deuteron energy increase, the cross-sections of $^{3}H(d, n)^{4}He$ and $^{2}H(d, n)^{3}He$ reactions become comparable, and the process of tritium substitution for deuterium can considerably change the spectrum of generated neutrons. Besides, when using the targets with Ti-layer thickness less than the deuteron range, an additional source of neutron background appears - the process of "drive-in" target formation. The calculations show that the relative values of neutron flux generated by deuterium implanted in Mo-backing of tritium-titanium target coincide very closely at E_d = 2-6 MeV with the similar values for deuterium-titanium target. At $E_d < 2$ MeV the cross-section of $^{3}H(d, n)^{4}He$ reaction inereases and neutron background generated by "drive-in" target decreases. At E_d = 1 MeV and $\Delta E_n/E_n$ = 0,05 the value of this neutron flux in relation to the neutrons produced by $^{3}H(d, n)^{4}He$ in titanium layer constitutes 2 %.

At $E_d > 3,71$ MeV, the ^{3}H + d reactions with break-up of one or both interacting particles may occur. Background neutron flux increases with E_d so sharply /3/ that the $^{3}H(d, n)^{4}He$ reaction could not be used without energy selection of produced neutrons.

In the present work the behaviour of thin tritium-titanium targets (P_{Ti} = 1-2 mg/cm^2) was investigated at 1,2 MeV deuteron bombardment. The total neutron flux at 0° was determined from the number of ^{238}U fission events in ionization chamber; the fraction of the flux caused by $^{2}H(d, n)^{3}He$ reaction was determined from the amount of protons produced in subsequent $^{2}H(d, p)^{3}He$ reaction neutron flux caused by $^{3}H(d, n)^{4}He$ reaction - from differencies in them.

At irradiation with immediate water-cooling of the target backing no decrease of tritium content in the titanium layer was observed within the experimental errors. Further investigations on substitution of tritium by deuterium were performed under conditions of poor water-cooling. The experimental results revealed that the amount of desorbed tritium $\mathcal{V}_T$ increased with irradiation time t_{ir} according to dependence $\mathcal{V}_T \sim t_{ir}^{1/2}$. In tritium - saturated targets the total tritium and deuterium volume in titanium layer remained constant during deuteron bombardment. The additive sorption of deuterium in titanium up to $n(^{3}H + ^{2}H)/n(Ti) \approx 2$ takes place in some targets with atomic ratio $n(^{3}H)/n(Ti) < 2$.

The carbon build-up on the target raduces the mean neutron energy from $^{2}H(d, n)^{3}He$ or $^{3}H(d, n)^{4}He$ reactions, changes the neutron flux value, and at $E_d \gtrsim 0,3$ MeV initiates added neutron flux from $^{12}C(d, n)^{13}N$ reaction with the energy $E_n \approx E_d - 0,27$ MeV. All changes in neutron flux can be taken into account from peak area of protons generated by $^{12}C(d, p)^{13}C$ reaction (Fig. 1). The amount of these protons may be estimated absolutely or from proton peak ratios for (d, p) reactions on carbon and deuterium in titanium layer. The necessary data on differential cross-sections for $^{12}C(d, p)^{13}C$ and $^{2}H(d, p)^{3}He$ reactions are available, e. g. /2, 5/. In the present work the target irradiation was carried out under typical experimental conditions of using oil-free magnete discharge vacuum pumps. In conducted experiments the thickness of carbon layer on the target increased directly with irradiation time and attained 190 μg/cm^2 in 12 hours at immediate water-cooling of target backings. Such carbon layer thickness led to appearance of additional neutron flux equal to 30 % of that from $^{2}H(d, n)^{3}He$ reaction in titanium layer at P_{Ti} = 0,5 mg/cm^2. In this case the neutron energy of the main group decreased by 65 keV. The rate of carbon build-up on the target surface is strongly dependent on its temperature and hence on beam density and cooling degree of the backing. So, the carbon build-up rate decreased over 10-fold at poor cooling of target by using the brass plate between water and target backing (Fig.6).

In conclusion it may be said that the considered procedure for registration of protons generated by (d, p)-reactions furnishes an useful method for continuous control over distortions of neutron spectrum shape as well as the characteristics of solid deuterium and tritium targets during bombardment.

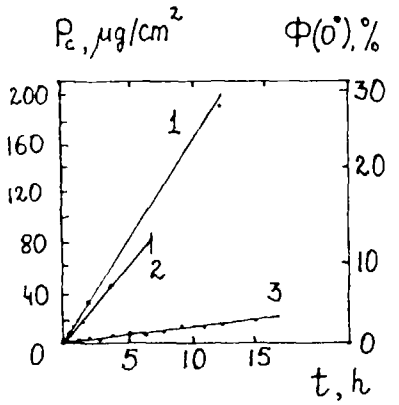

Fig. 6. The thickness of carbon layer and neutron flux produced by $^{12}C(d, n)^{13}N$ reaction under different operating conditions: 1 - immediate water-cooling; current 7 μA; 2 - immediate water-cooling; current 15 μA; 3 - poor cooling, current 15 μA. The density value of neutron flux generated by deuterium-titanium target with titanium layer thickness 0,5 mg/cm² is taken as 100 %.

References

1. Nemilov Ju. A., Selitsky Ju. A., Solovjev S. M. et al. Pribory I Tekhnika Eksperimenta, 1981, N 6, p. 23 (in Russian).
2. Marion J. B., Fowler J. L. Fast neutron physics. Part 1, N.Y.-London, 1960.
3. Drosg M. Nucl. Sci. and Eng-ng, 1978, v. 67, p. 190.
4. Vlasov N. A. Neutrons. M., 1971 (in Russian).
5. Huez M., Quaglea L., Weber G. Nucl. Instr. Meth., 1972, v. 105, p. 197.

SESSION III

CALIFORNIUM-252 PROMPT FISSION NEUTRON SPECTRA AND OTHERS

REVIEW OF MEASUREMENTS OF THE PROMPT FISSION NEUTRON SPECTRUM FROM THE SPONTANEOUS FISSION OF Cf-252*

J.W. BOLDEMAN
Lucas Heights Research Laboratories,
Australian Atomic Energy Commission Research Establishment,
Sutherland, New South Wales,
Australia

Abstract

A review is presented of experimental determinations of the prompt fission neutron spectrum from the spontaneous fission of ^{252}Cf. Special attention has been given to post-1979 measurements

1. INTRODUCTION

The prompt neutron spectrum from the spontaneous fission of ^{252}Cf has been defined as a standard neutron spectrum [1,2]. This standard has found considerable use in recent years in applications such as the energy calibration of neutron detectors [3] and reactor dosimetry via activation reactions [4]. The use of ^{252}Cf as a source of neutrons in environmental, medical and industrial applications is now widespread. Furthermore, the $\bar{\nu}$ value for the spontaneous fission of ^{252}Cf has been the reference for all $\bar{\nu}$ measurements and the accuracy of these measurements is influenced by the knowledge of the ^{252}Cf spontaneous fission neutron spectrum [5]. It is clear, therefore, that the spectrum requires accurate description.

There has been a large number of measurements of the spectrum since the potential value of ^{252}Cf as a neutron source was recognised. Table 1, taken from the review of Blinov [6] lists all measurements prior to 1979. Post-1979 measurements which are the principal concern of the present review, are listed in Table 2.

* Research supported in part by the Department of Foreign Affairs, Canberra, Australia

TABLE I

PRE-1979 MEASUREMENTS OF THE ^{252}Cf SPONTANEOUS FISSION NEUTRON SPECTRUM

(taken from Blinov [6])

Authors		Year	Neutron Energy Range (MeV)	Method, Neutron Detector	Results	
					T_{max} (MeV)	$\bar{E}$ (MeV)
Hjalmar et al	[7]	1955	2	Photoemulsion	1 40±0 09	-
Smith et al	[8]	1957	0.2-7.0	TOF, plastic scintillator, photoemulsion	-	2 36
Bonner	[9]	1961	<4	Integral (Bramblett counter)	1.367±0 030	-
Bowman et al.	[10]	1962	0.5-6 0	TOF, plastic scintillator	-	2 34±0.05
Condé & During	[11]	1965	0.07-7.5	TOF, ^{6}Li glass, plastic scint.	1.39±0.04	(2.09)
Meadows	[12]	1967	0.003-15	TOF, ^{6}Li glass, liquid scint.	1.52	2 348
Green	[13]	1969	-	Integral (Mn bath)	1.39	(2 09)
Zamjatnin et al.	[14]	1970	0.005-6.0	TOF, ^{6}Li glass, plastic. scint.	1.48±0.03	(2.22±0.05)
Jéki et al.	[15]	1972	0.002-1 0	TOF, ^{6}Li glass	1.57 (1.3)	-
Werle & Bluhm	[16]	1972	0.2-8.0	^{3}He spectrometer, Proportional counter	(1.42±0.015)	2.155±0.024 2.130±0.022
Green et al.	[17]	1973	0.5-13	TOF, organic scintillator	1.406±0.015	2.105±0.014
Knitter et al.	[18]	1973	0.15-15	TOF, organic scintillator	1.42±0.05	2.13±0.08
Spiegel	[19]	1974	-	Integral ("age")	-	2.21±0.05
Alexandrova et al.	[20]	1974	2.04-13 2	Single crystal spectrometer	1.42±0.03	(2.13±0 045)
Kotelnikova et al.	[21]	1975	0.5-7 0	TOF, liquid scintillator	1.46±0.02	(2.19±0 03)
Johnson	[22]	1975	2 6-15	Single crystal spectrometer	(1.42±0.02)	2.13±0 03
Csikai & Dezsö	[23]	1976	2.5-15	Activation detector (threshold reactions);	1.41±0.02	(2.12±0.03)
				"age" method	1.48±0.03	(2.22±0.05)
Batenkov et al.	[24]	1976	0.02-2.0	TOF, ^{6}LiI crystal	1.40	-
Blinov et al.*	[25]	1977	0.01-7.0	TOF, ^{6}LiI crystal, ^{235}U chamber	1.41±0.03	2.12
Oyachenko et al.	[26]	1977	<2	Amplitude, ^{6}Li(n,α)T reaction	1.18	-
Nefedov et al.†	[27]	1977	0.01-10	TOF, metal, ^{235}U, ^{235}U chamber	1.28	(1 92)
Bertin et al	[28]	1978	1-10	TOF, liquid scintillator	(1.51)	2.27±0.02
Starostov et al.	[29]	1978	0.01-10	TOF, metal ^{235}U; ^{235}U chamber	1.43±0.02	(2.15±0.03)

Note: The values of T_{max} and $\bar{E}$ in brackets are taken *not* from the reference works, but calculated according to their data by Blinov et al. [6].

*See Blinov et al. [30]

†See Starsatov et al. [37]

TABLE 2

POST 1979 MEASUREMENTS

Authors		Energy Range (MeV)	Flight Path (m)	Neutron Detector	Fission Detector	Timing Resolution FWHM (ns)
Time-of-Flight						
Blinov et al	[30]	0 03-1 0	0 0625-0 50	^{6}LiI (Eu)	gas scintillator	1.5
Blinov et al	[31]	0 04-11 4	0 25-1.0	^{235}U fission chamber	fast ion chamber	1.32
Li An-Li et al	[32]	0.45-15.0		NE213 (equivalent)	(scintillator)	
Poenitz & Tamura	[33]	0.2-10 0	2 58,3.47	black neutron detector	gas scintillator	≤4.0
Bottger et al	[34]	2.0-14 0	12 0	NE213, PSD	fast ion chamber	1.5
Laytai et al	[35]	0 025-1 18	0.30	^{6}Li glass scintillator	fast ion chamber	
Boldeman et al	[36]	1 0-14.3	3 015	NE102	fast ion chamber	2.6-3.0
		0.124-2.66	0 40	^{6}Li glass scintillator	fast ion chamber	2.9
Starostov et at	[37]	0 01-10 0	0.1-0.4	^{235}U fission chamber	gas scintillator	2.5,5 5
Boystov & Starostov	[38]	0.01-3 0		^{235}U fission chamber, anthracene crystal	fast ion chamber	3 5,5.0
Bottger et al	[59]	2 0-12 0	12.0	NE213 PSD	fast ion chamber	1.5
Marten et al	[39]	9.0-30.2	4 50	NE213 PSD	fast ion chamber	1.8
Bottger et al	[40a]	5 0-28.0	3.7,5.9	NE213 PSD	fast ion chamber	1.3,1.5
[Marten et al]	[40b]					
Chalupka et al	[60]	14-28	2 796	NE213 PSD	fast ion chamber	0.85
Proton Recoil Measurements						
Jasicek & Benck	[41]	0.9-10.0		proton recoil, gas counter		
Bolshov et al	[42]	1.0-11.0		proton recoil, stilbene crystal		

TABLE 3

SOME PREVIOUS REVIEWS AND EVALUATIONS

Year	Authors		Recommendations
1971	Smith Koster	[43] [44]	Consultants' meeting [2] recommended ^{252}Cf as a secondary standard
1972	Ferguson	[45]	Panel recommendations [1]. (i) ^{252}Cf should be the standard. (ii) Existing data poor. $\bar{E}$ from 2.085 to 2.35 MeV. Data not sufficiently accurate to define departures from Maxwellian.
1975	Grundl & Eisenhauer	[46]	Spectrum in energy range 0.25 to 8 MeV similar to Maxwellian with $\bar{E}$ = 2.13 MeV. Departures ≤5%. Recommended an empirical segmented fit. [NBS segmented fit]
1976	Knitter	[47]	In accord with Grundl & Eisenhauer [46]. Important to obtain improved data at low and high energies.
1980	Blinov	[6]	Consideration of error sources. Spectrum can be described by Maxwellian T = 1.42 MeV in range 1 keV to 10 MeV with deviations of ±10% at ends of this range.
1983	Klein & Blinov	[48]	For energy region 1 keV to 6 MeV, Maxwellian distribution with T = 1.42 MeV and deviations less than 10% (1-10 keV) and 5% (10 keV-6 Mev). For energy region 6-20 MeV, NBS segmented fit. Evaluation needed.
1984	Boldeman	[49]	Theoretical description now consistent with trends of experimental data. Use theoretical shapes pending full evaluation of experimental data

TABLE 4

CHARACTERISTICS OF NEUTRON DETECTORS USED FOR THE TIME OF FLIGHT MEASUREMENTS

Authors		Type	Dimensions ht x diam (cm)	Energy Range (MeV)	Special Features	Efficiency Determination	Accuracy
Blinov et al	[30]	^{6}LiI(Eu)	0.2 x 1.8 0.4	0.003-1.0 [20]	Corrections for multiple scattering	Calculated (Monte Carlo) using ENDF/B-V data for ^{6}Li(n,α)	
Blinov et al	[31]	^{235}U fission	1.2 x 10	0.01-11.4	Miniature design. Homogeneity of deposit.	^{235}U σ(n,f), Σ = 0.80 for fission fragments.	From ENDF/B-V for ^{235}U σ(n,f)
Li An Li et al	[32]	liquid scintillator	5.0 x 10.5	0.45-14.0			
Pomnitz & Tamura	[33]	black detectors (2)	17.7 x 15.24 27.0 x 20.0	0.2-4.0 0.6-10.0	Efficiency of BND ~100% based on design principle. Efficiency confirmed by extensive use.	98-83% (0.2-4.0 MeV) small detector 96-77% (0.6-10 MeV) large detector.	≤1-2% ≤1-2%
Bottger et al	[34]	4 x NE213	5.08 x 25.4	2.0-14.0	PSD. 4 Detectors separated by 12.5°. Optimised water collimators	Monte Carlo calculations including wall effects and detector resolution.	
Laytai et al	[35]	NE912 ^{6}Li glass scintillator	3.35 x 4.5	0.025-1.18	Thin wall Al cell to reduce neutron scattering.	Measured (TOF) relative to a thin NE908 ^{6}Li detector.	2-6% except on large resonances in ^{6}Li, ^{28}Si, ^{16}O.
Poiterman et al	[36]	NE102	2.54 x 5.08	1.0-14.3	Sliding bias used for analysis	Experimental. Absolute with assoc. particle 2-11 MeV. Calculation elsewhere	{2% absolute {1% relative 2% at low energy.
Boldeman et al	[36]	^{6}Li glass scintillator	0.20 x 5.08	0.124-2.66	Time response functions measured experimentally	Experimental TOF 0.124-1.349 MeV. Calculation 1.349-2.66 MeV	2% relative 0.5-1.4 MeV. 2-6% relative at lower energy.
Starostov et al	[37]	^{235}U(n,f) in (a) gas scint (b) ion chamber	(a) thick U target (11 x .01) (b) 1 mg cm^{-2} on 18 plates of 9 cm dia.			(a) ^{235}U σ(n,f) (b) fission frag. detector ~80-90% ^{235}U σ(n,f) is reference.	
Boystov & Starostov	[38]	^{235}U fission chamber anthracene crystal	1.5 mg cm^{-2} 8 layers 10 cm dia. 1.8 cm dia.	0.01-3.0		(a) ^{235}U σ(n,f) (b) calculation	4%
Bottger et al	[59]	NE213	5.08 x 25.4	2.0-12.0	PSD. 4 Detectors Separated by 12.5°.	Monte Carlo calculation. Confirmation by experiment.	1% 2% overall
Marten et al	[39]	NE213	12.7 x 12.7	9.0-30.2	PSD. Sliding bias.	Monte Carlo calc. Confirmed at low energies 0.4-7MeV.	5% at low energies.
Bottger et al [Marten et al.]	[40a] [40b]	NE213	3.81 x 12.7 12.7 x 12.7	5.0-28.0	PSD. 2 detectors 0°, 60° sliding bias PSD.	Monte Carlo calculation.	5% at low energies.
Chalupka et al	[60]	NE213	5.08 x 25.4	14-28	PSD.	Monte Carlo calculation.	

Historically, the spectrum has been approximated analytically by a Maxwellian distribution $N(E) \propto \sqrt{E} \exp(-E/T)$ in which the temperature $T = {}^{2}/_{3}\ \bar{E}$, where $\bar{E}$ is the average energy. Thus, the traditional way of treating the experimental data has been to determine the average energy $\bar{E}$ of a best fitted Maxwellian distribution and then to determine the deviation of the actual data either from the fitted Maxwellian or from a reference Maxwellian distribution with a defined temperature. Precise measurement of the spectrum presents serious experimental problems because of the range of energies involved. Thus the development of the subject has been accompanied by some disagreement. This has been reflected in the reviews of the subject. Table 3 lists some of the reviews and workshops, and the recommendations that were appropriate to the status of the experimental data at that time. It will be seen, for example, that the early work could be described by a Maxwellian distribution with an average energy which converged on 2.13 MeV, whereas more recent studies have tended to reveal widescale but small deviations from this shape. The evaluation of Grundl and Eisenhauer [46] produced the so-called NBS segmented fit which has been used extensively since then. The two most recent specialists' meetings [48,49] have recomended *temporary* descriptions of the spectrum, the first, empirical, and the second, a theoretical description, pending an evaluation of the recent experimental data.

2. GENERAL EXPERIMENTAL DETAILS

The recent measurements listed in Table 2 can be divided into two groups: time-of-flight measurements and measurements involving the analysis of proton recoil spectra. In the larger of these two groups, the spectrum was derived by measuring the inverse time-of-flight of neutrons over a specified flight path using the detection of a neutron in an appropriate detector as the start signal to a time-to-amplitude converter and a signal previously recorded (in real time) from the fission detector, suitably delayed, as the stop signal. The typical set-up is shown schematically in Figure 1. In assessing the accuracy of a particular experiment, the factors to be considered are the fission source and associated fission detector, the neutron detector and the corrections that must be applied to the experimental data.

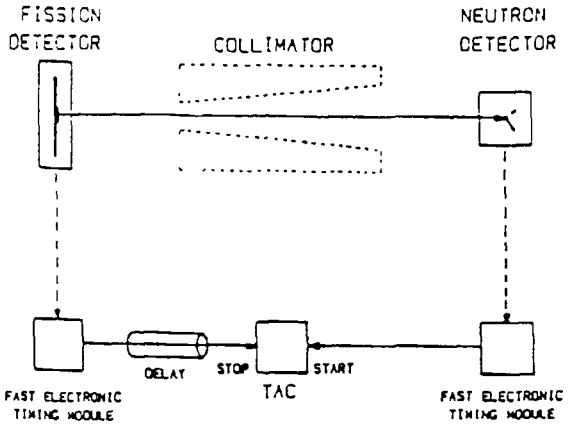

Figure 1

Details of the time-of-flight systems are listed in Table 2. It will be noted that the flight paths that have been employed vary greatly from as little as 6.25 cm to 12.0 m. The choice of the flight path was governed principally by the neutron energy range that was under study. The short flight paths, for example, were chosen for measurements emphasising the lower energy end of the spectrum. Long flight paths were used for the higher energy end of the spectrum, whereas measurements with flight paths between 1 and 4 m tended to be directed at determining the major component of the spectrum from about 0.5 to 10.0 MeV. The significance of different sources of error depends on the flight path. For example, for very short flight paths, the precision of the flight path itself and the downscatter of neutrons in the fission and neutron detectors are important. For the longer flight paths, accidental neutron fission coincidences are a major factor.

2.1 Neutron Detectors

For measurements covering the lower energy region of the spectrum, the neutron detectors were based either on the $^{6}Li(n,\alpha)$ reaction as in Li glass scintillators or LiI(Eu) crystals or ^{235}U fission chambers. Most of the detectors for measurements at higher energies were NE 213 liquid scintillators incorporating pulse shape discrimination to minimise the γ-ray background. One of the exceptions [36] used an NE 102 plastic scintillator, a

detector type which was frequently used in pre-1979 measurements. The other exception was the black neutron detector, based essentially on total neutron cross sections, which was used by Poenitz and Tamura [33].

The overriding feature to consider for the neutron detector was the method of determining either the relative or absolute neutron detection efficiency curves. Obviously, the accuracy of the shape of the spectrum is limited by the accuracy with which this is known. The efficiencies of the NE 213 liquid scintillators [34,39,40,59,60] were determined by calculation using Monte Carlo methods [50,53]. These calculations can produce extremely accurate data provided the full detector characteristics, such as the resolution function and the detector response function are specified [51]. The absolute neutron detection efficiency curve for the NE 102 plastic scintillator used in ref. [36] was determined experimentally in the energy range 2 to 11 MeV using the associated particle method and extended by calculation outside this region using Monte Carlo methods similar to ref. [50]. The alternative methods of determining the efficiency curves, experimental and calculational, have their virtues. The experimentally determined efficiency curve is directly applicable to experiment, although edge effects are difficult to take into account because of the collimation effect of the associated particle method. Calculation methods can bypass the edge effect problem but, in this case, the input data must be very accurate and the detailed structure of the detector system (PM tube, for example) must be incorporated into the calculation. Black neutron detectors as used by Poenitz and Tamura [33] are high efficiency devices based on total neutron cross sections which are known very accurately. Furthermore, extensive use of such detectors in other standards work such as the $^{235}U(n,f)$ cross section has led to very accurate calibration of their efficiency curves. The neutron detection efficiency curves of the ^{6}Li and ^{235}U based systems are generally related to the standard (n,α) and (n,f) cross sections for these isotopes. These cross sections are known to high accuracy (2-6%) in the first case and better than 4% in the latter case. Therefore, high accuracy can be obtained with such detectors, provided effects such as multiple scattering are taken into account.

A second factor that needs to be considered is the effects of neutron scattering in the structural elements of the neutron detector. Blinov et al. [52] have discussed this question in detail. In three measurements [33,34,59] collimators on the flight path were used reducing significantly scattering effects in both the neutron and fission detectors. Of course, such an arrangement introduces the necessity to design the collimator carefully to minimise scattering on the walls of the collimator. In the detectors based on the $^{235}U(n,f)$ and $^{6}Li(n,\alpha)$ reactions, scatter in the detectors was reduced by making the structural elements of each as small as possible. In ref. 36, scattering effects in both neutron detectors were included in the experimental determination of the efficiency curves.

2.2 Fission Counters

The critical features of fission counter design have been discussed recently by Chalupka et al. [54]. Greater attention has been paid to these requirements in recent years. Structural elements have been reduced as much as possible, great care has been taken with the preparation of the ^{252}Cf deposits to minimise fission fragment absorption and attention has been paid to the design to obtain fast response and a fission fragment detection efficiency close to 100%.

The detailed features of the fission counters are listed in Table 5. The most frequently used design has been the miniature fast ionisation chamber similar to that of Chalupka [55]. Except at very low energies, scattering effects in such fission detectors are negligible. The ionisation chamber used in ref. [36] was slightly heavier in construction, but here the principal component of the weight of the chamber was at a diameter of 7.5 cm and therefore the geometry and the relatively light design reduced the scattered component considerably. The body of the gas scintillator used by Poenitz and Tamura was shielded by the collimator on the flight path thereby making any correction exceedingly small.

A high efficiency in fission fragment detection is desirable because of the effects, discussed later, which result from the correlation of the neutron spectrum with the emission angle of the neutron relative to

TABLE 5

CHARACTERISTICS OF FISSION FRAGMENT DETECTORS

Authors		Type	Fission Rate (s^{-1})	Backing Material Thickness (cm)	Deposit Diameter (cm)	ϵ_f	Special Features
Blinov et al	[30]	gas scintillator	2 x 10^4 9.8 x 10^4	Pt. 0.02		0.99	
Blinov et al	[31]	miniature fast ionisation chamber 2 mm spacing	5 x 10^3	Pt 0.01	0.4	0.99	Calibrated via neutron yields with $MnSO_4$ bath. Noted small ageing effect. Anisotropy in detector taken into account.
Li-An Li et al	[32]						
Poenitz & Tamura	[33]	gas scintillator cylindrical ht 16 cm, dia 22 cm	1.43 x 10^3	Pt: 0.0254	<0.955	0.71 0.2 bias loss 0.09 frag.absorp.	Calibrated relative to absolute sources.
Bottger et al	[34]	miniature fast ionisation chamber	1 x 10^3	Au: 0.0254	0.5	0.954±0.003 experimental	"Golden" version of Vienna low mass detector
Laytai et al	[35]	fast ionisation chamber	1 x 10^4	SS. 0.01	0.6		
Boldeman et al	[36]	fast ionisation chamber	5-8 x 10^4	SS: 0.02	0.6	0.970	Efficiency determined using neutron coincidence counting with large liquid scintillator
Boldeman et al.	[36]	fast ionisation chamber	4.4 x 10^4	SS: 0.02		0.970	-do-
Starostov et al	[37]	gas scintillator miniature fast ionisation chamber	1.2-5.5 x 10^3	Au: 100 ug cm^{-2} SS: 0.01		≈0.95	
Bnystov & Starostov	[38]	miniature fast ionisation chamber		Pt: 0.01		0.97±0.02	
Bottger et al	[59]	miniature fast ionisation chamber	1.6 x 10^3	Pt		0.995±0.002	Special attention to reduce fragment loss.
Mârten et al	[39]	miniature fast ionisation chamber	3.4 x 10^4				
Bottger et al [Mârten et al]	[40a] [40b]	miniature fast ionisation chamber	7 x 10^4			0.9927±0.0005	
Chalupka	[60]	miniature fast ionisation chamber	1.4 x 10^3				

TABLE 6

CORRECTIONS TO EXPERIMENTS

Authors		Time Dependent Background Accidental Coincidences	Fragment Loss	Structural Materials	Attenuation Downscatter	Time Calibration
Blinov et al	[30]	Pulse pile up rejector used				
Blinov et al	[31]	Pulse pile up rejector used Effects very small and accurately corrected	(a) Correction for fragment registration effects in neutron detector (b) Fragment loss in fission detector very small	Corrections for chambers by calculation Maximum 3%	Air scattering by calculation Generally small but >10% below 0 1 MeV	Three separate methods to verify time calibration
Li An et al	[32]					
Poenitz & Tamura	[33]	Small effect Correction applied Renormalisation	Based on measurements of spectra at 0° and 90° Consistent with 7% absorption in target	Minimised by neutron collimator 0 1% scatter main collimator ≤0 2% for first shield collimator	Neutron collimator removes most components.	Corrections for timing effects on detector responses. Energy resolution. Energy scales verified experimentally (Carbon resonances)
Bottger et al	[34]	Exact correction for time dependent back ground	Correction based on experiment	Negligible for fission detector for E_n > 2 MeV	Air attenuation average 10%. Collimator minimises downscatter to ≤0 5%.	Energy scales verified by extensive inelastic scattering data
Laytai et al	[35]	Pulse pile-up rejector used		Response function correction	Shadow bar	
Boldeman et al	[36]	Very small effects Approx correction applied for time dependent background and renormalisation	Small correction based on experiment efficiency and nuclear data	Relatively large diameter lightweight fission counter Corrections mostly included in shadow bar measurement	Correction applied for air and resonances Downscattered from shadow bar measurement	Energy scale confirmed by carbon total cross section measurement. Resolution broadened
Boldeman et al	[36]	-do-	No correction applied Negligible relative to experimental accuracy	Assumed to be similar for calibration and experiment Effect much smaller than time effect in neutron detector	Correction automatically included in experimental efficiency determination.	Energy scale confirmed by ^{7}Li, ^{16}O resonances.
Starostov et al	[37]			Considerable attention to structural materials		
Boystov & Starostov	[38]			Mininimised by miniature detector	Shadow bar	
Bottger et al	[59]	Exact correction for time dependent background	Extremely small because of high efficiency 99 5%	Negligible for fission detector for E_n > 2 MeV	Air attenuation average 10% Collimator minimises downscatter to ≤0 5%.	Energy scales verified by extensive inelastic scattering data
Marten et al	[39]	Negligible because of low fission rate	Not of consequence for energy range of measurement	Minimised by use of small fission counter		Resolution broadened. Calibration via delay line.
Bottger et al	[40a]	as for Marten et al				
Marten et al	[40b]	[39]				
Chalupka et al	[60]	Special pile up Unit Very low hgj in Neutron Detectors	Extremely small because of high efficiency 99 5%.	Negligible		

flight direction of the fission fragments. Böttger et al. [34,59] have considered in detail factors such as the preparation of the backing surface which cause a reduction in the fission fragment detection efficiency. To improve the accuracy of the correction factor discussed in section 2.3, the fission fragment detection efficiencies were determined experimentally. In experiments [30,31,33] the total fission rate of the ^{252}Cf source was obtained using $MnSO_4$ baths to measure the total neutron emission $\bar{\nu}F$. Since $\bar{\nu}$ for ^{252}Cf is known to about 0.25%, the fission fragment detection efficiency can be determined very accurately. In experiment [36] neutron coincidence counting using a large liquid scintillator tank provided an accurate value for the fission fragment detection efficiency. Böttger et al [34] have measured the dependence of the fission fragment detection-neutron coincidence probability as a function of the angle of the neutron detector with respect to the perpendicular to the fission foil surface. In their more recent measurement Böttger et al [60] have shown that if special attention is paid to the preparation of the backing surface for the fission deposit a detection efficiency of 99.5% can be obtained.

2.3 Experimental Corrections

As the consensus between the different measurements has improved in recent years and with attention now turning to the deviations from a Maxwellian distribution, all corrections in time-of-flight measurements have received close scrutiny. The major ones are listed for post-1979 measurements in Table 6 and are discussed below.

2.3.1 Accidental neutron fission coincidences & renormalization

The events in a typical time-of-flight spectrum can be classified into three classes:- (i) Genuine fission neutron-correlated fission fragment counts, (ii) Genuine fission neutron-accidental fission fragment coincidences, (iii) Random background (γ-ray, neutron) fission fragment coincidences. Chalupka [56] has discussed the interaction of the three classes and formulated a method of analysis for typical data. Similar but independent analyses have been presented by other authors.

The specific procedure for the analysis differs according to the dead time of the stop pulse (generally the stop pulse width) τ relative to the time range of the time-to-amplitude converter T. In the case where $\tau \ll T$, the accidental coicidence gain to a channel i is given, in the formulation of Poenitz and Tamura [33], by

$$N_{aac}(i) = \sum_{\ell=i+1}^{\ell_{max}} \exp^{-N_f t} [1-\exp(-N_f \Delta t)] N(\ell) \qquad (1)$$

where N_f is the nett fission rate to the stop input of the TAC, t is the time associated with channel i and Δt is the channel width. The first exponential in equation (1) accounts for the probability that a random stop signal has not previously occurred in time t. Of course, these accidental coincidences mean that genuine neutron fission coincidences have been lost with the effect being larger for the higher energy channels. The shape of the spectrum requires a renormalisation factor $\exp(-N_f t)$ to account for this effect. The random background fission fragment coincidence probability can be determined from the higher end of the spectrum above the prompt γ-ray peak. However, this random background must also be renormalised. In the second case in which $\tau \geq T$, all channels in the time-of-flight spectrum have been equally affected by the accidental coincidence probability and the first exponential factor in equation (1) and the need for renormalisation are eliminated. As a general conclusion, it is clear that the magnitude of the corrections relate to the factor $N_f T$.

In the measurement of Böttger et al. [34], because of the flight path and the high fission rate necessary to obtain statistically significant data, the corrections necessary for the accidental coincidences were fairly large. Exact corrections were applied and their influence on the experimental data is illustrated in Figure 2. It should be noted that renormalisation was necessary only for the higher channels in this measurement because of the dead time associated with the stop trigger. Poenitz and Tamura [33] used a stop trigger dead time many factors smaller than the time range. In this measurement all the correction factors were fairly small and applied according to the formulation above. For measurement [36], the correction factors were smaller still. In this case, the use of a sliding bias on the neutron detector introduced an additional complication as the neutron detector spectrum associated with random coincidences

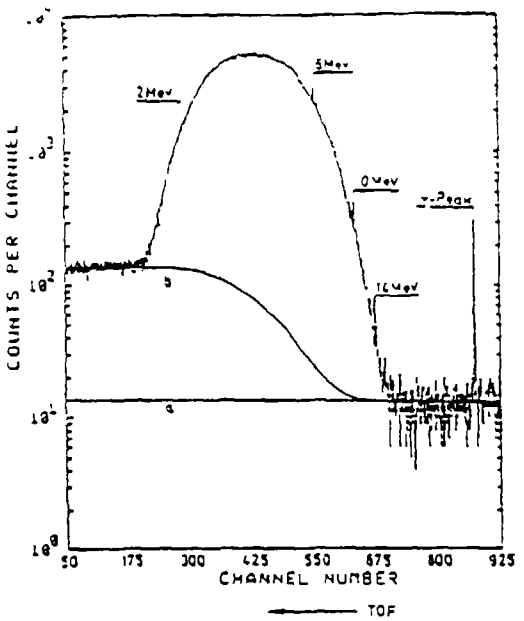

Figure 2

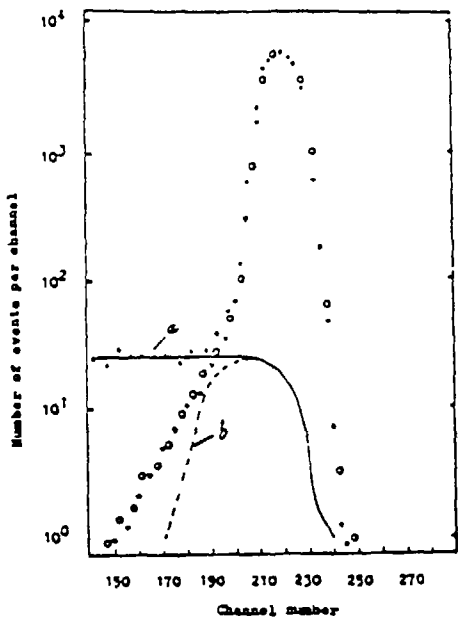

Figure 3

differs from that associated with the accidental neutron fission fragment coincidences. An approximation to an exact correction was applied and the data were also renormalised as $\tau << T$. In the measurements of Märten et al. [39] Böttger et al. [40] and Chalupka et al [60], the effects referred to above are negligible.

One consequence of the accidental neutron fission fragment coincidences seen in Figure 2 is that the background at low channel numbers, corresponding to the low energy part of the neutron spectrum, is increased. Thus accidental coincidences would seriously interfere with the data from measurements endeavouring to define the lower energy end of the spectrum. Blinov et al. [30] and subsequent measurements [31,35] have used pulse pile-up rejection so that the magnitude of the effect associated with accidental coincidences is reduced to one commensurate with the pulse pair resolution of the fission counter and associated electronics. Figure 3, taken from Blinov et al. [57] illustrates the background effects that are associated with experiments of this type.

2.3.2 Fragment loss

Neutron emission in the fission process is primarily evaporation from the fragments after they have reached their full velocities from Coulomb repulsion. Some of the neutrons, however, are emitted during the acceleration process and there is also considered to be a small component (~10%) which are emitted from the neck of the elongated fissioning system - the so-called "scission neutrons". For all of these reasons, the fission neutron spectrum varies with the neutron emission angle relative to the fragment direction. Therefore, if the neutron emission spectrum is measured with small geometry and there is an angular dependence to the discrimination against the fission fragments that can stop the TAC, a bias is introduced into the measurement of the spectrum.

Poenitz and Tamura [33] and Böttger et al. [34] have studied this effect experimentally. The latter have shown that even with highly polished deposit surfaces, a small proportion of the fission fragments travelling parallel to the plane of the source are still lost. The effects of such losses are clearly demonstrated in Figure 4 from Poenitz

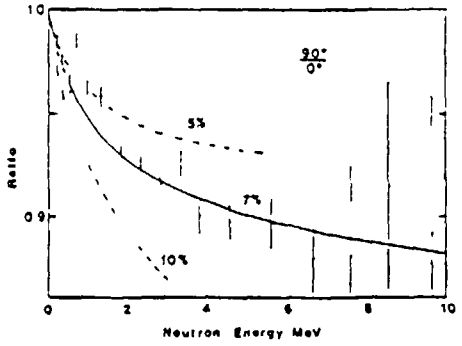

Figure 4

and Tamura [33]. The data show that fragment losses in the foil cause a hardening of the spectrum measured at 0° to the perpendicular to the plane of the source. It is also clear that the effect increases as the proportion of fission fragment absorption in the plane of the foil increases. Since almost all measurements were made at 0° corrections must be applied. The appropriate correction can be calculated from the fission fragment absorption probability and the data from Bowman et al. [10] on the density distribution of neutron emission angle with respect to fragment direction and the angular dependence of the emission spectrum.

Since the magnitude of the effect depends on the absorption probability, considerable effort has been devoted to the measurement of the fission fragment detection efficiencies as mentioned in section 2.2. In most cases, the fission fragment detection efficiencies were found to be close to 100% and therefore the corrections applied were quite small. In the case of Poenitz and Tamura [33] the fission fragment detection efficiency was 71%. A separate experiment was mounted by these authors to show that only 7% of the fragments were actually lost in the foil (Figure 4). A correction was applied on this basis.

2 3 3 Structural materials

Neutron scattering in the fission fragment and neutron detectors has been considered in detail by Blinov et al [52] and a number of other authors The distortion of the experimental spectrum caused by scattered neutrons increases rapidly at energies below about 1 MeV

As discussed previously, the precautions taken to minimse neutron scattering include miniaturisation of the fission fragment detector and the use of a collimator on the flight path. Neutron scattering in the body of the neutron detector alters its efficiency but, except at the lower energy end of the spectrum, does not significantly time shift the neutrons to lower energy In the measurements of Blinov et al. [30,31] and Starostov et al [37] which addressed the lower end of the spectrum, great attention was paid to the corrections necessary to account for neutron scattering Such effects are also taken into account in the calculation of the neutron detection efficiencies for measurement [35]. For the detector used for the lower energy measurement of ref. [36], the experimental determination of the neutron efficiency and time response functions overcame the scattering effects in the neutron detector.

2.3.4 Air attenuation, downscatter

Air attenuation is an important correction, especially for long flight path experiments such as that of Bottger et al. [34], where a correction of ~10% is mentioned Corrections for air attenuation appear to have been applied universally. A second aspect is the scatter of neutrons by the air outside the flight path into the neutron detector. The important consideration here is the time shift which makes a scattered neutron appear experimentally as one of lower energy. Such effects are fairly small at high energies where the scattered neutrons are adding to a spectrum which is increasing in intensity with lower energy. However, below 1 MeV or so, the effect starts to become quite significant. In the measurements using collimators [33,34,59] neutron scattering in the air is eliminated entirely. In other experiments [35,36] appropriate corrections were obtained by repeating the spectrum measurements with a shadow bar placed between the neutron source and detector to eliminate all direct sight neutrons.

2.3.5 Verification of energy scale

An important consideration in time-of-flight measurements is the verification of the energy scales Most experiments were performed with γ-ray sensitive neutron detectors and the prompt γ-ray peak in the time-of-flight spectrum can, with the use of time calibrators

or precision time delays, be used to define the energy scale An alternative method involves transmission measurements on, for example, a carbon sample using the experimental time-of-flight system The energy scale is then defined by the position of the narrow resonances in ^{12}C which have been defined by James [58] as reference energy standards For measurements of the lower energy part of the spectrum, the resonance in the $^{6}Li(n,\alpha)$ cross section can be used to define the energy scale, although the apparent peak in the cross section shifts if multiple scattering becomes significant Of course, the optimum method of calibration is to use such resonance data to confirm the energy scales determined using delay times etc.

Special problems arise in the use of neutron detectors based on the $^{235}U(n,f)$ reaction as there is no γ-ray signal here to provide an indication of zero time on the time-of-flight scale Blinov et al. [57] have discussed three methods of determining zero time in such systems. In the first method, identical fission shaped signals from a pulse generator were fed to the electrodes of the ^{252}Cf fission counter and the ^{235}U fission counter used as the neutron detector. The second method involved measuring the neutron time-of-flight spectrum over a flight path of only 6 mm with a single layer ^{235}U fission detector. The third method involved the comparison of the shape of the fission neutron spectrum measured over several different flight paths to obtain the optimum zero time position for minimum difference between the experimental data after all corrections Thus the zero time position was obtained with a reliability of the order of ±0.1 ns

2 3.6 Other sources of error

A number of other sources of error have been considered in the various experiments and dismissed as negligible. These include

(a) A contribution from delayed γ-rays from fission - shown to be negligible by Boldeman et al [36].
(b) Other californium isotopes in the ^{252}Cf target - dismissed by both Poenitz and Tamura [33] and Blinov et al. [57].
(c) The timescale in the fission process for the emission of neutrons - dismissed by Poenitz and Tamura [33].

3 PROTON RECOIL MEASUREMENTS

The second method of measuring the ^{252}Cf fission neutron spectrum utilised proton recoil spectrometers In the measurement of Jasicek and Bensch [41] two separate gas filled proportional counters were used, while Bolshov et al [42] used stilbene and antracene crystals. Both the proportional counters used by Jasicek and Bensch [41] were cylindrical in shape, the larger, covering the energy region 0.9 to 10 0 MeV, was filled with a mixture of methane and krypton, while the smaller, for the energy region 1 to 3 MeV, was filled with methane. Very small quantities of ^{3}He (0 1%) were added to each counter to provide an energy calibration via the 764 keV protons from the reaction $^{3}He(n,p)^{3}H$ induced by thermal neutrons Gas filled proportional counters of this type have been studied for many years and are capable of accurate measurements. The principal disadvantage is the need to unfold the proton recoil distribution which is distorted by wall and end effects. The details of the measurement by Bolshov et al. [42] were not available to this reviewer.

4 EXPERIMENTAL DATA

Recent reviews of the experimental data for the ^{252}Cf fission neutron spectrum have recommended that the optimum way to present the experimental data is relative to a reference Maxwellian distribution with T = 1.42 MeV. This recommendation has been followed in the present review.

For clarity, the experimental data are presented for three energy regions. 0-1.5 MeV, 1.0-15.0 MeV and 11.0-30.0 MeV. The data of experiments [31], [33], [35] and [36] for the energy region 0-1.5 MeV are shown in Figure 5. The data from experiment [30] were not included in this figure as they are in accord with the subsequent data [31] from the same group and because tabular data were not available. The data from Starostov et al. [37] are presented separately in Figure 8(a). The data from experiments [31], [33], [34], [36] and [39] for the energy range 1 0 - 15.0 MeV are shown in Figure 6(a). The extended data set from experiment [34] and recent data from the same authors [59], both reported at this conference, are shown in Figures 6(b) and 6(c) respectively. The data from [32] and [41] are shown separately in Figures 8(b) and (c) respectively. The data from ref. [39] are shown for the energy range

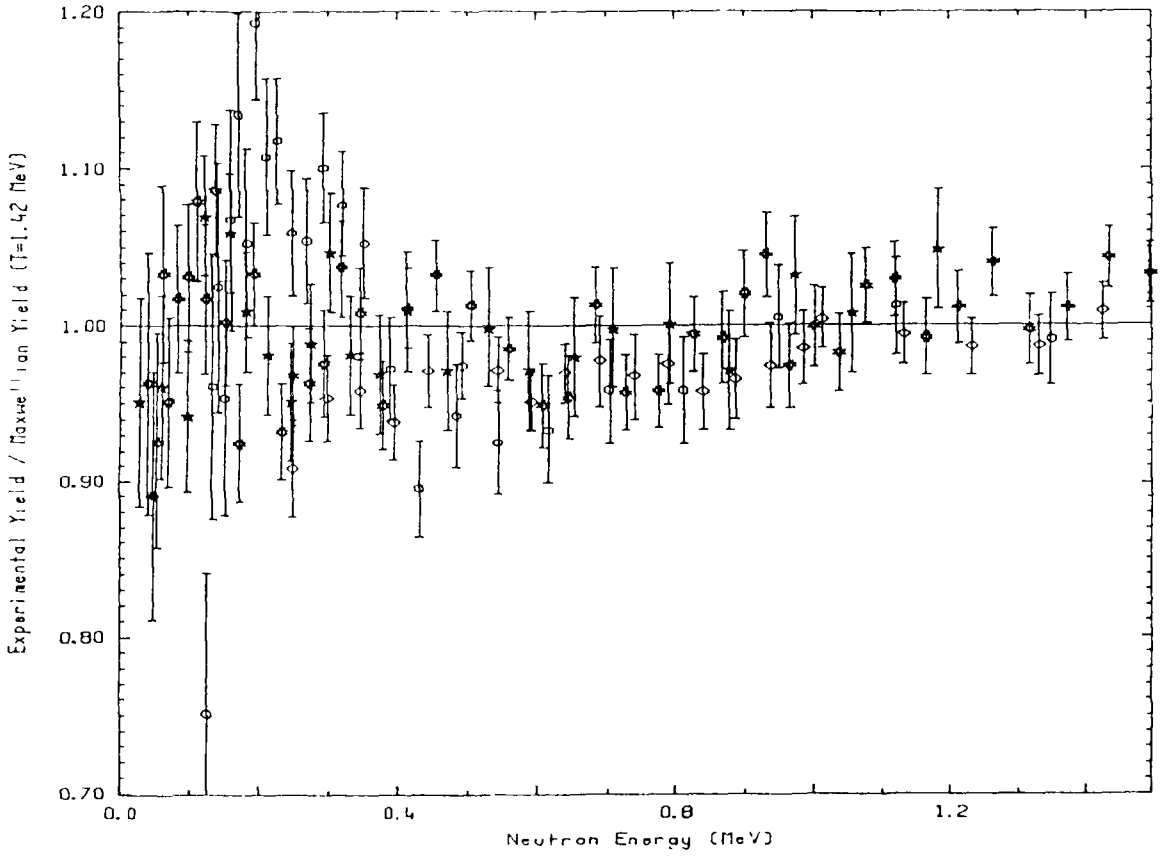

Figure 5

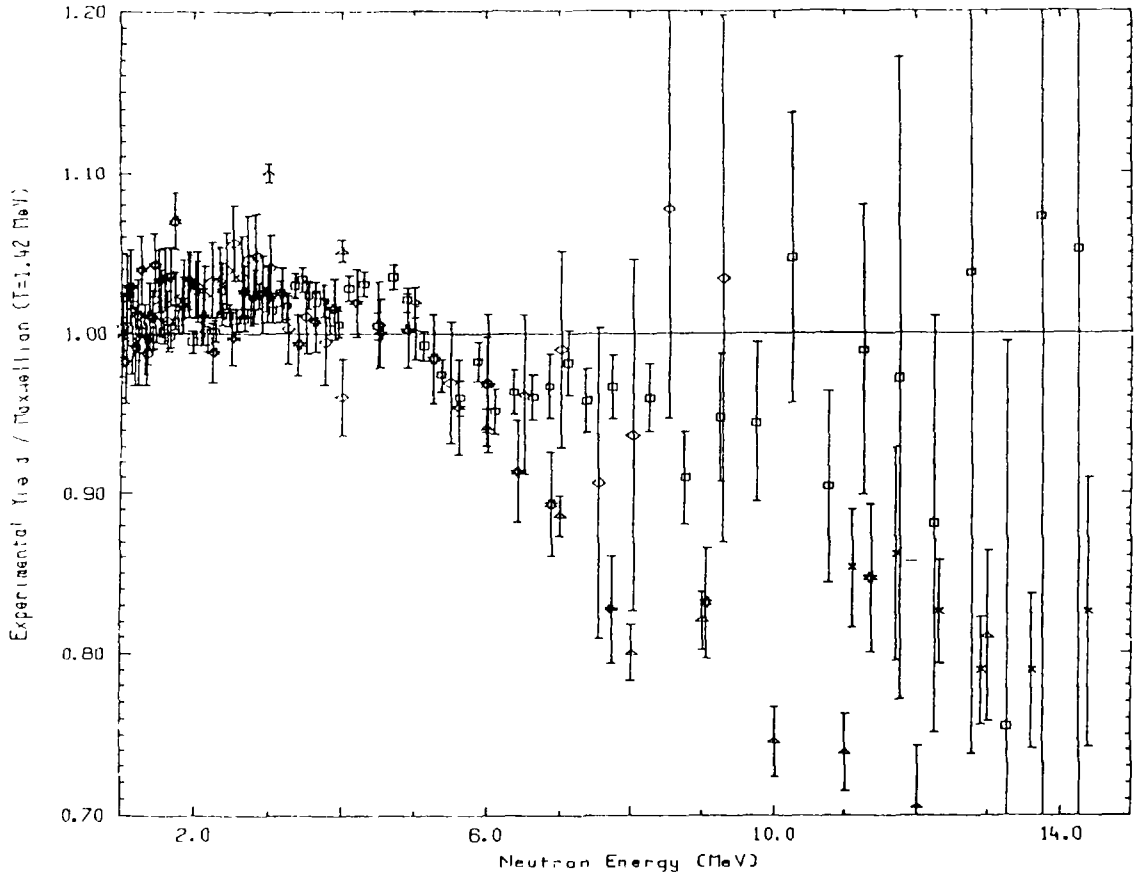

Figure 6(a)

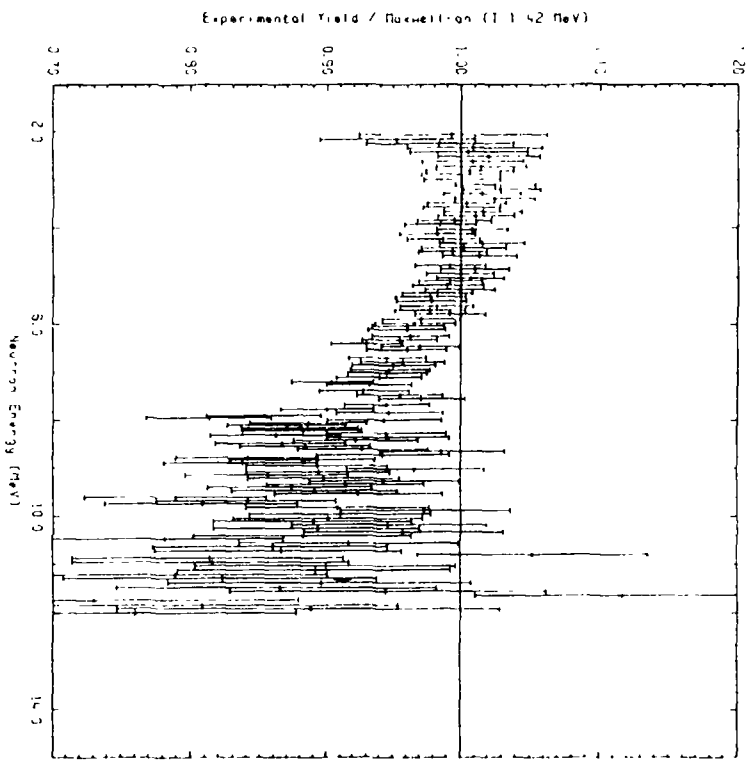

FIGURE 6(b)

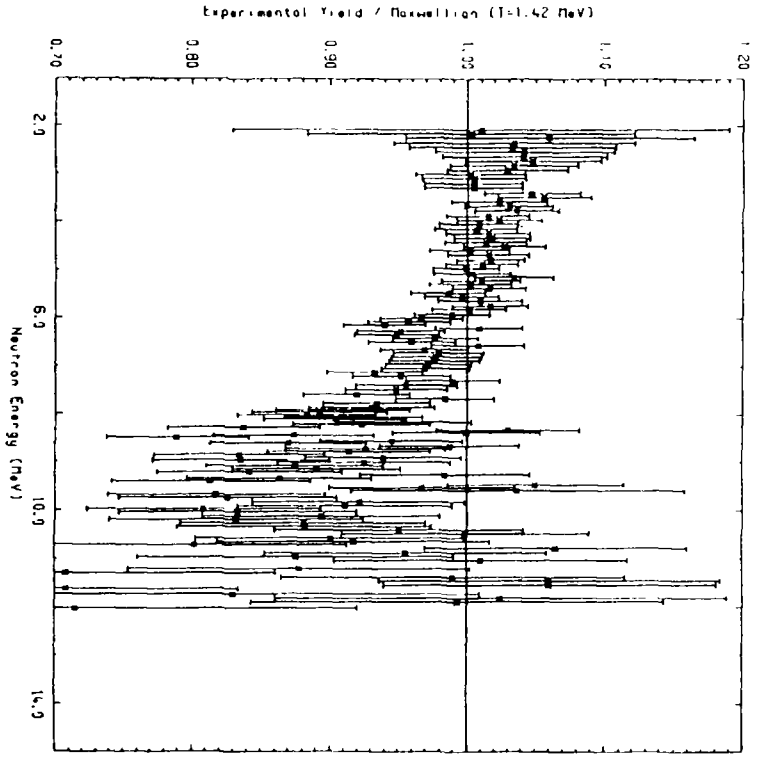

FIGURE 6(c)

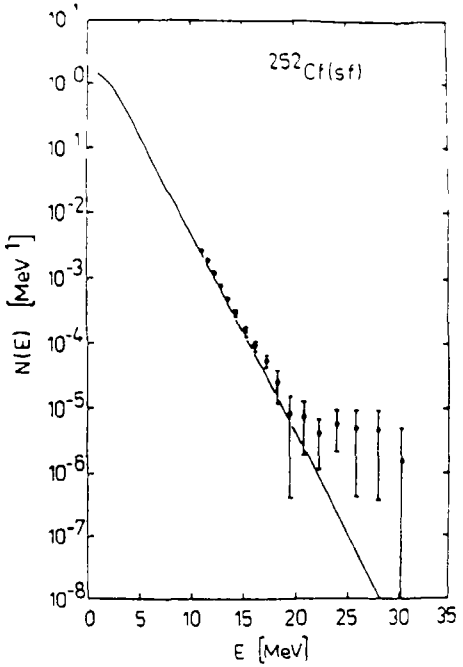

Figure 7

11.0-30.0 MeV in Figure 7. The experimental data of Böttger et al. [40a,b] give partial support to [39] but have not been shown in Figure 7 as the data were preliminary. The data from Chalupka et al. [60] were not available prior to the meeting.

It can be seen from a perusal of Figures 5-7 that the data show significant departures from the reference Maxwellian throughout the entire energy range. For the energy range 0.4-1.0 MeV, the four experiments, [31], [33], [35] and [36] consistently show a negative departure of the order of 2 to 4%. The departure is more pronounced in Poenitz and Tamura [33] and Boldeman et al. [36], but both Blinov et al. [31] and Laytai et al. [35] show a nett negative deviation.

Below 0.4 MeV, the data from Boldeman et al. [36] differ from the other three experiments in showing a positive deviation: however, the authors have pointed out problems with their experiment in this region. At lower energies, below 0.2 MeV, the data from Blinov et al. [31] and Laytai et al. [35] suggest that the spectrum may return to the reference Maxwellian. The experimental data from Starostov et al. [37] shown in Figure 8(a) support the trend of the data discussed above, except that at low energies they show a positive deviation. For the purpose of obtaining a representative spectrum, the four experiments [31], [33], [35] and [36] were given equal weight in small energy bins from 0.4-1.0 MeV and averaged. Below 0.4 MeV, the data of ref. [36] were excluded from the average.

The data from the six experiments [31], [33], [34], [36], [39] and [59] shown in Figures 6(a) (b) and (c) for the energy range 1.0-15.0 MeV are consistent in showing a positive deviation from 1.0-5.0 MeV with a peak at about 3.0 MeV. The deviation seen in the data of Poenitz and Tamura [33] is slightly larger than that of the other experiments. Above 5.0 MeV, all experiments show a negative deviation which increases with energy. The deviation seen by Böttger et al. [34 and 59] slightly exceeds that of the others. To arrive at a representation of the trend of the data, the data from each experiment were averaged in fairly broad energy bands and then all experiments were given equal weight and averaged. The exceptions were that above 10.0 MeV, the data of Boldeman et al. [36] were given half the weight of Marten et al. [39] and Bottger et al. [59]. It was also assumed that the data from Bottger et al [34] were included in the analysis presented in [59]. The data of Li-An Li et al. [32] are shown in Figure 8(b) in comparison with the reference Maxwellian. This data set shows the same general trend, except that the departures tend to be somewhat larger. The data from the proton recoil measurements of Jasicek and Bensch [41] are shown in Figure 8(c). Their data are consistent with the time-of-flight data in showing a negative deviation near 10.0 MeV; however, the shape of the spectrum at lower energy is not in accord with other measurements.

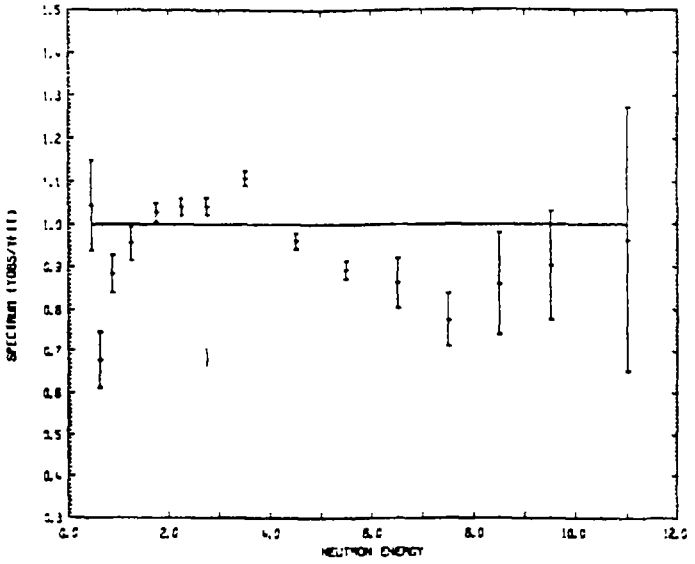

Figure 8(a)

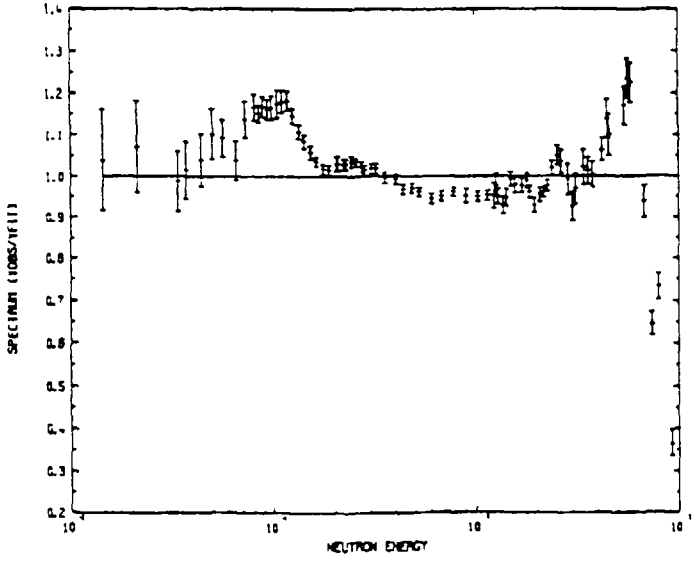

Figure 8(b)

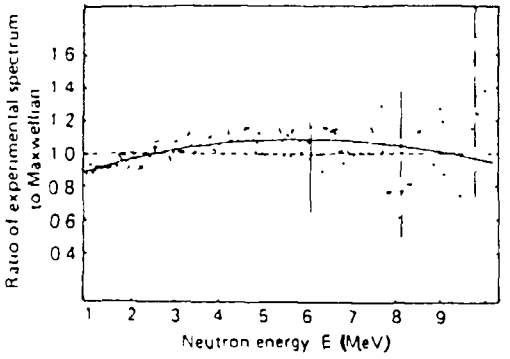

Figure 8(c)

5. CONCLUSIONS

The agreement between most of the post-1979 measurements is extremely good and the ^{252}Cf fission neutron spectrum can now be said to be known with reasonable precision as befits a reference standard. Figure 9 presents a representation of the majority of the experimental data between 0.01 and 20.0 MeV, but does not constitute a full evaluation. A full evaluation of the data will be presented at this meeting by Mannhart [61]. The errors shown essentially reflect the distribution of the data. The representation in Figure 9 shows a negative deviation from 0.2 to 1.0 MeV, a positive deviation between 1 and 5 MeV with a maximum at about 3 MeV and an increasingly negative deviation above 5 MeV. Above 20 MeV, the one experiment that has been finalised shows a large positive excess with respect to the reference Maxwellian. However the experiment of Chalupka et al.[60] which was performed in a mine at a depth of 600 m, giving a background reduction of approximately 5 orders of magnitude, did not see the large positive excess above 20 MeV. It is possible therefore that this effect may not be genuine. Below 0.2 MeV, two of the experiments produced data consistent with no deviation from the reference Maxwellian, while a third shows a positive excess. It may

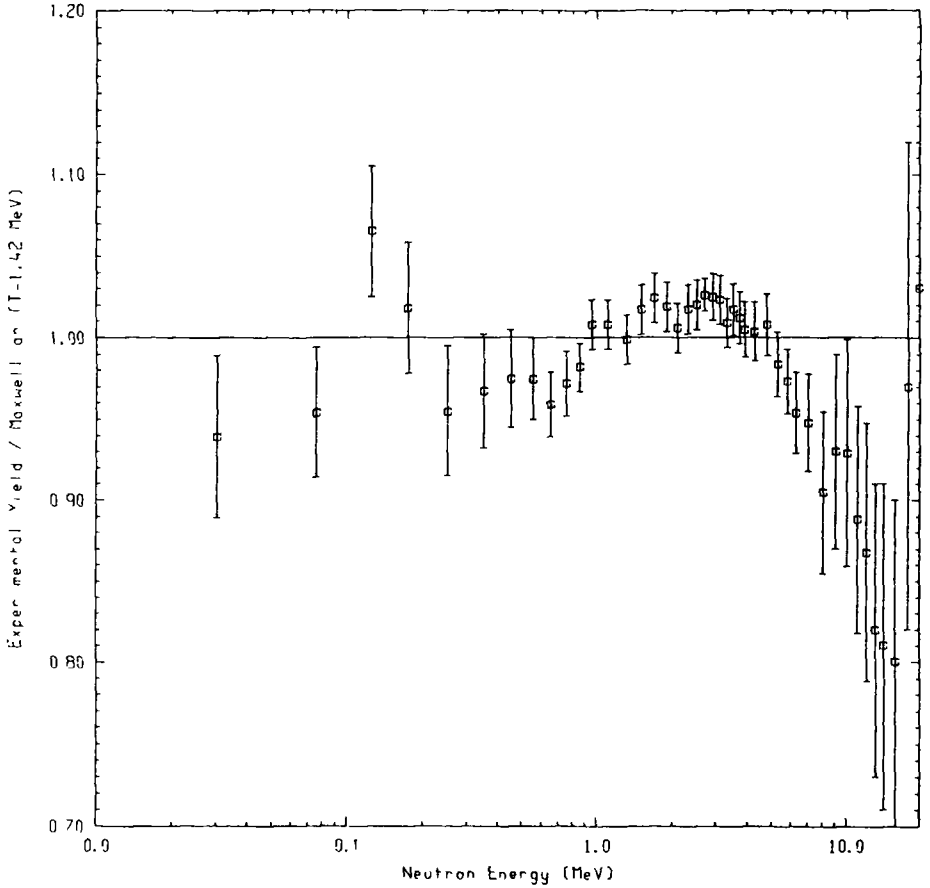

FIGURE 9.

be concluded, therefore, that between 0.2 and 20.0 Mev the spectrum is known sufficiently well that further measurements in this region are not necessary. Below 0.2 MeV further measurement could lead to an improvement in the status of the data.

6. REFERENCES

[1] Proc. IAEA Panel Neutron Standard Reference Data, Vienna, Austria 20-24 Nov 1972, CONF-721127, p. 362, International Atomic Energy Agency, Vienna (1973).

[2] Proc. IAEA Consultants' Meeting Prompt Fission Neutron Spectra, Vienna, Austria, 25-27 Aug 1971, p. 169, International Atomic Energy Agency, Vienna (1979).

[3] Smith, A. Günther, P., Sjoblom, R. (1977) - Nucl. Instrum. and Methods 140, 397.

[4] Mannhart, W. (1982) - Proc. Int. Conf. Nuclear Data for Science and Technology, Antwerp, Belgium, 6-10 Sept 1982, p. 429. (K.H. Böckhoff, Ed.) Reidel Publishing Company (1982).

[5] Boldeman, J.W. (1977) - Proc. Int. Specialists' Symp. Neutron Standards and Applications, Gaithersburg, Maryland, Special Publication 493, p. 182, National Bureau of Standards.

[6] Blinov, M.V. (1980) - Proc. IAEA Consultants' Meeting Neutron Source Properties, Debrecem March, International Atomic Energy Agency Report INDC(NDS)-114/GT, p. 79.

[7] Hjalmar, E.M. et al. (1955) - Ark. Fys. 10, 357.

[8] Smith, A.B., Fields, P.R., Roberts, J.H. (1957) - Phys. Rev. 108, 411.

[9] Bonner, T.W. (1961) - Nucl. Phys. 23, 116.

[10] Bowman, H.R., Thompson, S.G., Milton, J.C.D., Swiatecki, W.J. (1962) - Phys. Rev. 126, 2120.

[11] Condé, H., During, G. (1965) - Ark. Fys. 29, 313.

[12] Meadows, J.W. (1967) - Phys. Rev. 157, 1076.

[13] Green, L. (1969) - Nucl. Sci. Eng. 37, 232.

[14] Zamjatnin, Yu. S. et al. (1970) - Proc. 2nd Int. Conf. Nuclear Data for Reactors, Helsinki, 1970, p. 183, International Atomic Energy Agency, Vienna (1970).

[15] Jéki, L., Kluge, Gy., Laytai, A., Dyachenko, P.P., Kuzminov, B.D. (1972) - Atomnaya Energiya 33, 785 (Rus).
Jéki, L., Kluge, Gy., Laytai, A., Dyachenko, P.P., Kuzminov, B.D. (1972) - Proc. IAEA Consultants' Meeting Prompt Fission Neutron Spectra, Vienna, 1971, p. 81, International Atomic Energy Agency, Vienna (1972).

[16] Werle, H., Bluhm, H. (1971) - Proc. IAEA Consultants' Meeting Prompt Fission Neutron Spectra, Vienna, 1971, p. 62, International Atomic Energy Agency, Vienna (1972).

[17] Green, L., Mitchell, J.A., Steen, N.M. (1973) - Nucl. Sci. Eng. 50, 257.

[18] Knitter, N.N., Paulsen, A., Liskien, H., Islam, M.M. (1973) - Atomkernenergie 22, 84.

[19] Spiegel, V. (1974) - Nucl. Sci. Eng. 54, 28.

[20] Alexandrova, Z.A. et al. (1974) - Atomnaya Energiya 36, 282 (Rus).

[21] Kotelnikova, G.V. et al. (1975) - Report FEI-575 (Rus).
Kotelnikova, G.V. et al. (1975) - Proc. 3rd All Union Conf. Nejtronnaya Physica, Kiev, 1975, No.5; Obninsk 1975, p. 109 (Rus).

[22] Johnson, R.H. et al. (1975) - Trans. Am. Nucl. Soc. 22, 727.

[23] Csikai, J., Dezsö, Z. (1976) - Ann. Nucl. En. 3, 11/12, 527.

[24] Batenkov, O.I. et al. (1975) - Proc. 3rd All Union Conf. Netronnaya Physica, Kiev, 1975, No. 5, Moscow 1976, p. 114 (Rus).

[25] Blinov, M.V., Vitenko, V.A., Touse, V.T. (1977) - Proc. Int. Symp. Neutron Standards and Applications, Gaithersburg, 1977, Special Publication 493, p. 194, National Bureau of Standards.

[26] Dyachenko, P.P. et al. (1977) - Atomnaya Energiya 42, 25 (Rus).

[27] Nefedov, V.N. et al. (1977) - Proc. 4th All Union Conf. Netronnaya Physica, Kiev, 1977, No. 3; Moscow 1977, p. 205 (Rus).

[28] Bertin, A., Frehaut, J. (1978) - Report CEA-R-4895.

[29] Starostov, B.I. et al. (1978) - Report NJJAR P-22(356), Dimitrovgrad (Rus).

[30] Blinov, M.V., Vitenko, V.A., Yurevich, V.I. (1980) - Proc. 5th All Union Conf. Neutron Physics, Kiev, 1980, Moscow 1980 No. 3, p. 109.

[31] Blinov, M.V. Boykov, G.S., Vitenko, V.A. (1982) - Proc. Int. Conf. Nuclear Data for Science and Technology, Antwerp, Belgium, 6-10 Sept 1982, p. 465 (K.H. Böckhoff, Ed.) Reidel Publishing Company (1982).

[32] Li An-Li, Huang Tang-Zi, Bai Zi-Xang, Chen Guan-Ren, Wen Shen-Lin, Yao Ling (1982) - Chinese J. Nucl. Phys. 4, 145.

[33] Poenitz, W.P., Tamura, T. (1982) - Proc. Int. Conf. Nuclear Data for Science and Technology, Antwerp, Belgium, 6-10 Sept 1982, p. 465 (K.H. Böckhoff, Ed.) Reidel Publishing Company (1982).

[34] Böttger, R., Klein, H., Chalupka, A., Strohmaier, B. (1982) - Proc. Int. Conf. Nuclear Data for Science and Technology, Antwerp, Belgium, 6-10 Sept 1982, p. 484 (K.H. Böckhoff, Ed.) Reidel Publishing Company (1982).

[35] Laytai, A., Dyachenko, P.P., Kutzaeva, L.S., Kononov, V.N., Androsenko, P.A., Androsenko, A.A. (1983) - Proc. IAEA Consultants' Meeting ^{252}Cf Fission Neutron Spectrum, Smolenice, Czechoslovakia, International Atomic Energy Agency Report INDC(NDS)-146, p. 177, Vienna 1983.

[36] Boldeman, J.W., Clancy, B.E., Culley, D. (1986) - Nucl. Sci. Eng. 93, 181.

[37] Starostov, B.I., Semenov, A.F., Nefedov, V.N. (1980) - USSR Atomic Energy Committee Report on Nuclear Constants, No. 2, p. 37.

[38] Boystov, A.A., Starostov, B.M. (1984) - Proc. 6th All Union Conf. Neutron Physics, Kiev, 1983, Moscow 1984, No. 2, p. 298.

[39] Märten, H., Seeliger, D., Stobinski, B. (1982) - Proc. Int. Conf. Nuclear Data for Science and Technology, Antwerp, Belgium, 6-10 Sept 1982, p. 488 (K H Böckhoff, Ed.) Reidel Publishing Company 1982.

[40] Bottger, R., Fromm, W.D., Klein, H., Märten, H., Richter, H., Seeliger, D (1985) - Proc. Int. Conf. Nuclear Data for Basic

and Applied Science, Santa Fe, New Mexico, 13-17 May 1985 (to be published).
Märten, H., et al. (1984) - Proc. IAEA AGM Nuclear Standard Reference Data, Geel, Belgium, 12-16 Nov 1984, International Atomic Energy Agency Report TECDOC 335, p. 310.

[41] Jasicek, H., Bensch, F. (1981) - Nucl. Sci. Eng. 77, 51.

[42] Bolshov, V.I. et al. (1981) - USSR Atomic Energy Commission Report on Nuclear Constants, No. 3, p. 43.

[43] Smith, A.B. (1971) - Proc. IAEA Consultants' Meeting Prompt Fission Neutron Spectra, Vienna, Austria, 25-27 Aug 1971, p. 3, International Atomic Energy Agency, Vienna (1973).

[44] Koster, A. (1971) - Proc. IAEA Consultants' Meeting Prompt Fission Neutron Spectra, Vienna, Austria, 25-27 Aug 1971, p. 19, International Atomic Energy Agency, Vienna (1973).

[45] Ferguson, A.T.G. (1973) - Proc. IAEA Panel Neutron Standards Reference Data, Vienna, Austria, 20-24 Nov 1973, p. 337, International Atomic Energy Agency, Vienna (1973).

[46] Grundl, J.A., Eisenhauer, C.M. (1975) - Proc. Conf. Neutron Cross Sections and Technology, Washington, 1975, 1 NBS-425 (1975) 250, National Bureau of Standards.

[47] Knitter, H.H. (1976) - International Atomic Energy Agency Report IAEA-208, Vol. I, p. 183, Vienna.

[48] Proc. IAEA Consultants' Meeting ^{252}Cf Fission Neutron Spectrum, Smolenice, Czechoslovakia, 1983, International Atomic Energy Agency Report INDC(NDS)-146, p. 23, Vienna, Recommendations. Chairmen: Klein, H. and Blinov, M.V.

[49] Proc. IAEA AGM Nuclear Standards Reference Data, Geel, Belgium, 1985, International Atomic Energy Agency Report IAEA-TECDOC 335, p. 26, Recommendations. Chairman: Boldeman, J.W.

[50] Dietze, G., Klein, H. (1982) - PTB-ND-22.

[51] Dietze, G., Klein, H. (1982) - Nucl. Instrum. and Methods 193, 549.

[52] Blinov, M.V., Vitenko, V.A., Dushin, V.N., Yurevich, V.I. (1982) - Nucl. Instrum. and Methods 198, 455.

[53] Stanton, N.R. (1971) - COO-1545-92.

[54] Chalupka, A., Strohmaier, B., Klein, H., Bottger, R. (1983) - Proc. IAEA Consultants' Meeting ^{252}Cf Fission Neutron Spectrum, Smolenice, Czechoslovakia, 1983, International Atomic Energy Agency Report INDC(NDS)-146, p. 187, Vienna.

[55] Chalupka, A. (1979) - Nucl. Instrum. and Methods 164, 105.

[56] Chalupka, A. (1979) - Nucl. Instrum. and Methods 165, 103.

[57] Blinov, M.V., Boykov, G.S., Vitenko, V.A. (1984) - International Atomic Energy Agency Report INDC(CCP)-238, Vienna.

[58] James, D.G. (1977) - Proc. Int. Specialists' Symp. Neutron Standards and Applications, Gaithersburg, Maryland, 1977, Special Publication 493, p. 319, National Bureau of Standards.

[59] Böttger, R., Klein, H., Chalupka, A., and Strohmaier, B. (1986) Proc. IAEA Advisory Group Meeting on Properties of Neutron Sources, Leningrad, USSR, 1986, International Atomic Energy Agency Report

[60] Chalupka, A., Malek, L., Tagesen, S. and Böttger, R. (1986) Proc. IAEA Advisory Group Meeting on Properties of Neutron Sources, Leningrad, USSR, 1986, International Atomic Energy Agency Report

[61] Mannhart, W. (1986) Proc. IAEA Advisory Group Meeting on Properties or Neutron Sources, Leningrad, USSR, 1986, International Atomic Energy Agency Report

144 THEORETICAL DESCRIPTION OF THE Cf-252 FISSION NEUTRON SPECTRUM

H MARTEN
Technical University of Dresden,
Dresden, German Democratic Republic

Abstract

Starting with a characterization of the fission process related to fission neutron emission and corresponding theoretical concepts this review considers basic principles of a statistical-model approach to fission neutron spectra based on the assumption that all prompt fission neutrons are evaporated from fully accelerated fragments. Further possible emission mechanisms are discussed.
Recent theoretical descriptions of the Cf-252 (sf) neutron spectrum are summarized focusing on emission models (statistical formalism) as well as on the procurement of necessary fragment data. The present status of fission theory concerning the prediction of fragment distributions in nucleon numbers N, Z, kinetic energy E_k, excitation energy E^x, and spin I is evaluated.
Finally this review characterizes the applicability of the different fission neutron emission models considered to any fission reaction as well as their accuracy discussed on the basis of the Cf-252(sf) neutron spectrum calculation.

1. Introduction

As discussed in a recent review[1], the general understanding of prompt fission neutron emission requires some basic problems to be solved:

i) the role of friction in conjunction with large-amplitude collective motion, specifically diabatic single-particle excitation and particle emission due to rapid changes of potential (descent from saddle point to scission point),

ii) dissipation of excess deformation at scission into intrinsic excitation (main source of fragment excitation)

iii) correlation of fragment excitation with the scission configuration which defines a complex fragment probability distribution as function of N, Z(A = Z+N), total kinetic energy TKE, E^x, I, etc.

iv) neutron emission models for different mechanisms.

The stated questions indicate that prompt neutron emission is strongly connected with fission dynamics (paragraph 2). Neutrons emitted at a time close to scissen (cf. item i) are called "scission neutrons". Their existence predicted in the early paper of Bohr and Wheeler[2] was shown on the basis of the experimental energy and angular distribution $N(E,\theta)$ of fission neutrons[3], but considering a rough theoretical description as reference of this analysis. Experimental scission neutron data summarized elsewhere[1,4] exhibit large contradictions. In agreement with the general characteristics of experimental neutron emission distributions from fission, the evaporation from fully accelerated fragments is considered as the predominant mechanism of prompt neutron emission in fission commonly. However, statistical-model approaches published are based on different assumptions and formalisms. The complexity of fission and fission neutron emission is considered to a certain extent. We recapitulate recent treatments already reviewed[5] and discuss new modifications (paragraph 3). The application of these models requires the knowledge of different fragment data (cf. item iii) whose multitude depends on the kind of the model.
Generally experimental fragment data if available are more reliable than theoretical predictions. However, the determination of distributions in E^x on the basis of experimental neutron and γ-ray data depends on theoretical assumptions, too. The status of fission models relevant to neutron emission studies is discussed in paragraph 4.

2. The fission process and mechanisms of prompt fission neutron emission

Fission dynamics have been treated in the framework of different kinds of models. One extreme, the adiabatic model, excludes the excitation of single-particle degrees of freedom during the descent from the saddle point of the fission barrier to the scission point.[6] Assuming that the energy available at scission is shared among all degrees of freedom according to the laws of thermal equilibrium, one deals with the other extreme (statistical model)[7], i.e. strong single-particle excitation during the descent from saddle to scission point (viscous transition). Several intermediate models have been proposed[8-12]. They account for the coupling of the fission mode to different collective degrees of freedom and/or intrinsic degrees of freedom. The assumptions made are different and partly contrary. However, all these models are suited to describe the general features of nuclear fission more or less reasonably, but it is not possible to obtain a sufficiently good quantitative agreement with experimental data on fragment distributions (cf. paragraph 4). In any case, the consideration of shell effects is of fundamental importance for the understanding of low-energy fission and the diversity of scission configurations specifically.[13] The shell energies (depending on deformation and intrinsic temperature[11]) of complementary fragments define the ratio of their excess deformation at scission and, therefore, the value of their final excitation energy. This can be illustrated by the experimental data on neutron and γ-ray emission in fission as a function of TKE (elongation of the scission configuration) and A_1/A_2 (mass asymmetry).[14]

Different studies[15-19] of single-particle excitation due to the rapid change of nuclear potential in fission resulted in the qualitative conclusion that this appearance might be considerable. Nevertheless, quantitative estimations are quite uncertain. It is likely that the degree of single-particle excitation is correlated with the scission configuration defined by TKE and A_1/A_2 mainly.

The dissipation occuring during the descent from saddle point to scission can be of different types: one-body or two-body dissipation. Negele et al.[20] studied the evolution of the fissioning system applying the time-dependent Hartree-Fock (TDHF) method. The transition time between saddle point and scission was found to be in the order of some 10^{-21}s ($\approx 3 \cdot 10^{-21}$s). The corresponding fast change of deformation might give rise to a considerable single-particle excitation and, consequently, "scission neutron" emission.[15,16] Mädler[21] studied fast-particle emission in the framework of TDHF for scissioning nuclear systems (catapult mechanism) recently.

A new three-dimensional quantummechanical description based on a two-potential model yield energy and angular distribution of emitted neutrons.[22] A predominantly polar emission was obtained as in Mädler's model, i.e. similarity to the distribution of evaporated neutrons (main component). A verification of both theories is therefore very difficult.

In general, all hitherto published theoretical treatments of scission neutron emission give some first clues for an understanding only.

As mentioned above, experimental data on scission neutrons are poor and contradictory. It was shown recently[1] that the non-adequate theoretical treatment of the main fission neutron component, i.e. consideration of the complexity of fission reflected by an intricate fragment distribution, gives rise to systematic errors of data analysis.

The truth of earlier scission neutron data has been questioned, since they have been obtained on the oasis of rough evaporation models.

Ternary fission is connected with the preferred release of neutron-enriched light nuclei due to the neutron excess in the neck of the scissioning nucleus.[10]

Cheifetz et al.[23] found that about 11 % of alpha-particles from $^{252}Cf(sf)$ are originally emitted as n-unstable ^{5}He nuclei decaying in an alpha-particle and a neutron with a half-life of about 8.10^{-22}s. Such neutrons are predominantly directed in the equatorial plane obviously.

A calculation of their energy and angular distribution[1] has shown that this component is of minor importance. It doesn't disturb the total fission neutron distribution in energy and angle significantly.

Two simultaneous processes occuring after scission within some 10^{-20}s are of special interest: the fragment acceleration in the Coulomb field and the dissipation of excess deformation energy into intrinsic excitation. Neutron emission can occur in this time. The corresponding energy and angular distribution depends on time obviously.
Neutron evaporation during fragment acceleration was investigated on the basis of arbitrary assumptions concerning E^x as function of time[24-26]. The study of post-scission dynamics by Samanta et al.[27] resulted in an estimation of the dissipated energy depending on time (one-body friction). This was the basis of a new calculation in the framework of the statistical model.[1]
A remarkable influence of this component has been only found if assuming unreasonably short neutron life times (high nuclear temperatures $\gtrsim$ 2 MeV), i.e. simulation of non-equilibrium.
The role of non-equilibrium effects in the dissipation process of fragments is not yet clear.

The main mechanism of fission neutron emission, i.e. neutron evaporation from fully accelerated fragments, comes into action after the sufficiently high excitation of the originally deformed fragments (10^{-20}s).
The main sources of fragment excitation energy are[28]

- the excess fragment deformation at scission E_d,
- the velocity of collective degrees of freedom at scission,
- a contribution due to diabatic single-particle excitation before scission as already discussed,
- (in the case of induced fission) the excess excitation energy at the saddle point of the fission barrier ("heat" energy subdivided among the complementary fragments according to thermodynamics).

E_d contributes to E^x mainly in the case of low-energy fission. It is strongly dependent on shell effects[11,28,29] yielding the well-known saw-tooth curve of $\overline{E^x}(A)$.
The theoretical description of neutron evaporation from fully accelerated fragments requires the application of a statistical-model approach[1,4] to be attributed to a diversity of fragment configurations covering excitation energies up to 50 MeV.

3. Statistical-model approach to fission neutron emission

3.1. Basic principles

Calculations of fission neutron emission probabilities considering all possible emission mechanisms are infeasible at present. It was emphasized above that the description of the main mechanism, i.e. evaporation from fully accelerated fission fragments, is a complex task due to the necessary consideration of many characteristics of fission and fission neutron emission:

i) complex fragment distribution as discussed in paragraph 1, item (iii), i.e. $P(E^x,I,A,Z,TKE)$ depending on the characteristics of the fissioning nucleus,

ii) cascade neutron emission from highly-excited, neutron-enriched fragments in competition to γ-emission.

The fragment distribution P cannot be derived from fission theory completely and/or with sufficient accuracy (see paragraph 4). Therefore, one has to consider experimental data and/or special assumptions.
The CMS spectrum $\varphi(\varepsilon)$ is calculated in the framework of either the Weisskopf formalism[30] (without P(I) consideration) or the Hauser-Feshbach theory[31]. In any case, the level density $\varrho(U,I')$ of the residual nucleus with excitation energy U and angular momentum I' and the transition probabilities, i.e. the inverse cross section σ_c of compound-nucleus formation or the transmission coefficients respectively, have to be taken in account. Using the Weisskopf ansatz one can approximately consider the influence of the spin distribution on spectrum shape if assuming $\varrho(U,I) = \varrho(U,I=0)$[32].
The emission of fission neutrons is not isotropic in the center-of-mass system (CMS) of the fragments due to the fragment spin[33]. This influence is often neglected. The average spin amounts to about $(6 \div 8)\hbar$[34] yielding a CMS anisotropy close to 10 %[35].
The function $\varphi(\delta)$, i.e. CMS angular distribution, has been assumed to be independent on ε in Refs. 36, 4 and 37. According to the classical description of angular distributions of particles emitted from compound nuclei with a given average angular momentum[33], it is likely that the anisotropy is nearly proportional to ε (cf. paragraph 3.3).

The complex statistical-model approach to fission neutron emission based on the main mechanism can be stated by the following relation:

$$\varphi(\varepsilon,\delta : A,Z,TKE) = \sum_i \sum_I \int dE^x \cdot P_i(E^x,I:A,Z,TKE) \cdot \varphi_i(\varepsilon,\delta:E^x,I,A,Z), \quad (1)$$

i.e. the emission probability is calculated for a fixed fragment configuration defined by A,Z, and TKE. The sum over i (emission step index) means consideration of cascade emission.

The transformation of the CMS distribution into the laboratory system LS is carried out by the use of the formulae

$$N(E,\Theta)\, dE d\Omega = \sqrt{\frac{E}{\varepsilon}} \cdot \varphi(\varepsilon,\delta)\, dE d\Omega , \quad (2)$$

where

$$\varepsilon = E + E_f - 2 \cdot \sqrt{E \cdot E_f} \cdot \cos\Theta , \quad (3)$$

$$E_f = \frac{E_k}{A} = TKE \cdot \left[\frac{1}{A} - \frac{1}{A_{FN}}\right] \quad (4)$$

(E,Θ are the LS energy and angle respectively; A_{FN} is the mass number of the fissioning nucleus).

The weighted concentration taking into account the fragment occurance probability P(A,Z,TKE) yields LS emission probabilities for eligible fragment parameter bins. Specifically the total distributions $N(E,\Theta)$ and N(E) can be derived.

3.2. Recent theoretical treatments

The whole scheme of Eq. (1) has not yet been realized in praxis. Most of the hitherto published treatments rely on average fragment parameters, i.e. the diversity of fragment configurations is often neglected. The influence of several approximations is discussed in paragraph 3.3.

The Madland-Nix-Model (MNM)[38] is based on a simplified distribution P(T) in nuclear temperature of the residual fragments which is triangular in shape extending from 0 to the maximum temperature T_m. In this way, $P_0(E^x)$ and the cascade emission are considered roughly. It is assumed that P(T) is unique for the both considered fragment groups. σ_c and the CMS-LS transformation are considered in regard of average fragment group parameters. A model similar to the MNM was proposed recently[39]. Here, P(T) is modified to consider it more realistically. A further modified version of the MNM was used by Walsh[40]. He introduced the CMS anisotropy $B = 0.1$ (see Eq. 5) in this model.

The A dependence of T_m, E_f, σ_c, and the weight of the partial spectra is taken into account in the generalized Madland-Nix model (GMNM)[41], i.e. the complexity of fission fragment configurations is considered in more detail. Both the MNM and the GMNM are, however, rather rough models because of the assumption of an idealized temperature distribution and the use of a simplified Weisskopf ansatz based on the constant-temperature discription of nuclear level density. An extension of the GMNM has been worked out at TUD[42] recently to make the model applicable to any fission reaction (GMNM 2). The two-spheroid model is used to predict necessary fragment data ($\overline{E_k}$, $\overline{E^X}$) as a function of A. Further, the CMS anisotropy as well as a lower T limit in P(T) (to account for the influence of neutron/γ-ray competition roughly) is considered.

The concept of the complex cascade evaporation model (CEM)[5,37] corresponds to the scheme described in paragraph 3.1 but the explicit consideration of P(Z,I). Here, the Weisskopf formula is used to calculate $\varphi(\varepsilon: E^X, A)$ on the base of a semiempirical description of the level density $\varrho(U, I = 0)$ including shell and pairing correction. σ_c is calculated by the use of the optical model. Further, the initial distribution in excitation energy P_o (E^X : A, TKE) is assumed to be Gaussian for fixed A and TKE. The CMS anisotropy is considered roughly according to

$$\varphi(\varepsilon,\delta:A,TKE) = \varphi(\varepsilon:A,TKE) \cdot \frac{1 + \beta(\varepsilon) \cdot \cos^2 \delta}{1 + \frac{1}{3}\beta(\varepsilon)}. \qquad (5)$$

$\beta(\varepsilon)$ denotes the CMS anisotropy parameter.

Applying the Hauser-Feshbach theory for fission neutron spectrum calculations one is able to account for the competition of neutron and γ-ray emission as well as the initial distribution in fragment spin. The first study was presented by Browne and Dietrich[43]. Similar calculations have been done by the Leningrad group (HFC)[44] without consideration of CMS anisotropy and the spectrum dependence on Z and TKE.

Both the CEM and the HFC involve a more realistic consideration of $P_o(E^X)$ as well as improved semiempirical descriptions of the level density.

A review of earlier models of fission neutron emission was presented in Ref. 4.

3.3. Sensitivity of calculations in regard of approximations and input data variations

The study of sensitivity effects is a necessary precondition for the evaluation of the calculation accuracy as well as for the interpretation of systematic deviations between measured and calculated spectra. A first analysis in the framework of the CEM has been published in Ref. 4 for ^{252}Cf(sf) yielding the following conclusions:

i) The calculated average number of emitted neutrons is strongly changed by variations of $\overline{E^X}$ and the average neutron separation energy.

ii) The shape of the calculated spectrum is mostly sensitive to variations of $\overline{E^X}$, the width of $P(E^X)$, and the level density parameter.

iii) The calculated spectrum of the low-excited fragments with A close to 132 exhibits large uncertainties, specifically at energies higher than 3 MeV.

iv) The description of σ_c in the framework of the optical model reduces the average emission energy by about 5 % with reference to the calculation with constant σ_c.

v) If considering the TKE dependence of the spectra for fixed A, i.e. correct CMS-LS transformation (cf. Eq. 2-4), the calculated spectrum is strongly reduced at high energy (Fig. 1)

vi) The consideration of the CMS anisotropy yields an enhanced spectrum at low and high energy and a lower emission probability at intermediate energy (Fig. 2).

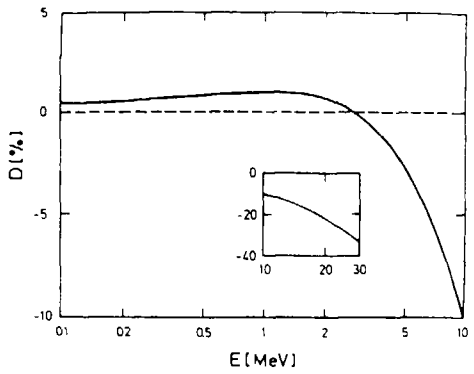

Fig. 1

Percentage deviations of the $^{252}Cf(sf)$ neutron spectrum calculated in the framework of the CEM including the full A, TKE-dependence from the Ef-approximated spectrum, i.e. neglection of the TKE dispersion at fixed A.

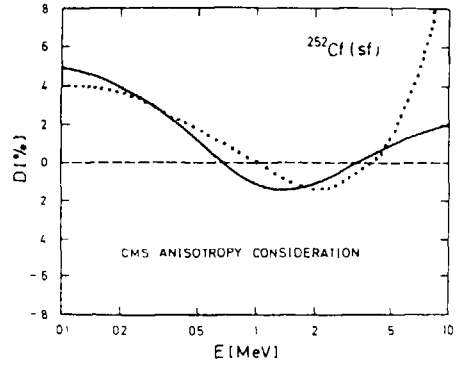

Fig. 2

Percentage departures of the $^{252}Cf(sf)$ neutron spectrum calculated in the framework of the CEM considering the CMS anisotropy from the ß = 0 calculation: ß = 0.1 (continuous line), ß = 0.1·E(dotted line).

3.4. The $^{252}Cf(sf)$ neutron spectrum and emission anisotropy

A comprehensive comparison of calculated $^{252}Cf(sf)$ neutron spectra (MNM, GMNM, CEM, HFC) with recent experimental data available with rather high accuracy in the 1 keV - 20 MeV energy region has been presented at the IAEA AGM on Nuclear Standard Reference Data.[5]

It has been shown that all statistical model versions considered yield similar results in the energy range 0.5 - 10 MeV.

The MNM and the HFC underestimate experimental data at high as well as at low energy.

The GMNM yields a clearly better description of the Cf spectrum at high energy. The result of the GMNM 2 calculation[42] is similar to the HFC spectrum at energies below 10 MeV. This new modification enables a very good description of the 10 - 20 MeV data.

The consideration of the neutron/γ-ray competition reduces the CMS spectra at low energy. This yields a diminution of the LS spectrum at E close to E_f, i.e. ≈0.55 MeV for the light fragment group, ≈0.98 MeV for the heavy one (cf. Eq. 2-4). This effect is present in both the HFC and GMNM 2 spectrum.

Furtheron, a comparison between experimental and theoretical anisotropy data for $^{252}Cf(sf)$ is presented. Fig. 3 shows measured points of different groups in comparison with calculations performed in the framework of both the CEM and the GMNM. Recent data[46,47] has been confirmed by the CBNM Geel group[48]. There is a good agreement between the statistical-model calculations and recent anisotropy data. Hence, all suggestions concerning the existence of a very hard emission component at equatorial direction ($\theta = 90^o$)[4] should be cancelled.

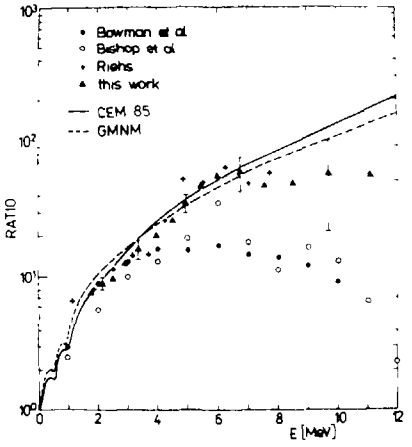

Fig. 3

Emission anisotropy ratio of $^{252}Cf(sf)$ neutrons defined by $[N(E,0^o) + N(E,90^o)] / (2.N(E,90^o))$: ● - Ref. 3, o - Ref. 45, + - Ref. 46, ▲ - Ref. 47.

4. On fragment data related to fission neutron models

The MNM is easily applicable to any fission reaction. No detailed fragment data are required. Average TKE values for the fission reactions concerned can be taken from systematics[49]

if not available from direct measurements. Nix et al.[50] use a dynamical calculation including dissipation described by a new surface-plus-window mechanism. Thus, they determine the average TKE value for the fission reaction considered. However, this treatment is only applicable to high-excitation fission, since single-particle shell and pairing effects which affect the potential energy, inertia, and dissipation in low-excitation fission are not taken into account.
All the other models characterized in paragraph 3.2 require the knowledge of a multitude of fragment data. Specifically the CEM including the full dependence on A and TKE is only applicable to $^{252}Cf(sf)$ and $^{235}U(n_{th},f)$, i.e. to well-studied fission reactions. The application of an approximative CEM discussed in the original paper[37] reduces the data procurement effort considerably.

The $\overline{E^x}(A)$ curve is usually deduced from measured neutron multiplicities and average γ-ray energies (total). The variance of the distribution in E^x can also be obtained from an analysis of neutron multiplicity functions.[14,37]

How accurate are, however, predictions of fragment distributions in the framework of fission theory? Specifically the scission-point model including deformed-shell effects[11] is successful in describing qualitative properties of fission for a wide range of fissioning nuclei at different incident energies. Nevertheless, the calculated fragment mass and kinetic-energy distributions are too narrow. Further, the deduced averages for the fragment groups deviate from experimental values appreciably. The consideration of dynamical aspects based on the use of the Fokker-Planck equation for the distribution function of collective variables (concerning the descent from saddle to scission) solves this discrepancy partly.[51] Besides the tabulation or parametrization of fragment distributions there has not yet been developed a comparatively simple model (semiempirical) to deduce fragment data with sufficient accuracy.

A new thermodynamical model for the description of the fission process, specifically mass yield distributions, was developed by Grashin et al.[52] They obtain a rather good agreement with measured mass yield curves.

The use of the simple two-spheroid model including shell effects is proposed by the TUD group[42]. Effective shell energies have been deduced from experimental data for the well-known fission reactions $^{252}Cf(sf)$ and $^{235}U(n_{th},f)$. Considering the diminution of shell effects at high excitation energies, $\overline{TKE}(A)$ as well as $\overline{E^x}(A)$ can be calculated. In this way, the GMNM has been made applicable to any fission reaction. The same formalism can be applied to the other models, on principle.

The saw-tooth-like $\overline{E^x}(A)$ curve yielding a similar dependence of $\overline{\nu}$ on A was qualitatively explained on the basis of different ideas (Ref. 36 and Refs. therein, Refs. 6, 11, 53). However, shell effects affecting the scission configuration have been considered as responsible for this dependence directly or indirectly.
Finally it is mentioned that the angular momentum distribution of fission fragments has been calculated in the framework of a dynamical model by Dietrich and Zielinska-Pfabe.[54] The average angular momentum has been found to depend on A in a saw-tooth form due to the influence of shell effects.

5. Conclusions

The present review on theory of fission neutron emission (emphasizing the spontaneous fission of ^{252}Cf) is the occasion to the following concluding remarks:

- The total emission distribution of prompt fission neutrons has to be understood as a superposition of different mechanisms. The evaporation of neutrons from fully accelerated fission fragments has been unambigiously pointed out as the most important one.

- The existence of scission neutrons has not yet been verified neither experimentally nor theoretically. The experimental study of this component requires the use of an adequate statistical-model approach for the description of the predominant evaporated-neutron distribution, i.e. consideration of the diversity of fragment configurations manifested by an intricate fragment occurrence probability distribution. Otherwise, systematic errors are the reason of wrong scission neutron data.[1]
- Neutron emission due to the ^{5}He decay (after ternary fission) was found to be of minor importance.
- The theoretical description of neutron evaporation during fragment acceleration is very sensitive about post-scission data ($\overline{E^{x}}(t)$ and $\overline{E_{k}}(t)$) as well as the fragment life time in regard of neutron emission. It is indicated that probable input data (based on statistical equilibrium) don't yield an important disturbance of the total emission distribution.[1]
- Several recent statistical-model approaches are suited to describe the ^{252}Cf(sf) neutron spectrum in a wide energy range rather accurately. However, only complex models reproduce the high-energy data (10 - 20 MeV) satisfactorily (GMNM, CEM).
- Recently measured ^{252}Cf(sf) neutron emission anisotropies as function of E indicate no hard emission component in equatorial direction as found in earlier works. The new data have been described on the basis of a pure statistical-model approach.
- The use of statistical-model approaches requires the knowledge of a multitude of fragment data. Known fission theories fail to reproduce most of the experimental data with sufficient accuracy. Reasonable semiempirical treatments are needed to predict necessary fragment data for practical purposes.

References

1 H. Märten et al., Proc. Conf. on Nucl. Phys., Gaußig (GDR), 1985, in press

2 N. Bohr, J.A. Wheeler, Phys. Rev. 56 (1939) 426

3 H.R. Bowman et al., Phys. Rev. 126 (1962) 2120

4 H. Märten et al., Proc. IAEA Consultants' Meeting on the U-235 Fast-Neutron Fission Cross-Section and the Cf-252 Fission Neutron Spectrum, Smolenice (CSSR), 1983, INDC(NDS)-146/L (1983), 199

5 H. Märten, D. Seeliger, Proc. IAEA AGM on Nucl. Std. Ref. Data, Geel (Belgium), 1984, IAEA-TECDOC-335 (1985) 255

6 R. Vandenbosch, Nucl. Phys. 46 (1963) 129

7 P. Fong, Statistical Theory of Nuclear Fission (Gordon and Beach, 1969)

8 J.R. Nix, W.J. Swiatecki, Nucl. Phys. 71 (1965) 1

9 J.J. Griffin, Proc. IAEA Symp. on Physics and Chemistry of Fission, Vienna, 1969 (IAEA, Vienna, 1969) 3

10 W. Nörenberg, ibid., p. 51 and Phys. Lett. 31 B (1970) 621 and Phys. Rev. C 5 (1972) 2020

11 B.D. Wilkins et al., Phys. Rev. C 14 (1976) 1832

12 U. Facchini, G. Sassi, J. Phys. G 3 (1977) 269

13 V.M. Strutinski, Nucl. Phys. A 122 (1968) 1

14 H. Nifenecker et al., Proc. IAEA Symp. on Physics and Chemistry of Fission, Rochester, 1973 (IAEA, Vienna, 1974) Vol. II, 117

15 R.W. Fuller, Phys. Rev. 126 (1962) 684

16 Y. Boneh, Z. Fraenkel, Phys. Rev. C 10 (1974) 893

17 S.E. Koonin, J.R. Nix, Phys. Rev. C 13 (1976) 209

18 T. Ledergerber et al., Nucl. Phys. A 275 (1977) 280

19 G. Schütte, L. Wilets, Nucl. Phys. A 252 (1975) 21

20 J.W. Negele et al., Phys. Rev. C 17 (1978) 1098

21 P. Mädler, Z. Phys. A 321 (1985) 343

22 B. Milek et al., loc. cit. (1)

23 E. Cheifetz et al., Phys. Rev. Lett. 29 (1972) 805

24 V.P. Eismont, At. En. 19 (1965) 113

25 G.A. Pik-Pichak, Yad. Fiz. 10 (1969) 321

26 D.J. Hinde et al., Phys. Rev. Lett. 52 (1984) 986

27 B.C. Samanta et al., Phys. Lett. 108 B (1982) 83

28 B.G. Geilikman, O.V. Zimina, Yad. Fiz. 23 (1976) 1175

29 M. Vildir, N.K. Aras, Phys. Rev. C 25 (1982) 365

30 J.M. Blatt, V.F. Weisskopf, Theoretical Nuclear Physics (New York, 1952)

31 W. Hauser, W. Feshbach, Phys. Rev. 87 (1952) 366

32 E. Nardi et al., Phys. Lett. 43 B (1973) 259

33 T. Ericson, V. Strutinski, Nucl. Phys. 8 (1958) L 84

34 J.B. Wilhelmy et al., Phys. Rev. C 5 (1972) 2041

35 A. Gavron, Phys. Rev. C 13 (1976) 2561

36 J. Terrell, Phys. Rev. 113 (1959) 527

37 H. Märten, D. Seeliger, J. Phys. G 10 (1984) 349

38 D.G. Madland, J.R. Nix, Nucl. Sci. Eng. 81 (1982) 213

39 A.F. Graschin, M.V. Lopeschkin, At. En. 58 (1985) 59

40 R.L. Walsh, private communication (1986)

41 H. Märten, D. Seeliger, INDC(GDR)-30/L (1984) and Nucl. Sci. Eng. (1986)

42 H. Märten et al., contributed paper to this AGM (concerning GMNM 2)

43 J.C. Browne, F.S. Dietrich, Phys. Rev. C 10 (1974) 2545

44 B.F. Gerasimenko, V.A. Rubchenya, loc. cit. (5), p. 280

45 C.J. Bishop et al., Nucl. Phys. A 198 (1972) 161

46 P. Riehs, Act. Phys. Austr. 53 (1981) 271

47 H. Märten et al., Proc. Int. Conf. on Nuclear Data for Basic and Applied Science, Santa Fe (USA), 1985

48 C. Butz-Jørgensen, H.-H. Knitter, ibid.

49 V.E. Viola et al., Phys. Rev. C 31 (1985) 1550

50 J.R. Nix et al., loc. cit. (47)

51 G.D. Adeev, I.I. Gonchar, Z. Phys. A 320 (1985) 451 and Z. Phys. A 322 (1985) 479.

52 A.F. Grashin et al., I zv. Akad. Nauk, SSSR, Ser. Fiz. 49 (1985), 188, Engl. Transl.: Bull Acad. Sci. USSR, Phys. Ser. 49 (1985) 197.

53 U. Brosa, Phys. Rev. C 32 (1985) 1438

54 K. Dietrich, M. Zielinska-Pfabe, Ann. Phys. (1979)

CALCULATION OF PROMPT FISSION NEUTRON SPECTRA FOR APPLIED PURPOSES

H. MARTEN, A. RUBEN, D. SEELIGER
Technical University of Dresden,
Dresden, German Democratic Republic

Abstract

An extended version of the generalized Madland-Nix model is used to calculate the energy spectrum of fission neutrons as well as multi-differential emission probabilities (energy and angular distributions for different fragment mass numbers A). Besides the consideration of the compound-nucleus formation cross-section and the model dependence on A we introduce the center-of-mass system (CMS) anisotropy of neutron emission and a definite lower limit of the temperature distribution to account for the influence of neutron-gamma competition roughly. Fission energetics are studied in the framework of a simple two-spheroid model including shell correction energy. This treatment can be used to deduce necessary fragment data for any fission reaction semi-empirically.
The new fission neutron spectrum model is applied to the spontaneous fission of ^{252}Cf.

1. Introduction

The Madland-Nix model (MNM) for the calculation of fission neutron spectra N(E) had been generalized concerning the model dependence on fragment mass number A (GMNM)[2]. The latter one was applied to the spontaneous fission of ^{252}Cf (nuclear standard), for which the input data (fragment kinetic energy E_k, average fragment excitation energy $\overline{E^x}$, the average number of emitted neutrons $\bar{\nu}$, the fragment yield Y(A)) are known with high accuracy. The Cf energy spectrum can be well reproduced in a broad energy range (1 keV - 20 MeV) if adjusting the constant C for the description of the level density parameter a = A/C.
However, the applicability of the GMNM as well as its approximation (reduction to two fragment groups and use of averaged input parameters)[2] has been restricted due to the insufficient knowledge of the stated input parameters for many fission reactions.

Therefore, we propose an extension of the GMNM to calculate necessary fragment data in the framework of a rather simple two-spheroid model following a treatment of Terrell[3]. Furtheron, we consider the fragment spin giving rise to an emission anisotropy[4] in the center-of-mass system (CMS) of fission fragments as well as an lower limit T_o of the idealized residual-temperature distribution P(T) to account for the influence of neutron/γ-ray competition of fragment de-excitation.

2. The neutron emission model

The original MNM serves for the calculation of the CMS spectrum $\varphi(\varepsilon)$ according to

$$\varphi(\varepsilon) \sim \sigma_c(\varepsilon) \cdot \varepsilon \cdot \int_{T_o}^{T_m} P(T) \cdot \exp(-\frac{\varepsilon}{T})\, dT, \qquad (1)$$

where σ_c - compound-nucleus formation cross-section (to be calculated in the framework of the optical model),
and

$$P(T) = \begin{cases} \frac{2 \cdot T}{T_m^2 - T_o^2}, & T_o \le T \le T_m \\ 0, \text{ otherwise.} \end{cases} \qquad (2)$$

The maximum value T_m of the distribution P(T) is connected with $\overline{E^x}$. The Fermi-gas model state equation yields

$$T_m = \left[\frac{\overline{E^x}}{a}\right]^{1/2} = \left[\frac{\overline{E^x} \cdot C}{A}\right]^{1/2}. \qquad (3)$$

The CMS anisotropy, i.e. $\varphi(\varepsilon,\delta)$ (δ - CMS angle of neutron emission) is assumed as

$$\varphi(\varepsilon,\delta) \sim (1+\beta(\varepsilon) \cdot \cos^2\delta). \qquad (4)$$

$\beta(\varepsilon)$ is the anisotropy parameter, whose average is close to 0.1.[4] The emission probability distribution $\varphi(\varepsilon,\delta)$ is normalized to $\bar{\nu}$ to be calculated by the use of the expression

$$\bar{\nu} = \frac{\overline{E^x} - \overline{E_\gamma}}{B_n + \bar{\varepsilon}}, \tag{5}$$

where

$$\bar{\varepsilon} = \frac{4}{3} \cdot T_m \tag{6}$$

(MNM approximation for σ_c = const.)[1].
The average γ-ray energy (total) can be deduced from

$$\overline{E_\gamma} = (6.6867 - 0.15578 \cdot Z_{FN}^2 / A_{FN}) \cdot \bar{\nu} + (0.11127 \cdot Z_{FN}^2 / A_{FN} - 2.2408), \tag{7}$$

where Z_{FN}, A_{FN} - charge and mass number of the fissioning nucleus, respectively.

Eq. (7) has been obtained from experimental data (cf. Ref. 5) for $^{252}Cf(sf)$ and $^{235}U(n_{th},f)$. It holds true as a function of A and total kinetic energy TKE of fragments, too.
Assuming neutron evaporation from fully accelerated fragments, the transformation of $\varphi(\varepsilon,\delta)$ into the laboratory system (LS) is

$$N(E,\theta) = (E/\varepsilon)^{1/2} \cdot \varphi(\varepsilon,\delta), \tag{8}$$

where

$$\varepsilon = E + E_f - 2(E \cdot E_f)^{1/2} \cdot \cos\theta \tag{9}$$

(θ - LS angle of neutron emission, $E_f = \overline{E_k} / A$).

All the parameters of the described model

(σ_c, T_m, T_o, β, $\overline{E^x}$, $\overline{E_\gamma}$, $\bar{\varepsilon}$, $\overline{E_k}$) can be considered as a function of A, so that we calculate $N(E,\theta:A)$ or $N(E:A)$ (after integration over solid angle).

Taking into account the fragment mass yield Y(A) we obtain $N(E,\theta)$ and $N(E)$, respectively, by weighted addition (cf. Ref. 2).

β is assumed either constant (β=0.1) or proportional to according to the classical description of Ericson and Strutinski[6]. Both approximations result in similar influences on N(E) but the higher enhancement at high E in the second case.[7]
The most crucial fragment parameters of the model are $\overline{E^x}$ (A) and $\overline{E_k}$ (A).
They are not available for a series of fission reactions. Therefore, we propose the following treatment.

3. Two-spheroid model including shell corrections

The total available energy in any fission reaction is equal to the sum of the Q value, the binding energy of the incidence particle B_i, and its kinetic energy E_i. The energy balance yields

$$\overline{Q}(A_1/A_2) + B_i + E_i = \overline{TKE}(A_1/A_2) + \overline{E_1^x}(A_1) + \overline{E_2^x}(A_2) \tag{10}$$

The sum of the average excitation energies of complementary particles is equal to the sum of

- deformation energies E_d at scission,
- the excess "heat" energy E_H above the fission barrier, which is distributed according to thermodynamics ($\sim$ A),
- a certain amount of intrinsic excitation due to nuclear friction during the descent from saddle to scission point (E_S, which is assumed to be distributed equally on both fragments).

Consequently, we have

$$\overline{F}(A_1/A_2) = \overline{Q}(A_1/A_2) + B_i + E_i - E_H - E_S = \overline{TKE}(A_1/A_2) + \overline{E_{d1}}(A_1) + \overline{E_{d2}}(A_2). \tag{11}$$

Following the ideas of Terrell (Ref. 3 and Refs. therein), we assume that E_d is quadratic in radius change, i.e.

$$\overline{E_d} = \alpha\,(D - R_o)^2. \tag{12}$$

α is the deformation parameter related to the stiffness parameter C_2 as

$$C_2 = \frac{5}{2\pi} \cdot \alpha \cdot R_o^2 . \tag{13}$$

D is the major semi-axis of a spheroid, R_o is the radius of the corresponding spherical nucleus. If we assume, that TKE is the same as the Coulomb interaction energy between two charges $Z_1 \cdot e$ and $Z_2 \cdot e$ effectively located at the centres of the fragments, we find

$$\overline{TKE} = \frac{Z_1 \cdot Z_2 \cdot e^2}{D_1 + D_2 + d} \tag{14}$$

d amounts to about 1 fm and accounts for the nuclear interaction at scission.[8]

Minimizing $\overline{F}$ (potential energy at scission) i.e. $\partial F/\partial D_i = 0$, we get a set of equations

$$\overline{E}_{d1,2} = \frac{\overline{TKE}^4}{4 \cdot \alpha_{1,2} \cdot Z_1^2 \cdot Z_2^2 \cdot e^4}, \tag{15}$$

$$\text{i.e.} \quad \frac{\overline{E}_{d1}}{\overline{E}_{d2}} = \frac{\alpha_2}{\alpha_1} \quad \text{(cf. Ref. 10).}$$

If knowing $\alpha(A)$, one is able to deduce $\overline{TKE}(A_1/A_2)$ and $\overline{E_d}(A)$ by solving

$$\overline{F} = \overline{TKE} + \frac{\overline{TKE}^4}{4 \cdot Z_1^2 \cdot Z_2^2 \cdot e^4} \cdot \frac{1}{\alpha_1} + \frac{1}{\alpha_2} \tag{16}$$

and using Eq. (15).

Here, we assume[9]

$$Z_1 = \frac{Z_{FN}}{A_{FN}} \cdot (A - 0.5) \text{ light fragment),}$$

$$Z_2 = \frac{Z_{FN}}{A_{FN}} \cdot (A + 0.5). \tag{17}$$

4. Shell correction energy

On the basis of the well-known $\overline{\nu}$ data for $^{252}Cf(sf)$[5] and $^{235}U(n_{th},f)$[11], we deduced $\overline{E^x}(A)$ for both fission reactions by the use of the Eqs. (5), (6), and (3).

Assuming E_S = 5 MeV, we obtained $\overline{E_d}(A)$. These data and experimental values of $\overline{TKE}$ (Refs. 12 and 13, respectively) were taken to calculate $\alpha(A)$. The results are represented in Fig. 1 showing the deviations from the liquid-drop model (LDM) curve[3] indicating the influence of shell effects.

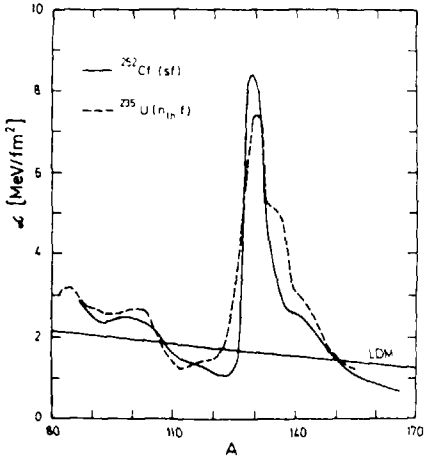

Fig. 1
Deformation paramter α as a function of A deduced from experimental fission data on the basis of the two-spheroid model (see text).

Mildir and Aras[10] considered the relation between C_2 and the shell correction energy δW by means of

$$C_2 = C_{2,LDM} \cdot \frac{K - \delta W}{K + \delta W} . \qquad (18)$$

The constant K was found to be equal to 8 MeV. Eq. (18) is also valid for α instead of C_2 (cf. Eq. (13)). Thus, $\delta W(A)$ can be deduced from the α data. Results obtained for the two analysed fission reactions are represented in Fig. 2.

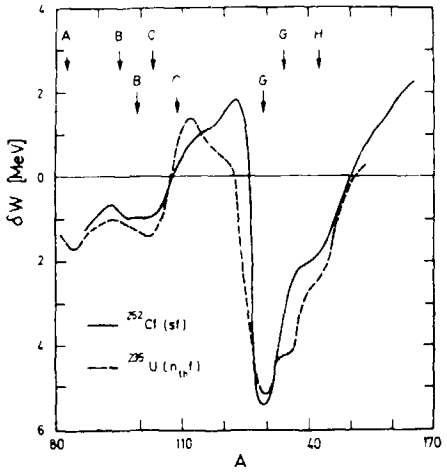

Fig. 2
Shell correction energies deduced from experimental fission data as a function of A. The arrows indicate the position of particular shell regions with negative sign as calculated by Wilkins et al.[8] The regions A and G correspond to closed neutron shells at N = 50 and N = 82, respectively. G is the closed-shell region for the proton system at Z = 50.

they can be understood on the basis of calculated shell corrections depending on deformation[8] (Strutinski method). Both $\delta W(A)$ curves deduced are quite similar. Distinctions are clear, if one takes into account the calculations of Wilkins et al.[8]

We propose the following semi-empirical treatment of shell corrections for any fission reaction in the actinide region. The actual $\delta W(A)$ curve is deduced by interpolation of the values deduced from Cf- and U-fission in terms of Z_{FN}^2 / A_{FN} (fissility parameter).

In the case of induced fission reactions, one has to consider the diminution of shell effects due to the enhanced temperature at scission (as a consequence of $E_H + E_S$).[8,14,15] The $\alpha(A)$ set and, finally, the $\overline{TKE}$ and $\overline{E}_d$ data are obtained by the use of the reversed procedure than that one described above. First calculations confirmed the applicability of the model. Here, we focus on the description of the Cf neutron spectrum according to the aim of the Advisory Group Meeting.

5. The ^{252}Cf(sf) neutron spectrum

Using the extended version of the GMNM (i.e. GMNM 2), N(E) and N(E,θ) of ^{252}Cf(sf) neutrons have been calculated.
We assumed the CMS anisotropy parameter β = 0.1, i.e. independent of $\mathcal{E}$. $\sigma_c(\mathcal{E}:A)$ has been calculated in the framework of the optical model accepting the Becchetti-Greenlees potential[16]. T_o was taken to be constant for all fragments and set to 0.2 MeV. We assumed C = 8.0 MeV (cf. Ref. 2).
For further input data, see paragraph 4 and Ref. 2.
The result is represented in Fig. 3 as percentage deviations from a Maxwellian distribution with kT = 1.42 MeV. The Cf spectrum calculated in the framework of the cascade evaporation model[17,18] is also shown for comparison. The shape of the GMNM 2 spectrum is quite similar to the result of the Hauser-Feshbach calculation of the RIL group.[19] This formalism includes the consideration of neutron/γ-ray competition which was simulated in our calculation by the lower temperature limit T_o. The GMNM 2 spectrum reproduces recent experimental data which are in good agreement with the CEM calculation for the energy range 1 keV - 20 MeV (see Fig. 3).[18]

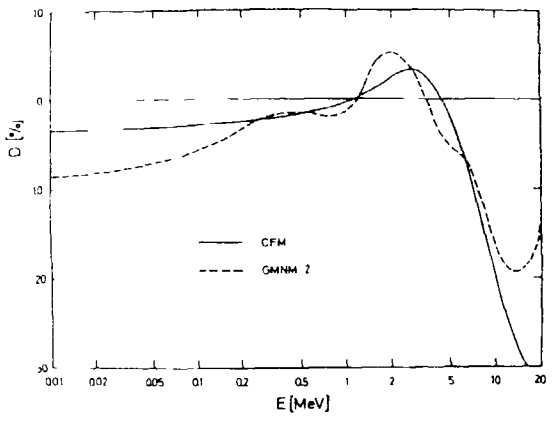

Fig. 3
Percentage deviations D of the calculated Cf spectrum (GMNM 2) from a Maxwellian distribution with kT = 1.42 MeV. The CEM spectrum[18] is shown for comparison.

6. Concluding remarks

The proposed extension of the GMNM concerning the consideration of CMS anisotropy and the lower temperature limit as well as its conjunction with the two-spheroid model including shell effects render it possible to calculate neutron spectra for any fission reaction in the actinide region. If the fragment mass yield curve is not known with sufficient accuracy, interpolation procedures based on the average masses of both fragment groups[26] and their variances $\sigma_A^2(E_i)$ can be used. In some cases, more accurate parametrizations are available.[13] Nevertheless, different fission theories fail to reproduce mass yield curves quantitatively, though they have been applied to explain a multitude of features of nuclear fission[8].
As an further alternative, the approximative GMNM[2] can be used, i.e. consideration of the two fragment groups represented by the averages of input data in each case.

In the present work, the $^{252}Cf(sf)$ and $^{235}U(n_{th},f)$ data have been considered to deduce effective shell correction energies. The $\delta W(A)$ curves obtained can be interpreted on the basis of shell energy calculations depending on deformation (Strutinsky method)[8].

Further, we introduced the dependence of shell effects on excitation energy (at scission) to make the model applicable to induced fission reactions. However, the energy E_S dissipated during the descent from saddle to scission can only be estimated roughly, since the actual value is not accessible neither experimentally nor theoretically. E_S is one of the controversional quantities in fission theory.

Acknowledgements

Fruitful discussions with Dr. R. Schmidt (TUD) and the help of Mr. D. Polster in calculating several quantities are greatfully acknowledged.

References

1 D.G. Madland, J.R. Nix, Nucl. Sci. Eng. 81 (1982) 213

2 H. Marten, D. Seeliger, INDC(GDR)-30/L (1984), Nucl. Sci. Eng. (1986)

3 J. Terrell, Proc. IAEA Symp. on Physics and Chemistry of Fission, Salzburg, 1965 (IAEA, Vienna, 1965), Vol. II, 3

4 A. Gavron, Phys. Rev. C 13 (1976) 2562

5 H. Nifenecker et al., Proc. IAEA Symp. on Physics and Chemistry of Fission, Rochester, 1973 (IAEA, Vienna, 1974), Vol. II, 117

6 T. Ericson, V. Strutinski, Nucl. Phys. 8 (1958) 284

7 H. Marten et al., Proc. Int. Symp. on Nucl. Phys., Gaußig (GDR), 1985, in press

8 B.D. Wilkins et al., Phys. Rev. C 14 (1976) 1832

9 J.P. Unik et al., loc. cit. (5), p. 19

10 M. Kildir, N.K. Aras, Phys. Rev. C 25 (1982) 365

11 J.W. Boldeman et al., Austr. J. Phys. 24 (1971) 821

12 H.W. Schmitt et al., Phys. Rev. 141 (1966) 1146

13 C.A. Strøde, Thesis, 1985 (CBNM Geel)

14 A.V. Ignatyuk et al., Yad. Fiz. 21 (1975) 485

15 A. Bohr, B.R. Mottelson, Nuclear Structure (Benjamin, New York, 1975), Vol. II., 607 (371)

16 F.D. Becchetti, Jr., G.W. Greenlees, Phys. Rev. 182 (1969) 1190

17 H. Marten, D. Seeliger, J. Phys. G 10 (1984) 349

18 H. Marten, D. Seeliger, Proc. IAEA Advisory Group Meeting on Nuclear Standard Reference Data, Geel (Belgium), 1984, IAEA - TECDOC-335 (1985) 255

19 B.F. Gerasimenko, V.A. Rubtchenya, Neutron Physics (Proc. All-Union Conf., Kiev, 1983), Moscow (1984) Vol. I, 349

20 K.F. Flynn et al., Phys. Rev. C 5 (1972) 1725

EVALUATION OF THE Cf-252 FISSION NEUTRON SPECTRUM BETWEEN 0 MeV AND 20 MeV

W MANNHART
Physikalisch-Technische Bundesanstalt,
Braunschweig, Federal Republic of Germany

Abstract

The results of seven recent measurements of the Cf-252 neutron spectrum were used in the evaluation. Based on the available information, for each experiment a complete uncertainty covariance matrix was generated. The data were combined by generalized least-squares techniques. The evaluation was carried out with 70 energy grid points between 25 keV and 19.8 MeV. The individual experimental data were extrapolated to these grid points by using the shape of a Maxwellian distribution specific for each experiment. The evaluation gave a value of χ^2 per degree of freedom of approximately unity and indicated no incompatibility between the experiments. The resulting relative uncertainty of the evaluation is smaller than 2 % between 180 keV and 9.3 MeV. A weighted spline interpolation between the discrete data points was used to generate a continuous shape of the evaluated neutron spectrum The result of the evaluation was compared with available theoretical descriptions of the Cf-252 neutron spectrum. None of the existing theories is compatible with the evaluation over the whole energy range.

1. Introduction

Measurements of the neutron spectrum of Cf-252 have been performed since 1955. In 1971/1972 the spectrum was defined as a standard /1, 2/ for neutron detector calibration and reactor dosimetry applications. Nevertheless, the shape of this neutron spectrum has not yet been unambigously defined. This discrepancy between definition and the actual state of the standard was a major problem for many years. A review of all experiments prior to 1979 /3/

reflects some of the difficulties. Historically based, most of the earlier experiments had been analyzed in terms of a Maxwellian. The resulting energy parameters showed a large spread in their value and were difficult to compare due to their restricted validity in different energy ranges. Another point which gave rise to problems was the wide energy range covered by this spectrum. Measurements of the Cf-252 neutron spectrum required the use of different kinds of neutron detectors to be able to cover the spectrum over the full energy range. In addition, many of the problems associated with the experimental determination of this spectrum have been recognized only recently /4/. Recent experiments performed with refined techniques and with improved corrections have therefore given more precise results. A comprehensive review of these post 1979 experiments is given elsewhere /5/. From time to time the status of the standard was discussed and temporary recommendations were given /6, 7/. The only systematic attempt to define the spectrum in its shape was an evaluation performed at the NBS /8/. This evaluation covered experiments before 1975 and stated piecemeal correction functions relative to a reference Maxwellian with an energy parameter of $T = 1.42$ MeV.

With improved experimental results and, at the same time, an increasing interest in describing the spectrum on a theoretical basis /9, 10/, the question of the adequacy of a Maxwellian in representing the spectrum lost its weight. It is todays' consensus that although the Maxwellian is convenient to scale experimental results, the shape of a Maxwellian is inappropriate for defining the Cf-252 neutron spectrum over a wider energy range.

Compared with the situation at the time of the NBS evaluation we now have the most favourable conditions. More experimental results obtained with improved techniques and a resulting higher precision are available and advanced evaluation methods based on generalized least-squares techniques /11, 12/ describe the present state-of-the-art. However, the last point in particular has produced a new class of problems in the form of documentation deficits. The new evaluation methods define obligatory requirements for the documentation of experimental data. Apart from comprehensive uncertainty listings, the correlations of the data, too, must be documented or sufficient details must be quoted to allow a deduction of these quantities.

Many of the older experiments lack a detailed description and it is sometimes necessary to re-analyze the data in order to take all corrections properly into account. This all results in serious restrictions, as it concerns the inclusion of such data into evaluations. The present evaluation had to be confined to more recent experiments where these problems have been, at least to some extent, circumvented.

2. Experimental data base

The data used in this evaluation comprise most of the post-1979 experiments. All of the experiments used were based on time-of-flight (TOF) techniques. A summary of the experiments is listed in Table 1. The energy range covered by each experiment and the number of available data points are given. A brief listing of a few characteristics of each experiment is given below.

Lajtai et al. /14/ (Fig. 1)

A flight path of (30.0 ± 0.1) cm was used for the experiment. The efficiency of the fission fragment detector was approximately 99 %. The neutron detector was a thick lithium glass scintillator (NE-912). The efficiency was experimentally measured relative to a thin lithium glass detector (NE-908). The efficiency of the thin detector was calculated using Monte Carlo methods.

The data of this experiment are plotted in Fig. 1 relative to a Maxwellian with an energy parameter of 1.42 MeV. This form of

Table 1: Experiments used in the evaluation

Authors	Energy range of the experiment	Number of data points
Lajtai et al. /14/	25 keV - 1.22 MeV	70
Böttger et al. /15/	2.00 MeV - 14.00 MeV	60
Poenitz/Tamura /16/	0.25 MeV - 9.25 MeV	51
Blinov et al. /17/	42 keV - 11.36 MeV	73
Boldeman et al. /18/ (Lithium glass)	124 keV - 2.66 MeV	28
Boldemann et al. /18/ (Plastic scintillator)	1.05 MeV - 14.25 MeV	59
Marten et al. /19/	3.89 MeV - 19.77 MeV	16
		Total: 357

representation also used in the following figures has been recommended /6/. The figure also contains the curves of recently developed theories. The dashed line represents the theoretical data of Madland and Nix in the version presented at the Geel meeting /9/. This theory has been adjusted with the experimental data of Poenitz and Tamura /16/ between 0.25 MeV and 9.25 MeV. The dot-dashed curve represents the cascade evaporation model of Märten and Seeliger /10/ obtained with an anisotropy parameter of $\beta = 0.1$. The discontinuity of this curve at 1.8 MeV is due to a numerical error in the transmitted data and is without any physical consequences /13/.

Böttger et al. /15/ (Fig. 2)

This TOF experiment was based on a flight path of 12 m defined with an uncertainty of 0.24 cm. The experiment used three or four large volume NE-213 scintillation neutron detectors in parallel. It was performed in two separate runs. During the first period in August

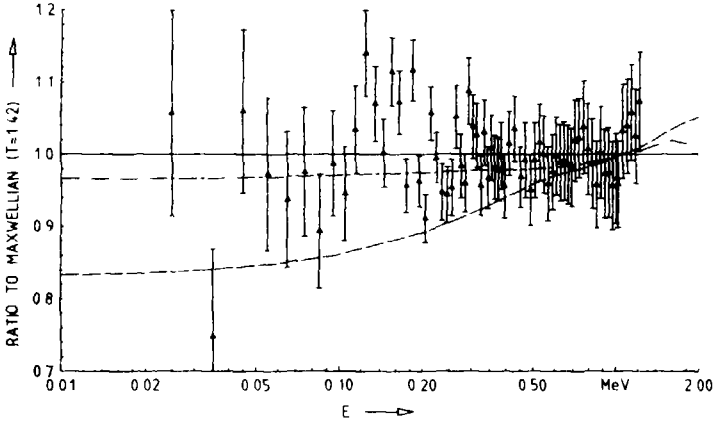

Fig. 1: Experimental data of Lajtai et al. /14/. Details in the text.

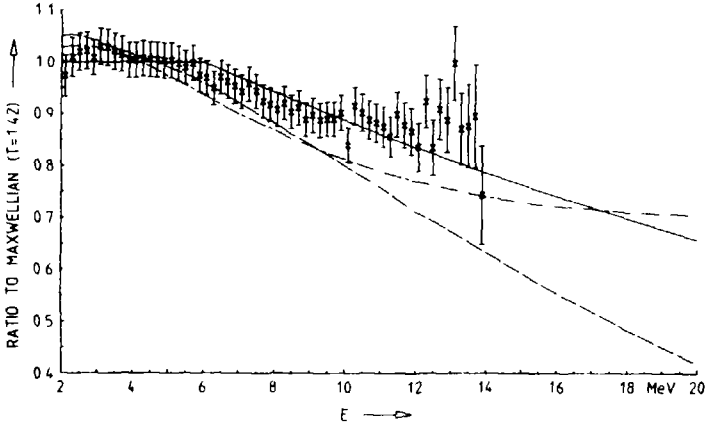

Fig. 2: Experimental data of Böttger et al. /15/. Details in the text.

1981 a fission fragment detector with an experimentally determined efficiency of 95.4 % was used. In this run the data of three neutron detectors were analyzed. The second run was in January 1986. Here an improved fission fragment detector of an efficiency of 99.5 % and four neutron detectors were used. The efficiencies of the neutron detectors were determined by Monte Carlo calculations. Between 3 MeV and 12 MeV the results were confirmed within ± 3 % by n-p scattering data.

Altogether, between 2 MeV and 14 MeV a total of 1018 data points at slightly different neutron energies due to different threshold and TAC calibration of the individual detectors was produced. Including all necessary corrections these data were available for the evaluation. First, the data of each detector of each series were handled separately. A two parameter fit (normalization constant and temperature parameter) with a Maxwellian was performed to obtain estimates of the energy-dependent shapes. Within the statistics the results for all detectors were identical. The shape parameters were used to transform the data of each detector from the individual energy grid to a common grid (steps of 200 keV between 2 MeV and 14 MeV) valid for all detectors. This process reduced the statistical uncertainties, whereas the systematic components remained unchanged and gave 420 data points. The common energy grid structure was the basis for further data compression. This was achieved step by step. First, the three detectors of run no. 1, then the four detectors of run no. 2 and finally the data of all seven detector sets were combined. In each step the compatibility of the data was tested. Within the uncertainties no inconsistencies between the different detectors and different series were found.

The 70 data points of this experiment finally obtained are plotted in Fig. 2. The representation in the figure is the same as in Fig. 1. However, the energy scale of this figure ranges from 2 MeV to 20 MeV. As in Fig. 1, the dashed curve corresponds to the theory of Madland and Nix /9/ and the dot-dashed curve represents the theoretical data of Marten and Seeliger /10/. The solid line above 6 MeV corresponds with the high-energy shape of the NBS evaluation /8/. It is interesting to note that the global trend of this old evaluation is in accordance with recent experiments and theories.

Poenitz and Tamura /16/ (Figs. 3 and 4)

The efficiency of the fission fragment detector in this experiment was only 71 %. It has been experimentally verified that the critical nonisotropic detection losses were of the order of 7 %. The neutron detectors used in this TOF experiment were two black detectors of different sizes. Data between 0.2 MeV and 4 MeV were obtained with the smaller detector and a flight path of 258 cm. In the energy range between 0.7 MeV and 10 MeV the flight path was 347 cm and the large detector was used. The efficiency of the smaller detector changed between 98 % and 83 %. For the large detector between 0.6 MeV and 10 MeV the corresponding efficiencies were between 96 % and 77 %. The uncertainty of the efficiency is very small and is of the order of 1 % to 2 %. The energy scale of the experiment has been verified with carbon resonances. The data of this experiment are plotted in Figs. 3 and 4.

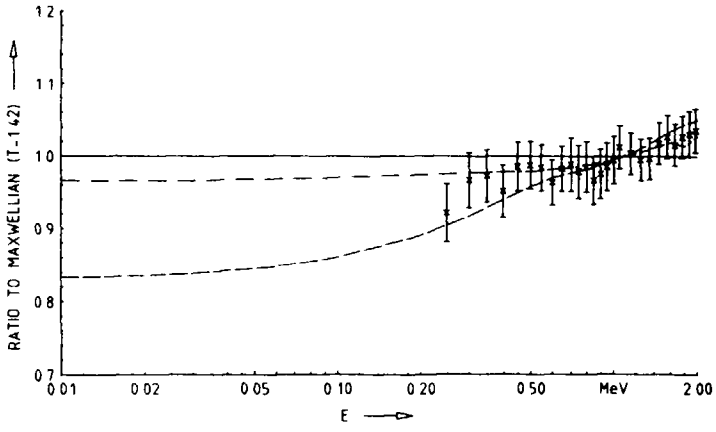

Fig. 3: Experimental data of Poenitz and Tamura /16/, below 2 MeV.

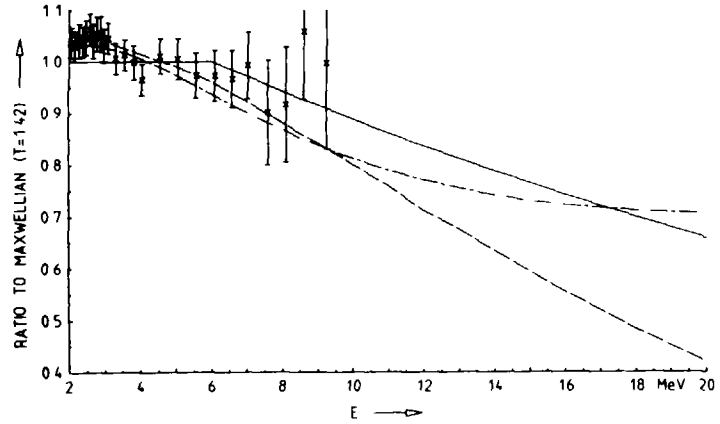

Fig. 4: Experimental data of Poenitz and Tamura /16/, above 2 MeV.

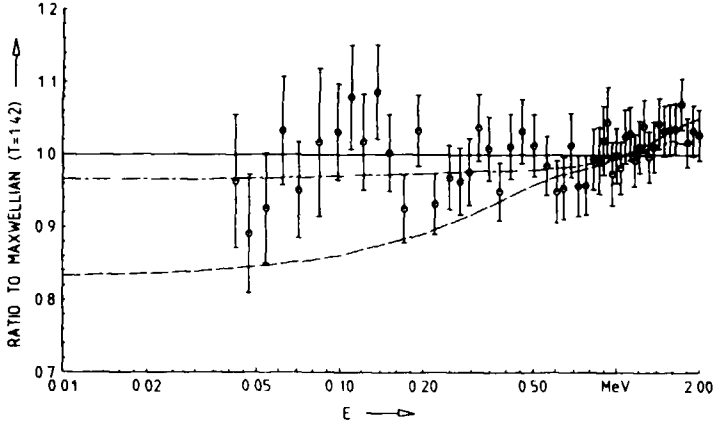

Fig. 5: Experimental data of Blinov et al. /17/, below 2 MeV.

Blinov et al. /17/ (Figs. 5 and 6)

The experiment was performed with different lengths of the flight path. The data used in the evaluation are based on a flight path of (50.00 ± 0.25) cm. The fission fragment detection efficiency was 99 %. A U-235 fission chamber acted as neutron detector. The efficiency of this chamber is proportional to the energy-dependent cross section of $^{235}U(n,f)$ and its uncertainty is given by the uncertainties of this cross section (ENDF/B-V). In the experiment, special attention was paid to calibrating the time scale precisely.

The authors prepared a comprehensive documentation of the experiment for the present evaluation. All corrections and the associated uncertainties were described in detail. The numerical data of this experiment are plotted in Figs. 5 and 6.

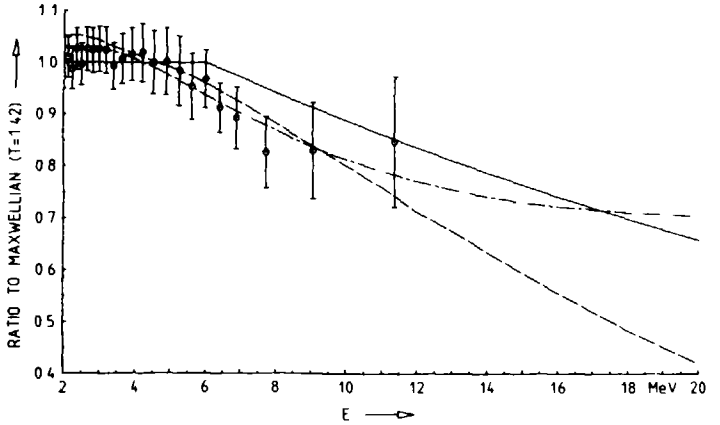

Fig. 6: Experimental data of Blinov et al. /17/, above 2 MeV.

Boldeman et al. /18/ (Figs. 7 and 8)

Data between 1 MeV and 15 MeV were measured with an NE-102 plastic scintillator as neutron detector and a flight path of 301.5 cm was used. The fission fragment detection efficiency was 97 %. Between 2 MeV and 11 MeV the efficiency of the neutron detector was experimentally determined using the associated particle method. The uncertainty is about 2 %. Between 1 MeV and 2 MeV the efficiency was measured relative to a long counter and above 11 MeV the efficiency is based on a Monte Carlo calculation which was tested between 2 MeV and 11 MeV. In all, seven different experiments were carried out. The data were combined by the authors and are plotted in Figs. 7 and 8.

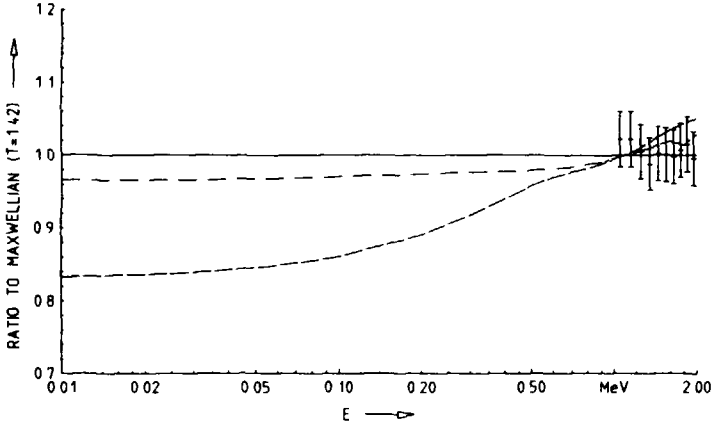

Fig. 7: Experimental data of Boldeman et al. /18/ (plastic scintillator)

Boldeman et al. /18/: ^{6}Li glass (Fig. 9)

In the low energy part of this experiment a lithium glass scintillator was used as neutron detector and a flight path of 40 cm. The fission fragment detector was the same. The efficiency of the neutron detector was measured relative to a long counter between 124 keV and 1349 keV. Above 1349 keV the efficiency is based on calculations. The experimental efficiency was determined with a time resolution similar to that of the later experiment. The results of this experiment were normalized to the plastic scintillator data between 1 MeV and 1.65 MeV. The data are plotted in Fig. 9. It is obvious that the structure of these data can be associated with the 240 keV resonance of $^{6}Li(n,\alpha)$, i.e., independent of the experimental determination of the detector efficiency, there remained some problems in taking the time resolution properly into account.

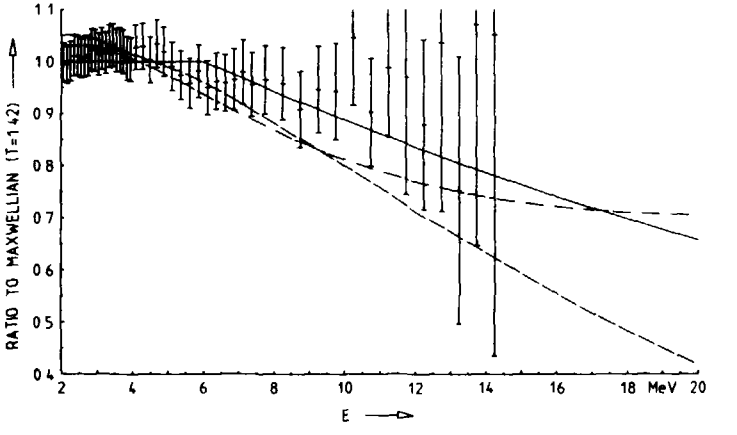

Fig. 8: Experimental data of Boldeman et al. /18/ (plastic scintillator)

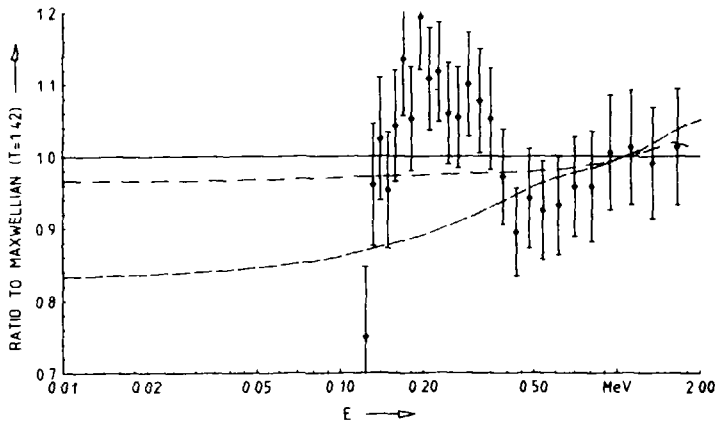

Fig. 9: Experimental data of Boldeman et al. /18/ (^{6}Li detector)

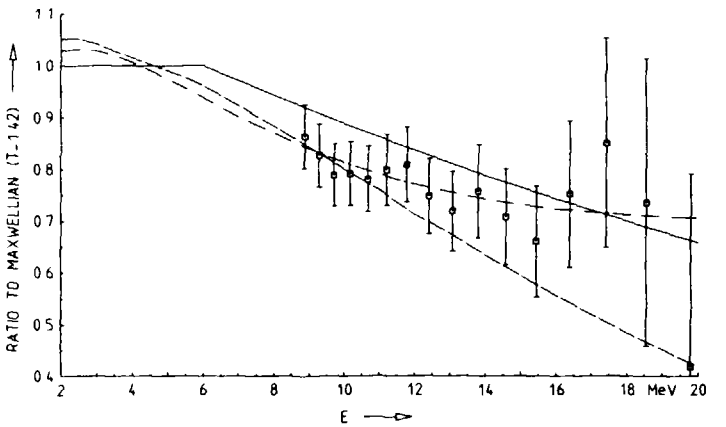

Fig. 10: Experimental data of Märten et al. /19/

Märten et al. /19/ (Fig. 10)

From this high energy experiment the data below 20 MeV were used. The fission fragment detection efficiency was 0.858 ± 0.010 derived from 0° to 90° measurements of the spectrum. The influence of the nonisotropic losses was corrected on the basis of angular distributions and theoretical models. A large NE-213 scintillator was the neutron detector. The flight path in the experiment was 450.0 cm. Similar to other experiments, pulse shape discrimination was used to reduce the background. The efficiency of the neutron detector was obtained from Monte Carlo calculations. The calculations have been checked with experiments between 4 MeV and 12 MeV by assuming the NBS evaluation /8/ as reference distribution. Above 12 MeV the efficiency is extrapolated. The uncertainty of the efficiency determination exceeds 5 % but the dominating uncertainty contributions in this experiment are from counting statistics, as can be seen from the data plotted in Fig. 10. The authors have prepared a detailed description of the experimental analysis for the present evaluation.

3. Steps of the evaluation process

An excellent review of all effects and corrections to be considered in sophisticated time-of-flight experiments is given in the paper of Poenitz and Tamura /16/ presented at the Antwerp conference. This information was used as a basis in checking the comprehensiveness of the analysis of the various experiments made use of in the present evaluation. Depending on the available documentation, no real deficits were identified. For all experiments, the calculation of the time resolution correction and the bin width correction has been repeated. Comparison of the present results with those expressly stated by the authors shows full agreement with the exception of the experiment of Boldeman et al. /18/ where the quoted time resolution correction factors were larger. This discrepancy may originate from an asymmetry in the time resolution function mentioned by the authors.

For each experimental data set, an uncertainty covariance matrix was generated, based on the documented uncertainty information and on additional information directly obtained from the authors. The dominating systematic uncertainty component of all experiments was due to the efficiency calibration of the neutron detectors. Another systematic contribution which was not expressly taken into account in most of the experiments is the uncertainty of the energy scale definition. This uncertainty has been transformed into a corresponding contribution to the neutron spectrum uncertainty with the following formula:

$$\left(\frac{\Delta N}{N}\right)^2 = \left[\left(\frac{1}{2} - \frac{E}{T}\right)^2 + \left(\frac{E}{\varepsilon}\frac{\partial \varepsilon}{\partial E}\right)^2 + 2\left(\frac{1}{2} - \frac{E}{T}\right)\left(\frac{E}{\varepsilon}\frac{\partial \varepsilon}{\partial E}\right)\right]\left(\frac{\Delta E}{E}\right)^2 \qquad (1)$$

$N = N(E)$ is the neutron energy spectrum and $\varepsilon = \varepsilon(E)$ the energy-dependent efficiency of the neutron detector. The first term on the right-hand side of eq. (1) is the relative derivative of the neutron spectrum with respect to the neutron energy valid for a Maxwellian with a temperature parameter T. (For the present purpose this approximation in describing the spectrum by a Maxwellian is of minor influence). The second term in the formula is the corresponding derivative of the detector efficiency. The third term is an interference term which enhances or decreases the transformation factor depending on the difference in the direction of the shape of $N(E)$ and $\varepsilon(E)$. The energy scale uncertainty comprises the flight path uncertainty, the uncertainty of the time channel width and the uncertainty of the definition of the zero time. For each experiment the uncertainties and correlations according to eq. (1) were calculated on the basis of the available data. Table 2 shows some results in form of the minimum and maximum value of this contribution to the spectrum uncertainty specific to each experiment. For a smooth efficiency curve the contribution of eq. (1) approaches zero for $E = T/2$ and increases towards lower as well as higher energies. For an efficiency curve rapidly changing with the energy, as for example in the case of the U-235 fission cross section used in the experiment of Blinov et al. /17/, the result of eq. (1) fluctuates strongly in some energy regions.

Table 2: Magnitude of the energy scale uncertainty contribution

Authors	Minimum value	Maximum value
Lajtai et al.	0.0 %	1.3 %
Bottger et al.	0.1 %	1.7 %
Poenitz/Tamura	0.0 %	1.7 %
Blinov et al.	0.0 %	13.4 %
Boldeman et al. (Lithium glass)	0.0 %	5.9 %
Boldeman et al. (Plastic scintillator)	0.2 %	13.2 %
Marten et al.	3.8 %	9.2 %

To obtain a common basis for the evaluation a fixed energy grid was established. The selection of the grid point energies was governed by the density of the available data points as well as by the necessity to represent the structure of the spectrum adequately. Altogether, 70 grid point energies were chosen. Each of the original data points was transformed to the neighbouring energy grid point. Before doing this, the approximate slope of the data was determined. This was done by fitting a Maxwellian to the original data of each experiment. The results of these fits are summarized in Table 3. Two parameters were obtained from the fit procedure: a normalization constant and an energy parameter. Both quantities were highly correlated or anticorrelated. All these fits were made over the whole energy range of each experiment (see Table 1) without differentiating in certain energy ranges. The strong variation of the individual temperature parameters and the values of chi-square per degree of freedom indicating inconsistency between experimental data and the Maxwellian were of minor importance because information of Table 3 was only used for auxiliary purposes. The specific Maxwellian of each experiment was

Table 3: Two parameter fit of a Maxwellian to the experimental data

Authors	Normalization factor	T (MeV)	χ^2/f
Lajtai et al.	1.009 ± 0.041	1.430 ± 0.044	0.48
Bottger et al.	1.054 ± 0.004	1.379 ± 0.002	3.09
Poenitz/Tamura	1.010 ± 0.004	1.429 ± 0.005	1.16
Blinov et al.	0.993 ± 0.005	1.395 ± 0.004	1.25
Boldeman et al. (Lithium glass)	0.976 ± 0.012	1.365 ± 0.014	4.13
Boldeman et al. (Plastic scintillator)	1.010 ± 0.001	1.410 ± 0.002	3.26
Marten et al.	0.984 ± 0.097	1.372 ± 0.018	0.24

Table 4: Shape experiments in the evaluation

Authors	Normalization by the authors	Integral Maxwellian	Normalization factor of the evaluation
Poenitz/Tamura	0.25MeV -9.25MeV Maxw. T=1.42 MeV	94.6 %	1.007 ± 0.013
Blinov et al	40 keV - 10 MeV Maxw. T=1.42 MeV	99.4 %	0.997 ± 0.009
Boldeman et al. (Lithium glass)	with plastic scintillator data between 1MeV and 1.65MeV	-	1.009 ± 0.024
Boldeman et al. (Plastic scintillator)	none	-	1.010 ± 0.012

applied in the transformation of a data point from its original energy to the grid energy. Due to small shifts in energy the uncertainty contribution of this procedure was almost negligible and the original structure of each data set, shown in the Figs. 1 to 10, was not essentially changed.

Based on the common energy grid, the data sets were combined by generalized least-squares techniques with regard to their uncertainties. The evaluation has been made with absolute data, i.e. without the scaling used in the figures. However, some of the data sets had to be regarded as shape data. These sets are listed in Table 4. Poenitz and Tamura /16/ as well as Blinov et al. /17/ normalized their result to the numerical value of the integral of a Maxwellian with T = 1.42 MeV taken over the energy range of the experiment. The energy range applied and the value of the integral are given in Table 4. The data of Boldeman et al. /18/ obtained with the lithium glass detector have been normalized to his plastic scintillator data in an overlap energy range. All these normalizations were ignored and the data were taken as shape data. The final normalization was part of the evaluation process. Because of a poor documentation of the efficiency calibration procedure, the second data set of Boldeman et al. obtained with the NE-102 neutron detector has also been regarded as a shape data set instead of an absolute one. In the last column of Table 4 the final normalization factors obtained from the evaluation process are listed.

4. Results and discussion

The evaluation resulted in a chi-square value of 264.5 which must be compared with 265 degrees of freedom. From a first glance at the different data sets shown in Figs. 1 to 10, one might have anticipated difficulties in obtaining a consistent result. The chi-square value indicating a full compatibility between the different data sets was therefore rather surprising. However, this result demonstrates that a mathematically consistent data combination

procedure with full regard to the uncertainties and correlations is superior to any eye-guided evaluation.

During the evaluation process a few difficulties arose. Nine of the seventy data points of the experiment of Lajtai et al. /14/ increased the chi-square contribution of this experiment by more than a factor of 4 and indicated a strong inconsistency with the remaining data from other experiments. These data points at neutron energies between 125 keV and 305 keV were within the range of the width of the broad $^{6}Li(n,\alpha)$ resonance at 240 keV. Difficulties in the handling of this resonance in the neutron detector efficiency calibration cannot be excluded. However, it was not understood why other data points at neighbouring neutron energies of the same range exhibited no problems. It has nevertheless been decided to remove these nine points from the evaluation set. The same has also been done with six data points of the lithium glass set of Boldeman et al. /18/ where similar problems were more obvious and have already been discussed in section 2. Finally, 3 of the 59 data points in the data set of Boldeman et al. /18/, measured with the plastic scintillator detector, made the same contribution to the chi-square as the remainder of these data. It was impossible to find a physical explanation of this, neither was it possible to have recourse to the original measurements, as the only data available was that which had already been combined. Here, the somewhat arbitrary opinion of the evaluator was the only justification for the rejection of these three data points. In all, 18 of the 357 data points available were neglected in the evaluation process.

The result of the evaluation at discrete neutron energies is plotted in Figs. 11 and 12. The representation is the same as in Figs. 1 and 2. The error bars given were obtained from the diagonal elements of the final covariance matrix of the present evaluation. These data represent the state of the available experimental data base and therefore a totally smooth behaviour as function of the neutron energy cannot be expected. Between 180 keV and 9.3 MeV the resulting relative uncertainty of the evaluated data is smaller than 2 %. Between 45 keV and 150 keV and between 9.8 MeV and 13.3 MeV the corresponding value remains smaller than 5 %. The evaluated data point at 25 keV has a relative uncertainty of 10 % and above 13.3 MeV the uncertainty increases strongly up to 77 % for the data point at 19.8 MeV.

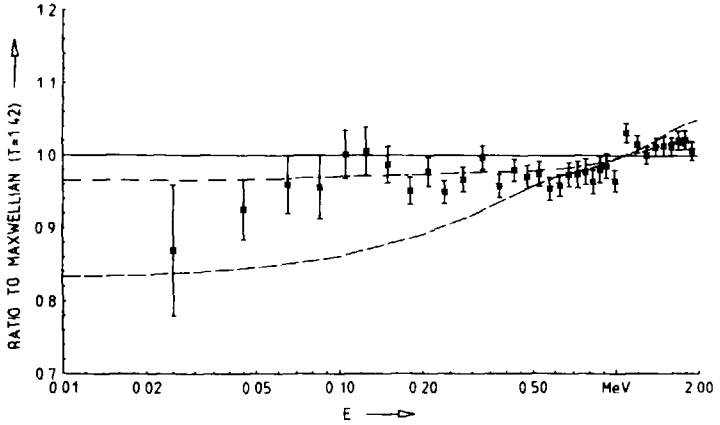

Fig. 11: Result of the evaluation at discrete neutron energies

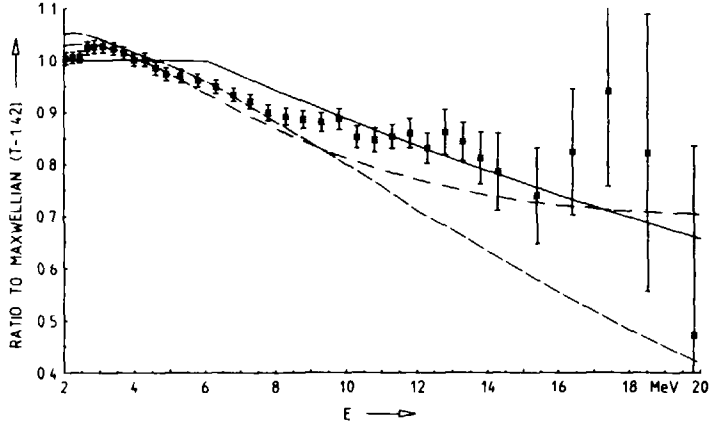

Fig. 12: Same as in Fig. 11, above 2 MeV.

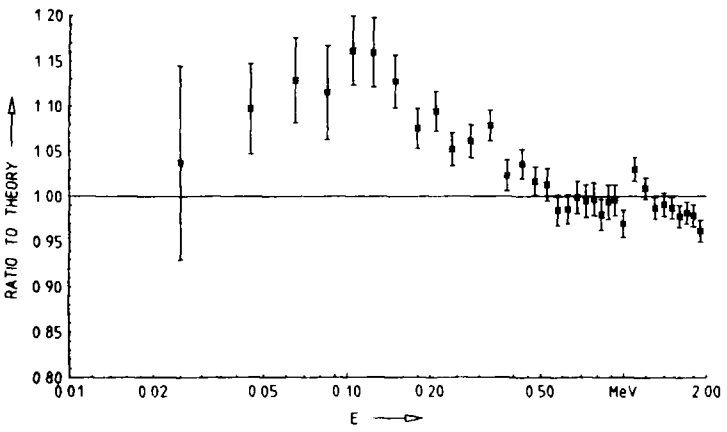

Fig. 13: Ratio of the evaluation relative to the theory of Madland and Nix /9/

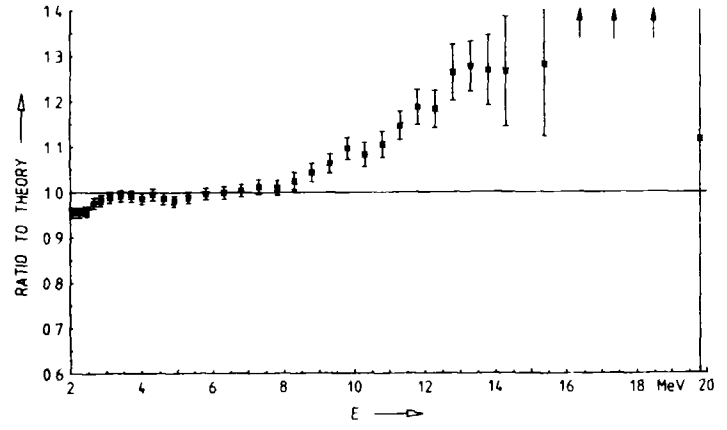

Fig. 14: Same as in Fig. 13, above 2 MeV.

The high accuracy of the evaluated data allowed differentation among some of the theoretical models. In the Figs. 13 and 14 the evaluated data are plotted relative to the theoretical model of Madland and Nix /9/ which is based on an adjustment to the experimental data of Poenitz and Tamura /16/. Below 0.4 MeV and above 8 MeV the theory underestimates the evaluated neutron spectrum. Above 11 MeV the deviation is larger than 10 %. Between 1 MeV and 3 MeV a slight overestimation of the theory can be identified. It cannot be excluded that a re-adjustment of this theory to the present evaluated data changes the global picture. However, it must still be proved if the level density parameter, the adjustable quantity of this theory, remains within physically reasonable limits.

The second theory used in this comparison is without freely adjustable parameters. The cascade evaporation model developed by Marten and Seeliger /10/ is based on a more detailed description of the physical processes and avoids some of the approximations used elsewhere /9/. The result used here is that with an anisotropy parameter of $\beta = 0.1$. In Figs. 15 and 16 the ratio of the evaluated data relative to this model is plotted. An overall agreement with the present data is given between 25 keV and 6 MeV. Above this energy the theoretical data is somewhat lower than the evaluated data, but the difference never exceeds 10 %. Recent improvements to this theory /20/ make it probable that these differences at high neutron energies can be further reduced.

At present, neither theory is adequate to describe within the uncertainties the evaluated data over the whole energy range. To obtain a smooth curve for the evaluated neutron spectrum a spline interpolation procedure was applied. This procedure used the variances of the evaluated neutron spectrum data at discrete energies as weights and generated a continous curve through the data points. The spline procedure has been applied to the complete data set between 25 keV and 19.8 MeV without any attempt to

interpolate between partial energy ranges. The result is plotted in Figs. 17 and 18 relative to a reference Maxwellian with T = 1.42 MeV in the form of a continuous curve. In addition, the data at the discrete energies are given. This curve represents the real final result of the present evaluation.

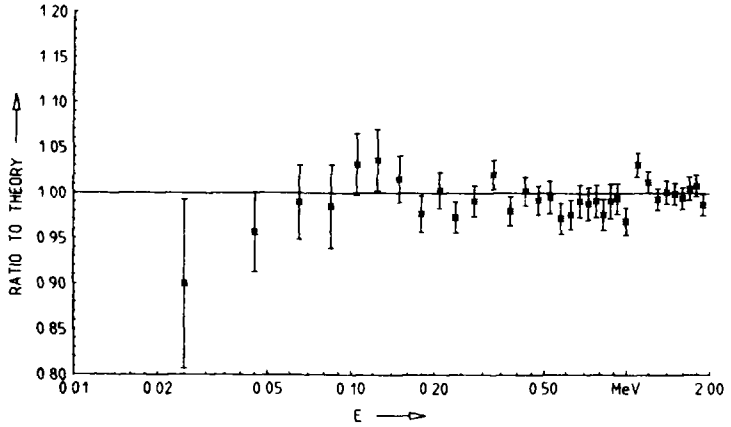

Fig. 15: Ratio of the evaluation relative to the theory of Märten and Seeliger /10/

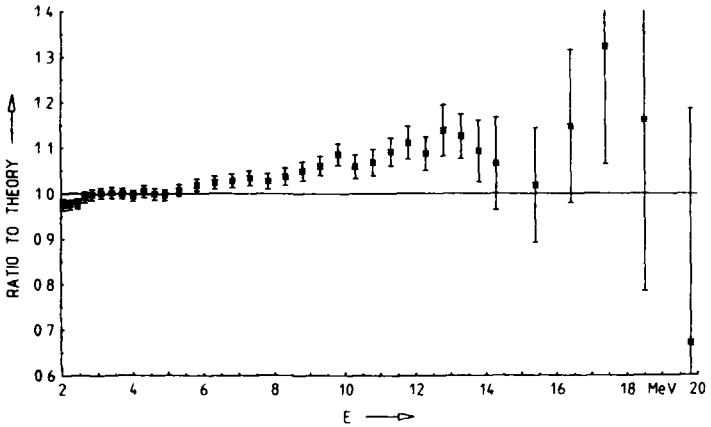

Fig. 16: Same as in Fig. 15, above 2 MeV.

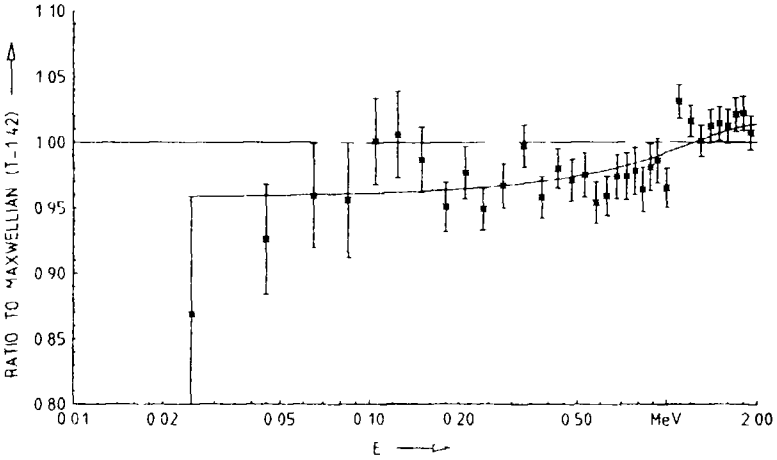

Fig. 17: Spline interpolated continuous form of the evaluation

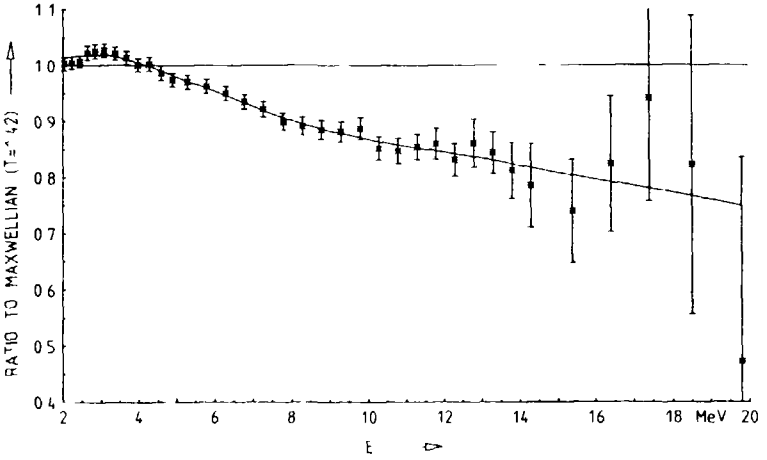

Fig. 18: Same as in Fig. 17, above 2 MeV.

5. Conclusions and future prospects

The neutron spectrum of spontaneous fission of Californium-252 has been evaluated on the basis of data of recent time-of-flight experiments. The result defines the spectrum with a precision never before obtained and supports the status of this spectrum as a standard. With the aim of further improving knowledge of this spectrum, in the near future it is planned to combine additional experimental data, especially the results of integral experiments and of recent TOF experiments performed at very high neutron energies, with the present evaluation.

The results of integral experiments (spectrum-averaged cross section data) have already been used in a preliminary evaluation of the Cf-252 neutron spectrum /21/. Instead of point-wise data, this evaluation yielded energy integrals over the spectral distribution. A comparison of these preliminary data /21/ with the present evaluation shows agreement within the uncertainties. The integral data were not considered in the present evaluation as this would have made necessary time consuming data transformation procedures which did not fit into the schedule of this work.

In addition, the analysis of two recent TOF experiments /22, 23/, which investigated the neutron spectrum up to 30 MeV, has not yet been finalized. The data of both experiments obtained below 20 MeV are believed to establish a sound basis for the reduction of the large uncertainties of the present evaluation between 14 MeV and 20 MeV. Both data sets are expected to be available very soon.

Before the end of 1986, the final version of the evaluation comprising the neutron spectrum and its covariance matrix will be released and transmitted to the Nuclear Data Section of the IAEA, for distribution to nuclear data centers.

References:

/1/ Proc. IAEA Consultants' Meeting on Prompt Fission Neutron Spectra, Vienna 1971, IAEA, Vienna (1972)

/2/ Proc. IAEA Panel on Neutron Standard Reference Data, Vienna, November 1972, IAEA, Vienna (1974)

/3/ M.V. Blinov: IAEA Consultants' Meeting on Neutron Source Properties, Debrecen, March 1980, Report INDC(NDS)-114/GT (1980) 79

/4/ "Nuclear Data for Science and Technology" (K.H. Bockhoff, ed.), Proc. Int. Conf., Antwerp, September 1982, D. Reidel, Publ. Comp., Dordrecht (1983)

/5/ J.W. Boldeman: contribution to the present meeting, review paper (1986)

/6/ Proc. IAEA Consultants' Meeting on the Cf-252 Fission Neutron Spectrum, Smolenice (CSSR), March 1983, Report INDC(NDS)-146/L (1983)

/7/ Proc. IAEA Advisory Group Meeting on Nuclear Standard Reference Data, Geel (Belgium), November 1984, IAEA-TECDOC-335 (1985)

/8/ J.A. Grundl, C.M. Eisenhauer: "Nuclear Cross Sections and Technology" (R.A. Schrack, C.D. Bowman eds.), NBS Spec. Publ. 425 (1975) 250
J. Grundl, C. Eisenhauer: Proc. First ASTM-EURATOM Symposium on Reactor Dosimetry, EUR 5667 ef (1977) 425

/9/ D.G. Madland, J.R. Nix: Nucl. Sci. Eng. 81 (1982) 213
D.G. Madland, J.R. Nix: Antwerp Conference /4/ (1983) 473
D.G. Madland, R.J. LaBauve, J.R. Nix: Geel Meeting /7/ (1985) 267

/10/ H. Marten, D. Neumann, D. Seeliger: Smolenice Meeting /6/ (1983) 199
H. Marten, D. Seeliger: Geel Meeting /7/ (1985) 255

/11/ W.P. Poenitz: Proc. Conference on Nuclear Data Evaluation Methods and Procedures, Brookhaven National Laboratory, September 1980, Report BNL-NCS-51363 (1981) 249

/12/ W. Mannhart: Report PTB-FMRB-84 (June 1981)
/13/ H. Marten: priv. communication (1986)
/14/ A. Lajtai, P.P. Dyachenko, L.S. Kutzaeva, V.N. Kononov, P.A. Androsenko, A.A. Androsenko: Smolenice Meeting /6/ (1983) 177
/15/ R. Bottger, H. Klein, A. Chalupka, B. Strohmaier: Antwerp Conference /4/ (1983) 484
R. Bottger, H. Klein, A. Chalupka, B. Strohmaier: contribution to the present meeting (1986)
/16/ W.P. Poenitz, T. Tamura: Antwerp Conference /4/ (1983) 465
W.P. Poenitz, T. Tamura: Smolenice Meeting /6/ (1983) 175
/17/ M.V. Blinov, G.S. Boykov, V.A. Vitenko: Antwerp Conference /4/ (1983) 479
M.V. Blinov, G.S. Boykov, V.A. Vitenko: Report INDC(CCP)-238/L (June 1985)
/18/ J.W. Boldeman, D. Culley, R.W. Cawley. Trans. Am. Nucl. Soc. 32 (1979) 733
J.W. Boldeman, B.E. Clancy, D. Culley: Nucl. Sci. Eng., 93 (1986) 181
/19/ H. Marten, D. Seeliger, B. Stobinski: Antwerp Conference /4/ (1983) 488
H. Marten, D. Richter, D. Seeliger: Report INDC(GDR)-28/L (September 1984)
/20/ H. Marten: contribution to the present meeting (1986)
/21/ W. Mannhart: Geel Meeting /7/ (1985) 294
/22/ H. Marten, D. Richter, D. Seeliger, R. Bottger, W.D. Fromm: Geel Meeting /7/ (1985) 310
R. Bottger, W.D. Fromm, H. Klein, H. Marten, D. Richter, D. Seeliger: Proc. Int. Conf. Nuclear Data for Basic and Applied Science, Santa Fe, USA, May 1985, to be published (1986)
/23/ A. Chalupka, L. Malek, S. Tagesen, R. Bottger: contribution to the present meeting (1986)

Cf-252 FISSION NEUTRON SPECTRUM AS AN INTEGRAL FIELD

I KIMURA, K. KOBAYASHI
Research Reactor Institute,
Kyoto University

O. HORIBE
Department of Reactor Engineering,
Kinki University

Osaka, Japan

Abstract

By making use of the average cross section data (Mannhart's evaluation) for twenty five reactions measured with the ^{252}Cf spontaneous fission neutron source, its spectral shape was unfolded by NEUPAC. As a whole, the result agrees with the predicted ones by Madland and by Marten and with the measured one by Pönitz and Tamura, but obviously differs from the Maxwellian spectrum with its average energy E_{av}=2.13 MeV. The influence of each cross section data to the shape of the unfolded spectrum was investigated.

The ^{252}Cf spectrum averaged cross sections for the above reactions were calculated by making use of energy dependent cross section data from ENDF/B-V (dosimetry file), JENDL-2 and internal library of NEUPAC and of six expressions of its spectral shape, (1) Maxwellian (E_{av}=2.13), (2) Madland's prediction, (3) Märten's predictions(CEM and GMNM), (4) Gerasimenko's prediction, and (5) the spectrum unfolded by NEUPAC. By comparison of the calulated values with the measured ones, checked were the shape of the ^{252}Cf fission neutron spectrum and the convergence between the measured and calculated cross section data.

The average cross section data for the above reactions were tried to be plotted by the Horibe's empirical rule Although the number of data is rather restricted, we can see good systematics for the (n,p), (n,α) and (n,2n) reactions similar to the case of the average cross sections to the ^{235}U fission neutron spectrum.

1. Introduction

Standard neutron spectrum fields or standard neutron fields have significant usefulness for the purpose of integral check of neutron reaction rate or cross section data, neutron detection efficiency and so forth

As an excellent standatd neutron field, it is required to fulfill the following conditions, (1) the neutron spectrum is known as precisely as possible, (2) its shape is gently-sloping without resonant peak and dip, (3) interlaboratory reproducibility of the spectrum, (4) the neutron flux in the vicinity is flat for position and angle, and (5) the absolute value of the flux can be obtained precisely

The most important standard neutron fields were defined by IAEA as/1/, (1) Maxwellian for the thermal neutron region, (2) 1/E distribution for the epithermal and intermediate energy range, and (3) ^{252}Cf spontaneous fission neutron spectrum in the fast neutron region Many attempts have been performed to develop other standard or reference neutron fields For example, there are (1) the neutron spectrum of thermal neutron induced fission of ^{235}U, (2) slightly softened one from the fission spectrum with some neutron moderator, and (3) broad neutron spectrum produced by the bombardment of thick light element target with monoenergetic protons or deutrons

Other than these spectra, it is regarded that the ^{252}Cf spontaneous fission neutron spectrum is more precise from 250 keV to 8 MeV However, errors below 250 keV and above 8 MeV are still considerably large/2/ Since the absolute number of total neutrons in these regions is extremely small, it can not be thought that these neutrons are very important for the main purpose of this field. But precise data of neutron spectra in these regions are needed for error analysis Furthermore, these data are of great significance for the study of fission phenomena Recently, fission neutron spectra have been theoretically derived by assumption of neutron emission from energetic fission fragments just after the scission From this standpoint, precise knowledge of fission neutron spectra is keenly expected

In the present work, we have tried to examine the shape of the ^{252}Cf spontaneous fission neutron spectrum by means of average cross sections for twenty five reactions Although two of the authors (I K. and K K) measured large number of average cross sections to the ^{252}Cf spontaneous fission neutron spectrum before, used here are the newest values of Mannhart/3/ evaluated by the covariance analysis of not only his original data but also ours/4/ and some others. Firstly, the shape of the ^{252}Cf spontaneous fission neutron spectrum is unfolded by NEUPAC code/5/ The ratios of the present result to the Maxwellian with 2.13 MeV of its average energy E_{av} are compared with measured values and theoretically predicted ones There appear a few peaks and dips, and hence the influence of each reaction cross section to the shape of the unfolded spectrum has been investigated

In the second place, we have calculated the ^{252}Cf fission neutron spectrum averaged cross sections for the above reactions by making use of energy dependent cross section data $\sigma(E)$ taken from three evaluated data libraries and of six types of the ^{252}Cf spontaneous fission neutron spectrum $\chi(E)$. For $\sigma(E)$ and $\chi(E)$, we adopted the followings.

$\sigma(E)$ (1) ENDF/B-V(dosimetry file)/6/,
(2) JENDL-2/7/,
(3) Internal data in NEUPAC/5/,

$\chi(E)$ (1) Maxwellian (E_{av}=2 13 MeV),
(2) Madland's prediction/8/,
(3) Márten's predictions(CEM and GMNM)/9/,
(4) Gerasimenko's prediction/10/,
(5) Unfolded spectrum by NEUPAC.

By the intercomparison between these average cross sections, the shape of ^{252}Cf spontaneous fission neutron spectrum is assessed Moreover, we examine the convergence of integral and differential cross section data for each reaction by comparison of the above calculated and measured values

Recently, one of the authors (O.H) proposed an empirical rule for the estimation of ^{235}U fission neutron spectrum averaged cross sections for the (n,p) and (n, α) reactions and showed

satisfactory result/11,12/. The applicability of this rule to the ^{252}Cf fission neutron spectrum has been attempted. We also try to apply this rule to the average cross sections for the (n,2n) reactions.

2. Unfolding of ^{252}Cf Spontaneous Fission Neutron Spectrum by Making Use of Average Cross Section Data

In order to unfold the shape of the ^{252}Cf spontaneous fission neutron spectrum, we used the NEUPAC code developed by Nakazawa, et al./5/. This code has been successfully applied to the neutron spectrum measurements in JOYO and EBR-II/13/ and in YAYOI, KUR and JMTR/14/. In the international comparison program of neutron spectrum unfolding codes by IAEA, NEUPAC showed satisfactory result. Present authors are now using this code to obtain neutron spectra in experimental facilities in KUR/15/.

The NEUPAC code contains energy dependent cross section data for main important neutron dosimetry reactions. These data have been mainly taken from the ENDF/B-V dosimetry file, but there are several reactions of which cross section data are originally evaluated in NEUPAC. The mesh size of correlation matrix in ENDF/B-V is rather coarse, therefore, larger correlation matrix with fine mesh is calculated in the NEUPAC code itself and is used in spectrum unfolding. We adopted 135 energy groups from 0.01 eV to 16.4 MeV, but the result obtained from 0.5 MeV to 16.4 MeV (68 groups) are plotted as shown later. As the input data for the measured values of the ^{252}Cf fission neutron spectrum averaged cross sections, we took the newest values of Mannhart's evaluation/3/ for twenty five reactions, which were obtained by the covariance analysis of his own original data and some other data including those by the present authors/4/. In his evaluated values, both variance and covariance data are presented, so we input all of these data together with the average cross sections into the NEUPAC code. We took the Maxwellian (E_{av}=2.13 MeV) as the initial guess spectrum in the first step. This calculation was executed by the KURRI terminal of the Computing Center of Kyoto University.

The neutron spectrum obtained by the NEUPAC code is compared with the Maxwellian and three predictions in Fig. 1. The ratio of the unfolded spectrum to the Maxwellian is depicted in Fig. 2. The ratios of the experimental values by Pönitz and Tamura/16/ and of the calculated ones by Madland/8/ and by Märten(CEM)/9/ to the Maxwellian are also shown in this figure. As a whole, the gross shape of the ratio of the present unfolded spectrum to the Maxwellian agrees with both the experimental values and the two predictions, however it shows a little peak around 6 MeV and oscillatory irregularity in higher energy region.

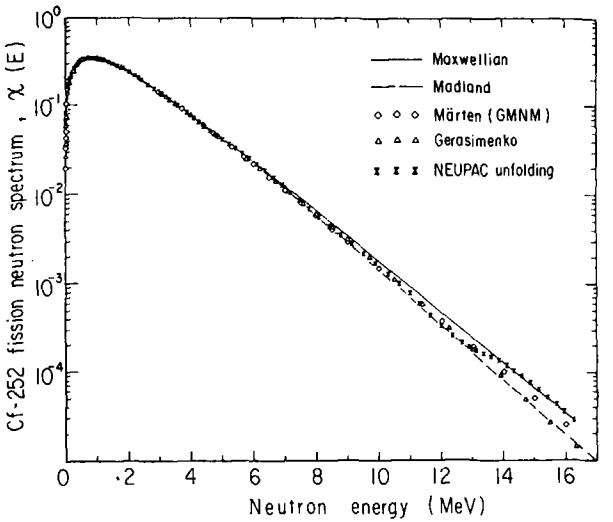

Fig. 1 Comparison of the unfolded spectrum by NEUPAC using Mannhart's evaluated average cross sections with the Maxwellian(E_{av}=2.13 MeV) and with three predictions.

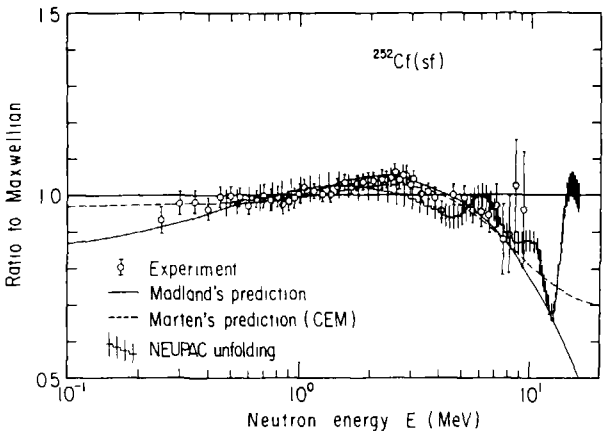

Fig. 2 Comparison of the ratio of the unfolded spectrum to the Maxwellian with those of the Madland's and Märten's predictions and of the Pönitz and Tamura's experiment.

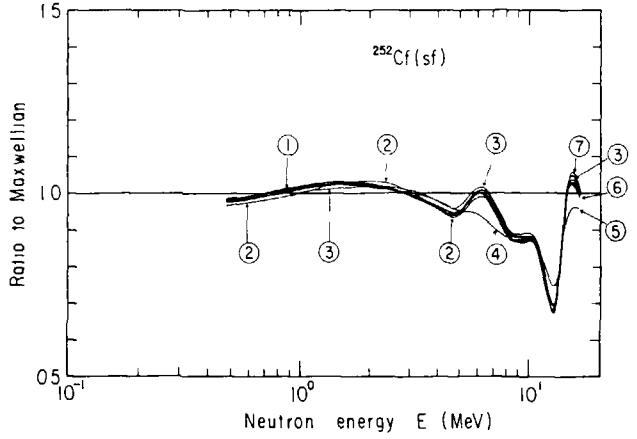

Fig. 3 Comparison of the ratios of the unfolded spectra to the Maxwellian. The meaning of each number is described in text.

In order to find out the reason of this irregularity and to investigate the influence of each reaction cross section to the shape of the unfolded spectrum, we tried to remove each reaction data step by step. Figure 3 shows the ratios in the following cases to the Maxwellian (E_{av}=2.13 MeV); (1) the unfolded spectrum with all data, (2) that without $^{47}Ti(n,p)^{47}Sc$ (its cross section data seem to have a problem as described later), (3) that without $^{115}In(n,\gamma)^{116m}In$ (not threshold reaction), (4) that without $^{56}Fe(n,p)^{56}Mn$, (5) that without $^{90}Zr(n,2n)^{89}Zr$, (6) that without $^{127}I(n,2n)^{126}I$, (7) that with the Winklers's data for $^{58}Ni(n,2n)^{57}Ni$ instead of its data from ENDF/B-V. Little change can be observed in the cases of (2), (3), (5), (6) and (7), but the peak around 6 MeV nearly disappears only in the case of (4).

3. Average Cross Sections to ^{252}Cf Spontaneous Fission Neutron Spectrum for Each Reaction

The average cross section to the ^{252}Cf spontaneous fission neutron spectrum was calculated for each reaction given in the previous section, and the result is compared with both that obtained with the Maxwellian (E_{av}=2.13 MeV) and the evaluated values by Mannhart. For data base of the energy dependent cross section $\sigma(E)$, we used the ENDF/B-V dosimetry file/6/, the JENDL-2 library/7/ and the internal library in NEUPAC/5/. As the shape of ^{252}Cf spontaneous fission neutron spectrum X(E), the following six expressions were used:

(1) Maxwellian with E_{av}=2.13 MeV.
(2) The Madland's prediction taken from the reference/8/.
(3) The Märten's prediction (CEM), the complex cascade evaporation model/9/.
(4) The Märten's prediction (GMNM), the generalized Madland-Nix model/9/. The numerical data of both Märten's spectra were offered by Märten/17/.
(5) The Gerasimenko's prediction, the Hauser-Feshbach calculation/10/. The numerical data were taken from the reference/23/.
(6) Unfolded spectrum shown in the previous section.

We practically calculated each average cross section by

$$\bar{\sigma} = \int_{1\ keV}^{20\ MeV} \sigma(E)\chi(E)dE \Big/ \int_{1\ keV}^{20\ MeV} \chi(E)dE$$

$$= \sum_i \sigma_i(E)\chi_i(E)\Delta E_i \Big/ \sum_i \chi_i(E)\Delta E_i$$

$$= \sum_i \sigma_i(E)\chi_i(E) \quad ,$$

$$\Delta E_i = \text{const} = 10\ keV \ .$$

Internal values of $\sigma(E)$ and $\chi_i(E)$ between two given data points taken from references are interporated by the linear approximation.

The obtained results are tabulated in Table 1. The ratios of the calculated value using each set to that with the Maxwellian (E_{av}=2.13 MeV) and to the Mannhart's evaluation are given in Table 2 and Table 3, respectively. The degree of convergence or the convergence factor given by the mean value of abs.$(1.0-(C/E)_i)$ is tabulated in the bottom row of Table 3. In Fig. 4, shown is the relationship between the 90 % confidence level which has been determined by the unfolded spectrum and the ratios of the Mannhart's evaluated value and the calculated value to that using the Maxwellian spectrum. From Tables 1 - 3 and Fig. 4, we can point out the followings

(1) The gross shape of the data points in Fig. 4 agrees with the Madland's and Marten's(GMNM) predictions for the ^{252}Cf spontaneous fission neutron spectrum, but does not agree with the Maxwellian (E_{av}=2.13 MeV).

(2) Most of the C/E ratios for the Maxwellian are larger than unity, and hence the convergence factor for that is much worse than others The best convergence factor is obtained for the combination of the unfolded spectrum by NEUPAC and its internal cross section data. If we compare the convergence factors for other spectral shapes in the case of ENDF/B-V, the ranking next to the unfolded spectrum is as follows, the Marten's(CEM), the Marten's(GMNM), the Gerasimenko's, the Madland's and the Maxwellian, although the difference is not very large.

(3) All of the convergence factors for ENDF/B-V are slightly better than those for JENDL-2 except in the case of the Madland's spectrum. However, there are a few reactions of which C/E ratios with JENDL-2 are closer to unity than those with ENDF/B-V, such as the $^{56}Fe(n,p)^{56}Mn$, $^{59}Co(n,\alpha)^{56}Mn$ and $^{63}Cu(n,\alpha)^{60}Co$ reactions.

(4) For the reactions with higher response energy such as (n,2n), the C/E ratios for the Maxwellian (E_{av}=2.13 MeV) are much larger than unity, while those for others with lower response energy are closer to unity. This fact can be explained by being smaller number of high energy fission neutrons than that in the Maxwellian distribution.

(5) Among these (n,2n) reactions, the C/E ratios for the $^{58}Ni(n,2n)^{57}Ni$ reaction are extraordinarily low. This is probably due to too small energy dependent cross section $\sigma(E)$ in both ENDF/B-V and JENDL-2. This tendency is pointed out by the present authors and by Ikeda, et al., recently/18,19/.

(6) The C/E values for the $^{47}Ti(n,p)^{47}Sc$ reaction are larger than 1.2 for all cases. Mannhart suggested the energy dependent cross section data for this reaction is too high in a few MeV/20/

Table 1 Comparison of the Cf-252 spectrum-averaged cross section (in mb)

Cf-252 spectrum σ(E) data	Maxwellian E_{av}=2.13 MeV ENDF/B-V	 JENDL-2	Madland's prediction ENDF/B-V	 JENDL-2	Märten's(GMNM) prediction ENDF/B-V	 JENDL-2	Märten's(CEM) prediction ENDF/B-V	 JENDL-2	Gerasimenko's prediction ENDF/B-V	 JENDL-2	Unfolded by NEUPAC Internal library	Measurement (% error) Evaluated by Mannhart	 Present authors
$^{27}Al(n,p)^{27}Mg$	5.27	4.65	4.97	4.40	4.89	4.30	4.93	4.36	5.00	4.41	5.04	4.885(2.14)	4.891(3.66)
$^{27}Al(n,\alpha)^{24}Na$	1.16	1.17	0.982	0.996	0.998	1.01	0.993	1.01	1.05	1.06	1.03	1.017(1.47)	1.006(2.17)
$^{46}Ti(n,p)^{46}Sc$	13.8		13.0		12.7		12.9		13.1		13.2	14.09(1.76)	14.04(4.36)
$^{47}Ti(n,p)^{47}Sc$	24.2		24.2		23.6		23.9		24.0		23.8	19.29(1.66)	20.36(5.44)
$^{48}Ti(n,p)^{48}Sc$	0.446		0.380		0.386		0.385		0.402		0.398	0.4251(1.89)	0.4153(3.80)
$^{55}Mn(n,2n)^{54}Mn$	0.557	0.568	0.387	0.395	0.456	0.465	0.440	0.449	0.405	0.413	0.431	0.4079(2.34)	
$^{54}Fe(n,p)^{54}Mn$	89.3	83.1	88.8	81.8	86.4	79.6	87.8	80.9	87.7	80.9	87.0	86.92(1.34)	87.63(4.97)
$^{56}Fe(n,p)^{56}Mn$	1.51	1.57	1.33	1.38	1.33	1.38	1.34	1.39	1.39	1.44	1.39	1.466(1.77)	1.440(4.86)
$^{58}Ni(n,p)^{58}Co$	116	113	115	112	112	109	114	111	114	111	112	117.6(1.30)	118.5(3.45)
$^{58}Ni(n,2n)^{57}Ni$	.00996	.00981	.00617	.00607	.00810	.00797	.00778	.00766	.00610	.00600	.00792	.008961(3.59)	
$^{59}Co(n,\alpha)^{56}Mn$	0.238	0.255	0.205	0.219	0.207	0.222	0.207	0.221	0.216	0.231	0.211	0.2220(1.86)	0.2176(6.44)
$^{59}Co(n,2n)^{58}Co$	0.512	0.473	0.352	0.327	0.417	0.387	0.403	0.373	0.367	0.341	0.400	0.4055(2.52)	
$^{63}Cu(n,\alpha)^{60}Co$	0.817	0.780	0.723	0.695	0.722	0.692	0.724	0.695	0.753	0.721	0.742	0.6893(1.98)	
$^{65}Cu(n,2n)^{64}Cu$	0.806	0.806	0.572	0.569	0.662	0.661	0.640	0.639	0.602	0.599	0.627	0.6587(2.24)	
$^{115}In(n,n')^{115m}In$	182		186		183		184		185		183	197.6(1.37)	201.0(4.08)
$^{127}I(n,2n)^{126}I$	2.76		2.07		2.29		2.23		2.23		2.23	2.071(2.75)	
$^{19}F(n,2n)^{18}F$		0.0261		0.0173		0.0213		0.0205		0.0178	0.0161	0.01613(3.40)	
$^{24}Mg(n,p)^{24}Na$											2.10	1.998(2.42)	1.940(4.79)
$^{63}Cu(n,\gamma)^{64}Cu$											9.86	10.45(3.24)	
$^{63}Cu(n,2n)^{62}Cu$		0.269		0.176		0.219		0.211		0.179	0.196	0.1845(3.98)	
$^{64}Zn(n,p)^{64}Cu$											38.7	40.63(1.64)	41.84(4.18)
$^{90}Zr(n,2n)^{89}Zr$											0.213	0.2212(2.90)	
$^{115}In(n,\gamma)^{116m}In$											124	125.7(2.23)	
$^{197}Au(n,\ )^{198}Au$											77.8	76.86(1.59)	
$^{197}Au(n,2n)^{196}Au$											5.69	5.511(1.83)	5.267(4.30)

Table 2 Comparison of the average cross section ratios

Reaction	90 % confidence level (eV) (by NEUPAC)	Ratios to Maxwellian spectrum-averaged cross section*									
		Madland		Märten (GMNM)		Märten (CEM)		Gerasimenko		Unfolded Internal library	Measurement (evaluated by Mannhart)
		ENDF/B-V	JENDL-2	ENDF/B-V	JENDL-2	ENDF/B-V	JENDL-2	ENDF/B-V	JENDL-2		
$^{27}Al(n,p)^{27}Mg$	3.52+6 - 9.83+6	0.943	0.945	0.923	0.924	0.935	0.937	0.948	0.948	0.955	0.926
$^{27}Al(n,\alpha)^{24}Na$	6.54+6 - 1.25+7	0.848	0.850	0.862	0.863	0.857	0.859	0.907	0.908	0.887	0.878
$^{46}Ti(n,p)^{46}Sc$	3.81+6 - 9.86+6	0.944		0.923		0.936		0.946		0.954	1.020
$^{47}Ti(n,p)^{47}Sc$	1.90+6 - 7.95+6	1.000		0.975		0.988		0.991		0.984	0.796
$^{48}Ti(n,p)^{48}Sc$	6.01+6 - 1.30+7	0.853		0.867		0.864		0.902		0.894	0.954
$^{55}Mn(n,2n)^{54}Mn$	1.12+7 - 1.57+7	0.695	0.695	0.818	0.817	0.790	0.789	0.727	0.727	0.774	0.732
$^{54}Fe(n,p)^{54}Mn$	2.37+6 - 7.96+6	0.994	0.985	0.967	0.958	0.982	0.974	0.982	0.974	0.974	0.973
$^{56}Fe(n,p)^{56}Mn$	5.55+6 - 1.18+7	0.884	0.884	0.883	0.882	0.885	0.885	0.918	0.919	0.919	0.972
$^{58}Ni(n,p)^{58}Co$	2.15+6 - 7.91+6	0.996	0.996	0.970	0.970	0.985	0.984	0.985	0.984	0.969	1.015
$^{58}Ni(n,2n)^{57}Ni$	1.32+7 - 1.61+7	0.619	0.619	0.812	0.813	0.780	0.781	0.612	0.611	0.794	0.899
$^{59}Co(n,\alpha)^{56}Mn$	6.01+6 - 1.27+7	0.858	0.861	0.869	0.870	0.866	0.869	0.907	0.909	0.886	0.931
$^{59}Co(n,2n)^{58}Co$	1.14+7 - 1.57+7	0.688	0.691	0.816	0.817	0.788	0.788	0.717	0.721	0.782	0.792
$^{63}Cu(n,\alpha)^{60}Co$	4.90+6 - 1.15+7	0.886	0.892	0.884	0.887	0.887	0.891	0.923	0.924	0.909	0.844
$^{65}Cu(n,2n)^{64}Cu$	1.08+7 - 1.55+7	0.709	0.706	0.821	0.820	0.794	0.793	0.746	0.743	0.777	0.817
$^{115}In(n,n')^{115m}In$	1.19+6 - 6.21+6	1.022		1.003		1.008		1.014		1.007	1.086
$^{127}I(n,2n)^{126}I$	9.76+6 - 1.50+7	0.751		0.830		0.807		0.808		0.809	0.751
$^{19}F(n,2n)^{18}F$	1.20+7 - 1.60+7		0.664		0.815		0.785		0.680		0.889
$^{24}Mg(n,p)^{24}Na$	6.56+6 - 1.21+7										0.857
$^{63}Cu(n,\gamma)^{64}Cu$	5.30+4 - 3.97+6										1.068
$^{63}Cu(n,2n)^{62}Cu$	1.20+7 - 1.60+7		0.652		0.812		0.782		0.664		0.822
$^{64}Zn(n,p)^{64}Cu$	2.50+6 - 8.01+6										1.027
$^{90}Zr(n,2n)^{89}Zr$	1.29+7 - 1.61+7										0.975
$^{115}In(n,\gamma)^{116m}In$	1.01+5 - 2.92+6										1.028
$^{197}Au(n,\gamma)^{198}Au$	5.44+4 - 2.94+6										0.993
$^{197}Au(n,2n)^{196}Au$	8.64+6 - 1.42+7										0.821

* In this case, the Maxwellian spectrum-averaged cross sections were obtained from NEUPAC calculation.

Table 3 Comparison of the C/E ratios of the Cf-252 spectrum-averaged cross sections

Reaction	Ratio of calculated value to experimental value (Mannhart's evaluation)										
	Maxwellian E_{av}=2.13 MeV		Madland's prediction		Märten's (GMNM) prediction		Märten's (CEM) prediction		Gerasimenko's prediction		Unfolded by NEUPAC
	ENDF/B-V	JENDL-2	ENDF/B-V	JENDL-2	ENDF/B-V	JENDL-2	ENDF/B-V	JENDL-2	ENDF/B-V	JENDL-2	Internal library
$^{27}Al(n,p)^{27}Mg$	1.080	0.953	1.018	0.900	0.996	0.880	1.010	0.892	1.023	0.903	1.031
$^{27}Al(n,\alpha)^{24}Na$	1.139	1.151	0.965	0.979	0.982	0.994	0.976	0.989	1.032	1.045	1.010
$^{46}Ti(n,p)^{46}Sc$	0.980		0.925		0.904		0.917		0.927		0.935
$^{47}Ti(n,p)^{47}Sc$	1.256		1.255		1.225		1.241		1.244		1.235
$^{48}Ti(n,p)^{48}Sc$	1.049		0.894		0.909		0.905		0.946		0.937
$^{55}Mn(n,2n)^{54}Mn$	1.366	1.393	0.950	0.969	1.117	1.139	1.079	1.100	0.993	1.101	1.057
$^{54}Fe(n,p)^{54}Mn$	1.028	0.956	1.021	0.941	0.994	0.916	1.010	0.931	1.009	0.931	1.001
$^{56}Fe(n,p)^{56}Mn$	1.029	1.069	0.910	0.945	0.908	0.943	0.911	0.945	0.945	0.982	0.946
$^{58}Ni(n,p)^{58}Co$	0.986	0.958	0.981	0.954	0.956	0.929	0.970	0.943	0.970	0.943	0.955
$^{58}Ni(n,2n)^{57}Ni$	1.112	1.095	0.688	0.677	0.903	0.890	0.868	0.855	0.681	0.669	0.883
$^{59}Co(n,\alpha)^{56}Mn$	1.074	1.147	0.921	0.988	0.933	0.999	0.930	0.997	0.974	1.042	0.951
$^{59}Co(n,2n)^{58}Co$	1.262	1.167	0.869	0.807	1.030	0.954	0.994	0.920	0.905	0.842	0.987
$^{63}Cu(n,\alpha)^{60}Co$	1.185	1.131	1.050	1.008	1.048	1.004	1.051	1.008	1.093	1.045	1.076
$^{65}Cu(n,2n)^{64}Cu$	1.224	1.224	0.868	0.864	1.005	1.004	0.972	0.970	0.913	0.909	0.951
$^{115}In(n,n')^{115m}In$	0.921		0.941		0.924		0.929		0.934		0.928
$^{127}I(n,2n)^{126}I$	1.332		1.001		1.105		1.075		1.076		1.077
$^{19}F(n,2n)^{18}F$		1.619		1.074		1.319		1.271		1.101	1.001
$^{24}Mg(n,p)^{24}Na$											1.053
$^{63}Cu(n,\gamma)^{64}Cu$											0.943
$^{63}Cu(n,2n)^{62}Cu$		1.460		0.952		1.186		1.141		0.969	1.065
$^{64}Zn(n,p)^{64}Cu$											0.952
$^{90}Zr(n,2n)^{89}Zr$											0.965
$^{115}In(n,\gamma)^{116m}In$											0.988
$^{197}Au(n,\gamma)^{198}Au$											1.012
$^{197}Au(n,2n)^{196}Au$											1.032
$\frac{\sum_{i}^{N}\lvert 1.0-(C/E)_i\rvert}{N}$	0.1405	0.1992	0.0895	0.0851	0.0701	0.0882	0.0683	0.0827	0.0806	0.0845	0.0532

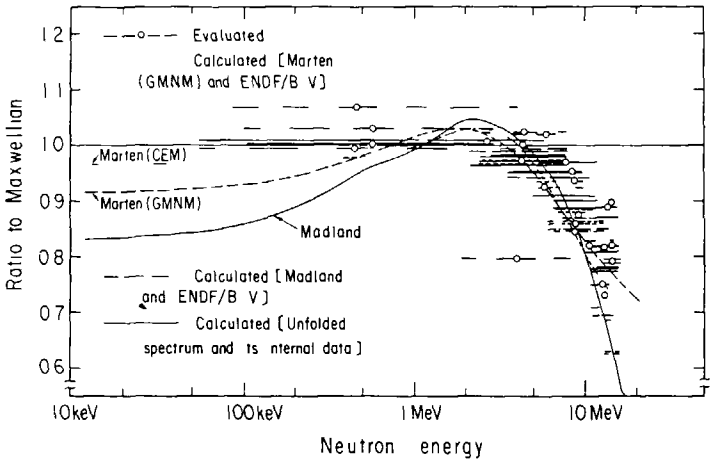

Fig 4 Plots of the response energy (90 % confidence level) and the ratio of each average cross section (evaluated and calculated) to the Maxwellian For comparison, those of the Madland's and Marten's(CEM and GMNM) predictions are shown

4 Plots of Average Cross Sections for ^{252}Cf Spontaneous Fission Neutron Spectrum by Horibe's Empirical Rule

Recently, one of the authors (O H) proposed an empirical rule for the estimation of ^{235}U fission neutron averaged cross sections for the (n,p) and (n,α) reactions and showed satisfactory results for large number of reacions/11,12/ By this rule, the average cross sections can be shown by

$$\sigma = A^{2/3} E_{eff}^{1/2} \exp(\alpha E_{eff} + \beta) ,$$

where A is the mass number of the nucleus and E_{eff} is the effective threshold energy defined by Hughes/21/ It was shown that most of the data points for the ^{235}U fission neutron averaged cross sections were clearly grouped by mass number (odd or even) and by neutron excess number t = N - Z

In this work, we investigated the applicability of this rule to the ^{252}Cf fission neutron spectrum averaged cross sections We also tried to apply this rule to the average cross sections for the (n,2n) reactions. In this case, the threshold energy E_{th} was used instead of E_{eff}

At first, the effective threshold energy E_{eff} to the Maxwellian spectrum (E_{av}=2 13 MeV) was calculated for each reaction by the same method described in the previous paper/11/ In this calculation, not actual integration but the summation was performed from 0 to 20 MeV with ΔE=50 keV All data, except that for the ^{52}Cr (n,p)^{52}V reaction/22/, are the evaluated values by Mannhart/3/ Although the number of the present data is less than that for the ^{235}U fission neutron averaged cross sections, most of the data points can be grouped into two lines as seen in Fig 5 The coefficients α and β were obtained by the least squares approximation and are tabulated in Table 4. The ratio of the predicted average cross section by using the empirical rule to that evaluated by Mannhart is also given in this table Most of the data points are close to the fitted line for even nuclei, but the results for the $^{48}Ti(n,p)^{48}Sc$, $^{56}Fe(n,p)^{56}Mn$ and $^{52}Cr(n,p)^{52}V$ reactions do not agree within the factor of 2 Similar tendency was seen in the case of the ^{235}U fission neutron averaged cross sections/11,12/ Agreement for odd nuclei seems to be satisfactory even for the $^{27}Al(n,p)^{27}Mg$ reaction (t=1)

The result for the (n,α) reactions is shown in Fig. 6 Three data points satisfactorily locate on the fitted line, which is parallel to that for the ^{235}U fission neutron averaged cross sections The fitted coefficients α and β and the C/E ratio for this case are tabulated in Table 4 The data point for the $^{27}Al(n,\gamma)^{24}Na$ reaction (t=1) is apart from the line

Similar plot was carried out for the (n,2n) reactions, where we took E_{th} for the abscissa instead of E_{eff}. The result obtained is shown in Fig 7 Although some t-values are quite large, most of data points are close to the fitted line for $t \geq 5$

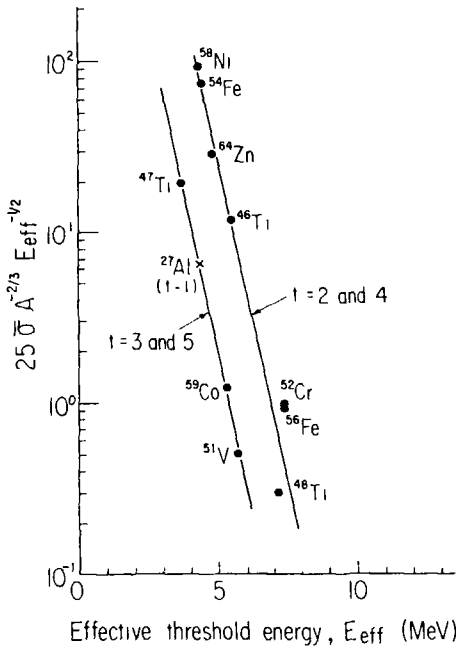

Fig. 5 Plots of $\log(25\,\bar{\sigma}A^{-2/3}E_{eff}^{-1/2})$ as a function of E_{eff} for the (n,p) reactions. Straight lines are the best fitted to the data points.

The numerical data are also given in Table 4. Except the cases of the $^{63}Cu(n,2n)^{62}Cu$ and $^{90}Zr(n,2n)^{89}Zr$ reactions, the C/E ratios converge to unity by about 10 %. The fitted line is parallel to that newly obtained for the ^{235}U fission neutron averaged cross sections. Two data points for $t \leq 2$ are apart from the above line.

Table 4 Comparison of effective threshold energy E_{eff} to the ^{252}Cf fission neutron spectrum, fitting coefficients α and β, and the ratio of the calculated average cross section using the empirical rule to the evaluated by Mannhart

Reaction	t	E_{eff}(MeV)	Ratio	α and β
$^{58}Ni(n,p)^{58}Co$	2	4.34	0.807	
$^{54}Fe(n,p)^{54}Mn$	2	4.41	0.988	
$^{64}Zn(n,p)^{64}Cu$	4	4.79	1.30	α=-0.740±0.073
$^{46}Ti(n,p)^{46}Sc$	2	5.54	0.903	
$^{48}Ti(n,p)^{48}Sc$	4	7.15	2.23	β=5.12±0.42
$^{56}Fe(n,p)^{56}Mn$	4	7.39	0.481	
$^{52}Cr(n,p)^{52}V$	4	7.40	0.451	
$^{47}Ti(n,p)^{47}Sc$	3	3.73	1.03	
$^{27}Al(n,p)^{27}Mg$	1	4.30	- - -	α=-0.785±0.058
$^{59}Co(n,p)^{59}Fe$	5	5.40	0.86	β=4.22±0.29
$^{51}V(n,p)^{51}Ti$	5	5.70	1.13	
$^{51}V(n,\alpha)^{48}Sc$	5	11.8	1.00	
$^{59}Co(n,\alpha)^{56}Mn$	5	10.6	0.98	α=-0.624+0.0073
$^{63}Cu(n,\alpha)^{60}Co$	5	9.83	1.01	β=5.675±0.078

Reaction	t	E_{th} (MeV)	Ratio	α and β
$^{197}Au(n,2n)^{196}Au$	39	8.12	1.00	
$^{127}I(n,2n)^{126}I$	21	9.21	0.89	
$^{65}Cu(n,2n)^{64}Cu$	7	10.1	0.94	α=-0.347±0.035
$^{55}Mn(n,2n)^{54}Mn$	5	10.4	1.05	
$^{59}Co(n,2n)^{58}Co$	5	10.6	0.93	β=2.97±0.36
$^{63}Cu(n,2n)^{62}Cu$	5	11.0	1.60	
$^{90}Zr(n,2n)^{89}Zr$	10	12.1	0.77	

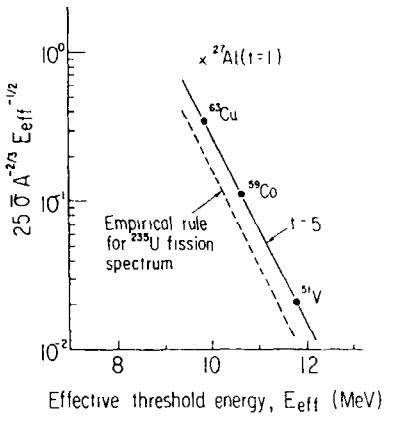

Fig. 6 Plots of $\log (25\,\bar{\sigma}\,A^{-2/3}\,E_{eff}^{-1/2})$ as a function of E_{eff} for the (n,α) reactions. Solid line is the best fitted to three data points for t = 5.

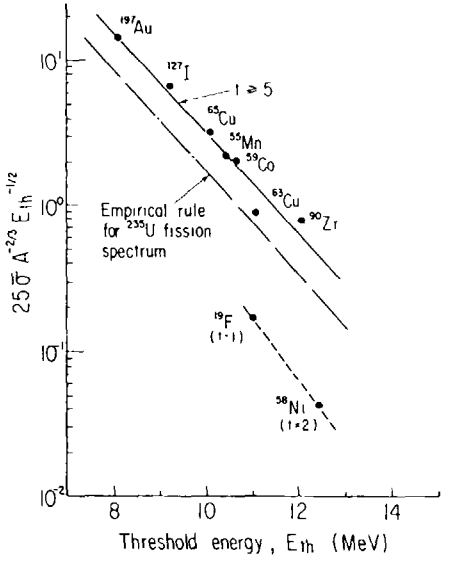

Fig. 7 Plots of $\log (25\,\bar{\sigma}\,A^{-2/3}\,E_{th}^{-1/2})$ as a function of E_{th} for the (n,2n) reactions. Solid and broken lines are the best fitted for $t \geq 5$ and t = 1, 2, respectively.

5. Conclusion

By making use of the twenty five ^{252}Cf fission spectrum averaged cross section data (Mannhart's evaluation), carried out were (1) unfolding the ^{252}Cf fission neutron spectrum by NEUPAC, (2) comparing them with the calculated average cross sections using three evaluated energy dependent cross section data and six expressions of the ^{252}Cf fission neutron spectrum, and (3) applying the average cross section data to the Horibe's empirical rule.

From these works, we can conclude:

(1) The gross shape of the unfolded ^{252}Cf spontaneous fission neutron spectrum is closer to the experimental values by Pönitz and Tamura and to the predicted ones by Madland and by Märten (CEM) than the Maxwellian (E_{av}=2.13 MeV), however there exists a little oscillatory structure. A peak around 6 MeV in the ratio of the unfolded spectrum to the Maxwellian nearly disappears, if we remove the cross section data for the ^{56}Fe(n,p)^{56}Mn reaction from twenty five data set. Little change was observed by the removal of other reaction data.

(2) The result of the comparison of the evaluated average cross section data with the calculated ones also supports the Madland's and Märten's predictions but does not agree with the Maxwellian. The best agreement is observed for the combination of the unfolded spectrum by NEUPAC and its internal data. The ranking next to this is ; the Märten's(CEM), the Märten's(GMNM), the Gerasimenko's and the Madland's, when we use ENDF/B-V. The convergence factors for ENDF/B-V are slightly better than those for JENDL-2 except in the case of the Madland's prediction.

(3) The evaluated energy dependent cross section data in ENDF/B-V and JENDL-2 for the ^{47}Ti(n,p)^{47}Sc and ^{58}Ni(n,2n)^{57}Ni should be improved.

(4) Applicability of the Horibe's empirical rule to the ^{252}Cf fission spectrum averaged cross section data for the (n,p) and (n,α) reactions has been demonstrated with a few exceptions. Similar rule to the data for the (n,2n) reactions is also observed.

Acknowledgments

The authors are deeply grateful to Prof. M Nakazawa and Dr. T. Iguchi of University of Tokyo for supplying the NEUPAC code. Thanks are due to Dr H Marten of Technical University of Dresden for his sending the numerical data. Kind arrangement for supplying nuclear data by Dr. T Asami of Nuclear Data Center in JAERI is heartly appreciated

They are very thankful to Dr W. Mannhart of PTB and to Dr. T Ohsawa of Kyushu University for fruitful discussions on this subject

REFERENCES

/1/ M.F.Vlasov(ed.), IAEA Consultants Meeting on Integral Cross Section Measurements in Standard Field, INDC(NDS)-81/L+M (1976).

/2/ J A Grundl and C M.Eisenhauer, Compendium of Benchmark Neutron Fields for Reactor Dismetry, Standard Neutron Field Entries, NBSIR 85-3151 (1986)

/3/ W.Mannhart, Proc. Fifth ASTM-Euratom Symp. on Reactor Dosimetry (J.P.Genthon and H. Rottger, eds.) Vol 2, p.801, D Reidel Publ. Co (1985)

/4/ K.Kobayashi, I Kimura and W.Mannhart, J. Nucl. Sci. Technol. 19, 341 (1982)

/5/ M.Nakazawa and A.Sekiguchi, Proc. Second ASTM-Euratom Symp. on Reactor Dosimetry, NUREG/CP-0004, Vol 3, p 1423 (1977)

/6/ ENDF/B-V Dosimetry File (TAPE=531) (1979).

/7/ JENDL-2, Japanese Evaluated Nuclear Data Library (1982).

/8/ D.G Madland and R.J.LaBauve, Preprint LA-UR-84-129 (1984), and private communication (1985).

/9/ H.Marten and D Seeliger, IAEA-TECDOC-335, p.255 (1985).

/10/ B.F Gerasimenko and V.A Rubchenya, ibid , p 280 (1985)

/11/ O.Horibe, Ann. Nucl Energy, 10, 359 (1983)

/12/ O Horibe, a paper presented at the Intern Conf on Nucl. Data for Basic and Applied Science, Santa Fe, May 1985, to be published in "radiation effects".

/13/ S.Suzuki, et al., Proc. Fourth ASTM-Euratom Symp. on Reactor Dosimetry, NUREG/CP-0029, Vol 1, p 171 (1982).

/14/ M.Nakazawa and A.Sekiguchi, Proc Third ASTM-Euratom Symp. on Reactor Dosimetry, EUR 6813, EN-FR, Vol.2, p.751 (1980).

/15/ K.Kobayashi, I Kimura, et al., to be published.

/16/ W P Pönitz and T.Tamura, Proc. Intern. Conf. on Nucl Data for Science and Technol., ed by K.H.Bockhoff, p.479, D Reidel Publ (1983).

/17/ H.Marten, private communication (1986)

/18/ K Kobayashi and I.Kimura, NEANDC(J)-116/U (unpublished) p.53 (1985)

/19/ Y Ikeda et al , ibid , p 16 (1985).

/20/ W Mannhart, a paper presented at the Intern. Conf. on Nucl. Data for Basic and Applied Science, Santa Fe, May 1985, to be published in "radiation effects".

/21/ D.J Hughes, "Pile Neutron Research", Addison- Wesley (1953)

/22/ K.Kobayashi, I Kimura, H Gotoh and H Tominaga. Ann Rep. Res. Reactor Inst , Kyoto Univ , 17, 15 (1984).

/23/ V A Rubchenya and B.F Gerasimenko, a paper presented at this meeting.

NEW EXPERIMENTAL AND THEORETICAL RESULTS OF THE ENERGY AND ANGULAR DISTRIBUTION OF Cf FISSION NEUTRONS

H. MÄRTEN, D. RICHTER, D. SEELIGER
Technical University of Dresden,
Dresden

W.D. FROMM, W. NEUBERT
Zentralinstitut für Kernforschung,
Rossendorf

German Democratic Republic

Abstract

Employing a direction-sensitive method of fission fragment detection in conjunction with neutron time-of-flight spectroscopy the energy and angular distribution of Cf fission neutrons has been measured. The correlation experiment and multiparameter analysis is briefly described. We present first experimental data which are compared with statistical-model calculations in the framework of the complex cascade-evaporation model as well as an extended version of the generalized Madland-Nix model.

1. Introduction

A detailed study of the mechanism of fission neutron emission is only possible on the base of a precise measurement of $N(E,\Theta:P_f)$ (P_f-fragment parameter set) or at least $N(E,\Theta)$ as recommended by an IAEA Consultants' Meeting.[1]
Such investigations are important because of open fundamental questions (scission neutrons) as well as for practical purposes (development of models for the calculation of fission neutron spectra).[2] Concerning asymmetric fission reactions, Θ is defined as the angle between neutron and light fragment direction commonly. In any case of $N(E,\Theta)$ measurements, the determination of the fragment direction and the distinction between the light and the heavy fragment group have to be arranged. On principle, the following methods of the $N(E,\Theta)$ measurement can be applied:

i) Detection of the fragments at a fixed direction; use of one neutron detector and consecutive measurement of the neutron energy spectra for selected angles.[3]

ii) As item(i), but use of several neutron detectors (multidetectorsystem) to measure $N(E,\Theta)$ at the selected angle points simultaneously (Ref. 4 but without distinction of light and heavy fragments).

iii) Use of only one neutron detector and application of a direction-sensitive method of fragment detection.

The method according to item (iii) implies the simultaneous measurement of the whole $N(E,\Theta)$ distribution applying only one neutron detector. Systematic errors concerning the other methods are avoided obviously. Two papers concerning a type-(iii) experiment have been published recently.[5,6] These arrangements rely on the use of a gridded ion twin chamber[5] and a double-PPAC set-up (one position-sensitive) - to be described in this paper in more detail - respectively.

2. Experimental arrangement

A scheme of the fragment-neutron correlation experiment is represented in Fig. 1.

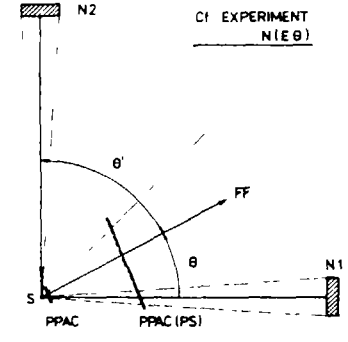

Fig. 1
Schematic representation of the experimental arrangement (S - ^{252}Cf source, PPAC - parallel-plate avalanche counter, PPAC(PS) - large PPAC, position-sensitive, N1,N2 - NE 213 scintillators for neutron detection, FF - fission fragment direction).

The fragment detection set-up consisting of two different parallel-plate avalanche counters[7] (PPAC) is mounted in a thin-wall chamber with low-pressure heptane ($\sim 10^3$Pa).
The single PPAC located beside the fission sample S (5 mm normal distance) provides a timing signal for fragment time-of-flight (TOF) and neutron TOF spectroscopy.
A large position-sensitive PPAC (35 x 180 mm^2), whose cathode is subdivided into 36 strips of 4.5 mm width, serves for the measurement of fragment direction (Fig. 1).
The PPAC(PS) strip signals are coupled into a delay line inductively (220 ns maximum delay). Measuring the time difference between the PPAC(PS) anode signal and the delay line pulse one gets the position (fragment direction) information (Fig. 3).
The normal distance between both PPAC amounts to 170 mm. The FF-TOF measurement enables the distinction between light and heavy fragment group.
Two identical neutron detectors consisting of NE 213 scintillator and XP 2040 photomultiplier are located as shown in Fig. 1. The neutron flight paths amount to 1.6 m. n/γ-discrimination is used to suppress the background.

Fragment TOF, fragment direction and neutron TOF of the two neutron detectors are measured employing a multi-parameter data acquisition system with KRS 4201 computer, magnetic disc and an universal microprocessor-controlled set-up for the handling of two-dimensional spectra.
Typical single spectra are shown in Fig. 2 and 3.

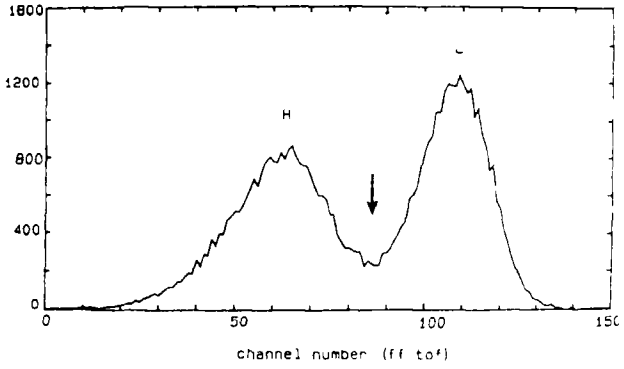

Fig. 2
Typical FF-TOF spectrum for a selected FF-direction. The arrow indicates the dividing point for the distinction of light and heavy fragment group (L, H).

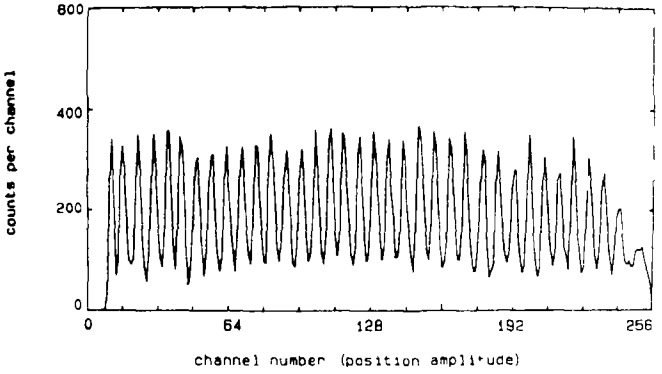

Fig. 3
Typical position spectrum exhibiting 36 resolved peaks which correspond to the PPAC(PS) strips.

3. Data analysis

The dividing line between heavy and light fragment group is a function of FF-direction (position amplitude) due to the position-dependent FF flight path (Fig. 1). The sorting code generates the two-dimensional (neutron TOF, position)-spectra for both fragment groups on the basis of channel limit table to be determined from the analysis of the non-correlated (FF-TOF, position)-spectrum. The latter one is also used to deduce the geometrical efficiency of the PPAC(PS), which was found to be identical for both fragment groups and equal to the geometric calculation (within the uncertainty of the PPAC(PS) strip area, i.e. about 1 %). The correlated position spectra deduced for selected neutron energy intervals are unfolded by the use of a rather simple Gaussian-fit algorithm. The peak area for a given FF direction (angle θ) and a selected E interval divided by the geometrical efficiency of the PPAC(PS) strip is proportional to $N(E,\theta)$.

4. Results

The experimental arrangement described above was employed to measure $N(E,\theta)$ of neutrons from ^{252}Cf(sf). This reaction represents a "standard" subject for the study of fission neutron emission.

Using the FF-TOF measurement for the L/H distinction (cf. Fig. 2) a small part of the fragments (about 2.5 %) is not correctly classified for physical (FF-TOF is a function of fragment kinetic energy per nucleon) as well as experimental reasons (time resolution). This effect concerning the uncertainty of $N(E,\Theta)$ data was estimated to be of minor importance. A part of the results of a 500-h-measurement carried out with a thin Cf source on Ta backing with 10^4 f/s strength is shown in Fig. 4.

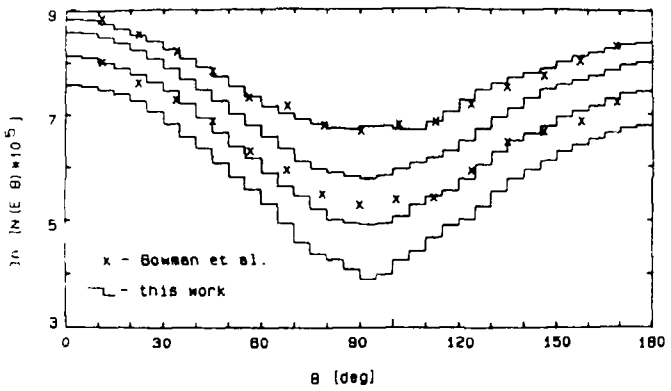

Fig. 4
Measured angular distributions (histograms) for 2, 3, 4, and 5 MeV in comparison with the data of Bowman et al.[3] The statistical errors are about 3 and 5-8 % in polar and equatorial direction, respectively.

The original data points (3.1 deg angular resolution) have been concentrated for 5 deg angle bins. We considered the random background and the background due to scattered neutrons. The latter part has been measured by the use of Fe shadow cones.
At energies below 3 MeV, the angular distributions are in excellent agreement with the data of Bowman et al.[3] The measured anisotropies for E above 4 MeV are considerably higher than previous data[3,8] in agreement with recent measurements carried out at CBNM Geel[5] and TU Dresden/CINR Rossendorf.[6] The angular distributions can be reproduced by calculations performed in the framework of the complex cascade evaporation model (CEM)[9] as well as an extended version of the generalized Madland-Nix model (GMNM 2) (Figs. 5, 6). No arbitrary normalizations have been included. Both the CEM and the GMNM yield a very good description of the $^{252}Cf(sf)$ energy spectrum.[2] Calculated angular distributions are similar.

A more thorough comparison between experiment and theory is in progress.

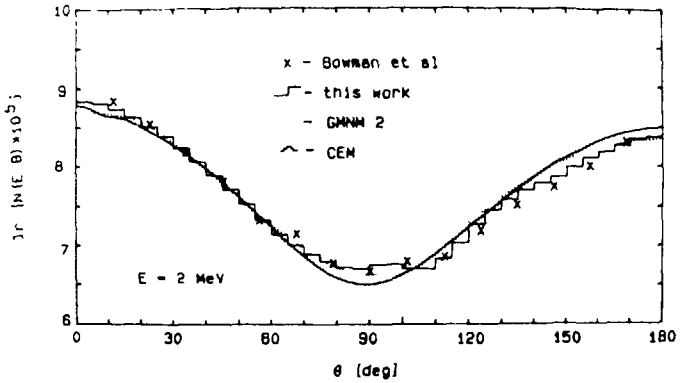

Fig. 5
$^{252}Cf(sf)$ neutron angular distribution at 2 MeV in comparison with statistical-model calculations (CEM, GMNM 2)[9,10].

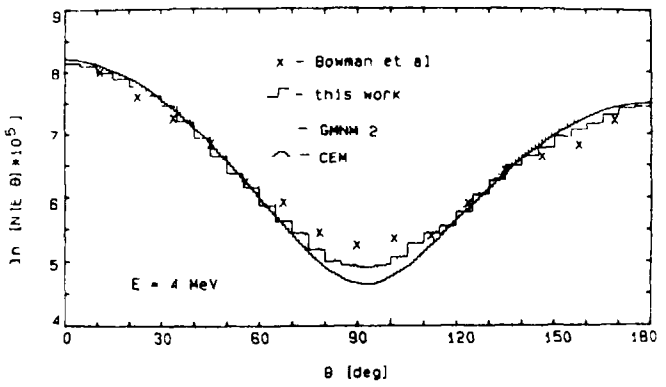

Fig. 6
As Fig. 5, but for E = 4 MeV

5. Conclusions

The experiment described render it possible to measure $N(E,\theta)$ for the whole angular range simultaneously. This guarantees a high accuracy of the shape of angular distributions. Complex statistical-model approaches, which are based on the assumption that all neutrons are emitted (evaporated) from fully accelerated fragments, have been used to reproduce the data satisfactorily. Within the uncertainty of experimental as well as theoretical results, no indications of other emission mechanisms have been found.

References

1 Proc. IAEA Cons. Meet. on the U-235 Fast-Neutron Fission Cross-Section and the Cf-252 Fission Neutron Spectrum, 1983, Smolenice (CSSR), INDC(NDS)-146/L (1983)

2 H. Märten et al., Proc. IAEA AGM on Nuclear Standard Reference Data, 1984, Geel (Belgium), IAEA-TECDOC-335 (1985) 255

3 H.R. Bowman et al., Phys. Rev. 126 (1962) 2120

4 E.A. Seregina and P.P. Dyachenko, Yad. Const. Vol. 1 (1985) 58

5 C. Budtz-Jørgensen and H.H. Knitter, Proc. Int. Conf. on Nucl. Data for Basic and Appl. Sci., 1985, Santa Fe (USA) and Proc. Int. Conf. on Nucl. Phys., 1985, Gaußig (GDR), in press

6 H. Märten et al., ibid.

7 W. Neubert et al., Nucl. Instr. Meth. 204 (1983) 453

8 C.J. Bishop et al., Nucl. Phys. A 198 (1972) 161

9 H. Märten et al., J. Phys. G 10 (1984) 349

10 H. Märten et al., INDC(GDR)-30/L (1984) and H. Marten et al., contributed paper to this AGM.

THE NEUTRON SPECTRUM OF THE SPONTANEOUS FISSION OF Cf-252 (3–12 MeV NEUTRON ENERGY)

R. BÖTTGER, H. KLEIN
Physikalisch-Technische Bundesanstalt,
Braunschweig, Federal Republic of Germany

A. CHALUPKA, B. STROHMAIER
Institut für Radiumforschung und Kernphysik,
University of Vienna,
Vienna, Austria

Abstract

A neutron spectrum of a source with 10^5 fissions s^{-1} installed in a miniatur ionization chamber was investigated at the PTB's time-of-flight spectrometer (flight path 12 m, 4 NE 213-type detectors, 25.4 cm x 5.08 cm). Some of the influences exerted on the neutron spectrum, such as efficiency of the ionization chamber for fission fragments, chamber material and corrections of the time-of-flight spectrum are discussed. The preliminary data presented in Antwerp in 1982 were re-analyzed on the basis of a modified efficiency of the neutron detector. The energy spectrum determined in this way is compared with various theoretical models. The Maxwellian distribution generally applied (E_o = 1.42 MeV) is incompatible with our results in the 3 to 12 MeV energy range.

The neutron energy spectrum from a Cf-252 source was measured in two series of experiments with a set of four identical, large volume NE 213 scintillation detectors (5.08 cm x 25.4 cm Ø) at the PTB time-of-flight (TOF) spectrometer. Measurement principles and results of the first experiment with the Vienna low mass fast ionization chamber have already been discussed, including the presentation of an improved analysis of the TOF spectrum (Ref. 1 - 5). For the second experiment performed more than four years later, the Cf source was replaced by a source of

about 50 % higher source strength and better fragment detection efficiency to generate the timing signal for the stop-channel in the TOF measurement.

The flight path of 12 m between the center of the scintillator and the source plate was the same for all detectors in all TOF experiments, thus achieving very high energy resolution with a TAC (time-to-amplitude converter) range of 1 μs and a TOF channel width of about 1 ns. The efficient n-γ discrimination is capable of separating the high photon background mainly originating from the surrounding of the unshielded detector from the few neutron events. Each event included light output (L(E) with charged particle energy E), particle identification signal, time-of-flight, and the energy loss signal of one of the two fission fragments. The data of only one detector were not included in the analysis due to instability of the TAC. For the other detectors excellent stability was found concerning time calibration, n-γ discrimination and thresholds in L(E) over more than three weeks.

The first fission fragment detector with a count rate of 110 000 s^{-1} had golden chamber walls with a golden backing, for which the effect of neutron absorption and production by the material was calculated on the basis of data evaluated with the STAPRE code. For $E_n \geq 2$ MeV the resulting corrections are of the order of $2 \cdot 10^{-3}$. The time resolution from the fragment detector together with a large scintillation detector with a bias of about 500 keV electron energy is 1.5 ns (FWHM). Extensive investigations were performed to study the influence of some parameters such as bias voltage polarity, roughness of the source backing and time pick-up on the fragment detection efficiency which was found to be 95.4 % for the golden chamber with a measured surface roughness parameter R_z = 2.0 μm. Computer simulations show that mainly the surface roughness is responsible for the loss of fragments because of fragment absorption or reduction of the pulse height below the threshold value which is set to separate α-particles and fission fragments. The second source (fission rate 160 000 s^{-1}) had a highly polished platinum backing and front plate. The roughness parameter was much smaller (R_z = 0.2 μm), resulting in a fragment detection efficiency of 99.5 % ± 0.2 %. As there is selective fragment absorption as far as the emission angle is concerned, an energy-dependent correction must be applied in the prompt neutron energy spectrum. This is taken into account for the first source (Ref. 1, 4), but can be neglected for the platinum source. The distortion of the neutron spectrum by the chamber material is similar for both sources for $E_n \geq$ 2 MeV. Excellent discrimination properties between α-particles and fission fragments are observed for both ionization chambers. Because of a different sealing system, the assembly or repair of the platinum chamber is easier, the higher mass being, however, a disadvantage.

After the random background has been subtracted from the measured TOF distribution, the background due to uncorrelated stops is analytically determined and subtracted. The difference between experiment and calculation for this background is less than 2 %. A channel-dependent renormalization factor must be applied to correct for the subtracted background with uncorrelated stops taking into account the dead time in the stop-channel. For the first experiment, the neutron energy distribution must be normalized by an energy-dependent factor due to neutrons whose associated fission fragments could not be detected.

The main problem involved in the measurement of the energy distribution is the normalization due to the neutron detection efficiency. The energy dependence is taken from MC simulations (NEFF5 code), which are based on carefully determined light output and resolution functions.

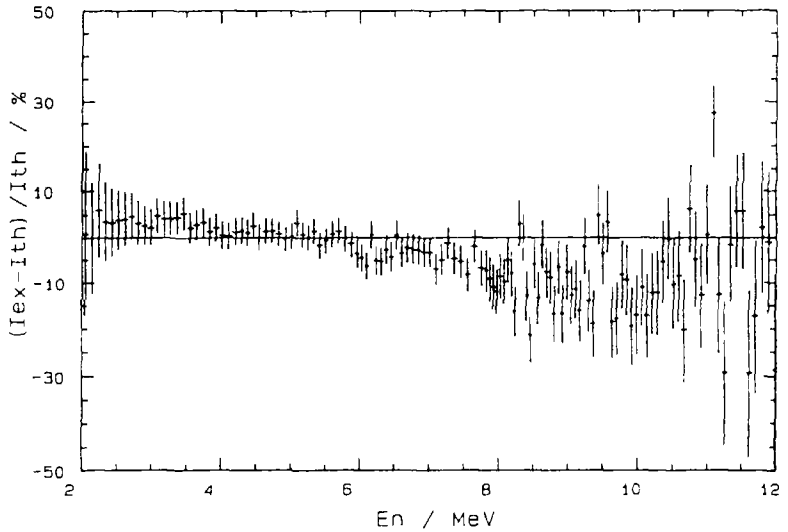

Fig. 1: Det. 3 / January 86: Relative difference between the experimentally determined spectral yield I_{ex} and I_{th} from a Maxwellian with E_o = 1.42 MeV

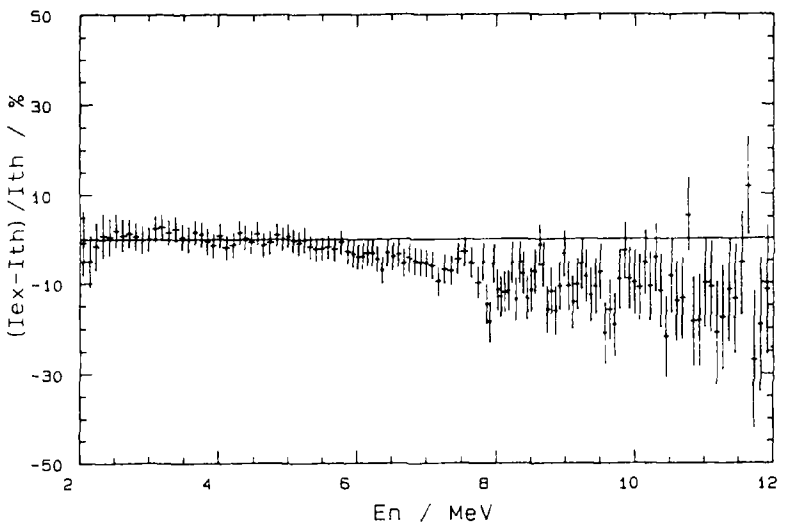

Fig. 2: Det. 3 / August 81: Experimental data from August 81 in comparison with a Maxwellian with E_o = 1.42 MeV

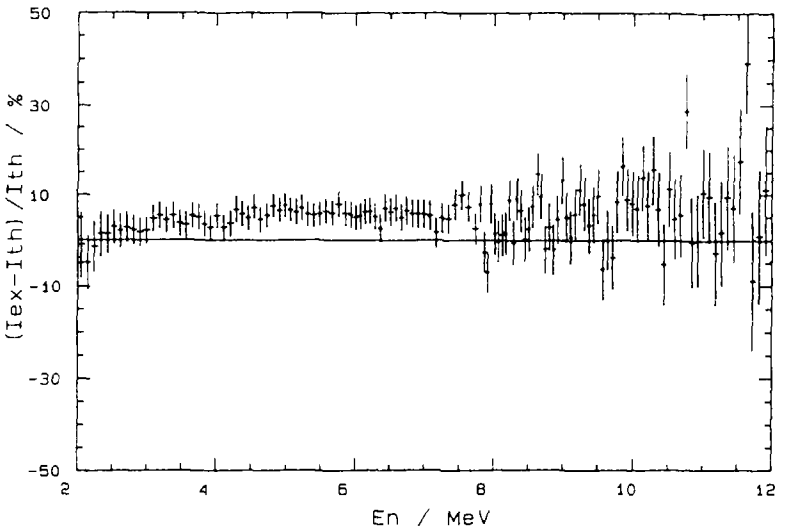

Fig. 3: August 81: Relative difference between the experimentally determined spectral yield I_{ex} and I_{th} from a Maxwellian with E_o = 1.375 MeV

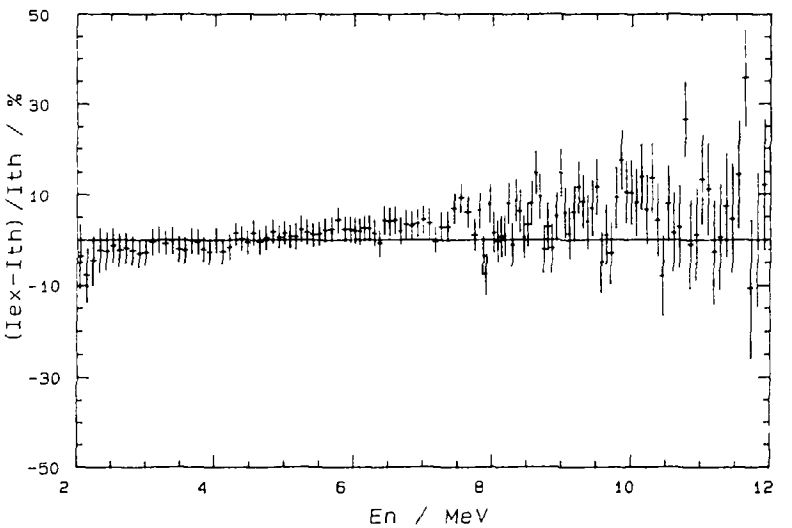

Fig. 4: August 81: Experimental data in comparison with CEM calculation (TUD)

The comparison of the neutron fluence determined with a proton recoil telescope (PRT) and the reference detector of the spectrometer (2.54 cm x 10.16 cm Ø) showed excellent agreement within uncertainties of ± 2 % for the energy range 6 MeV ≤ E_n ≤ 14 MeV. Cross reference measurements between the large volume detectors used for these investigations and the reference detector yielded an energy-independent normalization factor of 1.05 ± 0.02. These resulting efficiencies were confirmed by n-p scattering in the energy range 3 MeV ≤ E_n ≤ 12 MeV within the estimated uncertainties of ± 3 %, but a small energy-dependent correction cannot be excluded. Additional experiments are being analysed.

However, the preliminary experimental calibration which was chiefly based on the angular distribution of the D(d,n)^{3}He reaction, had to be revised.

Finally, the efficiency is given with uncorrelated uncertainties of the order of 1.0 % due to statistics and uncertainties in the calculation of the air attenuation of 0.8 ... 1.2 %. A common 2 % uncertainty must be considered in the absolute scaling.

The neutron energy distributions for one representative detector are displayed with a variable bin width of 50 - 100 keV and an absolute comparison with three reference spectra is carried out (Fig. 1 - 4). If a Maxwell distribution is assumed, we find for all detectors an energy parameter of E_o = (1.375 ± 0.005) MeV between 3 MeV and 12 MeV. Agreement between experimental data and theory is achieved if a normalization factor of 1.06 ± 0.02 is applied to the theoretical distribution. The comparison between our experimental data and the recommended Maxwellian distribution with E_o = 1.42 MeV shows good agreement between threshold and 6 MeV. For higher energies, deviations of up to 15 % are, however, measured. Also for the cascade evaporation model (CEM, TUD) no deviation is found within the statistical uncertainties up to 6 MeV. For 8 MeV ≤ E_n ≤ 12 MeV the ratio between the experimental and theoretical data is about 1.05. Our conclusion is that this theoretical spectrum provides best overall agreement with our experimental data. The experiments show in addition that there are no deviations in the results neither from the individual detectors nor from the two series of experiments.

References

1. R. Bottger et al., Nuclear Data for Science and Technology, Proc. of the Int. Conf. in Antwerp, ed. K.H. Bockhoff Reidel Publ. Comp., Dordrecht 1983, p. 484 - 487
2. H. Klein, Proceedings of the "XII. Intern. Symp. on Nuclear Physics", ed. R. Reif and J. Teichert ZfK-491, p. 113 - 121
3. H. Klein et al., Proc. of the IAEA Consultants Meeting, Smolenice, Report INDC (NDS)- 46 (1983), p. 191 - 194
4. A. Chalupka et al., Proc. of the IAEA Consultants Meeting, Smolenice, Report INDC (NDS)-146 (1983), p. 187 - 190
5. H. Klein et al., Proc. of the IAEA Advisory Group Meeting on Nuclear Standard Reference Data, Geel, Report IAEA-TECDOC-335, p. 433 - 436

190 Cf-252 FISSION NEUTRON SPECTRUM ABOVE 15 MeV*

A. CHALUPKA, L. MALEK, S. TAGESEN
Institut für Radiumforschung und Kernphysik,
University of Vienna,
Vienna, Austria

R. BÖTTGER
Physikalisch-Technische Bundesanstalt,
Braunschweig, Federal Republic of Germany

Abstract

The high energy tail (~ 15 to 30 MeV) of the neutron spectrum from the spontaneous fission of ^{252}Cf was measured with excellent shielding against cosmic radiation No significant deviation from Maxwellian shape (T = 1 42 MeV) and no indication of any neutron excess above 20 MeV was found

The high energy tail (up to ∿ 30 MeV) of the neutron spectrum from the spontaneous fission of ^{252}Cf was first investigated in 1982 by the TUD group /1/ using the time-of-flight (TOF) method. The authors found a clear deviation from a Maxwellian shape with a temperature parameter T = 1.42 MeV above 20 MeV neutron energy (see Fig. 1 and crosses in Fig. 6). A second TOF experiment was done in collaboration between the TUD and PTB /2,3/, and one set of results thereof ("detector 1 data") seemed to confirm the earlier measurement (Fig. 6, histograms 1 and 2) though the experimental uncertainty above 21 MeV amounts to 80 to 100 per cent (1 standard deviation).

Despite many advantages of the TOF method its applicability to the determination of this part of the spectrum suffers from the background due to cosmic particle radiation. Background reduction may be achieved by sophisticated apparative provisions or heavy shielding. We decided on the latter and performed a TOF experiment in a mine in Bad Bleiberg, Carinthia, early this year. Prior to the experiment, background measurements had been performed on sites in question for the experiment. A site at the end of an adit about 600 m below ground was chosen. Fig. 2 shows pulse-height spectra taken above (I,II) and below (III) ground with a neutron detector containing an NE213 liquid scintillator cell (Nuclear Enterprises Ltd., Edinburgh) 12.6 cm in diameter and 2.54 cm in height. The broad peaks are due to energy loss signals from cosmic radiation.

A micro-processor controlled measuring and data collection system capable of withstanding the environmental conditions in the mine was developed. A TOF experiment with a four parametric event by event data collection was performed applying a calibrated NE213 neutron detector (25.4 cm in diameter, 5.08 cm in height) from the PTB and a fast fission chamber. Besides TOF data, also light output and pulse shape information from the neutron detector signal and the energy loss signal from the fission chamber were recorded. A recently developed "pile up unit" /4/ allowed an identification of events with a unique time measurement. Characteristics of the experiment are summarized in Table 1.

Table 1

Median flight path	(279.6 ± 0.2) cm
Time channel width	0.2085 ns
TAC-range	400 ns
Time resolution (FWHM)	0.91 ns
^{252}Cf source strength (Jan. 1, 1986)	$1.564 \cdot 10^5$ fissions/s ± 0.2 per cent
Fission chamber efficiency	0.995 ± 0.002
Neutron detector: diameter	25.4 cm
thickness	5.08 cm
Run times: run 1	79.86 h
run 2	247.58 h
Bias setting: bias 1	4 MeV equiv. electron energy
bias 2	5 MeV equiv. electron energy
Background (TOF): bias 1	0.144 counts per channel ± 8 per cent
bias 2	0.088 counts per channel ± 10 per cent

* This work was supported by the International Atomic Energy Agency

Table 2

Energy bin in MeV	Calculated yield Maxwellian, T=1.42 MeV		Measured yield (counts)		Background (counts)		Ratio measurement to calculation		Relative uncertainty (per cent)
	Bias 1	Bias 2	Bias 1	Bias 2	Bias 1	Bias 2	Bias 1	Bias 2	
13.98 - 15.01	2004.70	1579.60	1749	1391	1.30	0.79	0.87	0.88	8
15.01 - 16.03	994.00	807.53	892	713	1.15	0.70	0.90	0.88	8
16.03 - 17.01	481.69	401.47	431	353	1.00	0.62	0.89	0.88	8
17.01 - 17.93	232.62	198.81	230	198	0.86	0.53	0.98	0.99	9
17.93 - 18.92	131.47	113.76	127	110	0.86	0.53	0.96	0.96	10
18.92 - 20.00	70.55	61.65	81	73	0.86	0.53	1.14	1.17	11
20.00 - 20.97	31.10	27.52	35	34	0.72	0.44	1.10	1.22	13
20.97 - 22.91	23.74	21.29	23	22	1.30	0.79	0.91	1.00	23
22.91 - 24.87	6.14	5.59	11	9	1.15	0.70	1.60	1.58	35
24.87 - 27.10	1.64	1.50	3	2	1.15	0.70	1.12	0.87	95
27.10 - 28.98	0.32	0.29	1	1	0.86	0.53	0.44	1.59	-

A comprehensive discussion of the design and properties of the fission chamber is to be found in earlier papers /5,6/. A short description is given in another contribution to this meeting /7/. The neutron detection efficiency of the scintillator in the energy region from 18 to 30 MeV was calculated from hydrogen cross section data /8/. For energies between 14 and 18 MeV, the result of the code NEFF4 /9/ was used. An uncertainty of 5 to 8 per cent was assigned to the efficiency data.

Off line data reduction was performed for two bias settings: at 4 MeV (bias 1) and at 5 MeV (bias 2) equivalent electron energy. Fig. 3 shows a three dimensional representation of the data. With respect to the bias the resulting TOF spectrum was generated from all the events within the area indicated . The position of the gamma-peak was obtained from all events above the bias and is plotted in Fig. 4.

The TOF spectrum after data reduction is shown in Fig. 5. The background was determined in the region from channel 2561 to channel 3740. In the energy region below 15 MeV neutron energy, the spectrum is in excellent agreement with previous measurements in that energy range /10/.

Assuming a neutron source with a Maxwellian energy distribution and taking the experimental parameters of Table 1, the efficiency function and a value of $\bar{\nu}$=3.77 for the mean number of neutrons per fission event /11/, we calculated the yield to be expected. The geometrical resolution function was taken to be rectangular with a width equal to the detector thickness, and the time resolution function was assumed to be Gaussian. The results are shown in Table 2 and Fig. 6 (bias 1 data only). We do not find any significant deviation from the Maxwellian shape. This finding is in accordance with recent results from integral measurements /12/ which do not indicate any neutron excess in the high energy wing of the ^{252}Cf spectrum.

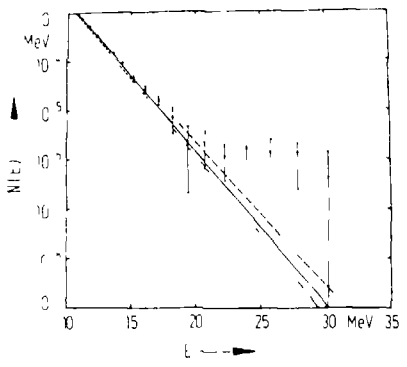

Fig. 1: This figure is taken from Ref. 1 (Fig. 8) and shows the measured spectral neutron yield N(E) of a Cf-252 source versus neutron energy E compared with the NBS spectrum (solid line) and the cascade evaporation model (dotted line). A Maxwellian with a temperature parameter T = 1.42 MeV (dashed line) is added.

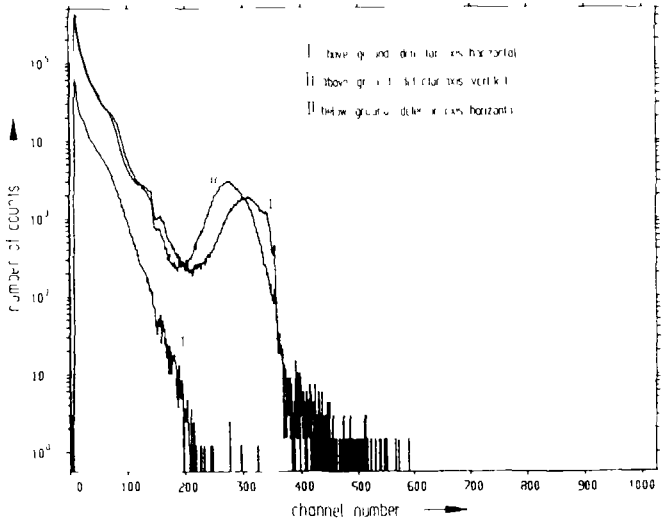

Fig. 2: Pulse height spectra as measured above ground with the scintillation detector axis horizontal (I), vertical (II) and 600 m below ground (III) normalized to 10^5 s collection time.

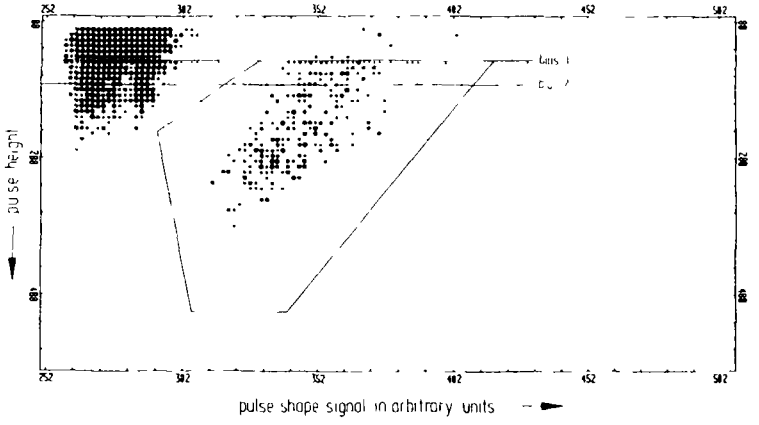

Fig. 3: Pulse height (38 channels correspond to 1 MeV equivalent electron energy) versus pulse shape signal.
smallest point stands for 1 event
largest point stands for 6 events and more
Events within the indicated area are interpreted as neutrons.

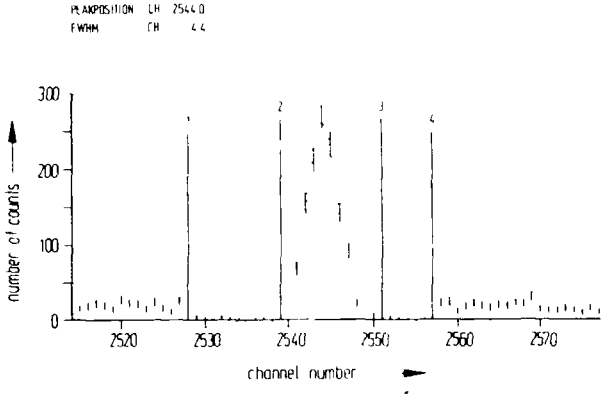

Fig. 4. Distribution of photon-induced events in the time-of-flight spectrum (bias 1). From marker 1 to marker 4 the contents of the channels must be multiplied by 10. The result of a fit between marker 2 and 3 is shown as a dotted line.

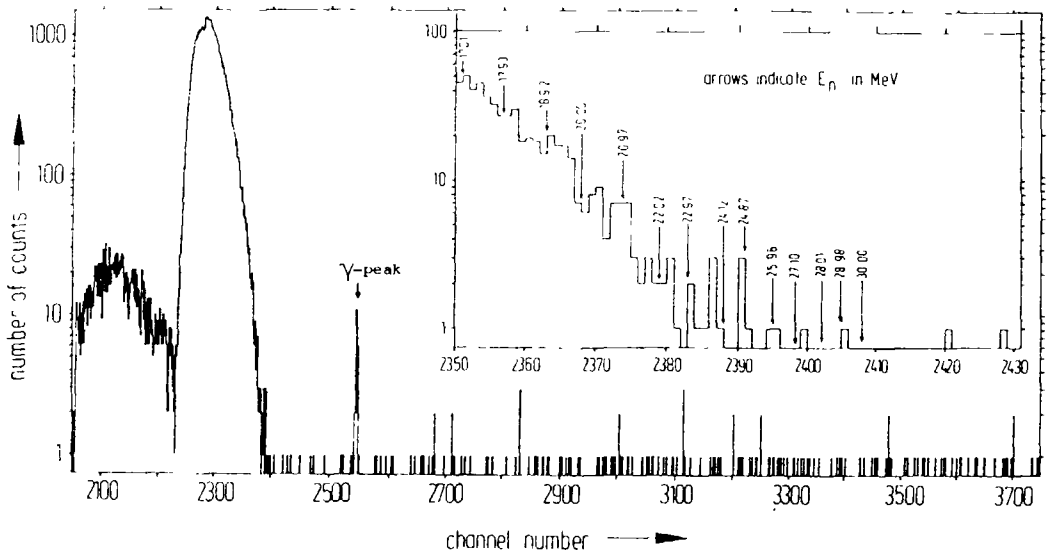

Fig. 5: Detector event numbers versus neutron time-of-flight (0.2085 ns/channel). Total time of accumulation was 327.44 h. (Sum of run 1 and 2).

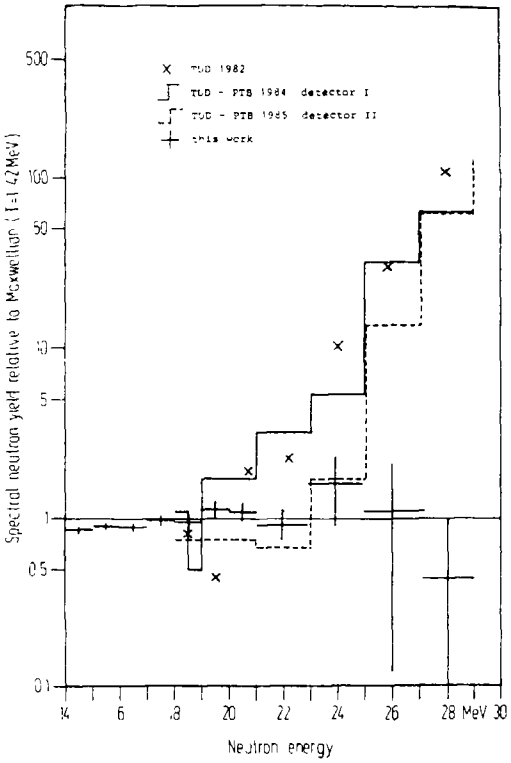

Fig. 6: Measured spectral neutron yield from Ref. 1 - 3 and this work relative to a Maxwellian with T = 1.42 MeV. Bars indicate the statistical uncertainty and the energy bin width, respectively.

Acknowledgements: Without the generous support of the Bleiberger Bergwerksunion this investigation would have been impossible. We also appreciate the help of many colleagues of the scientific and technical staff of the IRK.

References

/1/ H. Marten, D. Seeliger and B. Stobinski, INDC(GDR)-17/L, 1982

/2/ H. Märten, D. Richter, D. Seeliger, R. Bottger, W.D. Fromm, Proc. of an IAEA Advisory Group Meeting on Nuclear Standard Reference Data, Geel, 12-16 Nov. 1984, IAEA-TECDOC-335

/3/ R. Bottger, W.D. Fromm, H. Klein, H. Märten, D. Richter, D. Seeliger, Proc. of Int. Conf. on Nuclear Data for Basic and Applied Science, Santa Fé, USA, 13-17 May 1985, in press

/4/ A. Chalupka, S. Tagesen, Nucl. Instr. Meth. A245 (1986) 159-161

/5/ A. Chalupka, Nucl. Instr. Meth. 164 (1979) 105-112

/6/ A. Chalupka, B. Strohmaier, R. Bottger, H. Klein, Proc. IAEA Consultants' Meeting, Smolenice, INDC (NDS)-146 (1983) 187-190

/7/ R. Böttger, H. Klein, A. Chalupka, B. Strohmaier, paper contributed to the present meeting

/8/ A. Del Guera, Nucl Instr. Meth. 135 (1976) 337-352

/9/ G. Dietze, H. Klein, Ext. PTB Rept. ND-22 (1982)

/10/ R. Bottger, H. Klein, A. Chalupka, B. Strohmaier, Proc. of the Int. Conf. on Nuclear Data for Science and Technology, Antwerp, 6-10 Sep 1982, p. 484

/11/ R. R. Spencer, Rept. NBS-594 (1980) 728-732

/12/ W. Mannhart, paper contributed to the present meeting

THE HIGH ENERGY PORTION OF THE Cf-252 NEUTRON SPECTRUM DEDUCED FROM INTEGRAL EXPERIMENTS

W. MANNHART
Physikalisch-Technische Bundesanstalt,
Braunschweig, Federal Republic of Germany

Abstract

To investigate the validity of the neutron excess in the Cf-252 spectrum above 20 MeV first reported by the Dresden group in 1982, the responses of two (n,3n) reactions were measured in a Cf-252 neutron field. The reactions were $^{107}Ag(n,3n)$ and $^{169}Tm(n,3n)$ which are both sensitive to the shape of the spectrum above 20 MeV. In parallel, the (n,2n) spectrum-averaged cross sections of both reactions were also determined. The experimental results were compared with calculated ones based on various assumptions of the shape of the neutron spectrum. Due to low induced radioactivities and close sample-to-detector distances, extensive calculations of cascade-summing corrections were made in the radioactivity analysis process before deriving spectrum-averaged cross section data. The comparison of the corrected experimental results with calculated spectrum-averaged data did not confirm the neutron excess above 20 MeV as quoted.

1. Introduction

In 1982, a group from the Technical University of Dresden (TUD) published experimental data of the Cf-252 neutron spectrum /1, 2/ which above 20 MeV neutron energy showed a strong excess of neutrons compared with existing assumptions on the shape of the spectrum. This result was of some interest, contradicting as it does the present understanding of the fission neutron spectrum based on neutron evaporation from fully accelerated fission fragments. A second (non-equilibrium) mechanism in the neutron emission process has been assumed /3/.

Due to the low neutron yield of the Cf-252 neutron spectrum above 20 MeV, in this time-of-flight experiment careful discrimination against myon induced events was necessary to yield a measurable effect. In spite of the large relative uncertainties (> 60 %) of the measured data points there is a distinct significance in the neutron excess in this experiment. It was the aim of the present work to investigate the validity of this effect by another independent method. The availability of a strong Cf-252 neutron source (3×10^9 s^{-1}) mainly used for average cross section measurements /4, 5/ offered an opportunity to study the neutron excess on an integral basis. The only neutron reactions which are sufficiently sensitive to the spectral component above 20 MeV were those based on the (n,3n) process. The principle of the present experiment was to measure the integral responses (spectrum-averaged neutron cross sections) of such reactions and to compare the results with those calculated on the basis of different assumptions of the shape of the neutron spectrum above 20 MeV. The method specifically requires sufficient knowledge of the excitation functions of the (n,3n) reactions used in the experiment. This condition and the additional requirement of a convenient measurable radioactivity of the reaction product nucleus strongly reduced the number of possible candidates of (n,3n) reactions. Finally, the reactions of $^{107}Ag(n,3n)$ and $^{169}Tm(n,3n)$ were identified as being appropriate for the present purposes.

The (n,2n) reactions of both nuclides were also measured. These reactions are only sensitive to the neutron spectrum below 20 MeV. Nevertheless, the (n,2n) reactions were useful in detecting a possible bias in the experiment.

The present results supersede earlier published data /6/. These preliminary values have been obtained from a first rough analysis of the present experiment and did not include all the corrections applied in this work.

2. Experimental procedure

The general procedure is similar to that of previous work /4, 5/ and is only briefly reviewed.

2.1 Samples

Generally, the samples were high-purity metallic disks 10 mm in diameter. A summary is given in Table 1. Due to a slight instability of thulium in air, the thulium foils were fitted into cylindrical lucite containers with inner dimensions of 0.8 mm in height and 10.1 mm in diameter. The wall thickness of the lucite containers at the front and the rear side was 0.2 mm. Seven of the 0.1 mm thick thulium foils were fitted into each container.

Table 1: Sample characteristics

Material	Chemical form	Purity	Isotopic abundance	Thickness
Tm	metallic foil	99 9 %	Tm-169 100 %	0.1 mm
Ag	metallic powder enriched[a)]	-	Ag-107 98 22 % Ag-109 1.78 %	-
Ag	metallic foil	99 99 %	Ag-107 51 83 % Ag-109 48.17 %	1.0 mm

[a)] Obtained from the Isotope Distribution Office, ORNL, USA

The very low radioactivity of Ag-105 resulting from the $^{107}Ag(n,3n)$ reaction required a minimum background-to-photopeak ratio. With samples of natural silver this condition could not be met, due to strong background contributions resulting from photons of the reaction $^{109}Ag(n,\gamma)^{110m}Ag$ with a half-life of 250 days.

Therefore material highly enriched in Ag-107 was used in the experiment (see Table 1). This material was filled into lucite containers identical with those used for thulium. In addition, samples of natural silver were used for the investigation of the $^{107}Ag(n,2n)^{106m}Ag$ reaction.

2.2 Irradiation

The irradiation was carried out over a period of one month at our low-scattering outdoor Cf-252 facility in a position 12 m above ground. The neutron source encapsulated in a zircaloy cylinder with outer dimensions of 10 mm in diameter and 10 mm in height had an emission rate of 3×10^9 s^{-1} in 4 π during the experiment. The samples were placed perpendicular to the cylinder axis of the source and almost touched the convex surface of the source. Nickel foils (0.25 mm thick, 10 mm in diameter) were placed at the front and the rear of each sample and acted as neutron fluence monitors.

2.3 Radioactivity counting

The radioactivity of the samples was measured with a large volume Ge(Li) detector. The photopeak efficiency of the detector was calibrated with an extensive set of standard gamma-ray sources. Corrections were applied for the extended volume of the samples and for self-absorption within the samples. The decay parameters used for the different radionuclides are listed in Table 2. In the case of $Ag-106^m$ and Tm-167 the large uncertainty contributions from the photon emission probabilities of these radionuclides must be noted.

Due to low radioactivities, very close sample-to-detector distances were used in the counting process. Because of the complex decay schemes of $Ag-106^m$ and Tm-168 the counting losses due to cascade-summing effects were large. Extensive calculations were made to correct these effects. Based on the decay schemes

Table 2: Decay parameters and cascade-summing corrections

Nuclide	Ref.	$T_{1/2}$	E_γ (keV)	I_γ	$\Delta I_\gamma / I_\gamma$ %	C_Σ
Ag-105	/7/	41.29(7)d	280.4	0.310	1.1	1.08
			344.5	0.416	1.0	0.99
$Ag-106^m$	/8/	8.46(10)d	406.2	0.135	6.3	1.43
			451.0	0.283	6.2	1.53
			616.2	0.217	6.4	1.55
			717.3	0.290	6.3	1.37
			1045.8	0.297	6.6	1.41
Tm-167	/9/	9.24(2)d	207.8	0.410	14.6	1.04
Tm-168	/10/	93.1(1)d	184.3	0.163	2.2	1.35
			198.3	0.498	2.1	1.29
			447.5	0.218	3.0	1.41
			720.3	0.108	2.4	1.18
			741.3	0.112	2.3	1.12
			816.0	0.461	2.2	1.28
			821.1	0.111	2.3	1.09

/7 - 10/ the single branches of coincident photons were analysed and correction factors were derived. The decay scheme dependent part was combined with experimentally determined total and photopeak efficiencies to obtain the necessary correction factors. Terms of higher order were also considered (compare with ref. /11/). The specific cascade-summing correction factors of this experiment (C_Σ) are listed in the last column of Table 2. The measured photopeak areas were multiplied with these factors.

Table 3: Cf-252 spectrum-averaged neutron cross sections (in mb) and (n,2n) and (n,3n) reactions. The experimental data are compared with calculated ones based on various representations of the neutron spectrum.

Reaction	Threshold MeV	Experiment	Calculation				
			Madland-Nix	NBS spectrum	CEM β=0.1	Maxw. T=1.42	TUD spectrum
$^{169}Tm(n,2n)^{168}Tm$	8.11	6.69 ± 0.42	6.04	6.81	6.27	7.82	-
$^{107}Ag(n,2n)^{106m}Ag$	9.64	0.480 ± 0.037	0.506	0.595	0.553	0.718	-
$^{169}Tm(n,3n)^{167}Tm$	14.96	(1.56 ± 0.23) E-2	1.06E-2	1.55E-2	1.60E-2	2.25E-2	> 3.00E-2
$^{107}Ag(n,3n)^{105}Ag$	17.64	(1.12 ± 0.10) E-3	0.64E-3	1.07E-3	1.20E-3	1.70E-3	> 8.55E-3

3. Spectrum-averaged neutron cross sections

3.1 Experimental data

Based on the well-known value of the reaction $^{58}Ni(n,p)^{58}Co$ /5/, Cf-252 spectrum-averaged cross sections were derived for the reactions $^{107}Ag(n,2n)^{106m}Ag$, $^{107}Ag(n,3n)^{105}Ag$, $^{169}Tm(n,2n)^{168}Tm$ and $^{169}Tm(n,3n)^{167}Tm$. The experimental results are given in Column 3 of Table 3. For the reaction $^{107}Ag(n,2n)^{106m}Ag$ the results obtained with the natural and the enriched silver samples agreed within their statistical uncertainties. The final result was obtained by averaging these data.

The uncertainty quoted comprises the uncertainty contributions from counting statistics, gamma emission probabilities (see Table 2), photopeak efficiency calibration (1.5 %), cascade-summing corrections (5 % of the correction), geometric and self-absorption effects and from nickel monitoring (1.3 %). The uncertainties correspond to the 1σ-level (68 % probability).

3.2 Calculated data

3.2.1 σ(E) data

Energy-dependent cross section data of nuclear reactions are sparse above 20 MeV neutron energy. To avoid the use of excitation functions based on theoretical models alone, the experimental data

base was carefully investigated. For $^{169}Tm(n,2n)$ and $^{169}Tm(n,3n)$ experimental data between 14.7 MeV and 24 MeV were found in ref. 12. For both thulium reactions and for $^{107}Ag(n,2n)$ and $^{107}Ag(n,3n)$ another source with experimental data between 7.5 MeV and 28 MeV was available /13/. The experimental data of both works were used as the primary reference for the $\sigma(E)$ data used in the present analysis. Due to the lack of experimental data in certain energy ranges and relatively large energy gaps between the data, the results of model calculations were used to interpolate between the data. These calculations /13/ incorporated both compound-nucleus and prequilibrium decay modes.

For $^{169}Tm(n,2n)$ energy-dependent cross section data between threshold and 20 MeV were used. The experimental data of Ref. /12/ and Ref. /13/ agree within their uncertainties. Both data sets are also compatible with the model calculation of Ref. /13/ which was used in describing the excitation function of this reaction. With regard to the experimental uncertainties and the agreement with the model calculation, a relative uncertainty of 7 % valid over the whole energy range is estimated for this cross section.

For $^{169}Tm(n,3n)$ the situation was similar. Between reaction threshold and 28 MeV the model calculation of Ref. /13/ gave a good description of the experimental data. Here, an overall uncertainty of the order of 10 % is estimated.

The excitation function of $^{169}Tm(n,2n)$ used in the present work is in excellent agreement with other recent data /14/. The only data point of this work /14/ of $^{169}Tm(n,3n)$ fits well with the corresponding excitation function used here.

For the reaction $^{107}Ag(n,2n)^{106m}Ag$ only 8 data points between threshold and 20 MeV were available from Ref. /13/. Unfortunately the model calculation failed to describe the cross section curve adequately. To circumvent this problem a hybrid cross section curve was generated. This curve was based on precise $\sigma(E)$ data between 13.6 MeV and 14.7 MeV /15/ and was extrapolated to higher neutron energies with regard to the data of Ref. /13/. A similar extrapolation down to the threshold was done which was only weakly supported by available experimental data.

For $^{107}Ag(n,3n)$ the experimental data and the model calculation of Ref. /13/ were in agreement. Between threshold and 28 MeV the model calculation was used for representing the cross section curve. Here an overall uncertainty of 20 % is estimated.

3.2.2 Spectrum representations

Various representations of the Cf-252 neutron spectrum were used in the comparison between experimental and calculated data. It was the aim of the present work to discriminate between these representations and to obtain some information on their validity within certain energy ranges. The simplest assumption was that of a Maxwellian with a temperature parameter of 1.42 MeV. The NBS evaluation of Grundl and Eisenhauer /16, 17/ is based on this Maxwellian with additional energy-dependent correction functions within limited energy ranges. For the present purposes only the validity of the experimental correction function between 6 MeV and 20 MeV was of importance. The results of two theoretical model calculations were also used. The data calculated by Madland and Nix were used in the version as presented at the Nuclear Standard Reference Data meeting in Geel /18/. The second theoretical spectrum is the cascade evaporation model (CEM) of Marten and Seeliger /19/. The distribution obtained with an anisotropy parameter of $\beta = 0.1$ was used.

Compared with the neutron energy range below 20 MeV, information on the shape of the spectrum above 20 MeV is poor. Nevertheless, both model calculations /18, 19/ delivered data up to 40 MeV. It was also assumed that the exponential correction term of the NBS spectrum remains valid above 20 MeV. The TUD spectrum based on

experimental data /1, 2/ and used in the present analysis is identical with the NBS spectrum below 20 MeV. Between 20 MeV and 28 MeV a second exponential correction term was derived by the authors which essentially reflects the neutron excess measured in the experiment.

In the case of the model calculations uncertainties of the order of 10 % to 30 % can be estimated. However, it is quite difficult to give realistic uncertainty estimates of the various spectrum representations. This deficit seems of minor importance as long as the adequacy of the different spectrum representations in describing the experimental integral data is used to deduce trends instead of details.

3.3 Responses in the Cf-252 neutron spectrum

About 90 % of the total response of $^{167}Tm(n,2n)$ is between 8.6 MeV and 13.8 MeV and of $^{107}Ag(n,2n)$ between 10.1 MeV and 15.6 MeV. Therefore both these reactions allow conclusions only about the shape of the neutron spectrum below 20 MeV to be drawn.

In Fig. 1 and Fig. 2 the energy response curves of the reactions $^{169}Tm(n,3n)$ and $^{107}Ag(n,3n)$ are plotted. On the basis of the available excitation functions, the response curves were calculated for two different spectrum representations. The solid curves are valid for the NBS spectrum. In the case of the neutron excess of the TUD spectrum the response curves follow the dashed lines above 20 MeV and are identical with the solid curves below this energy. The integral over the curves is directly proportional to the expected spectrum-averaged cross section. Fig. 1 shows that in the case of the neutron excess the value of the $^{169}Tm(n,3n)$ reaction is enhanced by a factor of 2. For the reaction $^{107}Ag(n,3n)$, see Fig. 2, the numerical value of the spectrum-averaged cross section is quite sensitive to the neutron excess.

The upper limit of the available $\sigma(E)$ data is 28 MeV. In the case of the neutron excess (TUD spectrum) the response curves have at this energy a numerical value different from zero, i.e., the calculated spectrum-averaged cross sections based on the TUD spectrum remain incomplete and should be regarded as lower limit estimates.

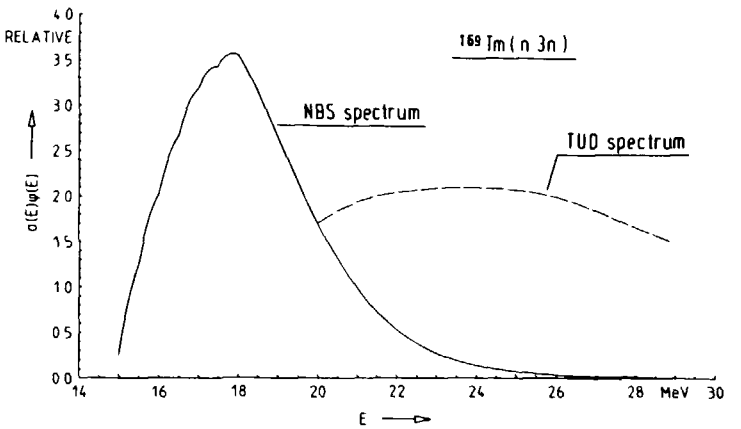

Fig. 1: Calculated response of $^{169}Tm(n,3n)$ without (solid curve) and with (dashed curve) a neutron excess above 20 MeV.

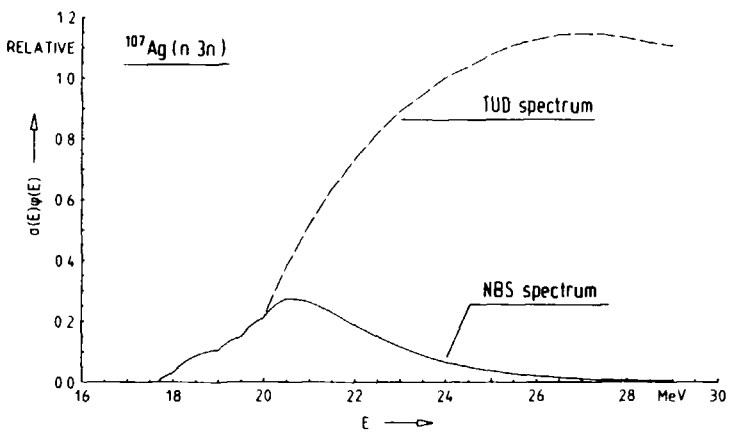

Fig. 2: Similar to Fig. 1, for the reaction $^{107}Ag(n,3n)$

4. Results and discussion

In Tab. 3 the experimental results are compared with calculated ones based on the various spectrum representations. For the reaction $^{169}Tm(n,2n)$ the best agreement between experiment and calculation is given for the NBS spectrum and for the CEM model. The theoretical model of Madland and Nix seems to underestimate and the Maxwellian to overestimate the neutron spectrum. These conclusions are fully consistent with the data of a recent evaluation of the Cf-252 neutron spectrum /20/. Between 9 MeV and 14 MeV the NBS spectrum is very similar to the evaluation. The data of the CEM model in this energy range follow the energy-dependent shape of the evaluation but are systematically lower. With the data of the Madland and Nix model the neutron spectrum is underestimated and this effect becomes more pronounced towards higher neutron energies. The agreement of the experimental value of $^{107}Ag(n,2n)$ with the calculated result based on the Madland and Nix model is therefore a virtual effect. The sensitive energy range of this reaction is between 10 MeV and 16 MeV. Here, the data of Madland and Nix deviate substantially from the evaluation. The increasing discrepancy of $^{107}Ag(n,2n)$ between experiment and calculation when using the CEM spectrum, the NBS spectrum and the Maxwellian is therefore due to the problems in defining the excitation function of this reaction between threshold and 13.6 MeV as already mentioned.

For both (n,3n) reactions a good agreement between experiment and calculation is given by using the NBS spectrum (extrapolated above 20 MeV) and the data of the CEM model. At present, our best knowledge of the shape of the Cf-252 neutron spectrum is given by the recent evaluation /20/ which ends at 20 MeV. When this spectrum is extrapolated by eye above 20 MeV the result is very similar to that of the NBS spectrum or the CEM model. Above 20 MeV the CEM data are slightly enhanced compared with the NBS spectrum. The difference between the experimental data of Tab. 3 and the calculations based on the Madland-Nix spectrum or the Maxwellian becomes quite large for the (n,3n) reactions and indicates that these representations are relatively bad descriptions of the spectrum at very high energies. The experimental result of $^{169}Tm(n,3n)$ is lower by a factor of 2 than that calculated with the neutron excess spectrum. For $^{107}Ag(n,3n)$ this factor is of the order of 8. Even assuming problems with the exact definition of the excitation functions (similar to that for $^{107}Ag(n,2n)$, see above) the differences are too large to be explained by this. The results of both (n,3n) reactions show the same tendency and contradict a neutron excess in the Cf-252 neutron spectrum above 20 MeV.

In summary, the author of the present work has reached the conclusion that a neutron excess with a magnitude such as that quoted by the Dresden group /1, 2/ does not exist. This statement is further confirmed by recent data of another time-of-flight experiment /21/ especially undertaken to study the same effect. It is obvious that a comparison between experimental and calculated spectrum-averaged cross section does not allow detailed conclusions about the exact shape of the Cf-252 neutron spectrum. However, the above discussion has shown that this method is relatively sensitive in recognizing global trends of the shape of the spectrum. The present analysis cannot exclude a small neutron excess but from the present data, it is believed that such an excess never exceeds the amplitude of a Maxwellian with a temperature parameter of 1.42 MeV.

References

/1/ H. Marten, D. Seeliger, B. Stobinski: Report INDC(GDR)-17/L (May 1982)

/2/ H. Marten, D. Seeliger, B. Stobinski: "Nuclear Data for Science and Technology", (K. H. Bockhoff, ed.), D. Reidel Publ. Company, Dordrecht (1983) 488

/3/ H. Marten, D. Seeliger: J. Phys. G, Nucl. Phys. 10 (1984) 349

/4/ W. Mannhart: "Nuclear Data for Science and Technology", (K.H. Bockhoff, ed.), D. Reidel Publ. Company, Dordrecht (1983) 429
/5/ W. Mannhart: "Reactor Dosimetry", (J.P. Genthon, H. Röttger, eds.), D. Reidel Publ. Company, Dordrecht (1985) 801
/6/ W. Mannhart: Progress Report NEANDC(E)-262 U, Vol. V (1985) 62
/7/ Nuclear Data Sheets 27 No. 1 (1979)
/8/ Nuclear Data Sheets 30 No. 3 (1980)
/9/ Nuclear Data Sheets 17 No. 1 (1976)
/10/ Nuclear Data Sheets 11 No. 3 (1974)
/11/ F.J. Schima, D.D. Hoppes: Int. J. Appl. Rad. Isot. 34 (1983) 1109
/12/ L.R. Veeser, E.D. Arthur, P.G. Young: Phys. Rev. C16 (1977) 1792
/13/ B.P. Bayhurst, J.S. Gilmore, R.J. Prestwood, J.B. Wilhelmy, N. Jarmie, B.H. Erkkila, R.A. Hardekopf: Phys. Rev. C12 (1975) 451
/14/ Lu Han-Lin, Zhao Wen Rong, Fan Pei Guo: Nucl. Sci. Eng. 90 (1985) 304
/15/ W. Mannhart, H. Vonach: Z. Physik A272 (1975) 279
/16/ J.A. Grundl, C.M. Eisenhauer: NBS Spec. Publ. 425 (1975) 250
/17/ J. Grundl, C. Eisenhauer: Proc. 1st ASTM-EURATOM Symp. Reactor Dosimetry, EUR 5667 ef (1977) 425
/18/ D.G. Madland, R.J. LaBauve, J.R. Nix: IAEA-TECDOC-335 (1985) 267
/19/ H. Marten, D. Seeliger: IAEA-TECDOC-335 (1985) 255
/20/ W. Mannhart: contribution to the present meeting
/21/ A. Chalupka, L. Malek, S. Tagesen, R. Bottger: contribution to the present meeting

STUDY OF THE MECHANISM OF Cf-252 SPONTANEOUS FISSION NEUTRON EMISSION

O.I. BATENKOV, A.B. BLINOV, M.V. BLINOV,
S.N. SMIRNOV
V.G. Khlopin Radium Institute,
Leningrad, Union of Soviet Socialist Republics

Abstract

The measurements of differential energy distributions of 252-Cf fission prompt neutrons have been carried out for different emission angles. The correlation of angular and energy distributions of neutronsfor different masses and total kinetic energies of the fragments is analysed for clearing up the mechanism of neutron emission. The velocities of the fragments during neutron emission have been determined from the experimental data obtained at small angles.

Introduction

In the process of nuclear fission and at establishment of the equilibrium shape of the fragments, a quick change of the shape of the nuclear surface and, respectively, of neutron emission is possible due to the effects of nonstatistical nature. Therefore the deviations from the evaporation model from equilibrium heated fragments moving at full velocities depend first of all on the time of separate steps of the fission process. Despite a number of works devoted to the study of the mechanism of spontaneous fission neutrons emission /1-7/, the full picture is not clear yet, as the results of the works differ much and sometimes are even contradictory.

In the present work precision measurements of differential energy spectra were carried out for different masses and total kinetic energies of the fragments at different flying out angles of neutrons. Special attention was payed to the neutron spectra at small angles (less than 6°). Using these data, for the first time by the direct method it was possible to determine the velo-

cities of the fragments during the neutron emission. The analysis of the same spectra enabled to obtain information on the behaviour of the cross-section of the reverse process (the capture of neutrons by the excited nucleus) for the region of low enrgies of neutrons. The comparison of the data for small and big angles enabled to specify the limits of applicability of the evaporation model.

The obtained data are very useful for correct formation of the 252-Cf integral spectrum-international standard, as it is possible only on the base of complete understanding of the mechanism of the neutron emission process.

Method

The measurements were carried out using multidimension spectrometer of spontaneous fission neutrons, on-line with a computer. For each fission event was determined the neutron energy (E), the masses of the fragments (M_1, M_2), the total kinetic energy of the fragments (E_k), the flying out angle of neutrons relative to the direction of the fragments motion (φ) in 1. s.

The fission source was made of high purity californium by the method of vacuum selftransfer on aluminium foil with the thickness 30 mg/cm^2. The intensity of the source was 10^5 fission/second, the diameter of the spot was 3 mm. Fragments were detected by two semiconductor surface-barrier silicon detectors (S. C. D.) with the area 300 mm^2. Energy calibration was done by the well-known Schmidt parameters /8/. The calibration was carried out automatically in each four hours, which excluded the influence of the radiation ageing of the detector on the correctness of measurements.

The energy of neutrons was determined by the time-of-flight method. A stilbene crystal (50 x 30 mm) with a photomultiplier (FEU-30) was used as a neutron detector. The efficiency of the detector was determined relative to the 252-Cf integral spectrum that was measured by three methods: by means of a fast ionization fission chamber, by direct applying of californium on the S. C. D. and by integration of neutron spectra, measured at different angles to the direction of the flight of the fragments in the laboratory system. The deviations in the integral spectra obtained by the three different methods did not exceed 2 %.

The threshold by the recoil protons for neutron energies less that 9 MeV was 0.15 MeV, for E_n 9 MeV - 1 MeV. This enabled to obtain the effect-background ratio not less than 10 for the energy range 0.3-15 MeV. The discrimination of neutrons and gamma-quanta was done by the pulse shape. The suppression coefficient at the neutron threshold 0.5 MeV was 10^4, and at the threshold 0.15 MeV - 10^2.

In this spectrometer threshold formers were used. The time - amplitude dependence was removed by means of the computer program. This allowed us to compensate the nonlinear dependence of the time shift on the pulse amplitude, to work in a wide dynamic range and to determine the correcting coefficients immediately in the course of the experiment.

In consequence during the whole series of measurements, lasting about 4 months, the shift of the time zero didnot exceed 0.1 ns. The dispersion determined by the width of the γ-quantum peak distribution, was 1 ns for neutron energy $E > 0.5$ MeV and 1.5 ns for $E < 0.5$ MeV.

For checking the energy calibration and the resolution of the neutron channel of the spectrometer a measurement of the neutron absorption curve by a carbon sample was carried out.

The value of neutron scattering on closely situated constructions is important characteristic influencing the corrections of measurements. In order to exclude this effect all the elements were made of minimum size; the thickness of the vacuum chamber was 0.3 mm, the thickness of the SCD was 0.2 mm. The measurements and calculations were carried out imitating the scattering on the construction elements. All this enabled to reduce the effect of neutron scattering and absorption to a small value ($\sim$2 %).

All the measurements of neutron spectra were doubled on three flight bases: 37.5, 75.0 and 150 cm. The use of the three bases increased the precision and reliability of the measurements; besides for increasing the precision two neutron detectors, situated collinearly, were used simultaneonsly. The measurements were done

for the angles of 2, 6, 15, 30, 45, 60, 75 and 90°. The angular resolution at measurements at the angle 0° was 2° or 6° in different experiments.

The treatment of the measurements consisted of two steps. During the first one, carried out immedeately in the course of the experiment, for each recorded event the mass (M), the kinetic energy (E_k), the velocity of the fragment (V_f) and the time of flight of the neutron (T) were determined. The accumulation was carried out of the matrix of fragment-fragment coincidences in the coordinates $N_f(M, E_k, I)$, where I - the number of the detector, of the matrix of fragment-fragment-neutron coincidences in the coordinates $N_n(T, M, E_k, I)$ and of the matrix of velocites $V_f(M, E_k, I)$. For each event was done: the compensation of the time-amplitude dependence of the connection, the fragment energies correction associated with the account of the neutron recoil effect, leading to a systematic shift of the coordinates of the N_n matrix relative to the coordinates of the N_f matrix. In the result of the treatment the neutron flux density distribution

$$\rho(V,\varphi) = T^3 * n/(R * e * L^3),$$

where I - the distance flown by the neutron, R - the number of registered fragments, n - the number of registered neutrons, - the efficiency of the neutron detector, V_n - the velocity of the neutron.

Results and discussion

The ^{252}Cf spontaneous fission neutrons emission mechanism is determined by the correlation of the three characteristic times: the fragment acceleration time (τ_o), the time of dissipation of collective energy of fragments - into the thermal energy (τd), the neutron emission time (τn). The main information on these times is obtained from the comparison of the shape and intensity of neutron spectra measured at different angles.

Almost in all the references /1-7/ a discrepancy is observed between the spectrum at small and big angles and, respectively, between the spectrum, obtained by means of integration by the angle in c. m. s. of diffential spectra, obtained from the measurements at small angles, and the sum of the spectra, obtained at all the angles. The value of this discrepancy varies from 10 % to 20 %. For explanation of this effect different suppositions are used: the presence of the neutrons associated with the process of neck breaking, neutron evaporation from unfully accelerated fragments, anisotropy of neutron emission in connection with great angular momenta. The most detailed studies of the "scission" component were carried out in the works, where its dependence on M and E_k of the fragment was studied. Yet, the results of those works have a contradictory character.

In this work for the first time the information on the correlation of the time τ_n and τ_o was obtained directly from the shape of the spectrum measured at the angle 2° in respect to the direction of the fragment motion. The advantage of those measurements is evident (Fig. 1).

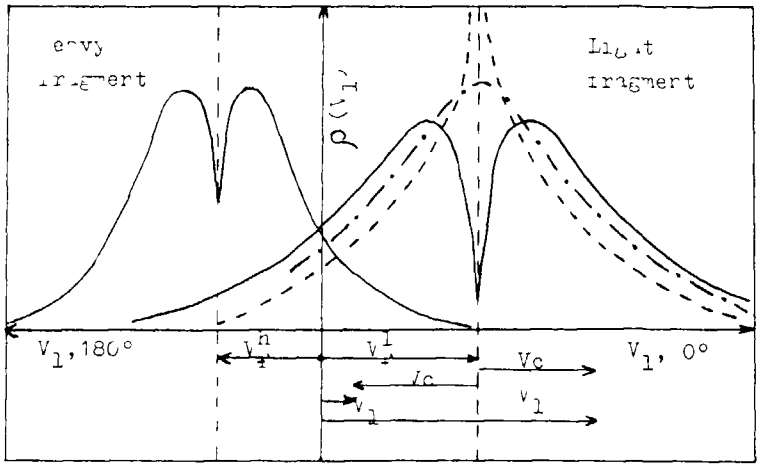

Figure 1. Neutron spectrum at small angles. Calculations of the spectra from the works: a - /10/, b - /11/, c - /12/

First, here the contribution of the neutrons from the opposite fragment is minimum and it is possible to account for it correctly, due to the additional velocity of the fragment the low-energy part the neutron spectrum is shifted to the region of energies of the order of 1 MeV and the relative yield of such neutrons increases sharply. Besides, there is a special point in the neutron spectrum at small angles. That point where the neutron's velocity (V_n) is equal to the transfer energy of the fragment (V_f), corresponds to the zero energy of the neutron in the c. m. s..

From the correlation

$$N(E) = N(\varepsilon) * \frac{\sqrt{E}}{\sqrt{\varepsilon}}$$

connecting the spectra in the laboratory system N(E) and in the system of mass center of the fragment $N(\varepsilon)$ it is seen that at $\varepsilon \to 0$ there is an uncertainty of the form 0/0, which can be differently disclosed in dependence on the spectrum form $N(\varepsilon)$ near the $\varepsilon = 0$. If the spectrum in the c. m. s. behaves as ε^{α}, then depending on the value of the parameter α in the laboratory spectrum a dip ($\alpha > 0.5$), a peak ($\alpha < 0.5$) or a smooth dependence ($\alpha = 0.5$) can be observed. Different theoretical calculations /10-12/ give a full set of these possibilities (Fig. 1).

If to use not an energy but a velocity reperesentation of the spectrum $\rho(V) = N(\varepsilon)/V$, then on condition of neutron emission from a fully accelerated fragment, a distribution symmetry must be observed relative to the point $V_i = V_f$ (back and forth symmetry).

In our work we have found a dip in the spectrum of light fragments (Fig. 2). The positions of the dips within the limits of measurement error coincides with the average velocities of the fragments for groups of light fragments isolated by their masses and kinetic energies, which confirms the hypothesis of neutron emission from a fully accelerated fragments.

The comparison of the spectra with respect to the symmetric point that divides neutrons emitted at the angles 0° and 180° in c. m. s. was carried out too. The data coincided within the limits of the measurement errors.

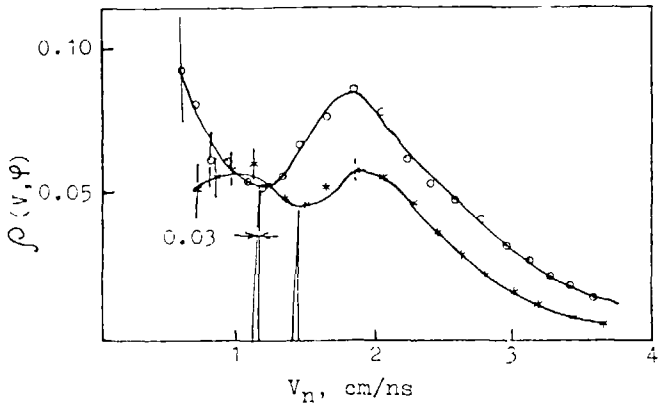

Figure 2. Spectrum of neutrons emitted at the angle 5°
* M = 98±4 m. u., E_k = 175±4 MeV, V_f = 1.44 cm/ns
o M = 117±4 m. u., E_k = 175±4 MeV, V_f = 1.22 cm/ns

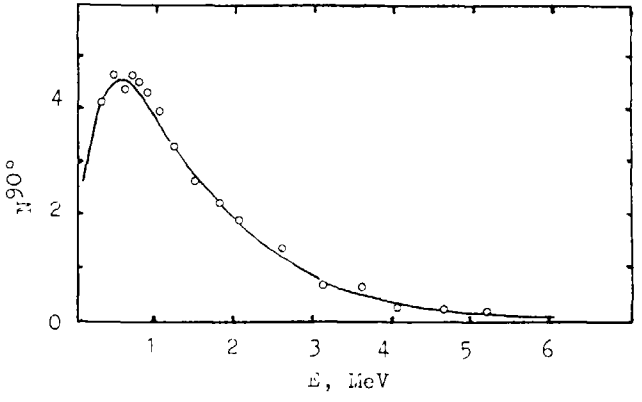

Figure 3. Neutron spectrum at the angle 90° in the l. s.
- - spectrum obtained from measurements at 0° angle in the l. s.
o - experimental data at 90° angle

In the work a comparision is presented of the spectra of neutrons emitted from the fragments at the angles 0° and 90° in the l. s. In Fig. 3 there are shown the spectra: the one measured at the angle 90° and the one calculated for the angle 90° from the data of the measurements at the angle 0° in assumption of neutron emission from a fully accelerated fragment.

Both spectra agree by the integral within the limits of statistical error (2-3 %).

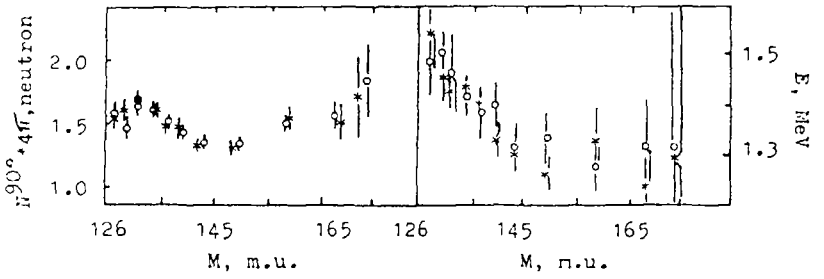

Figure 4. Neutron yield (N) and average energy (E) at the angle 90° in dependence on the fragment's mass for the sum of E_k
* - obtained from the data for the angle 0° (calcal.)
0 - obtained from the data for the angle 90° (exp.)

An analogous comparison of the spectra at 0° and 90° was carried out also for separate groups of fragments. In Fig. 4 the dependence of the neutron yield and the average energy on the fragment mass for the sum of E_k is shown.

Fission neutrons being present, one should expect a dependence of their number on the E_k and M of the fragment, which was noted in references /1-2/. But it is seen from the figures that within the error limits (3-10 %) the experimental and the calculated (from 0°) neutron yields coincide at the angle 90°.

We mark that in the initial stage of the given work the discrepancy of the measured and the calculated spectra for 90° composed 7 % by the integral /7/. The difference of the results of the work in question from the previous one can be explained by the following factors: the improvement of the spectrometer's characteristics, a thorough determination of the neutron detector's efficiency on the base of recent experimental data on the ^{252}Cf integral spectrum, the breaking of the whole range of fragments into 108 groups, for which the velocity of the fragment was determined immedeately in the course of the experiment, the development of the method enabling to account for the influence the neutron recoiling effect for each angle in each separately registered event (it was manifested most strongly in the comparison of 0° and 90° spectra where in case of a wrong account of the recoil effect the errors could reach 100 % for some groups of fragments), the introduction of anisotropy in the c. m. s., associated with the angular momentum of the fragment /17/ in the from $1 + \beta P_2(\cos\varphi)$, where $\beta = 0.04$.

In the present work there was also a comparison of the integral spectrum (Fig. 5), obtained from the data at small angles and measured by the direct method in the references /18-21/. In connec-

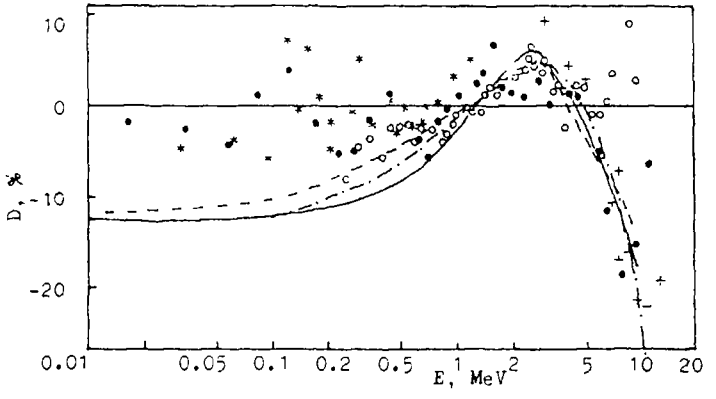

Figure 5. Deviation of the integral spectra from Maxwell distribution (T = 1.42 MeV)
• data of reference /18/, * /19/, o /20/, + /21/,
- data of the given work,
-•- calculation of reference /22/, - - - /23/

tion with the fact that the integral spectrum of ^{252}Cf fission neutrons is an international standard, the shape of this spectrum must be determined with a high precision. The highest precision in the determination of the spectrum is reached for the energy range 1-5 MeV. It seems interesting to determine the integral spectrum from our data for 0° in assumption that the neutron emission takes place only within the limits of the model of evaporation from fully accelerated fragments. In this case the correlation of the energy intervals for different angles of neutron flying-out due to the kinematic effect leads to the appearing possibility for the determination of the shape of the integral spectrum in the region of low and high energies, basing on a comparatively well known shape of the spectrum in the energy range 1-5 MeV. Besides, by means of an iteration procedure a description was carried out of the total in the energy range 0.2-1 MeV (in l. s.). The spectrum obtained in this way is shown in Fig. 5.

The theoretical calculation spectra obtained on the base of statistical models in reference /22-23/ are close by their shape to this distribution, which shows a reasonable degree of simplification in calculations. It is worth mentiong that in the energy range 1-10 MeV our integral spectrum (from 0°) goes close enough to a number of direct measurements experimental data /18-21/. In the low energy region (less that 1 MeV) our integral spectrum is somewhat lower than the data of direct measurements /18-19/. The difference in the low energy region can be associated with the influence of the anisotropy effect in the c. m. s., caused by the angular momentum of the fragments, and also with the presence of non-evaporating neutrons. The variation of the anisotropy coefficient, when using experimental spectra at 0° (l. s.) as the basis data, does not enable to reach an agreement of integral spectra in the whole energy region. The introduction of neutron of non-evaporating character (2% of the total number) enables to explain the discrepancy of the spectra.

Thus, the conclusion can be drawn that $\tau_n > \tau_o$, i. e. practically all the neutrons (except sevenal percent) are emitted from fully accelerated fragments for all measured groups of mass and total kinetic energies. Consequently, we can get the neutron spectrum in c. m. s. for neutron - rich nuclei - fragments in a wide excitation energy range.

Therefore it is very interesting to carry out the comparison of experimentally measured fission neutron spectra with equilibrium part of the neutron spectra, obtained from (n, n')(n, 2n)(p, n) and (α, n) reactions and with statistical calculations too at the corresponding excitation energies /25/.

The comparison carried out for the results of the first set of the experiment has shown that for high excitation energies the difference between the spectra was observed - the average fission neutron energy is lower than the average energy of the neutrons of nuclear reactions. This result was obtained for the first time in this paper. It shows that the values of τ_n (neutron emission time) and τ_d (the time of establishment of equilibrium shape of fragments) are possibly of the same order.

For low excitation energy a rather a good agreement was observed between the fission neutron spectra and the reaction neutron spectra. For this region the comparison of the experimental and the statistical calculation data was made /25/. There is a good agreement, except the region of low energy where the behaviour of the capture cross-section by an excited nucleus σ_c (inverse cross-section) has been unknown. For obtaining σ_c the spectrum in c. m. s. is given as in Ref. /13/ in the form: $\Phi(\mathcal{E}) = \int_0^\infty \Phi_c(\mathcal{E})P(T)dT$, $\Phi_c(\mathcal{E}) = \sigma_c(\mathcal{E})\mathcal{E}\exp(-\mathcal{E}/T)$, were P(T) is the residial distribution of fragment temperature. It was used as

$$P(T) = \begin{cases} 2T/T_m^2, & T \leq T_m \\ 0, & T > T_m \end{cases} \qquad E^* = aT_m^2$$

The excitation energy was determined from the experimentally obtained number of neutrons ν and the γ-rays total energy. The comparison of the obtained values σ_c with the values calculated for an urexcited nucleus was carried out /13/. Fig. 6 shows that they are in agreement qualitatively, though some quantitative difference is observed. It is necessary to specify both the experimental and the calculated data.

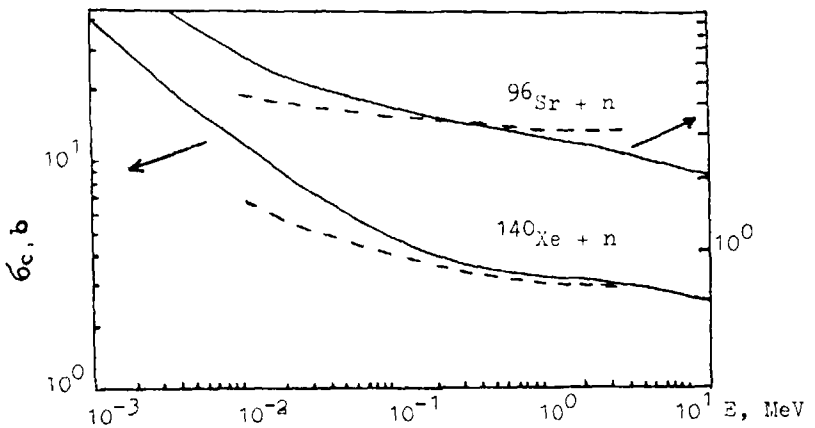

Figure 6. The cross-section of the neutron capture by an excited nucleus

— — — data of the this work calculation at the use of

——— the Bechetti-Creenles /13/ potential

Thus the information on the base correlations between the fundumental quantities that determine the neutron emission mechanism of ^{252}Cf spontaneous fission was obtained in this paper.

References

1. Y. S. Zamjtin, D. K. Rjzanov. Yad. Fiz., 29, 595 (1979).
2. V. M. Piksaikin, P. P. Dyatchenko and L. S. Kazaeva. Yad. Fiz., 25, p. 723 (1977).
3. Y. A. Vasiljev, A. V. Sidorov, Nejtronnaya Fizika (Moscow, 1976), part 5, p. 86.
4. M. V. Blinov, N. M. Kazarinov, Yad. Fiz., 16, p. 1155 (1972)
5. H. R. Bowman, S. G. Thompson, J. C. Milton, W. J. Swiatecki, Phys. Rew., 126, p. 2120 (1962).
6. P. Richs, Acta Physica Austriaca, 53, p. 271 (1981).
7. O. I. Batenkov, M. V. Blinov, V. A. Vitenko, Physics and chemistry of fission (Vienna, 1980), p. 267.
8. H. W. Smitt, W. M. Gibson, J. H. Neiler, F. J. Walter and T. D. Thomas, Proceedings of the Symposium on physics and chemistry of fission. Salzburg (IAEA, Vienna, 1965), vol. 1, p. 531.
9. V. M. Adamov et al., Phys. Lett. 48B 4 (1973) 331.
10. R. J. Le Cooter, Proc. Phys. Soc., v. A 65, p. 718, (1952).
11. G. M. Ahmedov, V. S. Stavinskij, Report (FEI-970, Obninsk, 1979).
12. V. F. Weiskopf, Phys. Rev., v. 52, p. 95 (1973).
13. G. Madland, J. R. Nix, Nucl. Sci. Eng., v. 81, p. 213, (1982).
14. G. A. Pik-Pichak, Yad. Fiz., 10, p. 321 (1969).
15. V. A. Rybchenj, Report (RI-28, Leningrad, 1974).
16. R. W. Fuller, Phys. Rev., v. 126, p. 684 (1962).
17. A. Gavron, Phys. Rev., 13, p. 2561 (1976).
18. M. V. Blinov et al., Proc. Int. Conf. on Nucl. Data for Sci. and Techn., editer by K. M. Bockhoff, D. Reichel (comp. Eindhoven, Antwerp., 1983).
19. A. Lajtai et al., IAEA Cons. Meet. on the U-235 fast-neutron fission cross-section, and the Cf-252 fission neutron spectrum. (proc. INDC(NDS)-146/L, 1983).
20. W. P. Poenitz, T. Tamura, loc. cit. (18), p. 465 and loc. cit. (19), p. 175.
21. R. Bottger et al., loc. cit. (7), p. 484.
22. D. J. Madland, R. J. Labauve, (Report, LA-UR-84-129, 1984).
23. B. F. Gerasimenko, V. A. Rybchenj, Nejtronnaya Fizika (Kiev, 1984), part 1, p. 349.
24. H. Märten et al., loc. cit. (7), p. 488.
25. O. I. Batenkov et al., Nejtronnaya Fisika (Kiev, 1984), part 1, p. 344.

208 THEORETICAL CALCULATIONS OF PROMPT NEUTRON SPECTRUM FOR Cf-252 SPONTANEOUS FISSION

B F GERASIMENKO, V A RUBCHENYA
V G Khlopin Radium Institute,
Leningrad, Union of Soviet Socialist Republics

Abstract

The results of theoretical calculations of promt neutron spectra and multiplicity distributions for ^{252}Cf spontaneous fission are reported. The calculations were carried out on the basis of Hauser-Feshbach statistical theory taking into consideration the angular anisotropy of neutron emission in the center-of-mass system of fragment and ignoring it. Nonequilibrium component was neglected in calculations. The theoretical results are compared with experimental ones. The effects of input data uncertainty and angular anisitropy consideration on the calculation results are discussed.

The interest for the study of prompt fission neutrons (PFN) spectra is connected with the fact that, on the one hand, they give information about atomic nuclei fission process and deexcitation of highly exc ted fission fragments, and on the other hand, the spectra of PFN are among important characteristics of fissionable nuclei wh ch are neutron sources.

One of the most widespread neutron sources is spontaneously fissionable ^{252}Cf. The neutron spectrum of ^{252}Cf spontaneous fission is the most studied one and is used as a neutron standard.

Numerous calculations of differential and integral PFN spectra for ^{252}Cf spontaneous fission are known; they were performed with different theoretical models /1-5/. In most of them a number of factors affecting PFN spectra formation are not taken into account or a series of substantial simplifications leading to more rough characteristics of PFN are used. The most well-founded and promissing approach to the calculation problem of PFN characteristics, which takes into account all basic factors having influence on the complex process of excited fission fragments deexcitation, is the use of Hauser-Feshbach statistical theory /5, 6/. The authors used this approach with a number of improvements, as compared with /5/, to calculate PFN characteristics for ^{252}Cf spontaneous fission /6, 7/. Fragment excitation energy and spin distribution as well as kinetic energy, charge and mass distribution are also taken into account in calculation. Cascade character of PFN emission from fission fragments is considered in detail, gamma-competition accompanying PFN emission from fragments is allowed for. An expression including shell structure of fragments and their nucleon pair correlations was used for density of excited fragment levels. Since the portion of nonequilibrium neutrons is small, the calculation was based on the supposition that PFN are emitted only by fully accelerated fragments. Angular anisotropy of PFN on centre-of-mass system of fragment was neglected. In our calculations the centre-of-mass energy spectrum of neutrons emitted from the fragment (A, Z) on K-th stage of the cascade with residual nucleus (A - K + 1, Z) formation was presented as /7/:

$$\varphi(\varepsilon, E^{*'}, A-K+1, Z, E_K) = \sum_I \omega(I, E^{*'}, A-K+1, Z) \times \quad (1)$$

$$\times \frac{\Gamma_n(\varepsilon, A-K+1, Z, E^{*'}, I)}{\Gamma_n^t(A-K+1, Z, E^{*'}, I) + \Gamma_\gamma^t(A-K+1, Z, E^{*'}, I)},$$

where $E^{*'}$ is the residual nucleus excitation energy;
ε is the kinetic energy of neutron in fragment centre-of-mass system;
E_K is the kinetic energy of fragment (A, Z);
Γ_n^t and Γ_γ^t are the total neutron and radiation widths;
Γ_n is the partial neutron width;
$\omega(I, E^{*'}, A-K+1, Z)$ is the spin distribution for the nucleus (A - K + 1, Z).

Excitation energy distribution $P_{K-1}(E^{*'}, A-K+1, Z)$ of residual nucleus was calculated, in distinction to /5/, taking

into account the (K - 1)th neutron spectrum:

$$P_{K-1}(E^{*\prime},\ A-K+1,\ Z) = \int dE_1^* P_{K-2}(E^*_1,\ A-K+2,\ Z)\ x$$
$$x\ \varphi\left[E_1^* - E^{*\prime} - B_n(A-K+2,\ Z),\ E^*_1,\ A-K+2,\ Z\right]. \qquad (2)$$

The spectrum (1) was averaged over the distribution $P_{K-1}(E^{*\prime},\ A-K+1,\ Z)$, and the resulting spectra ($K = 1, 2, \ldots, \nu_{max}$) were added (with corresponding weights) to PFN spectrum $\Phi(\varepsilon,\ A,\ Z,\ E_K)$ of the fragment (A, Z). Here ν_{max} - maximum number of neutrons in the cascade emission from the fragment (A, Z); the value of quantity ν_{max} is calculated within the limits of described model. The average energy $\bar{E}^*$ of initial distribution $P(E^*,\ A,\ Z,\ E_K)$ of excitation energy of fragment (A, Z) was calculated otherwise than in /5/ using the equation

$$\bar{E}^* = \bar{\nu}(\bar{B}_n + \bar{\varepsilon} + \bar{\delta}) + \bar{B}_n/2, \qquad (3)$$

where $\bar{\nu}$ and $\bar{\varepsilon}$ are the average prompt neutron multiplicity and average neutron kinetic energy for the fragment (A, Z), respectively. These values were taken from experimental or available evaluated data;

$\bar{B}_n$, $\bar{\delta}$ are the averaged over the cascade values of neutron binding energy and parity correction. These values are calculated within the limits of described method.

The use of equation (3) provide a means for a more correct calculation of PFN spectra parameters of individual fragments.

The neutron center-of-mass spectra obtained are converted to laboratory spectra $N(E,\ A,\ Z,\ E_K)$:

$$N(E,\ A,\ Z,\ E_K) = \frac{1}{\bar{\nu}} \int_{(\sqrt{E}-\sqrt{E_f})^2}^{(\sqrt{E}+\sqrt{E_f})^2} d\varepsilon\ \frac{\Phi(\varepsilon,\ A,\ Z,\ E_K)}{4(\varepsilon E_f)^{1/2}}, \qquad (4)$$

where $E_f = E_K/A$.

The integral spectrum is obtained by summation of E_K - distribution - averaged spectra (4) over independent fragment yields.

The calculations of PFN spectra made by the authors of this work for ^{252}Cf spontaneous fission /6-10/ with the use of described method showed a good agreement with experimental data in a wide range of neutron energies and fragment masses. The shape and mean energy experimental center-of-mass spectra were reproduced well in calculations. Mean energies of calculated and experimental spectra for fragments of ^{252}Cf spontaneous fission within the mass interval $96 \leqslant A \leqslant 156$ are compared in Fig. 1, and in Fig. 2 calculated values of PFN multiplicity distribution variances for fragment pairs are compared with experimental data. As can be seen from Fig. 1, the calculation reproduces well the experimental curve $\bar{\varepsilon}(A)$; and it supports the existence of a valley in the region of A = 130 found in the experiment /11/, which is connected with shell effects in fragments. The values of calculated variances in Fig. 2 are systematically lower than experimental ones, even though they reproduce a qualitative character of the A - dependence of experimental variances. This seems to be connected with the fact that PFN multiplicity distribution was calculated neglecting the correlation between the neutrons from paired fragments.

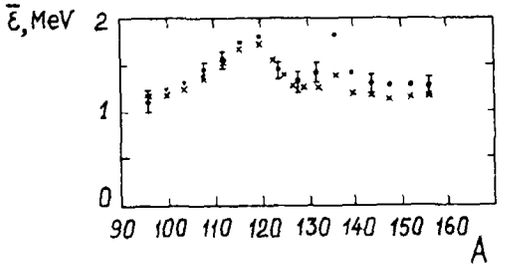

Fig. 1. Averaged center-of-mass neutron energies for ^{252}Cf spontaneous fission as a function of fragment mass number. I - experiment /11/; x - calculation of this work.

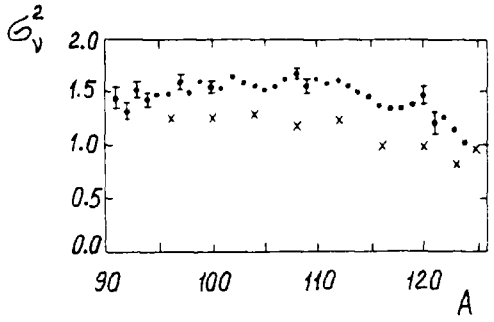

Fig. 2. Variances of PFN multiplicity distributions for ^{252}Cf spontaneous fission fragment pairs as a function of light fragment mass number.
I - experiment /16/; x - calculation of this work.

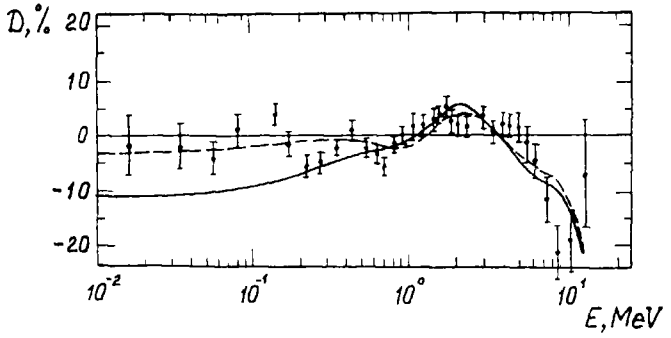

Fig. 3. Calculated and experimental integral PFN spectra for ^{252}Cf spontaneous fission relative to Maxwellian spectrum with T = 1.42 MeV.
——— - calculation of this work (b = 0.0);
- - - - calculation of this work (b = 0.15);
I - experiment /12/.

In the range of energies 10^{-3} MeV $\leq E \leq$ 30 MeV a detailed calculation of integral PFN spectrum for ^{252}Cf spontaneous fission was carried out. The results of this calculation in the form of ratio of calculated spectrum to Maxwellian distribution for T = 1.42 MeV are presented in Table, and also in Fig. 3 (solid line), where they are compared with the experimental data of /12/. The calculations show a strong dependence of high-energy-part of PFN spectrum or the variation of initial distribution parameters /7, 10/. Since the uncertainty of input data is of a random character, the averaging over many fragments at calculation of integral spectrum reduces the error of final result.

In the work /13/ it is shown that the angular distribution of particles with energy $\mathcal{E}$ emitted by an excited compound nucleus must have some anisotropy in the compound nucleus center-of-mass system, if the particles and the nucleus have angular moments different from zero. It is revealed that angular distribution of emitted particles is proportional to $(1 + b\cos^2\theta)$, where θ is particle emission angle in center-of-mass system; b - anisotropy parameter. In accordance with the above-mentioned it can be expected that center-of-mass angular distribution of PFN at energy $\mathcal{E}$ will be described by a dependence of the said form. For anisotropy parameter we can use the quasiclassical evaluation made in /13/:

$$b = \alpha_f \frac{\bar{I}^2 \bar{l}^2}{2}, \qquad (5)$$

where $\bar{I}^2$, $\bar{l}^2$ are the mean squares of fragment initial spin and orbital moment of neutron emitted respectively;
$1/\alpha_f$ is the variance of spin distribution for residual nucleus.

The value of α_f can be evaluated using the "rigid-body" value ($J_{r.b.}$) of nucleus moment of inertia and nuclear temperature T:

$$\alpha_f = \hbar^2/2J_{r.b.}T, \qquad (6)$$

E, MEV	N(E), 1/MEV	D,%
0.001	0.18540E-01	-12.0
0.002	0.26210E-01	-12.0
0.003	0.32089E-01	-12.0
0.004	0.37039E-01	-11.9
0.005	0.41395E-01	-11.9
0.006	0.45329E-01	-11.9
0.007	0.48942E-01	-11.8
0.008	0.52301E-01	-11.8
0.009	0.55452E-01	-11.8
0.010	0.58420E-01	-11.8
0.011	0.61256E-01	-11.7
0.012	0.63955E-01	-11.7
0.013	0.66540E-01	-11.7
0.014	0.69024E-01	-11.7
0.015	0.71418E-01	-11.6
0.016	0.73731E-01	-11.6
0.017	0.75969E-01	-11.6
0.018	0.78140E-01	-11.5
0.019	0.80249E-01	-11.5
0.020	0.82301E-01	-11.5
0.025	0.91828E-01	-11.4
0.030	0.10039E 00	-11.2
0.035	0.10821E 00	-11.1
0.040	0.11544E 00	-11.0
0.045	0.12219E 00	-10.8
0.050	0.12853E 00	-10.7
0.060	0.14022E 00	-10.4
0.070	0.15083E 00	-10.2
0.080	0.16057E 00	-9.9
0.090	0.16959E 00	-9.7
0.100	0.17800E 00	-9.4
0.110	0.18587E 00	-9.2
0.120	0.19328E 00	-8.9
0.130	0.20029E 00	-8.7
0.140	0.20691E 00	-8.5
0.150	0.21321E 00	-8.2
0.160	0.21920E 00	-8.0
0.170	0.22491E 00	-7.8
0.180	0.23037E 00	-7.6
0.190	0.23558E 00	-7.3
0.200	0.24056E 00	-7.1
0.225	0.25213E 00	-6.6
0.250	0.26253E 00	-6.1
0.275	0.27191E 00	-5.6
0.300	0.28034E 00	-5.2
0.325	0.28791E 00	-4.8
0.350	0.29468E 00	-4.4
0.375	0.30068E 00	-4.1
0.400	0.30599E 00	-3.8
0.425	0.31064E 00	-3.6
0.450	0.31471E 00	-3.4
0.475	0.31823E 00	-3.2
0.500	0.32123E 00	-3.1
0.525	0.32403E 00	-2.9
0.550	0.32637E 00	-2.8
0.575	0.32838E 00	-2.6
0.600	0.33009E 00	-2.5
0.625	0.33151E 00	-2.3
0.650	0.33264E 00	-2.2
0.675	0.33348E 00	-2.1
0.700	0.33425E 00	-2.0
0.725	0 33437E 00	-1.9
0.750	0.33446E 00	-1.8
0.775	0.33434E 00	-1.7
0.800	0.33403E 00	-1.6
0.825	0.33356E 00	-1.5
0.850	0.33295E 00	-1.5
0.875	0.33222E 00	-1.4
0.900	0.33139E 00	-1.3
0.925	0.33047E 00	-1.2
0.950	0.32946E 00	-1.0
0.975	0.32837E 00	-0.9
1.000	0.32722E 00	-0.8
1.025	0.32599E 00	-0.6
1.050	0.32471E 00	-0.5
1.075	0.32336E 00	-0.3
1.100	0.32194E 00	-0.1
1.160	0.31832E 00	0.3
1.220	0.31442E 00	0.8
1.280	0.31024E 00	1.3
1.340	0.30576E 00	1.8
1.400	0.30100E 00	2.2
1.460	0.29598E 00	2.7
1.520	0.29067E 00	3.1
1.580	0.28514E 00	3.5
1.640	0.27945E 00	3.9
1.700	0.27360E 00	4.2
1.760	0.26757E 00	4.5
1.820	0.26138E 00	4.7
1.880	0.25510E 00	4.9
1.940	0.24876E 00	5.0
2.000	0.24237E 00	5.1
2.060	0.23593E 00	5.2
2.120	0.22947E 00	5.2
2.180	0.22303E 00	5.2
2.240	0.21663E 00	5.1
2.300	0.21029E 00	5.0
2.360	0.20402E 00	4.9
2.420	0.19788E 00	4.8
2.480	0.19170E 00	4.7
2.540	0.18570E 00	4.5
2.600	0.17980E 00	4.3
2.660	0.17421E 00	4.1
2.720	0.16835E 00	3.9
2.780	0.16281E 00	3.7
2.840	0.15739E 00	3.5
2.900	0.15210E 00	3.2
2.960	0.14695E 00	3.0
3.020	0.14194E 00	2.7
3.080	0.13707E 00	2.5
3.140	0.13235E 00	2.2
3.200	0.12775E 00	2.0
3.260	0.12330E 00	1.7
3.320	0.11898E 00	1.5
3.380	0.11481E 00	1.2
3.440	0.11077E 00	1.0
3.500	0.10685E 00	0.7
3.800	0.89113E-01	-0.4
4.100	0.74154E-01	-1.4
4.400	0.61571E-01	-2.4
4.700	0.51055E-01	-3.3
5.000	0.42270E-01	-4.1
5.300	0.34933E-01	-4.9
5.600	0.28853E-01	-5.6
5.900	0.23799E-01	-6.3
6.200	0.19619E-01	-7.0
6.800	0.13323E-01	-7.9
8.000	0.61814E-02	-8.3
10.000	0.16205E-02	-12.1
12.000	0.38153E-03	-22.7
14.000	0.83429E-04	-36.0
16.000	0.18072E-04	-47.0
18.000	0.36992E-05	-58.2
20.000	0.68885E-06	-69.8
22.000	0.11519E-06	-80.3
24.000	0.18003E-07	-87.9
26.000	0.26134E-08	-93.1
28.000	0.26730E-09	-97.2
30.000	0.32715E-13	-100.0

Table.

Calculated integral PFN spectrum for ^{252}Cf spontaneous fission (b = 0.0).

$$J_{r.b.} = \frac{2}{5} mAR^2, \qquad (7)$$

where m is the nucleon mass;

R is the nuclear radius.

For typical fragments of ^{252}Cf spontaneous fission at $\bar{I}^2 \approx 64$, $\bar{l}^2 \approx 9$ with regard to mean excitation energies of fragments the evaluation of anisotropy parameter value can be made from (5-7):

$$b \approx 0.06\text{-}0.25, \qquad (8)$$

therefore the value $b \approx 0.15$ can be considered as a reasonable evaluation for ^{252}Cf spontaneous fission fragments. Experimental measurements of center-of-mass PFN spectra form ^{252}Cf spontaneous fission fragments reveal the existence of anisotropy /14/ evaluated in /14, 15/ and found to be close to the above mentioned one. We have made the calculations of PFN spectra for ^{252}Cf spontaneous fission using the foregoing statistical method but introducing in center-of-mass system of fragment the anisotropy over emission angle of neutrons relative to the direction of fragment motion with b = 0.15. Corresponding result for integral spectrum of PFN is shown in Fig. 3 (dashed line). As may be seen from Fig. 3, the phenomenological account for neutron angular distribution anisotropy in the fragment center-of-mass system improves the agreement of calculated results with experimental data, mainly in low-energy region, without changing the character of spectrum curve as a whole.

From the results of /6-10/ and the present data we can conclude that the main part of PFN is emitted from heated fully accelerated fragments. The 10 %-discrepancy between the calculation and the experiment in the low neutron energy region, possibly, may be reduced by means of consistent inclusion of angular distribution anisotropy of emitted neutrons and also of possible dependence of this anisotropy on the center-of-mass neutron energy. Furthermore, the above-mentioned discrepancy may be connected with neutrons emitted from fragments in the process of their acceleration, whose contribution is not accounted for in this calculation.

References

1. Lang D. W. Nucl. Phys., 1964, vol. 33, N 1, p. 113-127.
2. Zommer V. P., Savel'ev A. E., Zhikhareva C. V. Atomnaya energiya, 1 67, t. 23, vyp. 4, s. 327-333.
3. Marten H., Neumann D., Seeliger D. Proc. IAEA Consultants Meeting on the ^{235}U fast neutron cross-section and the ^{252}Cf fission neutron spectrum, Smolenice, Czechoslovakia, 28 March-1 April, 1983, Vienna: IAEA, 1983, p. 199-212.
4. Madland D. G., Nix J. R. Nucl. Sci. Eng., 1982, vol. 81, N 2, p. 213-271.
5. Dietrich F. S., Browne J. C. Phys. Rev., 1974, vol. 10C, N 6, p. 2545-2549.
6. Gerasimenko B. F., Rubchenya V. A., Pozdnyakov A. V. Neutron physics: Proc. 5th All-Union conference on neutron physics, Kiev, 15-19 September 1980, part. 3, M.: TsNIIatominform, 1980, p. 114-118. (In Russian).
7. Gerasimenko B. F., Rubchenya V. A. Atomnaya energia, 1985, t. 59, vyp. 5, s. 335-339.
8. Batenkov O. I., Blinov A. B., Blinov M. V., Gerasimenko B. F., Rubchenya V. A., Smirnov S. N. Neutron physics: Proc. 5th All-Union conference on neutron physics, Kiev, 2-6 October 1983, part 1, M.: TsNIIatominform, 1984, s. 344-349. (In Russian).
9. Gerasimenko B. F., Rubchenya V. A. ibidem, s. 349-353.
10. Gerasimenko B. F., Rubchenya V. A. Preprint RI-183, 1984.
11. Piksaikin V. M., Dyachenko P. P., Kutsaeva L. S. Yadernaya fisika, 1977, t. 25, vyp. 4, s. 723-731.
12. Blinov M. V., Boikov G. S., Vitenko V. A. Preprint RI-191, 1985.
13. Ericson T., Strutinski V. Nucl. Phys., 1958, vol. 8, N 3, p. 284-293.
14. Seregina E. A., Dyachenko P. P. Preprint FEI-1625, 1984.
15. Gavron A. Phys. Rev., 1976, vol. 13, N 6, p. 2562-2563.
16. Nifenecker H. et al. Proc. Symp. on Physics and Chemistry of Fission, Vienna: IAEA, 1974, vol. 2, p. 117-178.

ENERGY AND ANGULAR DISTRIBUTION OF Cf-252 FISSION NEUTRONS IN THE LOW ENERGY RANGE

H. MÄRTEN, D. RICHTER, D. SEELIGER
Technical University of Dresden

W. NEUBERT
Zentralinstitut für Kernforschung

Dresden, German Democratic Republic

A. LAJTAI
Central Research Institute for Physics,
Budapest, Hungary

Abstract

Experimental and theoretical investigation of the emission of prompt fission neutrons provides information of both practical and fundamental importance. Prompt neutrons from spontaneous fission of ^{252}Cf, adopted as an international standard have a special significance.

As it is well known the energy spectrum of prompt fission neutrons from spontaneous fission of ^{252}Cf can be described by a Maxwell distribution with a parameter of T=1-42 MeV. The different model calculations can reproduce the measured spectra within 10 percent. More precise double differential spectrum measurements are in progress at the TU in Dresden and at CENM in Geel.

In the low neutron energy range, 50 keV-1.2 MeV, NE-912 glass detectors enriched in ^{6}Li and with an absolutely determined efficiency at a distance of 350 mm from the target have been used for neutron detection. The fission fragments have been detected by two parallel-plate avalanche detectors, one of which, 5 mm far from the target gives the stop signal, while the other 35x180 mm large position sensitive detector at 72 mm far from the source divided into 36 segments of 4.5 mm width records the direction of fragment's flight. The distance between the two avalanche detectors, a flight path of 67 mm serves the distinction between the light and heavy fragments. The angular distribution of neutrons have been measured by a $\Delta\theta=6.5^{o}$ resolution in the 0^{o}-180^{o} region. The effect of scattered neutrons and delayed gamma-rays have been measured.

The experimental results have been compared with those of Bowman et al at two energies. The agreement is very good at 1 MeV, while at 0.5 MeV there is a small deviation.

Several years ago we have measured the energy distribution of neutrons from spontaneous fission of ^{252}Cf in the energy range of 0.03-1.2 MeV (1). In accordance with the measurements of Blinov et al (2) we found no excess neutrons at this energy region relative to the Maxwell distribution of T=1.42 MeV. However, to get absolute spectrum values the determination of the absolute efficiency of NE-912 ^{6}Li glass detector was unavoidable (3).

A new measuring method (4) has been worked out at the Technical University Dresden in cooperation with the Rossendorf Research Institute for the measurement of the energy and angular distribution of neutrons from ^{252}Cf for neutrons with energy above 0.8 MeV. So, it seemed to be obvious to combine this new method with ^{6}Li glass detector of known efficiency, to measure the neutron angular- and energy distribution in the 50 keV-1.2 MeV range.

The measurement was motivated by the following reasons:

1. There are no data at low energies in the full solid angle region.
2. The experimental data can be used to select between the different theoretical calculations of neutron emission probability, and especially to test the existence of the so called scission neutrons, and the reliability of the input nuclear data of the calculations.
3. IAEA NDS's recommendation in accordance with californium standardization program.

The measurement of californium prompt fission neutrons at low energies and different angles has been performed in Rossendorf. The neutrons have been detected by two NE-912 glass detectors enriched in ^{6}Li using time-of-flight method. The flight path was 350 mm. The fission fragments have been detected by two parallel-plate avalanche detectors, one of which, 5 mm far from the source gives the stop signal, while the other 35x180 mm^{2} large position sen-

sitive detector at 72 mm far from the source, divided into 36 segments of 4.5 mm width, records the direction of fragment's flight. The distance between the two avalanche detectors, (67 mm) ensures the distinction between the light and heavy fragments by time-of-flight method. The experimental setup is shown in Fig. 1. A special diaphragm system of thin aluminium foil reduced the fragment's angular dispersion in the polar direction. It diminishes the geometrical efficiency of fragment registration but it gives a better angular resolution for neutrons at 0° and 180°.

The geometrical efficiency of position sensitive avalanche detector with the diaphragm at the different angles is shown in Fig. 2.

The system provides 3-3.5° angular resolution for the fragment detection, while the NE-912 9.5 mm thick, 4.5 cm in diameter neutron detectors at 350 mm far from the source increase the total angular resolution up to 6.5°.

Among the disturbing background-effects the most important is the neutron scattering background. This can cause an enhanced neutron detection at low energies. We have determined this background with a 140 mm thick Fe shadow cone. The other part of the background is the contribution of delayed gamma-rays, which was measured separately by a NE-913 ^{7}Li glass detector of the same size.

We measured the neutron spectra ($P_1(t,\theta)$) with NE-912 for 900 hours, while with shadow cone for 100 hours ($P_2(t,\theta)$) and the delayed gammas for 107 hours ($P_3(t,\theta)$)

At the data evaluation we have assumed the approximate angular independence of scattered neutron spectra and delayed gamma spectrum, because the measuring conditions are the same for all direction of neutron detection.

We get the background-corrected neutron spectra at each of the 36 angles,

$$N(t,\theta) = P_1(t,\theta) - P_2(t-\theta) - P_3(t,\theta)$$

for the heavy and light fragments respectively.

The detailed procedure of data analysis is described in Ref. (5).

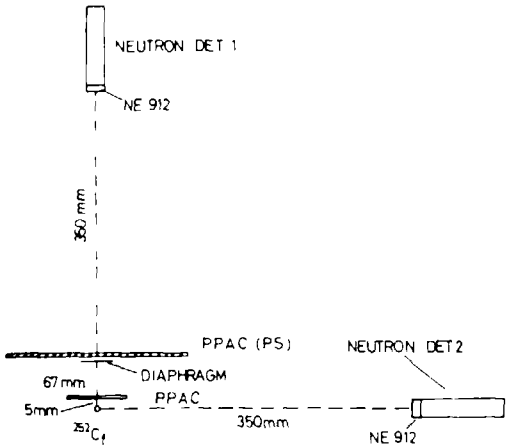

Fig 1

Experimental setup for the measurement of the neutron angular and energy distribution

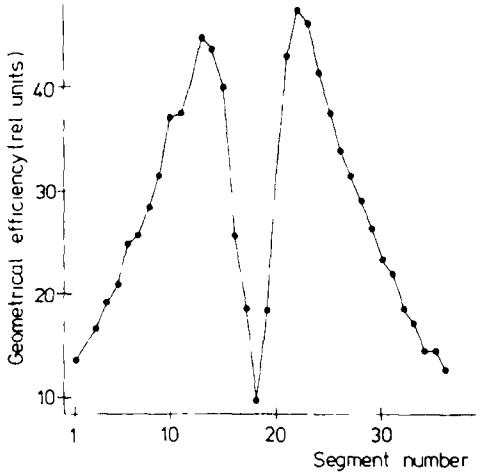

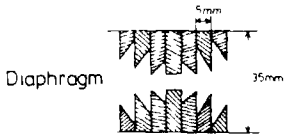

Fig 2

Geometrical efficiency of PPAC (PS) and diaphragm

Results

The experimental results can be seen in Figs. 3 to 6. At the lowest evaluated energy of E_n=0.125 MeV (energy bin 0.1-0.15 MeV) the angular distribution is practically isotropic (Fig. 3). The average statistical error at the angular bins of the histogram is about 5 %.

A small enhancement was found at 0° and 180° at E_n=0.25 MeV (energy bin 0.2-0.3 MeV) (Fig. 4). Because of the large neutron detection efficiency the statistical error in this case was only about 3 %.

At E_n=0.55 MeV (energy bin 0.5-0.6 MeV) the velocities of the neutrons are approximately equal to those of the heavy fragments, whose energy/nucleon is about 0.56 MeV. In agreement with Blinov (6) no dip was found at 180°. Instead of that we got a slowly arising distribution. That behaviour can have two different reasons. First is to mention the relatively large velocity dispersion of the heavy fragments which can smear out the possible effect. Second, the absence of any dip can be caused also by the possibly different behaviour of the compound-nucleus formation cross sections for light and heavy fragments. The statistical errors are of about 9 %. The shape of the measured distribution agrees with the result of Bowman et al (7), but the absolute values are somewhat different.

At 1 MeV (energy bin 0.95-1.05 MeV) the velocity of the neutrons are approximatly equal to those of the light fragments, whose energy/nucleon is about 0.99 MeV. In agreement with Blinov (6) dip was found at 0° (Fig. 6).

The shape of measured distribution well agrees with the result of Bowman et al (7).

The statistical errors are of about 11 %.

The above results are based only one part of the measured data. The evaluation of all the data and a comparison with theoretical calculations are in progress.

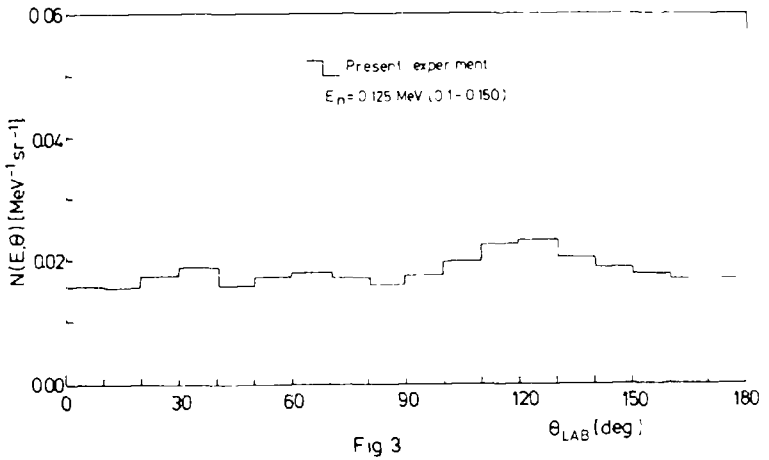

Fig 3

Angular distribution at E_n=0.125 MeV.

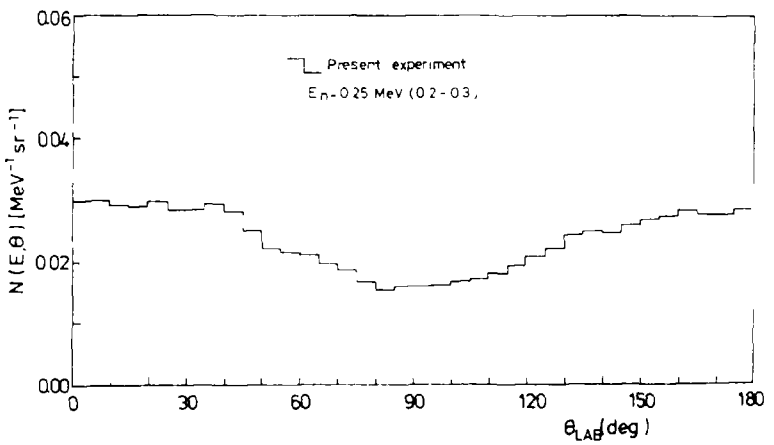

Fig 4

Angular distribution at E_n=0.25 MeV.

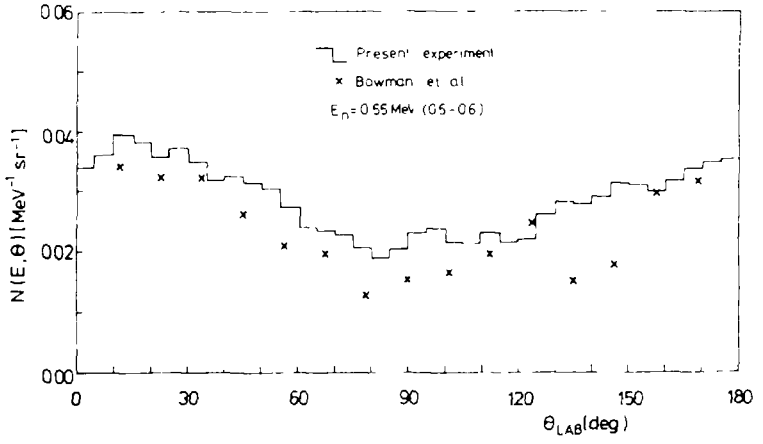

Fig 5

Angular distribution at E_n=0.55 MeV.

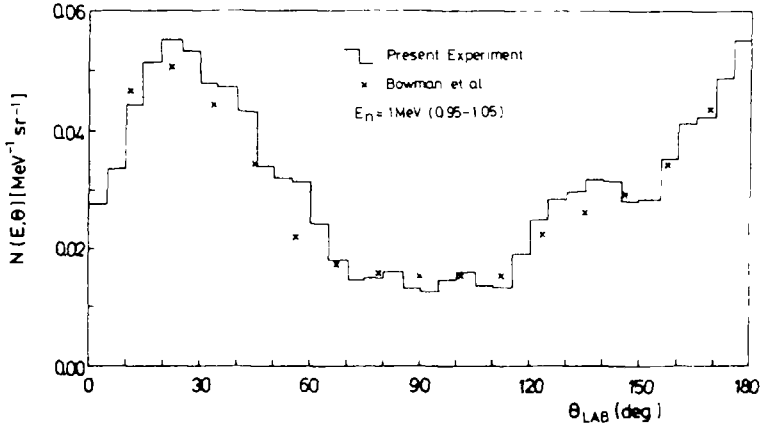

Fig.6

Angular distribution at E_n=1 MeV.

References

1. A. Lajtai et al, Proc. IAEA Meeting, Smolenice (CSSR)INDC (NDS)-146L (1983) 177
2. M.V. Blinov et al, NBS Spec. Publ. 493 (1977) 194
   M.V. Blinov et al, Proc. Antwerp Conference (1983) 479
   O.I. Batenkov et al, Proc. IAEA Meeting, Smolenice (CSSR) INDC(NDS)-146L (1983) 161
3. A. Lajtai et al, Proc. IAEA Meeting on Nuclear Reference Data, Geel (Belgium) IAEA-TECDOC-335 (1985) 122
   Kononov et al, Nucl. Instr. Meth. 234 (1985) 361
4. W. Neubert et al, Nucl. Instr. Meth. 204 (1983) 453
5. W.D. Fromm et al, Proc. Int. Symp. on Nucl. Phys. Gaussig (GDR) 1985 in press
6. M.V. Blinov, Proc. IAEA Meeting on Nuclear Reference Data, Geel (Belgium) IAEA-TECDOC-335 (1985) 281
   O.I. Batenkov et al, Proc. Inst. Symp. on Nucl. Phys. Gaussig (GDR) 1985 in press
7. H.R. Bowman et al, Phys. Rev. 126 (1962) 2110

ESTABLISHMENT OF SIMPLE NEUTRON REFERENCE CALIBRATION FIELD USING MODERATED Cf-252 SOURCE

S. IWAI
Omiya Technical Institute,
Mitsubishi Atomic Power Industries, Inc.,
Omiya, Saitama

A. HARA
Technical Research Institute,
Hazama-Gumi Ltd,
Saitama

T. NAKAMURA, T. OKUBO, Y. UWAMINO
Institute for Nuclear Study,
University of Tokyo,
Tokyo

Japan

Abstract

This paper describes the development and standardization of the neutron fields simply manufactured for detector calibrations used for radiation control and environmental measurement. These fields are the following: (1) bare ^{252}Cf fission field, (2) iron-moderated ^{252}Cf field, (3) carbon-moderated ^{252}Cf field, and (4) polyethylene-moderated ^{252}Cf field. These fields are most suitable for calibrating the detectors used in and around nuclear and radiation facilities, since the fields are designed to simulate the typical neutron fields in and around the facilities.

The direct neutron components of these fields have been standardized by the following two methods: (1) calculation by the ANISN code, and (2) measurements with and without a shadow shield, by detectors standardized in the national standard field at the Electrotechnical Laboratory (ETL). The neutron emission rates of the ^{252}Cf source have been calibrated also at ETL. We have standardized the energy spectrum of direct component because of its independency to room size and peripheral structures; the accuracies have also been evaluated to be 20% below 100 keV, 15% at 1 MeV, and 50% above 5 MeV.

The fields including room scattered components have also been characterized especially to calibrate the neutron detectors having high sensitivity to low energy room scattered neutrons; because large errors are included in the evaluation of low energy neutron components of the direct component field obtainable by shadow shield subtraction.

These two kinds of fields can be situated on the secondary standard fields traceable directly to the primary national standard fields in ETL.

1. Introduction

A simple neutron calibration field has been developed by using a ^{252}Cf source moderated with iron, carbon, or polyethylene sphere. The neutron energy spectra with and without room scattering at the reference calibration point, 1 m distant from the source center, have been calculated with a discrete ordinates code, ANISN-W [1], and a three-dimensional Monte Carlo code, MORSE-CG. [2]

This paper describes the characterization of these fields by comparing the calculated values with the measured values by using neutron detectors, which have been calibrated in the national neutron standard field at the Electrotechnical Laboratory (ETL).

The simple neutron calibration field[3,4] features the following points:

(1) The field has four different types of energy spectra close to those appearing commonly in and around various nuclear facilities.[5] The bare ^{252}Cf source forms a fission neutron fields, the polyethylene moderated ^{252}Cf source gives an nearly 1/E slowing-down neutron spectrum and the iron and carbon moderated source gives the spectra between these two.

(2) The neutron excluding room scattering, that is, the direct neutron components, have been standardized by calculations and experiments for detector calibration, because of its independency to room size.

(3) The neutrons including room scattering have also been characterized for the calibration of detectors having high sensitivity to low energy neutrons.

(4) This field may be constructed easily and at low cost, since this type of direct neutron field requires no large room and expensive equipments.

These simple calibration field may be situated as the secondary standard field,[6] because of its direct traceability to the primary national standard field in ETL.

2. Configuration of the Reference Calibration Field

A point isotropic ^{252}Cf fission neutron source of Amersham Co., Ltd. was used as a secondary standard neutron source. Its neutron emission rate was characterized to be 4.25×10^6 n/sec on August 16, 1985 at ETL. The fission neutron spectrum of bare ^{252}Cf source was fixed to be the following formula presented by the National Bureau of Standards,[7]

$$\chi(E) = 0.6672 * E^{1/2} * e^{(-E/1.42)} * \mu(E) \qquad (1)$$

where $\mu(E)$ is shown in Table 1 as a function of neutron energy, E. The ^{252}Cf fission source was encapsulated in double stainless steel capsule of 1.6 mm thickness, but the neutron slowing-down effect due to this capsule was neglected, because of its 1.6 mm thickness. This bare neutron source was contained in three types of spherical moderators of 20 cm diameter iron, 30 cm diameter carbon, and 45 cm diameter polyethylene shown in Fig. 1.

The source is set in the center of the concrete calibration room with dimensions of 7.0×7.0 m^2 size and 5.0 m height, whose concrete is 30 cm thick. The point of one meter from the center of the source is selected as a reference point for the detector calibration. This position is commonly used for calibrations. The distance of 1 m was selected as a kind of optimum value of two contradictory conditions that the ratio of room scattered neutrons to direct neutrons increases with the distance from the source but the neutron flux variation coming from the distance deviation decreases instead. The source and detector centers are both located 1.25 m above from the concrete floor, because of handling easiness.

A shadow shield was placed between the source and the detector so as to evaluate the contribution of room scattering by shutting off the direct neutron component. The shadow shield is assembled by iron borated polyethylene blocks of $5 \times 10 \times 20$ cm^3 and $5 \times 10 \times 10$ cm^3; the borated polyethylene includes 30 w/o B_2O_3 and has a density of 1.06 g/cm^3. The shadow shield is composed of 20 cm

Table 1 Values of $\mu(E)$ in Eq (1) cited from Ref (7)

Neutron Energy (MeV)	μ (E)
0 00 — 0 25	1 + 1 20 E — 0 237
0 25 — 0 80	1 — 0 14 E + 0 098
0 80 — 1 50	1 - 0 024 E — 0 033
1 50 — 6 00	1 — 6 2 × 10^{-3} E + 0 0037
6 00 — 20 00	1 0 exp [- 0 03 (E — 6 0)]

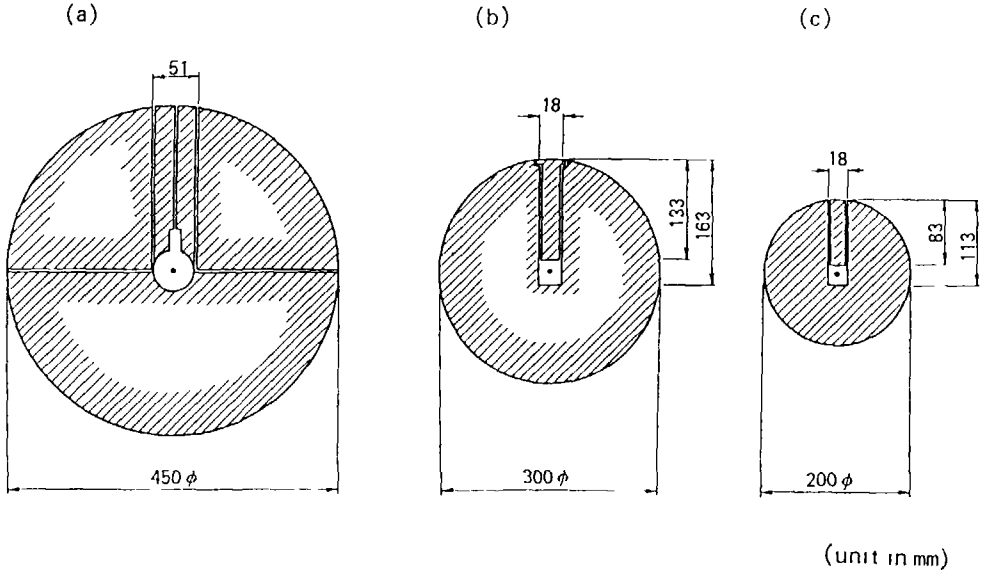

Fig. 1 Cross sectional views of spherical moderators surrounding the ^{252}Cf point source.
(a) Polyethylene moderator
(b) Carbon moderator
(c) Iron moderator

thick iron layer in the source side and 30 cm thick polyethylene layer behind; the iron layer is set for the source so as to decrease effectively neutron energy by iron inelastic scatterings. The shadow shield is constructed to have minimum thickness and configuration sufficient to shut off only the direct component from the source to the detector.

3. Standardization of Direct Neutron Energy Spectrum

Figure 2 shows the calculated energy spectra, $\phi_{dir}(u)$ in lethargy unit u, of direct neutron components at the reference calibration point which is 1 m away from the source. The spectra were calculated by ANISN-W code without regarding the concrete room. The figure clearly shows that the bare source gives the fission neutron spectrum field, the polyethylene moderated source gives almost 1/E - type spectra, and the carbon and the iron moderated sources give the intermediate spectra between the former two spectra. In the iron moderated source field, many resonance peaks can be seen between 5 keV and 1 MeV.

The neutron spectrum of direct neutron component without room scatterings $\phi_{dir}(u)$ at the reference calibration point, is obtained experimentally by the following equation:

$$\phi_{dir}(u) = \phi_{tot}(u) - \phi_{sc}(u) , \qquad (2)$$

where u = lethargy, $\phi_{tot}(u)$ = neutron spectrum measured without the shadow shield (direct component + room scattered component), $\phi_{sc}(u)$ = neutron spectrum measured with the shadow shield (room scattered component). Figure 3 shows comparisons of direct neutron spectra $\phi_{dir}(u)$ measured with the Bonner sphere[8] and the Bonner cylinder,[9,10] and those calculated by the ANISN-W code, in the energy range between the thermal to 15 MeV for the four types of simple neutron calibration field. Figure 4 shows finer intercomparisons of $\phi_{dir}(u)$ calculated by the ANISN-W code, and those measured by the Bonner sphere, the Bonner cylinder, NE-213,[11] and two types of hydrogen counters[12,13] in the energy range from 10 keV to 15 MeV.

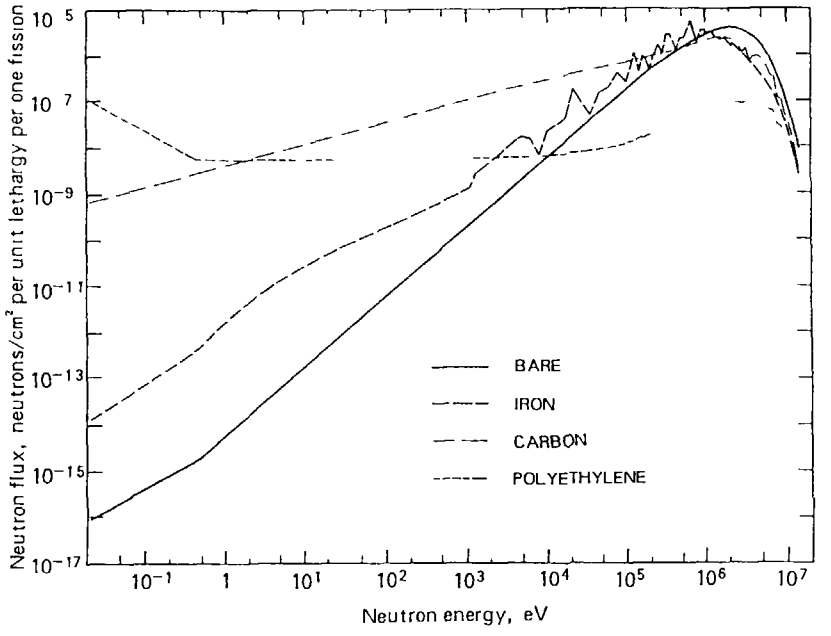

Fig. 2 Direct neutron energy spectra, $\phi_{dir}(u)$, per one fission at the reference point 1 m distant from the source, calculated by the ANISN-W code.

Bare : Bare ^{252}Cf fission field
Iron : Iron moderated ^{252}Cf field
Carbon . Carbon moderated ^{252}Cf field
Polyethylene: Polyethylene moderated ^{252}Cf field

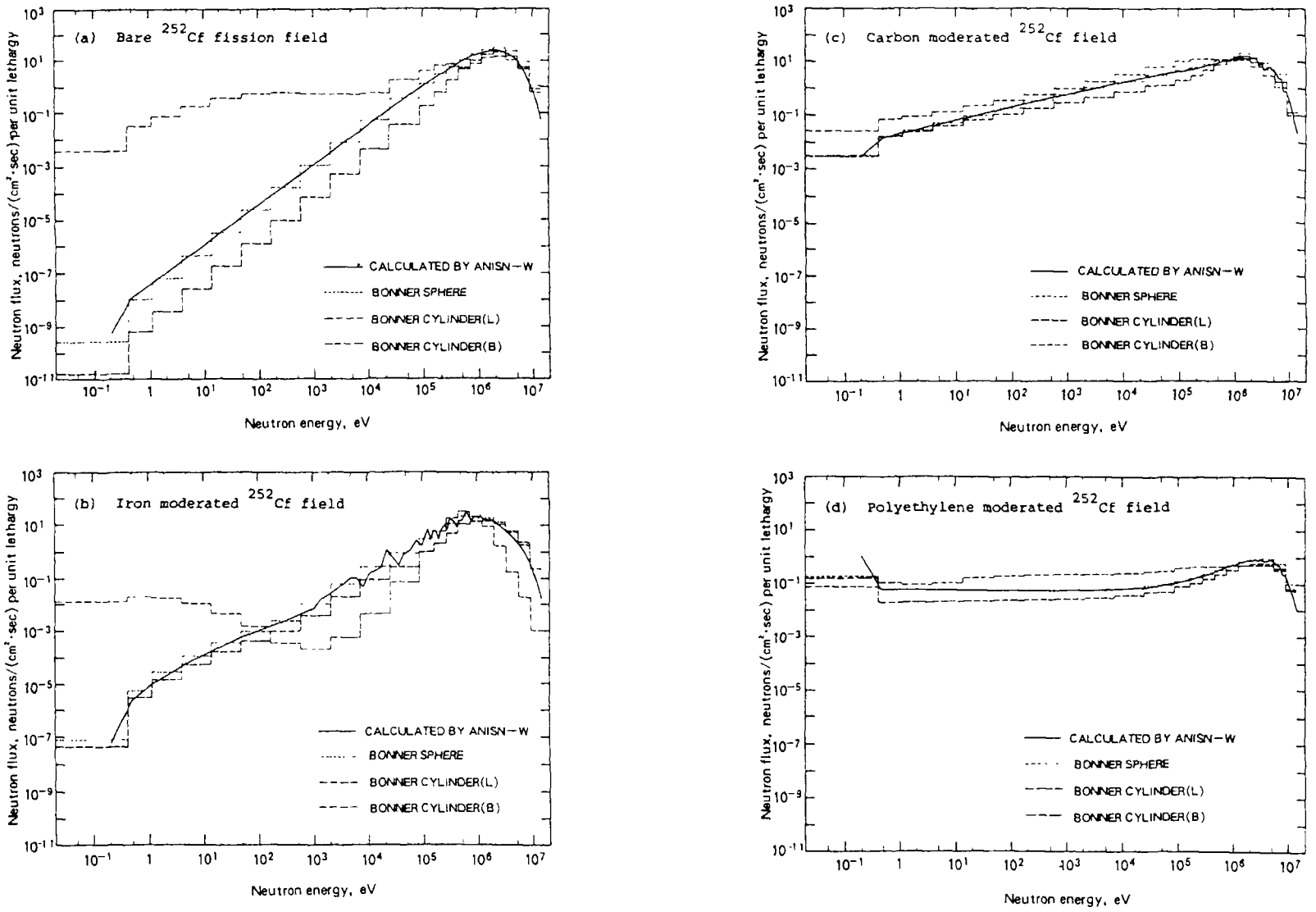

Fig. 3 Comparison of calculated and experimental direct neutron spectra (thermal - 15 MeV) at the reference calibration point in the fields having ^{252}Cf source intensity of 6.09×10^6 n/sec on April 1, 1984. (L) means neutron incidence from lateral surface and (B) from bottom surface.

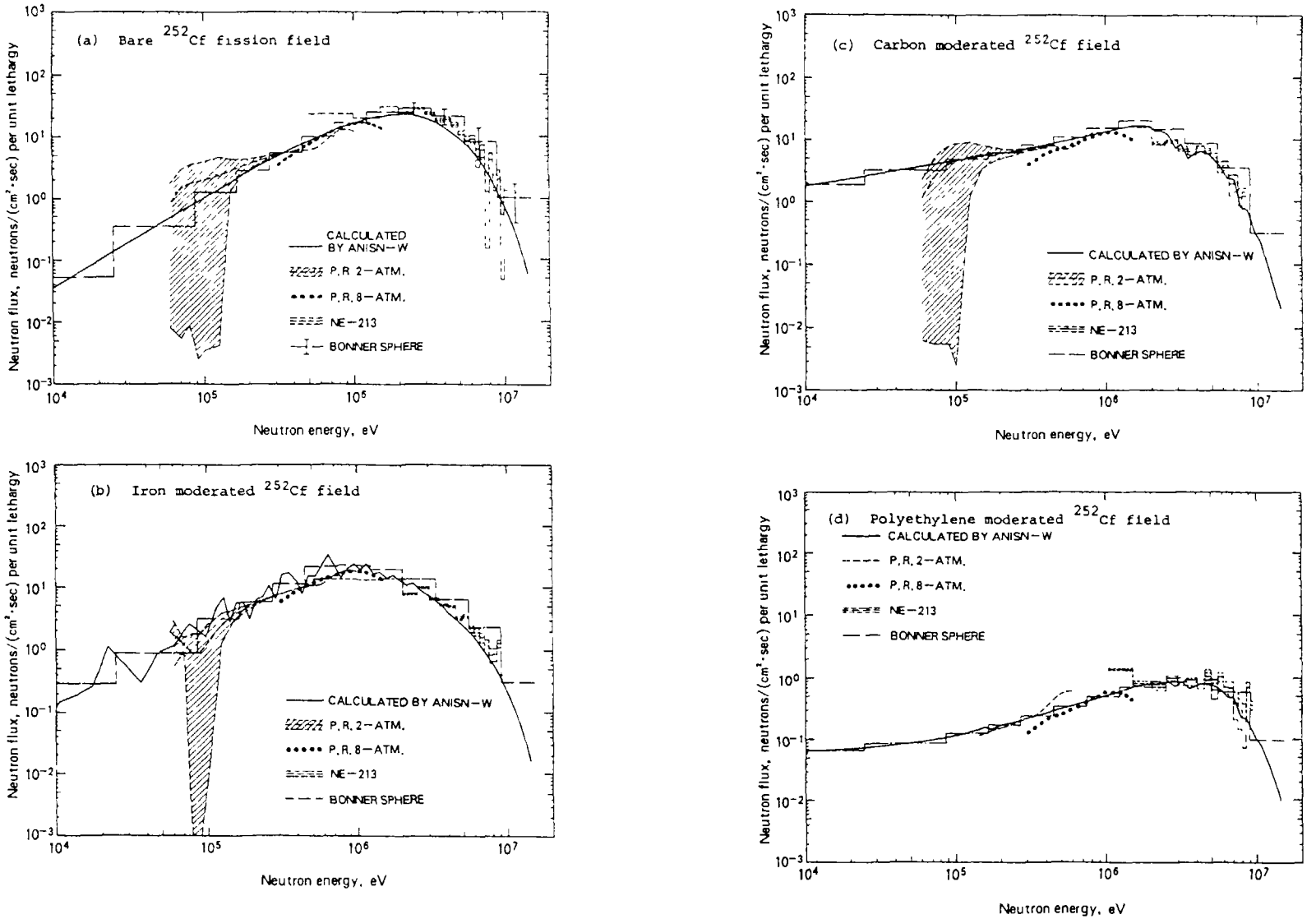

Fig. 4 Comparison of calculated and experimental direct neutron spectra (10 keV - 15 MeV) in the same condition as in Fig. 3. P.R. 2-ATM is 2-atm hydrogen counter and P.R. 8-ATM is 8-atm hydrogen counter.

The following results can be found from these figures:

(1) The spectra calculated with the ANISN-W code agree well with the results measured with the NE-213 scintillator exceeding 1 MeV for the four calibration fields.

(2) In the four calibration fields, the spectra calculated with the ANISN-W code agree well with the results measured with the 2 atm hydrogen counter in the energy range from 70 keV to 1 MeV, and in the energy range from 400 keV to 1.5 MeV the calculated spectra agree with the results measured with the 8 atm hydrogen counter.

(3) The spectra calculated with the ANISN-W code in a range below 2 MeV are in good agreement with the results measured by the Bonner sphere in the iron-, carbon-, and polyethylene-moderated fields; although in the bare ^{252}Cf field, the measured spectrum gives a factor from 30% to 90% lower value to the calculated result in a range below 1 keV. The spectra calculated with the ANISN-W code in a range above 2 MeV are approximately 50% of those measured by the Bonner sphere.

(4) The spectra measured with the Bonner cylinder for neutron incidence from its lateral surface show nearly equal or a little larger (about 50%) values to the spectra calculated with the ANISN-W code in a range above 2 MeV. In a range below 2 MeV, however, these measured spectra show about 50% values of the ANISN-W code calculated spectra for the three moderated fields, and about only 5% values for the bare ^{252}Cf field.

(5) The spectra measured by the Bonner cylinder for neutron incidence from its bottom surface are quite different from calculated spectra, especially for the bare ^{252}Cf and iron-moderated fields.

These results prove that the direct neutron energy spectra calculated by the ANISN-W code have good accuracy.

The spectra measured by the Bonner cylinder are not in good agreement with the calculated values, especially for the bare ^{252}Cf and iron moderated fields. This disagreement is attributable to the inadequate application of response functions. In these experiments, neutron spectra were unfolded by use of the Bonner cylinder response functions for paralleled incidence to the detector surface, nevertheless the detector were set 1 m distant from a point or point-like isotropic source.

The spectra measured by the Bonner sphere give higher values than those measured by the NE-213 and calculated by the ANISN-W code in the energy region exceeding 2 MeV. We consider this disagreement originates in the large unfolding errors caused by use of the response functions having similar slopes above 2 MeV. As shown in Fig. 4(a), the spectra by the Bonner sphere are in agreement with the other two spectra within the error evaluated by the LOUHI code.[14]

It was verified experimentally that the spectra of direct neutrons calculated with the ANISN-W code have good accuracy, since the calculated spectra agree well with the spectra measured by NE-213 above 2 MeV, by hydrogen counters in the energy from 50 keV to 1.2 MeV, and by the Bonner sphere below 2 MeV down to the thermal energy.

Only in the bare ^{252}Cf fission field, the direct neutron spectrum calculated by the ANISN-W code shows larger values than that measured by the Bonner sphere below 1 keV, as shown in Fig. 3(a). This discrepancy may be attributable to the neutron leakage through the shadow shield. Considering this leakage, we have determined the spectrum measured by the Bonner sphere to be an evaluated value below 1 keV in the bare ^{252}Cf fission field. For all other cases, the spectra calculated by the ANISN-W code have been finally determined to be evaluated spectra of direct neutron components at the reference point.

We have roughly estimated the errors of the neutron spectra to be about ±20% below 100 keV, ±15% at 1 MeV, and ±50% above 5 MeV. We have estimated these errors from differences between calculations and experiments, since it was quite difficult to determine quantitatively all errors from many sources.

4. Characterization of Neutron Spectrum Including Room-Scattered Component

These spectra including room scattered components have also been characterized especially to calibrate the neutron detectors having high sensitivity to low energy room scattered neutrons, because large errors can be caused in the low energy neutron components by shadow shield subtraction.[15]

Fig. 5 shows the three types of neutron lethargy spectra at the reference point for the four different calibration fields: (1) total neutron spectra including room-scattered components $\phi_{tot}(u)$, measured without the shadow shield by the Bonner sphere, (2) total neutron spectra including room-scattered components calculated without the shadow shield by the MORSE-CG code, and (3) direct neutron spectra $\phi_{dir}(u)$ calculated by the ANISN-W code in a free air.

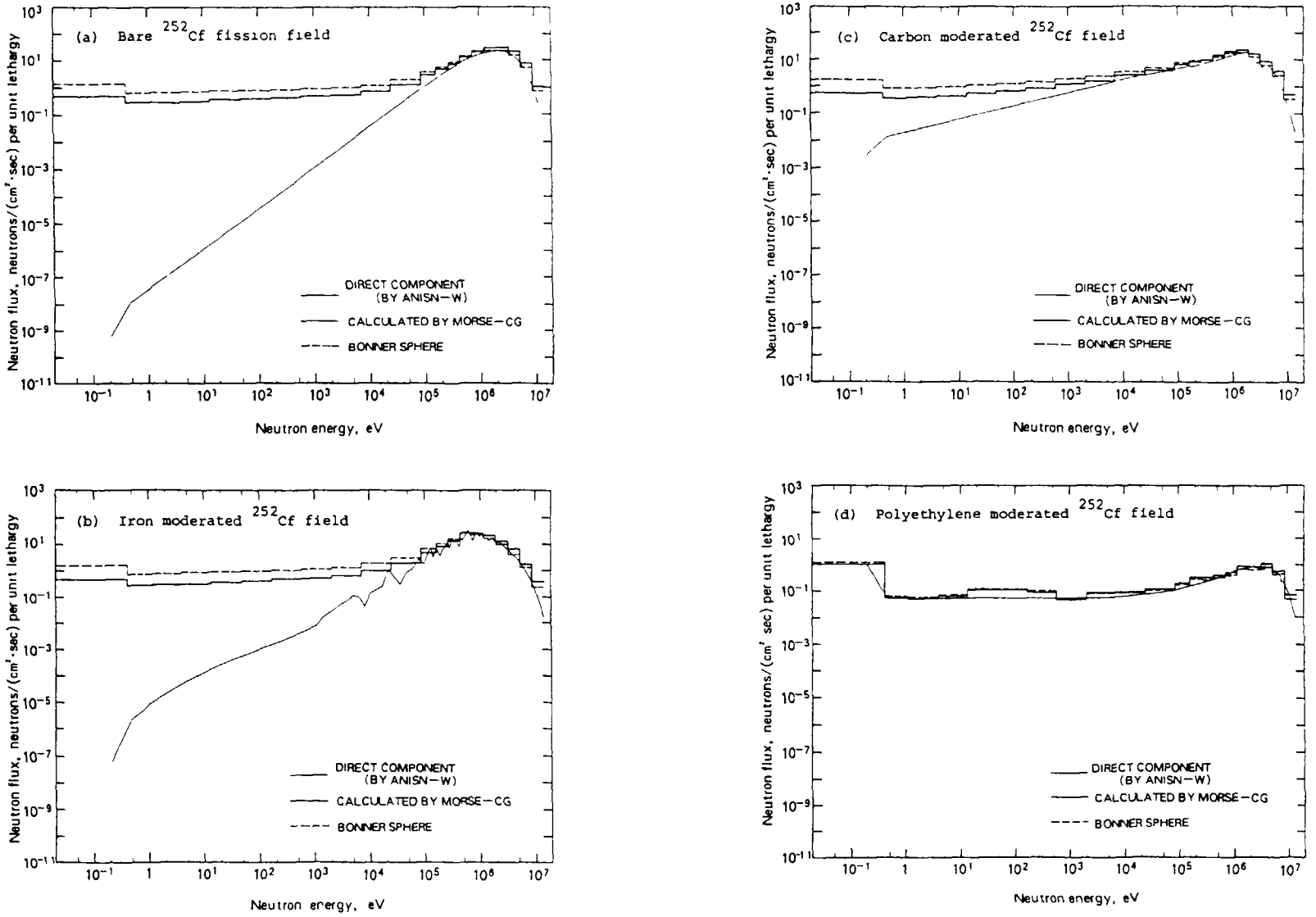

Fig. 5 Comparison of calculated and measured neutron spectra including room-scattered components in the same condition as in Fig. 3.

The following results have been proved from Fig. 5.

(1) The total neutron spectra for the four different fields are similar each other, owing to the 1/E-type slowing-down spectra (<500 keV) caused by room scatterings; although the direct component spectra are mutually different.

(2) The results calculated by the MORSE-CG code are at maximum 20% higher than the experimental results and results calculated by the ANISN-W code above 500 keV.

(3) The MORSE results below 10 keV are in good agreement with the experimental values in the polyethylene moderated fields, but in the other three fields, the values calculated by the MORSE-CG are about 50% higher than the experimental results.

The discrepancy is found between the MORSE spectra and the ANISN spectra of experimental spectrum above 500 keV, although the neutrons exceeding the energy of 500 keV is mostly direct components. This discrepancy is not yet explainable at present.

The experimental results are higher than the MORSE results in the low energy scattering components. We assume this fact may be ascribed to the neglection of a little complicated room structure such as irradiation tables, beams, and pillars in the MORSE calculational model. This assumption have led to the findings that the experimental results are more accurate than the MORSE calculated results. Then, we have determined that neutron spectra measured by the Bonner sphere are the evaluated spectra $\phi_{tot}(u)$ including room scatterings at the reference calibration point.

5. Summary

The four kinds of neutron fields have been developed for neutron detector calibration. These fields have been designed to simulate typical neutron spectra appearing in and around nuclear facilities. The absolute values of spectra have been accurately standardized from calculations and experiments for direct neutron components without room scatterings. The direct neutron field can be used for calibrations by the subtraction method of the shadow shield. We have standardized direct components because of its independency to room size and structure.

The direct neutron calibration fields are not adequate to be applied to the calibration of neutron detectors having high sensitivity to low energy room scattered neutrons, because of large errors caused by subtraction. These detectors should preferably be calibrated in the fields including room scattered components, by a comparison with the results measured with standardized detectors. Therefore, the energy spectra including room-scatterings have been characterized from calculations and experiments.

The simple neutron calibration field developed in this study is very useful in eliminating the need for large rooms and expensive apparatuses.

References

1) R. G. Soltese and R. K. Disney, revised WANL ANISN Program User's Manual: WANL-TMI-1967 (1969).
2) M. B. Emmett, ORNL-4972 (1975).
3) E. Teranishi et al., Electrotechnical Lab. 41 (1977) 693, in Japanese.
4) O. Yura, A. Katoh, and T. Michikawa, RADIOISOTOPES 28 (1979) 70, in Japanese.
5) R. B. Schwartz, G. W. R. Endres and T. M. Cummings, NUREG/CR-2233 (1982).
6) Y. Moriuchi; J. At. Energy Soc. Japan, 19 (1977) 218, in Japanese.
7) J. Grundl and C. Eisenhauer: Neutron Cross Sections for Reactor Dosimetry, Technical Document IAEA-208, 1, p53 (1978).
8) Y. Uwamino, T. Nakamura and A. Hara, Nucl. Instr. Meth., A.239 (1985) 299.
9) T. Nakamura, T. Kosako, and S. Iwai, Health Phys., 47, (1984) 729.
10) T. Kosako, T. Nakamura and S. Iwai, Nucl. Instr. Meth., A232 (1985) 103.
11) W. R. Burrus and V. V. Verbinski, Nucl. Instr. Meth., 67 (1969) 181.
12) P. W. Benjamin, C. Dkemshall, and A. Brickstock, AWRE O-9168 (1968).
13) J. F. Janni, Part 2 Proton Range-Energy Tables, 1 keV-10 GeV Energy Loss Range, Path Length, Time-of-Flight, Straggling, Multi-Scattering, and Nuclear Interaction Probability: Atomic Data Tables, 27 (1982) 341.
14) J. V. Sandberg and J. T. Routti, TKK-F-A 488 (1982).
15) Y. Onai, RADIOISOTOPES 28 (1979) 57, in Japanese.

THE HALF-LIFE AND THE AVERAGE NUMBER OF NEUTRONS PER AN ACT OF CF-252 FISSION

E.A. SHLYAMIN, I.A. KHARITONOV
V.G. Khlopin Radium Institute,
Leningrad, Union of Soviet Socialist Republics

Abstract

The manganese bath method has been used with fragment counting over a small solid angle to measure the value of $\bar{\nu}[^{252}Cf]$. The improved quality of the source active layers has reduced the error in determining the fission rate. The value obtained for $\bar{\nu}[^{252}Cf]$ is 3,749 ±0,016. An analisis of the results and methods of californium-252 half-life measurement has been carried out.

The value T=(2,6473±0,0028) years can be recommended as evaluated by the results of the considered publications.

1. Measurement of $\bar{\nu}(^{252}Cf)$

For many years the average number of neutrons per an act of ^{252}Cf fission has been a standard, in relation to which the measurement of the $\bar{\nu}$-values of "fuel" isotopes of uranium and plutonium was done. However, despite the status of a standard for $\bar{\nu}(^{252}Cf)$, there is a long disagreement of the experimental results obtained by different methods. For the recent one and a half decades the discrepancy of the results exceeds the claimed error of measurements by the methods of manganese bath and large liquid scintillator. A reevaluation of the results and introduction of corrections for the case of these main methods has improved the situation, but hasn't brought a final agreement. Thus, $\bar{\nu}(^{252}Cf)$ measurements with the highest precision both by the manganese bath method and by the large liquid scientillator is the only a way for detection of systematic errors and for obtaining the required agreement of the results. The works on $\bar{\nu}(^{252}Cf)$ measurement have been carried out at the V.G.Khlopin Radium Institute since 1972 /1,2/.

The flowing manganese bath is used for measuring the neutron flux /3/, and the fragments of californium sources fission are measured by means of a small solid angle chamber.

Californium sources were prepared by the method of thermopulverization of californium chloride with the contect of the A=252 isotope ~85% on platinum substrates 0,4mm thick. Rotation of a substrate at californium pulverization provided a 5% homogeneity of the layer at the spot diameter 8mm. The mass of the active substance of different sources was within the limits (0,4 -0,8) μg; this provided a reasonable counting value both at measuring the neutron flux and at measuring the counting rate of fissions in the small solid angle chamber.

The calibration of the chamber was done by the reference target of americium-241; it's α-activity was measured by the $\alpha-\gamma$ coincidence method with the error 0,1 %.

A specially manufactured surface-barrier silicon detector with a small level of the low-energy "tail" of the fission fragments spectrum was used as the detector of the fission fragments. At determining the counting rate of fissions in the californium target the spectrum of the fission fragments was extrapolated to the zero energy of the linear dependence.

The neutron flux of the californium sources hermetized by means of titanium containers was neasured on the flowing manganese bath of the Radium Institute.

The counting device of the bath was calibrated, i. e. the registration efficiency of the full induced activity of manganese-56 was determined, by absolute measurements on $4\pi\beta-\gamma$ setting of the aliquots of the manganese sulphate activated solution added to the bath.

The corrections used for calculation of the neutron flux of californium sources by the results of measurements of the saturated activity of the solution of the bath, had the following values:
$1 + g\bar{r}s = 1.0137$ /4/ for $n_{Mn}\gamma_{n_H} = 0.023417$ - the correction for the resonance neutron capture by manganese;

$1 + l = 1.00216$ /5/ - correction for the neutron leakage from the bath;

$1 + \varkappa = 1.00437$ /3/ - correction for the capture of fast neutrons by nuclei of sulpher and oxygen;

$1 + m = 1.00388$ /3/ - correction for neutron absorption in the casing material of the source and in the aluminium hollow sphere, where the source was encased during measurements;

$K_1 = 1.00003$ /3/ - correction for neutron absorption in steel rods-holders of the aluminium hollow sphere;

$K_2 = 1.0027$ /3/ - correction for neutron absorption by the solution admiztures.

At counting the share of the neutrons captured by manganese - coefficient F - the following cross-section values were used:

$$\sigma_S = (0.53 \pm 0.01) \cdot 10^{-24} \text{ cm}^2 \text{ /6/},$$

$$\sigma_{Mn} = (13.3 \pm 0.2) \cdot 10^{-24} \text{ cm}^2 \text{ /7/},$$

$$\sigma_H / \sigma_{Mn} = 0.02486 \pm 0.00009 \text{ /8/}.$$

The concentration of the solution was obtained 0.281897 $\pm$ $\pm$ 0.00014 g/g of solution.

The components of the error of the neutron flux determination had the values:

- counting statistics of the γ-detector ± 0.05 %;
- efficiency determination of the γ-detector ± 0.3 %;
- coefficient F ± 0.2 %;
- neutron absorption in the source and aluminium sphere ± 0.01 %;
- neutron absorption by oxygen-16 and sulphur-32 ± 0.01 %;
- neutron leakage ± 0.02 %;
- neutron absorption by the solution admixtures ± 0.03 %;
- neutron absorption in the rods ± 0.0001 %.

The components of the error of the fission rate measurement were:

- counting statistics ± 0.1 %;
- extrapolation of the energy spectrum of fission fragments to zero energy $\pm 0,1$ %;
- californium self-diffusion ± 0.1 %;
- determination of the solid angle ± 0.15 %.

The value of the average number of neutrons per an act of californium-252 fission by the results of measurement of the neutron flux and the counting rate of fissions of different californium target was:

$$\bar{\nu}(^{252}\text{Cf}) = 3.749 \pm 0.016.$$

For agreement of the measurements the value was used

$$T_{1/2}(^{252}\text{Cf}) = (2.651 \pm 0.004) \text{ years /17/}.$$

In 1979-1984 international intercomparison of the neutron source on the base of californium-252 "SR-CF-144" belonging to the NBS (USA) was carried out on the initiative of the International Bureau of Measures and Weights. 14 laboratories from 9 countries took part in the intercomparison. The Soviet Union was represented by the D. I. Mendeleyev Metrology Institute and the V. G. Khlopin Radium Institute.

The summary results of the intercomparison are published in the document CCEMRI (III)/85-2.

From Fig. 1, 2 of the document a conclusion can be made about a good agreement of the results of the RI (symbol VGK) with the average-weighed value of the flow of the "SR-CF-144" source, and about a correct account of the corrections of the manganese bath method, which it its furn characterized the reliability of the obtained value of $\bar{\nu}(^{252}\text{Cf})$ in the field of neutron measurements.

2. Californium-252 half-life: data analysis and formulation of requirements to the experiment providing a measurement with a necessary precision

An analysis of the results and methods of californium-252 half-life measurement from eleven works /9-19/ published in the period 1965-1985 has been carried out.

A comparison of the half-life values shows that the error of the result evaluated by the authors in from 0.08 % to 0.38 %; deviation of individual values from the recommended, for instance /20/,

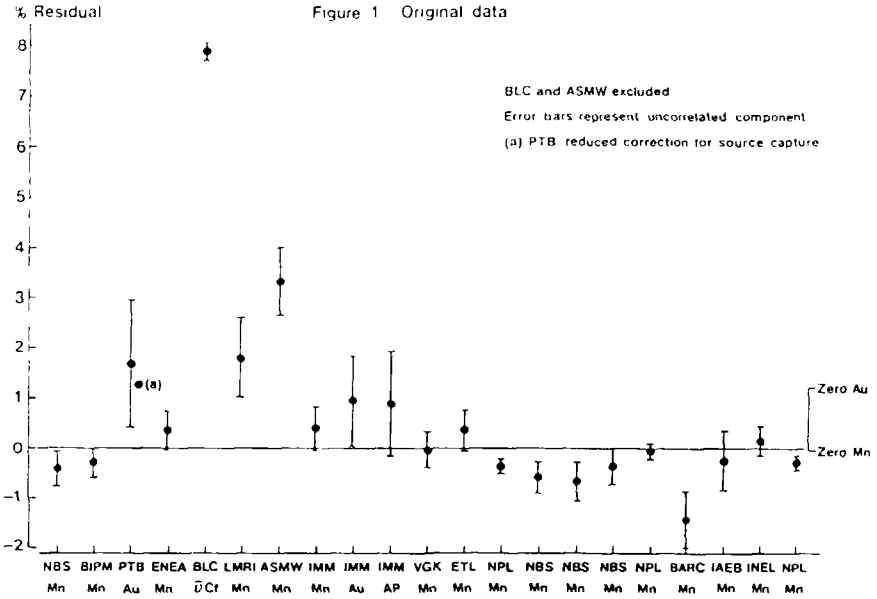

Figure 1 Original data

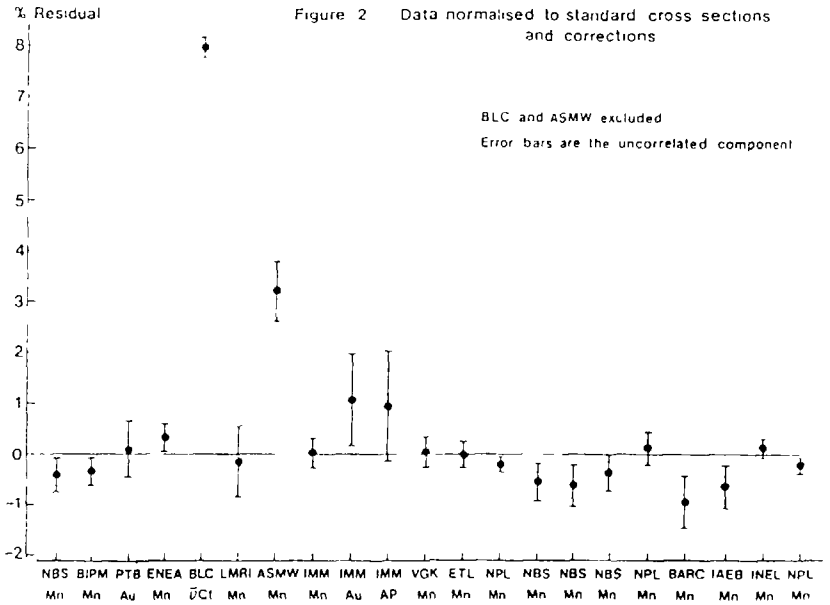

Figure 2 Data normalised to standard cross sections and corrections

value reaches 0.7 %; the swing of the results is 1.5 %; the results of the later works /16-19/ are grouped around the average value which exceeds the recommended one by 0.3 %.

Thus, the divergence of the results exceeds considerably the indicated by the authors errors, which gave grounds to Reich /21/ to characterize the existing situation with the californium-252 half-life as a "highly confused".

In 1985 Smith /23/ analyzed the results of the measurements and evaluated the half-life; however in connection with the publication of the results of works /18, 19/ this evaluation requires specification.

In prologed experiments on measuring of constants, where californium-252 is used as a standard, the error in the value of the half-life directy influences the results of measurements. For instance, as shown in reference /19/, at the experiment on measuring the $\bar{\nu}$ of ^{252}Cf the data accumulation may take the time comparable with the half-life. Since the required error of measurement of the $\bar{\nu}$ is fixed 0.25 % /22/, one can suppose that the error of the half-life shouldn't exceed 0.1 %.

One and the same method of determining the half-life is used in the experimental works: calculation of the decay constant from the results of relative measurements of the activity (or the neutron flux) of the radionuclide in the source for a certain time interval.

In all the works side by side with the random error of measurement one can suppose the presence of a systematic error stipulated by the influence of ^{250}Cf and ^{254}Cf nuclides and by instability of the measurement condidions.

In most works the influence of the concomitant nuclides is accounted for by introducing the correction calculated on the base of the initial product composition determined by the mass-spectrometric method; however in some references /10, 11, 13, 16/ the composition of the initial product isn't quoted and the correction wasn't introduced.

Although to provide constant conditions of measurements, special neasures had been taken in the course of the experiment: fixed geometry of the source's location in relation to the detector,

the coincidence method at measuring the activity, stable equipment or normalization for the neutron flux of the sources with long-lived radium, nevertheless the influence of the long-time instability can't be excluded completely.

For nonampuled sources one should take into consideration the specific cause of systematic error, connected with the noncontrolled losses of californium resulting from the agregate product transfer from the substrate of the cource.

Thus, in each experiment the presence of nonexcluded remainders of the systematic error, the combined action of which leads to the experimental result displacement from the "true" value and is the cause of divergence of the results beyond the error limits, cited by the authors.

In some references /12, 14, 19/ the evaluation of the systematic error, established by the authors, is included in the error of the result side by side with the standard deviation. Therefore, although in the other works this hasu't been done, the first approximation in our method of evaluation is the half-life evaluation calculated only with an account of the error cited by the authors.

By the calculation results $T_1 = (2.6457 \pm 0.0026)$ years.

In some works /10, 11, 13, 16/ the influence of other nuclides wasn't accounted for, and the composition of the initial product was either not cited at all, or cited in the form not enabling to introduce the correction. From analysis of the works where the composition was studied and the corrections were carefully calculated it follows that the minimum error because of non-accounting of californium-250 can be 0.2 %, and because of californium-254 - 0.1 %. These additional error were summed up with the "authors" ones in the works where the influence of the attendant nuclides was neglected. Besides, in the work of Spiegel /14/ a correction of the value cited by the authors was introduced, with the account of the californium-254 content and the measurement procedure.

The second approximation in the accepted method of evaluation is $T_2 = (2.6468 \pm 0.0021)$ years, calculated with an account of the additional error through the influence of the attendant nuclides.

At comparison of the results of the works certain difficulties arise because of great variety of the experiment duration chosen by the authors (from 0.5 to 7 years) and of the number of measurements (from 2 to 50), because both parameters influence the precision of the calculation of the decay constant by the least square method.

In absence of a criterion enabling to give preferance to certain values of the parameters a concept of a conditional rational experiment was formed. If we suppose that the measurement of the activity (or the flux) are carried out in equal time intervals with a fixed statistical error σ and choose the length of the interval on the condition that the relative change of activity should exceed 2σ (an account of the resolution of the apparatus), it is possible to show that there exist an optimal duration and the number of measurements for such an experiment. In particular, for californium the optimal duration corresponds to the half-life and the number of measurements equals 33.

The duration and the number of measurements in each real experiment were compared with the paremeters of a rational one, and the difference was evaluated by a certain method as a factor of additional error of measurement. It was by this that all the experiments were conditionally reduced to the rational one.

The third approximation to the accepted method of evaluation is the value $T_3 = (2.6473 \pm 0.0028)$ years, calculated with an account of an additional error due to the difference of the measurement procedure from the "rational" experiment.

Comparison of the values T_1, T_2, T_3 shows that introduction of additionsl error because of ignoring the influence of other nuclides and digression from the procedure of the "rational" experiment leads to the increase of the mean weighted value of the half-life at keeping the mean-square deviation of the calculation result 0.1 %.

The value $T = (2.6473 \pm 0.0028)$ years can be recommended as evaluated by the results of the considered publications.

The analysis of the "weight" coefficients bear witness that the contribution of the results of Alberts /18/ and Axton /9/ peblished after the analysis of Smith/23/to the T_1, T_2, T_3 was over 50 %.

It would be desirable to reduce the summary "weight" of the results of those works in T_3 to the level of 25 %, for this it is necessary to do, at least, two more independent experiments the requirements to which could be worded as follows.

The measurement method: activation of the detectors, preferably gold foil, by an ampulled source in fixed geometry in a moderator: water, graphite or polythylene. The activity of the foils should by measured by the $4\pi\beta-\gamma$ coincidence method. The choice of the method excludes an agregate self-atomization of the product and decreases the probability of measurement aonditions instability.

Product composition: californium-250 content isn't limited, but it must be measured with an error not more 5 %; the content of ^{254}Cf in the initial product before the ampulation of the source not more 0.02 % and should be determined with an error not more 30 %; the time interval between the ampulation and the first measurement not less 14 months.

Measurement procedure: experiment duration - 2.7 yeas, the number of measurements - 33, the interval between measurements - 1 month, according to the plan of the "rational experiment".

One can suppose that carrying out of purposeful experiments will enable to establish the value of the half-life of californium-252 with an error less 0.1 %.

References

1. B. M. Aleksandrov et al., Proceeding, Kiev Conf. 5 (1975) 166.
2. B. M. Aleksandrov et al., Proceeding, Kiev Conf. 4 (1980) 119.
3. J. M. Kramarovski et al., "Flowing manganese bath", Leningrad RI-160 (1983).
4. Axton E. Y., Rives T. B., Journ. Nucl. Energy, 21 7 (1967) 543.
5. A. V. Sorokina et al., Atomic Energy, 45 (1978) 459.
6. L. Koester, K. Knopt, W. Waschowski, Z. Physika, 289 (1979) 399.
7. BNL 325 (1978).
8. J. R. Smith. EPRI. NP-1098 (1979) 5-1.
9. Metta D., Diamond H., Barnes R. F. et al., Journ. Inorg. Nucl. Chem. 27 1 (1965) 33-39.
10. Volpi A. de., Poeges K. G., Inorg. Nucl. Chem. Letters, 5 2 (1969) 111-113.
11. Volpi A. de, Porges K. G., Inorg. Nucl. Chem. Letters, 5 8 (1969) 699-700.
12. Mijnheer B. J., Hauten-Zuidema E., Vande, Intern. Journ. Appl. Radiat. Isotopes. 24 3 (1973) 185-187.
13. V. T. Schebolev et al., Atomic Energy, 36 5 (1974) 339.
14. Spiegel V., Nucl. Sci. Eng. 53 3 (1974) 326-327.
15. V. K. Moshaev, Atomic Energy, 40 2 (1976) 174.
16. Lagoutin F., Legrand J., Intern. Journ. Appl. Radiat. Isotopes, 33 9 (1981) 711-713.
17. Smith J. R., BNL-NCS-31052, May 1982.
18. Alberts W. G., Matzke M., PTB-Mittelungen, 93 (1983) 315-319.
19. Axton E. J., Bardell A. G., Metrologia, 21 (1985) 59-74.
20. Vaninbroukx R., LorenzzA., IAEA, Vienna, STI/DOC 10/227 (1983) 69.
21. Reich C. W. IAEA, Vienna, TECDOC-335 (1985) 390-393.
22. Spencer R. R., Gwin R., Nuclear Sci. Eng., 80 (1982) 603-629.
23. Smith J. R. INDC/NDS/-147/GE, 1983.

SESSION IV

MONOENERGETIC SOURCES AND FILTERED BEAMS

POSSIBILITIES OF EXPERIMENTAL DETERMINATION AND THEORETICAL PREDICTION OF DIFFERENT PROPERTIES OF ACCELERATOR BASED NEUTRON SOURCES

N V KORNILOV
Institute of Physics and Power Engineering,
Obninsk, Union of Soviet Socialist Republics

Abstract

The paper considers the possibilities of theoretical description of various neutron source characteristics on the example of a gas deuterium target.

It has been shown, that with proper models adopted not only the first moments but the function of neutron flux energy distribution can be calculated with good accuracy. There is a review of experimental measurement methods for incident particle energies, mean neutrons energies and distribution functions. Attention is paid to the systematic disagreement between the experimental and theoretical neutron fluxes from the gas target.

A monoenergetic neutron source is totally determined by a distribution function of the neutrons by the energy and the angle of escape $\Phi(E,\theta)$. In many cases, when the value $\sigma(E)$ investigated is independent on an angle and can be described by a linear function in the range of averaging it is enough just to take into account the first moment of distribution. In this case

$$\bar{E} = \int_{E_{min}}^{E_{max}} E\,dE \int_{\Omega} \Phi(E,\theta)\,d\Omega = \int_{E_{min}}^{E_{max}} \Phi(E)\,E\,dE \qquad \bar{\sigma} = \sigma(\bar{E})$$

where

However, on these assumptions, for $\bar{\Phi}$, $\bar{E}$ calculation the distribution function should be determined correctly. For this purpose the following factors should be taken into account:

1. Space distribution of incident particles;
2. Energy losses in target materials, energy and angle straggling, surface inhomogenety.
3. Energy and reaction cross-section variation with on the angle of neutron escape.

Same of the above factors are often ignored at neutron source calculation, which may result in systematic energy shifting, may alter the neutron flux dependence on a distance etc. At the same time all the factors affecting $\Phi(E)$ are calculated with the sufficient accuracy. That is the consideration of theoretical models of calculation and experimental methods of neutron source characteristics measurement the present work is devoted to.

Theoretical Models for Calculation

I. Distribution Function Calculation

Let the possibilities of neutron source characteristics calculation be illustrated on the example of a gas deuterium target focusing attention on the analysis of the factors mentioned above in points 2,3, and let the main relations usable for practical calculations be listed.

I.I. Interaction of Particles in target entrance foil

A mean particle energy after the entrance foil is calculated on the basis of stopping power tabulated in a number of references /1,2/, and a known thickness of foil. However, with essential energy losses it is reasonable to define energy E_1 after the foil from the equation:

$$R(E_0) - \Delta R = R(E_1)$$

where ΔR - foil thickness,

$R(E_0)$, $R(E_1)$ - particle paths with the energy E_0, E_1

The function $R(E)$ is described fairly accurately by the formula:

$$R(E) = a\,E^{b}$$

The coefficients a, b are defined from the description of tabulated values $R(E)$. As a rule, two sets of coefficients are enough to describe $R(E)$ with an accuracy $\lesssim 0.15\%$ in the incident particle energy range from 2 to 8 MeV.

At the expense of statistical nature of charged particle interaction its energy will be properly distributed in the vicinity of the mean energy E_1.

The interaction is characterized by an average number of collisions K.

$$K = 0.150\ \Delta R\ Z_p^2 Z/A\,(2E_0/m_p c^2)^2 \qquad /3/$$

where Z_p, m_p - projectile charge and mass,
E_0 - kinetic energy (MeV),
Z, A - charge and mass number of stopping material nuclei.

At $K \lesssim 1$ the distribution has an asymmetric form, that is an excess of large energy losses. The importance of taking the distribution into accont was paid attention to in Ref /4/, when investigating neutron distribution of thin metallic lithium targets. The problem of interactions for small K was considered by Vavilov. The resulting distribution fanctions were tabulated e.g. in Ref /5/.

At $K \gtrsim 10$ the distribution is described by a Gaussian. If the incident particle velocity essentially exceeds the Bohr one $v_0 = e^2/\hbar$, the energy losses are determined by interaction with electrons and the interaction cross-section is proportional to ΔE^{-2} -the energy dispersion is calculated by the Bohr formula.

$$\sigma_B^2 = 4\pi e^4 Z_p^2 Z N_0 \Delta R/A$$
$$\sigma_B = 0.395\, Z_p (Z\,\Delta R/A)^{1/2},\ [\sigma] = MeV,\ [\Delta R] = g/cm^2 \qquad 1$$

where N_0 -is Avogadro's number.

High-energy limit (1) is predicted in all theoretical calculations. More ambiguous is the behaviour of σ at low energies. Let certain models be considered in more detail. The total review of theoretical and experimental analysis of the energy straggling is given in Ref /6/.

In Ref /7/ it was suggested to calculate the energy straggling with the formula:

$$\sigma^2/\sigma_B^2 = \begin{cases} 0.5\,L(x) = 0.68\,x^{1/2} - 0.08\,x^{3/2}, & x \le 3 \\ 1, & x > 3 \end{cases} \qquad 2$$

where $x = (v/v_0)^2/Z = 36.7\,E_0/Z A_p$

It should be emphasized that the function $L(x)$ defines the material stopping power formula

$$-\frac{dE}{dx} = \frac{4\pi e^4 z_p^2 z}{m_e v^2} \frac{N_0}{A} L$$

Hence for low energies $x \leq 3$, σ^2 can be defined from the equation

$$\sigma^2 = (\Delta E E_0) m_e / m_p$$

The behavior of σ^2 close to expression 2 is also predicted in more rigorous theories /8,9/. So for deutrons with $E_0 \sim 6$ MeV going through a molybdenum foil $\sigma^2/\sigma_B^2 \sim 0.8$ /8/. The critical energy determined by formulae 2 is ~ 7 MeV.

The comparison of the theoretical model with the experimental data is hindered due to incressing contribution of surface inhomogeneity at low particle energies. The experimental data given in Ref /6/ exceed the theory prediction by a factor of 1-4 for $x \leq 3$. In /6/ the data for varions incident particles experimentally obtained with one set of foils were analyzed, which enabled the inhomogeneity contribution to be taken into account. The data are in a good agreement with the predictions of Ref /8/. However, these results cover the area $x \geq 2$ and their accuracy is defined by the accuracy of heavy particle (ions ^{6}Li) ionization loss knowlegde.

Work /10/ experimentally showed the nouniformity contribution to be well below straggling. The experimental data for nickel show (Fig.I), that $\sigma = \sigma_B$ up to the energies corresponding to the velocity 3.6 Vo (0.7 MeV for deutrons). The deuterium target investigations with molibdenum foil performed in our institute do not contradict an assumption on the Bohr formula validity up to $E \sim 3$ MeV.

Thus for source under consideration the application of expression 1 is justified at energy straggling calculation. When destribing a source with other structural materials the possibility of essential decrease of σ^2 at low incident particle energies should be kept in mind. Besides, the material's structure affecting the value of straggling is quite feasible /6,10/.

The foil non-uniformity essentially affects particle energy distribution. The distribution formed in this case is well- - described by the Gaussian (Fig.2). Dispersion as a function of the initial energy can be calculated from the equation

$$\sigma_R^2 = \left[\frac{dE}{dx}^2(E_0) + \frac{dE}{dx}^2(E_1) \right] \delta_R^2 \qquad 3$$

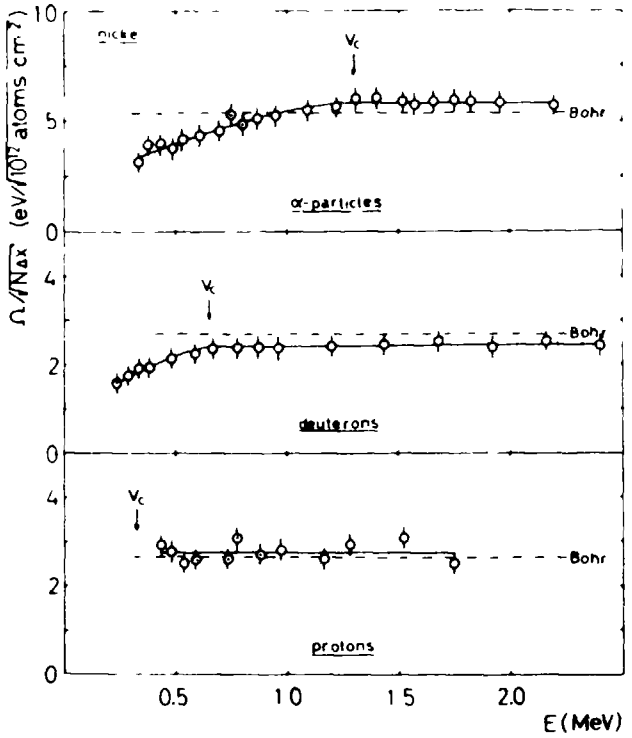

Fig.I. Energy straggling depending on incident particle energy according to the data of Ref /10/. The arrows indicate energies corresponding to the velocity 3.6 Vo.

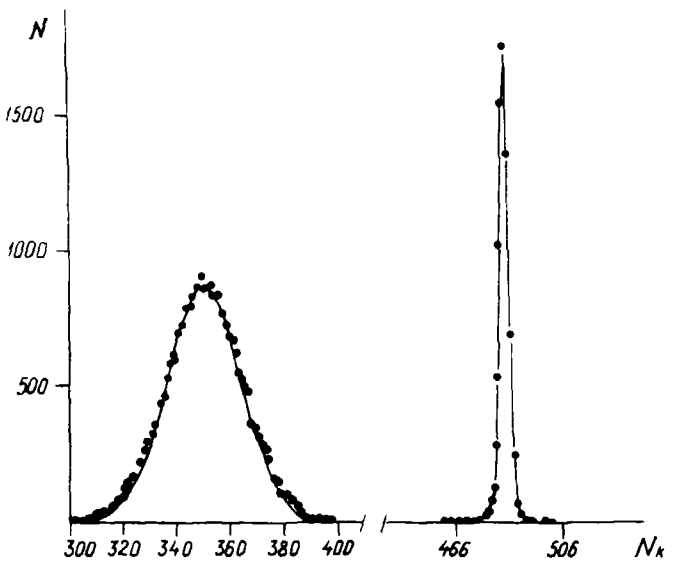

Fig.2. α - particle spectra with E=7.68 Mev measured by a semi-conductor with molibdenum foil ΔR = 6.45 mg/cm^2, δ_R = 0.46 mg/cm^2 (a) and without foil (b). σ_B = 42.1 KeV, σ_R = 201 KeV. The solid line shows the function of normal distribution.

Equation (3) is valid, if non-uniformities of the inlet and outlet foil surfaces δ_R are non-intercorrelated. It should be pointed out, that value δ_R can be essentially varied for different foils, that is why it should be determined experimentally.

An important factor affecting not only the distribution, but also the mean neutron energy is the angular straggling. A detailed analysis of theoretical models is given in Ref /11/. According to this wirk 90% of particles in the angular range $0° \sim \theta < 6°$ are described by the normal distribution function. For these angles the assumption $\sin\theta \simeq \theta$ is valid and

a particle escape frobability in the interval of angles $\theta \sim \theta + d\theta$ is determined by the Expression:

$$P(\theta) = (2\theta/\theta_c^2)\, exp(-(\theta/\theta_c)^2) \qquad 4$$

where θ_c - is an angle of the e-fold distribution decrease. For practical calculations it is reasonable to adopt approximated expression (4), after the value θ_c determination on the basis of consistent theoretical models /11/. The parameters required for the angle θ_c calculation are: θ_1 is the angle for which on an average there is only one scattering with the angle $\theta > \theta_1$,

θ_0 - is the critical angle associated with shielding and the function B, which is the solution of the equation $B = b + \ln b$

$$\theta_1^2 = 0.1569\, z(z+1)\, Z_p^2\, \Delta R / A (pv)^2$$

$$\theta_1^2/\theta_0^2 = 2730\, z^{2/3}(z+1)\, Z_p^2\, \Delta R/A\beta^2, \quad [pv]=\text{MeV} \quad [\Delta R]=g/cm^2 \qquad 5$$

$$b = \ln(\theta_1^2/\theta_0^2) - 0.1544, \quad \beta \; v/c$$

p, v - are the pulse and particle rate. Upon determining the parameters from equation (5) (the function B is tabulated in Ref /11/), the value θ_c can be calculated from the formula:

$$\theta_c^2 = \theta_1^2 (B - 1.2) \qquad 6$$

Ref /11/ determines the limits of the theory applicability:

1. The value e^b is approximately equal to the number of collisions in the foil. The theory is inherently statistical, so this value must be suffeciently high 10-20. If $e^b \sim 15$, then $b \sim 2.7$.

2. The theory does not take into accomt the energy variation when particle goes through the foil. The theory is supposed to be valid if $\Delta E/E_0 \leq 20\%$. In this case it is required apply the mean energy

$$\bar{E} = E_0 - 0.5\, \Delta E$$

The theoretical calculations were verified in a number of experimental investigations, e.g. /12,13/. At low energy losses $\Delta E/E_0 < 0.2$ a good agreement of the theory and experiment is observed. The disagreements increase as E_0 decreases and Z increases. In Ref /13/ the correction functions allowing the theory and experiment being in agreement with an accuracy $\sim 5\%$ are determined .

$$\widetilde{\theta}_e = \theta_e \; f(Z)\,[1 + C(Z)\,(E_0 - 3)^{1/2}]$$
$$f(Z) = 1.02 - 6.7\,10^{-3} Z + 3.75\,10^{-5} Z^2$$
$$C(Z) = 0.017 + 7.6\,10^{-4} Z$$

θ_e - is calculated by formulae (5,6).

1.2. Reaction kinematics and Geometrical factor

The factors considered in this section essentisly vary with the experimental conditions. Qualitative consideration of the typical distribution functions is qiven in Ref /14/. In the case of a point detector and an extended target, at distance to the detector comparable with the target length: $\varphi(E) \sim (const + E)^{-2}$ At large distances the distribution has an retangular form. In the case of a point source and a cylindrical detector the energy distribution is close to the uniform one. To obtain distribution functions in the real geometry a dependence of neutron formation reaction cross-section and their energy an the angle of escape should be taken into consideration. For the accurate calculation it is convenient to apply cross-sections /15/ recommended, which are represented in the form of Legendre polynomial expansion of the angular distribution in the system of the centre of mass. The neutron energy and the reaction cross-section in the laboratory system can be calculated by formulae /16/

$$\sigma(\mu) = \sigma'(\mu')\, d\mu'/d\mu$$

where σ', μ' - is the cross-section and cosine of the angle in the system of the centre of mass. For the reaction $M_2(M_1, M_3)M_4$

$$\mu' = \beta(\mu^2 - 1) + \mu(1 - \beta^2(1 - \mu^2))^{1/2}$$

$$\beta^2 = \frac{M_1 M_3}{M_2 M_4} \; \frac{E}{E + Q + \frac{M_1}{M_2} Q}$$

$$d\mu'/d\mu = [2\beta\mu\alpha + \beta^2(2\mu^2 - 1) + 1]/\alpha$$

$$\alpha = [1 - \beta^2(1 - \mu^2)]^{1/2}$$

$$E_3 = E_T B\,[\mu + (\vartheta/B - 1 + \mu^2)^{1/2}]^2, \quad E_T = E + Q$$

$$Q = (M_1 + M_2 - M_3 - M_4)\,c^2$$

$$B = \frac{M_1 M_3}{(M_1 + M_2)(M_3 + M_4)} \cdot \frac{E}{E_T}$$

$$\vartheta = \frac{M_2 M_4}{(M_1 + M_2)(M_3 + M_4)} \left(1 + \frac{M_1}{M_2} \frac{Q}{E_T}\right)$$

Equations (9) were obtained in the quasiclassical approximation which is valid with an accuracy 0.1-0.3% for the initial energies $\leq$ 10 MeV.

1.3. Neutron Flux Distribution Calculation

The most natural way for distribution function calculation taking into account all the above peculiarities is the Monte-Carlo modelling. The results of this calculation using the code developed in IPPE are shown in Fig.3. They were obtained for the

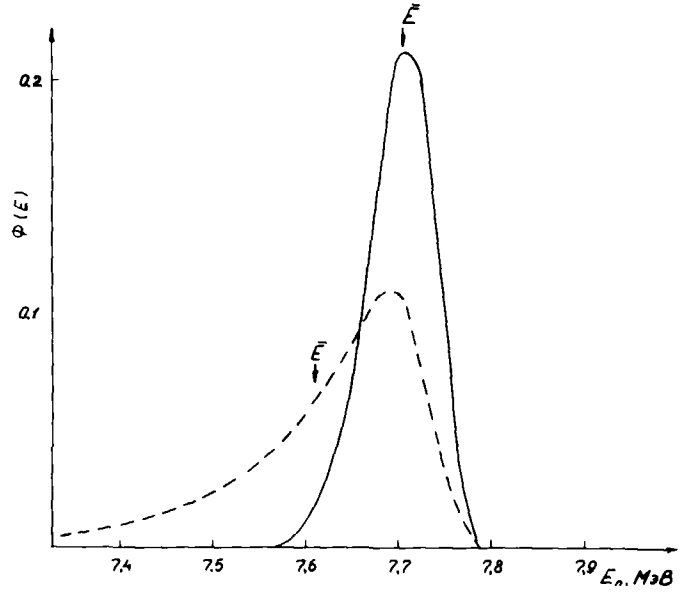

Fig.3. Neutron flux energy distribution function for various distances from the target to the detector 7 cm ------ and 2 cm - - - - -.

following conditions: incident particles are uniformly distributed over a circle of a diameter 0.5 cm, the entrance foil is of Mo of a thickness 8.08 mg/cm^2, δ_R = 0.1 mg/cm^2, the gas pressure is 210 torr, the target length is 5 cm, a distance from the target end to the detector is L = 7 cm, 2 cm, the detector diameter is 1.9 cm, the thickness - is 0.11 cm, the deutron energy is 4.5 MeV. The detector is located at an angle 0°.

Depending on the experimental conditions the above-mentioned factors have different influence upon the mean energy and it's dispersion. For example taking into account the angular straggling varies the mean neutron energy by ~ 8 KeV. Partial components of neutron energy dispersion for the montioned conditions are listed in Table I.

Table I.

Value under examination	σ, KeV
1	2
Scattering due to neutron escape angle (L=7 cm) and energy losses in the target	19.8
Charged particle beam size	7.4
Angular straggling	19.9
Energy straggling	23.5
Non-uniformity of foil	9.0

2. Experimental Determination of Neutron Source Characteristics

The experimental technique may be adopted both for all most essential values required for neutron source calculation: accelerated particle energy, energy loss in target materials, geometrical factors; and the mean neutron energy, the distribution function of the neutron, energy dispersion. Let the methods of determining these values be considered.

2.2 Incident Particle Energy Determination

The most accurate measurement of charged particle energy, to be more exact analyzing magnet calibration, is made in the method of thereshold and resonance reactions. Nowadays an accuracy ~40 ev (~ 0.01%) has been reached. A review of reference energies as well as methods of measurement is given in Refs./17-19/, that is why there is no need to discuss this method in detail.

The requirement to the energy determination accuracy in the neutron experiments is more moderate - 0.2%, this accuracy can be achieved in other in certain cases more convenient methods.

Ref /20/ suggests a method, which enables the proton energy to be measured with an accurace ~ 0.4 KeV in any point of the interval 0.9 - 2 MeV. It is based on measuring the γ-ray energy formed in the direct proton capture reaction $^{16}O(p,\gamma)$. In this case a γ-rays energy is $E_\gamma = E + Q$ (Q = 600.7 ± 0.4 KeV). This energy is in the range of well-know standards, which allows the spectrometer scale to be accurately calibrated.

The anthors of Ref /21/ suggested employing an inelastic scattering reaction for energy measurement. For certain nuclei, e.g. ^{27}Al, ^{56}Fe the lowest level's energies are known with high accuracy (Table 2) and are well-separated from each other.

Table 2

Scheme of Nuclear Levels

N°	^{27}Al /22/ KeV	^{56}Fe /23/ KeV
I	843.76 ± 0.03	846.755 ± 0.014
2	1014.46 ± 0.04	2085.05 ± 0.03
3	2210.5 ± 0.60	2657.52 ± 0.04
4	2734.0 ± 0.99	
5	2981.1 ± 0.90	

A semi-conductor detector is located at an angle 90° to the incident particle beam. In this case, equation (9) is transformed to the form :

$$E_L = E\frac{A-1}{A+1} - \frac{A}{A+1}Q_L \qquad 10$$

where Q - is the excitation energy of the i-th level (i=0-k).

$$A = M_2 / M_1$$

$$M_1 + M_2 \simeq M_3 + M_4$$

On the basis of ratio (10) a set of equations for the scale calibration and energy measurement can be obtained:

$$E\frac{A-1}{A+1} - a x_i - b = \frac{A}{A+1} Q_i + \Delta_i$$

where x_i - is the number of the channel of a centre for the i-th peak,

Δ_i - is the energy loss correction in the scattering foil.

Therefore there are 4-6 equations from which E,a,b can be determined with the least-square method. This method of energy measurement can be employed for the determination of charged particle energy in a wide energy range 3-10 MeV for various accelerated particles. The accuracy of the method is (0.1 - 0.2)%.

The similar ratios were applied in Ref /24/ to measure the energy in the backscattering method.

The time-of-flight method was realized in IPPE. It requires pulsed mode (1-2 nçec) and an ion path of flight > 5 m. A small part of the accelerated particle beam hits the slits after the analyzing magnet, another portion goes through the slits and hits the target located at the ion-pipe end. Near the slits and the target there are two scincillation detectors of γ-quanta and neutrons.

A distance from the source to the detectors is chosen so as to provide good separation of events from the γ-quanta and neutrons.

The starting pulses from the detectors arrive at a single time converter. The frequency of stopping pulses is reduced by a factor of two relative to the accelerated particle pulse frequency. This lay-out of the experiment permits the simulteneons measurement of the particles'time-of-flight and the time converter channel width. The inter-detector time shift is measurable if they are placed together in the vicinity of a single source. With the path length 6 m and the accuracy of its determination ~0.5 cm, this method provides the energy measurement with an accuracy (0.2-0.3)% in the deutron energy range ≤9 MeV. The method is absolute, simple in realization, allows measuring an energy of any particles in a wide energy range. The energy measurement accuracy basically is determined by the path length available.

2.2. Measurement of neutron energy and distribution function

The mean neutron energy can be determined through measuring the near-resonance transmission in the total cross-section with well-known energy. If the resonance width is well below the neutron flux distribution function width, then these experiments may also result the information on the distribution function. A list of resonances with the well-known energy is given in /28/. The experiments on the determination of neutron energy from the gas deuterium target held in IPPE utilized a resonance ^{12}C(6.293 ± ± 0.005) MeV in the total carbon cross-section. The measurements were conducted with time-selection mode to reduce the background. The accuracy of transmission measurement ~3% was basically determined by the peak integration accuracy. The experimental set-up is typical for measuring the total cross-sections in the transmission method. Fig.4 shows the experimental data and the result of the theoretical calculation of transmission on the basis of the rations given in section I. A good agreement of the calculated and experimental function shows that the distribution function of a neutron flux from the source is determined properly. Note, that there were no free parameters in the calculation, all the values required were determined experimentally or calculated from the theoretical models.

The neutron energy can be determined in the transmission method in separate points, however a good agreement of the theory and experiment enables us to assume, that the mean energy can be determined fairly accurately (10-15) KeV in a wide energy range.

In /25/ on the basis of the time-of-flight experiments a neutron energy dispersion was determined depending on the angle of escape. The results are in a satisfactory agreement with the analitical approach taking into account all the factors considered in section I. The neutron distribution function can also be measured in the similar experiments. Ref /26/ gives the results of the like

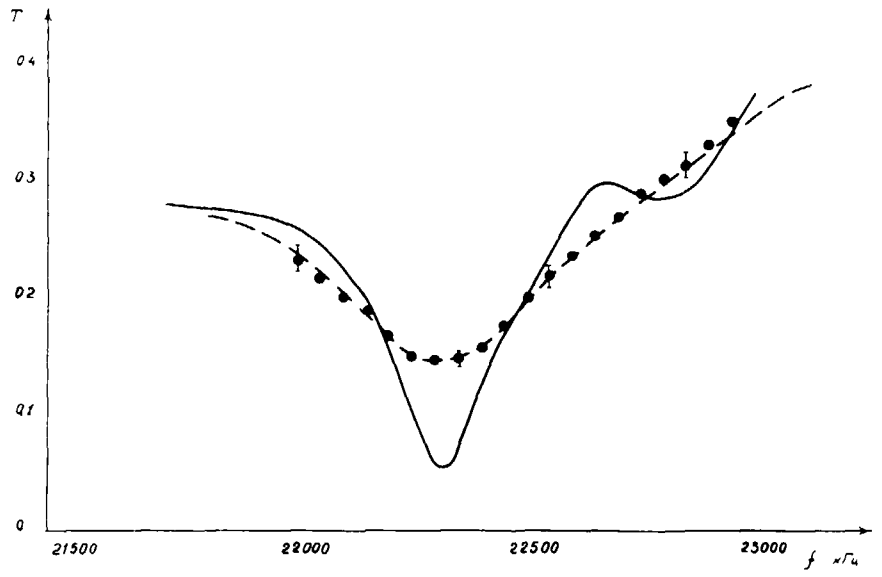

Fig.4. Carbon transmission functions depending on nuclear-magnetic resonance frequency. Points - experiment. The solid line shows transmission without averaging, the broken one - calculation taking into account distribution functions. The carbon cross- section is taken from ENDF/B-V.

measurements for 2.7 MeV energy neutrons formed in the litheum target. The measurent were performed at a path length ~ 40 m. A satisfactory egreement with the theoretical calculation is pointed ont.

3. Theoretical Predictions of Absolute Yield from the Source

The gas deuterium target is a well-simulated neutron source. The D(d,n) reaction cross-section is known with an accuracy (1.5-2)% for deutron energies 5-10 MeV /15/. The nuclear density in the target is measured with an accuracy ~ 1%. Taking wito account the geometrical factor error and the current measurement (1-2)%, the absolute neutron yield can be expected to be calculated by an error ~ 3%. However, only relative flux variation on the distance to the target can be calculated with a good accuracy (~ 2%).

In Ref /27/ it is noted, that the neutron yield is systematically below the calculated one, the difference increase with the gas pressure in the target. A lower neutron yield observed in our investigations as well. The data given in Fig.5 indicates not only of the presence of the yield dependence on pressure, but probably of its decrease as the mean particle current increases. A great

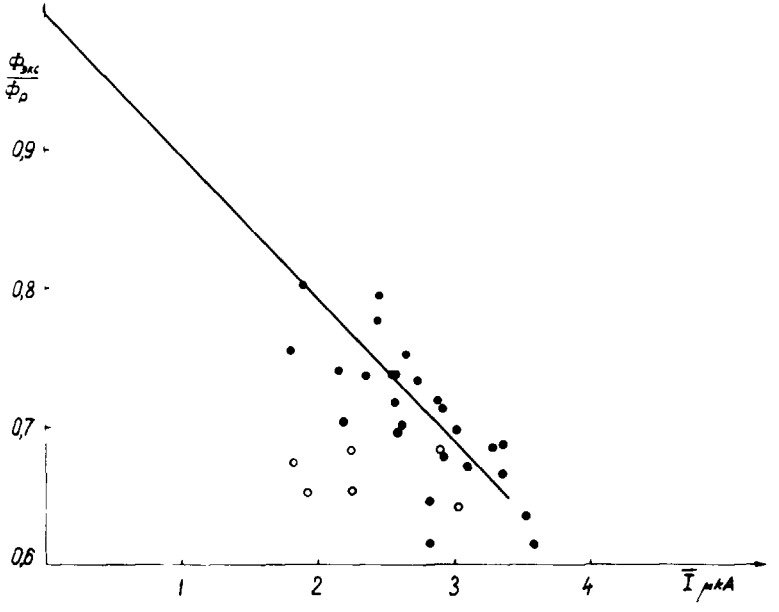

Fig.5. Dependence of neutron yield observed on the mean current value for pressures 200 torr • and 800 torr ○ . The line is drawn by eye through the experimental points and $\phi_{exp.} / \phi_{cal.} = 1$.

spread of points, which essentially exceeds the experimental accuracy, is paid much attention to. This is indicative of the existence of the unknown factor affecting the neutron flux.

If the yield decrease is associated with the energy dessipation in the target resulting in local increase of the gas temperature and density reduction, the mean neutron energy increase must be observed. This phenomenon is currently the main source of mean neutron energy calculation uncertainty in the gas target, and its investigation must be paid a serious attention to.

References

1. Janni J.F., Atomic and Nucl Data Tables, 1982, 27, 2-5.
2. Nemets O.F., Gofman Jn.V. " Handboon of Nuclear Physics". Naukova Dumka, Kiev, 1975.
3. Maccabee H.D., Raja M.R., Tobias C.A. Phys. Rev., 1968, 165, 2, 469.
4. Meadows J.W., ANL/NDM-25, 1977.
5. Deconinck G. Introd. to radioanalytical phys. Amsterdam, 1978.
6. Beserdacher F., Andersen J.U., Bondcrup E., NIM, 1980, 168, 1-3.1.
7. Lindhard J., Scharff M., Mat.Fis.Medd.,Dan.Vid.Selsk., 1953, 27,15.
8. Bonderup E.,Hvelplund P.,Phys.Rev, 1971, A4, 562.
9. Chu W.K., Phys. Rev. 1976, A13, 2057.
10. Friedlund E., Lombaard J.M., NIM, 1980, 168, 1-3.25.
11. Marion J.B., Zimmerman B.A., NIM, 1967, 51.
12. Vincour J., Bem P. NIM, 1978, 148, 2, 399.
13. Dixon D.R. NIM, 1983, 213, 525.
14. Uttley C.A. Neutron sources for Basis Phys. and Appl. Pergamon Press, 1982.
15. Drosg M., Nucl. Science and Engin., 1978, 67, 190.
16. Marion J.B., Young F.C. Nucl.React, Analysis, Amsterdam, 1968.
17. Marion J.B. Reviews of Modern Phys. 1966, 38, 1, 660.
18. Overley J.C., Parker P.D., Bromley D.A. NIM, 1969, 68, 61.
19. Simakov S.P., Spirin V.I., Trufanov A.M. et al. PTE, 1979, 5, 36.
20. Rolfs C., Rodney W.S. Nucl.Phys., 1975, A240, 221.
21. Baryshnikov A.I., Abramov A.I. Certificate of anthorship N° 317969, 1970.
22. Atomic Data and Nucl. Data Tables, 1975, 15, 5, 425.
23. Nucl. Data Sheets, 1977, 20, 3, 286.
24. Klein H., Brede H.J., Siebert B.R.L. NIM, 1982, 193, 635.
25. Scott D.M., Pain B.M. NIM, 1983, 218, 154.
26. Meadows J.W., Smith D.L. Consultunt's meeting on neutron source properties. Debrecen, 11-21, 1980, INDC(NDS)-114/GT, 1980.
27. Klein H. Nuclear standard reference Data, IAEA-TECDOC-335, Vienna, 1985, 454.
28. Nuclear Data Standards for Nucl. Meas. 1982. INDC/NEANDC, Tech. reports, 227, Vienna, 1983.

PRODUCTION OF FAST NEUTRONS WITH TARGETS OF THE HYDROGEN ISOTOPES - SOURCE PROPERTIES AND EVALUATION STATUS OF THE CROSS-SECTIONS

M. DROSG
Institut für Experimentalphysik,
University of Vienna,
Vienna, Austria

Abstract

An updating survey of the three basic monoenergetic neutron sources $^{3}H(p,n)^{3}He$, $^{2}H(d,n)^{3}He$ and $^{3}H(d,n)^{4}He$ is given including the inverse reactions $^{1}H(t,n)^{3}He$ and $^{2}H(t,n)^{4}He$. Source properties and the accuracy of the differential cross sections are discussed. In addition fast neutron production by t-T and by inverse (p,n) reactions (e.g. $^{1}H(^{7}Li,n)^{7}Be$) and inverse (d,n) reactions is considered.

I. INTRODUCTION

Evaluations of the differential cross sections for fast monoenergetic neutron production by the hydrogen isotopes have been ameliorated from time to time[1,2,3] by incorporating new data. At the same time the highest neutron energy covered by the evaluations was increased. Since the last survey of these reactions[4] only few papers became available. Nevertheless, the reliability of the evaluated data now appears to be much increased.
Other fast neutron sources using targets of hydrogen isotopes include the (white) t-T reaction and the inverse (p,n) and (d,n) reactions. The interest in the inverse reactions has been increasing in recent years due to the development of bunched heavy ion sources that allow neutron time-of-flight (TOF) technique for neutron detection. This is true especially for the $^{1}H(^{7}Li,n)^{7}Be$ source.

II. MONOENERGETIC NEUTRONS FROM REACTIONS AMONG THE HYDROGEN ISOTOPES

The sources and their properties are discussed with some length in a contribution to the new Handbook on Nuclear Activation Cross-Sections[3]. There also the presently recommended absolute differential cross sections of the reactions can be found for projectile energies up to 16 MeV. Additional overview information is given in the forerunner of this paper[4] (including break-up neutrons and neutron production up to 40 MeV) and in other recent publications [2,5]

The basic figure of merit of a clean monoenergetic neutron source is the specific neutron yield, i.e. the number of neutrons with the right energy (whithin the desired energy resolution) per projectile particle. A general comparison of various sources must therefore start out with this property. Usually neutrons emitted at 0° are used. Therefore Fig.1 gives the energy dependence of the specific 0° neutron yield in pure targets for various popular sources for an energy resolution of 10 keV.

Starting out with the specific yield, some more individual parameters must be taken into account to establish the "best" source (i.e the most intense source, if background is negligible)
Under the assumption that projectiles of the correct type and energy are available, the following characteristics of the set-up must be considered[3]

current capability of the accelerator
- maximum local heating (current density) in the target (or entrance foil in gas targets)
- maximum global power dissipation in the target
degradation of energy resolution (by straggling in the target structure, by the finite time resolution in TOF experiments, etc)

To give an example of how the actual neutron flux is connected with the specific neutron yield, Table 1 compares neutron fluxes of the p-T and the d-D reaction in an energy range where specific neutron

yields of the two reactions do not differ much. From this it is clear that in this energy range p-T is better by about a factor of two. The smaller background and the better time resolution (because of the higher projectile velocity) in the p T case, gives even an appreciable higher factor (at least in TOF experiments).

TABIF 1

Yield Comparison for Equal Total Neutron Energy Spread (FWHM=100 keV) and for the Same Power (0.2 W) in a 5.3 mg/cm^2 Molybdenum Entrance Foil of a Gas Target. (All energies in MeV.)

	Projectile data				Neutron data					
	E_m[a]	ΔE_f[b]	ΔE_{gas}	ΔE_{ge}[c]	I_m[d]	ΔE_{st}[e]	ΔE_{gas}	ΔE_{geo}	Y[f]	F[g]
8 MeV Neutrons.										
p T	8.957	0.136	0.040	0 012	1.47	0.051	0.080	0.024	8.36	1.0
d D	5 115	0.307	0.043	0.013	0.65	0.040	0.083	0.026	7.66	0.4
10 MeV Neutrons.										
p-T	10.941	0.118	0.040	0.015	1.70	0.052	0.079	0.030	10.9	1.5
d D	7.134	0.252	0.043	0.017	0.79	0.043	0 082	0.032	12.5	0.8

a) energy of accelerated projectile
b) energy loss in entrance foil
c) correction of beam energy to give the correct mean neutron energy at an opening angle of ±5°
d) maximum current for a power of 0.2 W dissipated in the entrance foil
e) FWHM of energy smearing due to energy straggling
f) specific yield n.sr^{-1}. pC^{-1} for an energy loss in the gas resulting in a 10 keV neutron energy spread
g) flux in units of 10^8n.sr^{-1}.s^{-1}

II.A. PROTON-TRITON REACTION

Table 2 summarizes measurements not included into previous evaluations. New data[6] by this author, measured mainly by the inverse reaction ^{1}H(t,n)^{3}He, formed the backbone for a reevaluation at lower energies which included also the recent Chinese data[7] giving improved Legendre coefficients[3,6].

TABLE 2

^{3}H(p,n)^{3}He Differential Cross-Section Measurements Which are Not Included in Previous Evaluations (Symbols in accordance with Ref.1)

Symbol	Author(s)	Ref.	Method	Ang.Range (c.m.,deg.)	Proton Energy (lab.,MeV)
	Absolute Data				
DR85	Drosg et al.	6	n,TOF	47...180	2...6.4
	Relative Distributions				
YI81	Chen Ying et al.	7		0...120	1.3,1.8
DR85	Drosg et al.	6	n,TOF	0...144	2.22,3.00
	Break-up Data				
TH82	Thambidurai et al.	8	n,TOF	0	9.77...14.77

New integrated break-up data[8] confirm the previous solution[4] extending the energy range by 1 MeV down to 9.77 MeV. Unfortunately the new double differential break-up data were not compared with previous spectra[9], although 5 of the 6 projectile energies coincide. Another aspect of the new evaluation is the removal of the data labeled JA56B[10] in the evaluation of Liskien and Paulsen[1]. After studying the Progress Reports of the Physics Division of LASL[11] of the late fifties, it became clear that the data labeled PE59[12] contain the revised JA56B data so that they are not independent data sets.

As shown in Table 1 , the p-T reaction is superior to the d-D reaction even for neutron energies where the specific neutron yield (see Fig.1) is smaller For special applications (e.g. elastic scattering) it is also by far superior to the d-T reaction, even at the "14 MeV" resonance. There its specific yield is 27 times higher. In TOF experiments this advantage is further greatly enhanced by a much better time resolution

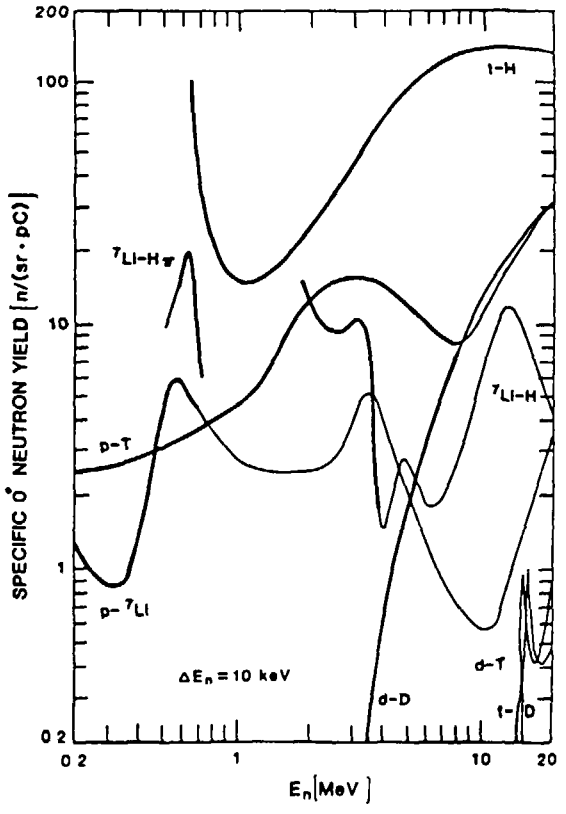

Fig. 1. Energy dependence of the specific 0° neutron yield for an energy resolution of 10 keV. Except for d-T and t-D the thick curves indicate the monoenergetic range. The index π denotes the second neutron group (at 180° in the c.m. system).

An even better source than p-T is the reaction $^{1}H(t,n)^{3}He$ as shown in Fig 1 Its specific neutron yield at 0° is the highest of all competitive sources over practically all the energy range between 0 6 and 20 MeV. Its practical use as monoenergetic source has been demonstrated several times[9,13-15] There not only the high yield but also the special kinematic situation of this reaction is very advantageous neutrons are only emitted into a forward cone giving less room background and simplifying shielding
The half angle θ of this cone at the projectile energy E_p can be derived from the (nonrelativistic) equation

$$\sin^2\theta = \frac{M_2\, M_4}{M_1 . M_3}\ (1 - \frac{E_{th}}{E_p})$$

The masses M_1 are those of the projectile, the target, the neutron and of the residual nucleus resp , E_{th} is the threshold energy of the reaction (here, E_{th} = 3.051 MeV). The monoenergetic range extends to 17 64 MeV neutron energy. Actually there are two neutron groups at 0° with the lower energetic one negligible in energy and intensity[3,16] in most cases. The background from (t,n) reactions in the target structure can usually be corrected for by a separate background run with the empty target.

The t-H source is probably the best source for neutron radiotherapy because of the possibility to tailor the neutron emission spectrum by chosing target thickness and projectile energy in such a way that intrinsically no neutrons below 10 MeV are produced[17,18]. At the same time, the neutron yield is comparable with other choices (see Table 3). With a gas target allowing the dissipation of 100 W[19] 1.10^{12}n $sr^{-1}sec^{-1}$ can be achieved in the 0° direction. Below 10 MeV only neutrons from the target structure and the second line [3,16] are present. The intensity of the latter is only 5 10^{-4} of the primary line and its average energy is 0.03 MeV (for the conditions given in Table 3). The neutron background from the target structure cannot be predicted without experimental data.

TABLE 3

Comparison of Neutron Yield and Energy Data for the $^{1}H(t,n)^{3}He$, $^{2}H(d,n)$ and $^{9}Be(d,n)$ Reactions in the Forward Direction for Particle Beams of 25 MeV and an Effective Target Thickness of 10 MeV

Reaction Type	Neutron Yield (10^{10} n.sr^{-1}.μc^{-1})	Average Neutron Energy (MeV)
t H	10.5	13.8
d D[a)]	15.5	13.2
d-Be[b)]	11	11

a) from Table 1 of Ref. 19

b) derived from values given in Table 1 of Ref. 19

One could also consider using t-H with a thick target as a "white" fast neutron source. For the monoenergetic range (neutrons between 0.6 and 17.6 MeV) the spectrum can easily be predicted (full line in Fig. 2). It is worthwhile to compare this neutron yield with that of the spallation source of WNR at Los Alamos under the assumption of equal dissipated power in the target (800 W) as done in Fig. 2. In this figure some more information is given: the meagre yield of the "14 MeV" d-T resonance (even for a gas target), and the continuation of the specific monoenergetic neutron yield of t-H beyond the break-up threshold. At higher energies the break-up cross section becomes increasingly larger than that of the two-body reaction (see e.g. Ref.20) so that for triton energies sufficiently higher than the threshold energy of 25 MeV the 1 μA specific yield curve of t-H will grossly underestimate the reality.

When the total neutron output (integrated over solid angle) of p-T and t-H at the same center-of-mass energy is compared, a curious fact appears: although the cross sections involved are the same, the neutron output for t-H is threefold! The explanation is simple: at the same c.m. energy the triton energy is thrice that of the proton energy so that the absolute energy loss in the target becomes the same (because of the same velocity of the projectiles). Thus, the relative energy loss is only on third in the t-H case giving thrice the neutron yield in the same cross section range.

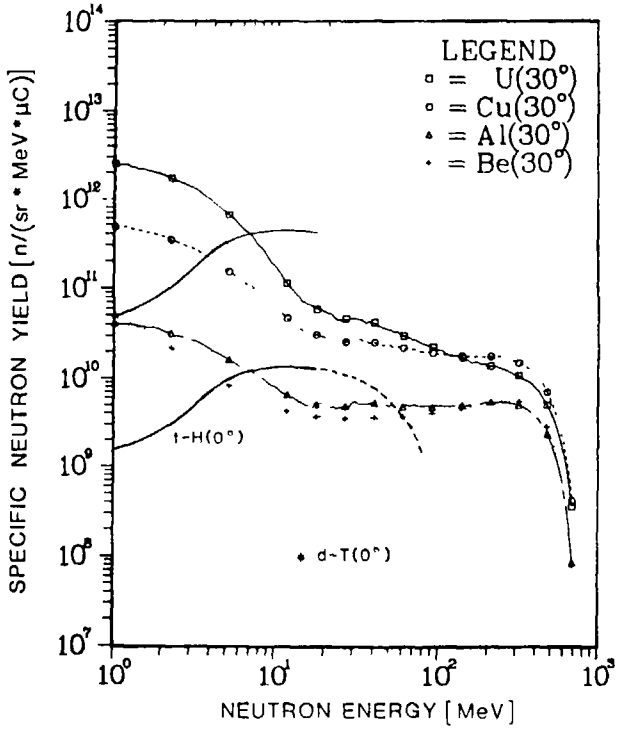

Fig. 2. Specific neutron yield of a spallation source (LAMPF, 800 MeV) at 30° and of the t-H source at 0° (lowest curve). The solid part of the curve covers the "monoenergetic" range. Adjustment to the same dissipated power in the target gives a yield according to the upper solid curve. The maximum specific yield of the "14 MeV" d-T resonance is given, too.

II.B. DEUTERON-DEUTERON REACTION

Table 4 summarizes measurements not included into previous evaluations.

TABLE 4

$^{2}H(d,n)^{3}He$ Differential Cross Section Measurements Which are Not Included in Previous Evaluations (Symbols in accordance with Ref. 1)

Symbol	Author(s)	Ref.	Method	Ang. Range (c.m.,deg.)	Deut. Energy (lab.,MeV)
		Absolute Data			
OK79	Okihana et al	26	^{3}He	6...90	13.2
JA85	Jarmie et al.	21	^{3}He	25...125	0.02...0.12
		Relative Distributions			
JO80	Jones	22	^{3}He	20...95	18...26

The main activities were at very low energies[21] and at higher energies[22]. The former data were included into the recent evaluation[3] of this reaction. The latter confirmed a previous evaluation between 20 and 39.8 MeV[23] based on a rather incomplete data set [24] which, however, agreed very well with the postulated energy dependence of the integrated cross section[25] as shown in Fig. 3. The low energy data support the anisotropy given by Liskien[1] so that a revision which seemed necessary [4] was superfluous. The new data at 13.2 MeV[26] agree with the current evaluation reasonably well, if the scale of the data is raised by 4.8% and the zero degree position adjusted by +0.4°.

II.C. DEUTERON-TRITON-REACTION

Table 5 summarizes measurements not included into previous evaluations.

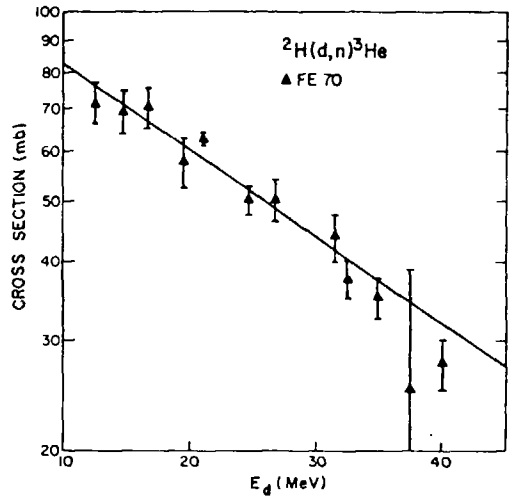

Fig. 3. Predicted integrated cross sections of $^{2}H(d,n)^{3}He$ (solid line, Ref. 25) and verifying data (FE70, Ref. 24).

TABLE 5

$^{3}H(d,n)^{4}He$ Differential Cross Section Measurements Which are Not Included in Previous Evaluations (Symbols in accordance with Ref.1)

Symbol	Author(s)	Ref.	Method	Ang. Range (c.m.,deg.)	Deut. Energy (lab., MeV)
		Absolute data			
IV68	Ivanovich et al.	27	^{4}He	120...150	4.....11
JA84	Jarmie et al.	29	^{4}He	30...135	0.01...0.08

The three charged particle excitation functions[27] between 4 and 11 MeV proved very valuable for checking the 1978 evaluation[2] because they provide back angle data. There the neutron data are

expected to have the biggest systematic errors. After a single scale adjustment of +2.8 % (the scale uncertainty given for these data is 3 %) all three excitation functions coincided very well with the predictions of the evaluation[28]. Inclusion of these new data gave only small changes below 7 MeV down to 3 MeV[28]. These changes together with those due to the new very low energy data[29] were included in the latest evaluation [3].

The use of this reaction for producing "14 MeV" neutrons is subject of a special session at this Meeting. Therefore it will not be covered in this paper.

For the same reasons as explained in part A the integrated neutron yield from $^{2}H(t,n)^{4}He$ is 1.5 times that of d-T when the same portion of the center-of-mass cross sections is involved. This can also be noticed in Fig. 4 where neutron yields of d-T at 0° and 90° are compared with those of t-D at the same angles, and with that of t-H at 0°. From this figure it is clear that t-D at 90° is quite advantageous even if the peak in a practical application will be lower and wider because of beam straggling which was not taken into account in this figure. Thus, t-H has at least an order of magnitude higher yield and additional advantages, like lower room background and better timing characteristics.

Another advantage of t-D over d-T is the higher monoenergetic energy limit[3], namely 23.0 MeV rather than 20.5 MeV.

II.D. TRITON-TRITON-REACTION

The $^{3}H(t,n)$ reaction does not produce monoenergetic neutrons. However, it is of some importance in the fusion program. Therefore its low energy cross sections were measured recently[21].
At high enough energy one would expect an intense white neutron spectrum due to the fact that two thirds of the nucleons are neutrons[30]. For complete break-up tritons of at least 34 MeV are necessary. Data only up to 19 MeV have been taken[31]. So it is still unclear how good such a source would be.

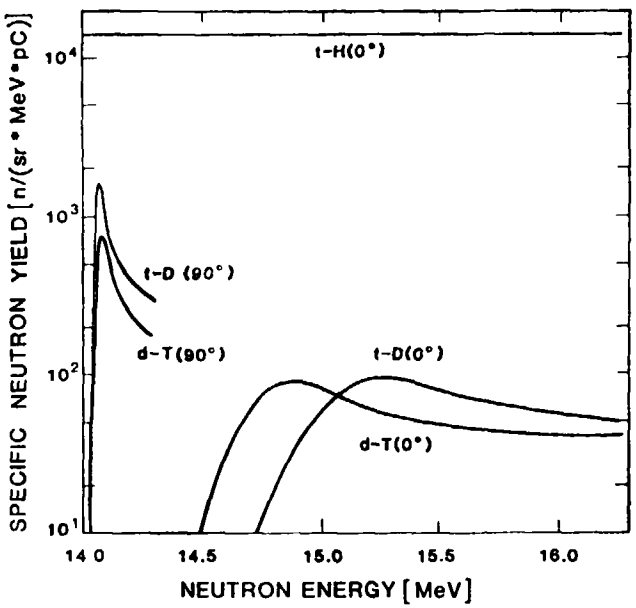

Fig. 4. Comparison of specific neutron yields of monoenergetic sources near 14 MeV for pure targets. Inclusion of beam straggling into the calculation would lower the maximum and widen the width of the peaks.

III. INVERSE REACTIONS WITH HYDROGEN AND DEUTERIUM TARGETS

Nowadays, the technology is available to produce bunched heavy ion beams with sufficient intensity for neutron work. Therefore inverse (p,n) and (d,n) reactions should be considered for neutron production[32].
The advantage of inverse reactions is

a) the wider monoenergetic neutron production range
b) the containment of neutron emission into a forward cone, if the two body reaction is endothermic.

The advantage of such a containment was discussed above (see II.A.). There, the general formula for the opening angle of the cone is given, too.

III.A. INVERSE (p,n) REACTIONS

Most of the practical (p,n) reactions are endothermic. In these cases the neutrons from the inverse reactions are contained into a forward cone, thus enhancing the zero degree yield kinematically and simplifying the experimental set-up because of the reduced background.

Table 6 gives relevant data for some selected reactions involving lighter nuclei. The range of monoenergetic neutron production is given and the maximum opening angle θ_m (at the upper limit of this range) Fig. 5 shows that a reaction requiring a high projectile energy must be chosen if the neutrons of a given energy should be contained in a narrow cone.

TABLE 6

Reaction Data for Monoenergetic Neutron Production by Some Inverse (p,n) Reactions at 0°

Reaction	Threshold		Upper Limit[a]		
	E_p(MeV)[b]	E_n(MeV)	E_p(MeV)[b]	E_n(MeV)	θ_m(deg)
$^1H(t,n)^3He$	3.051	0.573	25.011	17.640	69.6
$^1H(^7Li,n)^7Be$	13.095	1.439	25.732	8.184	44.5
$^1H(^{10}Be,n)^{10}B$	2.478	0.206	51.267	16.659	77.2
$^1H(^{10}B,n)^{10}C$	48.492	4.031	92.284	21.924	43.5
$^1H(^{11}B,n)^{11}C$	32.967	2.534	122.986	32.659	58.8
$^1H(^{14}C,n)^{14}N$	9.323	0.584	121.821	29.449	73.9
$^1H(^{14}N,n)^{14}O$	98.302	5.533	157.248	27.298	41.5
$^1H(^{15}N,n)^{15}O$	56.177	3.316	172.138	33.806	55.1
$^1H(^{18}O,n)^{18}F$	45.980	2.310	129.284	21.156	53.4
$^1H(^{19}F,n)^{19}Ne$	79.824	3.821	149.908	20.386	43.1

a) Limit for 3-body break-up with neutron emission

b) projectile energy

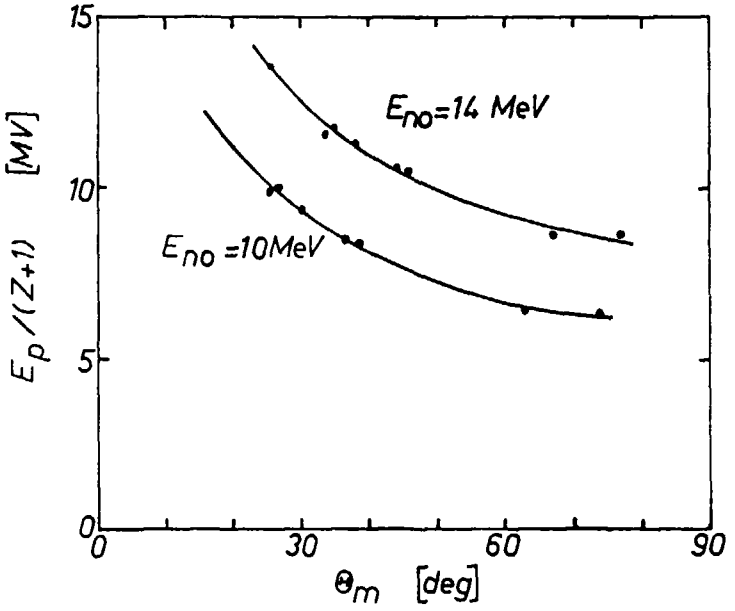

Fig. 5. Required terminal voltage of a tandem Van de Graaff for the acceleration of fully stripped heavy ions (with charge Z) to produce neutrons of a maximum energy E_{no} inside a cone with a maximum opening angle θ_m via inverse (p,n) reactions. The curves are only meant to guide the eye.

The most prominent inverse (p,n) reaction is $^1H(t,n)^3He$. It has been dealt with in Sec. II.A. The only other reaction of this table used up to now[33] is the $^1H(^7Li,n)^7Be$ reaction [3,34]. Its specific yield at 0° is compared with that of the other reactions in Fig. 1. Except near the threshold (i.e. for neutrons between 1.4 MeV and 1.9 MeV), the p-T reaction and the t-H reaction have a higher yield. Contrary to t-H the second neutron group at 0° (corresponding to 180° c.m.) is in most cases not negligible, neither in energy nor intensity. Around 0.55 MeV neutron energy this second line is even the most intense "monoenergetic" neutron source (see Fig. 1). The center-of-mass cross sections can be calculated from the Legendre coefficients of the $^7Li(p,n)^7Be$ reaction[35] after adjustment of the energy by a factor of 6.9637 and changing the angle θ to 180°-θ. The status of the eva-

luation of this reaction will be presented independently at this Meeting[36]. However, it is worthwhile to note that there seems to be an energy shift of about 50 keV between measured ^{7}Li-H data[33] and the evaluated p-^{7}Li data[35] (see Fig.6). This figure shows the energy dependence of the anisotropy of p-^{7}Li for the two cases.

III.B. INVERSE (d,n) REACTIONS

No measurements have been reported. Some reactions have been suggested as relative standards[32] providing multiline neutron spectra (see Table 7).

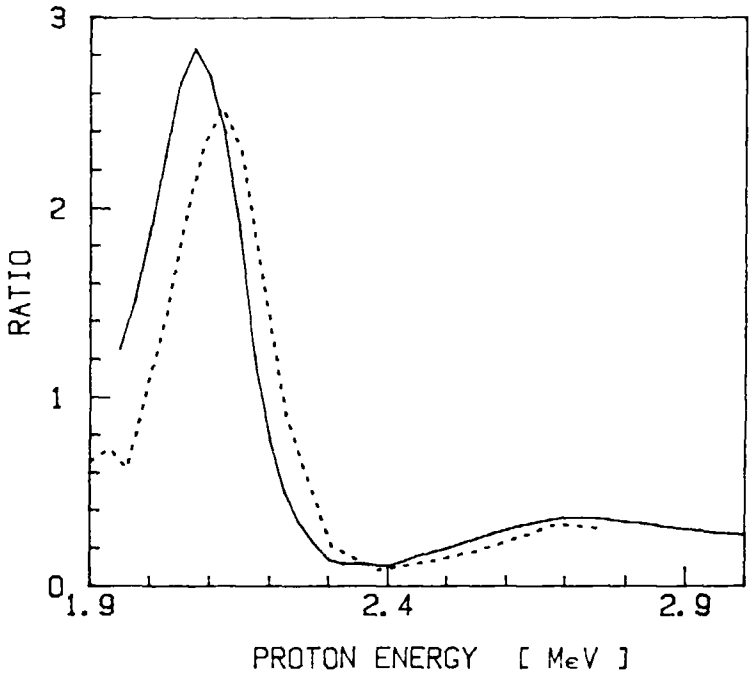

Fig. 6. Ratio of the center-of-mass cross sections at 180° and 0° of the ^{7}Li(p,n)^{7}Be reaction. Full line from Ref. 35, broken line from Ref. 33.

TABLE 7

Kinematics Data for Selected Multiline Neutron Sources by Inverse (d,n) Reactions (All energies in MeV)

Reaction Type	2-Body Reaction		3-Body Neutron Reaction	
	Q	$E_n(0°)$*)	Threshold	Q
^{2}H(^{13}C,n)^{14}N	5.326	13.236	16.587	-2.225
^{2}H(^{27}Al,n)^{28}Si	9.361	13.288	8.987	-0.624
^{2}H(^{30}Si,n)^{31}P	5.072	13.561	35.331	-2.225
^{2}H(^{31}P,n)^{32}S	6.640	8.836	5.057	-0.309
^{2}H(^{10}B,n)^{11}C	6.466	10.895	6.442	-1.079
^{2}H(^{9}Be,n)^{10}B	4.361	4.908	0.547	-0.100

*) Maximum zero-degree neutron energy, at the 3-body threshold energy

---

Advantages of inverting the reaction are:
At the same center-of-mass energy higher neutron energies are obtained so that the energy gap between primary neutrons and neutrons from the deuteron break-up is appreciable larger. In parallel, the spacing between the neutron lines from the excited levels is wider in the inverse case which is beneficial for a multiline reference spectrum.

IV. EVALUATION STATUS AND DATA NEEDS

Evaluations using Legendre polynomials for the presentation of the absolute differential cross sections are available for neutron production by the hydrogen isotopes[1-3,23] and for the ^{7}Li-H reaction[35]. The status of the latter reaction will be discussed independently at this Meeting[36].

IV.A. PROTON-TRITON REACTION

The most recent evaluation[3,6] gives Legendre coefficients for proton energies up to 16 MeV. The scale error of the evaluated data increases from about ±1.5 % between 10 and 16 MeV to about ±4 %

at 3 MeV and below. The shape error of the angular distributions is less than ±3 % over most of the energy range (see Fig.7). The uncertainty in the 0° position is typically ±0.1° with a maximum of ±0.6° near 3 MeV. The energy uncertainty is about ±0.02 MeV, decreasing with decreasing energy.

When measuring differential cross sections of this reaction it is very important to determine the effective energy and the effective 0° direction accurately. Otherwise the data will contribute only little to an improvement of the present evaluation.

Especially at lower energies angular and beam straggling[37] could play an important role. When measuring the charged particle branch of the reaction, the magnitude of the multiple scattering correction might be appreciable larger than the combined uncertainties. Properly corrected new accurate measurements are worthwhile below 10 MeV, especially near the threshold, around 3 MeV and near 8 MeV. Above 20 MeV only few data are available[4] so that less accurate data will be acceptable there.

IV.B. DEUTERON-DEUTERON REACTION

The latest evaluation[3] gives Legendre coefficients for deuteron energies up to 15 MeV. The energy range up to 40 MeV is covered in a separate report[23].

The scale uncertainty between 5 and 17 MeV is about ±1 % increasing to about ±5 % at 1.5 MeV and at 20 MeV (and above). Below 0.1 MeV the scale error is ±1.5 %. The shape error is ±1 % between 5 and 10 MeV, increasing to about ±4 % at 17 MeV and ±10 % at 20 MeV and above. Below 3 MeV the maximum shape uncertainty[1] can be read from Fig. 7. The 0° position has an error of ±0.1° and the projectile energy a typical uncertainty of ±0.02 MeV decreasing with decreasing energy

The accuracy of the differential cross sections of the $^{2}H(d,n)^{3}He$ reaction around 5 MeV is so good that it has been recommended as a standard[38].

Deviations of new measurements[39] of the order of 5 to 10 % have no bearing because these (preliminary) data have internal inconsistencies (in c.m. they are not symmetric around 90°).

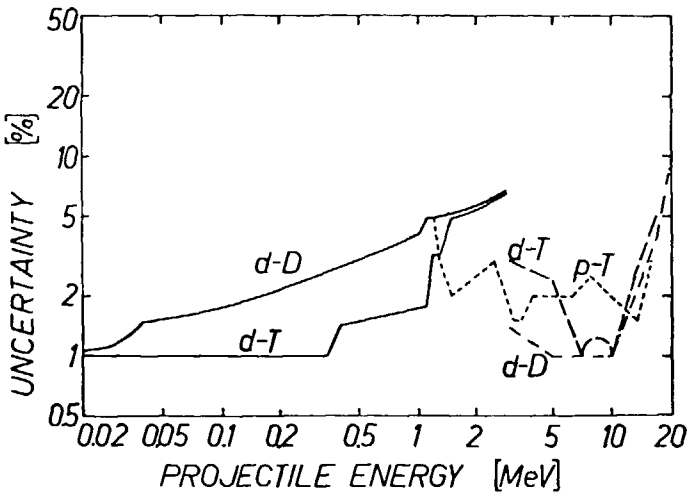

Fig. 7. Shape uncertainties of the angular distributions of monoenergetic neutron sources. The full curves give worst case errors, the others give estimated probable errors.

The evaluation at energies above 20 MeV[23] is strongly suppported by later data[22] when taken as relative angular distributions. Not reproduced is the energy dependence which was established previously[25] and verfied afterwards[24] (see Fig.3). An explanation for this discrepancy might be an insufficient charge collection in the Faraday cup because of the high deuteron energy (it must collect the protons of the break-up, too'). This would give a deviation increasing with energy as observed.

A main problem with data of the $^{2}H(d,n)^{3}He$ reaction lies in the uncertainty of the 0° direction as demonstrated in Table 8. A change in the 0° direction by only 0.1° (in the c.m. system) results in cross

TABLE 8

Systematic Deviations of Selected $^{2}H(d,n)^{3}He$ Data at Higher Energies from the Evaluation

Symbol[a]	Energy (MeV)	Scale Dev. %	Dev. of 0° Position (deg.,lab)
JA76	12.305	+1.1	0.0
OK79	13.2	+4.8	-0.4
HE77	17.5	-2.0	-0.17
JO80	18.0	b)	0.7
JO80	20.0	b)	0.4
JO80	22.0	b)	0.1
JO80	24.0	b)	0.0
VA63	25.3	-2.9	-0.57
JO80	26.0	b)	0.0

a) for symbols not included in Table 4 see Ref. 2 and 4.
b) relative data only

section changes from 1 % at 4 MeV to 2 % at 20 MeV. When the ^{3}He particle is detected, the changes are even more severe due to the kinematic compression. In this case, also uncorrected multiple scattering contributes to discrepancies as indicated in some data at higher energies.

The data base for $^{2}H(d,n)^{3}He$ appears to be in a very good shape. The accuracy seems to be sufficient even up to 40 MeV. One accurate absolute differential cross section measurement near 1.5 MeV would be helpful to reduce the uncertainty in this region. However, all precautions and corrections mentioned in part A and B of this section should be adhered to to make the data worthwhile. The analytical description[40] of the neutron energy spectra from the three-body break-up (i.e. up to 8.9 MeV) appears to be very promising. It should help with the correct background subraction in experiments where d-D must be used beyond its break-up threshold

IV.C. DEUTERON-TRITON-REACTION

The latest evaluation[3] gives Legendre coefficients for deuteron energies up to 16 MeV. The coefficients for energies between 3 and 10 MeV have been published before[28] and those between 7 and 19 MeV in the 1978 evaluation[2].

The scale uncertainty is about ±1.3 % below 0.1 MeV rising to about ±4 % near 2 5 MeV, falling to 2 % at 4 MeV and to 1.5 % at higher energies. As pointed out before[28] there is an indication that the scale at higher energies might be high by (1.5 + 0.8)%.

The worst case shape error[1] increases from ±1.4 % at 0.4 MeV to ±6.5 % at 2.9 MeV. The probable shape error is estimated to be ±3 % at 3 MeV, decreasing to ±1 % between 7 and 10 MeV and then increasing again (±2.5 % at 13 MeV, ±5 % at 16.5 MeV). The 0° position has an error of ±0.1° and the projectile energy a typical uncertainty of ±0.02 MeV decreasing strongly with decreasing energy.

In the 1.5 to 2.5 MeV range new data, measured with the precautions mentioned in parts A and B of this section, could improve the confidence level . Double differential neutron spectra from the break-up are sparse[4]. An increase of the data base would be quite welcome.

V. CONCLUSION

The evaluation of the three hydrogen reactions producing monoenergetic fast neutrons appears to be very reliable for energies up to about 20 MeV. There are some small energy ranges left, where the total uncertainty is ±5 % or more. Most cross sections are known absolutly to about ±3 % or even better (down to ±1.9 % for d-D at 5 MeV[32]). This accuracy was acknowledged by recommending[38] that the "absolute differential cross sections (complete angular distributions) of the $^{2}H(d,n)^{3}He$ reaction for projectile energies around 5 MeV and the zero degrees cross section for projectile energies above 3 MeV be applied as a neutron flux standard using a gas target". New measurements of cross sections of these reactions are worthwhile only, if the projectile energy is known to better than

0.5 %, the zero-degree position to better than 0.1° and the individual angles to about 0.1°. In addition, corrections for beam straggling (energy and angle) and multiple scattering (of the outgoing charged particle beam, if applicable) must be applied if they are not negligible.

Among the inverse reactions, the $^{1}H(t,n)^{3}He$ reaction has outstanding properties. The t-H source is practically monoenergetic up to 17.6 MeV with the highest specific neutron yield of all monoenergetic sources. Furthermore it can be used as intense "white" neutron source. There, the possibility to tailor the spectrum in such a way that practically no neutrons below a given limit (e.g. 10 MeV) are produced, makes it a potential source for neutron radiotherapy.

Among the other inverse (p,n) reactions which emit neutrons into a forward cone only, up to now only the $^{1}H(^{7}Li,n)^{7}Be$ reaction has been used. Although its specific neutron yield is appreciable smaller than that of t-H, it can be useful in specific applications. The $^{1}H(^{11}B,n)^{11}C$ source appears to be very promising in the interesting neutron energy range between 10 and 20 MeV[41]. It is basically a two-line source up to 11.9 MeV and a four-line source up to 20.6 MeV with a rather high specific yield. So it would be worthwhile to realize it.

The inverse (d,n) reactions could provide multiline neutron reference spectra. However, their development as a source depends on the ready availability of ion sources delivering bunched heavy ions which are only now appearing in neutron installations.

REFERENCES

1) H. Liskien and A. Paulsen, Nucl.Data Tables 11, 569 (1973)
2) M. Drosg, Nucl.Sci.Eng. 67, 190 (1978)
3) M. Drosg and O. Schwerer, "Production of Monoenergetic Neutrons Between 0.1 and 23 MeV Neutron Energies and Cross Sections", in Handbook on Nuclear Activiation Cross-Sections, K. Okamoto, Ed , IAEA, Vienna, in press
4) M. Drosg, pp.201 Proc IAEA Consultants Meeting on Neutron Source Properties, Debrecen, Hungary, Report INDC(NDS)-114/GT (1980)
5) C.A. Uttley, "Sources of Monoenergetic Neutrons", pp.19 of Neutron Sources for Basic Physics and Applications, S. Cierjacks, Ed , Pergamon, Oxford (1983)
6) M. Drosg, G. Haouat, W. Stoeffel and D.M. Drake, "Differential Cross Sections of $^{3}H(p,n)^{3}He$ and of $^{6}Li(n,t)^{4}He$ by Using Triton Beams Between 5.95 and 19.15 MeV and a Reevaluation of the p-T Neutron Production Cross Sections up to 12 MeV", Los Alamos National Laboratory report LA-10444-MS (1985)
7) Ch. Ying, Zhu Shengyun, Luo Dexing and Jiang Songsheng, Chinese Journal Nucl.Phys. 3 375 (1981)
8) P. Thambidurai, A.G. Beyerle, C.R. Gould, Nucl.Instr. Meth.Phys.Res. 196, 415 (1982)
9) M. Drosg, G.F. Auchampaugh, and F. Gurule, "Neutron Background Spectra and Signal-to-Background Ratio for Neutron Production Between 10 and 14 MeV by the Reactions $^{3}H(p,n)^{3}He$, $^{1}H(t,n)^{3}He$, and $^{2}H(d,n)^{3}He$", Report LA-6459-MS, Los Alamos Scientific Laboratory (1976)
10) G.A. Jarvis, see JA56B in Ref. 1
11) I am indebted to D.M. Drake of LANL for providing me with copies of the relevant pages of the P-Division Progress Reports
12) J.E. Perry, E. Haddad, R.L. Henkel, G.A. Jarvis, and R.K. Smith, see PE59 in Ref. 1
13) D.M. Drake, G.F. Auchampaugh, E.D. Arthur, C E. Ragan, and P.G. Young, Nucl.Sci.Eng. 63, 401 (1977).
14) P.W. Lisowski, G.F. Auchampaugh, D.M. Drake, M. Drosg, G. Haouat, N.W. Hill, and L. Nilsson, "Cross Sections For Neutron-Induced, Neutron-Producing Reactions In ^{6}Li and ^{7}Li At 5.96 And 9.83 MeV", Los Alamos Scientific Laboratory report LA-8342-MS (1980).
15) M. Drosg, P.W. Lisowski, D M Drake, R.A. Hardekopf, and M. Muellner, "Cross Sections For Neutron-Producing Reactions Induced By 6- and 10- MeV Neutrons on ^{10}B and ^{11}B", Los Alamos National Laboratory report LA-10665-MS (1986)
16) W. Deuchars, J.L. Perkin and R Batchelor, Nucl.Instr.Meth. 23, 305 (1963)
17) M. Drosg, Z.Physik A298, 297 (1980)
18) G. Zago, Lett. Nuovo Cim. 32, 327 (1981)

19) W. von Witsch and J.G. Willaschek, Nucl.Instr.Meth. 138, 13 (1976)
20) A.V. Blinov et al., J.Phys G. Nucl.Phys. 8, 223 (1982)
21) N. Jarmie and R.E. Brown, Nucl.Inst.Meth.Phys.Res. B10/11, 405 (1985)
22) A.B. Jones, Aust.J.Phys. 33, 203 (1980) and Report ANU-P/744, Oct. 1979
23) M. Drosg, "The $^{2}H(d,n)^{3}He$ Differential Cross Sections for Deuteron Energies Between 20 and 40 MeV", Los Alamos Scientific Laboratory report LA-8538 (1980)
24) R.W. Fegley, "Differential Cross Sections for D(d,d)D Elastic Scattering and the D(d,^{3}He)n, D(d,t)p Reactions between 12.5 and 40.0 MeV", Thesis, Univ. California, Davis (1970)
25) M. Drosg , Nucl.Sci.Eng. 65, 553 (1978)
26) A. Okihana, N. Fujiwara, H. Nakamura-Yokota, T. Yanabu, K. Fukunaga, T. Ohsawa and S. Tanaka, J. Phys.Soc.Jap. 46, 707 (1979)
27) M. Ivanovich, P.G. Young and G.G. Ohlsen, Nucl.Phys. A110, 441 (1968)
28) M. Drosg, Z.Phys. A300, 315 (1981)
29) N. Jarmie, R.E. Brown and R.A. Hardekopf, Phys.Rev. C29, 2031 (1984)
30) M. Drosg, "Neutron Sources", Proceedings XIth Internat. Symp. on the Interaction of Fast Neutrons with Nuclei, Rathen near Dresden, Report ZfK-476, p.80, July 1982.
31) M. Drosg et al., data reduction not finished yet
32) M. Drosg, "Candidates for Fast Neutron Standards Among Neutron Producing Reactions", report IAEA-TECDOC-335, p.456 (1985)
33) J.H. Dave, C.R. Gould, S.A. Wender, S.M. Shafroth, Nucl.Instr.Meth.Phys.Res. 200, 285 (1982)
34) M. Drosg, " The $^{1}H(^{7}Li,n)^{7}Be$ Reaction as a Neutron Source in the MeV Range", Report LA-8842-MS, Los Alamos Scient.Lab. (1981)
35) H. Liskien and A. Paulsen, Atomic Data and Nucl. Data Tables 15, 57 (1975)
36) Y. Yamanouti, this meeting
37) H. Klein, H.J. Breda, B.R.L. Siebert, Nucl.Instr.Meth.Phys.Res. 193, 635 (1982)
38) Summary of Working Group Session II, H. Klein, chairman, p.42 of report IAEA-TECDOC-335 (1985)
39) H. Klein, oral presentation at IAEA Adv. Group Meeting on Nuclear Standard Reference Data, Geel, Nov. 1984, and personal communications.
40) A.B. Kagalenko and N.V. Kornilov, this meeting
41) M. Drosg, companion paper, this meeting

NEUTRON SOURCES WITH LITHIUM TARGET

Y. YAMANOUTI
Japan Atomic Energy Research Institute,
Tokai, Ibaraki,
Japan

Abstract

The $^{7}Li(p,n)^{7}Be$ reaction is widely used as a source of monoenergetic neutrons. Usefulness of the $^{7}Li(p,n)^{7}Be$ reaction as a monoenergetic neutron source can be evaluated from the characteristics on zero-degree energy spectra, zero-degree cross sections, angular distributions, and total reaction cross sections of the reaction. The $^{7}Li(p,n)^{7}Be$ reaction on a thin lithium target is the most practical source of monoenergetic neutrons with neutron energy spread of about 400 KeV at proton energies above 30 MeV.

It is also to be noticed that the ^{7}Li + p and ^{7}Li + d reactions on thick lithium targets are useful sources of intense neutron beams for applications where the monoenergetic characteristics are not required. In these reactions the ^{7}Li + d reaction produces the zero-degree neutron yield higher than the ^{7}Li + p reaction at the same projectile energy.

In this paper characteristics of the $^{7}Li(p,n)^{7}Be$ reaction as a monoenergetic neutron source and production of intense neutron beams from the ^{7}Li + p and ^{7}Li + d reactions are presented.

---

1. Introduction

Nuclear data measured with monoenergetic neutron sources are needed for technological applications and medical programs as well as studies of neutron nuclear physics. The monoenergetic neutron source is required to have only one peak in its energy spectrum with small energy spread. The $^{7}Li(p,n)^{7}Be$ reaction is widely used as a source of monoenergetic neutrons. This reaction produces monoenergetic neutrons at proton energies between 1.92 and 2.37 MeV. A second group of neutrons leading to the first excited state of ^{7}Be at 0.429 MeV is emitted at proton energies above 2.37 MeV. Liskien and Paulsen have evaluated neutron production cross sections for the $^{7}Li(p,n_0)^{7}Be$ and $^{7}Li(p,n_1)^{7}Be$ reactions for proton energies up to 7 MeV [1]. Groups of neutrons leading to the higher excited states of ^{7}Be are produced at higher proton energies. However, these groups of neutrons have relatively weak intensity compared with neutrons leading to the ground and first excited states. At higher proton energies unresolved neutron groups leading to the ground and first excited states are usually used as a monoenergetic neutron source with energy spread of about 400 KeV. Usefulness of the $^{7}Li(p,n)^{7}Be$ reaction as a monoenergetic neutron source can be evaluated from following characteristics of the reaction:

1) Zero-degree energy spectra
2) Zero-degree cross sections
3) Angular distributions
4) Total reaction cross sections

Haouat and Cance have given a review of the $^{7}Li(p,n)^{7}Be$ reaction data in the previous meeting on neutron source properties held at Debrecen[2].

It is to be noticed that the ^{7}Li + p and ^{7}Li + d reactions on thick lithium targets are useful sources of intense neutron beams for applications where the monoenergetic characteristics are not required. Data available up to 1977 for the ^{7}Li + p and ^{7}Li + d reactions on thick lithium targets have been summarized in an article by Lone[3].

In this paper characteristics of the $^{7}Li(p,n)^{7}Be$ reaction as a monoenergetic neutron source and production of intense neutron beams from the ^{7}Li + p and ^{7}Li + d reactions are presented.

2. Monoenergetic neutrons from thin lithium targets

2.1. Energy spectra

The Q-value of the $^{7}Li(p,n)^{7}Be$ reaction is -1.644 MeV. The characteristics of the $^{7}Li(p,n)^{7}Be$ reaction as a monoenergetic neutron source can be seen in the zero-degree energy spectra of the

reaction at different proton energies. The energy spectra from the $^{7}Li(p,n)^{7}Be$ reaction have been observed in the energy range from 10 to 63.8 MeV[4-13]. Incident proton energies, authors and comments for the measurements of the energy spectra are listed in table 1. Fig.1 shows a zero-degree time-of-flight (TOF) spectrum for the $^{7}Li(p,n)^{7}Be$ reaction at E_p=33 MeV. This TOF spectrum was measured at the JAERI tandem accelerator fast neutron facility[14]. As is seen in fig.1, the zero-degree TOF spectrum has a main peak corresponding to the ground and first excited states, and has very weakly excited peaks corresponding to the second and higher excited states at this proton energy.

Table 1
Energy Spectra at 0°

Proton Energy Range (MeV)	Authors	Comments	References
10.45	M.Anwar	20°,120°	4)
10,22	C.Poppe		5)
15,20,30	M.McNaughton		6)
30	DeVito	TOF spect.	7)
30,50	C.Batty	10°,40°	8)
30,50	C.Batty		9)
50	J.Jungerman		10)
50	M.Bosman	20°	11)
61.8	F.Brady		12)
40.6,63.8	J.Wachter		13)

The neutron peaks corresponding to the second and higher excited states are small compared with the main peak. At proton energies of 10 and 22 MeV neutron groups corresponding to the second and higher excited states become relatively large[5].

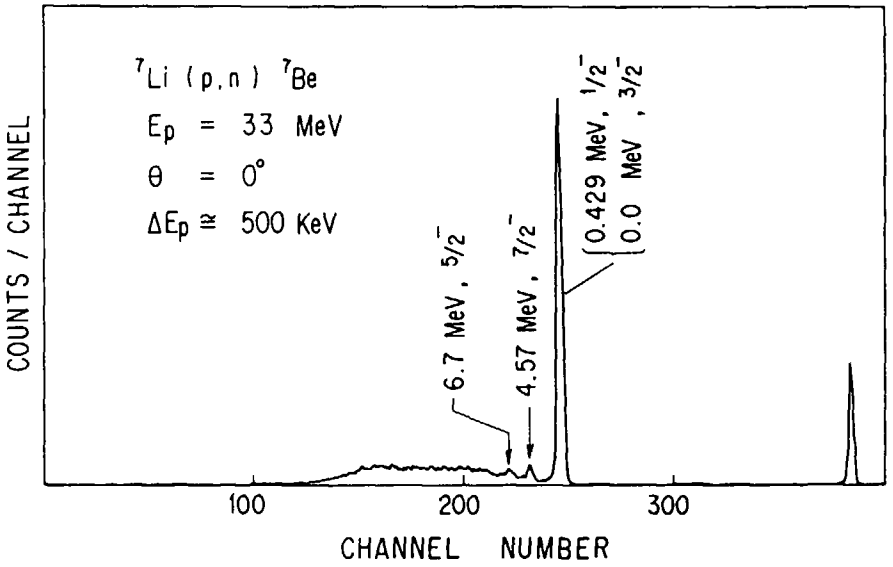

Fig. 1. Zero-degree time-of-flight spectrum for the $^{7}Li(p,n)^{7}Be$ reaction at E_p=33MeV.

2.2. Zero-degree cross sections

The zero-degree cross sections of the $^{7}Li(p,n)^{7}Be$ reaction are directly related to the neutron yields of the source. Measurements of the zero-degree cross sections for the $^{7}Li(p,n)^{7}Be$(g.s.+ 0.429 MeV) reaction have been recently extended to 160 MeV[15]. The measurements of the zero-degree cross sections are summarised in table 2. In fig.2 the zero-degree cross sections for the $^{7}Li(p,n)^{7}Be$ (g.s.+ 0.429 MeV) reaction are plotted as a function of proton energy. The zero-degree cross section increases with increasing proton energy in the energy range from 13 to 30 MeV, and approaches approximately 30 mb/sr at

Table 2

0° Cross Section Measurements

Proton Energy Range (MeV)	Authors	Comments	References
4.2-26	C.Poppe	3.5°	5)
15,20,30	M.McNaughton		6)
30,50	C.Batty		9)
30,40,50	J.Jungerman		10)
30,40,50	J.Romero		16)
50	M.Bosman		11)
39,60	J.Wachter		13)
135,160	J.Watson		15)

the proton energy of 29 MeV[5]). In fig.2 in the energy range higher than 30 MeV the zero-degree cross section hardly change as a function of proton energy. Neutron yields from the $^{7}Li(p,n)^{7}Be$ (g.s.+ 0.429 MeV) reaction can be predicted from these zero-degree cross sections in the energy range up to 160 MeV.

2.3. Angular distributions

Angular distributions of the source reaction are one of the most fundamental information needed for calculating other properties in

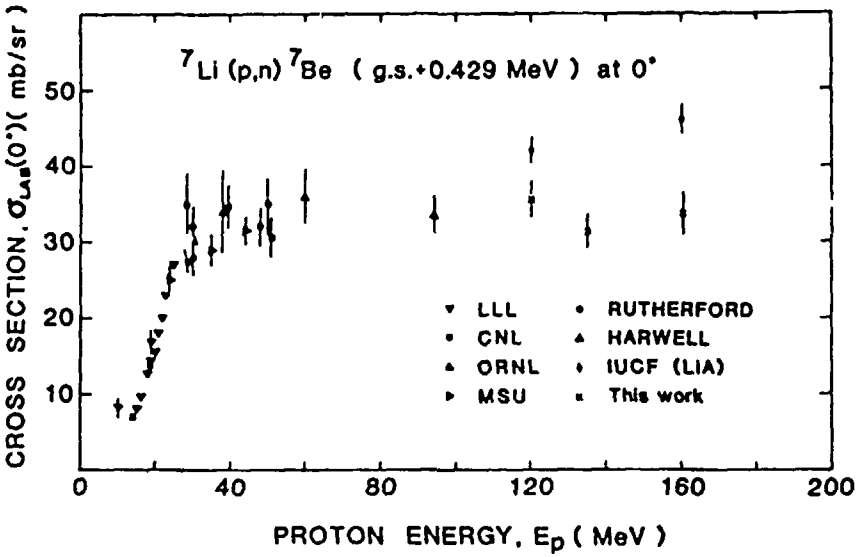

Fig. 2. The laboratory cross section at 0°, $\sigma_{lab}(0°)$, for the $^{7}Li(p,n)^{7}Be$ (g.s. + 0.429 MeV) reaction as a function of laboratory bombarding energy; ref. 15)

applications. Measurements of the angular distributions for the $^{7}Li(p,n)^{7}Be$ reaction are listed in table 3. The angular distributions for the $^{7}Li(p,n)^{7}Be$ reaction are forward peaked at proton energies above about 15 MeV, and become more forward peaked with increasing proton energy[5,8]). Theoretical analyses of the angular distributions at proton energies of 26 and 45 MeV have been performed within the framework of the microscopic folding model[17]).

2.4. Total reaction cross sections

The total reaction cross sections are related to the 4π integrated yields of the neutron sources. The $^{7}Li(p,n)^{7}Be$ (g.s.+ 0.429 MeV) total reaction cross sections have been measured recently up to 480 MeV by using the activation technique[21]). Measurements of the total reaction cross sections are listed in table 4. The measured total reaction cross section shows a striking 1/E energy dependence[21,22]).

Table 3

Angular Distribution Measurements

Proton Energy Range (MeV)	Authors	Comments	Reference
1.95-7	H.Liskien	compilation	1)
10.45	M.Anwar	n_0+n_1, n_2	4)
9.8,19.6	J.Anderson		18)
4.2-26	C.Poppe		5)
24.8,35,45	S.Schery		19)
30.2,49.4	C.Batty	n_0+n_1	8)
119.8	C.Goulding	n_0+n_1	20)
134.2	J.Watson	n_0+n_1	15)

Table 4

Total reaction Cross Sections

Proton Energy Range (MeV)	Authors	Comments	Reference
4.2-26	C.Poppe		5)
25-45	S.Schery	n_0+n_1	19)
60-200	T.Ward	n_0+n_1	22)
60-480	J.D'Auria	n_0+n_1	21)

3. Intense neutron beams from thick lithium targets

The Q-value of the $^7Li(d,n)^8Be$ reaction is 15.03 MeV. Zero-degree neutron yields of the ^7Li + p and ^7Li + d reactions on thick lithium targets have been measured in the energy range from 2 to 65 MeV[23-30]. The reaction type, incident energy range and authors for these measurements on thick lithium targets are given in table 5.

Table 5

Neutron yield measurements from ^7Li + p and ^7Li + d reactions on thick lithium targets

Projectile	Incident energy range	Authors	References
p	14.8-23	M.Lone	23)
p	15	C.Nelson	24)
p	35,65	H.Amols	25)
d	2	D.Jones	26)
d	5-19	K.Weaver	28)
d	8,12,15	C.Nelson	24)
d	13.42,34.06	A.Goland	27)
d	14.8-23	M.Lone	23)
d	35	H.Amols	25)
d	35	D.Johnson	30)
d	40	M.Saltmarsh	29)

3.1. Spectral distributions

At the proton energy of 65 MeV the spectral distribution for the ^{7}Li + p reaction shows a broad peak at a neutron energy of about 22 MeV[25]. At proton energies below 23 MeV, however, the spectral distributions for the ^{7}Li + p reaction decrease monotonically with increasing neutron energy. While in the spectral distributions for the ^{7}Li + d reaction a broad peak appears. The neutron energy of the broad peak is always about $0.4E_d$, where E_d is the incident deuteron energy[3]. Very few neutrons are emitted at neutron energies higher than incident deuteron energy, in spite of the high Q-value of 15.03 MeV for the ^{7}Li(d,n)^{8}Be reaction[30].

3.2. Angular distributions

The angular distributions of neutron yields integrated over neutron energy for the ^{7}Li + p reaction are essentially isotropic at proton energies below 23 MeV[23,24]. On the other hand the angular distributions for the ^{7}Li + d reaction become more forward peaked with increasing deuteron energy[23,30]. The broad peak in the spectral distribution and the forward peak in the angular distribution of the ^{7}Li + d reaction can probably be accounted for with the deuteron stripping theory[31]. Fig.3 shows neutron yields at zero-degrees from the ^{7}Li + p and ^{7}Li + d reactions as a function of projectile energy. The neutron yields from the ^{7}Li + d reaction at zero-degrees are obviously higher than those from the ^{7}Li + p reaction at the same projectile energy. The neutron yield at zero-degrees from the ^{7}Li + d reaction approaches 2.50×10^{17} n/(sr A sec) at the deuteron energy of 35 MeV[30].

4. Conclusions

The ^{7}Li(p,n)^{7}Be reaction on a thin lithium target is the most practical source of monoenergetic neutrons with neutron energy spread of about 400 KeV at proton energies above 30 MeV, because the contribution of lower energy neutrons corresponding to the second and higher

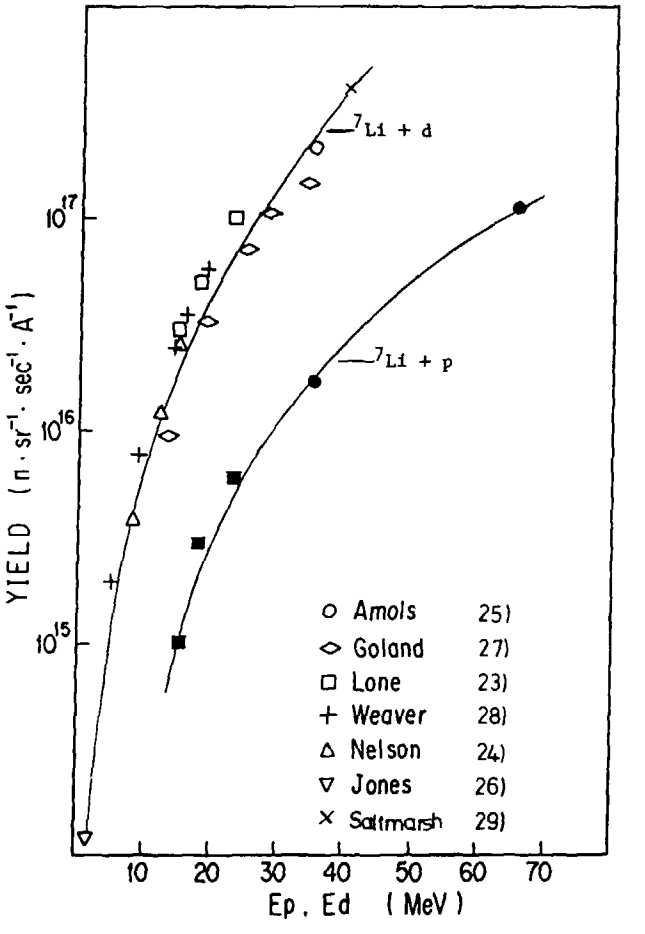

Fig. 3. Zero-degree neutron yields as a function of the projectile energy. Solid circles and solid squares represent data for the ^{7}Li + p reaction.

excited states of ^{7}Be becomes relatively small, and the zero-degree cross section approaches its highest value in this energy range.

The ^{7}Li + p and ^{7}Li + d reactions on thick lithium targets are useful sources of intense neutron beams. The ^{7}Li + d reaction produces the zero-degree neutron yield higher than the ^{7}Li + p reaction at the same projectile energy.

References

1) H.Liskien and A.Paulsen, Atomic Data and Nucl.Data Tables 15(1975)57
2) G.Haouat and M.Cance, Proc. of IAEA Consultant's Meeting on Neutron Source Properties, Debrecen, 1980, INDC(NDS)-114/GT
3) M.A.Lone, Symposium on Neutron Cross Sections from 10 to 40 MeV, Edited by M.R.Bhat and S.Pearlstein, (1977),BNL-NCS-50681, p79
4) M.Anwar Chaudhri, J.Templer and J.L.Rouse, IEEE Trans. on Nucl.Sci. NS-26 (1979) 2287
5) C.H.Poppe, J.D.Anderson, J.C.Davis, S.M.Grimes and C.Wong, Phys.Rev. C14 (1976) 438
6) M.W.McNaughton, N.S.King, F.P.Brady, J.L.Romero and T.S.Subramanian, Nucl.Instr.Meth 130 (1975) 555
7) R.P.Devito, Dissertation, Michigan State University (1979)
8) C.J.Batty, B.E.Bonner, E.Friedman, C.Tschalär, L.E.Williams, A.S.Clough and J.B.Hunt, Nucl.Phys. A120 (1968) 297
9) C.J.Batty, B.E.Bonner, A.I.Kilvington, C.Tschalär, L.E.Williams and A.S.Clough, Nucl.Instr.Meth. 68 (1969) 273
10) J.A.Jungerman, F.P.Brady, W.J.Knox, T.Montgomery, M.R.Mcgie, J.L.Romero and Y.Ishizaki, Nucl.Instr.Meth. 94 (1971) 421
11) M.Bosman, P.Leleux, P.Lipnik, P.Macq, J.P.Meulders, R.Petit, C.Pirart and G.Valenduc, Nucl.Instr.Meth. 148 (1978) 363
12) F.P.Brady, T.D.Ford, G.A.Needham, J.L.Romero, C.M.Castaneda and M.L.Webb, Nucl.Instr.Meth. 228 (1984) 89
13) J.W.Wachter, R.T.Santoro, T.A.Love and W.Zobel, Nucl.Instr.Meth. 113 (1973) 185
14) Y.Yamanouti, M.Sugimoto, S.Chiba, M.Hyakutake and S.Iwasaki, JAERI Tandem, Linac and VdG Annual Report, JAERI-M86-112 (1986) 159
15) J.W.Watson, B.D.Anderson, A.R.Baldwin, C.Lebo, B.Flanders, W.Pairsuwan and R.Madey, Nucl.Instr.Meth. 215 (1983) 413
16) J.L.Romero, F.P.Brady and J.A.Jungerman, Nucl.Instr.Meth. 134 (1976) 537
17) F.Petrovich, R.H.Howell, C.H.Poppe, S.M.Austin and G.M.Crawley, Nucl.Phys. A383 (1982) 355
18) J.D.Anderson, C.Wong and V.A.Madsen, Phys.Rev.Lett. 24 (1970) 1074
19) S.D.Scherry, L.E.Young, R.R.Doering, S.M.Austin and R.K.Bhowmik, Nucl.Instr.Meth. 147 (1977) 399
20) C.A.Goulding, M.B.Greenfield, C.C.Foster, T.E.Ward, J.Rapaport, D.E.Bainum and C.D.Goodman, Nucl.Phys. A331 (1979) 29
21) J.D'Auria, M.Dombsky, L.Moritz, T.Ruth, G.Sheffer, T.E.Ward, C.C.Foster, J.W.Watson, B.D.Anderson and J.Rapaport, Phys.ReV. C30 (1984) 1999
22) T.E.Ward, C.C.Foster, G.E.Walker, J.Rapaport and C.A.Goulding, Phys.Rev. C25 (1982) 762
23) M.A.Lone, C.B.Bigham, J.S.Fraser, H.R.Schneider, T.K.Alexander, A.J.Ferguson and A.B. McDonald, Nucl.Instr.Meth. 143 (1977) 331
24) C.E.Nelson, F.O.Purser, P.Von Behren and H.W.Newson, Phys.Med.Biol. 23 (1978) 39
25) H.I.Amols, J.F.Dicello, M.Awschalom, L.Coulson, S.W.Johnsen and R.B.Theus, Medical Phys. 4 (1977) 486
26) D.T.L.Jones and C.M.Bartle, Nucl.Instr.Meth. 118 (1974) 525
27) A.N.Goland, C.L.Snead,Jr., D.M.Parkin and R.B.Theus, IEEE Trans. on Nucl.Sci. NS-22 (1975) 1776
28) K.A.Weaver, J.D.Anderson, H.H.Barschall and J.C.Davis, Nucl.Sci.Eng. 52 (1973) 35
29) M.J.Saltmarsh, C.A.Ludemann, C.B.Fulmer and R.C.Styles, Nucl.Instr.Meth. 145 (1977) 81
30) D.L.Johnson, F.M.Mann, J.W.Watson,F.P.Brady,J.L.Ullmann and J.L.Romero, Symposium on Neutron Cross Sections for 10 to 50 MeV, Edited by M.R.Bhat and S.Pearlstein, BNL-NCS-51245, P99
31) L.S.August, F.H.Attix, P.Shapiro, R.B.Theus, G.Herling and C.C.Rogers, Phys.Med.Biol. 21 (1976) 931

FILTERED MEDIUM AND THERMAL NEUTRON BEAMS AND THEIR USE

V.P. VERTEBNYJ, A.V. MURZIN, V.A. PSHENICHNYJ,
L.L. LITVINSKIJ, PAK EN MEN*
Institute for Nuclear Research,
Ukrainian Academy of Sciences,
Kiev, Union of Soviet Socialist Republics

Abstract

Application of the filtered neutrons beams for nuclear and reactor physics field is reviewed. Experiments have been carried out at Kiev atomic reactors using interference and monocrystall filters.

Some results of these experiments are given for the germanium - 74 monocrystall, inelastic scattering cross Sections on the first 2^+ levels of ^{238}U and ^{232}Th, etc.

A Review of filtered neutron beams use for nuclear data measurements is given. Results of new experiments which have been carried out at Kiev atomic reactor WWR-M are reported. In particularly ^{232}Th and ^{238}U neutron inelastic and elastic scattering cross sections, ^{74}Ge single crystal filter properties are discussed.

Neutron filters are used at stationary atomic reactors and time-of-flight neutron pulsed sources in order to tailor intense quasimonochromatic intermediate and thermal neutron beams.

Filter quality is determined with peculiarities of the neutron cross section energy dependence of the filter material. Filter material choice depends upon of the experiment purpose. It has been shown that filtered beam experiments allow to get an additional information to one which is usually obtained in time-of-flight method experiments or to get new possibilities. The filtered neutron beams properties and their earlies applications have been reviewed in /1,2/. This paper deals for the most part with new uses of filters and only for clarity a few information is given about their properties.

1. Filtered intermediate neutron beams

Filtered neutron beams have been widely used after the pioneer Simpson and Miller paper /3/. For example let consider the idea of the Scandium filter. Scandium total cross section upon neutron energy is shown in fig.1 (Wilson Data 1966). It is seen that the 2 keV interference minimum cross section value is equal approximately zero. If to insert a long scandium rod ("the scandium filter") inside an atomic reactor neutron beam tube there will be tailored quasimonoenergy neutron beam with the mean energy 2 keV at excit end of the filter (see the lowest curve in fig.2);

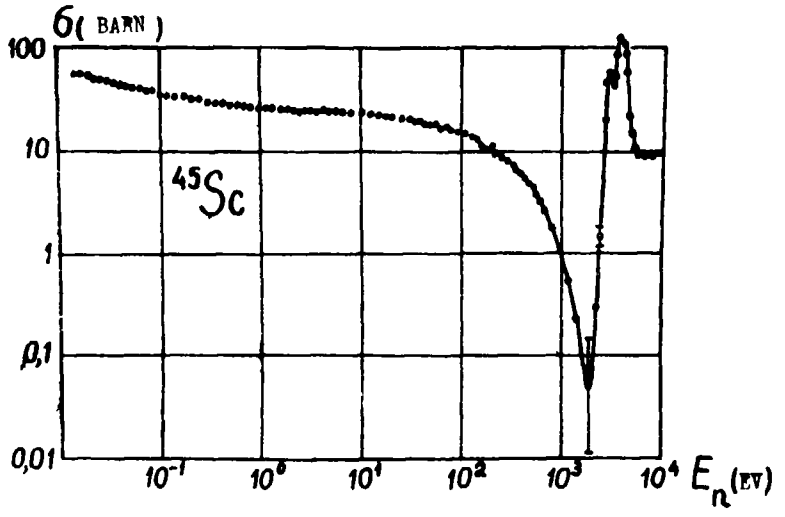

Figure 1. Scandium total cross section upon neutron energy (see (2), Wilson 1966).

* Visiting scientist from the Democratic People's Republic of Korea.

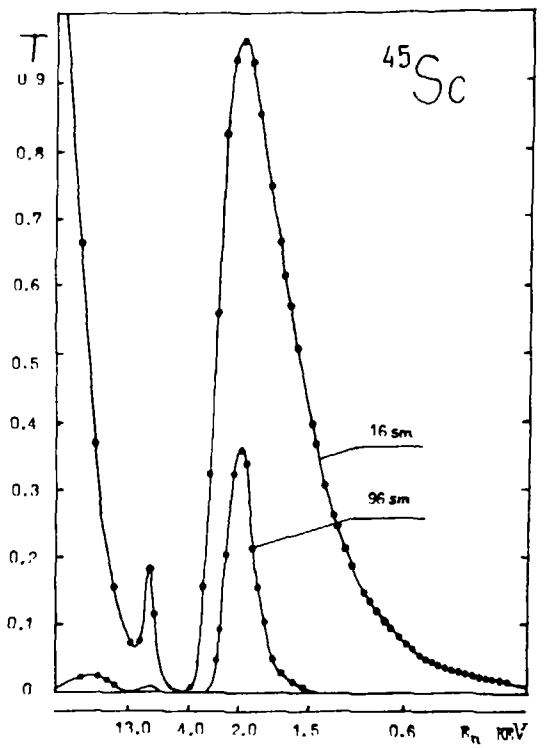

Figure 2. Transmission of scandium filters of different thickness upon neutron energy (time-of-flight) (A.L.Kiriljuk measurements).

the line half-height width is nearly 0.6 keV.

The iron is usually used to get 24-keV neutron beams. The 24-keV iron interference minimum is well known for reactor shield designers as "neutron window". Slabs of aluminium and sulfur are added to the iron filter if necessary to suppress other "windows" which have been well investigated by Filippov /4/. The intensity of the 24.3 keV neutron beam may be essentially increased if to use pure ^{56}Fe isotope instead natural iron. Other iron isotopes increase the minimum value from 7 mb to 450 mb. The pure Fe-56 filters have been used at the HFBR in Brookhaven /5/ and at WWR-M in Kiev.

Silicon has two "windows" at 144 keV and 55 keV. 144 keV beam first was obtained in /3/ and 55 keV one was obtained in /6/. Using of silicon single crystal permits to tailor high quality thermal neutron beams /7,9/. This possibility is discussed in the section 3

Few examples of filtered beams are given in table 1. Filtered beams are well collimated (beam diameters were used in the 4 ÷ 40 mm range); other energy neutron background is ussually equal 2-3% (a scandium filter is exception, which background is 10-40%). Thick filters suppress strongy reactor gamma-rays and background is usually low. Filtered neutron beams should be considered as intensive and stable those because research atomics reactors belong to very high average intensity and stable neutron sources.

Half-height-line width of a filtered neutron beam is usually wide that many neutron resonances of heavy and some medium isotopes fall into this energy interval. Consequently, cross section values are averaged on many resonances in investigations of nuclear reactions with the filtered beams. As this energy interval is wider than the one for resolved resonances so we can obtaine average values of strongly fluctuated resonance parameters with the better accuracy than in time-of-flight method experiments.

Many other filters have been proposed after /3/. Mill and Harvey /10/ proposed to use separated isotopes ^{170}Er, ^{184}W, ^{68}Zn, ^{86}Sr, ^{64}Zn, ^{60}Ni, ^{54}Fe, ^{58}Ni, ^{52}Cr for beam tailoring with differeni energies in the 0.06-48 keV range. Some of these and some other isotopes have also been used at the Kiev atomic reactor in the neutron energy 1-144 keV range. We have also observed the interference minima for ^{74}Ge near 4 keV, which probably may be used for filter beam getting.

Mill and Harvey /10/ collected so many proposes to use filtered neutron beams that they even considered a possibility of Specilized atomic reactor design.

In addition to the above mentioned of filtered beams tailoring it was proposed to use resonance scatterers /11-12/ Broder, Gamaliy, Zemtsev, et al. used wide ^{23}Na neutron resonance to get a filtered beam 2,7 keV neutron energy and 0.52 keV

Table 1.1.

Parameters of some filtered neutron beams (examples)

Filter	E_n, keV	E_n, keV	Composition, thickness in mm	Diameter in mm	(n/sec)
Scandium:					
1. Idaho, U.S.A. /1/	2	0.6	Sc 1067, Ti 14 ;	25	$\sim 10^7$
2. Kiev, U.S.S.R. /2/	2	0.6	Sc 960, B^{10} 0.2 g/cm^2	20-40	$3 \cdot 10^7$
3. Kiev, U.S.S.R. /2/	2	0.8	Sc 850, 60, Co 30, T 2	20-40	$\sim 10^7$
Iron:			B^{10} 0,2 g/cm^2		
1. BNL, U.S.A /1,3/	24,3	2	^{56}Fe 3,05, Al 7.8	72.7	$4 \cdot 10^7$
2. -"- /1,3/	"	"	Fe 228, Al 362, S 63	S = 7,27 cm^2	$\sim 10^7$
3. Kiev, U.S.S.R. /2/	"	"	Fe 250, Al 350, S 65	40	$\sim 10^7$
Silicon:			Single, crystal		
1. Kiev, U.S.S.R. /2/	55	2	Si 875; S 205, B^{10} 0.2 g/cm^2	30÷42	$2,0 \cdot 10^7$
-"-	144	25	Si 875; B^{10} 0,2 g/cm^2 Ti 875	30÷42	$\sim 4 \cdot 10^7$
-"-	thermal neutrons		Si single crystal 875 S 205; Ti 18	30÷42	$\sim 10^8$ n/cm^{2}sec
Oxygen:					
1. Massachusetts, U.S.A. /1/	2350	100	O_2 1830; Bi 80;	-	$\sim 5 \cdot 10^5$

width at the Dimitrovgrad SM-2 reactor /10/. Dilg and Vonach also used this filter at Garching-Munich reactor /12/. The both methods combination allows to increase quality of filtered beam, for example to achieve better background suppression.

Some investigators improved experimental conditions using filters of different type at lineacs and other pulsed neutron sources (See Muradjan, Adamchuk et al /13/), Tsubone et al /14/, Popov and Samosvat /15/ experiments).

2. Experiments with filtered neutron beams

Examples of different earlier investigations with filters are given in /1,2/. Here we consider only relatively new examples of experiments, which high stable intensity of filtered beams was important for.

Inelastic scattering of 144 keV neutrons for the first excited levels of ^{238}U and and ^{232}Th isotopes

There are the lowest excited 2^+ states 45 keV and 49 keV ^{238}U and ^{232}Th nuclei correspondingly.

Inelastic scattering for these levels was investigated not very surely in former time, differential data for ^{238}U were in some contradiction with integral experiments /16/. Recently angular distributions of elastic and inelastic ^{238}U scattering of 144 keV neutrons have been investigated at atomic reactors of the Missoury Universite /17/ and Kiev Institute for Nuclear Research /18/. Both results are nearly the same. Experiment arrangement in /18/ is shown in fig.3, U238 angular distributions are shown in fig.4 and Th-232 those in fig.5.

It is possible to show that σ_{in} - value strongly depends only upon p-strength function value S_1 and practically is independent upon other average resonance and potential parameters for ^{238}U and ^{232}Th isotopes. Large correlations between value S_1 and other parameters there were in methods, which used previously for S_1 evaluation. By this reason we hope that $_{in}$ - measurements for the lowest states of some heavy nuclei allow to evaluate S_1-values with a better accuracy than in other measurements.

In addition we have studied as a neutron resonance transmission selfshielding at 55 and 144 keV energy so angular distribution of the elastic scattering.

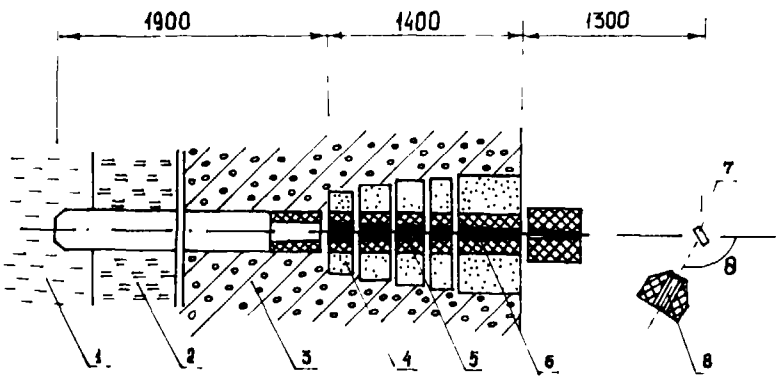

Figure 3. Experimental arrangementof ^{238}U and ^{232}Th neutron scattering investigations with Si-filters.

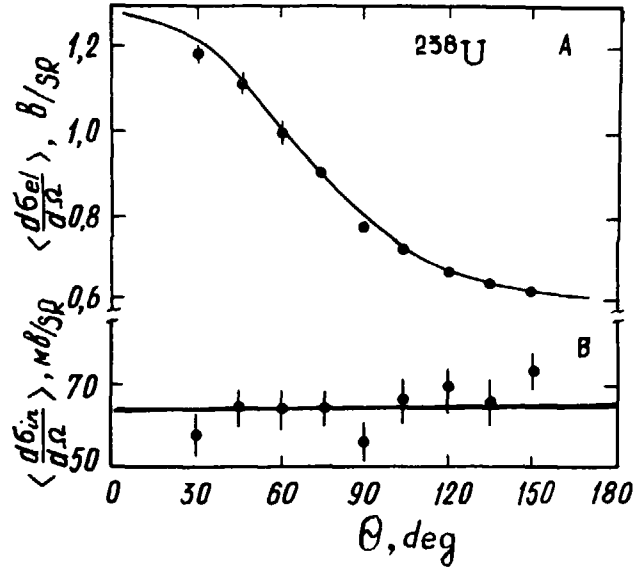

Figure 4. Angular distributions for ^{238}U elastic (upper curve) and inelastic (lower curve) scattering.

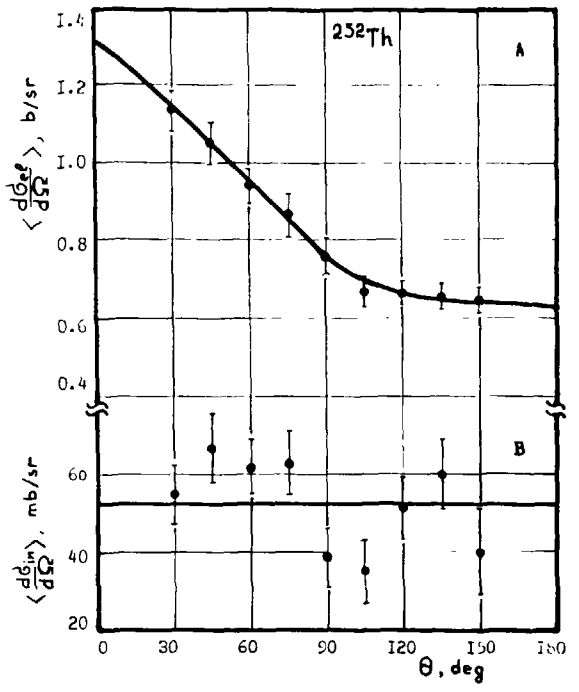

Figure 5. Angular distributions for ^{232}Th elastic (upper curve) and inelastic (lower curve) scattering.

Everything was done with silicon filters. It has been also measured U-238 neutron resonance self-shielding with the Scandium filter. (See /19/ and fig.6). The obtained average parameters for ^{238}U and ^{232}Th isotopes are listed in table 2.1.

Intermediate neutron capture gamma-ray spectra — Neutron capture primary gamma-ray transitions are being widely investigated with the help of filters /19/. Porter-Thomas partial gamma- width fluctuations are essentially less in the case of filtered neutron capture in compare with those for thermal neutron capture, for which only one or two of the nearest to zero e energy neutron resonances are important. A typical arrangement of

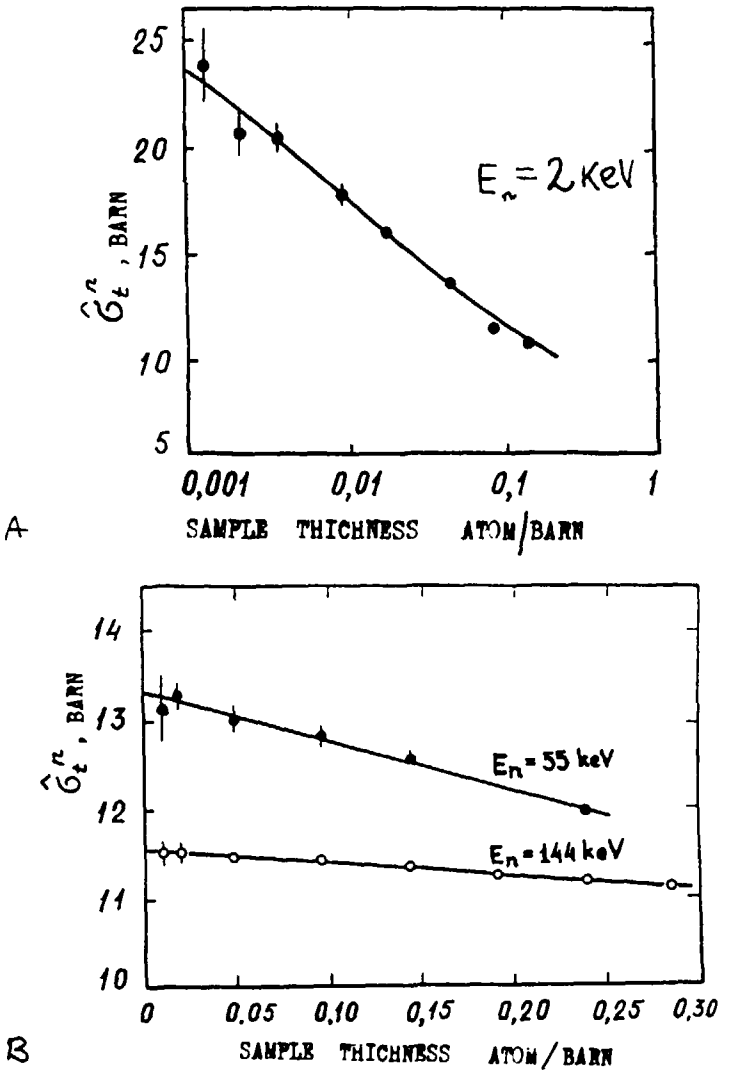

Figure 6. Observed total cross section σ_t of ^{238}U upon sample thickness (resonance self-shielding) at 2 keV neutron energy (results of V.F.Razbudey, A.V.Muravitsky, A.L.Kiriljuk), 55 keV and 144 keV.

Table 2.1

^{238}U and ^{232}Th average resonance and potential parameters

Value	:	^{238}U	:	^{232}Th
$10^4 \times S_1$, $eV^{-1/2}$		2,42 ± 0.09		2.12 ± 0.11
R_0', f		9.15 ± 0.24		8.56 ± 0.41
R_1^∞		0.257 ± 0.027		0.360 ± 0.054
R_2^∞		0.82 ± 0.71		1.2 ± 3.3
σ_t (144 keV), b		11.55 ± 0.02		11.38 ± 0.13
σ_t (55 keV), b		13.34 ± 0.05		12.98 ± 0.17
σ_t (2 keV), b		24.70 ± 0.30		-
σ_{el}(144 keV), b		10.57 ± 0.09		10.23 ± 0.12
σ_{el} (55 keV), b		12.9 ± 0.2		-
σ_{in} (144 keV), b		0.815 ± 0.024		0.667 ± 0.030

capture gamma-ray spectrum experiment is shown in fig.7 /20/. We have the Sc-(E_n=2 keV), Fe-(E_n=24.3 keV) and Si-(E_n=55 keV) filters and Ge(Li) pair gamma-spectrometer. The 2 keV-neutron capture gamma-ray spectrum for ^{238}U is given in fig.8 /20/, for example.

Uranium-238 gamma-spectra transformations connected with neutron energy change from thermal up to 55 keV are shown in fig.9. Primary transitions to the ground and near -ground states are not observed for thermal neutrons but they are well observed for filtered neutrons. It is worth to note our 2 keV and 24.3 keV data ^{238}U gamma-spectra are in agreement with the results of /21/. The neutron energy dependance of average E1 primary gamma-ray transition reduced intensities has been investigated for S- and p-waves in /20/. It has been observed that reduced intensity of primary E1 transitions, which are induced with S-neutrons, from compound states to the final states $1/2^-$ and $3/2^-$ abnormally increases at the 24.3 keV energy in compare with 2 keV one (see fig.10). Reduced intensities for ^{143}Nd neutron capture gamma-ray spectrum is shown in fig.11 at E_n=2 keV. Similar investigations allow to cor-

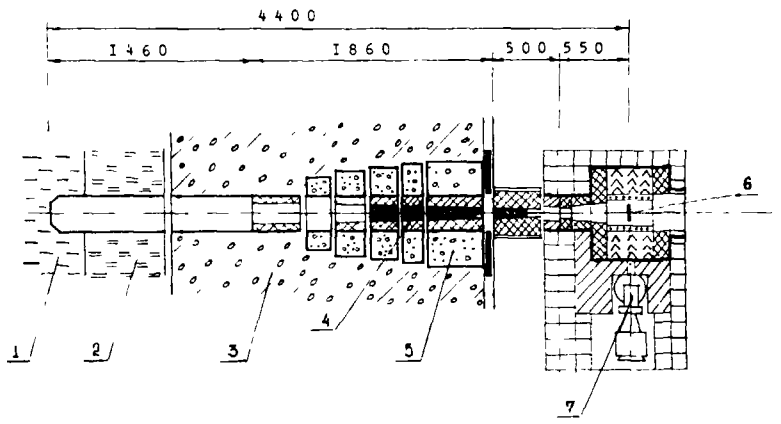

Figure 7. Neutron capture gamma-ray spectrum experiment with filtered beams at Kiev atomic reactor.
1 - core; 2,3 - shield; 4 - filter; 6 - sample, 7 - Ge(Li) pair spectrometer.

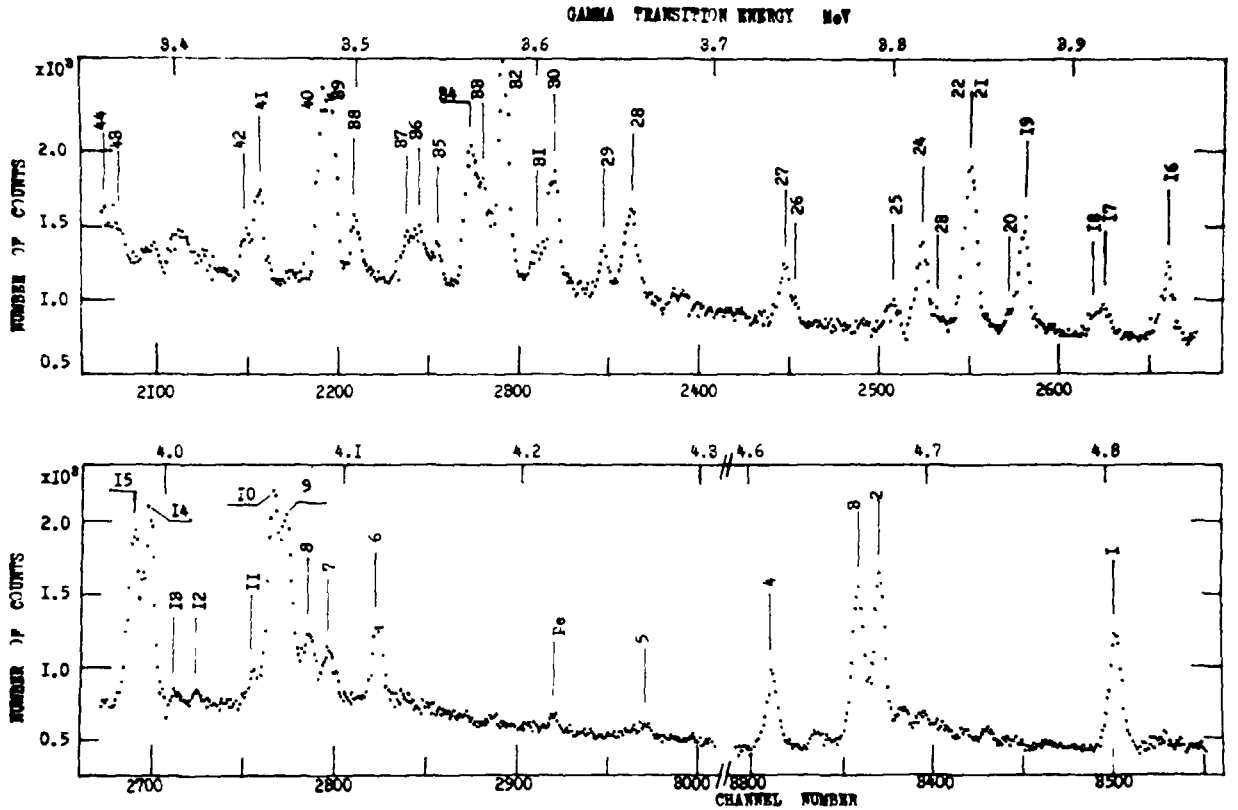

Figure 8. ^{238}U neutron capture gamma-ray spectrum at E_n = 2 keV (Sc); numerals above peaks mean ordinal numbers of observed gamma transitions. (288 hours exposition) 307 g mass sample; 47 mm dia., 10 mm thick.

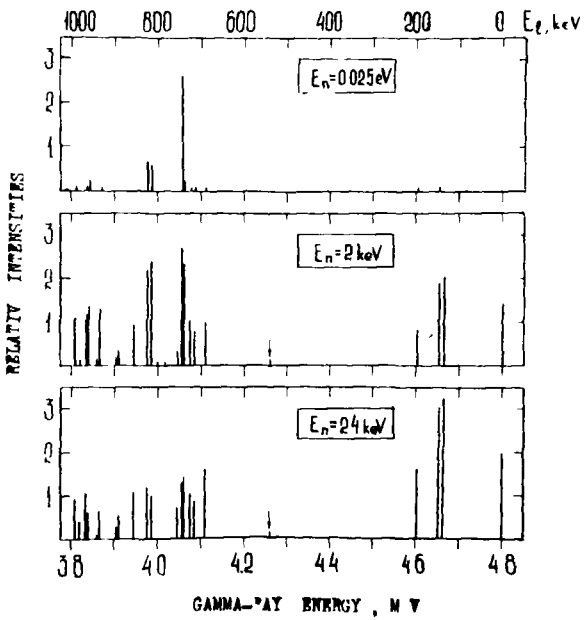

Figure 9. Neutron capture gamma-ray spectra for ^{238}U at different energies of neutrons in spectrum arbitrary units. Upper spectrum relates to thermal neutrons, medium one relates to 2 keV-neutrons and lower one relates to 24 keV neutrons.

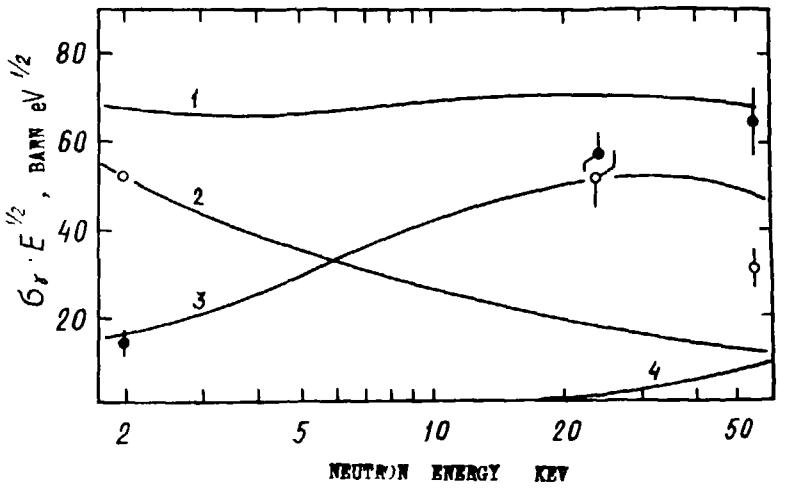

Figure 10. Reduced gamma-ray intensity for transitions from capture of S- and p-neutrons in ^{238}U upon neutron energy; 2 - S neutrons (transitions from compound states to $1/2^-$, $3/2^-$ those); 3 - p-neutrons (transitions from compound state to $1/2^+$, $3/2^+$ states); 1 - total capture cross section.

rect transition schemes and to study energy dependence of a gamma-ray transitions rate for a given multiplicity /22/.

Neutron resonance self-shielding in transmission and partial cross sections experiments

Such experiments allow for large level density nuclei to evaluate average neutron resonance parameters with a good accuracy /23,24/. Gnidak, Pavlenko et al /24/ have evaluated from experiments with thin samples (n σ_t < 0.01) in addition to $\langle\sigma_t\rangle$, $\langle\sigma_s\rangle$, $\langle\sigma_\gamma\rangle$, also generalized dispersions $\langle\sigma_t\sigma_s\rangle - \langle\sigma_t\rangle\langle\sigma_s\rangle$; $\langle\sigma_t\sigma_\gamma\rangle - \langle\sigma_t\rangle\langle\sigma_\gamma\rangle$. Using Lukjanov calculations /25/ they have evaluated at 2 keV energy all the average S-wave resonance parameters for ^{181}Ta in unresolved resonance region. The experimental results for scattering are shown in fig.12 and the data are listed in Table 2.2. in comparison with resolved resonance region from BNL-atlas /26/.

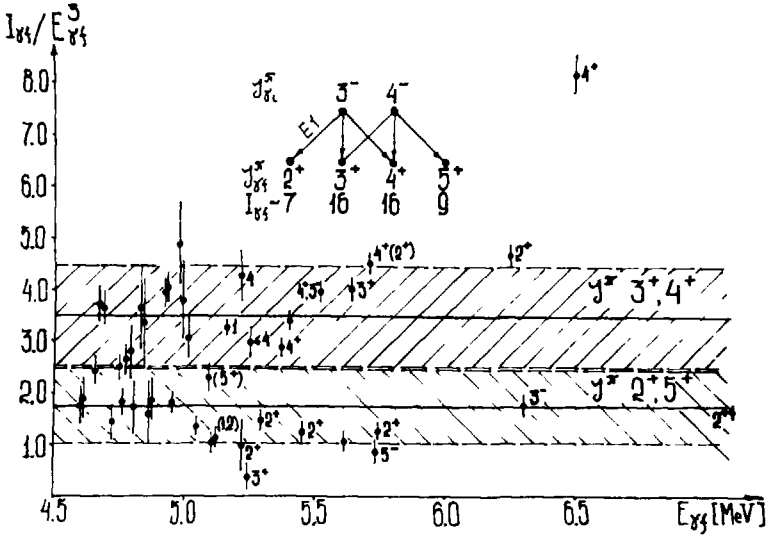

Figure 11. ^{143}Nd (n,γ) reduced intensity $I\gamma_f/E\gamma_f^3$ at ? keV neutron energy.

Gnidak and Pavlenko /27/ taking in account a high neutron intensity of Sc-filtered beam have proposed a new absolute method of capture cross section measurement.

Neutron fission cross sections of ^{233}U, ^{235}U and ^{239}Pu isotopes have been measured in Obninsk /30/, Dimitrovgrad /31/ and Kiev /32/ Murzin et all. /32/ observed resonance self-shielding in fission cross sections of $^{233,235}U$ even at the 24.3 keV neutron energy.

Investigations of (n,α) reactions

These experiments are difficult to make because ratio $\langle\Gamma_\alpha\rangle/\langle\Gamma_\gamma\rangle \sim 10^{-6}$ is very small. Yu.P.Popov et al at pulsed reactor IBR-30 in JINR (Dubna) has first carried out many experiments on neutron resonance spectroscopy of (n,α)-reactions /28/. Joint Dubna and Kiev group has measured (n,α) cross sections ^{147}Sm, ^{95}Mo, etc. and evaluated $\langle\Gamma_\alpha\rangle$ /29/.

Filtered beam applications at pulse neutron sources

Tsubone et al /13/ have measured average total cross section of ^{238}U up to 1 MeV neutron energy with iron beam. Zo INOK, Popov and Samaswat also have used 24 cm-iron filter and 50 cm-aluminium filter to measure total cross sections of Mo and Cd /30/. Muradjan, Adamchuk and Schepkin measured accuratly Pb total cross sections with the help of the Sb-resonance scattering

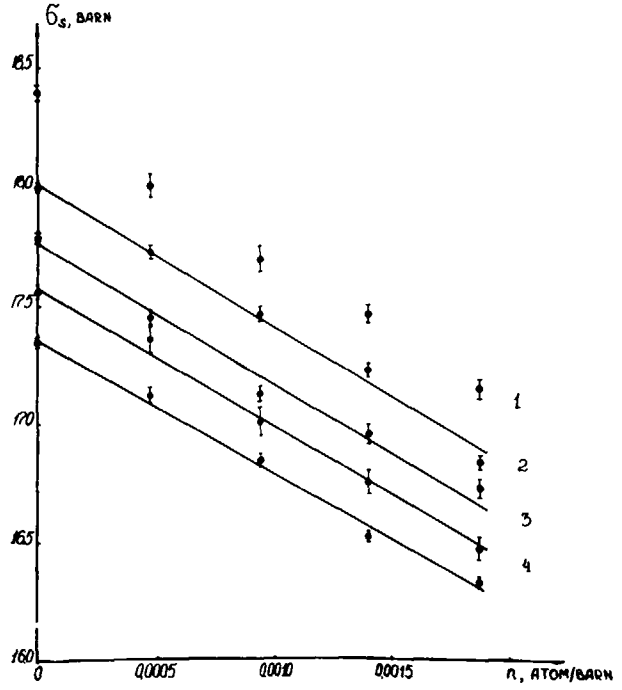

Figure 12. Self-shielding in self-indication scattering cross section measurements. ^{181}Ta observed total scattering cross sections upon thickness (nucl/barn) n_1 of shielding sample for different thickness n_o ^{131}Ta scatterers: 1 - n_o = 0.000464 nucl/b; 2 - n_o = 0.00925 nucl/b; 3 - n_o = 0.001387 nucl/b; 4 - n_o = 0.001848 nucl/b; 5 - n_o = 0.002308 nucl/b.

Table 2.2

^{181}Ta cross sections and neutron resonance parameters

Parameters	:	Results [24]	[26]
$10^4 \times S_o$, $eV^{-1/2}$		1.64 ± 0.07	1.70 ± 0.12
D_o, eV		4.3 ± 0.3	4.17 ± 0.04
Γ_γ, meV		57 ± 4	57 ± 3
R'_o, f		8.1 ± 0.2	7.8 ± 0.2
$\langle\sigma_t\rangle$ = 23.0 ± 0.3 b;	$\langle\sigma_t\sigma_s\rangle - \langle\sigma_t\rangle\langle\sigma_s\rangle$	= 652 ± 12 b^2 ,	
$\langle\sigma_s\rangle$ = 18.43 ± 0.03 b;	$\langle\sigma_t\sigma_\gamma\rangle / \langle\sigma_\gamma\rangle$	= 56 ± 1 b.	

filter at well definite energies. Background conditions have been essentially improved in all these experiments using filters.

3. Single crystal filters of thermal neutrons

Perfect single crystals with low capture, inelastic and incoherent cross sections and with high cross sections for epithermal and fast neutrons work as high quality thermal neutron filters. They are often used to receve only slow neutron beams from "white" reactor neutron beam. The slow neutrons penetrate though perfect coherent single crystal without intensity attenuation if neutron wave length does not satisfy Wolf-Bragg condition ($\lambda = 2d\sin\theta$). Neutron, which satisfy this condition go out of the beam of course but their intensity part is relatively low. It is this reason that total cross section of a single crystal is demnished neutron energy decreases. Total cross section energy dependences of Si and Ge single crystal are good examples of the above statesment (fig.13,14).

Probably Brockhouse /32/ was first who had been used such type filter in experiments. It was single quartz crystal (SiO_2) cooled with a liquid nitrogen in order to suppress neutron inelastic scattering on atomic thermal motion.

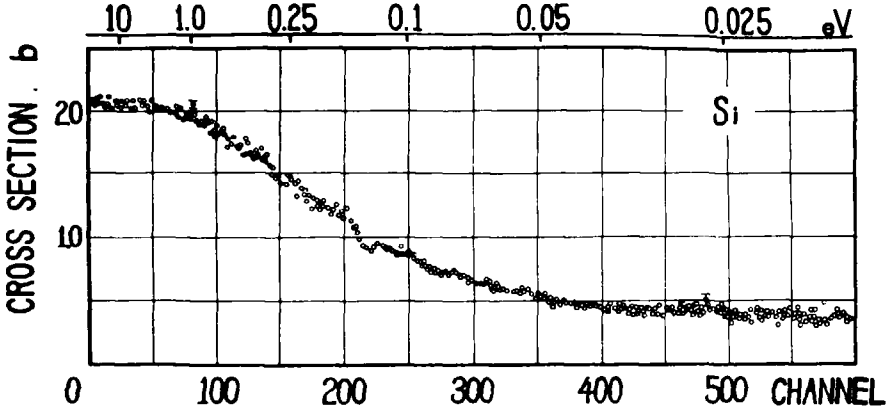

Figure 13. Si single crystal total cross section upon neutron energy (time of flight).

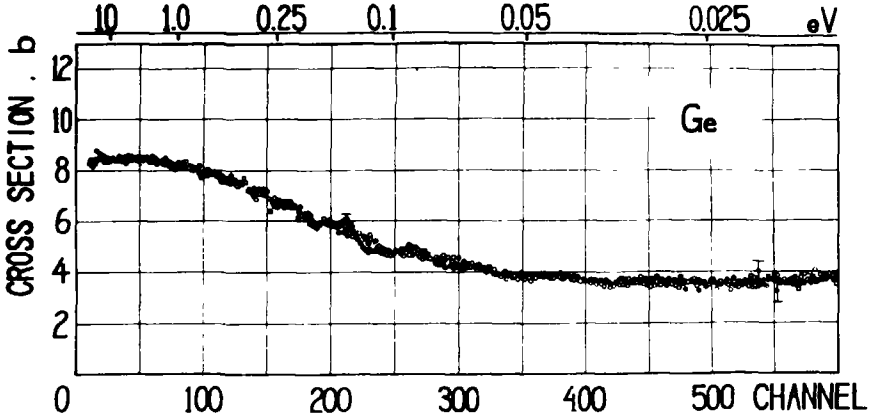

Figure 14. Ge single crystal total cross section upon neutron energy (time of flight)

Vertebnyi, Vlasov and Koloty /7/ after measurements of Ge total cross section upon neutron energy /33/ have concluded, that easy available industrial Si and Ge single crystal may be used as neutron filter even without liquid nitrogen cooling /3/. For Si this was shown in /7/ then in /8/ by R.M.Brugger. The first use of Si-single monocrystal filter was reported in paper of Barchuk et al /34/. A filter quality may be suggested if to evaluate σ_{in} for slow neutrons. In first approximation σ_{in} is determined by value of Debye temperature θ /35/: $\sigma_{in}=\sigma_0-\sigma_\Delta$, where σ_0 - total scattering cross section for free nuclei, σ_Δ = $= \sigma_{coh}(1-e^{-\alpha})/\alpha$; $\alpha = 4E/\mu\varepsilon$, ε- Einstein energy, is characteristic energy, which is a function of T/θ ; T is filter temperature, μ is nucleons mass in units of neutron mass; is practically equal to elastic cross section (without energy loss). In table 3.1. listed evaluated σ_{in}, capture cross section σ_a for 50 MeV neutron energy and some other parameters of filters. It is seen from this table that silicon gives the lowest neutron attenuation and this is cause of silicon application success in /7,8/. Other experimental and evaluated data are listed

Table 3.1

Inelastic and capture cross sections for neutron energy 50 meV and temperature 293°K

(evaluation)

Material	Θ, °K	Cross sections, barn			Material	Θ, °K	Cross sections, barn		
		σ_{in}	σ_a	$\sigma_{in}+\sigma_a$			σ_{in}	σ_a	$\sigma_{in}+\sigma_a$
Be	1160	1,5	10^{-2}	1.5	Pb	111	5.2	0,17	5,4
C	1580	0,5	3 10^{-3}	0,53	Bi	119	4,1	0,05	4,15
Mg	400	1,2	65 10^{-3}	1,27	U	200	1,8	2,7	4,5
Al	428	0,5	0,235	0,74	MgO	825	1,4	0,067	1,5
Si	640	0,4	0,16	0,56	Al_2O_3	1025	1,5	0,44	2,0
Ge	310	2	2,3	4,6	SiO_2	562	2,8	0,16	3,0
Zr	370	1,3	0,19	1,49	^{74}Ge	310	1,65	0,35	2
Sn	199	1.65	0,63	2,28	^{76}Ge	310	?	0,10	?

Slow neutron filter comparative parameters

Table 3.2

Single crystal	Thickness cm	Attenuation of neutrons (times)			Attenuation of gamma-rays at E_γ = 2 MeV
		E_n = 50 meV	E_n = 1 eV	E_n = 1 MeV*	
Ge	7	2,5	10	4	5.5
Si	25,5	1,8	10	50	12
SiO_2	10	2,9	10	6	3.3
MgO	9	3	10	14	4
^{74}Ge					
^{76}Ge					

* Calculated

in table 3.2. Silicon single crystal filters successfully used in (n,) experiments at Rzesh, Kiev atomic reactors and in solid state physics experiment in Obninsk /9/.

It is always desirable to have a filter of high Z material in order to suppress gamma-ray intensity. Kley et all /36/ investigated properties of Bi-single crystal filters (thickness 20 and 40cm), which were cooled by liquid nitrogen. Bi-single crystal transmission at the neutron energy 50 meV was very low, T 0.05; neutron spectra were cutted with Wolf-Bragg's "Steps" and maxima of these spectra were displaced to the cold neutron region. Cadmium ratio for these filters was equal approximately 5000. Bi-single crystal filter was also used by Lowde /37/.

In /7/ it has been suggested that pure even-even (74 or better 76) germanium have isotope single crystal filters would have good properties. It is this reason we have measured with time-of-flight method a transmission of a pure ^{74}Ge single crystal (Enrichment 98.3%; nongermanium impurities 3 10^{15} cm^{-3}; sample thickness 3.25 cm or 0.144 nuclei/b). The incident neutron beam direction was normal to the planes (1,1,1). The total cross section σ_t of this sample is shown for the 0.02-10 eV neutron energy range in fig.15. For comparison the natural germanium single crystal total cross section is shown in fig.14. It should be mentioned that for natural germanium the results were nearly the same for normal and parallel incident neutron beam directions to the planes (111). The thickness of the Ge single crystal in normal directions was nucl./barn. Our new results are in agreement with those of /7/.

Appearance of the Bragg peaks on curve in fig.15 mean that our ^{74}Ge single crystal is still not perfect as natural Ge one is. However we have been able to evaluate the total cross section for perfect ^{74}Ge single crystal from the curve which was drawn through minimum points. At E = 50 meV this value for ^{74}Ge single crystal is equal 2 barn, for Ge one is equal 38barn. We have evaluated the free nucleous total scattering cross sections σ_o: for Si 2.04±0.06 barn; for Ge 8.1±0.2 barn, for ^{74}Ge 6.9±0.2 barn.

Untill now be Si-single crystal filters lengthes were equal 25 cm in /7/, up to 200 cm in other experiments at Kiev reactor without any cooling and up to 200 cm in /8/ with nitrogen cooling.

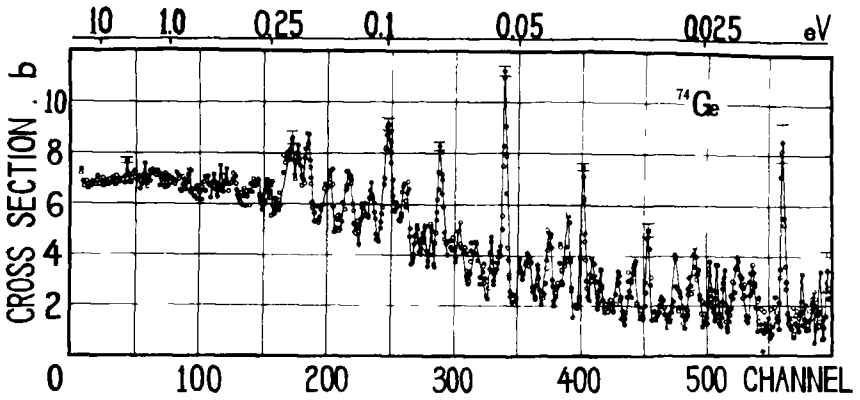

Figure 15. ^{74}Ge single crystal total cross section upon neutron energy (time of flight).

It should be concluded at the end that the filtered neutron beams which can be tailored at stationary atomic reactors and pulsed neutron sources are very promised for many applications not only in nuclear physics experiments, but also in other fields.

Aknowlegements

Authors are thankful all the fellow-workers who helped in measurements and discussed the results to dr. Vorobkalo F.M. for pure ^{74}Ge-single crystal giving, to dr. Gavriljuk V.I. for the attention to and support of investigations.

REFERENCES

1. R.C.Block, R.M.Brugger, Filtered Beams in Neutron Physics and Nuclear Data in Science and Technology, v.2, Chapter 5; Pergamon Press.
2. V.P.Vertebnyi, Neutron resonance investigations at stationary atomics reactors, Proc. of the 4 International School on Neutron Physics, Dubna 1982; D3, 4-82-704, p. 66-86; Applications of Intense Filtered Neutron Beams for Physical Research, Proc. of the 14 Nuclear Physics Symp. 1984, Dresden, DDR.

3. O.D.Simpson, L.G.Miller

Nucl. Instr. Meth. 1968, 68, 245.

4. V.V.Filippov, Investigations of iron total cross section minima, Preprints FEI-823, 1978; FEI-685, 1976.
5. T.Bradley, Z.Parza, M.L.Stelts, R.E.Chrien, NBS. Sp.P.H. 599; Neutron Cross Sections for Technology, Proc. Conf. 1980, 344-347.
6. E.N.Kuzin et al., Atomnaja Energia 1973, 35, 66.
7. V.P.Vertebnyi, M.F.Vlasov, V.V.Kolotyi, Thermal neutron single-crystal filters, Ukr. Fiz. Journ., 1974, 19, 510-513.
8. R.M.Brugger, A single crystal silicon thermal neutron filter, Nucl. Instrum. Meth., 1976, 135, 289-291.
9. V.V.Sulin et al., Silicon filter in solid state physics experiments, Pribory i Technika Experimenta 1985, N 5, 1983.
10. A.I.Mill and I.R.Harvey, A Proposed International Filtered Beam Project Nucl. Data in Sci and Techn., Proc. Conf. Antverp., 1982, p.999-1004.
11. D.L.Broder, A.F.Gamaliy, B.V.Zemtsev, B.N.Nesterov, L.P.Chamjanov, Yadernaj physica 1971, 13, 3.
12. W.Dilg and H.Vonach, Neutron Resonance Parameters Measured with ^{23}Na filtered beam, Proc. Int. Conf. on Stat. Phys. of Nucl., New York 1980.
13. G.V.Muradjan, Yu.V.Adamchuk, Yu.G.Schepkin, Neutron physics total cross section measurements, p.1, Proc. Conf., Kiev, 1972, 124-127.
14. I.Tsubone, Y.Nakajima, Y.Punta, Neutron total cross sections of ^{181}Ta and ^{238}U from 24.3 keV to 1 MeV and average resonance parameters, Nucl. Sci. Eng., 1984, 88, 579-591.
15. Zo In Ok, A.B.Popov, G.Samosvat, Mo and Cd cross sections measurement in 20-1100 keV energy range with filtered neutron beam, Preprint JINR, P3-84-669, 1984.
16. Constant for Reactor Calculations, (Russ.), Moscow, Energoizdat, 1981.
17. F.Y.Tsang, R.M.Brugger, The Differential Neutron Scattering Cross Sections of ^{238}U at 144 keV, Nucl. Sci. Eng. 1978, 65, 70-75.
18. L.L.Litvinsky, A.V.Murzin, V.A.Libman, Preprint KIJAI-85-35, 1985.
19. R.E.Chrien et all, The HFBR tailored-beam facility, Sec. Int. Symp. on neutron capture gamma ray spectroscopy, 1974, Petten 99-103; R.C.Greenwood, R.E.Chrien, K.Rimawi, Radiative capture of neutrons in the keV Region NBS Sp. Public. 425, Nuclear Cross Sections and Technology, Proc. Conf., 1975, 912-915.
20. A.V.Murzin, V.A.Libman et al., ^{238}U (n,) gamma-ray spectra for neutron energies 2, 24 and 55 keV; Neutron Physics v.2, Proc. Conf., Kiev, 1983; M-1984, 313-317.
21. R.E.Chrien, J.Kopecky, The nuclear structure of ^{238}U, Nucl. Phys. A 414, 1984, 281-300.
22. Yu.E.Loginov, V.V.Martynov, A.V.Murzin, E.I.Fedorov, ^{128}I gamma-ray transitions, Neutron Physics, v.3, Proc. Conf., Kiev 1983; M. 1984, 20-24.
23. Vertebnyi V.P., N.L.Gnidak, A.V.Grebnev et al., Resonance self shielding experiment with Sc-filtered neutron beam.
24. V.P.Vertebnyi, N.L.Gnidak, A.V.Grebnev, A.L.Kiriljuk, G.M.Novoselov, E.A.Pavlenko, T.A.Senchenko, ^{181}Ta self-indication measurements of resonance selfshielding with Scandium filter, Neutron Physics, v.3, Proc. Conf., Kiev 1983; M. 1984, 28-32.
25. A.A.Lukjanov, Slowing down In and capture of resonance neutrons, Atomizdat, 1974.
26. S.F.Mughabghab, Neutron cross sections v.1, p.13. Pergamon Press, 1984.
27. N.L.Gnidak, E.A.Pavlenko, A new absolute method of neutron capture cross section measurements, Neutron Physics, v.2, 198, M., 1977, 248-251.
28. In Review of V.J.Luschikov, L.B.Pikelev, Yu.P.Popov et al., NBS Sp. Publ. 593, Proc. Conf., 1980, 385.
29. V.A.Vtjurin et al., ^{95}Mo (n,) reaction for intermediate neutrons, Neutron Physics v.2, 1983; M. 1984, 342-345.
30. K.D.Juravlev, N.I.Kroshkin, ^{233}U, ^{235}U and ^{239}Pu Fission cross section measurements with filtered neutron beams at the reactor SM-2. Sov. At. En., 1977, N1, p42.

31. A.V.Murzin et al., ^{233}U and ^{235}U fission cross section and neutron resonance selfshielding, Neutron Physics, v.2, M. 1980, 257-261.
32. Brockhouse, SiO_2 single crystal filter, Can. J. Phys. 37, 893, 1959
33. V.P.Vertebnyi et al., Nuclear Data for Reactor, Proc. Conf., 1980 IAEA, Vienna; Report SN-26/37.
34. Barchuk I.F. et al., Yadernaja Physica, 1970, 11, 934.
35. V.F.Turchin, Slow Neutrons (Russ.), M., Atomizdat, 1963.
36. S.Menardi, R.Haas, W.Kley, Transmission of Thermal Neutrons through Large Single crystal of Bi at Liquid Nitrogen Temperature, Symposium on In. Scat. of Neutrons in Solids and Liquids, Chalk River 1962, Report S.M. 30/65.
37. R.D.Lowde, IAEA, Symposium, Vienna, 1960.

MONOENERGETIC NEUTRONS FROM THE $^{45}Sc(p,n)^{45}Ti$ REACTION

M COSACK, H LESIECKI
Physikalisch-Technische Bundesanstalt,
Braunschweig, Federal Republic of Germany

J B HUNT
Division of Radiation Science and Acoustics,
National Physical Laboratory,
Teddington, Middlesex,
United Kingdom

Abstract

The $^{45}Sc(p,n)^{45}Ti$ reaction was investigated with good energy resolution by a DC-beam method and the time-of-flight technique at both PTB and NPL. A number of isolated resonances were found in the energy region from 8 to 40 keV. The energy width of the levels is well below 1 keV (FWHM). The reaction was used for the calibration of instruments in the keV region.

Introduction

Monoenergetic neutron sources in the low keV region are needed for the calibration of radiation protection instruments. Several methods of neutron production have been used for this purpose, e.g. the radionuclide neutron source $SbBe(\gamma,n)$[1], reactor filtered neutron beams[2] and nuclear reactions induced by charged particles[3]. The $^{45}Sc(p,n)^{45}Ti$ reaction appeared especially suitable[4] - [7] as scandium is monoisotopic, the targets have good stability, the cross section is comparatively large and changes little with incident proton energy. The reaction threshold at 2.908 MeV can easily be reached with small particle accelerators. Measurements using this neutron source led to difficulties which made a thorough investigation necessary. The quantity of interest in connection with neutron sources is the

neutron yield, Y, of the target, which is the quotient of dN by $d\Omega$, where dN is the number of neutrons propagating in a specified direction within the solid angle $d\Omega$

$$Y = \frac{dN}{d\Omega}$$

The spectral neutron yield, Y_E, is the quotient dY by dE, where dY is the increment of neutron yield in the energy interval between E and E + dE

$$Y_E = \frac{dY}{dE}$$

Experimental Method

The spectral neutron yield, Y_E, of the $^{45}Sc(p,n)^{45}Ti$ reaction has been determined as a function of the incident proton beam energy using both conventional DC beam and time-of-flight techniques. For the DC-beam measurements, the charged particle beam from the Van de Graaff accelerator (HVEC, KN 3750) had an energy resolution of 2 keV (FWHM). Scandium metal targets with a mass per area of 5 $\mu g/cm^2$ were used, corresponding to an energy loss of about 0.3 keV for incident proton energies near the reaction threshold of 2.908 MeV. The proton energy was increased in steps of 0.3 keV. The neutron fluences were measured with two previously calibrated long counters[8)9)] (NPL, DePangher). The spectral neutron yield determined with the NPL long counter at 0° and 60° with respect to the direction of the charged particle beam is shown in Fig. 1. The effects of the scattered neutron background were taken into account by placing a shadow cone between the target and the detector. Other spurious neutrons were identified by blank target measurements. The structure observed could be reproduced in different measurements with other targets giving the same resonance energies within 1.5 keV. The line width of different measurements depended upon the adjustment of the accelerator's voltage stabilizer.

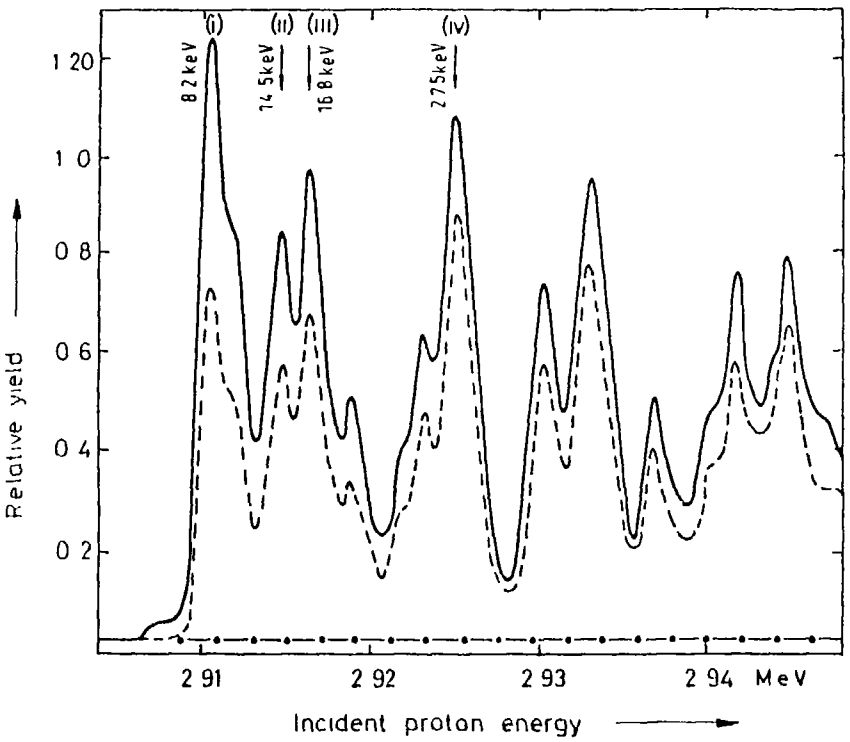

Fig. 1 Relative spectral neutron yield as a function of proton energy for a thin target at angles of 0° (——) and 60° (- - -) with respect to the incoming proton beam measured with a long counter. The indicated background was determined with a shadow cone and by reducing the proton energy below the reaction threshold.

Another confirmation of the spectral neutron yield was obtained by the neutron time-of-flight technique with a pulsed charged particle beam. The klystron bunching system of the Van de Graaff accelerator was operated at a pulse repetition rate of $6.25 \cdot 10^5$ s^{-1} with an approximate pulse width of 2 ns. When a thick target (mass per area about 0.5 mg/cm^2) on a tantalum backing (0.5 mm thick)

was used the slowing-down of the charged particles caused the excitation of the spectral yield over a correspondingly broad energy range. The resulting neutron groups could easily be separated by time-of-flight measurements. The detectors were two lithium glass scintillators (Nuclear Enterprises, NE 912, 3 mm thick, 38 mm in diameter, and 6 mm thick, 25 mm in diameter) coupled to photomultipliers (Philips, PM 2232 B and XP 2020). An overall time resolution of the system of 3.5 ns (FWHM) was achieved. The flight paths were 0.3 m to 1.2 m. The background in the time-of-flight measurements was determined by shadow cone measurements and by reducing the proton energy below the threshold for neutron production. Pulse height discrimination reduced the detection of photon radiation considerably. The spectral neutron yield obtained at a distance of 1.2 m and an angle of 0° to the direction of the incoming protons is shown in Fig. 2. The spectral neutron yields measured by the two methods agree very well, and exhibit very pronounced resonances with very little neutron production between the lines. The independent determination of the neutron energies gave differences smaller than 0.1 keV for neutron energies below 20 keV, 0.5 keV at 27.4 keV, and 1.3 keV at higher energies. The neutron energies, at 0°, of the observed peaks, based upon the time-of-flight measurements, are 8.15, 9.1, 10.9, 13.2, 14.4, 16.7, 19.4, 20.2, 23.3, 25.2, 27.4, 33.4 and 36.7 keV. Three isolated neutron groups with energies well suited for detector calibrations are at 8.15 keV, 16.7 keV and 27.4 keV. With these three resonances the neutron energy can be continuously varied from 2 keV to 27.4 keV measuring at different neutron emission angles from 0° to 80°. Neutrons with an energy of 0.5 keV can be produced at an angle of 120° using the first neutron group with an energy of 8.15 keV at 0°.

The angular distributions of these main resonances have been determined using both the long counters and the lithium glass scintillators. From the time-of-flight measurements, the change of neutron energy with the emission angle was consistent with the kinematics calculated for the individual levels. The measurements

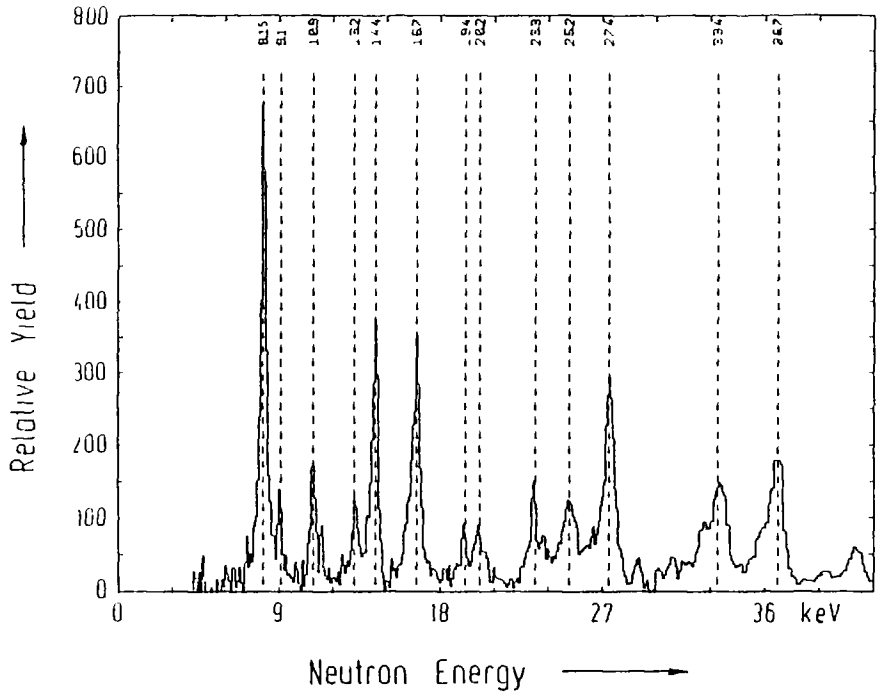

Fig. 2 Relative spectral neutron yield from a thick target measured by the time-of-flight technique using a lithium glass scintillator. The measurement was at 0°; background has been subtracted.

indicate that the angular distributions are isotropic in the centre of mass frame.

The neutron yields from the individual resonances have been determined with a calibrated DePangher long counter. Typical values for a scandium target (10 $\mu g/cm^2$) bombarded by a proton

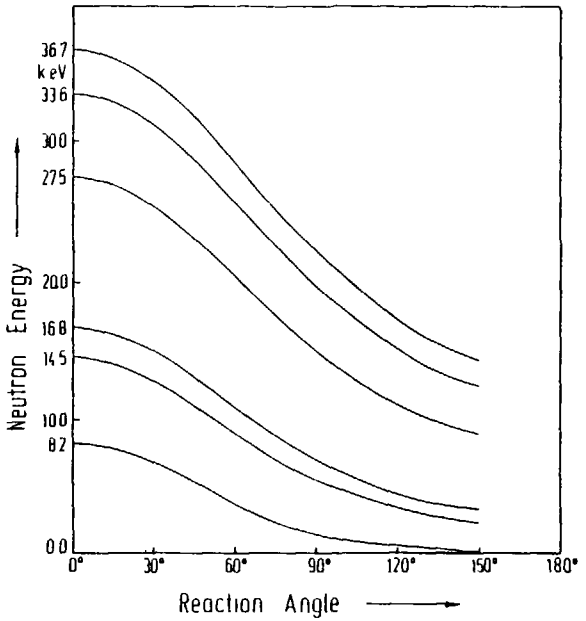

Fig. 3 Neutron energy as a function of emission angle for the most prominent neutron groups. The emission angle is the angle between the directions of the outgoing neutron and the incoming proton.

beam of 50 μA, vary from about $3 \cdot 10^4$ sr^{-1} s^{-1} at 2 keV to about 10^5 sr^{-1} s^{-1} at 8.15 keV and 27.4 keV. It should be kept in mind that several levels may be excited with thicker targets, but this may be insignificant if the quantity to be measured is a smooth function of energy.

Acknowledgements

The authors wish to express their gratitude to the accelerator operating staff, in particular to Dr. H. Schölermann and Dipl.-Ing. H. Strzelczyk, for their support. The presentation of the paper at this meeting by Dr. R. Böttger is gratefully acknowledged.

References

1.) T.B. Ryves, J.C. Robertson, J. Nucl. Energy, 25 (1971) 557
2.) J.R. Harvey, A.J. Mill, Fourth Symp. on Neutron Dosimetry EUR 7448 EN I (1981) 431 - 441
3.) J.B. Marion, Fast Neutron Physics, I, Intersc. Publishers Inc., New York (1960)
4.) R.M. Brugger, T.W. Bonner, J.B. Marion, Phys. Rev. 100 (1955) 84
5.) D.W.O. Rogers, Nucl. Instr. and Meth. 142 (1977) 475 - 478
6.) M. Cosack, H. Lesiecki, J.B. Hunt, Fifth Symp. on Neutron Dosimetry, Neuherberg 1984, CEC, EUR 9762 EN (1985) 597
7.) J.B. Hunt, M. Cosack, H. Lesiecki, Fifth Symp. on Neutron Dosimetry, Neuherberg 1984, CEC, EUR 9762 EN (1985) 607
8.) J.B. Hunt, NPL Report RS5, Nat. Phys. Lab., UK, (1976)
9.) J. DePangher, L. Nichols, Report BNWL-260, Pac. North West Lab., Richland, Washington (1976)

274 TARGET SCATTERING IN THE PRODUCTION OF MONOENERGETIC NEUTRONS AT ACCELERATORS

H. LESIECKI, M COSACK, B R L SIEBERT
Physikalisch-Technische Bundesanstalt,
Braunschweig, Federal Republic of Germany

Abstract

When monoenergetic neutrons are produced at accelerators, a contribution of neutrons scattered from the target backing and the vacuum chamber must be taken into account. Monte Carlo calculations and time-of-flight experiments were carried out for the quantitative determination of the spectral distribution of the fluences of scattered neutrons

Introduction

Monoenergetic neutrons are most frequently produced via nuclear reactions with charged particles from accelerators The thin layer of target material is usually supported by a backing and surrounded by a vacuum chamber As this material is close to the spot of neutron production, it gives, in particular, rise to neutron scattering. This results in a non negligible contribution of low energy neutrons[1)2)3)]

It is not possible to separate the primary and these scattered neutrons by shadow cone measurements or variation of the target-to-detector distance. The importance of this background may be enhanced by the dependence on energy of the cross section or the response under study. The influence of target-scattered neutrons appeared to be quite important in recent international inter-comparisons of fluence measurements[4)5)]. In order to obtain reliable correction factors, a Monte Carlo code has been written which allows the spectrum of primary and secondary neutrons to be computed by simulating the target assembly. Experiments were performed to test the reliability of the computer code. In the following we will confine ourselves to a few[6)] standard monoenergetic neutron fields with typical target assemblies.

Monte Carlo Calculation

The Monte Carlo simulation of the neutron production and neutron scattering within the target assembly is similar to the calculations performed by Ryves[1)]. In addition we calculated the time-of-flight distribution of neutrons as seen by a lithium glass detector to make a comparison with measurements possible. The following effects are considered in the Monte Carlo simulation:

- energy loss of charged particles in the target material prior to neutron production,
- angular distribution of the neutron producing reaction,
- attenuation of primary and secondary neutrons in the target construction;
- angular distribution of neutrons from reactions with the material of the target construction,
- lithium glass detector, response of which is taken to be proportional to the cross section of the reaction $^{6}Li(n,t)^{4}He$ in a first order approximation with multiple scattering being neglected,
- geometry of backing, mounting ring and tube of vacuum chamber.

The nuclear data were taken from Liskien and Paulsen[7)] for the neutron producing reaction and from ENDF/B[8)] for the other cross sections.

Comparison with Experiment and Results

The spectral distributions of neutron fluences were measured with the neutron time-of-flight technique employing the pulsed particle beam of the Van de Graaff accelerator and a lithium glass scintillation detector. The Van de Graaff pulsing was described earlier[9)]. The scintillation detector consisted of a lithium glass scintillator NE 912 (Nuclear Enterprise) of the following

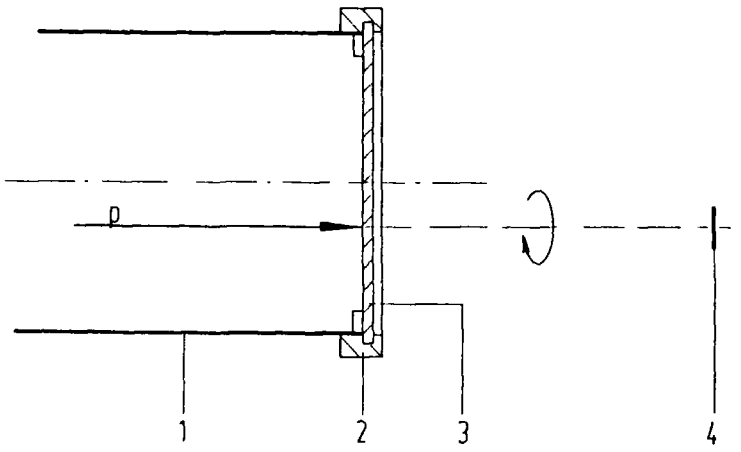

Fig. 1 Target assembly as considered in the Monte Carlo calculation. (1 - Tube of vacuum chamber; 2 - Mounting ring of target backing; 3 - Target backing; 4 - Detector)

dimensions: diameter: 2.5 cm, thickness: 0.6 cm; it was coupled to a photomultiplier of the Philips XP 2020 type. This system had a pulse height resolution of 20 % FWHM for the peak related to thermal neutrons. The time resolution of the system comprising essentially the charged particle beam pulse width and the detector time resolution was typically 3 ns FWHM, as could be observed in the γ-ray peak of the time-of-flight spectra. For neutrons an additional uncertainty in time was introduced by the primary charged particle energy distribution, the energy loss of the charged particles in the target layer, the kinematic broadening of the neutron energy distribution with solid angle and the time-of-flight of neutrons in the scintillator. These phenomena deteriorated the time resolution considerably.

The contribution of photon radiation in the time-of-flight spectra was reduced by selecting only pulse heights in the detector spectrum which corresponded to neutrons. Scattered neutron background from air, from the walls of the building and other equipment was determined by shadow cone measurements. This background was found to be uniformly distributed in the time-of-flight spectra.

A comparison of a measurement and the corresponding calculation is given in Fig. 2. The Li(p,n)Be reaction was used with a proton energy of 2.04 MeV, a target with a mass per area of lithium of 120 $\mu g/cm^2$ and a backing of tantalum, 1 mm thick. The mean primary neutron energy was 144 keV at a reaction angle of 0°. The target to detector distance was 1.5 m, and the time resolution 0.8 ns/channel. While the main peak in the experiment is much broader since some effects had not been implemented in the Monte Carlo calculation, the region of lower-energy scattered neutrons is reproduced very well. The agreement of the measurements with calculations at other energies was of varying quality. The main reasons for the discrepancies are:

- the response of the lithium glass scintillator was assumed to follow the Li(n,t)^{4}He cross section as a function of energy, although deviations had to be expected[10], especially at resonances of oxygen or silicon,
- neutron scattering in the vicinity of the scintillator has not been considered,
- the material at the target was assumed to consist only of pure elements such as: Ag, Al, Fe, Ta
- the geometry was not realistically simulated in all details,
- some of the neutron-producing reaction cross sections and the neutron reaction cross sections were affected by large uncertainties.

The calculated energy spectra are shown in Figs. 3, 4, 5, 6 for neutron energies of 0.144, 0.25, 0.57 and 1.2 MeV, respectively. Target configurations most frequently used in this laboratory and

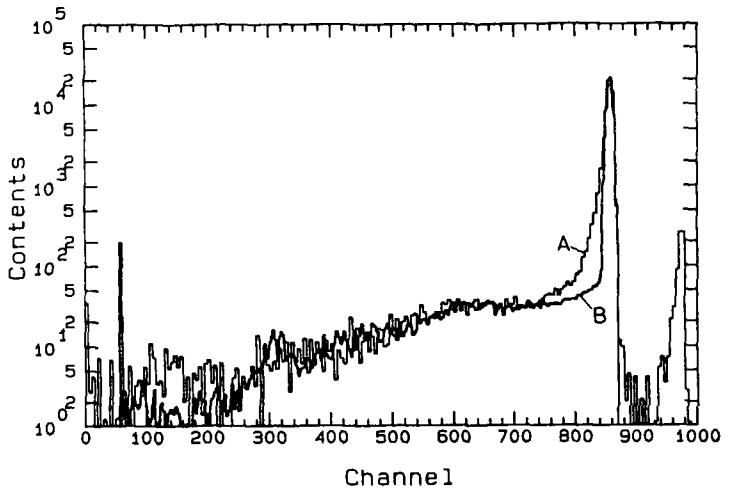

Fig. 2 Time-of-flight spectra for neutron energy of 144 keV
A - measured with lithium glass detector
B - simulation by Monte Carlo code

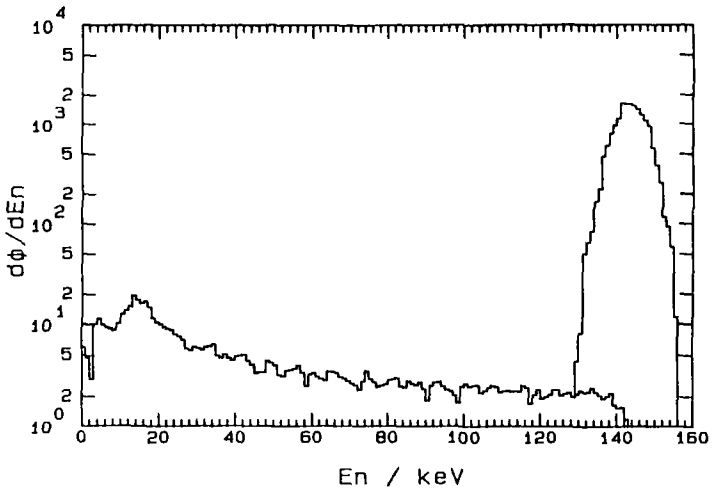

Fig. 3 Calculated spectral distribution of neutron fluence for E_n = 144 keV, lithium (50 µg/cm^2) on backing of tantalum (1 mm)

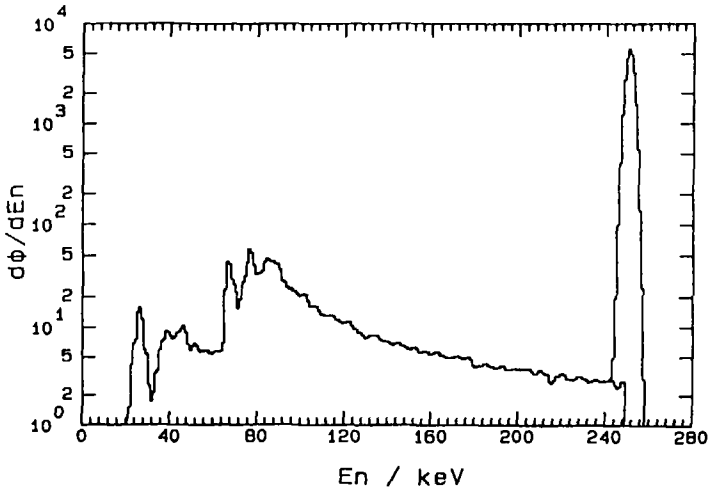

Fig. 4 Calculated spectral distribution of neutron fluence for E_n = 250 keV, lithium (50 µg/cm^2) on backing of tantalum (1 mm)

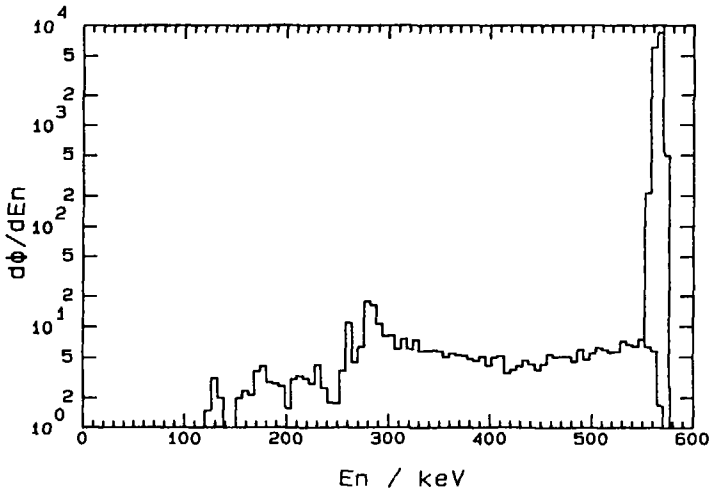

Fig. 5 Calculated spectral distribution of neutron fluence for E_n = 570 keV, lithium (50 µg/cm^2) on backing of tantalum (1 mm)

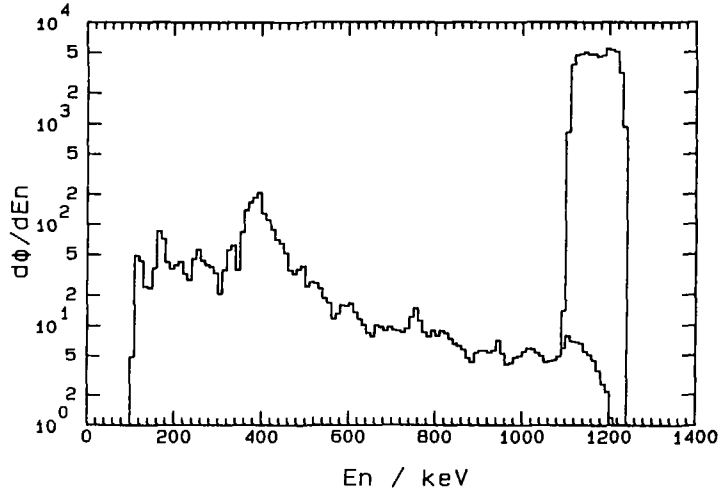

Fig. 6 Calculated spectral distribution of neutron fluence for E_n = 1.2 MeV, titanium-tritium (0.9 µg/cm^2) on backing of silver (1 mm)

typical of neutron production were selected. The results of these calculations are summarized in the table, which gives the relative contributions of the spectral distribution of neutron fluences in different energy regions.

The change of the scattering effect with the target backing thickness is illustrated in Fig. 7. As can be expected from solid angle considerations and the attenuation of neutrons, the target scattering is not proportional to the target thickness. This must be taken into account if the target scattering effect is measured by mounting additional discs to the target backing.

Further investigations are planned which may help to reduce uncertainties in the knowledge of fields of monoenergetic neutrons.

Table

E_n keV	Back.-Mat.	BG %	1. Region E_n keV	1. Region BG %	2. Region E_n keV	2. Region BG %	3. Region E_n keV	3. Region BG %	4. Region E_n keV	4. Region BG %
144	Ta/1mm	3.72	0 -36	1.97	36-72	0.77	72-108	0.54	108-144	0.44
250	Ta/1mm	9.64	0 -62	1.15	62-125	6.17	125-187	1.53	187-250	0.79
565	Ta/1mm	2.41	0-141	0.05	141-282	0.59	282-423	0.97	423-565	0.83
1200	Ag/1mm	5.35	0-300	1.41	300-600	3.20	600-900	0.47	900-1200	0.27

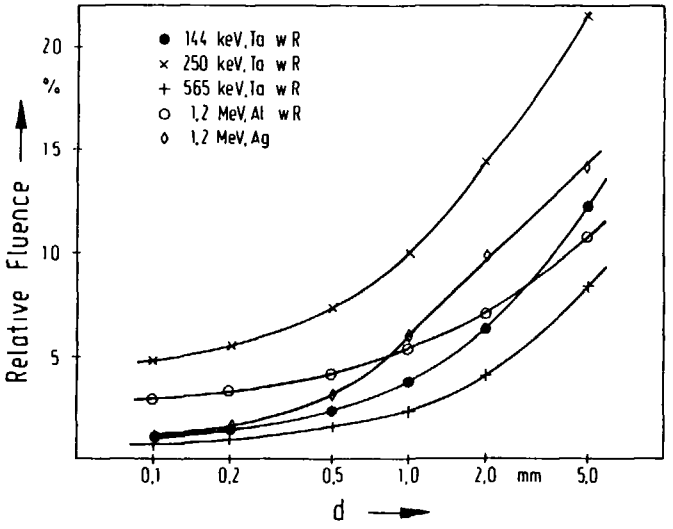

Fig. 7 Contribution of target scattering neutron background as function of backing thickness for different energies and target mountings (w.R.: is with a scraw cap mounting, otherwise soldered)

Acknowledgements

The authors wish to express their gratitude to the accelerator operating staff, in particular to Dr. H. Scholermann and Dipl.-Ing. H. Strzelczyk, for their support. The presentation of the paper at this meeting by Dr. R. Bottger is gratefully acknowledged.

References

1) T.B. Ryves: Calculations on the Scattering of keV Neutrons from the $^{7}Li(p,n)^{7}Be$ Reaction in a Typical Target Assembly. Journ. of Nucl. Energy 27 (1973) 365
2) H. Lesiecki, M. Cosack, B.R.L. Siebert: Influence of Target-Scattered Neutrons on Cross Section Measurements. Proc. Adv. Group Meeting, Geel 1984, IAEA-TECDOC-335 (1985) 144
3) P. Andersson, R. Zorro, I. Bergquist: Neutron Capture Cross-Section Measurements for ^{197}Au and ^{115}In in the Energy Region 2.0 - 7.7 MeV using the Activation Technique. ibidem, p. 143
4) H. Liskien: International Fluence-Rate Intercomparison for 2.5 MeV and 5.0 MeV Neutrons. Metrologia 20 (1984) 55 - 59
5) H. Lesiecki, H. Cosack: International Intercomparison of Fluence of Fast Neutrons using $^{115}In(n,\gamma)$ Activation. PTB-ND-25 (1985)
6) M. Cosack: Neutron Energies Selected by ISO for the Calibration of Radiation Protection Instruments. Proc. Adv. Group Meeting, Geel 1984, IAEA-TECDOC-335 (1985) 388
7) H. Liskien, A. Paulsen: Neutron Production Cross Sections. Nucl. Data Tables 11 (1973) 569 and Atomic Data Tables 15 (1975) 57
8) D. Garber et al.: ENDF-102, BNL-NCG-50496, Brookhaven (1975)
9) H.J. Brede et al.: The Braunschweig Accelerator Facility for Fast Neutron Research. Nucl. Instr. and Meth. 169 (1980) 349
10) G.F. Lamaze: Special Problems with ^{6}Li-glasses. Proc. Spec. Symp. Neutron Standards and Application, NBS Special Publ. 493 (1977) 37

THE Be(d,n) SOURCE AT A MODEST FACILITY*

A.B. SMITH, D.L. SMITH, J.F. WHALEN
Applied Physics Division,
Argonne National Laboratory,
Argonne, Illinois,
United States of America

Abstract

Source characterization for deuteron energies less than 8 MeV is discussed including: intensity, spectrum and angular distributions. Pulsed and steady-state applications of the source to the acquisition of fast-neutron data are illustrated by energy-averaged neutron total cross-section and spectrum-averaged activation cross-section measurements. Source utilization, measurement techniques, and experimental results are described with attention to self-shielding effects, background suppression and specification of uncertainties. These illustrations are extrapolated to broader-scope studies, taking advantage of the high fast-neutron intensities. The present and future potential is determined more by detection capability than by source properties.

I. INTRODUCTION

There are a number of basic and applied fast-neutron problems that require a fast-neutron source of high intensity. Such sources are available at large machines, but they often do not have the character or utility to be rapidly responsive to the needs. It is our objective to show that the Be(d,n) source at a modest facility can meet many of these needs effectively and at low cost. Illustrative applications are: i) pulsed white-source microscopic neutron-cross-section measurements such as neutron total, (n:n',gamma) and radiative-capture studies, ii) the production of well-characterized standard neutron fields, iii) the determination of activation processes in integral fields, and as differential cross sections using unfolding techniques, and iv) benchmark integral studies such as tests of fusion blankets and fast-reactor neutronics.

* This work was supported by the US Department of Energy

II. CHARACTERIZATION OF THE SOURCE

The Q-value of the Be-9(d,n)B-10 reaction is +4.362 MeV (1). The predominant mechanism for exciting low-lying levels in B-10 via deuterons on Be is the stripping reaction. Excitation of the higher-excited B-10 states involves a combination of direct and compound-nucleus mechanisms. When a beryllium target thick enough to stop the incident deuterons is used, most of the neutrons are emitted in a broad distribution with an average energy approximately 40% that of the incident deuteron. In addition, there is a lower-yield, higher-energy component extending to the kinematically-allowed neutron-energy limit. This spectral shape is illustrated in Fig. 1. The neutron emission is generally peaked forward with the anisotropy governed by the angular momentum of the (d,n) processes for the particular levels involved. The high-energy component is dominated by contributions from the first few levels in B-10. The respective stripping reactions proceed primarily by ℓ=1 transitions (excepting only the 4.77-MeV, ℓ greater than 2, and 5.11-MeV, ℓ=0, levels) (2). The predominance of ℓ greater than 0 transitions leads to anisotropic high-energy distributions with smaller yields at zero degrees than at angles away from zero. The energy dependencies of such angular distributions are illustrated in Fig. 2. These anisotropic spectral distributions can

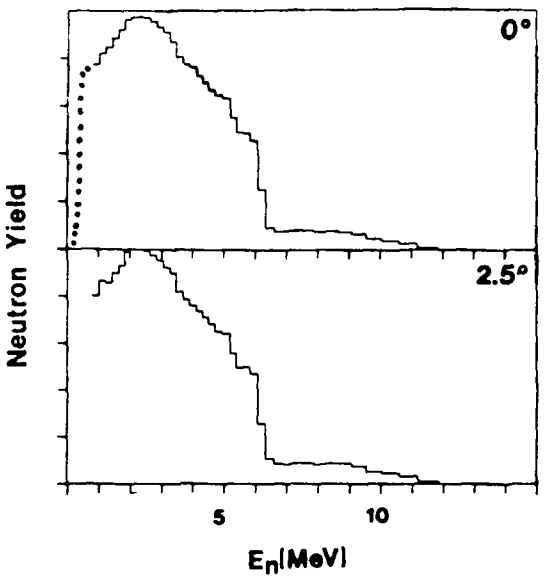

Fig. 1. (up) Forward-Angle Spectra Resulting from 7 MeV Deuterons Incident on a Thick Be Target.

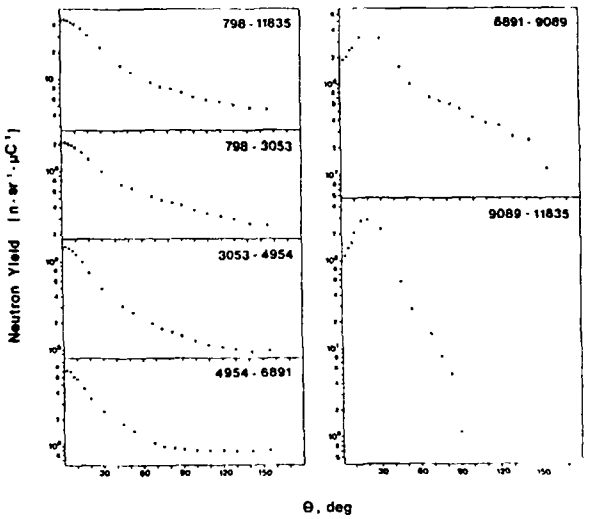

Fig. 2. (up) Meutron Angular Distributions Resulting from 7 MeV Deuterons Incident on a Thick Be Target.

produce important consequences in some applications. The neutron yield is very intense. For example, at a 7 MeV deuteron energy approximately 3 × 10**9 neutrons per steradian-microcoulomb (3) are emitted near zero degrees. At many installations, the maximum intensity is primarily dictated by target power-handling capabilities. Some proposed special-purpose facilities have projected yields as high as 1 × 10**16 (4), but such estimates involve very specialized targets and accelerators.

First attempts to predict the spectrum from basic principles were semi-empirical (5). Lately, DWBA theory has been used, correlated with thin-target measurements (3). None of these fundamental approaches is a substitute for direct measurement of thick-target spectra. Detailed quantitative spectrum-mapping efforts have been systematically carried out at only a few lower energies, notably near 7 MeV (6,7). At CBNM, time-of-flight measurements were made using a liquid scintillator (6) and the results were reasonably consistent with integral Cu-63(n,alpha)Co-60 measurements (8). More recently, detailed data have been obtained at Argonne with the results shown in Figs. 1 and 2 (7). In this later work it was shown that the spectral angular distributions are an important consideration in activation-cross-section measurements. However, even with this new detail, consideration of activation responses in this spectrum, particularly comparisons of low- and high-threshold reaction rates, has raised questions concerning the spectral shape (13). Most of the reported

spectrum measurements have utilized time-of-flight techniques and calibrated organic scintillators to measure the velocity spectrum. The low-energy response of organic scintillators varies rapidly with energy, is difficult to determine with reliability, and can be unstable with time. Very recent measurements at Argonne employed time-of-flight methods, with approximately-flat response U-235 fission chambers as the neutron detectors, to give improved definition of the low-energy portion of the spectrum (9). It was found that at zero degrees the spectrum yield falls to essentially zero below approximately 200 keV (see Fig. 1). When this result is factored into the above-cited activation results, much better agreement is obtained between differential and Be-field measurements. These new results should be extended to higher energies using scintillation detectors, but they already give valued and long-sought after spectral definition.

III. ENERGY-AVERAGED FAST-NEUTRON TOTAL CROSS SECTIONS

Energy-averaged neutron total cross sections are the starting point for applications evaluations, and they are essential to the development of fundamental models. They have been measured for many years, most recently at large white-source facilities using time-of-flight techniques with pulsed beams. Despite this effort, disturbing discrepancies remain. In a number of cases, the experimental values are sparse, discrepant, and of poor quality. Self-shielding effects have distorted many results, and some of the evaluations leave much to be desired. An illustration of such problems is shown in Fig. 3A. A contemporary evaluation of Co (10) shows a great many fluctuations but an energy dependence inconsistent with physical behavior, for example as indicated by an optical model. The discrepancies are large (10-20% at a few MeV). In this particular example, all three of the above factors probably contributed to this discrepancy. It has long been evident that a systematic, precise and comprehensive study of energy-averaged total cross sections over the energy range from the unresolved resonance region to 20+ MeV is needed. The requirement is for "true" (as contrasted to the "observed") cross sections.

The Be(d,n) reaction can provide a very-intense pulsed-neutron source for energy-averaged total cross section measurements using modest deuteron energies. With flight paths of the order of tens of meters, relatively-good energy resolution can be realized using conservative pulse durations of approximately 1 nsec. This potential has been routinely exploited using the novel experimental arrangement shown in Fig. 4 (11). A small (several mm in diameter) and intense neutron beam is defined at the transmission samples by a collimator. Samples and a void are rapidly stepped through the beam. The samples may be quite small, e.g., separated isotopes, and a number of sample thicknesses may be used concurrently, making possible accurate corrections for self-shielding effects. A conventional scintillation detector, placed 10-30 m distant, provides energy resolutions of 0.1-0.03 nsec/m, sufficient for energy-averaged cross-section measurements. Background control is very good, with little gamma-ray "flash" and no high-energy-particle contamination, and the circuitry corrects for dead-time effects. Neutron detection is correlated with sample position using a digital computer which provides real-time

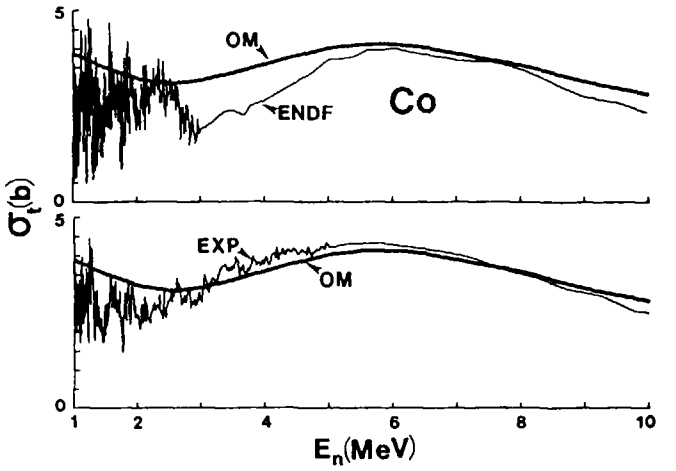

Fig. 3. Co Total Cross Sections. Up=Comarison of Evaluation and Optical-model calculation. Lower=Measured and Optical-model Results.

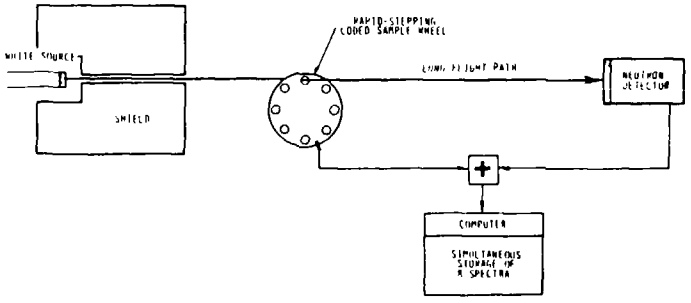

Fig. 4. Argonne Total-Cross-Section Apparatus

cross-section information. The result is the concurrent determination of the total cross sections of up to 8 samples in real time, with no requirement for beam monitoring, and with identical energy scales and resolutions.

Obviously, the total-cross-section measurements are self-normalizing. However, measurement fidelity is verified by the concurrent observation of the well-known carbon total cross sectons with results such as shown in Fig. 5. This illustration was obtained with a relatively-short flight path (11 m), and it does not have the resolution of the ENDF evaluation; nevertheless, the energy-average magnitudes and the energy scales are in good agreement. Results obtained over a wide range of the periodic table are illustrated in Fig. 6, where experimental corrections for self-shielding effects have been made using results obtained with various sample thicknesses. Fig. 7 extends the illustrative observations to the actinide region, where these particular results have led to major revisions of evaluated files (e.g., that of Pu-239). Another example of the resolution of discrepancies associated with evaluations and/or physical interpretations is the cobalt case of Fig. 3. The above methods can be extended to higher energies using composite Li and Be targets, and to lower energies using thick Li targets and protons beams, as illustrated in Fig. 7 (11).

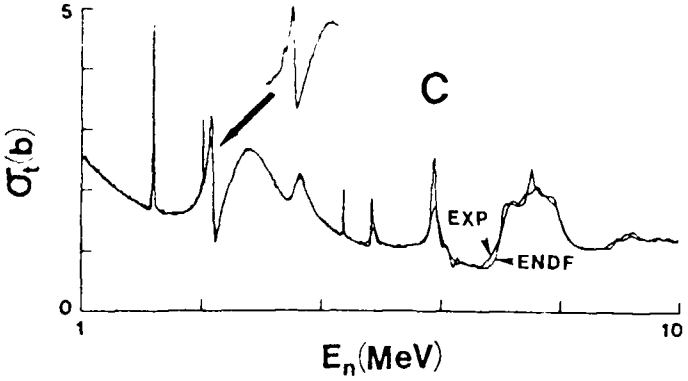

Fig. 5 Comparison of Measured and Evaluated Carbon Total Cross Sections.

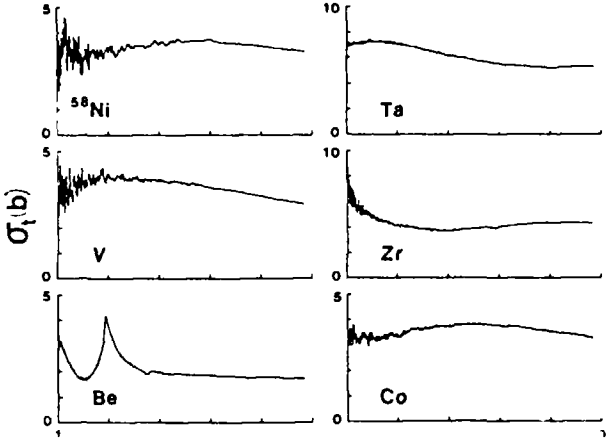

Fig. 6 Illustrative Neutron Total Cross Sections.

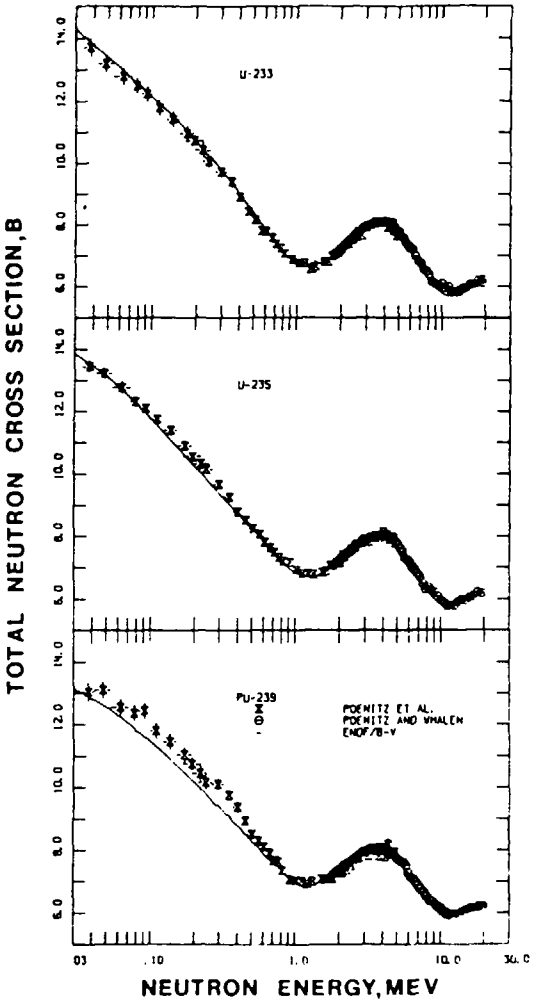

Fig. 7. Actinide Neutron Total Cross Sections.

The above results were obtained with flight paths of less than 12 m, yet they have adequate resolutions for the objective of determining precise energy-averaged total cross sections in the MeV energy range. Measurements have been made at 30 m (see carbon inset of Fig. 5), with commensurate resolution improvements. An important measurement problem is neutron intensity--too much intensity. Special instrumentation is required to make optimum use of the source at flight paths of 30 m or less. Alternatively, flight paths can be greatly extended, with consequent improvement in resolutions and the elimination of an annoying technical problem.

The essential point is that the high specific brightness of the Be(d,n) source in the MeV energy range makes a modest facility highly competitive in energy-averaged total cross section measurements and, indeed, such a facility has been a major source of such information.

IV. STANDARD FIELDS AND REFERENCE ACTIVATION CROSS SECTIONS

There is a need for intense benchmark fields for resolving existing activation cross-section discrepancies and for studying low-yield and long-lived reactions not otherwise accessible. The Be(d,n) reaction is ideal for providing such fields for it has the advantages of high intensity and, contrasted to fixed spectra such as Cf-252, the capability to be tailored to the needs of the particular investigation. These are attractive attributes. Many of the most-needed fusion activation data may well not be determined in any other manner. In some cases data are obtained at isolated energies, e.g., 14 MeV, and they are then model-extrapolated over ride energy ranges. Such extrapolations can easily differ by an order of magnitude. Measurements in reference fields can give considerable guidance to such model extrapolations. Even "well determined" activation cross sections can (and should) be validated in standard reference fields.

The high yield of the Be(d,n) source is such that special facilities must be established to assure biologically tolerable environments for personnel. Such a facility has been constructed at Argonne, providing a very-heavily-shielded cavity within which accurately-calibrated neutron fields can be is produced (12). Particular attention was given to the reduction of room-return effects. The field can be varied to reasonably represent the environments encountered in "hard" fast reactors and fusion blankets. The target assemblies are low mass, scattering only a few percent of the emitted neutrons, and yet are capable of dissipating several hundred watts of beam power. Cavity walls are lined with polyethelene and cadmium to reduce neutron room return. Measurements using U-235 and U-238 (threshold) fission detectors indicate that the return of neutrons above 1 MeV in the cave is relatively small (e.g., less than 0.1% of the direct yield 10 cm from the target). Below 1 MeV the room-return fraction can increase to 10% at 10 cm, but that is of little concern in the threshold measurements for which the facility was primarily designed. The general concept of this facility is illustrated in Fig. 8.

The above facility is presently being used in spectral characterizations and integral cross-section measurements for a number of prominent dosimetry and radiation-damage activation processes with a 7-MeV incident deuteron beam. The objectives are: i) to establish a well-known benchmark field, ii) to explore applications of the field, and iii) to develop new and innovative methods for the provision of nuclear data. The immediate problem is mathematical specification of the benchmark spectrum consistent with the measured spectrum and the experimentally-determined responses of well-known activation cross sections. The next step is the determination of the neutron-emission spectra for a number of additional incident-deuteron energies, using time-of-flight techniques with fission and

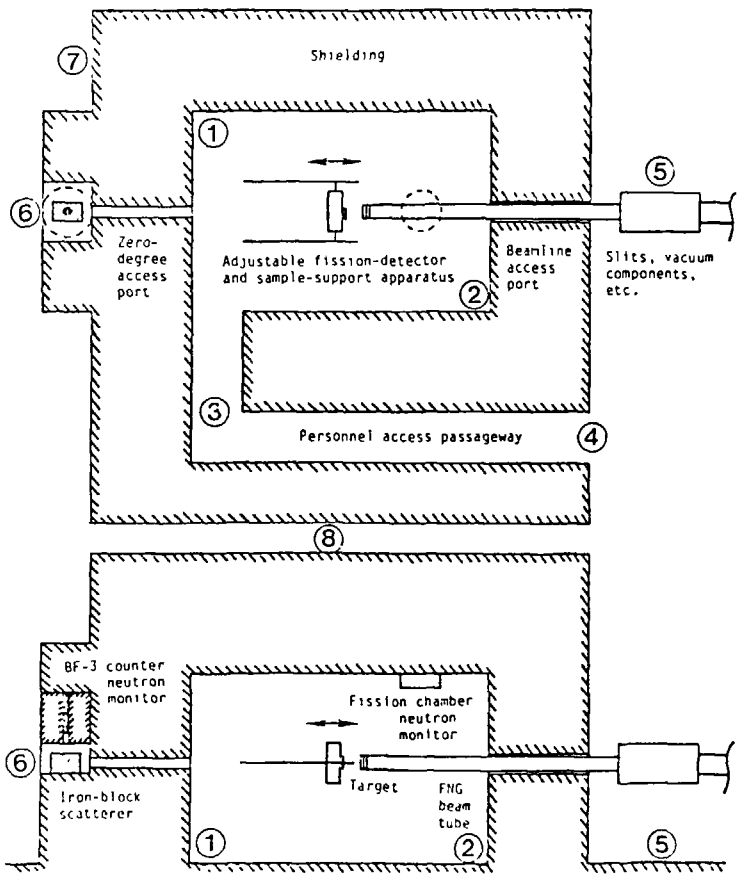

Fig. 8. Facility for the Production of Intense Be(d,n) fields.

scintillation detectors. Complete covariance information is also sought. Concurrently, activation cross sections for low-yield reactions in high-atomic-number elements are to be measured, e.g., for Ta, W and Re. Such cross sections are very small, but are of interest in high-temperature applications.

Integral tests of differential data for the reactions Li-7(n;n',t)He-4, Al-27(n,p)Mg-27, Al-27(n,alpha)Na-24, Ni-58(n,p)Co-58 and Ni-60(n,p)Co-60 relative to U-238(n,f) have been carried out to good precisions (13). These results are indicated in Fig. 9. Some interesting conclusions have emerged from this work: i) It was observed that the high threshold reactions (all other than Ni-58 and U-238) are internally consistent, providing a reasonable test of both the differential cross sections and the high-energy portion of the Be(d,n) field. ii) There is an apparent discrepancy between low- to high-energy threshold C/E comparisons. This suggests some problems with the Be(d,n) spectrum representation previously reported in the literature (6). However, as pointed out above, a very recent Be-spectrum measurement at Argonne with a U-235 fission chamber has led to a representation that reduces this discrepancy considerably. iii) There appears to be somewhat of a problem with the Ni-58(n,p) reaction. It is not clear at present whether this is associated with the differential or integral data, or both. Additional measurements have also been made for the structural materials, e.g., Nb, Fe, Cu and Al and these data are being analyzed.

It is anticipated that integral tests of activation cross sections in the Be spectrum will provide a useful supplement to the extensive body of 14 MeV experimental cross section data and to nuclear-model calculations in the threshold region, as mentioned above. These investigations extend over the full neutron-spectrum range encountered in fusion-energy applications. It is often said that 14-MeV measurements and model calculations are adequate for many applications, but experience indicates that this is not clearly so in the threshold region.

V. FUTURE POTENTIAL

As noted above, the intensity of the source is too great to fully utilize its capabilities in total-cross-section measurements at relatively-short flight paths, using conventional circuitry and detection equipment. Therefore, flight paths are being extended to 50+ meters and will thereby provide resolutions of 0.02 nsec/m or better, even with conservative 1-nsec bursts. Large white-source facilities have nominally (though not exclusively) employed 5-10 nsec bursts in such measurements, therefore they must have 250-500 m flight paths for equivalent performance. Moreover, the 1 nsec burst durations used in the present work can be reduced by factors of 2-4 without undue trouble (14). Thus, the potential for performing energy-averaged neutron-total-cross-section measurements using the Be(d,n) source at modest facilities is good and can be realized at low cost. It is not a new concept as some of the most comprehensive and most reliable data of that type were obtained more than 15 years ago using a very modest Van de Graaff accelerator (15). However, it is a concept limited to higher energies and should not be construed as a capability for low-energy resonance studies.

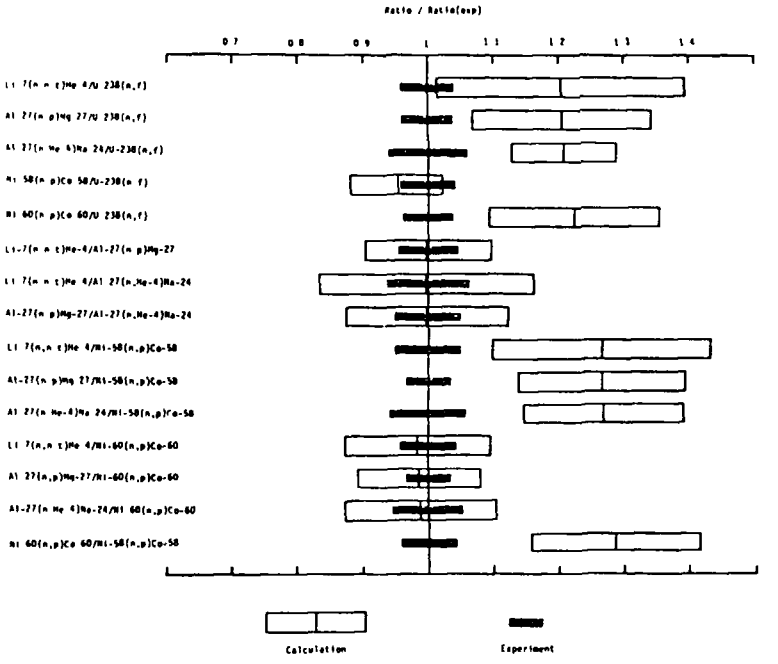

Fig. 9. Relative Activities in the Be(d,n) Field Induced by 7 MeV Deuterons.

Effective access to the difficult 8-14 MeV neutron-energy region remains a problem in many monoenergetic measurements. The Be(d,n) source provides a vehicle for reaching this region at a modest facility, particularly so if supplemented with higher positive Q-value reactions such as the Li-7(d,n)Be-8 process (as was used in some of the above total cross section measurements). An important aspect of this approach is the ability to combine integral and differential data determinations. A statistical method for unfolding integral neutron-reaction data to obtain differential information has been proposed (16), and initial use of the methods in tritium production studies (17) is encouraging. An essential requirement for the application of statistical unfolding methods is a complete covariance specification of uncertainties for both the integral data and the spectrum representation. As noted above, a goal of the Argonne program is the development of such information for the Be(d,n) spectrum for deuteron energies up to 7.5 MeV.

Benchmark integral studies remain an essential test for microscopic data bases. Accelerator-based fields will play an increasing role in such studies as fission-reactor "physics" integral experiments become sparse and interest in fusion-energy grows. Their value is illustrated by the 14-MeV pulsed-sphere program at Lawrence Livermore Laboratory (18). The high intensities, and the ability to vary the spectral distribution obtained with the Be(d,n) reaction, make this source very attractive for integral studies supporting fusion- and fission-energy development. As noted, the source spectrum can be tailored to represent very "hard" fission reactors or fusion blankets. In all such work the characterization of the spectral- and angular-dependence of the source is important. A program of such measurements is in progress at Argonne, with the initial objective of testing Be as a fusion-blanket multiplier.

With the intensity and spectral distribution of the Be(d,n) source, it is interesting to consider the potential for alternate types of differential-data measurements. For example, time resolutions of a few nsec obtainable with intrinsic germanium detectors could be exploited to make precise measurements of (n;n',gamma) cross sections for applied and basic purposes, and the energies are high enough so that there is a potential for examining the decay properties of transmutted nuclei (19). Another option is the study of neutron-induced prompt-charged-particle production using timing techniques to determine the incident neutron energies. More generally, the source is, at a modest facility, competitive for white-source measurements at higher energies.

V. SUMMARY REMARK

One of the outstanding limitations of neutron physics remains source intensity. In the Be(d,n)B-10 reaction, nature has provided an intense source of neutrons which appears to be relatively easy to control and characterize. Thus far efforts to do so have been modest, and the potential of this source is far from fully exploited. Doing so should be a priority activity of fast-neutron physicists during the coming decade.

References

1. J. K. Tuli, "Nuclear Wallet Cards", Brookhaven National Laboratory (1985).
2. F. Ajzenberg-Selove, Nucl. Phys. A413 1 (1984).
3. K. A. Weaver et al., Nucl. Sci. Eng. 52 35 (1973).
4. P. Grand et al., Nucl. Technol. 29 327 (1976).
5. R. Serber, Phys. Rev. 72 1008 (1947).
6. A. Crametz et al., Nuclear Data for Science and Technology, ed. K. Boeckhoff, D. Reidel Pub. Co., Dordrecht, Holland, p-902 (1983).
7. D. L. Smith et al., Argonne Report ANL/NDM-90 (1985).
8. H. Liskien et al., ibid. ref. 8, p-409.
9. D. L. Smith and J. W. Meadows, (to be published).
10. ENDF Summary Documentation, compiled by R. Kinsey, ENDF-201, 3rd Ed., Brookhaven National Laboratory (1979).
11. W. P. Poenitz et al., Argonne Report ANL/NDM-80 (1983).
12. D. L. Smith and J. W. Meadows, Argonne Report ANL/NDM-95 (1986).
13. D. L. Smith et al., Argonne Report ANL/NDM-93 (1985).
14. A. Crametz et al., CBNM Annual Report, NEANDC(E) 262"U" (1986).
15. D. G. Foster and D. W. Glasgow, Phys. Rev. C3 576 (1971).
16. D. L. Smith, Argonne Report ANL/NDM-77 (1982).
17. R. Woelfe et al., Nucl. Sci. Eng. 91 162 (1985).
18. C. Wong et al., Lawrence Livermore Report UCRL-51144, Rev. II (1971).
19. D. C. Larson, Proc. Conf. on Nucl. Data for Basic and Applied Sci., Santa Fe, NM (1985).

UPDATING SURVEY OF SOME LESS COMMON FAST NEUTRON SOURCES: $^{9}Be(p,n)^{9}B$, $^{11}B(p,n)^{11}C$, $^{51}V(p,n)^{51}Cr$ AND $^{9}Be(\alpha,n)^{12}C$

M DROSG
Institut fur Experimentalphysik,
University of Vienna,
Vienna, Austria

Abstract

Production of fast neutrons by the reactions $^{9}Be(p,n)^{9}B$, $^{11}B(p,n)^{11}C$, $^{51}V(p,n)^{51}Cr$ and $^{9}Be(\alpha,n)^{12}C$ is surveyed with an upper neutron energy limit of about 30 MeV More recent cross section measurements are included into the data base and their impact on the results of previous reviews is investigated Besides the use of $^{1}H(^{11}B,n)^{11}C$ as a monoenergetic source for 11.4 MeV neutrons and as a two-line source between 11.9 and 20.6 MeV is discussed.

I. INTRODUCTION

In most cases fast monoenergetic neutrons are produced by charged particle reactions among the hydrogen isotopes[1]. Other common sources are $^{7}Li(p,n)^{7}Be$, $^{9}Be(d,n)$ and $^{45}Sc(p,n)^{45}Ti$[2-4].
In this paper some less common sources are reviewed. For $^{9}Be(p,n)^{9}B$ and $^{51}V(p,n)^{51}Cr$ this is an updating of a previous review[5], for the others it is a survey of recent experimental results.

II. PRESENT STATUS

The sources dealt with in this paper have quite different applications like
- "monoenergetic" neutron production at higher energies (e.g. p-^{9}Be)
- monoenergetic neutron production at lower energies (e.g. p-^{51}V) and
- thick target "white" neutron production (e.g. p-^{9}Be).

They have little in common except that most of them are (p,n) reactions. As pointed out in the companion paper[1] the exchange of projectile and target nuclei often results in improved source properties. Therefore one can expect that in the near future (as soon as bunched heavy ion sources of enough output are also available in neutron installations) inverse (p,n) reaction will have increased importance.

II.A. THE $^{9}Be(p,n)^{9}B$ REACTION

The situation has much improved since the last survey[5] A more recent survey[6] covers cross section and neutron yield measurements until 1983 for neutron energies up to 120 MeV Table 1 adds some more references[7-10] to this survey with emphasis on very recent work[11,12]. A thorough evaluation using Legendre coefficients to present the data up to 30 MeV is available[11]. Discrepancies in the data base of the order of 25 % make it, however, unlikely that the accuracy of the Legendre presentation is better than ±10 %. At higher energies even this value seems optimistic because recent measurements around 17 MeV[12] (measured in the same laboratory) differ by about 20 % from the Legendre values.

Table 1. Additional Experimental $^{9}Be(p,n)^{9}B$ Data Which are Not Included in the Survey of Ref.6

E_p (MeV)	Symbol	Ref.	Ang.Range (c.m.,deg.)	Remarks
4....14	BA64A	7	integral	rel.tot.yield
6.3,7.4	BA64B	8	0..112	TOF
14.9,17.8	BA80	9	0...90	
	GU82	10		indent. data
8.2...15.7	BY83	11	0...162	incl. evaluation
16.4,17.6	MU86	12	0...162	Lane model

II.B. THE $^{9}Be(\alpha,n)^{12}C$ REACTION

The differential cross sections and neutron energy spectra following the break-up reaction $^{9}Be(\alpha,\alpha n)^{8}Be$ have been evaluated for energies up to 7.7 MeV to allow the simulation of the neutron spectra of radioactive α-Be sources[13,14]. Since then low energy total cross

sections have been measured with a 4π counter[15]. These results agree within error limits with the integral of previous angular distributions[16].

The thick target yield at 0° for alpha particle energies between 12 and 30 MeV has been measured recently to investigate the usefulness of this source in neutron radiotherapy[17]. For this purpose the source is much inferior to both the p-Be and the d-Be source not only with regard to the total yield but even more so with regard to the neutron energy distribution, i.e. the average neutron energy.

II.C. THE $^{51}V(p,n)^{51}Cr$ REACTION

Since the last survey[5] two papers[18,19] dealing with the integrated cross section of this reaction became available. Because of the near-isotropy[20] at not too high energies the differential cross sections are usually obtained from the integrated values by dividing by 4π. The shapes of the two new excitation functions agree rather well. However, the data of Zyskind et al.[18] are lower by about 40 % in rough agreement with others[21,22]. These data were measured at 90° with a BF_3 counter. Also the higher excitation function[19] agrees in scale with previous data[23,24]. In this case the measurement was done with a 4π neutron detector consisting of a 60 cm diameter polyethylene sphere in which eight BF_3 counters are embedded. In an earlier experiment in which also a 4π neutron detector was used, the scale was an additional 30% higher[25].

Even if this highest solution which is not reproduced by other work is excluded, no unique solution for the correct scale is evident. Until further reliable data become available or a more detailed analysis allows the exclusion of some of the data it is advisable to use the mean of the two lower data sets and to assign a 20 % scale error to it.

II.D. THE $^{11}B(p,n)^{11}C$ REACTION

This reaction supplements the $^{7}Li(p,n)^{7}Be$ reaction for neutron energies between 2 and 3 MeV where the other reaction is not monoenergetic any more (see Fig.1). Some kinematic properties of this source are summarized in Table 2.

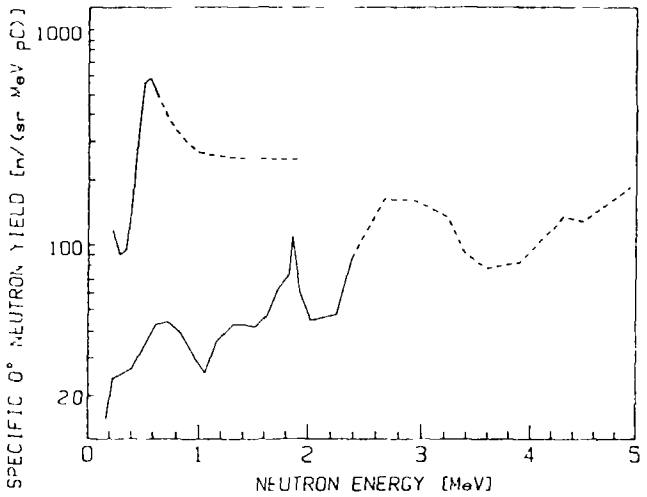

Fig. 1. Energy dependence of the specific zero-degree neutron yield of $^{7}Li(p,n)^{7}Be$ (upper curve) and $^{11}B(p,n)^{11}C$. The full curves cover the monoenergetic range, the dotted part indicates the presence of a neutron continuum.

There are quite a few cross section measurements available[26-38] (see Table 3). Below proton energies of 10 MeV agreement between the data sets within the order of 10 % is achieved[34,36].

The p-^{11}B excitation function does not show very narrow resonances (see Fig.1 and 2). Therefore one can profit from the relatively high yield at the maxima of the resonances (at 1.9 MeV and around 3 MeV neutron energy) even with energy resolutions somewhat above 0.1 MeV. At 1.9 MeV the specific yield of p-^{11}B is about one half of that of the p-^{7}Li reaction but it has the advantage of a pure single line spectrum. The maximum around 3 MeV lies in the double line range which extends to about 5 MeV. In this energy range the p-^{7}Li source is already plagued by the neutron continuum of the ^{7}Be break up.

Table 2. Kinematic Data of the $^{11}B(p,n)^{11}C$ Reaction. (All energies in MeV)

		Ground St. (n_0)	1st Exc.St. (n_1)	2nd Exc.St. (n_2)	Break-up Thr.
C^{11}-Exc.Energy		0.000	2.000	4.319	7.544
Q-Value		-2.765	-4.765	-7.083	-10.308
Forward Reaction:					
Proj.Energy		3.018	5.202	7.734	11.252
E_{n0}	0°	0.021	2.388	4.941	8.469
	180°c.m.	0.021	1.350	3.080	5.499
E_{n1}	0°		0.037	2.860	6.425
	180°c.m.		0.037	1.497	3.881
E_{n2}	0°			0.055	3.999
	180°c.m.			0.055	2.060
Inverse Reaction:					
Proj.Energy		32.977	56.839	84.510	122.947
E_{n0}	0°	2.536	11.879	20.646	32.646
	180°c.m.	2.536	0.542	0.313	0.198
E_{n1}	0°		4.371	16.082	28.473
	180°c.m.		4.371	1.189	0.672
E_{n2}	0°			6.497	23.021
	180°c.m.			6.497	1.835

The real potential of $p-^{11}B$ lies in its inverse reaction $^1H(^{11}B,n)^{11}C$.[39] In this case the neutrons are collimated into a forward cone as detailed in the companion paper[1]. In addition, the neutron energy at the same center-of-mass energy is appreciable higher for the inverse reaction (see Table 2) so that break-up neutrons start to appear only when the primary neutron energy becomes larger than 32.6 MeV. The monoenergetic range extends from 2.5 to 11.9 MeV. Actually it is a two-line range, because also the neutrons emitted under 180°c.m. occur at 0°lab. However, this second line is typically two orders of magnitude less intense and its energy decreases strongly with increasing primary neutron energy as can be seen from Table 2.

Table 3. Survey of Experimental $^{11}B(p,n)^{11}C$ Data.

E_p (MeV)	Symbol	Ref.	Ang.Range (c.m.,deg.)	Remarks
8.1...14.1	HI60	26	10...140	proton rec.spectrometer
2.9... 4.3	AL61	27	0...130	long ctr.,rel.data[a]
4.9...11.4	LE61	28	integr.	activ.techn.[b]
17,18.5	AN64	29	3...155	TOF
4...14	BA64A	7	integr.	4π ctr.,rel.yield
4...11.5	OV65	30	0...170	TOF[c]
7.1,8.2	WA65	31	0...155	TOF
30,50	CL70	32	2... 65	TOF
18.0	AN74	33	2...144°	TOF
3.1...4.8	VA78	34	0...165	prot.recoil, data comp.
10.9..27.5	AN81	35	integr.	activ.techn.
5.4...7.5	HO81	36	22...162	TOF
14.0...14.6	SC84	37	22...162	TOF
16...26	GR85	38	4...147	TOF

a) dubious data; lowest energy 0.12 MeV below threshold'
b) data are high by a factor 1.71[34]
c) normalization is high by at least a factor 1.71[36]

Special attention deserves the relatively high yield around 11.4 MeV (with a width (FWHM) of 0.8 MeV) which is in the 8 to 14 MeV "gap". There the second line has an energy of about 0.6 MeV and an intensity which is only 1 % of that of the primary line.
Also the two-line range (actually it is four-line range if the 180°c.m. groups are considered, too) up to 20.6 MeV could be useful. The specific yield is higher than that of the truely monoenergetic d-T source by an order of magnitude. If solid tritium targets are used then it is even higher by about two orders of magnitude. In addition, the natural collimation of the neutrons into a forward cone is very beneficial because it simplifies shielding.

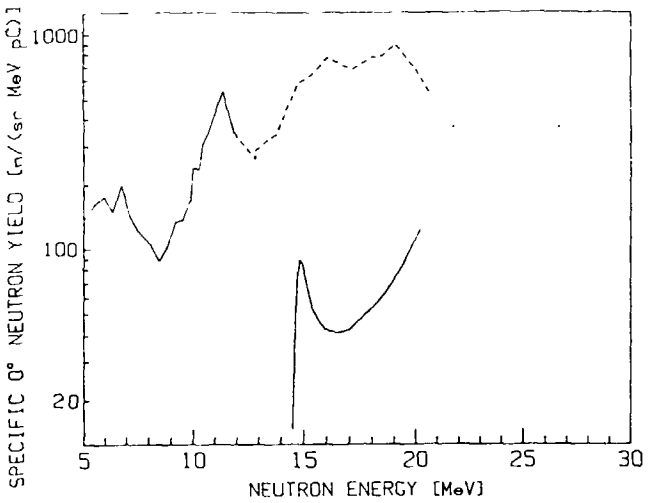

Fig. 2. Energy dependence of the specific zero-degree neutron yield of $^{1}H(^{11}B,n)^{11}C$ (upper curve) and $^{3}H(d,n)^{4}He$. The full curves cover the monoenergetic range, the dotted portion of the d-T curve indicates the presence of a neutron continuum.

III. DISCUSSION

The neutron sources considered in this paper are used for very different purposes. The usefulness of the two Be sources (p-Be and α-Be) for neutron radiotherapy has been investigated[17]. The reaction α-Be appears to be much inferior in such an application. However, the α-Be cross sections have been successfully used to calculate the neutron spectra of radioactive α-Be sources[13,14].

The data base for the p-Be reaction is already quite good as can be seen from a recent evaluation[11] and the quite successful application of the Lane model to these data[12].

For neutron production below 120 keV both $^{51}V(p,n)^{51}Cr$ and $^{45}Sc(p,n)^{45}Ti$ are being used. The latter reaction is subject of a contribution to this Meeting[4]. The ambiguity of the p-^{51}V data is discussed in Sect.II.C. A thorough investigation is necessary to clarify this 40 % discrepancy.

The $^{11}B(p,n)^{11}C$ reaction appears to be quite a useful monoenergetic source. Even more so if the inverse reaction is considered. Its specific yield at the resonances is comparable with that of the p-T reaction when solid T_2 targets are used. (With gas targets the yield from p-T is about an order of magnitude larger.) So the p-^{11}B reaction is a good one-line source for 1.9 MeV neutrons and a two-line source between 2.4 and 5 MeV.

Although the acceleration of heavy ions has become a tool in many technical fields, it has not been used much for monoenergetic neutron production, despite the availability of bunched beams (e.g. Ref. 40). The only work in this field is a measurement of the $^{1}H(^{7}Li,n)^{7}Be$ reaction[41]. The need of a source between 8 and 14 MeV (aside from the prolific t-H source[1]) together with the available technology (boron beams in the above μA range have been obtained[42,43] and have been accelerated to be required energies[43,44]) should speed up the development of the $^{1}H(^{11}B,n)^{11}C$ source. However, the seriousness of the neutron background from the interaction of the ^{11}B beam with the target structure can be assessed only after a bunched ^{11}B beam has become available in a neutron time-of-flight installation.

ACKNOWLEDGEMENT

Thanks are due to Mr. W. Penits and Mrs. R. Libiseller for the technical assistance in preparing this report.

REFERENCES

1) M. Drosg, this Meeting
2) Y. Yamanouti, this Meeting
3) A.B. Smith, D.L. Smith and J.F. Whalen, this Meeting
4) M. Cosack, H. Lesiecki and J.B. Hunt, this Meeting
5) M. Drosg, "Properties of monoenergetic neutron sources from proton reactions with nuclei other than tritons", pp.241 Proc. IAEA Consultants Meeting on Neutron Source Properties, Debrecen, Hungary (1980), report INDC (NDS)-114/GT, IAEA, Vienna

6) M. Allab, "A survey of neutron energy spectra and angular distributions of the $^{9}Be(p,n)^{9}B$ reaction for fast neutron radiotherapy", report INDC(NDS)-153/L, IAEA, Vienna, 1984.
7) J. K. Bair, C.M. Jones and H.B. Willard, Nucl.Phys.53, 209 (1984)
8) R.W. Bauer, J.D. Anderson and C. Wong, Nucl. Phys. 56, 117 (1964)
9) A.G. Baryshnikov, M.G. Gulyamov and S.P. Krekoten, Izv. Akad. Nauk SSSR, Ser. Fiz , 44, 2421 (1980)
10) M. Gulyamov, G. Kim and S.M. Bekbaev, Yad.Fiz. 36, 572 (1982)
11) R.C. Byrd, C.E. Floyd, P.P. Guss, K Murphy and R.L. Walter, Nucl Phys. A399, 94 (1983)
12) K. Murphy, R.C. Byrd, C.E. Floyd, P.P. Guss and R.L. Walter, Nucl. Physics, in press (1986)
13) K.W. Geiger and L. van der Zwan, Nucl.Instr.Meth.131, 315 (1975)
14) K.W. Geiger, "Radioactive Be(α,n) and Be(γ,n) neutron sources", pp. 43 of report INDC (NDS)-114/GT, IAEA Vienna, 1980
15) E. Ramstrom, "Excitation Functions of the $^{9}Be(\alpha,n)^{12}C$, the $^{13}C(p,n)^{13}N$ and the $^{13}N(n,p)^{13}C$ Reactions", report NFL-6, Studsvik Science Research Lab., Sweden (1979)
16) C.N. Davids, Nucl. Phys. A110, 619 (1968)
17) M.A. Lone, A.J. Ferguson and B.C.Robertson, Nucl. Inst. Meth. 189, 515 (1981)
18) J.L. Zyskind, C.A. Barnes, J.M. Davidson, W.A. Fowler, R.E. Marrs and M.H. Shapiro, Nucl.Phys. A343, 295 (1980)
19) F. Gabbard and R.L. Hershberger, "Total (p,n) and (α,n) Cross Sections for Nucleosynthesis and Nuclear Applications", report DOE/ER/10642-2 (1983)
20) G Deconninck and J. Royen, Nucl.Instr.Methods 75, 266 (1969)
21) K.K. Harris, H A. Grench, R.G. Johnson and F.J. Vaughn, Nucl.Instr.Methods 33, 257 (1965)
22) J H Gibbsons and R.L. Macklin, Nucl.Instr.Methods 37, 330 (1965)
23) J. Wing and J.R. Huizenga, Phys.Rev.128, 280 (1962)
24) C H. Johnson, A. Galonsky and C.N. Inskeep, "Cross Sections for (p,n) Reactions in Intermediate-Weight Nuclei", Report ORNL-2910, p 25 (1960)
25) M.K. Mehta, S. Kailas and K.K. Sekharan, Pramana 9, 419 (1977)
26) K. Hisatake, Y. Ishizaki, A. Isoya, T. Nakamura, Y. Nakano, B. Saheki, Y. Saji and K. Yuasa, Journ.Phys.Soc.Jap. 15, 741(1960)
27) R.D. Albert, S.D. Bloom and N.K. Glendenning, Phys.Rev. 122, 862 (1961)
28) G.J.F. Legge and I.F. Bubb, Nucl. Phys. 26, 616 (1961)
29) J.D. Anderson, C. Wong, J.W. McClure and B.D. Walker, Phys.Rev. 136, B 118(1964)
30) J.C. Overley and R.R. Borchers, Nucl.Phys. 65, 156 (1965)
31) B.D. Walker, C. Wong, J.D. Anderson and J.W. McClure, Phys.Rev. 137B, 1504, (1965)
32) A.S. Clough, C.J. Batty, B.E. Bonner and L.E. Williams, Nucl.Phys. A143, 385(1970)
33) J.D. Anderson,"Charge exchange reactions", Nuclear Spectroscopy and Reactions, Part B, p.613, Academic Press, New York (1974).
34) L. van der Zwan and K. Geiger, Nucl.Phys. A306, 45 (1978)
35) B. Anders, P. Hergers and W. Scobel, Z. Phys. A301, 353 (1981)
36) J. Hohn, J. Kayser, W. Pilz, D. Schmidt and D. Seeliger, J.Phys.G. Nucl.Phys. 7, 803 (1981)
37) H.R. Schelin, E. Farrelly Pessoa, W.R. Wylie, J.L. Cardose Jr. and R.A. Douglas, Report IFUSP/P-451, Univ Sao Paulo (1984)
38) S.M. Grimes, J.D. Anderson, J.C. Davis, R.H. Howell, C. Wong, A.W. Carpenter, J.A. Carr and F. Petrovich, Phys.Rev. C31, 1679 (1985)
39) M. Drosg, to be published
40) F.-J. Bergmeister, K.-P. Lieb and D. Straeter, Nucl.Inst.Meth. Phys.Res. A244, 176 (1986)
41) J. H. Dave, C.R. Gould, S.A. Wender and S.M. Shafroth, Nucl.Inst.Meth.Phys.Res. 200, 285 (1982)
42) R. Middleton, Nucl.Inst. Meth. Phys. Res. 220, 105 (1984)
43) R.I. Cutler, K.W. Kemper and K.R. Chapman, Nucl.Inst.Meth. 164, 605 (1979)
44) W.R. Fahrner, K. Heidemann and P. Schottle, Phys.Stat.Sol. 70, 463 (1982)

290 NEUTRON SOURCE FOR 3-25 MeV ENERGY RANGE BASED ON EGP-10M ACCELERATOR AND GAS TRITIUM TARGET

G.N. LOVCHIKOVA, O.A. SALNIKOV, S.P. SIMAKOV,
A.M. TRUFANOV, A.V. POLYAKOV
Institute of Physics and Power Engineering,
Obninsk, Union of Soviet Socialist Republics

Abstract

The report describes the design and operating principle of a gas tritium target installation on the EGP-10M FEI pulsed accelerator. Neutron fluxes in the energy range of 3-8 MeV in the $^{3}H(p,n)^{3}He$ reaction and in the energy range of 20-25 MeV in the $^{3}H(d,n)^{4}He$ reaction are being obtained with the help of this target. The basic physical neutron flux parameters, from a target, the comparison with a solid tritium target and the examples of using a gas target in neutron experiments are given.

A study of the fast neutron interactions with nuclei is of great scientific interest and significant practical importance. This requires the neurton source with an energy readily varied, sufficient monoenergeticity and intensity of a neutron yield. The gas tritium target made by the authors [1, 2] using the $^{3}H(p,n)^{3}He$ and $^{3}H(d,n)^{4}He$ reactions for obtaining some neutrons satisfies these requirements. The EGP-10M recharged electrostatic accelerator is used as a source of protons and deutrons. From the references we know the works [3-6] devoted to a description of the gas target constructions but a little attention is given to a study of some characteristics of the neutron flux created by targets. The present work gives a comprehensive description and study of the physical characterictics of the gas tritium target as a source of neutrons.

The target depicted in Fig.1 represents a steel cylinder filled with gaseous tritium of 10 mm in diameter, 40 mm in length and 0,2 mm of wall thickness. The two windows with cool helium circulated between them isolate tritium from the vacuum system of an accelerator.

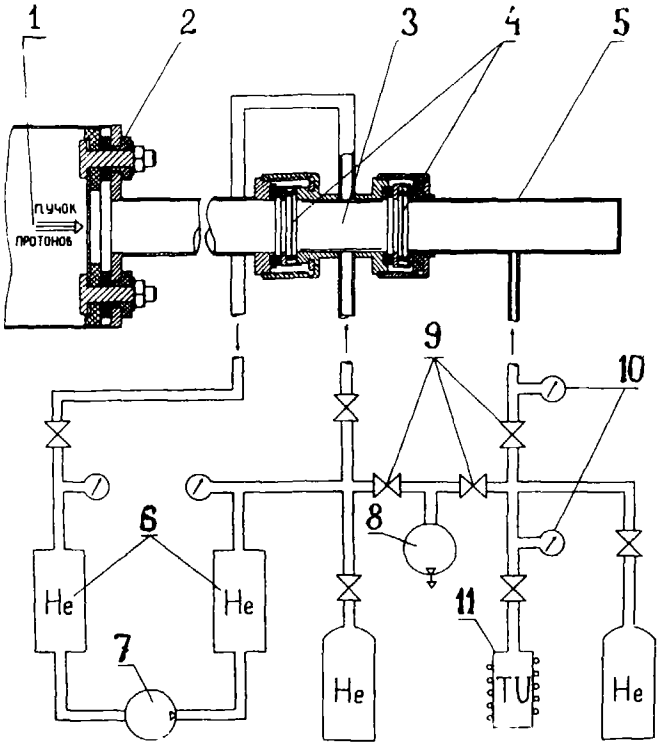

Fig.1. The arrangement of a gas target:
1 - a beam of charged particles,
2 - lamellae, 3 - a cooling cell,
4 - foils, 5 - a steel cylinder,
6 - ballastic volumes with helium,
7 - a compressor, 8 - a fore pump,
9 - valves, 10 - a pressure indicator,
11 - a balloon with uranium tritide.

In case of using the T(p, n) reaction for obtaining neutrons the windows have been made of the ^{58}Ni - milling foils 9,2 μm thick sealed with the ring-type indium spacers. Geometric demensions of a proton beam incident on the target are restricted by lamellae with a hole of 7 mm in diameter and positioned at a distance of 10 cm in front of the target. The inner surfaces of the target, a cooling cell as well as a side of lamellae faced to a proton beam have been covered with the ^{58}Ni - layer (with an enrichment of 96%) 0.2÷0.3 mm thick. This has been accomplished for decreasing neutron yields from the (p, n) reaction on the construction materials of the target since a threshold of the ^{58}Ni(p, n) reaction is sufficiently high (9,51 MeV).

The gas target is similar in constraction when obtaining neutrons from the T(d, n) reaction. In this case the molybdenum foils of 7,9 and 14 mg/cm^2 thick have been used for the entrance windows. Also, the lamellae have been covered with molybdenum (60 mg/cm^2). A disk of platinum 580 mg/cm^2 thick served as the bottom of the target. The materials selected with large Z allow to decrease the yield of background neutrons from the (d, n) reaction.

Before the target has been filled with tritium it is evacuated by a fore pump (Fig.1) and then the balloon containing uranium tritide is heated to a temperature of 500°C. The gaseous tritium, being released in the decay of a compound, is entered a target via a system of electromagnetic valves. When the given tritium pressure has been reached the target is cut off by a valve and uranium tritide is cooled absorbing tritium that has been left in the system. To avoid the diffusion of tritium via foils during heating with a beam of the passing charged particles the provision has been made to cool these ones with a flow of helium drifted through a closed circuit by a microcompressor.

The inner layer in a cooling cell of the target is laid out so that to direct a flow of helium to both the foils uniformly.

The target of a described construction is found to be stable and reliable in operation during some months of continuous work at the bombarding proton and deutron currents of 1.5 ÷ 2.5 μA. In a neutron energy range of 5 ÷ 8 MeV and at an energy of 21 MeV the target characteristics are studied as a source of neutrons. Results presented in the table are obtained at the following conditions: the pressure of tritium in the target is 2 atm, the pressure of helium in a cooling cell is 1 atm. There have been determined the energies of charged particles [7], the energy losses in foils and gas, the energy and neutron yield at an angle of 0° to a beam incident on the target. The angular divergence of a beam occured as a result of a multiple Coulomb interaction in foils and gas leads to an added energy spread of 10 keV in case of the T(p, n) reaction and of 20 keV in the T(d, n) reaction.

table The characteristics of a gas target as a source of neutrons in a range of 5 ÷ 8 MeV and at an energy of 21 MeV

1. Reaction	T(p, n)				T(d, n)
2. Energy of neutrons escaped forward, MeV	5,00	6,00	7,00	8,00	21,0
3. Yield of neutrons at 0°, 10^8n/sr·μK	1,31	0,95	0,76	0,68	0,54
4. Accelerated particle energy, MeV	6,51	7,42	8,37	9,33	5,54
5. Losses of particle energy in foils and gas, MeV	0,74	0,65	0,60	0,56	1,44
6. Root-mean-square angle of particle beam divergence in gas, degrees	3,5	3,0	2,7	2,4	5,2
7. Neutron energy uncertainty, MeV	0,07	0,06	0,05	0,05	0,20
8. Neutron yields from background reactions to yields from basic ones, %	0,03	0,08	0,03	1,00	85

The initial neutron energy uncertainty (a root-mean-squre deviation) presented in the Table is composed of the energy particle losses in a half-value layer of gaseuos tritium, the fluctuation of ionization proton losses when passing through foils and the energy uncertainty occured because of a non-uniform entrance window thickness. Should a quantitative estimation can be given to first two components on a base of the well-known relations, then a non-uniformity of the used foil thickness can be estimated experimentally only. For this we have measured the graphite sample transmission functions at the neutron energies close to resonances in a total neutron interaction cross-section with carbon. This resonance parameters are well-known [8] : E_{res}= 5,369 ± 0,003; 6,293 ± 0,003; 6,56 MeV, Γ_{res}= 28 ± 3; 57 ± 4; 40 ± 4 keV, respectively. The graphite samples of 10 and 18 cm long have been placed between a tritium target and detector; monitoring has been carried out using a long counter. In the Fig.2 are shown the experimental points obtained during measuring the transmission functions for the mentioned above resonances and graphite sample thickness.

The smooth curves show the same sample transmission functions calculated on an assumption that the energy neutron flux line from a target has a normal distribution with appropriate standard deviations. (See the numerals near the curves in the Fig.2). It is seen that at the 5,4 and 6,3 MeV energies of neutrons escaped from a target the total initial energy uncertainty accounts for 70 and 50 keV, respectively. Taking into account the energy tritium half-value layer thickness and the ionization proton losses fluctuations in foils (all together is accounted for ≈ 30 keV) one obtain an energy spread introduced by a non-uniformity of foils being equal to 60 and 40 keV that corresponds to relative non-uniformity in thickness ± 8%.

Monoenergeticity of a neutron flux from the target is characterized by a ratio of the neutron yield (with the energies from a detector threshold 0,7 MeV to a maximum one) originated in the interaction of protons or deutrons with structural materials of a target to the neutron yield from the basic T(p,n) or T(d,n) reactions.

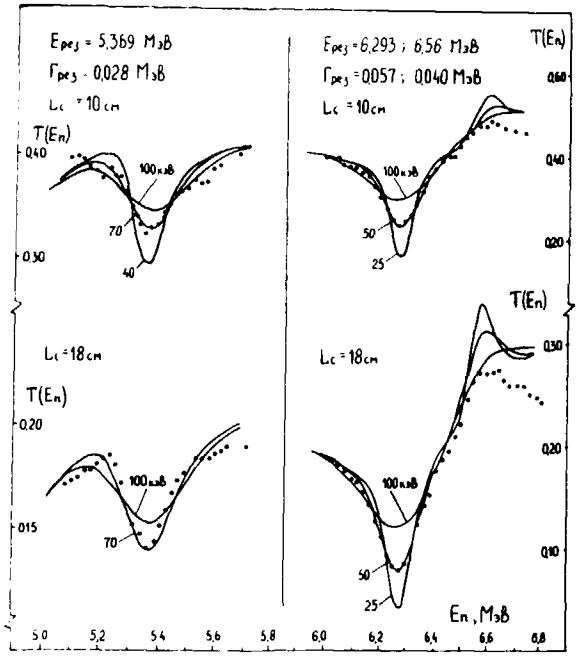

Fig.2. Transmission functions of graphite samples: the experimental points and the transmission curves calculated with different dispersions of the neutron energy distribution from the tritium target.

The energy spectra of these "background" neutrons, i.e., neutrons at 0° from an evacuated target are shown in Fig.3 for the two incident proton energies of 6.00 and 8.77 MeV. The arrows and figures show the peak energy of neutrons produced in the (p,n) reaction on the proper Ni -isotopes. The correlation of

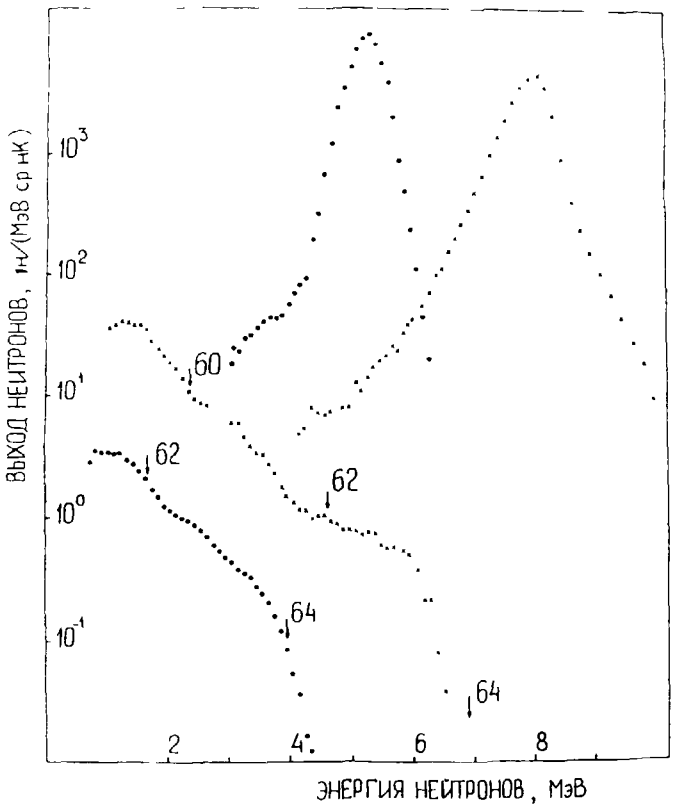

Fig.3. The spectra of neutrons escaped from the evacuated and the neutron peaks from the target filled with tritium up to 2 atm. The energy of incident protons in the target 6.00 (·) and 8.77 (x) MeV.

these ones with the rise of "background" neutrons in the energy spectra points out to the origin of neutrons that disturb "the purity" of a target. For comparison the same figure shows the neutron peaks from the target filled with tritium to 2 atm. The measurements have performed using a time-of-flight method by a scientillation detector [9] placed in the shield at a distance of 2.1 m in front of the target. A visible width of the neutron peaks exceeding in some times a true width of energy distribution of neutrons is determined by a time resolution of a detector (≈ 3 ns) and by the effects of neutron interactions with a collimator of a shield.

One of an added neutron source with energies differed from the basic one can be reactions on impurity gases which are inevitable present in tritium or can penetrate into a target during measurements. To illustrate this in Fig.4 are shown the neutron spectra measured from the air-filled target to 1 atm and the evacuated one. The energy of incident protons in a

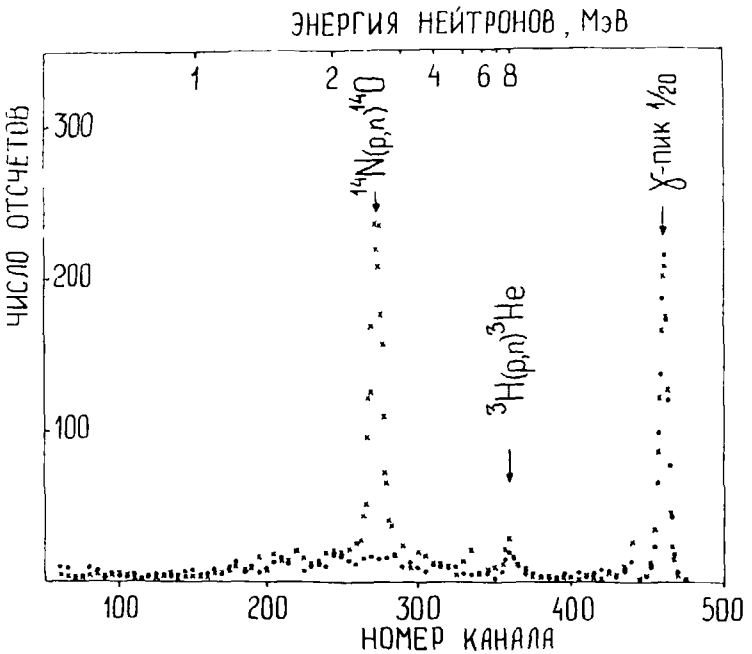

Fig.4. The time spectra of neutrons escaped from the evacuated target (·) and the target filled with air up to 1 atm (x) at the proton energy of 8.77 MeV in the target.

target is equal to 8.77 MeV. The sole additional peak appeared on the spectrum corresponds to neutrons from the $^{14}N(p,n)^{14}O$ reaction (E_{thresh}= 8.35 MeV). The evacuation of this target even to ≈ 1 mm of mercury column reduces a peak from these neutrons to a level of the contribution from residual background reactions.

At the neutron energies of 8 MeV the T(p,n)D tritium break-up reaction (Q= - 6.26 MeV) became energetically possible, in this case a maximum energy of neutrons from this reaction is equal to 1.5 MeV. Apparently, proceeding from this small value of a tritium break-up reaction cross-section [10, 11] a contribution of these neurtons at the considered energies is not detected.

At the proton energies below a tritium break-up reaction threshold in the instrumentation neutron spectra in an energy range of 1,5 MeV a wide peak with an area of 100 times lower than the area of a basic neitron peak from the T(p,n) reaction is observed. The similar effect has been observed by the authors in the work [12]. The reason of these neutron occurence is not established. The estimations made by us show that the neutrons with such an approximately low energy can be formed in the T(p,n) reaction with the beam protons scattered back into a gas volume by the bottom of a target.

When bombarding a gas target by a deutron beam for the reason of obtaining neutrons with energies near to 20 MeV a contribution of background neutrons, as is seen from the table, becomes considerably higher as compared to the experiment with a proton beam. In the Fig.5 is shown the instrumentation spectrum of neutrons from the gas target filled with tritium at E_d= 5.5 MeV. Besides neutrons from the basic T(d,n) reaction a complex spectrum of background neutrons is seen. There have been displayed sharply the peaks of neutrons formed in the (d,n) reaction on oxygen, carbon, nitrogen (oxides, scales, residual gases) and on deuterium (packing of a deutron beam, impurities in gases). The continuous part of a neutron spectrum is formed at the expense of deutron break-up reactions on the structural element nuclei of a target.

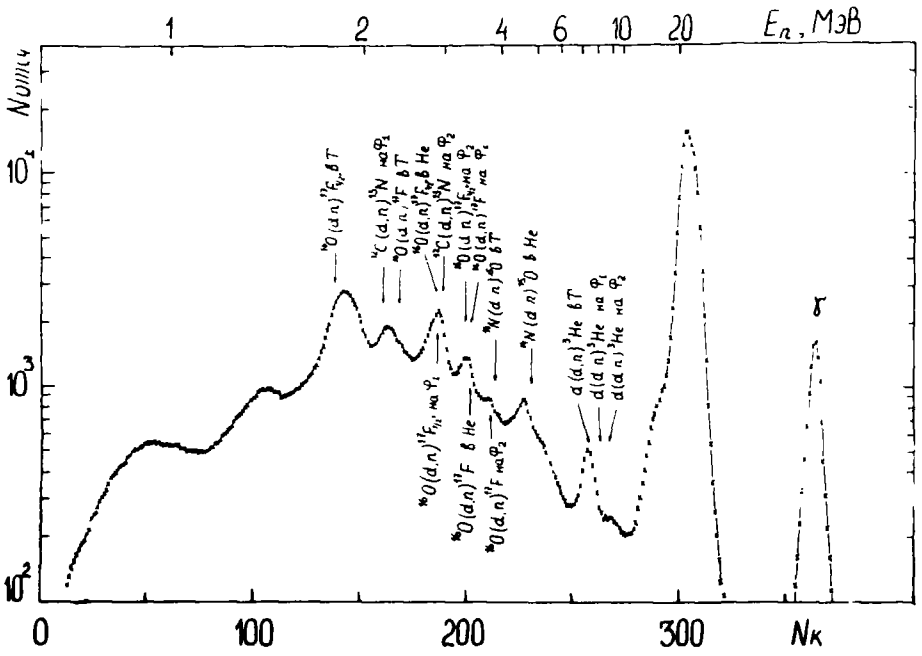

Fig.5. The instrumentation spectrum of neutrons from the gas tritium target measured at an angle of 0° and E_d= 5.5 MeV.
The arrows indicate neutron energies from the (d,n) reaction for different elements existed in helium (He) and tritium (T) volumes as well as in foils from molybdenum (Φ_1 and Φ_2).

It is interesting to compare a possibility of obtaining neutrons with the energies greater 5 MeV using the gas and solid tritium target since the considered ones are used widely for obtaining the neutrons of lesser energies. We have used a solid target with a titanum-tritium layer of 0.96 mg/cm^2 thick on a molybdenum backing.

To obtain an energy resolution comparable to that one from a gas target the TiT layer thickness should be taken

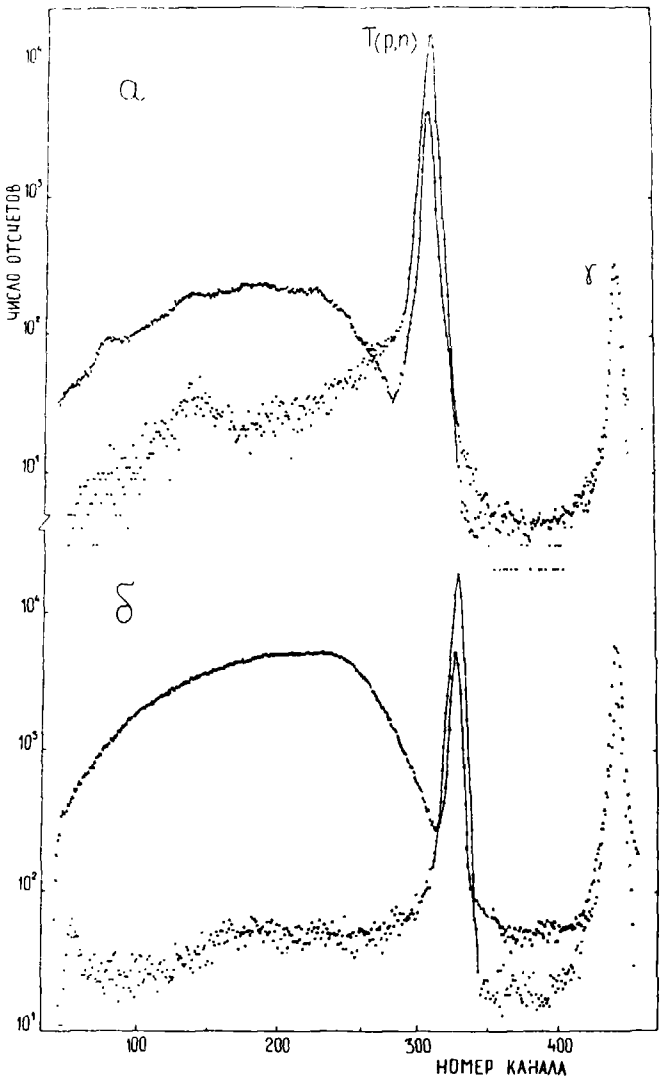

Fig.6. The time spectra of neutrons escaped at an angle of 0° to the incident proton beam from the gas target (•) and the TiT (Mo) target (x). The energy of neutron peaks from the T(p,n) reaction is equal to 5,3 MeV(a) and 7,2 MeV(b).

approximately four times greater; in this case a neutron yield from the T(p,n) reaction should be increased, respectively. It has been taken into consideration by normalizing time spectra in Fig.6 (amplitudes of neutron peaks are related as 1:4), which illustrates the relation of background neutrons for the gas and solid tritium target.

It is seen from the figures that for the solid target a ratio of neutron yields from the (p,n) reaction on structural materials to the neutron yields from the T(p,n) reaction exceeds the appropriate ratio for a gas target in the one or two orders of magnitude. It makes impracticable to use solid targets for obtaining monoenergetic neutrons with energies greater 5 MeV.

The gas tritium target as a constituent part of a neutron-time-of-flight spectrometer [9] is actively used for a study of the fast neutron interaction cross-sections with nuclei. The differential elastic and inelastic neutron scattering cross-sections in the range of initial energies 5-8 MeV on a number of construction [13] and fissile [14] nuclei have been investigated. The elastic scattering cross-sections on carbon [15] and neutron spectra from the ^{93}Nb(n,xn) reaction [16] have been measured at an energy of neutrons 21 MeV.

REFERENCES

1. Fetisov N.I., Simakov S.P. et al. Pribory I Tekhnika Eksperimenta, 1980, N 6, p.22.
2. Lovchikova G.N., Polyakov A.V. et al. Preprint FEI-1483, Obninsk, 1983.
3. Haouat G., Lachkar J. et al. Neutron Physics, v.6, Kiev, 1975, p.236.
4. Cramer D.S., Cranberg L. Nucl. Instr. & Meth., 1971, v.93, p.405.
5. Biryukov N.S., Zhuravlev B.V. et al. PTE, 1971, N 3, p.66.
6. Holmqvist B., Wiedling T. Nucleonik, 1964, v.6, p.183.
7. Simakov S.P., Spirin V.I. et al. PTE, 1979, v.5, p.36.

8. Galati W., Brandenberger J.D., Well J.L. Phys. Rev., 1972, v.C5, p.1508.
9. Trufanov A.M., Nesterenko V.S. et al. PTE, 1979, N 2, p.50.
10. Drosg M., Auchampaugh G.F. Nucl. Instr. & Meth., 1977, v.140, p.515.
11. McDaniels D.K., Drosg M. et al. Phys. Rev., 1972, v.C5, p.1593.
12. Thambidurai P., Beyerle A.G. et al. Nucl. Instr. & Meth., 1982, v.196, p.415.
13. Simakov S.P. Synopsis of thesis for competition of candidate's degree of physico-mathematical sciences. Leningrad, 1983.
14. Lovchikova G.N., Polyakov A.V. et al. Preprint FEI-1564, Obninsk, 1984.
15. Lovchikova G.N., Polyakov A.V. et al. "Neutron Physics", M., CSRIAS, 1984, v.3, p.230.
16. Lovchikova G.N., Polyakov A.V. et al. Preprint FEY-1603, Obninsk, 1984.

INVESTIGATIONS ON THE PROPERTIES OF D+D AND D+T NEUTRON SOURCES*

J. CSIKAI, Zs. LANTOS, Cs.M. BUCZKÓ**
Institute of Experimental Physics,
Kossuth University,
Debrecen, Hungary

Abstract

Simple analytical expressions are given for the calculation of the energy and angular distributions of neutrons emitted in the reactions $^{2}H(d,n)^{3}He$ and $^{3}H(d,n)^{4}He$ for the 20-500 keV deuteron energy range. The results obtained were compared with the measured and calculated thin and thick target energy and angular distributions of D+T neutrons at 75, 125, 150, 175 and 210 keV deuteron energies. The energy spread of D+T neutrons as functions of emission angle and deuteron energy is also given for thick TiT target.

1. INTRODUCTION

The accurate knowledge of the energy and angular distributions of neutrons emitted in the D+D and D+T reactions is needed especially for the precise measurement of cross sections around 14MeV and for the design of thermonuclear devices. The aim of this work was to find simple analytical expressions for the description of

* This work was performed under the "14 MeV Co-ordinated Research Programme" organized by the International Atomic Energy Agency.

** Permanent address Isotope Laboratory, Kossuth University, Debrecen, 4010 Hungary.

the source yield and the energy of neutrons emitted in the widely used D+D and D+T reactions below 500 keV bombarding deuteron energy as well as to check these expressions by experiments and calculations both for thick and thin targets.

2. FITTING PROCEDURE

The thin-target data recommended[1] for the energy (E_n) and angular (Y_n) distributions of neutrons emitted in the D+D and D+T reactions in laboratory system were approximated by the following expressions[2]

$$E_n(E_d,\theta) = E_o(E_d) + \sum_{i=1}^{n} E_i(E_d)\cos^i\theta \qquad (1)$$

$$Y_n(E_d,\theta) = Y_o(E_d) + \sum_{i=1}^{n} Y_i(E_d)\cos^i\theta \qquad (2)$$

In eqs.(1) and (2) n=5 and 3 for D+D while n=3 and 2 for D+T reactions, respectively. It was found that the evaluated data[3] for the energy and angular distributions in the case of thick target can also be described by eqs.(2) and (1). The values of Y_o, Y_i, E_o and E_i coefficients obtained from a least-squares fit are given in Tables 1-5 for the 20-500 keV deuteron energy range.

Table 1. Values of the parameters in Eq.(1) for the calculation of thin target neutron energy vs. emission angle in lab. system

E_d [keV]	D-T			D-D			
	E_o	E_1	E_2	E_o	E_1	E_2	E_3
50	14.04814	0.47679	0.00834	2.46073	0.24848	0.01282	0.00031
100	14.06732	0.67488	0.01719	2.47303	0.35237	0.02524	0.00062
200	14.10711	0.95596	0.03320	2.49771	0.50072	0.05044	0.00242
300	14.14704	1.17282	0.04923	2.52289	0.61581	0.07530	0.00589
400	14.18670	1.35640	0.06527	2.54798	0.71456	0.10013	0.00757
500	14.22569	1.51899	0.08249	2.57246	0.80285	0.12592	0.01024

Table 2. Values of the parameters in Eq.(1) for the calculation of thick target neutron energy vs. emission angle in lab. system

E_d [keV]	D-T			D-D			
	E_o	E_1	E_2	E_o	E_1	E_2	E_3
50	14.06520	0.42329	0.00682				
100	14.07883	0.57613	0.01222	2.46674	0.30083	0.01368	-
150	14.08942	0.66776	0.01600	-	-	-	-
200	14.09680	0.72427	0.01908	2.47685	0.39111	0.04098	0.02749
250	14.10286	0.76661	0.02167	-	-	-	-
300	14.10803	0.80001	0.02374	2.49712	0.47697	0.05124	0.02957
325	14.10723	0.79477	0.02347	-	-	-	-
400	-	-	-	2.50981	0.55825	0.07125	0.02474
500	-	-	-	2.52140	0.62147	0.09816	0.03307

Table 3. Recommended parameter values for the calculation of the thin target angular dependence of D-T source yields in lab. system by Eq.(2) normalized to 90°

E_d[keV]	Y_o	Y_1	Y_2	$\sigma(90^\circ)$ [mb/sr]
20	1	0.0220	0.00025	4.2942
30	1	0.0227	- 0.0093	19.6126
40	1	0.0310	0.0007	52.8382
50	1	0.0344	0.0010	105.4180
60	1	0.0518	- 0.0035	173.2630
70	1	0.0407	0.0011	249.3768
100	1	0.0482	0.0011	393.3834
150	1	0.0599	0.0009	316.3704
200	1	0.0678	0.0005	198.4180
250	1	0.0685	- 0.0104	132.8133
300	1	0.0818	0.0005	95.0878
350	1	0.0904	0.0028	77.3864
400	1	0.1003	- 0.0008	63.4112
450	1	0.1140	- 0.0101	53.0290
500	1	0.1273	- 0.0187	45.5970

Table 4 Coefficients for the calculation of the thin target angular dependence of D-D source yields in lab system by Eq (2) normalized to 90 degree

E_d [keV]	Y_o	Y_1	Y_2	Y_3	Y_4	Y_5	$\sigma(90^o)$ [mb/sr]
50	1	0 11787	0 58355	- 0 11353	0 04222	0 16359	0 32016
100	1	0 01741	0 88746	0 22497	0 08183	0 37225	1 01828
200	1	- 0 03149	1 11225	0 38659	0 26676	0 11518	1 95031
300	1	- 0 10702	1 64553	0 63645	0 67655	0.35367	2.66479
400	1	- 0 02546	1 05439	0 21072	0 81789	0.59571	3 32222
500	1	- 0 10272	1 09948	0 29820	1 09435	0 76159	3 63084

Table 5 Coefficients in Eq (2) for the calculation of the thick target D-T neutron yield vs emission angle normalized to 90 degree

E_d [keV]	Y_o	Y_1	Y_2	$\sigma(90^o)$ [mb/sr]
50	1	0 03003	0 00035	105
100	1	0 04087	0 00062	393
150	1	0 04727	0 00083	316
200	1	0 05124	0 00096	198
250	1	0 05419	0 00110	132
300	1	0 05651	0 00119	95 1
325	1	0 05616	0 00119	86 2

The E_o and E_1 values for the D+T reaction have been determined between 20 and 70 keV in 10 keV steps. The angular dependence of D+D source yield at different deuteron energies normalized to 90 degree is shown in Fig.1. In the insert of Fig.1. the energy dependence of the Y_1 coefficients are demonstrated.

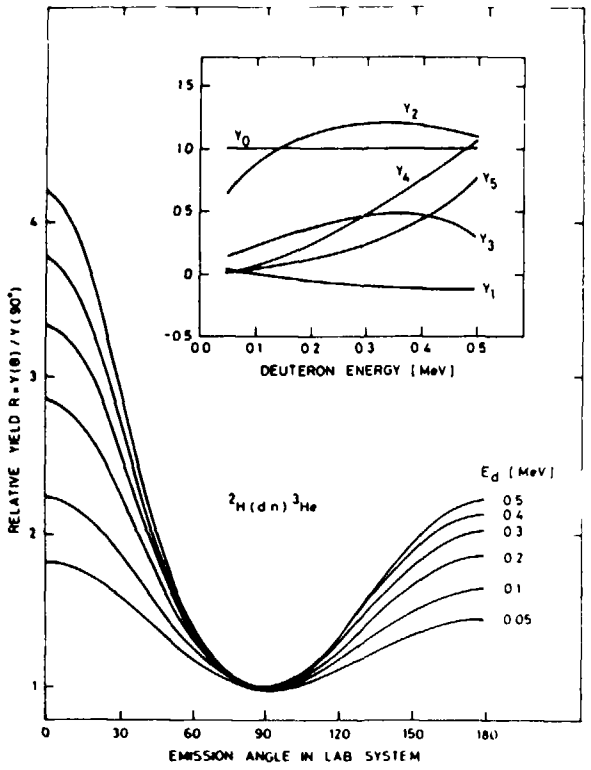

Figure 1.

3. EXPERIMENTAL PROCEDURE

The effect of target thickness on the source yield and on the energy of neutrons as a function of emission angle in D+T reaction was investigated in an improved experimental arrangement shown in Fig.2. This scattering-free irradiation facility rendered it possible to measure the source yield and the neutron energy in 2π interval. The details of the foil activation method used for the determination of the neutron energy around 14 MeV are described in Ref.[4]. The neutron energy and the yield as functions of

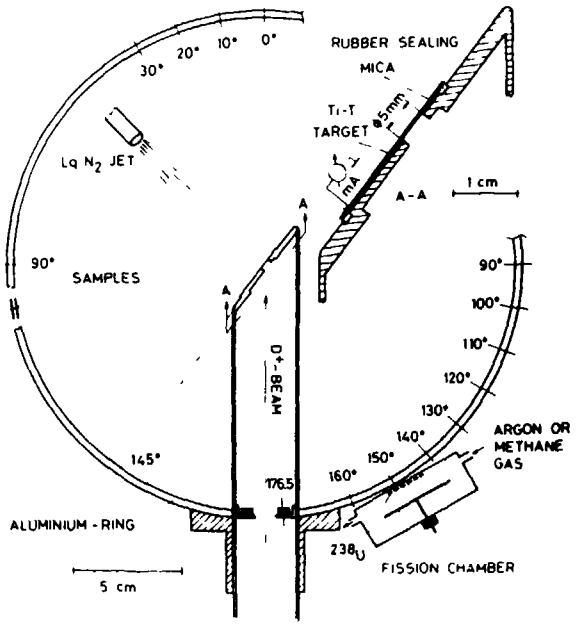

Figure 2.

emission angle were determined from the measurements of the activity ratios $^{89}Zr/^{92m}Nb$, $^{89}Zr/^{180m}Ta$ and $^{89}Zr/^{196}Au$ produced in (n,2n) reactions. The measured energy values together with those obtained by relativistic[5] and nonrelativistic[6] calculations at E_d=150 keV are indicated in Fig.3. The calculated[5,6] energy spreads (δ E) of neutrons as a function of emission angle for thick TiT target are shown in Fig.6 for 125, 150, 175 and 220 keV bombarding deuteron energies. The energy spreads are the 1/2 FWHM values of the distributions at different emission angles. Further investigations are needed for the determination of the shape and magnitude of the $\delta E(E_d,\Theta)$ functions.

4. RESULTS AND DISCUSSION

Figure 3 shows that good agreement exists between the measured and calculated neutron energies. As it can be seen the

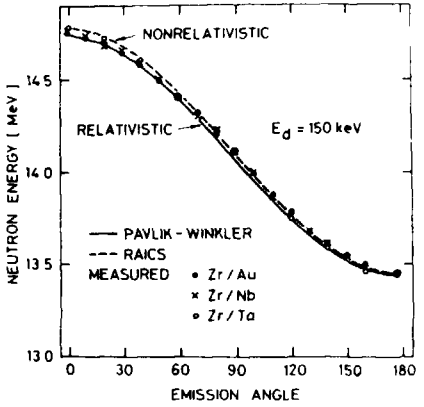

Figure 3.

Zr/Nb ratio gives the best agreement with the relativistic calculation. The coefficients obtained for the $E_n(\Theta)$ function by calculation and experiment for thick TiT target at different deuteron energies are summarized in Table 6. An analysis of the

Table 6 Coefficients of the $E_n(\Theta)$ function for thick TiT target

Method	Coefficients					
	E_d=125[keV]			E_d=150[keV]		
	E_o	E_1	E_2	E_o	E_1	E_2
Calculated Pavlik-Winkler[5]	14.0617	0.6283	0.0149	14.0645	0.653	0.016
Raics[6]	14.0847	0.6279	0.0142	14.0894	0.668	0.016
Measured						
Nb/Zr	14.0602	0.6046	0.0469	14.0862	0.658	0.010
Ta/Zr	14.0894	0.5984	0.0166	14.0820	0.644	- 0.001
Au/Zr	14.0777	0.5963	0.0192	14.0846	0.649	0.008
	E_d=75[keV]			E_d=150[keV] D^+(74%)+D_2^+(26%)		
Nb/Zr	14.0715	0.507	0.008	14.074	0.581	0.051

data at different energies led to the conclusion that the deviation from the relativistic calculation does not exceed 30 keV for D+T and D+D neutrons if $E_d \leq 500$ keV. The shapes of the source yield curves measured by Nb, Ta and Au foils deviate slightly from each other indicating that the (n,2n) excitation functions of the flux monitor reactions are not constant around 14 MeV (see Fig.4). Accepting the calculated angular distributions[5,6] for thick target we have deduced the shapes of the monitor reactions around 14 MeV. As it can be seen in Fig.5 the relative change in the cross section curves for the ^{93}Nb, ^{181}Ta and $^{197}Au(n,2n)$ reactions between 13.5 and 14.8 MeV is +0.35 %, -2.4 % and +1.6 %, respectively.

The authors are grateful to Dr.G.Winkler and Dr.P.Raics for the valuable discussions. Thanks are due to Mrs.M.Juhász, Mr.A.Halmi and Mr.J.Szegedi for their kind assistance during the measurements.

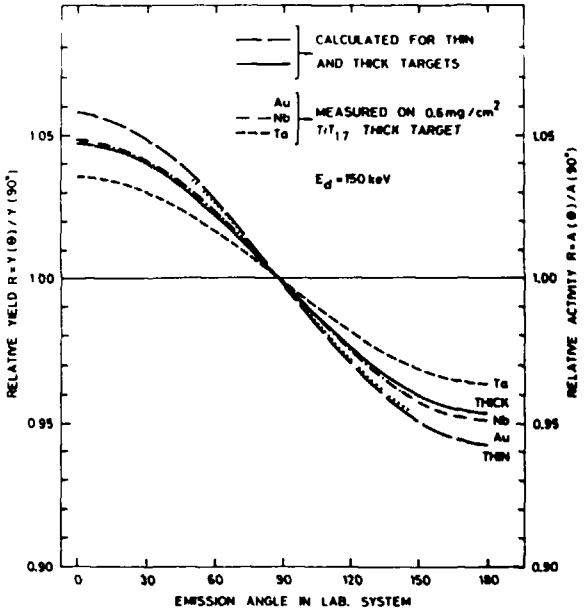

Figure 4.

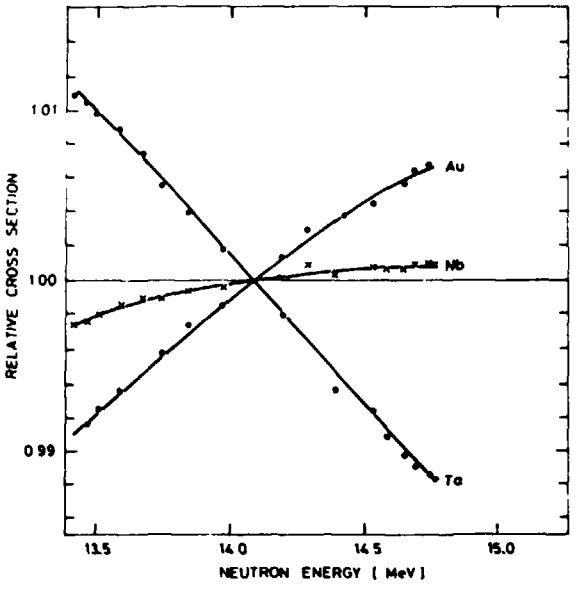

Figure 5.

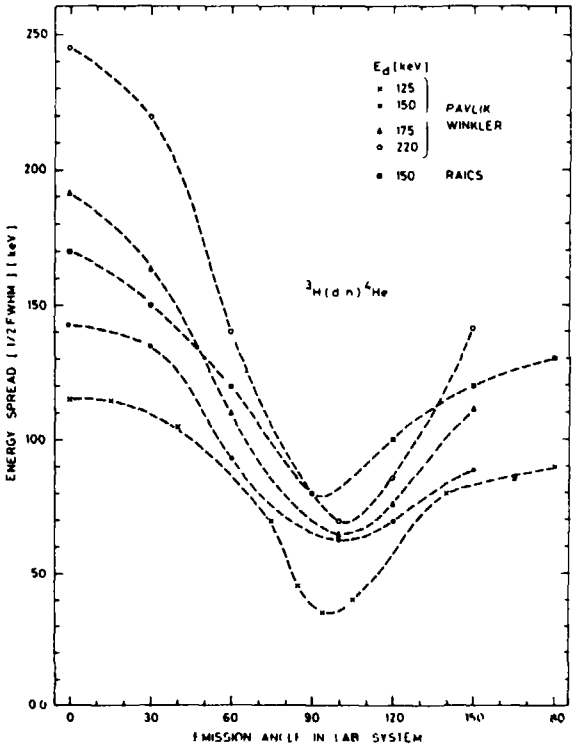

Figure 6.

REFERENCES

1. Liskien,H. and Paulsen,A., Nucl.Data Tables, 11(569)1973
2. Csikai,J., Handbook of Fast Neutron Generators, CRC Press Inc., USA, (in press)
3. Seagrave,J.D., Graves,E.R., Hipwood.S.J. and McDole,C.J., LAMS-2162, Los Alamos (1958)
4. Csikai,J., in Proc. of the Int. Conf. on Nuclear Data for Science and Technology, Antwerp, Ed. Böckhoff,K.H., Reidel,D., Publishing Company, Dordrecht (1983)p.414
5. Pavlik,A. and Winkler,G., private communication
6. Raics,P., private communication

DEUTERIUM GENERATOR FOR GAS TARGET

A.A. GOVERDOVSKIJ, A.K. GORDYUSHIN, V.F. MITROFANOV
Institute of Physics and Power Engineering,
Obninsk, Union of Soviet Socialist Republics

Abstract

The device filling gas targets with deuterium is described. The working substance of the device is titanium powder. The tests of the device have shown that the gas coming out of the powder does not contain impurities.

The $D(d,n)^3He$ reaction provides a perspective source of fast neutrons in the energy range from 4 to 10 MeV. The targets for this source can be deuterium gas target , which is more preferable in comparison with the metal-deuteride deposit. Their advantages are connected with a higher yield for a given energy loss, target backgrounds being correctly measured .

A generator-accumulator of deuterium for gas target filling has been constructed (Fig.1). Its operation is based on the property of titanium to absorb and to adsorb hydrogen isotopes with heating. The former process is more intensive at T=300°C, the latter increases very rapidly in the temperature range T from 500°C to 1100°C. Therefore, at low temperatures (T 300°C) titanium is an accumulator of deuterium, and a generator at high T=500°C. Other gaseous components were not found in the deuterium released.

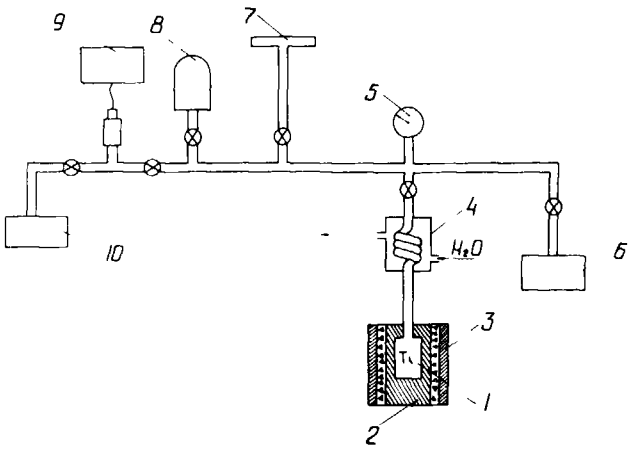

FIGURE. Schematic diagram of the experimental arrangement :

1) titanium powder;
2) stainless-steel container;
3) electrical heater;
4) refrigerator;
5) manometer;
6) emergency bolloon tire;
7) gas target;
8) thermocouple vacuum-gauge;
9) hydrargyrum manometer;
10) vacuum - pump.

Titanium has several advantages over uranium [1,2], for example, as a deuterium generator working substance. These are :

1) titanium is not radioactive ;

2) in case of emergency and dehermetization of the working volume the explosion of the uranium-hydride is not impossible;

3) titanium absorbs about 430 cm^3/1g(Ti) of the deuterium, while uranium - only 230 cm^3/1g(Ti);

4) titanium is more available in practice than uranium;

5) oxygen is not released by titanium with heating .

At the temperature T=700°C the formation and explosion of the combustible mixture (oxygen+hydrogen) was quite possible. Therefore, a considerable amount (about 200g) of titanium was available and the temperatures T were about 550-600°C. In the refrigerator (R) deuterium cools down to T_d=40°C.

In the identical experimental conditions more than 20 refillings were performed; small decrease of the gas-adsoption rate from 5 to 10% was found (T_{Ti}=600°C), while the change in the absorption intensity was negligible (T_{Ti}=300°C). It was concluded that the dominant mechanism was a leakage of deuterium through the stainless-steel walls of the working volume. The time-operation interval of the device was 2000^h. At the heating temperatures T_{Ti} 1000°C the surface layer of titanium powder can be baked, titanium absorption capability can decrease, but slightly - from 20 to 25% .

The inspection of quality of the deuterium released was done by means of neutron time-of-flight method. The flight path was more than L=2,6 m. A scintillation detector was used for measurements in the neutron energy range E_n 1 MeV; in the energy range E_n 1 MeV a double-ionization fission chamber with the ^{235}U and ^{238}U-radiators was used (L=0,7 m). General Conclusion : gas-cell was filled by pure deuterium.

REFERENCES

1. Fast neutron physics.Ed. by J.B.Marion and J.L.Fowler, INC., New York, 1960, v.1, p.87.
2. Birjukov N.S.ea. -PTE (Sov.), 1971, v.3, p.66.

SESSION V

14 MeV NEUTRON SOURCES

RTNS-II: EXPERIENCE AT 14 MeV SOURCE STRENGTHS BETWEEN 1×10^{13} AND 4×10^{13} n/s*

J C DAVIS
Lawrence Livermore National Laboratory,
Livermore, California,
United States of America

Abstract

The RTNS-II Facility was built at LLNL from 1976 to 1978 to provide two 14-MeV sources dedicated to irradiation of materials and components for the Magnetic Fusion Program of the United States Department of Energy Initial experiments began in early 1979 with a single source operating at a strength of 1×10^{13} n/s In 1982, a five-year agreement was signed between the US DOE and the Ministry of Science, Education and Culture of the government of Japan to operate the facility jointly for fusion irradiation experiments Under this agreement, both neutron sources became operational with source strengths rising to near the original design goal of 4×10^{13} n/s Nominal source design parameters are 150 mA of D^+ focused to a 1-cm diameter spot on a 5000 rpm titanium tritide target, producing a maximum useful flux of 1.3×10^{13} n/cm^{2}s In the past eight years, approximately one hundred 23-cm targets and seventy-five 50-cm targets have been produced and used Target output decays with a half-life varying from 75 to 200 hours at currents near 125 mA Average initial yield on a new target is 2.1×10^{11} n/s-mA, average total yield of a target before replacement is 1.1×10^{19} neutrons Lifetimes of ion source components range from 200 hours for cathode assemblies to as much as 1200 hours for extraction electrodes Power supplies, acceleration columns, most beam transport components and radiological systems have imposed no significant operational limitations Maximum fluence delivered in irradiations to date has been 1×10^{19} n/cm^2

Operation of the facility is currently scheduled to cease at the expiration of the joint agreement in February of 1987 The operational experience gained with accelerator, target and radiological systems will be reviewed, as well as design options and changes appropriate for inclusion in solid target 14-MeV generators designed to operate at higher source strengths The prospects for upgrading a source of this type to 4×10^{14} n/s will be discussed

---

* Work performed under the auspices of the US Department of Energy by the Lawrence Livermore National Laboratory under Contract No W-7405-ENG-48

INTRODUCTION

Ten years have passed since the design of the two RTNS-II (Rotating Target Neutron Source-II) 14-MeV neutron sources. These sources have now operated for a total of almost twelve accelerator years, providing irradiation services for a wide variety of nuclear physics and materials science experiments. With the closure of this irradiation facility scheduled for next year, a review of the successes and failures of its design concepts is particularly appropriate. Originally designed to operate at a peak neutron source strength of 4×10^{13} n/cm^{2}s, the sources have basically reached that goal. Essential in design of the sources was not just the production of high fluxes in themselves, but development of a facility that could support complex and changing irradiation experiments. The facility was to operate at high plant factor and at an acceptable cost in both dose delivered to operating staff and releases to the environment. The success of this endeavor is reviewed as well.

The possibilities of higher source strengths are discussed in light of the operating experience to date and of new technologies that may be applied to the problems of high flux generators of this type. Similarly, changes in the ancillary equipment that would provide more efficient or safe operation are also indicated.

1. Original Design Concepts and Expectations: 1974-78

Fundamental to the design of the RTNS-II sources was the experience with the RTNS-I source. Booth and Barschall[1] were the first to explain that the apparently anomolous target lifetime of up to 100 hours obtained with RTNS-I was a consequence of the use of a monoatomic deuteron beam. This beam produced the maximum useful neutron yield from the solid target without displacement of the tritium contained in the target by accompanying molecular species. As the RTNS-I source utilized an accelerator designed for both pulsed neutronics and intense flux production, this monoatomic beam existed as a result of a somewhat fortuitous design feature; the high-current duoplasmatron ion source in the high voltage head utilized a bending magnet to separate the ion species and provide monoatomic beam to simplify the bunching optics. Development of a clever splash-cooled 15-cm titanium-tritide target rotating at 1100 rpm provided a source strength near 2×10^{12} n/s at D^+ currents of 8 mA.[2] The accelerator was modified to produce D^+ beams up to 20 mA, and the target was enlarged to a diameter of 23 cm. By 1973, peak source strengths of 6×10^{12} n/s were produced routinely, and a variety of fusion-related materials irradiations and cross-section measurements had been performed.

The successful operation and understanding of RTNS-I, coupled with the energy crisis-induced expansion of the fusion programs of the United States, led the Livermore Laboratory to propose construction of a new intense source based upon the principles of RTNS-I. The final proposal, funded for construction in 1976, envisioned two neutron sources. Each source was to be capable of peak strengths of 4×10^{13} n/s with potential to be upgraded to 1×10^{14} n/s. Design concepts for the facility were discussed at some length in 1977;[3] a brief summary is given here. The arrangement of major accelerator and target systems is shown in Fig. 1.

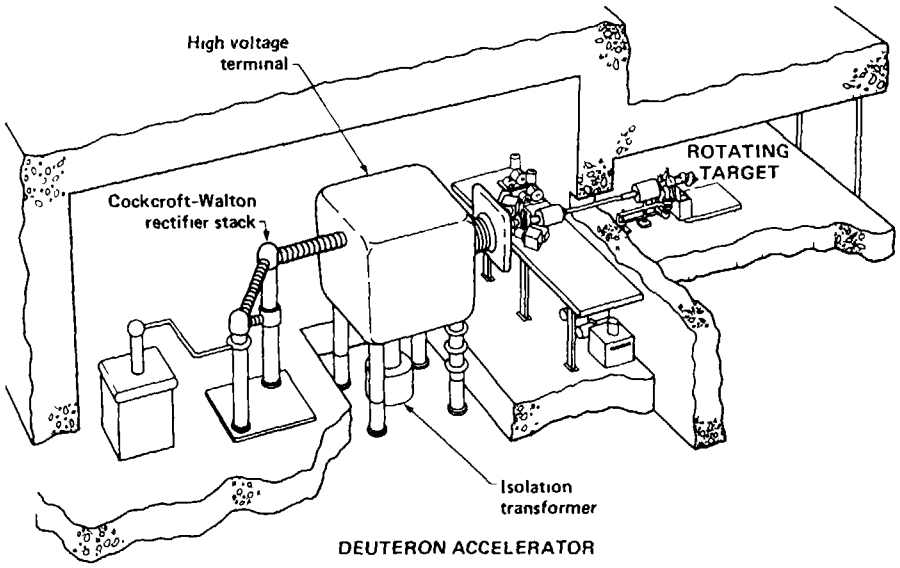

Figure 1
RTNS-II Neutron Source Schematic

Accelerators

Each accelerator was to produce a beam of 150 mA of D^+ at 400 keV, which was to be transportable to a target room several meters from the high voltage platform and able to be focussed to a spot size of 1 cm in diameter Rather than the magnetically coupled 60 Hz power supply of RTNS-I, 1500 Hz solid state voltage multiplier supplies purchased from Emile Haefele et Cie were utilized Each supply is rated at 300 mA and is upgradable to 500 mA by the addition of a second rectifier string To provide power in the 10 m^2 high voltage platform, a 75 kVA three phase isolation transformer is used Inside the high voltage platform, voltages of 480, 220 and 115 are distributed at single or three phase as required by electronics and power supplies Control of all components in the high voltage terminal is by robust single-channel fiber optic links, readout of terminal parameters is by both a multiplexed fiber optic link and a backup television link also transmitted via fiber optics

The ion source selected for use is a seven aperture reflex arc source The extraction supply installed originally was rated at 25 kV, 0 5A In operation on a test stand duplicating the 90° double focussing magnet selected for species separation, the source produced currents of up to 100 mA of H^+, suggesting its adequacy for this application The acceleration tube design is uniform gradient, utilizing five electrodes of 10-cm aperture with an active length of 25 cm Actively cooled electrodes fabricated of chromium-coated copper with molybdenum inserts shape the accelerating field The vacuum envelope of the acceleration tube is a 46-cm diameter ceramic vacuum brazed into four sections, O-ring joints join the separate sections Pumping was originally by directly coupled turbomolecular pumps A single 2000-l/s pump was installed in the high voltage terminal behind the analysis magnet and two 2000-l/s pumps on a plenum directly following the acceleration tube The original vacuum system was all stainless steel with O-ring seals near the ion source and metal seals in the section between accelerator and target Two 1000 l/s turbomolecular pumps removed the gas load at the target

Currents in the transport section in the ion source terminal are read from both fixed and insertable electrodes, while beam position is determined with a television viewer that observes the recombination light from ionization of residual gas in the beam line Beam diagnostics in the transport system at ground potential utilize graphite limiting apertures on which power can be read both electrically and calorimetrically, and optical monitors similar to those in the terminal The beam spot on the rotating target is observed by a television camera looking down the transport system from behind the bending magnet in the terminal All elements in the entire accelerator system are shown in Fig 2

Target

The tritium containing target layer selected from trials on the RTNS-I machine was chosen for these sources After evaluating several thicknesses and types of tritium occluders, a nominal thickness of 10 μm of titanium was found to retain tritium for the longest useful lifetime while minimizing tritium inventory Targets lasted for an average of 100 hours before the yield decayed to half the initial value After that time, the neutron output of the target decayed more rapidly Initial yield from a fresh target was $2\ 5 \times 10^{11}$ n/mA

Mechanical design of the target system envisioned operating the target layer within the envelope of the same thermal cycle experienced on RTNS-I, thus achieving the same lifetime To accomplish this, the target diameter had to be increased to 50 cm, and the speed of rotation increased to 5000 rpm At this speed, cooling of the target by immersion in a thin film of water was no longer possible because of drag considerations, thus, an internally cooled target was required with rotating fittings for water feed and drain Target substrates were made by diffusion bonding of two layers of copper alloy, one etched to contain the cooling channels Initial substrates were 23 cm in diameter To reach the high rotating speed desired, a differentially pumped bearing was built to support the target Mechanical loads are carried by a large aperture precision ball bearing assembly, and an air-levitated differentially pumped seal provides vacuum isolation The bearing assembly is driven by an air turbine The assembly is mounted on a cart with all utility interfaces running through a single panel to allow for remote changeout The target cart was also designed to support the irradiation experiment and provide utility services to it as well

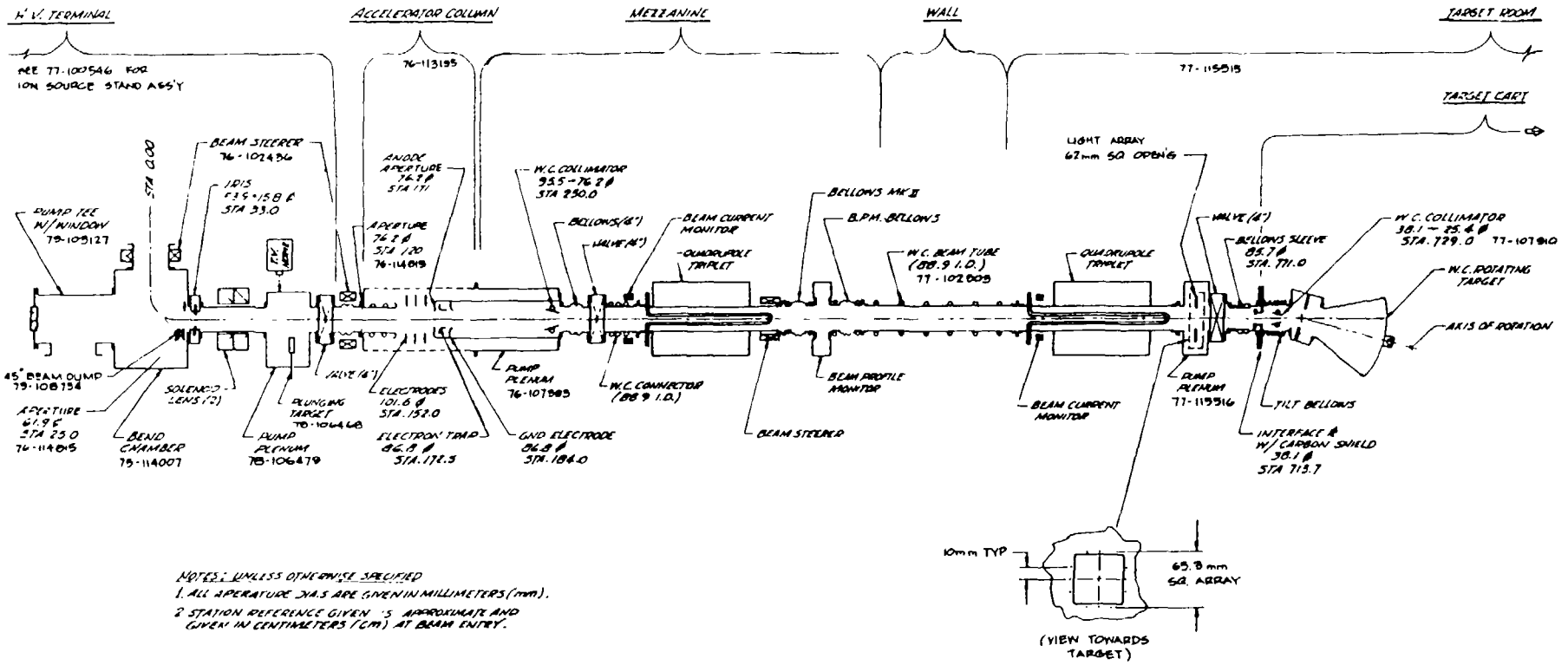

NOTES: UNLESS OTHERWISE SPECIFIED
1. ALL APERATURE DIA.S ARE GIVEN IN MILLIMETERS (mm).
2. STATION REFERENCE GIVEN IS APPROXIMATE AND GIVEN IN CENTIMETERS (cm) AT BEAM ENTRY.

Figure 2

Beam Transport System

Ancillary Systems

Containment and control of prompt and residual radiation without compromising convenient access to the working points of the sources were important design criteria for this facility The floor plan of the facility is shown in Fig 3 To contain the prompt radiation, walls of the target cells were made 2 5 m thick, yielding an attenuation factor of 10^8 Reinforcing bars in the cell walls were placed no closer to the surface of the concrete that 40 cm to reduce the dose in the target room contributed by activation of the iron Target rooms are kept at negative pressure during operation, and the exhaust from them passed through particulate filters to minimize the inventory of airborne species and activated dust released up the facility stack Temperature in the target rooms was stabilized by wholly contained cooling systems in each room

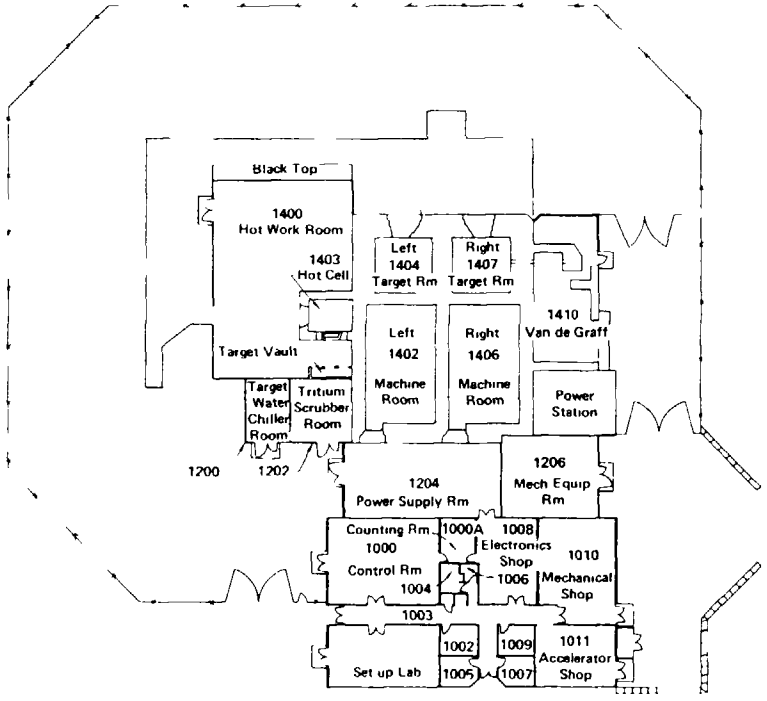

Figure 3

RTNS-II Facility - Bldg 292

Controlled access work space for the repair and storage of activated or contaminated irradiation assemblies and target assemblies was built into the facility Included in this 300 m^2 hot workroom were a hot cell with traditional remote manipulators, a storage vault for temporary storage of used targets, fireproof vaults for longer term storage of new targets, and hoods for maintenance of tritium contaminated equipment A remote handling system was included to transport target carts between the hot cell and the target rooms

Protection against tritium released by the targets during operation and reduction of the amount exhausted up the facility stack is provided by online catalytic tritium scrubbers through which the exhaust of all pumps in the facility passes Tritium content of the air in all accelerator and target rooms, in the maintenance areas, in the enclosures around the scrubbers and in their input and output streams, and in the facility exhaust stack itself, is continuously monitored and recorded The presence of tritium throughout the facility and in the body tissues of the operating staff is monitored by a combination of swipe tests and urine analyses Fortunately, the 10 years experience gained with RTNS-I provided useful guidance in establishing protocols for contamination control All target containers are opened under hoods in case of particulate release, and respirators and gloves are used in all target changing operations A fundamental goal in establishing rules for all handling of radioactive materials was to keep individual annual dose below 0 5 rem Except in emergencies, no entry to target pits was to be made for the first 8 hours after extended operation

2 Operating Experience and Modifications 1978-1986

The construction phase of the RTNS-II project reached completion in November of 1978 [4] Unfortunately, the Magnetic Fusion Program was able to provide only 60% of the funding estimated necessary to operate the two sources in the 24-hour per day mode for which they were designed Consequently, only one source was operated for the next 4 years for 16 hours per day Since the accelerator had been tested successfully by operating one system as a prototype with hydrogen beams during the construction project, the accelerator design staff were reassigned to different Laboratory activities Operation

during the first few years reached source strengths of about 1 5 x 10^{13} n/s and the first few 50-cm targets were produced Because of the reduced operating week and low source strength, maintenance could be easily accomplished, and the systems were not stressed to their design levels

In February 1982, a joint agreement to operate RTNS-II was signed between the Ministry of Science, Education and Culture (Monbusho) of the Government of Japan and the Department of Energy of the United States For the first time, resources adequate to operate both sources continuously and to push them to higher strengths were available Since that time, source strengths have reached nearly 4 x 10^{13} n/s and availabilities of about 85% have been obtained in 24-hour per day operation for 5-day weeks [5] Initial and current parameters of the sources are given in Table I The agreement between the US and Japan expires in Feburary 1987 At that time, the facility will be shut down and preserved for possible future use

Table I

Initial and Present Characteristics of RTNS-II Neutron Sources

	Initial	Present
Total energy of beam	360 keV	365 keV
Ion source extraction voltage	25 kV	35 kV
Ion source arc current	40 A	50 A
Maximum beam current	45 mA	150 mA
Maximum neutron production	10^{13} n/s	3 5 x 10^{13} n/s
Target substrate size	23 cm	50 cm
Target tritium content	4 4 x 10^{7} MBq	1 8 x 10^{8} MBq

Accelerators

In general, the accelerators have operated with excellent reliability and simplicity The limiting feature has been the atomic species output of the ion source In early operation, this fraction was as low as 30% of a total extracted current of 150 mA In 1982, the original 25-kV extraction supplies were replaced by 35-kV supplies of the same 0 5 A rating This modification, combined with raising the arc power from 2 5 kW to 5 kW has raised the atomic species current available for acceleration to over 150 mA, with target currents of up to 150 mA possible Successive developments have produced extraction grid sets that last over 1000 hours and cathode assemblies that run for up to 250 hours before replacement Atomic fraction still remains below 50%, however, and the terminal pumping system has been upgraded to a total of 4000 l/s capacity

The acceleration columns have operated without modification or failure except for three occasions two when insulators shorted on the electron suppression electrode at ground and one when a cooling line in the accelerator terminal failed into the vacuum system However, the sparking rate of the tubes is very nonlinear with current and voltage Sustained operation at the design voltage of 375 kV (nominal beam energy of 400 keV) is not possible without excessive sparking Lowering the column voltage to 330 kV reduces the sparking rate to 4 5 per hour at currents near 135 mA, and produces little penalty in neutron output The cause of the sparking is throught to be x-ray induced charging of the smooth inner surfaces of the insulators A new tube of identical electrostatic geometry, but with thicker electrodes and ceramics with convoluted inner surfaces has been built This tube will be installed and tested if the operating schedule allows Sections of the two tube types are shown in Fig 4

Operation of all high voltage systems and power supplies has been excellent Only nominal maintenance has been necessary for components in the high voltage terminals Less transient induced damage has been observed than expected, a tribute to the excellent power distribution and grounding protocols in the design The main high voltage supplies have required occasional replacement of diode sections, and each isolation transformer was opened shortly after initial operation to correct grounding errors on the secondary leads Use of highly derated equipment has yielded excellent reliability

Transmission through the acceleration tube and the transport system to the target is virtually 100% However, the occasional thermal loading of elements during tuning caused welds to fail in the original hard-sealed stainless steel beamline Gradually, most of the stainless steel transport system has been replaced by water cooled copper components with elastomer seals The two 1000-l/s pumps at the target were replaced by two 2000-l/s

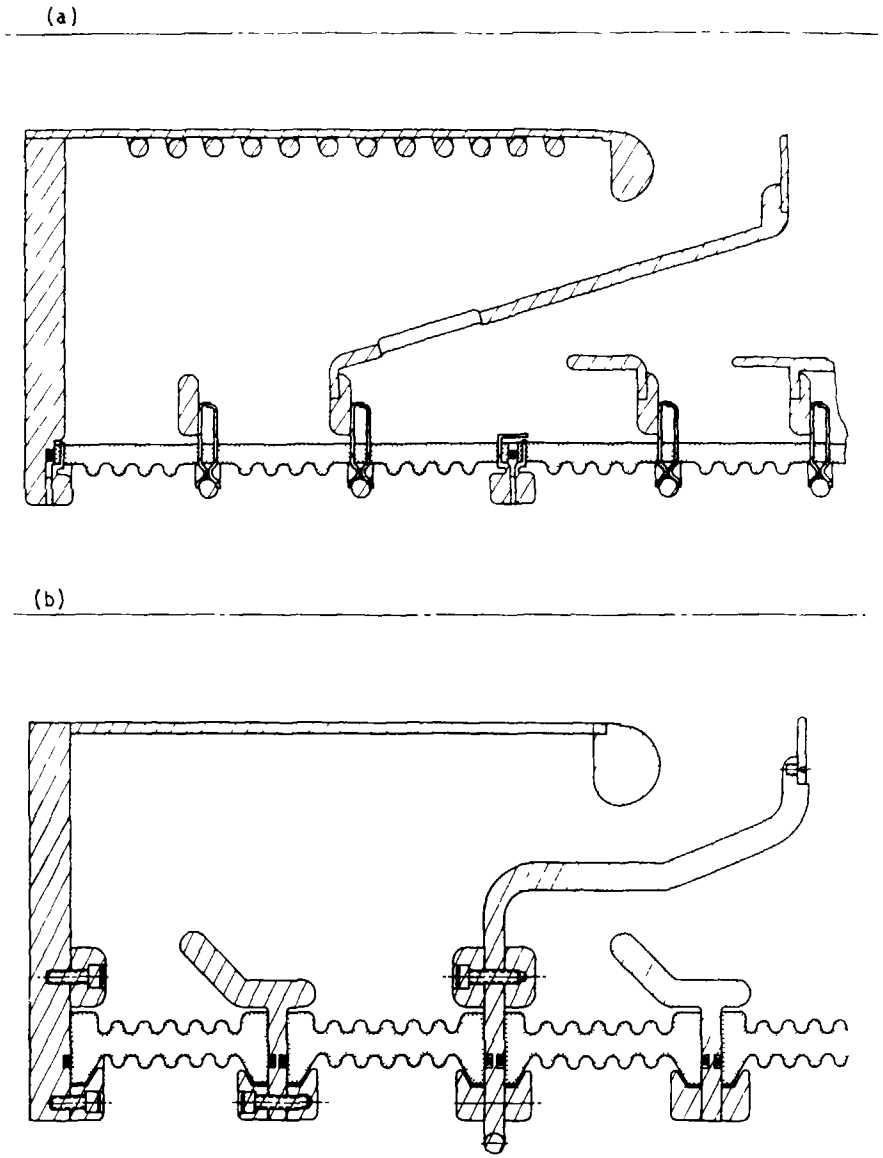

Figure 4
Old and New Acceleration
Tube Details

pumps to improve operating vacuum there. Static pressure throughout the system is in the low 10^{-7} Torr range. Operating pressures are typically 10^{-4} Torr near the ion source, 10^{-6} Torr in the transport region and 10^{-5} Torr at the target. All of the original Sargeant-Welch turbo pumps have been replaced by Balzers pumps.

No satisfactory visual diagnostic has been developed for tuning the beam spot on the rotating target. The light produced by the beam on the target varies with target and gas pressure, and has never been successfully correlated with the fluence measured by radiographic means. A combination of sputtering and radiation damage rapidly darken the window through which this light is observed. Similarly, there is no real time flux diagnostic; fluence is still measured for each irradiation by foil activation. The geometry of the target assembly and the irradiation packages precludes use of the sort of neutron imaging systems that might otherwise be thought useful.

Target

Original operation was with 23-cm targets whose substrates were fabricated at LLNL and then shipped to Oak Ridge National Laboratory for titanium deposition and tritium loading. At currents in the 40-70 mA range, these targets did indeed have useful lifetimes of 100-150 hours; however, considerable variation in target quality (as evidenced by failure early in operation) and in lifetime was observed. In parallel with the operation on 23-cm targets, the production sequence for 50-cm targets was developed. Approximately one hundred 23-cm targets were used before operation with them was discontinued.

Difficulties in control of the diffusion bonding, hydrostatic deformation and pressure testing processes involved in production of the target substrates led to unacceptable losses in the process. The diffusion bonding technique was abandoned and replaced with an electrodeposition process. Target substrates are now made by depositing a thin copper layer over etched cooling channels that are filled with conductive wax. The wax is subsequently melted and blown out. High success rates are obtained now, and the resulting target has slightly better thermal properties as the electrodeposited copper has higher conductivity than the alloy previously used. Partly because of the variation observed with the ORNL loaded targets and partly to establish total

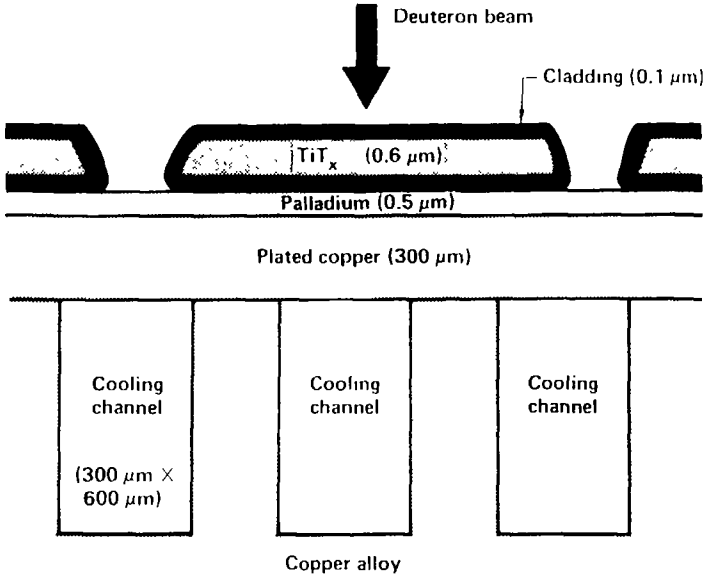

Figure 5
Schematic of Layered Target

control of the thermal cycles to which the targets were subjected in all preparation steps, we decided to perform the tritium loading operations for the 50-cm targets at LLNL. A dedicated loading system was built in the LLNL Tritium Facility for this mission.

Routine operation with 50-cm targets began in 1982. To date, a total of 75 of these targets have been produced. Average initial yield of a new target is 2.1×10^{11} n/s-mA; average total yield before replacement is 1.1×10^{19} neutrons. In this period of operation, two targets have failed mechanically while in operation by collapsing under atmospheric pressure and loading caused by rotation. These failures are thought to have resulted from radial expansion of the target rim. The design of the target system relies on radial stiffening by a graphite composite hoop into which the target is installed. Elastic deflection of the target shell under vacuum loading brings the target rim into contact with the stiffening hoop. An undersized target may deflect too far before contacting the stiffener, then buckle under the additional loads imposed by rotation. More careful control of target dimensions has prevented a reoccurrence of this failure. In both incidents, the rotating bearing suffered major damage, but there was no violent disassembly of the target system.

Ancillary Systems

Performance of the various supporting systems has ranged from vital and excellent to irrelevant and virtually useless. The tritium scrubbers have functioned with very little maintenance, removing tritium from the exhaust of the vacuum systems at factors approaching 10^6:1. After several years of operation, it became evident that the annual release of 20-80 curies resulted from roughing out operations during which the scrubbers are bypassed. Installation of a large volume tank in the roughing system allows these surges of gas to be buffered from the scrubbers. The stored gas is then slowly processed by the scrubbers. Release of tritium from the facility is expected to be less than 10 curies per year with this modification.

Because of the complexity of the experiments fielded (typically multi-week irradiations under high vacuum and at carefully controlled temperatures ranging from 20° K to 720° K), the original concept of withdrawing the target assembly and experiment for weekly target changes has never been used. The weekly cooldown period over each weekend has allowed access to the target rooms on Monday mornings for both target changes and repair or adjustment of experiments. Neither the remote handling equipment nor the hot cell have ever been used as originally intended.

Radiological Experience

Dose levels to operating staff remained below the 0.5 rem annual target during the first few years of operation of the facility with the average annual dose to workers actually handling maintenance operations being typically 100-150 mrem. The contribution to total dose from tritium retained in the body tissues was 10% of the total dose. No neutron dose has ever been recorded for any staff member.

After switching to 50-cm targets and beginning 24-hour operation of both sources, the average annual dose climbed to 250 mrem. Three or four

individual doses in the 500 mrem to 1 25 rem range were recorded in the years 1983 and 1984 This increase in dose resulted from higher residual activities caused by higher source strengths, extra maintenance operations in debugging larger target assemblies, and the more delicate operations and longer times required to change the larger targets More stringent control of personnel entry to the activated areas, increased hardware reliability, more carefully defined target replacement procedures and rotation of staff have reduced the annual doses to their previous levels

In this period, both the long lifetime activation and tritium contamination levels in the target cells increased More elaborate entry and exit and protective clothing requirements were instituted to prevent the spread of contamination However, in the summer of 1984 a major spread of tritiated particulates (perhaps 100 microcuries total inventory) was detected throughout the facility A shutdown of several weeks was required to clean the facility before operation could be resumed The origin of the particulates (determined to be from a target) and the exact mechanism of spread of them throughout the facility remains uncertain What was clear was that the daily sequence of swipe testing had failed to detect the contamination because of the exceedingly low exchange of tritium from the particulates to the scintillation solution used in the swipe testing The particles represented little biological hazard because of this low exchange rate and because they were not of the size to be retained in the lungs Procedures were modified to require careful and slow scanning of personnel and equipment with thin window x-ray detectors before leaving contaminated areas Full body suits, gloves, boots and face shields are now used in target areas Flow paths of people and components through the facility were modified to provide more limited pathways for particulate spread and a convenient station for monitoring for contamination Since that time, no further spread of contamination has occurred

3 Future Possibilities

Discussions of improvements or upgrades of the technology of this particular source technology are somewhat colored by the scheduled termination of operations at RTNS-II This closure will leave RTNS-I at Livermore, Oktavian at Osaka and FNS at Jaeri, all operating in the 4 x 10^{12} n/s range as the strongest 14-MeV sources available until Oktavian-II becomes operational Nevertheless, as there are no plans for the construction of more intense neutron sources in this energy range for any applications in the near future, it is perhaps useful to document the ideas relevant to the further development of this approach

Accelerators

Design of the RTNS-II sources anticipated the possibility of an upgrade to 1 x 10^{14} n/s in the power supplies and shielding of the accelerator systems By adding another rectifier stack to the high voltage supply, it is possible to raise the current rating of the supplies to 500 mA at 400 kV Similarly, a second isolation transformer can be added to the high voltage platform to increase the power available at 400 kV to 150 kVA, adequate for any likely ion source Utilization of this capability requires an ion source producing 0 5 A of atomic deuterium without excessive molecular components At present, developments in the use of large RF ion sources suggest that this step may be possible Sandia Albuquerque is currently debugging a 50 A RF source built by TRW Corporation for thermal testing of tokamak limiter materials Initial short pulse operation of the source is encouraging [6] LLNL has discussed with TRW the purchase of a version of this source rated at 2 A of D^+ Sufficient power exists in the high voltage terminal to operate the source The new acceleration tube would probably accelerate at least 0 5 A of current, above that level the redesign of the electrostatic optics might be required The main attractions of the RF source are high atomic fraction and absence of cathode structures Recent experiments with RF sources having ceramic arc chambers and external antennas offer the hope that erosion of antenna insulators may be avoided as a limiting problem

The balance of the present accelerator system is adequate for operation at higher currents unless a newer ion source generates a significantly greater gas load It would be difficult to increase the delivered pumping speed on the accelerator without major and unwieldy rebuilds of the vacuum system The optical components of the transport system presently operate at fields indicating complete space charge neutralization of the ion beam, no serious problems are expected at currents a factor of ten higher Total costs of the

changes necessary to try to produce 10^{14} n/s are under $750K The reconfiguration of an accelerator to produce 1 5 A of D^+ at 400 keV for a 4×10^{14} n/s source is estimated to cost $5-6M All projected costs assume continued operation of at least one source

Target

Construction of a target able to operate at higher powers with an acceptable lifetime is the major uncertainty in the extension of this technique to higher source strengths A major study[7] of such an extension has been performed by David Tuckerman of LLNL His modeling of the present target suggests that improvements in the aspect ratio of the cooling channels, thinning the layer between water and target layer, doubling the target speed and diameter, and using microfabrication techniques to encapsulate the tritium-bearing material in refractory layers and place a palladium drain layer in the target would produce a target able to operate at the 750 KW/cm^2 necessary for a 4×10^{14} n/s source The development and fabrication costs for this target system are estimated to be $4 5M

Ancillary Systems

Most outstanding of the problems for a source operating at higher source strengths will be the need for fully automated exchange of targets At present, we are operating near the limit of the duty factor-dose tradeoff If complicated experiments are to be exchanged and positioned remotely, the cost of the utility support and remote handling systems will easily exceed the cost of the source itself The point may rapidly be approaching where it will be more cost effective to relocate the source than the experiment because the former has a lower activation level and can be more easily serviced The failure of the conventional hot cell to be useful for maintenance operations at the present source strengths suggest that ample storage space, spares and a clever glove box system would meet these needs in a more cost effective and realistic manner Costs of facility improvements adequate for operation at 4×10^{14} n/s are estimated at $5M

Summary

The RTNS II Facility has met the technical and program goals set out at the time of its proposal in 1974 The solid target neutron generator technology still has reserve for further development An investment of $15M could provide yet another factor of ten enhancement in source strength As RTNS-II provides both irradiation data and valuable operating experience with high duty factor tritium contaminated systems, a further investment in this technology seems appropriate if the fusion budget enters another period of growth

Acknowledgements

The operation and improvement of RTNS-II has been made possible only through the efforts of a dedicated group of scientists, engineers and technicians over a long period Clint Logan, Dale Heikkinen, Bruce Schumacher, Dexter Massolletti and George Harter are particularly appreciated for their contributions to the success of RTNS-II in general and to this review in particular The author looks forward to working with them on future projects with great pleasure

REFERENCES

1 R Booth and H H Barschall, Nucl Instr Meth 99, 1 (1972)

2 R Booth, IEEE Transactions NS14, 938 (1967)

3 R Booth, J C Davis, C L Hanson, J L Held, C M Logan, J E Osher, R A Nickerson, B A Pohl and B J Schumacher, Nucl Instr Meth 145, 25 (1977)

4 J C Davis, D W Heikkinen, J L Held, C M Logan and J E Osher, IEEE Transactions NS26, 3058 (1979)

5 D W Heikkinen and C M Logan, Nucl Instr Meth B10/11, 835 (1985)

6 J Whitley, private communication

7 Fusion Materials Science at Reactor 14-MeV Neutron Fluxes, D B Tuckerman, UCID 2040 (1984)

Review Paper

INTEGRAL STUDIES BY 14 MeV NEUTRON SOURCES

K SUMITA
Faculty of Engineering,
Osaka University,
Osaka, Japan

Abstract

In these five years, the integral studies by D-T Neutron Source were carried out mainly to resolve the problems of fusion reactor neutronics In addition to RTNS-I, OKTAVIAN, FNS and LOTUS were newly built for this area Recent remarkable progresses in several fusion neutronics integral experiments are introduced here as well as to the neutron source properties and experimental methods

Those new machines have the very similar neutron intensity of 5×10^{12}n/s order and proved that their neutron intensities were enough to resolve the problems concerned with neutron spectrum However to measure the Tritium Breeding Ratio directly, it may be helpful for us to have higher intensity with nearly point-source characteristics

RTNS-II with the highest D-T neutron intensity of 6×10^{13}n/s has mainly served for the fundamental studies of radiation damage, however, it has been sometimes very useful for fusion neutronics integral experiments

---

1 Introduction[1~4]

D-T Neutron Sources have a long and respectable history for serving traditional nuclear studies from the early age On the way to develope the nuclear fission reactor after World War II they have contributed to many integral neutronic experiments in reactor physics due to their easier and economical production of neutrons even though there exists a large difference of source energy between D-T reaction and nuclear fission It must be remarked that such difference did not cause any difficulty in analyzing the results of integral experiments because of the unique characteristics of major problems in fission reactors (i e , solving eigenvalue problems) The technique so called Pulsed Neutron Method (neutron die away experiments) has been a convenient way to measure the diffusion parameters and thermalization costants of moderators by a small pulsed neutron generator Those ways have been developed to measure the degree of of criticality by using a small sealed D-T source in a subcritical reactor Such method can be applied for both thermal and fast reactors It should be noted that the pulsed neutron intensity of D-T source over $10^{6\sim8}$ n/s is not required for such integral experiments in multipling medium For neutron thermalization studies, the intensity is optionally required to be $\sim10^{6\sim9}$ n/s and most ambitious experiments such as a time dependent spectrum measurement in multipling medium demand the intensity close to 10^{11}n/s

Now, it is clearly required for us to have 14 Mev Neutron Sources for promoting various neutronic researches and developement works for D-T fusion reactors and large scale facilities serving D-T fusion studies The most typical example is the source to measure neutron cross section of fusion materials in the high energy region, where accuracies of cross section is not satisfactory The D-T source is sometimes inconvenient due to its fixed energetic characteristics, and mono-energetic neutron sources with wide energy selection may be required for such needs

Since 1980, however, in the fusion neutronics area many integral works have been performed The efforts have been concentrated so far on the following categories, Neutron Transport Problem (including Tritium Breeding Problems, Neutron Shielding & Streaming) and Material Problems (mainly Induced Activity and Radiation Damage Fundamentals) Such experiments ask for 10^2 times higher intensity to get accurate and useful results for reactor design than in fission reactor studies

Several experiments were carried out in the early stage using the sources at our hands for fission reactor physics Generally their results are lacking in the good statistics Requirement of energy condition is rather strict in realizing fusion reactor conditions and also the point source condition is very optional to make a simple system for easy analysis These requirements may be difficult terms to be satisfied by other type neutron sources except for the D-T reaction itself

Then, urgent construction of neutron sources with higher intensity was requested as the first step[5] In addition to the first D-T neutron source, RTNS-I (LLNL, USA)[6] of 10^{12}n/s order with a rotating solid tritium target, two nearly same type intense sources, OKTAVIAN (OSAKA UNIV Japan)[7](Fig.1) and FNS (JAERI, Japan)[8](Fig.2), were constructed for fusion studies LOTUS (EPFL, Switzerland)[9](Fig 3.4), was also built for fusion studies by introducing another type of machine, using the D-T mixed beam injection on a fixed conical target developed for cancer therapy These neutron sources have intensities very close to each other of about $5x10^{11}$n/s, and first three sources can supply pulsed neutrons of nano-second width Presently the

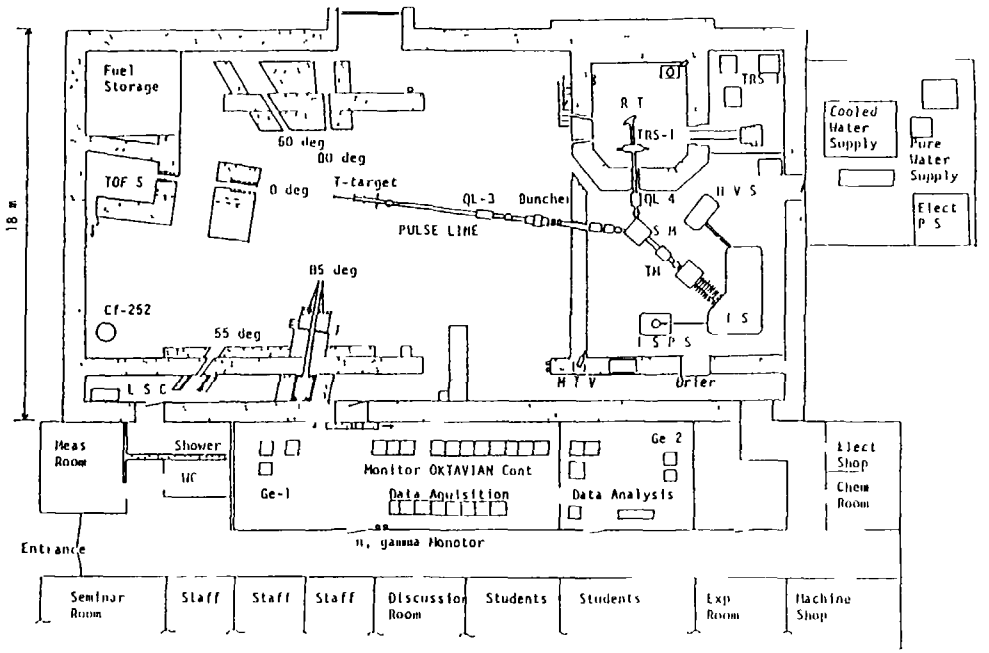

Fig.1 OSAKA UNIVERSITY INTENSE 14 MeV NEUTRON SOURCE FACILITY (OKTAVIAN)

world most itense D-T source is RTNS-II (LLNL, USA)[10], which can supply $5x10^{13}$n/s with a large diameter rotating target, but it is operated in the DC mode only The activities of such newly constructed D-T sources are aiming at studies on fusion neutronics (see Table I) They have highly contributed to the integral experiments in these 5 years. Through these experiments and analyses, significant improvements have been made, for example, in the tritium production cross section of Li Recently the source energy characteristics of these water cooled complex target construction have been investigated, and the results indicated that careful corrections on experimental data should be considered

For the next stage, several proposals to build more intense new D-T sources for integral experiments have been announced, but no project has been establishd so far on the budgetally background Power increase of present machines are also proposed. Technically, it seems to be fairly difficult, but not impossible to get 10~50 times jump in intensity and to solve the problems in prolonging the target life. Even if this modification is possible only in the short pulsed operation mode, very fruitfull results are expected In the future, we hope to use more intense D-T sources for D-T fusion study, especially for integral experiment in fusion neutronics.

From the last 1985 fisical years, it was started to design OKTAVIAN-II as a new national facility for university researchers, by Osaka Univ. group with industrial volunteers. At present conceptional design, we intend the 10 times of continious neutron yield, and 100 times of pulsed neutron yield of the presemt OKTAVIAN-I, the former characteristics of our design is near value of US RTNS-II, the latter may be very unique characteristics for time dependent damage experiment and calibration of pulsed fusion diagnotics as well as many precise fusion neutronic experiment. Major R&D items may include developements of Tritum Target and High Beam Current Pulsing Technique Total budget to be requested for whole project is very breafly estimated between 15 and 20 M$

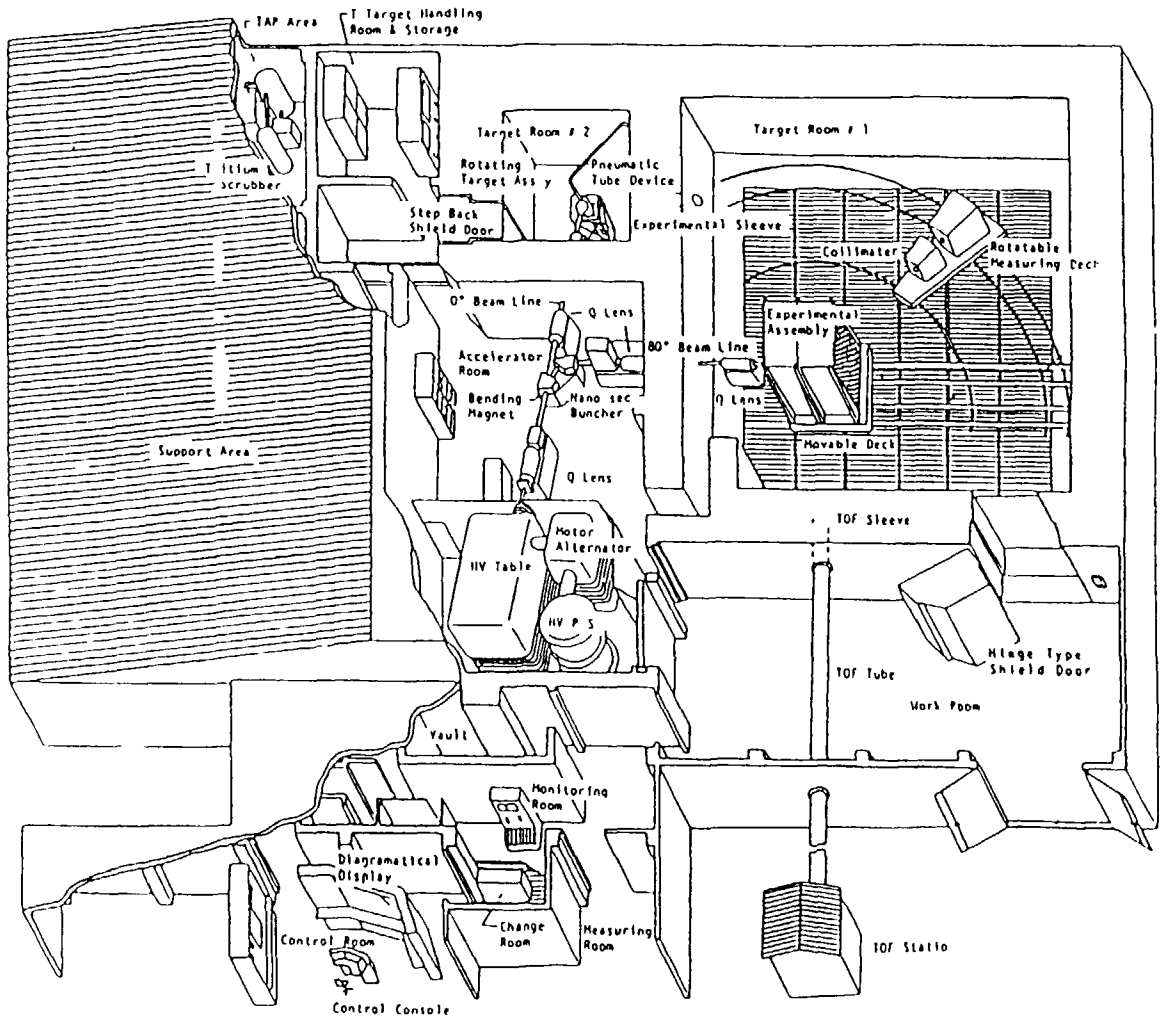

Fig.2 Top view of FNS point neutron source facility.

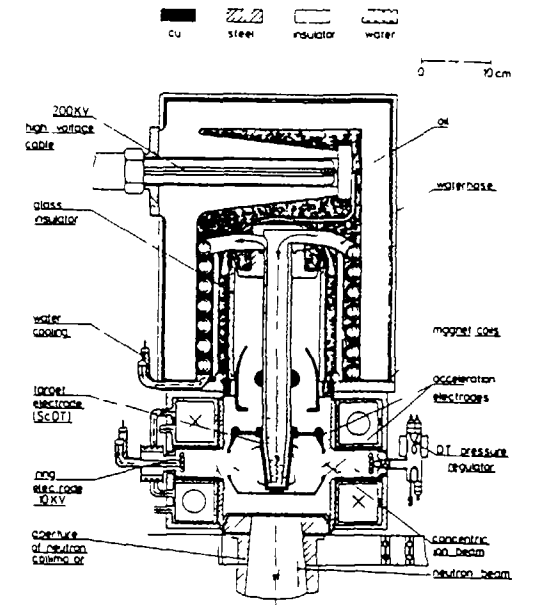

Fig.3 Schematic diagram of sealed neutron tube and accessories for a high-intensity neutron generator. A mixed beam of deutrons and tritons from a toroidal ion source is focused by magnetic fields onto a conical target at the centre.

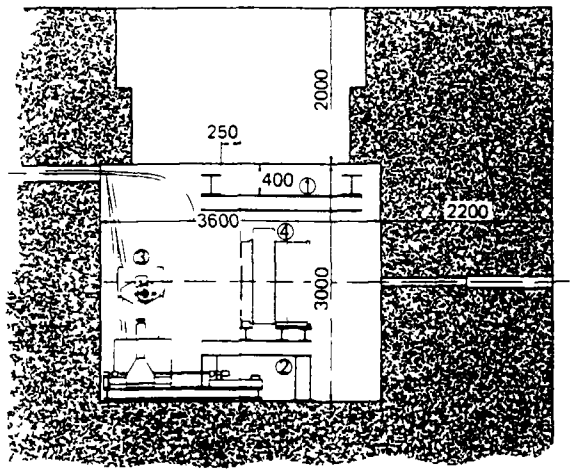

Fig.4 Schematic diagram of the LOTUS test chamber showing upper and lower support structures and neutron generator (1= upper support structure; 2=lower support platform; 3=neutron generator; 4=LOTUS blanket assembly).

Table I D-T Neutron Sources for Integral Experiments in Fusion Neutronics Studies

Accelerator Name (Status) Location & Facility	RTNS I (in operation) U S A LLNL	RTNS-II (in operation) U S A LLNL	FNS (in operation) JAPAN JAERI	OKTAVIAN (in operation) JAPAN Osaka Univ	LOTUS (in operation) SWITZ EPFL
High Voltage(KV)	400	380	400	300	250
Ion Source Data					
Type	Duoplasmatron	Duoplasmatron	Duoplasmatron	Duoplasmatron	Toroidal
Ion beam	D^+	D^+	D^+	D^+	$D^+ + T^+$
Current(mA)	40	150~400	35	35	500
Analyzing Magnet at Ion Source Outlet	with	with	with	with	without
Target Data					
Diameter (cm)	23	23 (50)	23	20	4 (conical)
Beam spot size in diam (cm)	0 6	1 0 (1~2)	1 5	3	50 cm^2
Beam current (mA)	25	130	20	23	500
Rotating speed (rpm)	1100	5000	1100	800	——
Cooling medium	Water	Water	Water	Water	Water
Tatget lifetime (h)	100	100	100	100	500
Continuous Neutron Yield (n/sec)	6×10^{13}	3×10^{13} (10^{14})	5×10^{12}	4×10^{12}	5×10^{12}
Pulsed Beam Width (nsec in FWHM)	1 5	— ——	2	1 5	——

Table II Aiming accuracy and the estimated uncertainty of the quantities related to nuclear design proposed by designer side [11]

Quantity	Aiming accuracy	Estimated uncertainty	Major limiting factors and cause of uncertainty
a Tritium breeding ratio	1%	10%	Nuclear data, heterogeneity
b Nuclera heating rate			
Vacuum vessel	20%	100%	Transport calculation
Tritium breeder	5%	50%	heterogeneity
c Bulk shielding			
Superconducting magnets	10%	100%	Nuclear data, design criteria
Biological shield	50%	350%	Nuclear data, skyshine
d Streaming effect			
SCM(Cu insulator)	10%	500%	
NBI(Insulator)	20%	100%	Transport calculation
Instrumentation (window, semiconductor)	10%	100%	Gamma-ray production data
Cryopanels (heating)	20%	100%	
e Induced acivity			Activation cross sections
NBI	50%	200%	
Instrumentations	50%	200%	Impurity content
Dose rate distribution	50%	500%	Transport calculation Corrosion Products

2 Neutronic Tasks for Fusion Reactor Design

There are many candidates for a future fusion reactor in energy balance competition However, neutronic works are ,so far, mostly common in each reactor design Major tasks of nuclear design of a fusion reactor are abstracted as follows.[11]

1 Estimate the accurate net tritium breeding ratio
2 Estimate Nuclear Heating in the component
3 Protect radiation sensitive component,e g ,superconducting magnet
4 Protect public and personnel from irradiation during reactor operation and at shutdown
5 Analyze fusion neutrons for plasma diagnostics
6 Aiming accuracy

The aiming accuracy and the estimation of the presentlly achievable accuracy of quantities related to the above tasks are presented in Table-Ⅱ[11] With some comments on the limiting factors of accuracy and the cause of uncertainty It should be noted that there is still a large difference between the aiming accuracy and the estimated uncertainty

To improve the accuracy of tritium breeding ratio, nuclear data improvement and heterogeneity treatment of the breeding blanket composition are requested Especially, improvement of energy and angular distribution data of secondary neutrons from the composite nuclides of the blanket is required (so called, DDX Measurement)[12]

In the calculation of neutron transmission through bulk shielding, the accuracy of neutron transport cross sections seems to be the limiting factor Duct streaming and skyshine problems are serious matter for design The γ-ray production data should be improved for calculation of nuclear heating in superconducuting magets and cryopanels

For the induced activity calculation, the accurate activation cross sections are needed not only for the major component elements but also for impurity elements

3 Double Differencial Cross Section (DDX) Measurement for D-T Neutron

First extensive measurements of DDX by D-T neutron source around 14 MeV incident neutron energy were carried out by using a fairly small source at Dresden[13] in 1970 s, their massive data book was only one systematic compilation for DDX for 14 Mev neutrons Of cource, several endeavors have been reported element by element independently

DDX data of 25 elements for fusion reactor materials have been measured at the OKTAVIAN facility in these five years [14] These measured data have been also useful to point out guide lines for re-evaluating nuclear data libraries like ENDF/B-IV and JENDL-2, although the incident neutron energy varies with the change of scattering angle Through the comparison work with available evaluated nuclear data libraries, we have contributed to the present jobs of ENDF/B-VI, JENDL-3PR2, etc

It has become clear that the direct and semi-direct processes are important for the secondary neutron emisson data at 14 MeV For beavier elements, excitations of discrete and collective levels by inelastic scattering should be further investigated It is expected to collect angular differential data for individual levels at specfied neutron energy For light elements, angle-energy correlation data (DDX) are important for continuum neutrons Hence, a high resolution DDX measurements with fixed incident energy are required A new deg and 8 m TOF system[15] (Fig 5) was constructed for this purpose at the OKTAVIAN facility Using this system, re-measurements have been planned for some of the 25 elements (Fig 6) and new measurements will be started for other elements than the 25 By the new system, reaction cross section data for individual reaction channel will be expected to evaluate due to the fixed incident neutron enargy Besides the activities of OKTAVIAN, A dynamitron of Tohoku Univ have also served to DDX measurements of about 10 elements which included B F and Si [16]

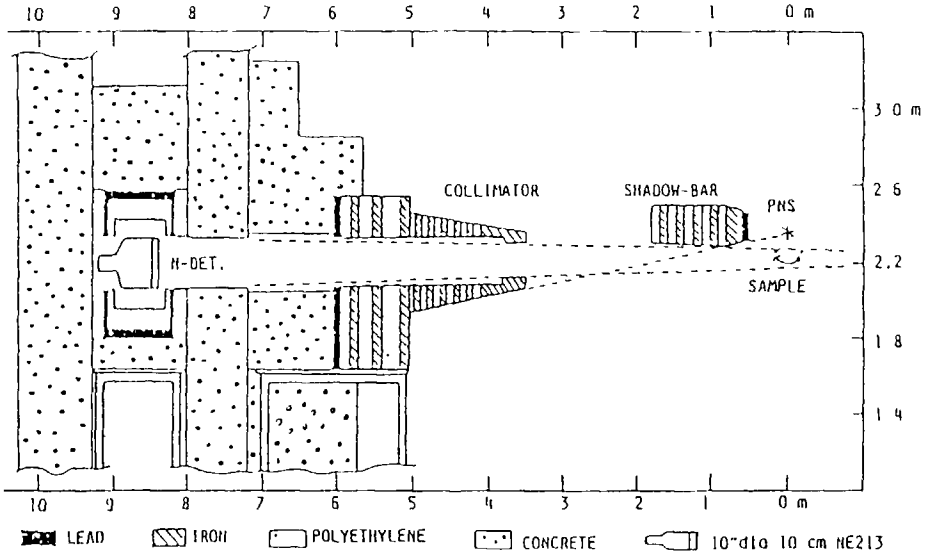

Fig.5 Schematic view of shield for TOF experiment

4 Integral Experiments for Blanket Design of Fusion Reactor

Neutron integral experiments are useful to assess nuclear data and transport codes for calculating important reaction rates and neutron flux distributions in fusion reactor blanket. There have been reported remarkable works on breeding and neutron multiplication bassed on the integral experiments and analyses of a lithium sphere and a beryllium assembly, which have shown fairly large discrepancies between experiments and calculations with evaluated nuclear data at that time.

The "Pulsed Sphere"[17] experiment with RTNS-I was the well known first integral experiment served for fusion neutronics as a good supplement to verify microscopic data. In this experiment a pulse of D-T neutrons about 1.5ns was produced at the center of a sphere made of the material (i.e., ^{6}Li, ^{7}Li, etc) to be studied. The diameter of the sphere, less than 45cm, is a several mean free path length for 14-MeV neutrons. The spectrum of neutrons

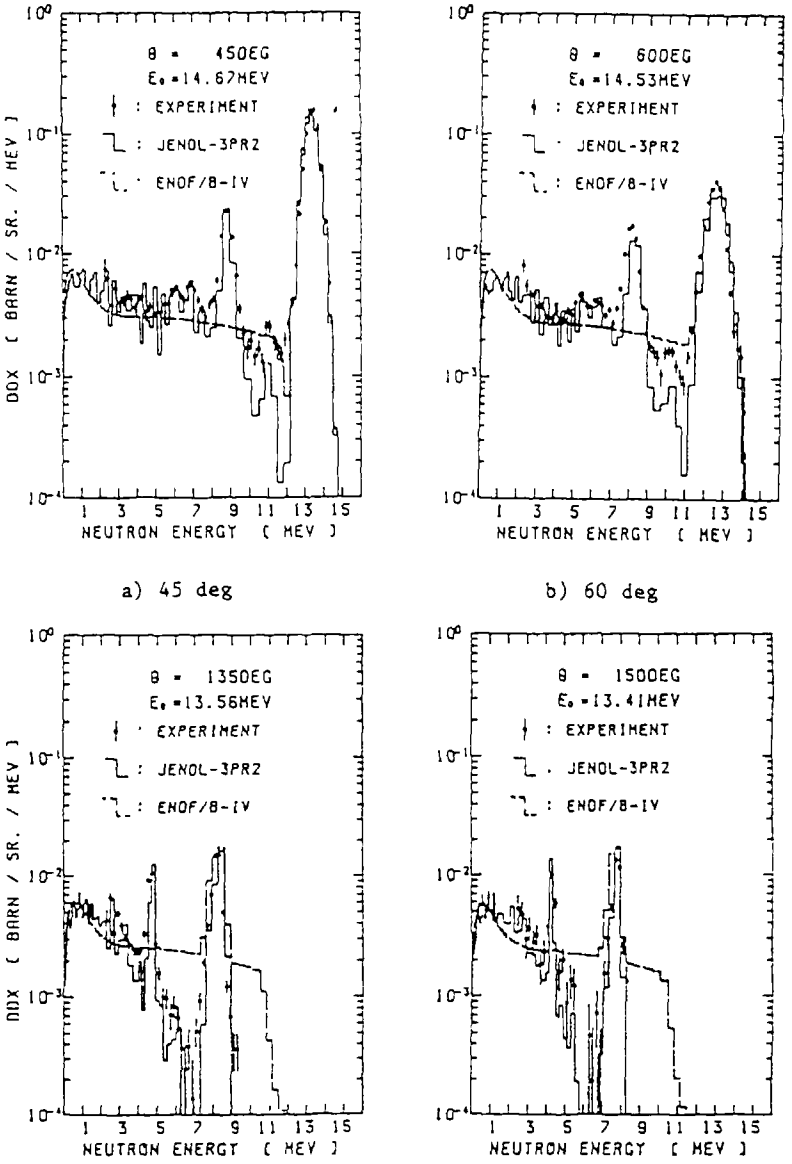

a) 45 deg b) 60 deg

c) 135 deg d) 150 deg

Fig.6 DDX of natural lithium, compared with JENDL-3PR2

leaked from the sphere is measured by T O F method with about 10 m flight path In addition, spectra of gamma rays produced in the sphere may be measured with gamma-ray spectrometer The objectives of this experiment itself might be different from others, and the results of the very neutron-leaky system may be not directly applicable to fusion reactor blanket design

Karlsruhe group carried out the same type experiment with a larger sphere of 100cm diameter [18] The preliminary measurement of Tritium breeding ratios (TBR) has been done In this case, neutron source intensity was not enough to give accurate data as a benchmark experiment

Then, re-measurements of ^{7}Li(n,n t) cross sections and other differential neutron emission cross sections have been required New nuclear data libraries like ENDF/B-V, EFF and JENDL-3PR2 were compiled for fusion reactor design For accurate prediction of Tritium breeding ratio of fusion reactor, it is required for nuclear data that high priorities for improvement are given to ^{7}Li(n,n t), Be(n, 2n), Pb(n, 2n) cross sections and double differential neutron emission cross sections of breeder, multiplier and structure material elements Concerned with neutron multipliers, Pb[19-21] and Be[21] measurements of neutron multiplication factors have been carried out and most results had large discrepancies with calculational predictions

Since 1982, many neutronics integral experiments have been carried out at the OKTAVIAN facility using spherical and slab assemblies, with which were a natural lithium Sphere with 120cm diameter[22](Fig 7)including a lead shell for neutron mulitiplier, a iron Sphere with 100 cm diameter, 30cm thick litium slab and so on In the early stage, numerical analyses for the experiments have been done using ENDF/B IV and recently using JENDL-3PR2 nuclear data libraries

In the lithium sphere experiment[22] for analyses by calculation, 1-d transport codes ANISN and NITRAN and 3-d Monte Carlo codes MCNP and NIMOS have been used with nuclear data sets processed from ENDF/B-IV and JENDL-3PR2 NITRAN, NIMOS and MCNP utilize the DDX-type data set The order of Sn is S16 for ANISN and S19 for NITRAN Measured source neutron spectra by TOF method were used for calculations (Fig 8 and 9)

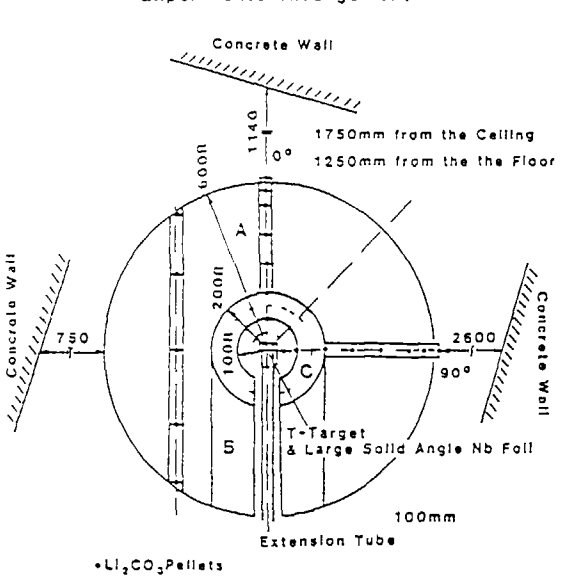

Fig.7 Experimental Arrangement of TBR measurement.

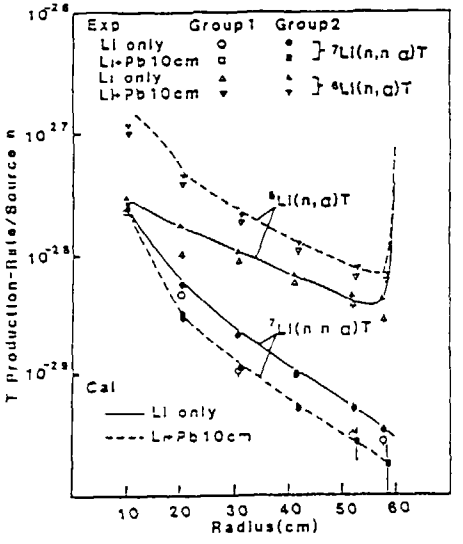

Fig 8 TBR spacial distribution at 0° degree

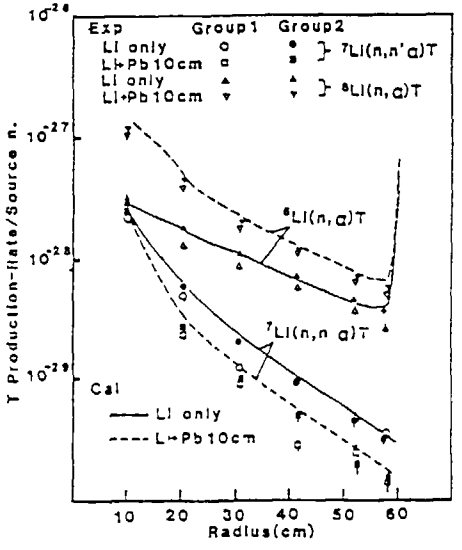

Fig.9 TBR spacial distribution at 90° degree

Lithium carbonate pellets (enriched ^{6}Li and ^{7}Li,) and many activation foils were irradiated with 1~2 mA deuteron beam current (average 14 MeV neutron yield was 10^{11} n/s)for about 10 hours The absolute number of produced 14 MeV neutrons was determined by the activation of a Nb cup (large solid angle foil) Tritium measurements of the pellets were done by the Dierck s method based on the liquid scintillation counting technique Tritium atoms produced in different samples were measured in two different laboratories to ascertain consistency, a very good agreement between experiment and calculation has seen for the tritium breeding ratios (TBR), T-6 by $^{6}Li(n,t)$reaction For the T-7 from $^{7}Li(n,n\ t)$reaction, the calculation with ENDF/B-IV data overestimates the experiment while the calculation with JENDL-3PR1 data shows fairly good agreement TBRS were deduced by integrating production rate distribution curves TBR is normalized to triton per 14 MeV source neutron

At OKTAVIAN, re-measurement and analysis of multiplication factors of Pb shells were also carried out[21] Neutron spectra of leakage currents from Pb Shell (3~12 cm thick) were measured by TOF method with NE213 and lithium glass detector (14KeV~2MeV) By integrating absolute leaking current spectrum (current/MeV/source neutron)over the whole energy, we can obtain the leakage multiplication factor which is very close to the real neutron multiplication factor in the case of Pb or Be where parasitic absorption is negligible It was checked by calculation that the existence of Pb shell affected monitor counts only by less than 1 % Monitor counts by $^{27}Al(n,\alpha)$ and ^{24}Na reaction were finally adopted due to high counting statistics

At FNS(JAERI), U S -Japan joint experiments[23] on tritium breeding began in 1983 Most of the Phase 1 experiments (cylindrical Li_2O assemblies, (Fig 10 and 11) stainless steal first wall, and beryllium multiplier) have been completed The phase 2 experiments will start in 1986 These experiments hav e demonstrated that point neutron sources are very useful because many neutronics issues can be treated in a low neutron fluence For example, the fluences at the front surface of the assemblies in the Japan-U S experiments are $7x10^{11}$ n/cm^2 over 50 hrs of operation in Phase 1 and $7x10^{12}$ n/cm^2 over 50 hrs of operation in Phase 2

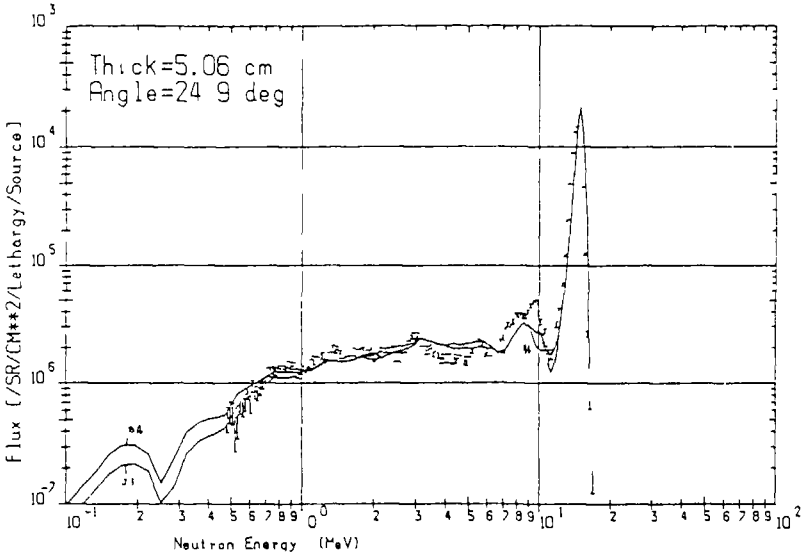

Fig.10 Measured and calculated leakage spectra from the 5.06-cm thick Li_2O slab.

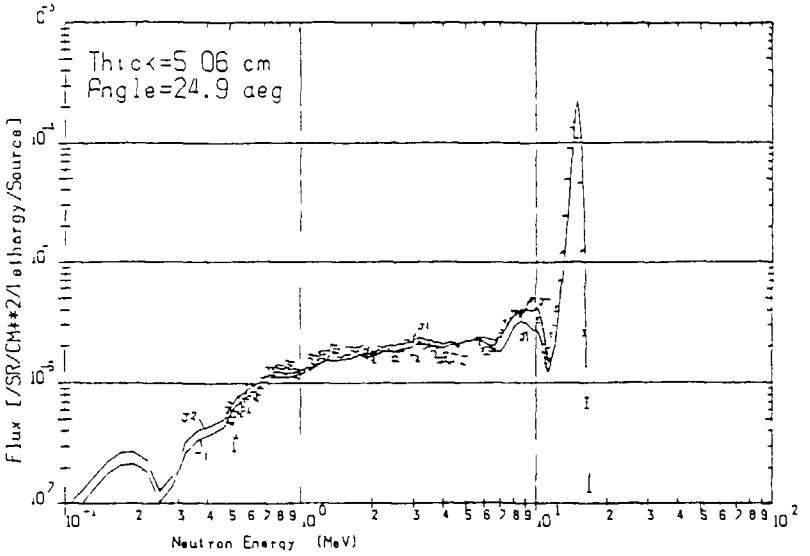

Fig.11 Measured and calculated leakage spectra from the 5.06-cm thick Li_2O slab.

The clean benchmark experiments[24] also conducted at FNS include: (a) integral experiments, e.g., measurement of reaction-rate distributions, and spectra in an assembly (Fig. 12 & 13) and (b) TOF experiments for measurement of angle-dependent spectra of neutrons leaking from a slab assembly. The integral experiments have been carried out on the following three asssemblies: (1) 60-cm thick Li_2O cylindrical slab assembly (Li_2O assembly) (2) 60-cm thick graphite cylindrical slab assembly (C assembly), (3) 60-cm thick Li_2O cylindrical slab assembly followed by 20cm thick graphite reflector (Li_2O+C assembly).

As for the TOF experiments, measurements of Li_2O, graphite and lithium metal slab assemblies have been done The work on the Li_2O slabs and its analysis using DOT3.5 transport code with the ENDF/B-IV nuclear data file has been published[25]. In the case of the lithium metal experiment, the lower limit of measured enegy was extended to the range from 500keV to 50Kev. An additionl experiment is planned in the near future to measure the efficiency curve. The final result will be obtained using this efficinecy curve.

LOTUS(Switz.) is the test facility designed for integral experiments in fusion neutronics. Experimental data for slab assemblies representative for fusion or hybrid blanket concepts were supplied by using a sealed high intensity D-T neutron generator, so called Haefley type. Somepreliminary results[26] from a set of spectrum measurements with a NE-213 scintillator spectrometer were reported. Neutron spectra were given for measurements made behind individual slabs of stainless steel, beryllium, lead and graphite. These experimental results were compared with 2-d transport calculation based on the discrete ordinates code DOT 3.5 and neutron cross sections derived from the ENDF/B-IV library. The agreement between the calcurated and measured spectra is reported to be satisfactory in general.[28]

6. Neutron Shield, Streaming and Skyshine

Some experiments[27] had been carried out at the FNS to study the radiation shielding. To fast neutron streaming experiments were carried out. The main objectives of the experiments are to acquire fundamental data on the performanced of two experimental ports which will be used extensively

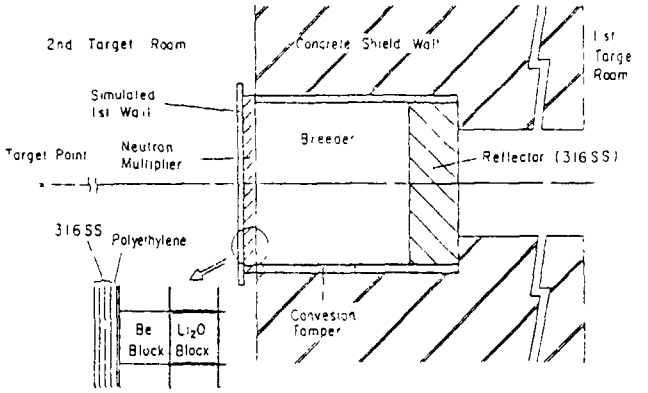

Fig.12 Typical Configuration in Crean Benchmark Test Experiments

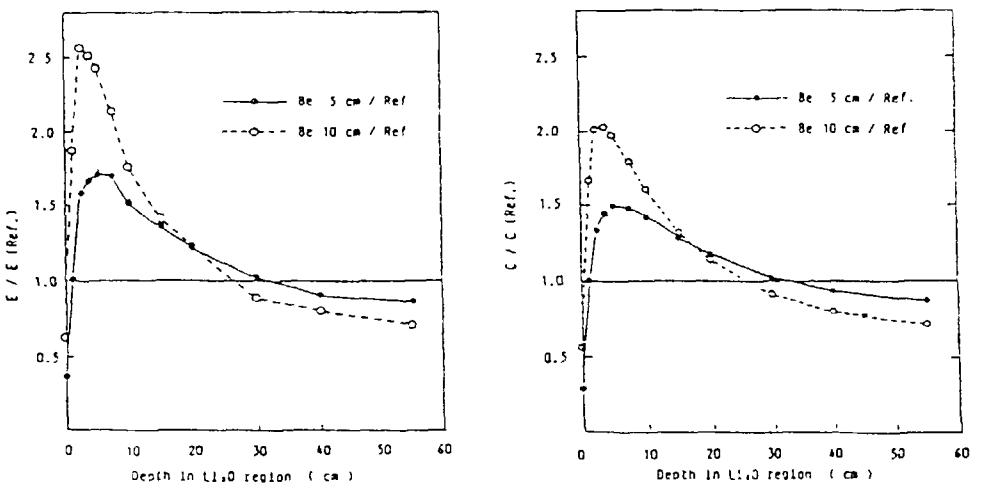

Fig.13 Ratios of TPR for ^6Li of Be System to That of the Reference.

for coming shielding research program. The experiments provide also the data appropriate to examine the current data and methods in both large small diameter penetration probrems.

The one experiment is on a straight experimental port of 42 cm in diameter , which is lacated in thick shield wall at a distance of 2.5m form a ratating target. The detailed spatial distribusions were measured across the fast neutron beam streaming through the port as well as the spectra at selected locations with putting the emphasis on the slope and tail of the profile. The other is an experiment on the group fo parallel, small-diameter long holes prepared on the shield plug of another experimental port. The axial fast neutron distribution was measured in each hole into which the source neutrons entered with a different angle of incidence. In both casses, a small spherical NE213 liquid scintillations detector was applied in order to achieve a good spatial resolution and obtain spectral information at the same time. (Fig. 14. &15)

Measurement of leakage neutron spectra from slabs of typical shielding materials were carried out by means of time-of-flight technique with pulsed D-T neutrons at OKTAVIAN [8]. The present experimental program was designated as a benchmaek experiment with simple geometry shields to assess neutron cdross section data and method for shielding calcurations of D-T neutrons. The slabs of single material were prepared using ordinary concrete, limestone concrette, (Fig. 16) stainless steel 316 , polyethlene and water, respectively. Neutron spectra obtained with good statistics and adequate energy resolution in the energy range 0.7 to 05 MeV can be used for the experimental benchmark data. The assessment was don for leakage neutron spectra calcurated with one-dimensional Sntransport codes, ANISN and NITRAN, using the ENDF/B-IV and the B-V library. Three-dimensional calcurations by Monte Carlo code were also compared with experiments. Uncertainties in differential cross section data were discussed as for energy-distributions of secondary neutrons from neutroninduced reactions by D-T neutrons.

The dose distribution and the spectrum variation of neutrons due to the skyshine effect[9] (Fig. 17) have been measured with the high-efficiency rem counter, the multisphere spectrometer, and the NE-213 scintillator in the enviroment surrounding the OKTAVIAN facility. The dose distribution and the

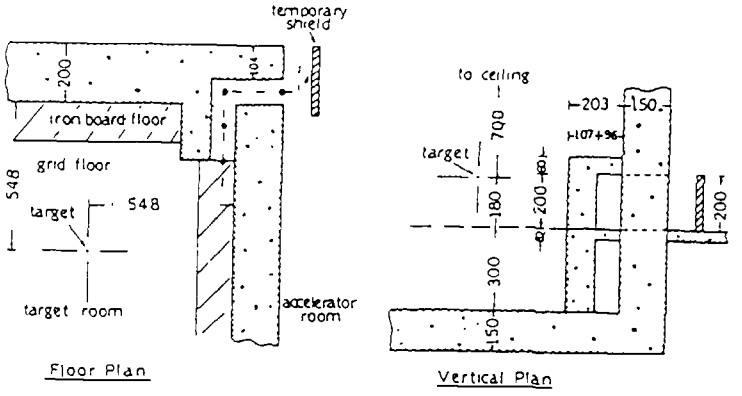

Fig.14 Layout of the Streaming Duct (Personnel Acces Way)

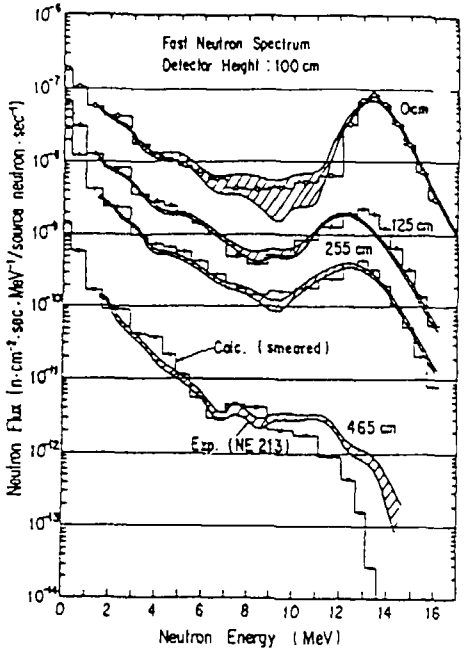

Fig.15 Fast Neutron Spectra (Calculation Smeared) at 4 Locations in the Duct.

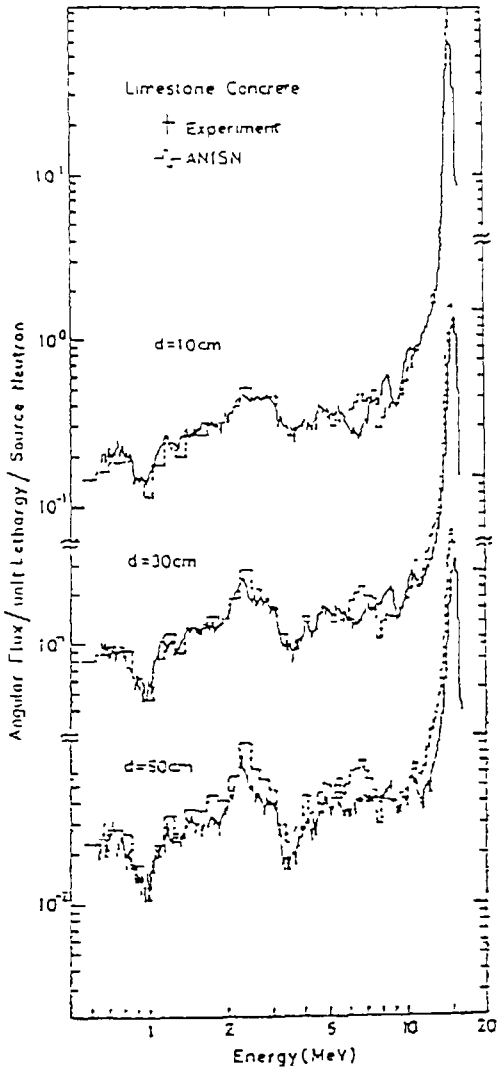

Fig.16 Comparison between measured and calculated neutron spectra from limeston concrete slabs.

energy spectra of neutrons around the facility used as a skyshine source have also been measured to enable the absolute evaluation of the skyshine effect.

The skyshine effect was analyzed by several transport codes NIMSAC and MMCR-2 are the multigroup Monte Carlo Codes. ANISN and DOT 3.5 are the discrete ordinates code. and SKYSHINE-II is the shield structure design code for skyshine. The calculated results show good agreement with the measured results in absolute values These experimental results should be useful as of fusion facilities. This work is the first experimental work on neutron skyshine from a 14-MeV D-T neutron source facility and will be useful in providing benchmark data for the skyshine analysis and for shielding design of fusion reactors.

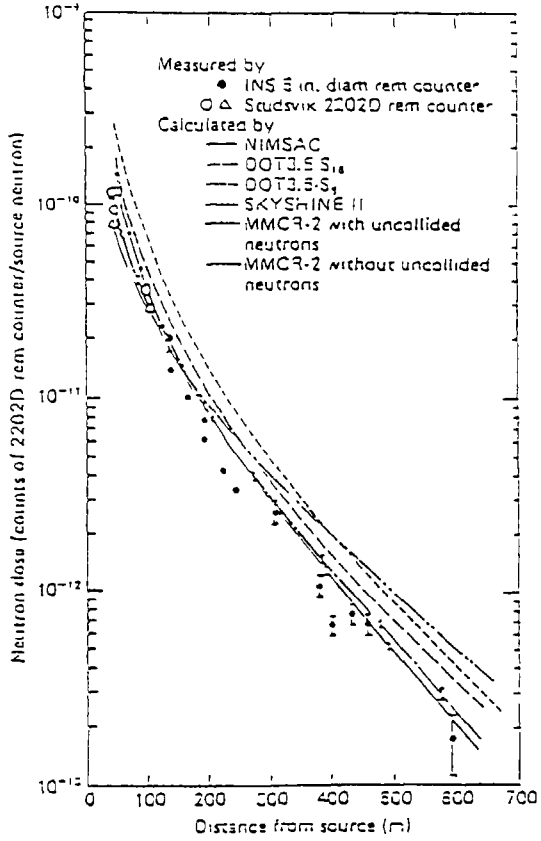

Fig.17 Comparison of measured and calculated neutron dose distributions in the field around the OKTAVIAN buildings.

D-T neutron cross sections for many reactions on several elements[30] contained in fusion reactor materials have been already measured with sufficient accuracy by the activation method with few exceptions. An intense neutron source and simultaneous irradiation[23] reduced the statistical and systematic errors as well as the irradiation time A computer code that uses cross section datawas developed, and adopted to caluculate dose rates of some practical irradiated alloys. (Fig.18) The results agree very well with experimental results. RTNS-II have served for mainly material test, however, it could contribure to residual activity measurement on a lot of miniature tensile test specimens. The residual activityof the tensile test specimens which had been irrrdiated for a long term in high fluences (10^{17}~10^{18} n/m^2) were carried out at 1.5 year after irradiation. The activities were compared with the calcurations using the cross sections based on the ENDF/B-V dosimetry libaray, or other experimental data.

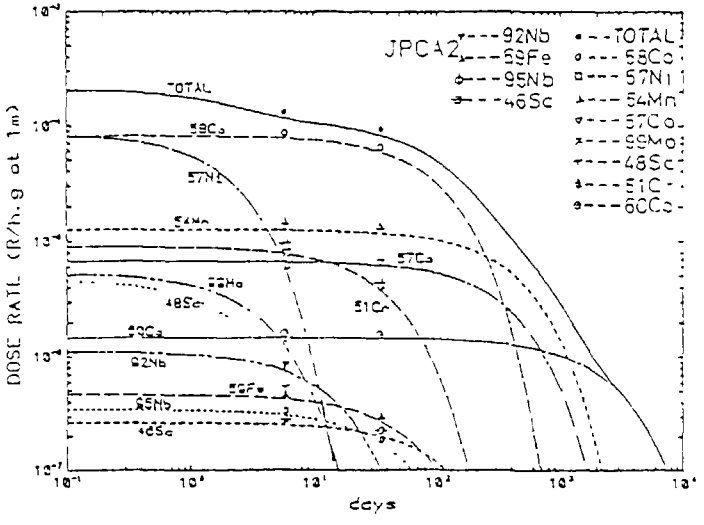

Fig.18 Calculated and measured dose rate at 1m of JPCA-2
Fluence was 1.92x10^{17} n/cm^2 for 46 days.
Data Points are measured.

Thousands of tensile test specimens had been packed together with disksfor the TEM observation in an aluminum cylinder container of 50mm dia. with very thin front window by using many aluminium disk spacer which have many circular and rectangular holes to hold the specimes. Among the specimens, a lot of iron dosimetry foils were also inserted. The container was evacuated and sealed to prevent the contamination and oxidization, and placed just in front of the rotating target of 50cm dia. We have chosen 14 kinds of materials including pure metals, of which had two specimens whose neutron fluences were ranging form 1 5 to 2.4×10^{17} and from 0.8 to 3×10^{18} n/cm^2 The irradiated specimens were shipped to Tohoku University at about one year after irradiation Residual activities were measured by a high solution Ge(Li) detector system.

8 Source Properties and Neutron Field

The source spectrum is selected at 14 MeV in the neutronics calculations of fusion reactor However, in fusion neutronics experiments, the D-T neutrons are generated with a low energy tail in addition to the 14 MeV peak. Several types of targets are currently in use at RTNS-II, FNS and OKTAVIAN with various water-cooling conditions. To perform the analysis of benchmark experiments chosen for geometrical simulation the reactor blanket, such observed external source spectra should be adopted As an example, recent dosimetry experiments[31] in RTNS-II may be introduced here. The measuremant had two subjects, ( ) neutron fluence characterization for the material irradiation experiments at the very near position from the rotating target, called as the primary positions", and ( ) the neutron source spectrum determination works for the neutronic experiments such as the neutron reaction cross section measurements and somefurther neutronic benchmark experiment for the tritium breeding rate evaluation Neutron fluence has been determined by the activation data of ^{93}Nb(n,2n) reaction and special attention has been paid for determination of source neutron spectra

Source neutron energies have been determined by the newly proposed activation-rate method based on the two reactions of ^{90}Zr(n,2n)^{89}Zr and

^{93}Nb(n,2n) ^{92m}Nb, which is called as the Zr/Nb ratio method The calibration curve between the neutron energy and the activation-rate ratio data, which has been obtained using the international standard neutron source

Another important point in prepareing the TBR measurement is an accurate absolute measurement of source intensity, rather different from relativemeasurement for spectrum The detail was already introduced in the preceding page for integral experiment of OKTAVIAN and FNS

9 Conclusion

D-T sources have served for the several integral experiments of fusion neutronics The contribution may increase in the future support the accurate design of a fusion reactor in detail Present intensity is still unsatisfactory to assure the precise experimental results such as benchmark experiments More intense D-T neutron sorces are expected to resolve many experimental difficulties in determining key design parameters of blanket

A Newly planned D-T sources, even the modification of existing sources may add remarkable progresses in fusion neutronics and its related fields If the fusion age arrives, then a large scale D-T fusion machine can supply enormous numbers of neutrons, but the essential importance of the D-T neutron source with simple geometry is not diministished

If further requirements for the problems like as secondary produced charged particles are considered, we must require surely more intense D-T sources with $10^{14\sim15}$n/s intensity with or without pulsed operation

References

1)Von Dardel G F ,Trans Royal Insti Techn No 75 Stockholm (1954)
2)Antonov A V et al Proceed of the 1st Geneva Conf Vol V P 3(1955)
3)Beckurts K H and Wirtz K Neutron Physics,p 22 (Springer,1964)
4)Egelstaff P A and Poole M J Experimental Neutron Themalization (Pergamon Press,1969)
5)Barshall H H , 14 MeV D-T Source p 57 OECD Report Neutron Sources (OECD 1983)
6)Booth R et al,Rev Sci Inst & Methods, Vol 145,p 25 (1977)
7)Sumita K et al Proceed 12th SOFT 1982 Vol 1,p 675 (Pergamon Press,1982)
8)Nakamura T et al Proceed of the International Ion Engineering Congress, Vol 1 p 567 (Kyoto,1983)
9)Haldy,P A et al,Atomkernenergie Kerntechnik Vol 44,No 1,p 65 (1983)
10)Davis J et al IEEE Trans NS-26 p 1240 (1980)
11)Seki T ,Proceedings of Specialist Meeting on Nuclear Data for Fusion Neutronics at Tokai 1985 p 52 (1986)
12)Takahasi A :To be published in Proceed of JNDC 1985 Seminar on Nuclear Data at Tokai (1986)
13)Hermsdorf D et al,ZFK Report(L) (1975)
14)Takahasi A et al OKTAVIAN REPORT,A-8301 (1983), & J Nucl Sci & Tech Vol 21,p 577 (1984) and some recent results reported in Proceed of JNDC 1985 Seminar on Nuclear Data for Fusion Neutronics at Tokai,p 99(1986)
15)Takahasi A et al OKTAVIAN REPORT,C-8607 (1986) or To be appeared in Proceed of Int Conf on Fast Neutron Physics at Dubronik (1986)
16)Baba M ,Proceed of JNDC 1985Seminar on Nuclear Data for Fusion Neutronics at Tokai,p 119(1986)
17)Hansen L F et al,Nucl Sci & Eng ,Vol 60,p 27 (1976)
18)Bachmann H et al,ibid Vol 70,p 74 (1978)
19)Takahasi A Proceed 12th SOFT 1982,Vol 1 p 687 (Pergamon Press,1982)
20)Antonov S et al,Atomnaya Energiya Vol 58 p 280 (1985)
21)Takahasi ,To be published in Proceed Int Conf on Nucl Data for Basic and Applied Sci at Santa Fe (1985)
22)Sugiyama K et al,Nuclear Fusion Vol 8,p 1491 (1985)
23)US/JAERI Fusion Neutronics Calculational Benchmarks for Nuclear Data and Code Intercomparison JAERI-M 85-201 (1985)
24)Maekawa,Y et al Proceed of Specialist Meeting on Nuclear Data for Fusion Neutronics at Tokai 1985 p 171 (1986)
25)Nakamura,T et al Proceed of Specialist Meeting on Nuclear Data for Fusion Neutronics at Tokai 1985 p 183 (1986)
26)Haldy P A et al To be published inInt Conf on Nucl Data for Basic and Applied Sci at Santa Fe (1985)
27)Seki T et al,Proceed of 6th Int Conf on Radiation Shieldibid Vol II p 898 (JAERI 1983)
28)Yamamoto J et al, ibid Vol I P 464 (JAERI 1983)
29)Nakamura T et al Nucl Sci & Eng Vol 90 p 281(1985)
30)Iwasaki S et al,Annual Resaearch Report of Japanese Contributions for Japan-US Collaboration on RTNS-II Utilization p 1 (Monbusho,1986)
31)Nakazawa M et al,Annual Resaearch Report of Japanese Contributions for Japan-US Collaboration on RTNS-II Utilization p 33 (Monbusho,1986)

BASIC AND APPLIED STUDIES WITH MODEST 14 MeV FACILITIES

H VONACH
Institut fur Radiumforschung und Kernphysik,
University of Vienna,
Vienna, Austria

Abstract

Properties and applications of modest (total neutron production $<10^{11}$/sec) 14 MeV facilities are discussed in detail. In addition to neutron generator and tritium target properties the discussion includes the problems of laboratory design, shielding radiation safety and the properties and quality of the neutron field which can be produced with such machines. Application to basic nuclear physics, measurement of nuclear data for fusion and radiobiology to activation analysis and some more special subjects like fusion diagnostics or calibration of neutron detectors are discussed in some detail. Some important applications such as integral studies for fusion and to geophysical problems - especially addressed in some other talks of this meeting - are mentioned very briefly only.

---

1) Introduction

Since almost 40 years the $^{3}He(d,n)^{4}He$ reaction is used as convenient source of 14 MeV neutrons. The large cross-sections for this reaction at low energies permit high yields of fast neutrons to be obtained with relatively cheap low energy accelerators. Such neutron generators have since then been widely used both in basic nuclear physics and applications especially activation analysis and measurement of nuclear data for fusion. These generators do however have the important disadvantage that the energy range of neutrons which can be produced is quite limited to about 13.5 - 15 MeV.

Therefore the development of more flexible accelerators allowing production of a wide range of particle species and energies, as also discussed in a number of lectures in this conference, has made 14 MeV neutron generators less and less attractive for nuclear physicists especially in the Western countries. In addition also neutron activation analysis has in many cases proved not to be competitive with other methods like X-ray fluorescence or proton induced X-ray analysis. Accordingly a large number of such neutron generators were put out of operation in Europe and the U.S. in last decade; actually in Western Europe our neutron generator in Vienna will by next year probably be the only one devoted to basic nuclear physics and fusion nuclear data research. On the other hand in Eastern Europe there is still a much stronger activity existing in the 14 MeV neutron field, although there also the trend towards increasing use of other neutron energies is present. In a number of developing countries this situation is quite different. Neutron generators have been given by the IAEA to many countries such as Algeria, Bangladesh, Bolivia, Cuba, Malaysia, Mongolia, Marocco, Northkorea, Peru, Sudan, Thailand and Zambia as a relatively inexpensive starting point for training of scientists and start of a nuclear program and a number of them are just now becoming really operational.

Thus there is now the serious question how these neutron generators can be used best both in basic and applied nuclear physics and whether further neutron generators should be distributed by the IAEA. In the following I will try to address these problems. In order to do this I will at first briefly talk about the technique of 14 MeV neutron production and the requirements of shielding and radiation safety for such laboratories. Then in somewhat more detail I will summarize the properties of the neutron fields produced by DT machines and then I will talk about applications of 14 MeV neutrons, giving both examples of recent studies and future possibilities. In all this I will restrict myself to modest neutron sources, that is source strength less than a few times 10^{11} n/sec as intense sources for radiation damage studies and radiotherapy have just been discussed by J.C. Davis /1/. Likewise I will not address the applications in geophysics which are the subject of a separate contribution /2/.

2) 14 MeV Facilities

2.1. "Modest" Neutron Generators

Concerning the technical problems of modest neutron generators I will remain very short. No new developments have been reported in the last 10 years and the subject has been reviewed recently by several authors, e.g. Prof. Barshall and Prof. Csikai /3,4/. Due to the energy dependence of the DT cross-sections (s. fig. 1) the most economical deuteron energy in term of neutron output relative to beam power is about 180 keV. Accordingly standard neutron generators are deuterium accelerators with energies of 150-300 keV and currents around 1 mA which allow a neutron source strength around 10^{11}/sec. Radiofrequency ion sources are used in most cases because of their high D^+ content. Neutrons are produced by irradiating TiT targets with the accelerated deuterons. Such targets with a composition of about $TiT_{1.5}$ and thickness sufficient to stop the deuterons are commercially available from a number of sources /5/. These targets can be operated with air cooling up to 100 μA and water cooling up to some mA. The useful lifetime of the targets depends critically on the composition of the deuteron beam Using pure magnetically analysed D^+ beam typical half-lives are ∿20 mA.hours/cm², whereas only ∿ 2 mA.hours/cm² are observed if such targets are bombarded with unanalyzed accelerator beams which contain comparable amounts of D^+, D_2^+ and D_3^+ and heavy ion contaminations /6,7/. Thus both for reason of operating cost and to reduce the tritium contamination problems neutron generators should only be operated with pure D_2 beams.

Such standard neutron generators have been manufactured by a number of companies; due to the decreasing demand however most manufacturers have left the field. At present there is essentially only one company, Irelec (former Sames) is left producing neutron generators in the West and even this compary might stop its operation in this respect. This situation causes severe repair and maintanence problems for neutron generator laboratories using commercial neutron generators especially in developing countries.

For many applications in nuclear physics and measurement of nuclear data for fusion a n-sec pulsing system is required. Such systems are not commercially available, they have, however, been developed in several laborato-

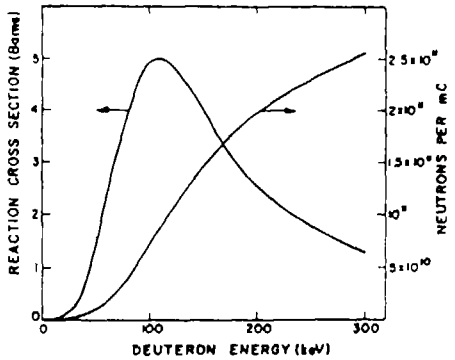

Fig. 1. The total cross section of the reaction $^3H(d,n)^4He$ and the total neutron yield of the reactions $^3He(d,n)^4He$ induced by neutrons stopping in a Ti target for an atomic ratio of tritium to titanium of 1.6 (from ref. 3).

ries and described in detail /8,9/. Using the discussed "standard" neutron generator it is possible to produce pulses of about 2 nsec (FWHM), frequencies of ∿ .1-10 MHZ and intensity of about 10^3 neutrons/pulse.

2.2. Shielding and Radiation Safety

Even "standard" neutron generators are intense radiation sources. A source strength of 10^{11}/sec produces an equivalent dose of 2 Sieverts/h at 1 meter distance. In addition the conventional tritium targets do contain ∿ 10^{11}-10^{12} Bq of tritium which to a large extent is released during operation into the forepump exhaust. Therefore rather high demands on shielding and radiation safety are necessary. Shielding will have to reduce the neutron dose by a factor ∿ 10^5 if the exposure limit of .6 μSiev/h for the general population is to be reached in 10 m distance from the source. The cheapest and best material for this is concrete, a thickness of ∿ 1.5 m is needed for the walls of the target room /10/, in addition also the roof has to be shielded by not much less (∿ 1 m) because of the so-called sky-shine caused by the air scattering of the fast neutrons /10/. The use of the described tritium targets requires a number of precautions:

1) Such targets, both new and used ones, have to be stored in a well ventilated glove-box.

2) The forepump exhaust has to be connected to a separate chimney which guarantees that this main source of tritium release is sufficiently diluted.

3) The air in the neutron generator itself should be renewed several times per hour during accelerator operation in order to assure that the tritium concentration remains below the tolerable limit.

4) All parts of the accelerator, especially target construction will eventually be highly tritium contaminated and should only be deposed as radioactive waste.

5) The procedures to be used when changing targets are still somewhat of an open problem. Very different experiences have been reported obvious strongly dependent on target quality. Our own procedure has been to always remove the whole target assembly and do the target change itself in a ventilated glove-box

Induced activities will not be a serious problem for source strength $< 10^{11}$ n/sec. It should however be kept in mind that quite high dose rates due to short lived activities in the hour to day range will be present from induced activity near the target after longer irradiations and all work with such parts has to be done under supervision of a radiation safety officer and some cooling time should be allowed for after long irradiations. Finally it is to be mentioned that an effective interlock system is needed to prevent unwanted irradiation of persons.

2.3. General Laboratory Requirements

The general requirements in the design of the neutron generator building and the necessary auxiliary equipment depends strongly on the planned applications. For a pure activation analysis installation they are very modest, for a multi-pupose neutron generator these demands may be quite high If the neutrons are to be used for nuclear physics and nuclear data studies the shielded room for neutron generator and experiment should have at least the size of 10 x 10 x 5 m in order to allow a sufficiently clean neutron field (s. section 2.4.) in addition it will be necessary to have air-conditioning both in the neutron generator and the control and measuring room. In addition neutron and gamma-detectors, standard nuclear electronics and a reasonably large computer system are required. This means that in this case the cost of the neutron generator ($\sim$ 100.000 US $) itself may be only one relatively small part (10-20%) of the total facility cost and this fact has to be taken into account if the purchase of a neutron generator is to be compared with other possibilities e.g. small Van de Graaff machines

2.4. Output characteristic of the DT reaction and quality of 14 MeV neutron field

The main features of the neutron field produced by a typical DT neutron generator are summarized in fig. 2. Neutrons are emitted with average energies of about 13.5-14.5 MeV depending on emission angle θ relative to the deuteron beam. The differential n-production cross section is isotropic in the c.m. system, accordingly the neutron intensity decreases slightly with emission angle as shown in fig. 2b. The energy width of the neutrons (fig. 2c) is determined by two effects.

1) As the deuterons are completely stopped in the target the reaction may occur at any energy between the accelerator energy and zero. This causes different lab energies especially in forward direction.

2) Small angle scattering of neutrons within the target. This causes a certain emission angle to correspond to different reaction angles and introduces an energy spread due to the neutron energy dependence on emission angle (fig. 2a). This effect dominates the neutron energy width around $\theta = 90°$.

These properties of the neutron field, also the detailed neutron energy distribution at any emission angle, can be calculated very accurately from the deuteron energy, the $T(d,n)^4He$ cross-section and the specific energy loss dE/dx of deuterons in Ti and T /11,12/. Fig 3 shows typical examples for such energy distributions for different emission angles. The main source of uncertainty in these calculation is the lack of detailed knowledge on the tritium distribution within the targets. Nevertheless average energies

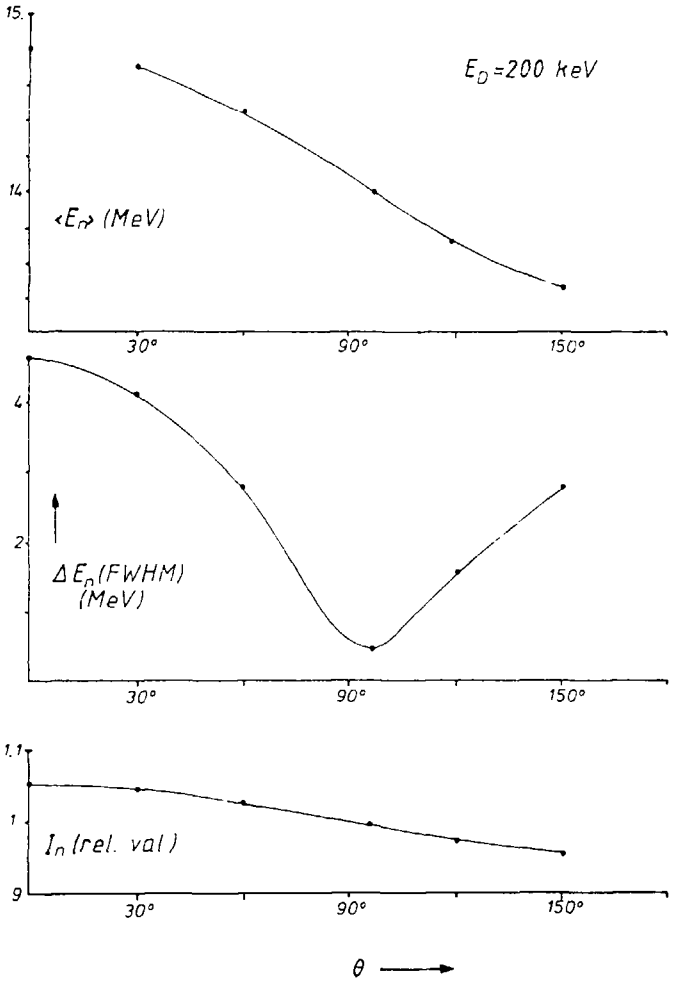

Fig. 2. Properties of the neutron field of a typical neutron generator with E_d = 200 keV.

(a) Dependence of the mean neutron energy on emission angle

(b) Dependence of the neutron energy spread (FWHM) on emission angle

(c) Dependence of neutron intensity on emission angle

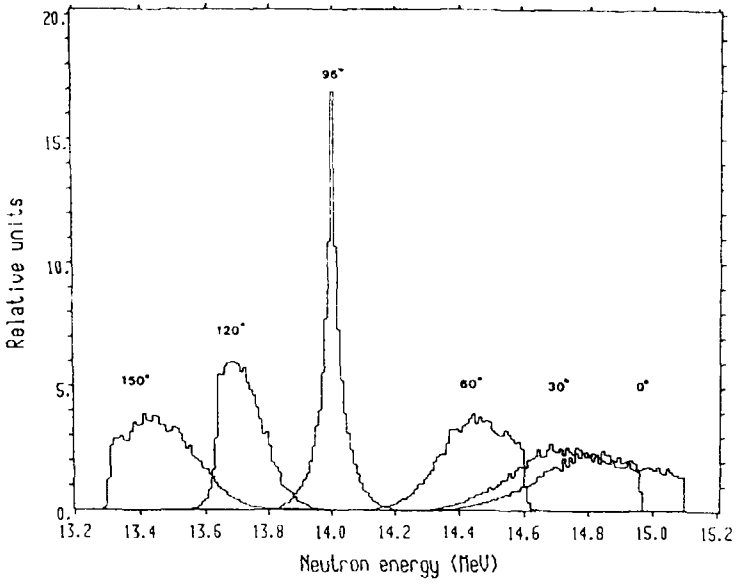

Fig. 3. Energy distributions of the neutrons produced from the $^{3}H(d,n)^{4}He$ reaction at E_d = 200 keV in a thick Ti target at different emission angles (calc. according to ref. 11).

can be calculated to about ± 10-20 keV and relative neutron intensities for different angles to ∿ ± .5%, the width of the energy distribution can be predicted to about 10-20%.

The absolute source strength of DT sources can be measured very accurately (< .5%) by means of the so-called associated particle methods that is be observing the number of recoil α-particles per solid angle in a certain direction /13/. Accordingly it has been possible to make cross-section measurements with similar accuracy. Thus for eaxmple the $^{27}Al(n,\alpha)$ cross-section /14/ known to better 1% for the whole discussed energy region and allows an easy measurement of absolute neutron flux with this accuracy as also confirmed by the last international neutron flux comparison.

In practice it has to be taken into account that this ideal 14 MeV neutron

field is always contaminated by lower energy neutrons to some extent. The most important sources of these parasitic neutrons are:

1) Inelastic neutron scattering in the air and from the walls of the accelerator room.

2) DD (∿ 2.5-3 MeV) neutrons from reactions of the deuteron beam with the deuterons accumulated in the target, amounting to ∿ .1-1% of the DT yield depending in age of the target /6/.

3) DD neutrons from self-target formation in apertures.

4) Low energy neutrons from inelastic scattering and (n,2n) reactions of the source neutron with the target backing and other materials near the target.

In order to keep these contributions small the target should have distance of at least 3 meter from the walls and most important the mass around the target is to be minimized e.g. by use of an air-cooled low mass target-construction attached to the accelerator by a thin walled tube of at least 20 cm length. Under these circumstances the contamination of the 14 MeV field can be kept at the percent level in vicinity (∿ up to 10-20 cm) of the target /15/.

Neutron generators using massive water cooled target constructions and sealed neutron generators will however be much worse in this respect and may well produce low energy contributions in the 10% range /16/.

3) Applications

3.1. Basic Nuclear Physics

Despite the work of the last 30 years there are still a number of open questions also in basic physics with 14 MeV neutrons I will just mention two examples, few body systems and precompound reactions in heavy nuclei.

As an example of the first kind fig. 4 shows the result of a recent study of the ^{6}Li(n,αx) and ^{7}Li(n,αx) reaction from Prof. Miljanic and co-workers /17/. In this study the short-lived ^{4}H was clearly identified in the α-spectrum from ^{7}Li in coincidence with the triton from the decay of ^{4}H into t+n and both position and width of ^{4}H could be determined. The reaction mechanism in an number of other reactions of 14 MeV neutrons with light nuclei is still an open question.

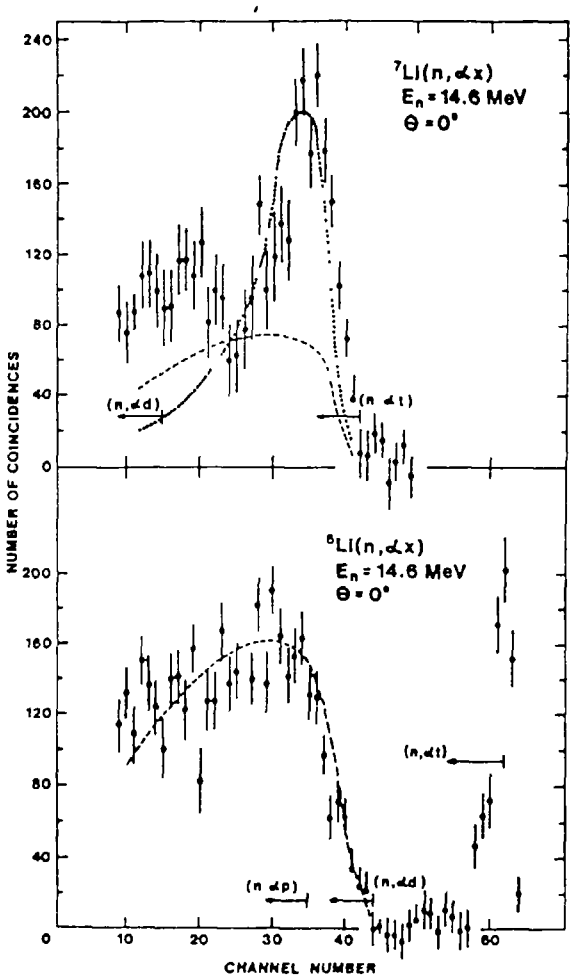

Fig. 4. Coincident α-particle spectra from ^{6}Li(n,αx) and ^{7}Li(n,αx) reactions. The dashed lines represent calculated three-body phase space distributions for the ^{6}Li(n,αx) and ^{7}Li(n,αt)n reactions, respectively. The dotted line shows the calculated ^{7}Li(n,α_0)^{4}H reaction contribution (E_r = 2.7 MeV, γ^2 = 2.3 MeV for ^{4}H ground state). (From ref. 17).

Likewise there are still open questions concerning the comparative role of direct, precompound and compound reactions in the interaction of 14 MeV neutrons with heavy nuclei. Especially for the angular distribution of emitted neutrons and protons very few reliable angular distributions have been determined.

As an example of such work fig. 5 shows the angle-integrated neutron and proton spectra from the interaction of 14 MeV neutrons with Niobium determined recently in Osaka and Vienna /18,19/. These measurements indicate that in this case the conventional precompound and compound particle emission is unable to explain both spectra and a third direct mechanism is needed for the (n,n') channel. Similar comparisons for other nuclei would be very interesting. Concerning the angular distributions studies of the (n,p) reactions on Nb, Ag and In performed recently at our institute in Vienna /20/ showed an intersting systematic feature (s. fig. 6). All angular distributions showed a very similar shape; irrespective of proton energy and nucleus the angular distributions are compatible with the simple form $d\sigma/d\Omega = a_o(1+b_1P_1(\cos\,0) + .5\ b_1P_2(\cos\,0))$ with the constant b_1 and thus the forward-backward asymmetry increasing with proton energy. Extension of these measurements to other nuclei and especially equally accurate neutron angular distributions would be highly desirable.

Thus there are still a number of interesting experiments to be done which however require in most cases the determination of double-differential particle emission spectra for either neutrons or charged particles and thus require rather sophisticated experimental methods.

3.2. Nuclear Data for Fusion

As all present designs of fusion reactors are based on the DT reaction, cross-sections for 14 MeV neutrons are needed with rather high accuracy for many materials, especially those relevant to the so-called tritium-breeding. At present the World Request List for nuclear data contains more than 350 requests for neutron cross-section measurements, more than 90% involve energies including the 14 MeV region, thus there is still considerably work to be done. However most of the requests demand measurement of secondary neutron spectra which requires source with n-sec pulsing. Some data for

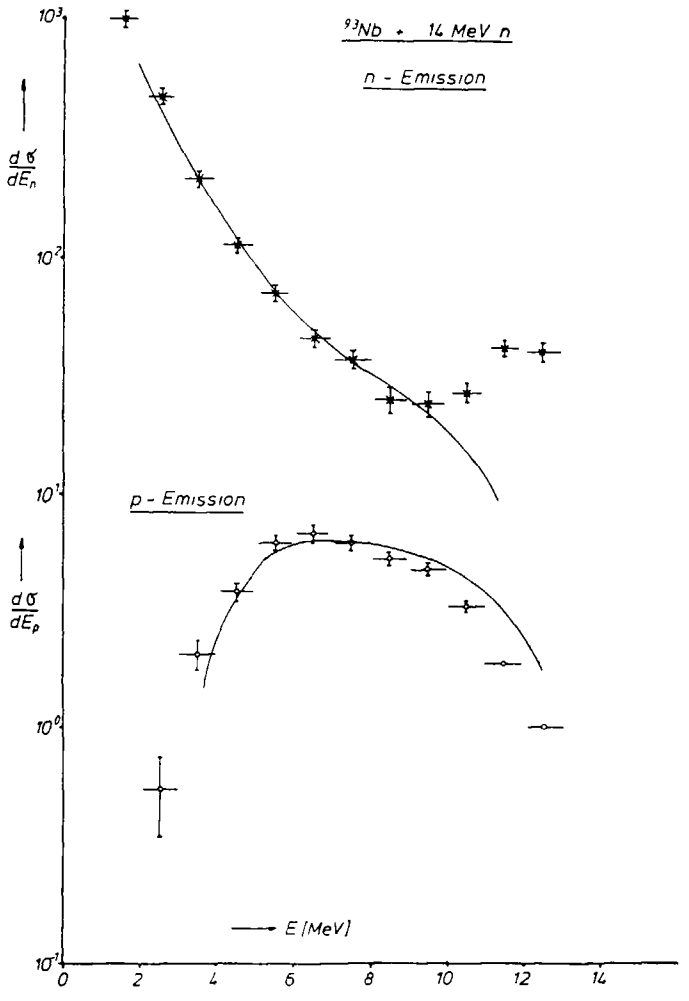

Fig. 5. Angle-integrated proton and neutron emission spectra from the interaction of 14 MeV neutrons with ^{93}Nb. Experimental values for protons from ref. 18, for neutrons from ref. 19, solid lines: prediction of the statistical model of nuclear reactions, sum of preequilibrium and equilibrium contributions.

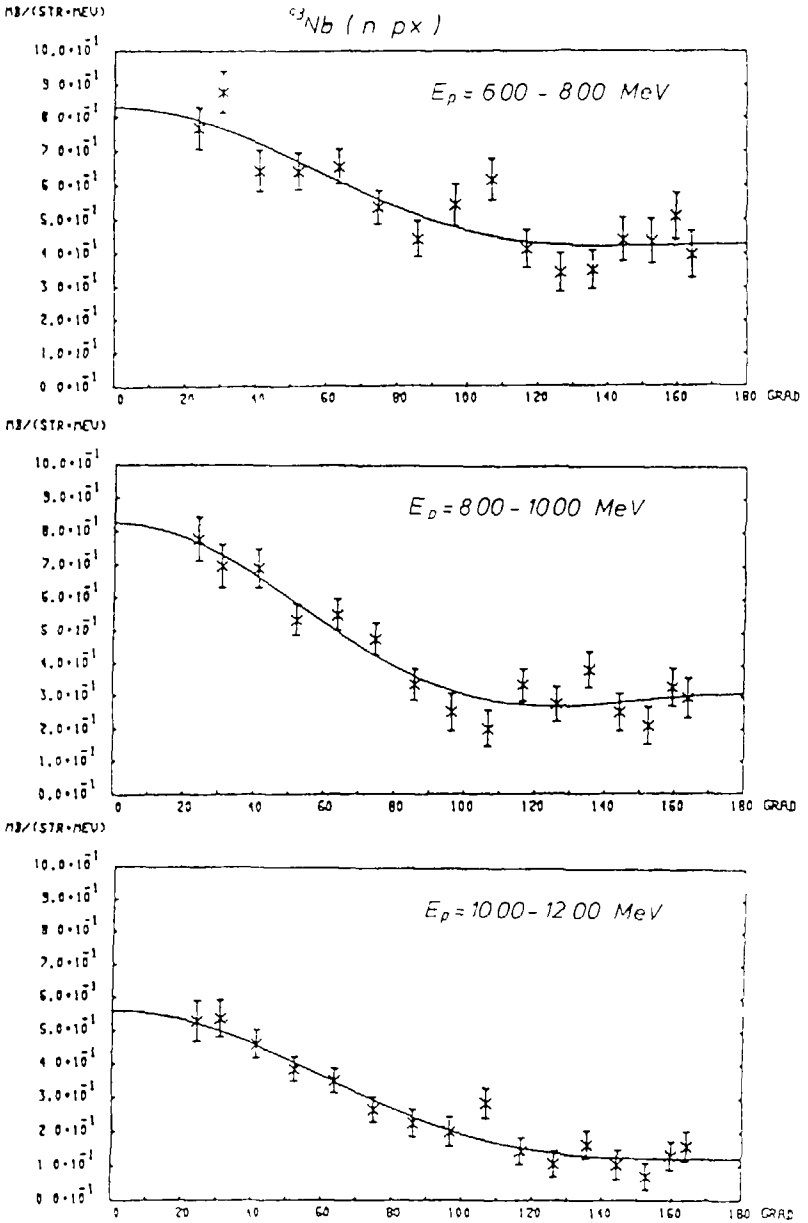

Fig. 6. Angular distribution of protons from the ^{93}Nb(n,px) reaction at E_n = 14.1 MeV. Experimental values from ref. 18, solid lines· second order Legendre fits.

total proton and Helium production cross-sections and for photon production cross-sections could also be obtained with d.c. machines; practically no further 14 MeV activation cross-sections are required for fusion purposes. Thus fusion nuclear data will remain an important field of application for neutron generators suitable for time-of-flight neutron spectroscopy. The accuracy demanded for these measurements is generally of the order of 5-10% and requires - as in the case of basic nuclear physics studies - both rather expensive equipment and great care and experience of the scientists involved.

3.3. Calibration of Neutron Detectors and Spectrometers

The described properties of the neutron field make it very suitable for calibration purposes. Neutron detectors for accurate flux measurements such as proton recoil telescopes or fusion chamber can be calibrated to better 1% in a clean 14 MeV field, e.g. by use of the ^{27}Al(n,α) standard reaction and subsequently be used at other neutron energies. In this way only the error of the ratio $\sigma(E_n)/\sigma(14\ MeV)$ adds to the uncertainty at the other energies and the difficult exact absolute determinations of the hydrogen of Uranium masses of such detectors can be avoided. It appears that in FNDFB/VI the uncertainties of the ratios $\sigma(E_n)/\sigma(14\ MeV)$ will be of the order of 1-2% for the standards H, ^{235}U and ^{238}U over most of the fast neutron range, thus absolute flux measurements in the 2% range seem feasible in the whole MeV range At the IRK Vienna we have done such a calibration for a ^{238}U fission chamber to be used for accurate measurements of activation cross-sections in the 3-12 MeV range /21/.

3.4. Radiobiological Studies

The well defined nature of the 14 MeV neutron field makes it also very suitable for radiobiological studies, dose rates are quite sufficient for this purpose even for generators in the 10^{10} n/sec range. As an example fig. 7 shows the results of an investigation of chromosome aberations in human lymphocytes produced by both X-rays and fast neutrons (the neutron irradiations were done at IRK Vienna /22/). The results indicated give a RBE value for 14 MeV neutrons and indicate a possibly important difference in the dose-effect relation between X-rays and fast neutrons,which certainly deserves further study.

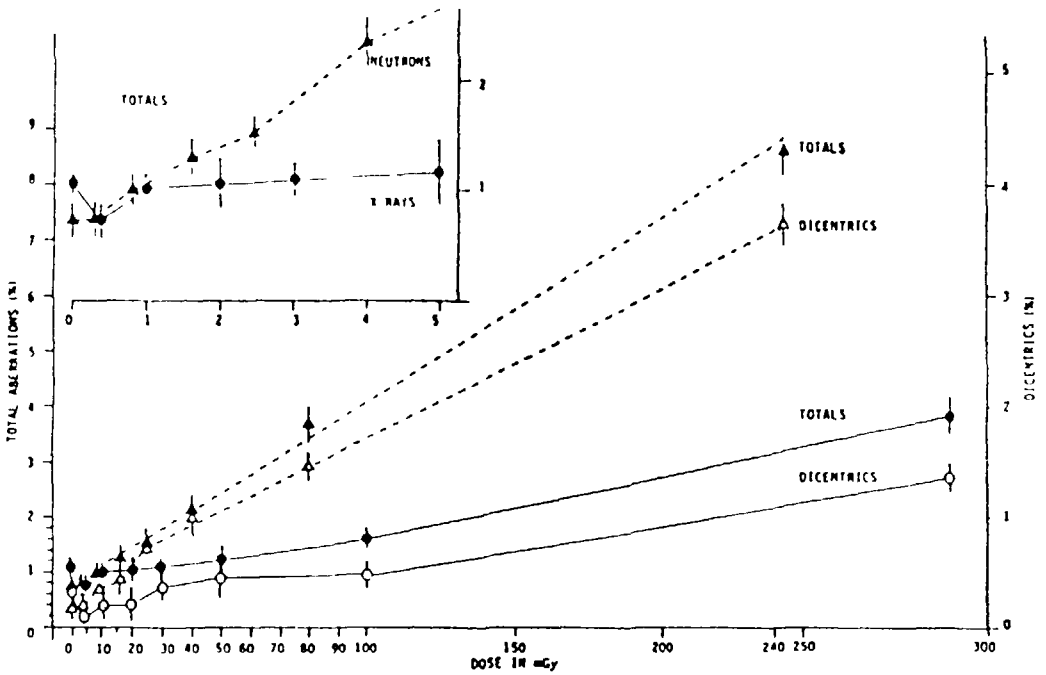

Fig. 7. Frequencies of chromosome aberrations per 100 metaphases induced by irradiation (from ref. 22).

- ● totals caused by 250 kV X-rays
- o dicentrics "
- ▲ totals caused by 14.8 MeV neutrons
- Δ dicentrics "

3.5. Activation Analysis

One of the classical applications of neutron generators has for a long time been activation analysis. Nondestructive elemental analysis by 14 MeV neutrons is possible for more than 90% of the elements with sensitivities in the 10^{-3}-10^{-5} g range /23/. It is especially useful for a number of light elements such as oxygen, nitrogen, phosphorous, aluminium and magnesium for which the normally more sensitive thermal neutron activation analysis is not possible. A number of problems in agriculture, biology, geology, hydrology, metallurgy have been successfully studied by 14 MeV neutron activation analysis - typical examples are determination of nitrogen and phosphorous in fertilizers and of nitrogen in grain or other agricultural products, fluorine analysis in biological materials and organic compounds, trace analysis of fluorine in water, elemental analysis of river sediments for their major elemental constituents, determination of oxygen down to the ppm level in a variety of metals.

Further need for such investigations certainly exists. A promising field is perhaps the analysis of coal for oxygen and nitrogen /24/. Nevertheless the use of fast neutron activation analysis has been decreasing considerably in the Western countries in the last decade. Reasons for this are the rapid development of other instrumental methods of elemental analysis like X-ray fluorescence and Pixe and automated fast chemical methods, e.g. for nitrogen and excessive radiation safety regulations increasing considerably the cost of neutron generator operation.

In the case of developing countries the situation if certainly somewhat different and the possibility to analyze most of the elements with one facility is certainly quite important, even if the sensitivity may only be moderate in many cases. In the long run however also there will be the trend towards using the optimum method for any special case and thus towards decreasing importance of fast neutron activation analysis.

3.6. Development of neutron spectrometers for the diagnostics of DT fusion devices

The energy spectrum of the DT neutrons in controlled thermonulear reaction depends strongly on the neutron temperature. The halfwidth of the neutron distribution increases from ca. 200 keV at T=10 keV to about 700 keV at T=30 keV (s. fig. 8). Measurement of the spectrum thus allows an accurate temperature determination. Development of suitable neutron spectrometers which can measure this temperature sufficiently fast with the required resolution of $\sim$ 100 keV will therefore be a challenging task which can be done with 14 MeV neutron generators.

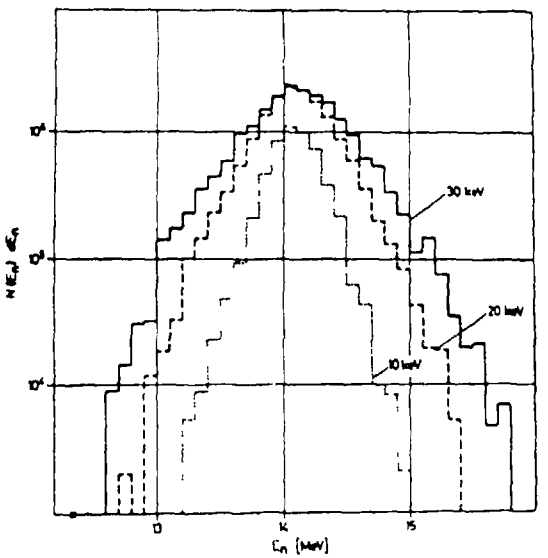

Fig. 8. Energy spectra of neutrons from a D-T plasma of temperature T = 10, 20 and 30 keV (from ref. 4).

3.7. Other applications

For completeness I would just like to mention that some other more exotic applications have been suggested such as their use in safeguards to detect and analyze fissionable materials /3/ and the detection of explosives in airports /26/ using nitrogen detection by means of the $^{14}N(n,2n)$ reaction. Neither of these suggestions however seem to have been really implemented.

I hope I have shown that there are at present a number of intersting applications also for modest 14 MeV neutron sources, but also that in the long run the use of such sources does not seem to be an expanding one and the foundings of new neutron generator laboratories has to be considered with some caution.

References

/1/ J.C. Davis, contribution to this meeting

/2/ C.G. Clayton, contribution to this meeting

/3/ H. Barshall, Neutron Sources for Basic Physics and Applications, Pergamon Press 1983, General Editor A. Michandon, S. Cierjacks and R.E. Chrien, p. 57-80

/4/ J. Csikai, Proc. IAEA Consultants' Meeting on Neutron Source Properties, Debrecen 1980, INDC(NDS)-114/CT (1980)

/5/ For example Safety Light Corporation, 4250A Old Berwick Road, Bloomsburg, PA17815, USA

/6/ G. Stengl, H. Vonach and H. Fabian, Nucl. Instr. Meth. 126, 235 (1975)

/7/ G. Stengl and H. Vonach, Nucl. Instr. Meth. 140, 197 (1977)

/8/ G. Stengl, Thesis, Technical Univ. Munich (1976)

/9/ D. Lehmann, D. Seeliger, A. Sgonina, ZfK-268, Dresden 1974

/10/ S.S. Nargolwalla and P. Przybowicz, Activation Analysis with Neutron Generators, Wiley N.Y. 1973, chapter 4

/11/ A. Pavlik and G. Winkler, IAEA-Report, to be published

/12/ J. Csikai, Proc. Int. Conf. on Fast Neutron Physics, Dubrovnik, 1986

/13/ H. Vonach et al., Z.f.Physik 237, 155 (1970)

/14/ H. Vonach, IAEA Technical Report Series Nr. 227, IAEA Vienna 1983, p. 59

/15/ D. Leithner, M. Uhl and H. Warhanek, Anz. Österr. Akad. Wiss., math.-nat. Klasse 107, 121 (1970)

/16/ B.M. Bahul and H.U. Fanger, Nucl. Instr. Meth. 211, 469 (1983)

/17/ D. Miljanic, S. Blagus and M. Zadro, Phys. Rev. C33, 2204 (1986)

/18/ G. Traxler et al., Nucl. Sci. Eng. 90, 174 (1985)

/19/ A. Takahashi et al., Oktavian Report A-83-03 Osaka University, Osaka 1983

/20/ R. Fischer, M. Uhl and H. Vonach, to be published

/21/ G. Winkler, priv. comm.

/22/ J. Pohl-Rühling et al., IAEA-SM 266/4, p. 171 (1983)

/23/ Ref. 10, chapter 7

/24/ G.E. Miller and A. Vollbarth, Proc. 4th Conf. on the Scientific and Industrial Use of Small Accelerators, North Texas Univ., Oct. 1976, IEEE report 76 CH 1175-9 NPS 288 (1976)

/25/ H. Barshall, priv. comm.

TECHNIQUES FOR 14 MeV SOURCE UTILIZATION

D. SEELIGER
Technical University of Dresden,
Dresden, German Democratic Republic

Abstract

This review considers recent development of those techniques which are used for the utilization of DT-neutron generators usually not being a part of commercially delivered low voltage accelerators. Such techniques are needed for maintaining a high stability of operation, high quality of experiments, radiation protection and flux monitoring. Moreover, a few modern techniques for the utilization of neutron generators in nuclear data measurements are presented.

---

1. Introduction

The state of the development of DT-neutron sources based on low voltage accelerators is well described in many review papers over the past years, for instance in [1 - 5]. The status of this neutron sources was discussed in detail also at the IAEA Consultants Meeting on Neutron Source Properties in Debrecen, March 1980 [6]. Moreover, since many years several types of neutron generators are commercially available [7]. Therefore, the author of this review does not recognize the necessity of a new broad-scale review on this subject here. The main development in the field - high intensity DT-generators - is reviewed by J.C. Davis and applications of modest DT-generators for basic and applied studies - by H.K. Vonach. Consequently the present paper concentrates on the discussion of the progress in those techniques which usually are neither part of commercially delivered neutron generators nor a typical part of only one specific application but which can be used as standard multi-purpose equipment in a 14-MeV neutron source laboratory.

Among this techniques the recent development of the ion beam control, computer control of the neutron generator, for tritium handling, ion beam pulsing, neutron flux monitoring are discussed. Finally a few examples for techniques of modern nuclear data measurements at 14 MeV neutron sources are presented.

2. Techniques for ion beam control and automation

2.1. Ion beam transport and its control

The application of neutron generators in physical experiments usually requires an analysed ion beam focussed in a stable, well-defined beam spot at the target. Therefore, commercially available neutron generators have to be additionally equipped with a beam transport system including focussing lenses (magnetic as well as electrostatic quadrupole doublets or triplets), deflecting magnets (which can be replaced by a Wien filter) and equipment for ion beam diagnostics [8].

As the most suitable ion beam monitor for many years in neutron generator laboratories was used a quartz disc which was turned into the beam and observed by a TV-camera. However, this method can be used up to ion beam currents in the order of 100 µA only due-to the melting of quartz glass at higher power densities. Therefore, in connection with the development of high flux neutron generators new techniques for the high-current ion beam diagnostics have been developed. A few of them should be mentioned here:

(i) For determination of the ion beam emittance at high current and moderate power the multislits-probe or multidiaphragm-probe methods are used in combination both with photocopying paper or solid states diodes for registration of the ion beam [9,10,11].

(ii) A crude information about the ion beam profile at a beam power up to a few kW easily can be obtained by an arrangement of a few water-cooled isolated concentric diaphragms made from copper or tantalum as shown on fig. 1a [12].

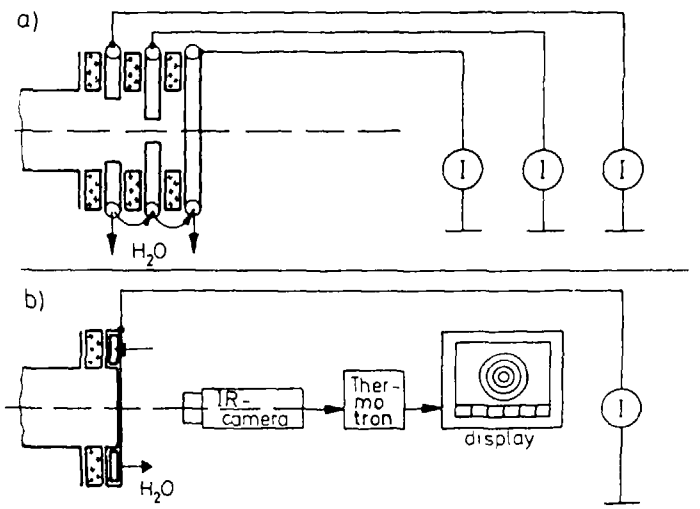

Fig. 1
Methods of intense ion beam diagnostics [12]
a) multidiaphragma-method;
b) infrared thermography method

(iii) The harp monitor displays the intensity distribution of the ion beam by means of two orthogonal sets of thin parallel tungsten or wolfram wires (diameters $\leq$ 0.1 mm) without interruption of the beam transport to the target. The applicability is limited by the power absorption per wire [13].

(iiii) The most elegant method of high intensity beam profile measurements is the contactless videofrecuency scanning of the infrared radiation emitted from the surface of the target by means of infrared thermography, as shown on fig. 1b [13-15]. This method was used for ion beam measurements up to 5 kW power [12].

2.2. Computer controlled operation

Both the requirements for a long-time stability of the beam conditions in nuclear data measurements and the broad availability of microcomputer techniques promoted the development of computer based control systems for neutron generators during the last years [8].
In [16] the on-line closed or open loop control of the high flux neutron generator INGE-1 is provided by three microcomputers of the type AMCA-80 (within the CAMAC-standard) and of type K 1520. Through optical transmission lines based on glass fibre optics all the important parameters in the high-voltage terminal as well as on ground potential are controlled by the microcomputer and the operator is provided with information about the important physical parameters of the accelerator on the graphical display (see fig. 2).
Parameters controlled are: beam currents at the target and diaphragms, temperature and circulation rates of cooling water, vacuum conditions, voltage and current of power supplies, neutron flux, tritium monitors a.o.
Another control system presented in [17] is based also on a CAMAC-microcomputer. The system is capable to control about 20 analog and 100 digital quantities.
No doubt, in the future a growing number of neutron generators will be equipped with this comparatively cheap technique providing a higher reliability for experiments.

3. Tritiumhandling

3.1. General considerations

The tritium content of an usual solid state Ti-T-target used at standard neutron generators is in the order of magnitude of $(1\text{-}5) \cdot 10^2$ GBq. In the high flux neutron generators the tritium content per target is increased up to 20 TBq. An essential part of this ammount of tritium is released from the target during its storage, transport, change and operation. The main mechanism of the release of tritium from the target is the displacement of

tritium by impinging deuterons. Measurements by Barschall and Booth [18] obtained a release rate of about 6 GBq/h · mA. In case of closed vacuum systems the main part of this tritium gas is absorbed in the getter pumps. Moreover, practically all inner surfaces of the vacuum system will be covered with tritium.

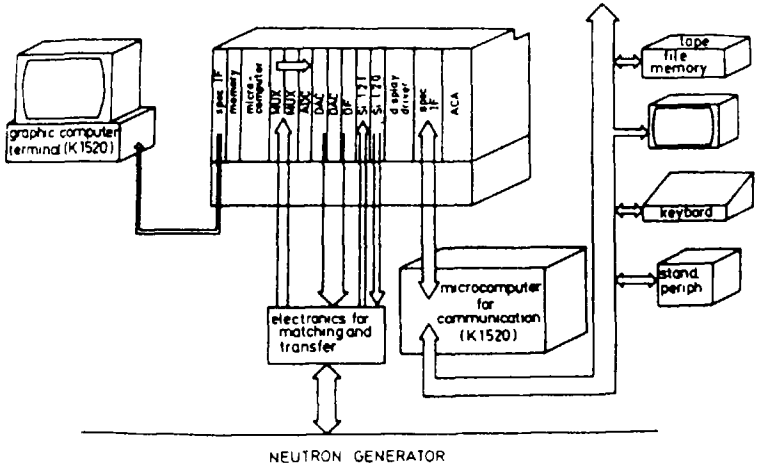

Fig. 2
Scheme of the computer control electronics for the intense neutron generator INGE-1 [16]

In the case of open vacuum systems the main part of gaseous tritium release is exhausted through the diffusion and fore pumps contaminating the oil of the diffusion pump as well as the surrounding air of the neutron generator.

At the other side, the derived air concentrations (DACs) are strongly limited by the ICRP regulations. The annual limits of DACs for Tritium in the case of occupational work (fourty-hour week) are

$$0{,}8\ \mathrm{MBq/m^3} \text{ and } 20\ \mathrm{GBq/m^3}$$

for HTO and T-gas, respectively [19].

Therefore, besides shielding against external neutron and γ-ray radiation and protection against induced radioactivity handling of tritium is one of the major radiation protection problems with neutron generators.
Besides the gaseous tritium contaminations occur also in form of tritiated water (cooling water), water vapour and metal tritide aerosols or sputtered particles from the target. However, in the case of neutron generators the main part of tritium released is in the form of T_2-gas for which the DAC limits are much higher than in the case of tritiated water. New estimates assuming particle contamination and gaseous release showed that in comparison with more conservative estimates (basing on a complete HTO-contamination) the current limits could be relaxed by several orders of magnitude [20]. Nevertheless, in case of the use of any pumped DT-neutron generators the following measures have to be considered (and at least partially realized) to meet the ICRP regulations concerning radiation protection against tritium contaminations:

- handling of contaminated getter pumps in the same way as tritium targets;
- handling of all other parts of the accelerator vacuum system as being contaminated;
- appropriate storage and transport of fresh and used targets;
- high-speed exhaust of the air from the generator room, the fore pump outlet and from all places where contaminated parts of the accelerator or targets are stored;
- special regulations must be foreseen for procedures of opening of the vacuum system and changes of targets to avoid high-level contaminations and incorporations;
- use of tritium absorption systems for reduction of the tritium emission to the open air;
- continuous control of the tritium concentration in the generator room, of the tritium emission to the air, in the cooling water and at other places as well as surface

contaminations at the floor (especially near the target) and the walls of the generator rooms;

- measures of personnel dosimetry like urine analysis and others.

3.2. Tritium monitoring

Since many years methods for measurements of tritium including low-level measurements are well-developed and described in the literature. They can be divided into two groups:

(i) direct counting of tritium in the form of water vapour or hydrogen gas in air using flow-through ionisation chambers or proportional counters and

(ii) indirect registration of tritium containing samples from the air, preferably using liquid scintillation counters.

Essential improvements in the tritium proportional counting techniques decreasing the background produced by Compton electrons have been obtained many years ago [21,22]. Recently a new type of counter for radionuclides emitting soft beta-radiation has been developed by Povinec et al. [23]. In this case the single wire inner counter has been replaced by many counter elements separated from each other by thin cathode wires. This multielement low-level proportional counters enable to reach a very high sensitivity and long-term stability of tritium counting.

Recently the measurement of Tritium activity concentration in air by a new method - by means of the electret ionisation chamber - was proposed [24]. In this case the annulative tritium activity release in air with high sensitivity by means of a comparatively simple system could be measured over a long time. Fig. 3 shows the mechanical construction of the PTFE-electret chamber and fig. 4 shows the radiation induced electret voltage decay ΔU_E as function of exposure time Δt.

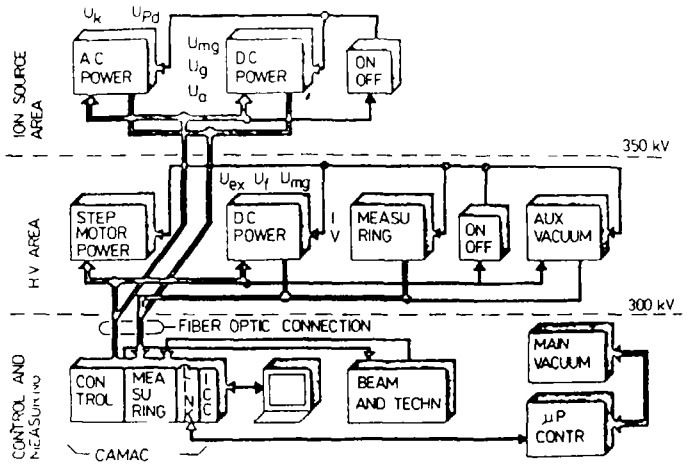

Fig. 3
Control scheme of the Bratislava intense neutron generator project [17]

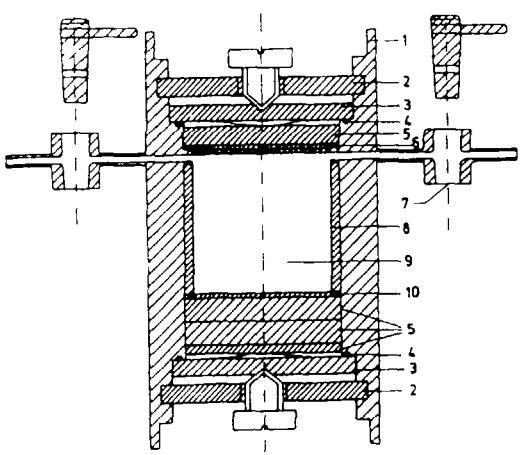

Fig. 4
Construction of a simple electret detector for the measurement of the tritium content in the air [24]
1 - capsule; 2 - lid with screw; 3 - lid with spring; 4 - gasket ring; 5 - spacing disc; 6 - electret with rear electrode; 7 - opening with trap; 8 - spacing ring; 9 - chamber volume; 10 - opposite electrode

3.3. Tritium absorption

During the operation of a high-flux generator with an open vacuum-system, in case of emergency and in other cases (f.i. opening of the target chamber in the glowe-box) the tritium has to be extracted from the air exhaust to guarantee the upper limit of tritium concentration in the air outside of the neutron generator building.
Absorption systems for this procedure are well-described in the literature [25-30] . Fig. 5 shows the principle scheme of such an absorption system. It includes filters for the oil from the vacuum pumps, the stove for burning the tritium gas by means of a catalyst (Cu, Pd, Mn or others), the absorber for the resulting HTO or T_2O and the tritium monitor controlling the proper function of the whole unit.

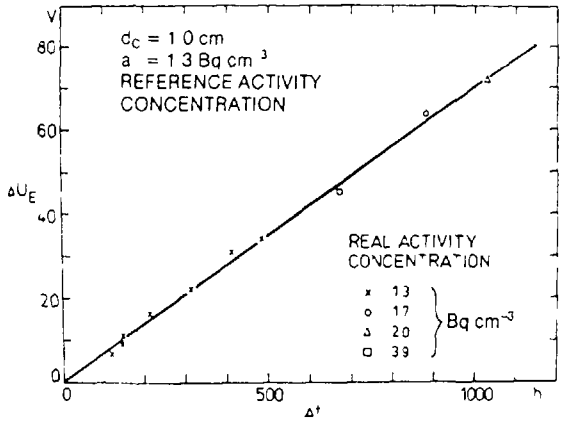

Fig. 5
Radiation induced electret voltage decay U_E as function of the exposure time t for an inter-electrode spacing distance d_c = 1.0 cm and a reference activity concentration of 1.3 Bq.cm^{-3} [24]

4. Beam pulsing

Since the pioneering work by Cranberg and Levin [31] the nanosecond ion beam pulsing used for neutron time-of-flight spectroscopy became a widely used technique also in connection with DT-generators [32,33] . The main advantages of the pulsed-beam method of fast neutron spectroscopy are the high energy resolution as well as high intensities accessible. Among the different methods of beam pulsing and their combination between each other [34] in the case of DT-generators the most reasonable solution consists of the combination of RF-deflection with RF-klystron bunching of the ion beam after acceleration at the same frequency. In this case more than 20 % of the ion beam can be concentrated into 1 ns ion bursts at the target due to a compression factor higher than 40 [35] . A drawback of systems like this is the need for a comparatively long drift path for ion bunching in the order of several meters. Nevertheless, new pulsing systems of this type succesfully started operation recently. As an example the pulsing system of OKTAVIAN at the Osaka University is shown on fig. 6 [36] . With this system 1,5 ns ion pulses with 16 mA peak current are produced at the target.
A more compact construction of the pulsed neutron generator is possible, if klystron bunching is introduced into the beam at the low energy end of the accelerator [6,37] . In this case the period of bunching voltage has to be chosen much higher than the needed period of neutron bursts at the target, resulting in a lost of average neutron intensity.
Altogether one can conclude that during the last years no remarkable changes in the techniques of nanosecond beam pulsing have been introduced. To realize proposed multiple klystron bunching which promises a compression of more than 60 % of the ion beam [33] , the combination between short ion source pulsing with klystron buncning and other advanced techniques are still open to the future.

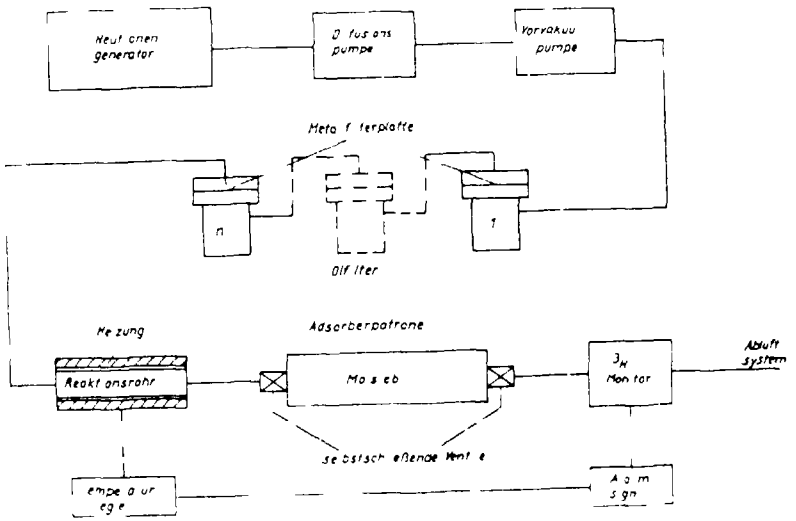

Fig. 6
Principle scheme of a tritium absorption unit including metallic filters for the fore pump oil, the reaction stove with catalyst molecular absorption unit and tritium monitor [5]

5. Neutron flux monitoring

For modest-level neutron flux monitoring in 14MeV laboratories long counters and proton recoil scintillation counters are used. Without special measures the accuracy of this type of flux monitoring is in the order of 10% or even worse due-to the sensivity of this detectors to self-target DD-neutrons ,background radiation,uncertainties of the efficiency calibration and other reasons.For high-level flux monotoring special techniques have to be used,a few of them are mentioned below.

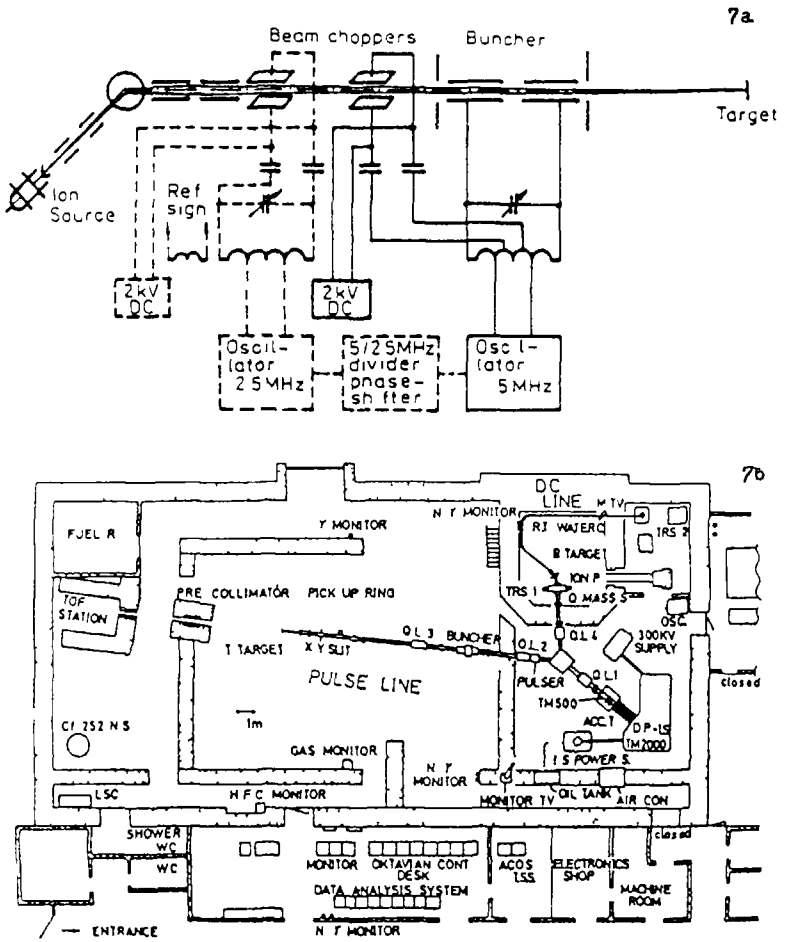

Fig. 7
Post acceleration nanosecond beam pulsing systems at 14 MeV neutron generators
a - scheme of the pulsing system at the TUD [35,8]
b - TOF-laboratory at Osaka University [36]

5.1. Associated particle method

Counting the associated α - particles from the $T(d,n)^4He$ reaction by a solid state or plastic scintillator detector easily uncertainties of the determined neutron flux (fluence) below 5% can be obtained, and this was done since many years (for instance in [54]). Using more refined methods the accuracy can be improved, in this case uncertainties in the order of 1,5% are realistic [39,56]. The use of 'electronically marked' neutrons for a fast coincidence with a neutron detector (fission chamber or scintillation counter) was named 'time correlated associated particle method' (TCAPM) [38,55]. This method can be used for the absolute neutron detector efficiency calibration, but also for very precise fission cross section measurements (in the order of 1%), for (n,2n)-tof-measurements and in other cases.

5.2. Proton recoil telescope

The proton recoil telescope (PRT) has been a standard method for flux (fluence) measurements of fast neutrons up to 20MeV for many years [57].
Recently Brede et al. [40] presented a proton recoil telescope consisting of two gaseous proportional ΔE-couters combined with a surface barrier E-detector. In comparison with experiments an extensive Monte-Carlo simulation of the whole process [41] was carried out yielding a deviation of the response values of the PRT of about 2% for typical experimental conditions.

5.3. Thin scintillators

The cross section of the reaction $^6Li(n,t)^4He$ is known with an accuracy of 0.5...2% below 100 keV. Moreover, lithium glasses have a high neutron detection efficiency and are capable of fast timing. For minimizing of multiple scattering effects compact materials must be kept out of the neutron beam. With an arrangement from Harwell [42] shown on fig. 10 uncertainties as low as 2...3% can be obtained below 100 keV neutron energy. Due-to the decrease of the cross section and its increasing uncertainties such flux monitors cannot be used at 14MeV incident energy.

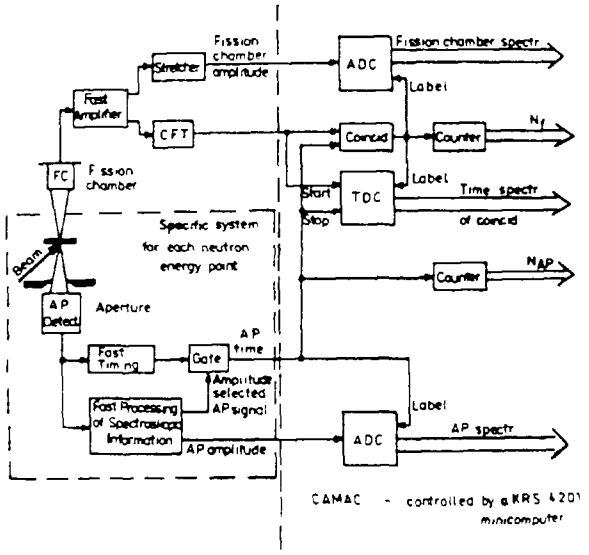

Fig. 8
Associated particle method used for absolute flux monitoring in a fission cross section measurement [38]

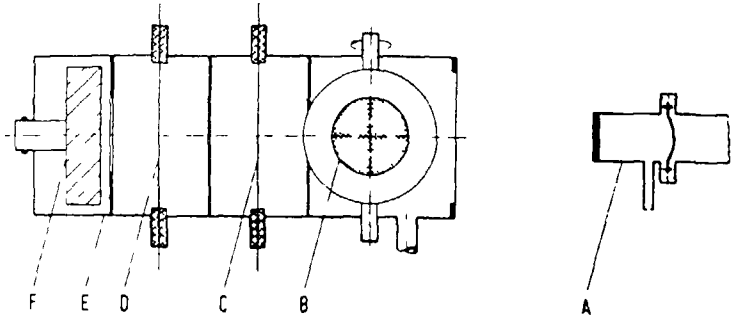

Fig. 9
Absolute neutron flux measurement by the proton recoil method using a E - E - telescope [40,41]
A - gas target; B - polyethylen radiator; C + D - proportional counters; E - aperture; F - silicon detector

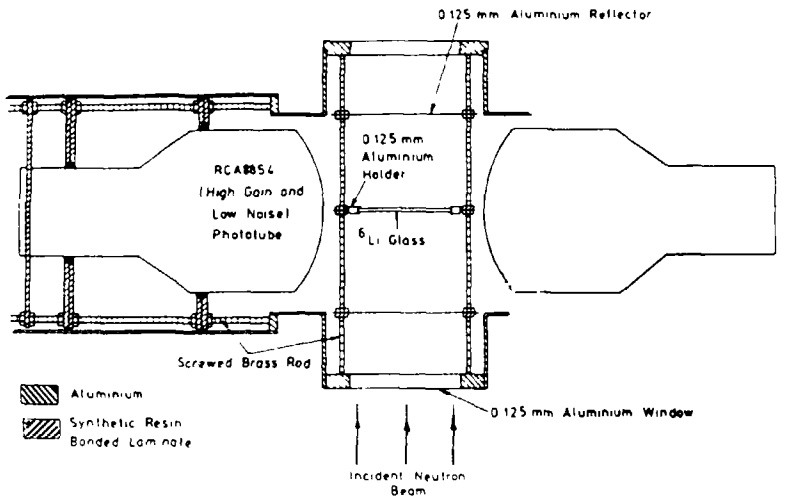

Fig. 10
Neutron flux measurement using a ^{6}Li - glass - scintillator [42]

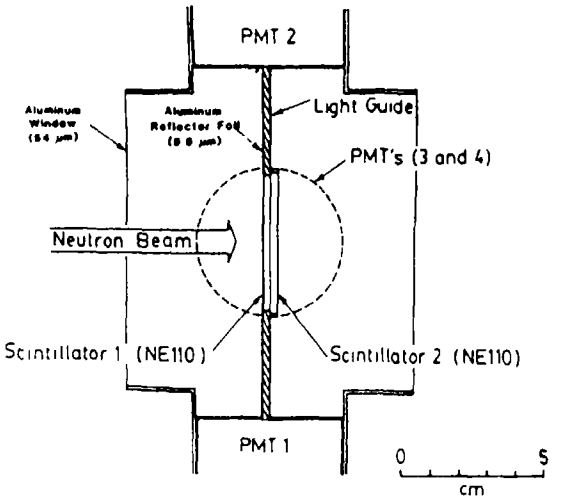

Fig. 11
Neutron flux measurement using two thin recoil scintillators [43]

For higher energies the most accurately known neutron standard reaction is the elastic neutron-proton scattering(o.5...1.o%). The angular distribution is known to an uncertainty of 2% only. Therefore, The most accurate results can be expected with a detector counting the proton recoils in the whole angular range which at the same time is thin enough to avoid effects of double-scattering of the incident neutrons. This thin proton recoil scintillator technique is widely used.
An improvement of this standard method recently was proposed in the NBS with a dual thin scintillator in which events with incompletely absorbed recoil protons are excluded by anticoincidence. (see fig.11) [43]. The uncertainty of the detection efficiency in the energy range between 1 and 15 MeV is within 1...2%.

5.4. Black detector

The 'black neutron detector' [44] consisting of a thick scintillation counter with an entrance channel is suitable for precise neutron flux measurements mainly below 1oMeV where its detection efficiency is well above 8o%. At 14MeV its behaviour becomes similar to that of a usual thick proton recoil scintillator.

5.5. ^{235}U fission detectors

The ^{235}U fission cross sction is a standard in the energy range up to 2oMeV which is known to an accuracy of 2...3%. Therefore, fission fragment detectors , mainly gridded fissionionization chambers, are widely used as neutron flux monitors withan uncertainty of a few percent [45].

6. Typical experimental arrangements for nuclear data measurements

DT-neutron generators are widely used for nuclear data measurements especially for the fusion reactor program. At the following figures some typical examples for such experiments are presented. The list of cited references 46,- 57 is far from being complete. These examples are selected to show the big amount of different research work which is carried out at 14 MeV neutron sources at present.

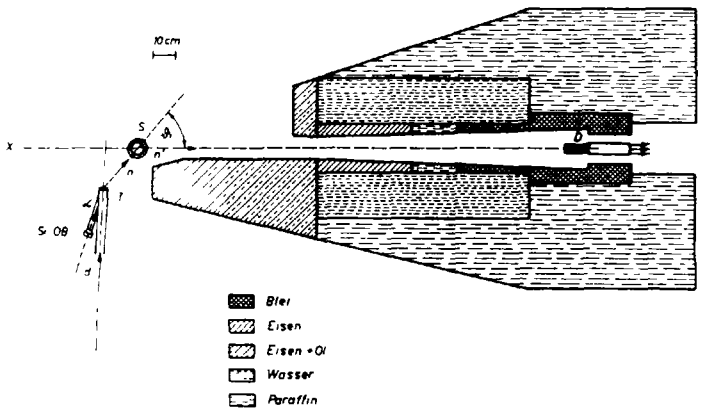

Fig. 12
Typical arrangement for a fast neutron TOF spectrometer [47]

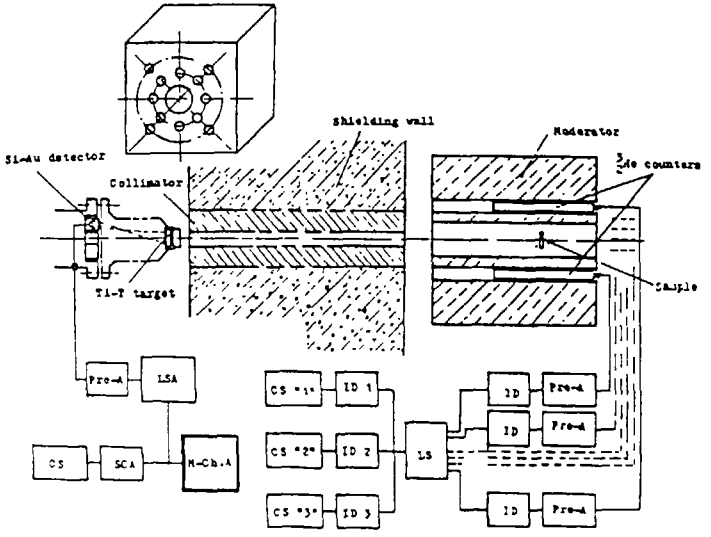

Fig. 13
Arrangement for the measurement of multiplicity of secondary neutrons from 14 MeV induced reactions [46]

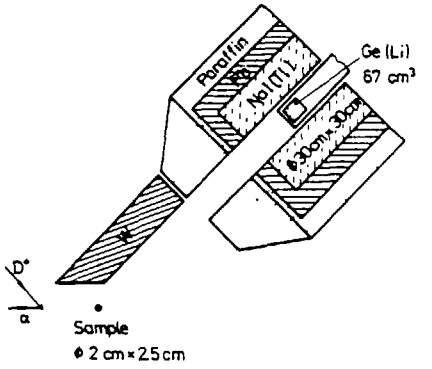

Fig. 14
Arrangements for the measurement of γ-ray spectra emitted in 14 MeV induced reactions using a Ge(Li)-Detector with NaJ(Tl)-anticoincidence shield [48]

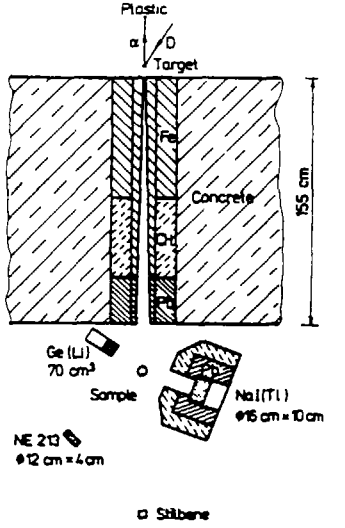

Fig. 15
Arrangement for measurement of secondary n-γ-correlations using different detectors [50]

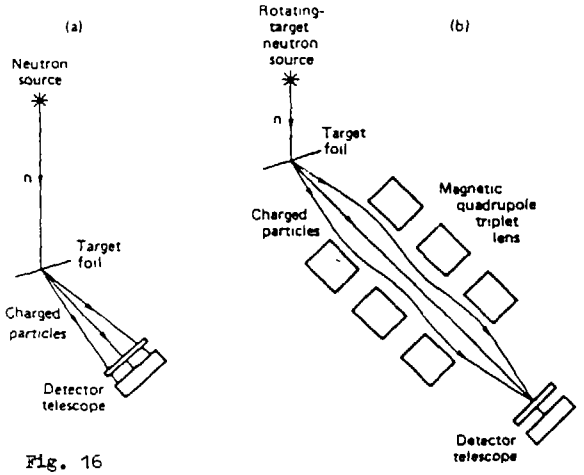

Fig. 16
Techniques for the measurement of charged particle spectra resulting from 14 MeV induced reactions [52]
a - telescope technique
b - quadrupole spectrometer

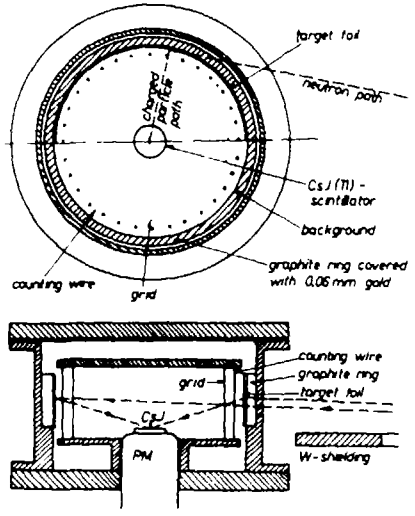

Fig. 17
Ring detector for the measurement of the angular distribution of charged particles resulting from 14 MeV induced reactions [53]

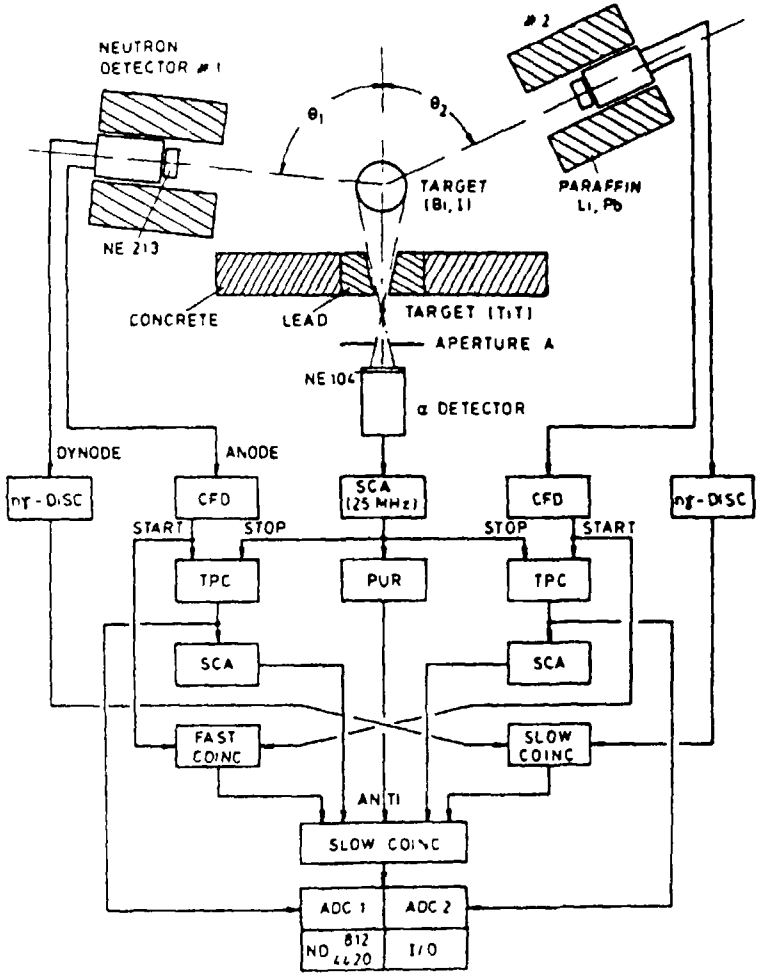

Fig. 18 Experimental arrangement for the measurement of secondary neutron spectra from the (n,2n) reaction by means of a double-tof-spectrometer using the associated particle method [57].

References

[1] S.S. Margowalla, E.P. Przybylowicz
Activation Analysis with Neutron Generators
Wiley, New York, 1973

[2] J. Csikai, Atom. En. Rev. 11 (1973) 415

[3] T. Sztaricskai, Atomki Kozlemenyek 22 (1980) 47

[4] H.H. Barschall, Neutron Sources for Basic Physics and Applications., Chap. IV DT-Sources, in the Series Neutron Physics and Nuclear Data in Science and Technology. Oxford,1983

[5] U. Jahn, E. Paffrath, D. Schmidt and D. Seeliger Kernenergie 28 (1985) 433

[6] J. Csikai, Proc. IAEA Cons. Mtg. on Neutron Source Properties INDC(NDS)-114/GT, Debrecen,1980, p. 265

[7] Nucleonics 23, 4 (1965) 60

[8] Proc. of the XIV-th International Symposium on the Interaction of Fast Neutrons with Nuclei - Neutron Generators and Application, Gaussig, Nov. 1984, ZfK-562, July 1985

[9] U. Wroe, Nucl. Instr. Meth. 52 (1967) 67

[10] Sun Biehe, Wang Fulin, Chen Qin in [8] , p. 33

[11] A. Tunia, U. Jahn, E. Paffrath, in [8] , p. 52

[12] U. Jahn et al., Exp. Techn. and Physik, 1986, to be published

[13] W. Adam and H. Buttig, ZfK-443 (1981) 155

[14] H. Buttig, in [8] p. 56

[15] H. Buttig, Nuclear Instr. Meth. 203 (1982), 69

[16] P. Eckstein et al., in [8] , p. 63

[17] J. Pivarc et al., in [8] , p. 16

[18] R. Booth, H.H. Barschall, Nucl. Instr. Meth. 99 (1972)

[19] Safety Series Nr. 9, Safety Standards
Basic Safety Standards for Radiation Protection, 1982, Edition, IAEA, Vienna, 1982

[20] B. Lorenz, Radiation Protection Problems with Tritium in High Flux Neutron Generators, in [8] , p. 68

[21] F.G. Houtermans, H. Oesdiger, Helv. Phys. Acta 31 (1958) 117

[22] A. Moljk, R.W.P. Drewer, S.C. Curran, Proc. Roy. Soc. A 239 (1957) 433

[23] P. Povinec, J. Szarka, S. Msacev, Nucl. Instr. Meth. 163 (1979) 269

[24] P. Povinec, Nucl. Instr. Meth. 176 (1980) 111
G. Pretzsch, B. Dorschel, H. Seifert, T. Streil and D. Seeliger Radiation Protection Dosimetry Vol. 12 N. 4 (1986) 345

[25] R. Booth et al., Nucl. Instr. and Meth. 145 (1977) 25

[26] D.W. Heikkinen, C.M. Logan, UCRL-86747, Lawrence/-Livermore-Lab., USA, 1982

[27] T. Nakamura et al., Proc. IVth Symp. on Accel. Sci. and Technology, Saitana, Japan, 1982

[28] K. Sumita, J. Atom. Energy Soc. Japan, 20 (1978) 613

[29] D. Dale et al., Nucl. Instr. and Meth. 145 (1977) 127

[30] M. Schuler et al., KFA-Bericht, Inst. f. Chemie, Julich, 1977

[31] L. Cranberg and J.S. Levin, Phys. Rev. 103 (1956) 343

[32] J.H. Neiler, W.M. Good in "Fast Neutron Physics" part I eds. J.B. Marion and J.L. Fowler, New York, 1960

[33] D. Seeliger in "Nuclear Theory for Applications - 1980" IAEA-SMR-68/I, Trieste, 1981, p. 255

[34] D. Lehmann, D. Seeliger, A. Sgonina, Nanosekunden-Pulsung stationarer Teilchenbeschleuniger, ZfK-268, 1974

[35] D. Seeliger, K. Trutzschler, Nucl. Instr. Meth. 66 (1968) 157

[36] K. Sumita et al., 12th SOFT, Julich, Sept. 1982
A. Takanashi et al., in Proc. Int. Conf. on Cross Sections

for Science and Technology, Antwerp, 1982
Ed. K.H. Bocknoff, Reidel Publ. Comp., p. 360

[37] V.B. Anufrienko et al., Prib. Tekh. Eksp. 3 (1971) 46.

[38] R.Arlt et al. in Nuclear Standard Reference Data, IAEA-TECDOC-335, Vienna, 1985, p.174

[39] V.D.Huynh as 38 ,p.338
V.D.Huynh Metrologia 16(1980)31

[40] H.J.Brede et al. as 38 ,p.340

[41] B.R.L.Siebert et al. PTB-Report ND 23 (1982)

[42] D.B. Gayther Annals Nucl.Energy 4(1977)515

[43] M.S.Dias et al. Nucl.Instr.Meth. 224(1984)532

[44] W.P.Poenitz Nucl.Instr.Meth. 109)1973) 413

[45] H.H.Knitter ,C,Budtz-Jorgenson in Nuclear Cross Sections for Technology, NBS Spec.Publ.594, Proc.Knoxville Conf., 1980, p.947
H.H.Knitter et al. Nucl.Sci.Eng.83(1983)229

[46] T.T.Panteleev et al. INDC (BUL) - 010/GI INT(86) - 1

[47] D.Hermsdorf et al. ZfK-277 U ,1975

[48] J.Lachkar et al. Nucl.Sci.Eng. 55(1974(168

[49] D.M.Drake et al. Report LA- 5983 -MS ,Los Alamos,1975

[50] S.Hlavac ,P.Oblosinsky Nucl.Instr.Meth. 206(1983)127

[51] S.M.Grimes et al. Phys.Rev. C19 (1979) 2127

[52] R.C.Haight in Techniques of Measurement, Analysis and Instrumentation for 14MeV Neutron Nuclear Cross Sections INDC(GDR)- 34/GI, Oct.1985, p.1

[53] H.Vonach in Nuclear Theory for Applications-1980 IAEA -SMR -68/I, Trieste, 1981.p-269

[54] W.Haussen et al. Nucl.Instr.Meth. 88(1970)251

[55] R.Arlt et al-in Nuclear Cross Sections for Technology, NBS Spec.Publ. 594, Proc.Knoxville Conf.1980, p990

[56] D.J.Thomas, V.E.Lewis Nucl-Instr.Meth.179(1981)397

[57] Schroeder et al.Ztschr.Phys. A287(1978)353

ASSOCIATED PARTICLE METHOD FOR 14 MeV NEUTRON DATA MEASUREMENT

YUAN HANRONG
Institute of Atomic Energy,
Beijing, People's Republic of China

Abstract

The application of associated particle method for 14 MeV neutron data measurement is discussed. The improvements of the AEP associated particle type fast neutron TOF spectrometer are presented. A new AEP value of 2.078±0.040 b for the fission cross section of ^{235}U induced by 14.2 MeV neutrons using the time correlated associated particle method is given and the "back-to-back" TCAP method for direct measurement of fission cross section ratio of ^{238}U to ^{235}U is described. In the latter experiment a "correlated neutron beam wrapping up samples" geometry has been adopted to eliminate the effect of the ununiformity of the samples. The initial experimental results indicate that this method is feasible.

The $T(d,n)^4He$ reaction used in neutron generators provides a good condition for utilization of associated particle method. The main applications of associated particle method for 14 MeV neutron data measurement are concentrated in the following fields:

- To determine the 14 MeV neutron flux by associated alpha particle method;
- To establish the fast neutron time-of-flight spectrometer for the measurement of neutron energy spectrum and angular distribution of elastically and inelastically scattered fast neutrons by associated alpha particle method;
- To determine the fission cross sections induced by 14 MeV neutrons with the time correlated associated particle method.

The application of the associated alpha particle method in 14 MeV neutron flux measurement has achieved great success. Its accuracy for the neutron flux determination is better than that of the other methods used in this neutron energy region. Since the sixties the associated alpha particle method has been applied to determine the 14 MeV neutron flux at the Institute of Atomic Energy, Beijing (AEP) and the determination with an accuracy of 1% has been obtained.

As compared with the TOF spectrometer using the pulsed-beam method, in the case of the TOF spectrometer using the associated particle method the intensity of the neutrons cannot be used to be so high and the flight path cannot be used to be so long[1,2]. This is because the ratio of the effect to background is approximately inversely proportional to the squares of the neutron strength and the flight path. However, the neutron backgrounds are comparatively low and structureless because the correlated neutrons are emited to a small spatial cone and it is very easy to reduce the data from the spectrum. The width of the neutron spectrum and the dynamic range of the spectrometer may not be influenced by the functional changes of the accelerators, and the time resolution may be slightly better than that with the pulsed-beam method. It is thus clear that the associated particle method can yet be regarded as a worthy method for constructing the TOF spectrometer. In the last few years some improvements of the associated particle type fast neutron TOF spectrometer have been made at the Institute of Atomic Energy, Beijing[3,4]. To put it in a nutshell, they are the following:

1, A liquid scintillator ST-451, 105 mm in diam. and 50 mm in height, coupled with a XP 2040 type photomultiplier tube was used as the neutron detector instead of the plastic scintillator, and the neutron detector was shielded with a special purpose paraffin, iron and lead block, thus improving the uniform angular response and detection efficiency of the detector and reducing the neutron backgrounds coming from the surroundings.

2, The risetime to pulse height converter was applied to realize the pulse shape discrimination between gamma rays and neutrons. The risetime to pulse height converter discriminates not only gamma ray pulses but also pulses, especially those originated from the photomultiplier tube.

3, The constant fraction timing circuit was adopted, thus improving the time resolution of the spectrometer.

4, A new time to amplitude converter was used and the occasional coincidence counts were reduced.

5, A goniometer with air cushion was disposed to the TOF spectrometer. It convenienced for changing the angles for measurements.

This TOF spectrometer has been used for the measurements of the secondary neutron spectra and differential scattering cross sections of 14 MeV neutrons. The resolution time of the spectrometer is about 1 ns and the efficiently maximum flight path is more than 3 m.

In spite of that one can put forward a question on reliability in making use of time correlated associated particle method, on the present level of understanding the TCAPM may be still the best mothod for measuring the fission cross sections in the 14 MeV neutron energy region. It enabled us to get the data of some fission cross sections with an accuracy of 1% or so. As mentioned elsewhere, the absolute measurements of fission cross sections for ^{235}U and ^{239}Pu induced by 14.7 MeV neutrons using the associated particle method [5] were completed at the AEP. As a part of the IAEA co-ordinated programme of research concerned, the absolute measurement of the fission cross section of ^{235}U for 14.2 MeV neutrons by TCAPM has been carried out and the measurement of the fission cross section ratio of ^{238}U to ^{235}U for 14.7 MeV neutrons is in progress. The experimental conditions of the absolute measurement of the fission cross section of ^{235}U for 14.2 MeV neutrons were similar to that of previous work [5] and a value of (2.078 ± 0.040) b has been obtained[6]. The main feactures of this

experiment are given in table 1. Comparing this value with that of "modern" measurements[5,7-13](as shown in table 2), it can be seen that the ^{235}U fission cross section is nearly constant over the 14 MeV neutron energy region.

Besides the few fission events induced by background neutrons, one of the main advantages of the TCAPM used for absolute measurement of fission cross sections is that the exact knowlege of the alpha particle detection efficiency is not necessary. As is known to all, in this case such prerequisites must be satisfied: the fissionable sample should be large enough to make the base of the neutron cone to be situated inside the fissionable sample and the fissionable sample should be uniform enough. This is because in the absolute measurement by TCAPM the important thing is that to know exactly the number of fission events induced by the whole neutrons correlated with the alpha particles and the number of fissile nuclei per cm^2.

In the case of determination of the fission cross section ratio, when the "back to back" method is used and the whole fissile nuclei of the two kinds of samples to be irradiated by the same correlated neutron beam can be satisfied, the whole numbers of the fissile nuclei of the samples can be used in calculation instead of the numbers of fissile nuclei per cm^2 of the samples. That means, the errors caused by ununiformities of the samples can be avoided and the errors caused by background neutrons can be reduced by a big margin when the "back to back" TCAPM with "correlated neutron beam wrapping up samples" geometry is applied. Of course, the distance between the samples and the target should be enlarged for enabling the samples to be wrapped in the correlated neutron beam and prolonging the measuring time appropriately is neccessary under these circumstances.

The "back to back" TCAPM with "correlated neutron beam wrapping up samples" geometry are adopted to determine the fission cross section ratio of ^{238}U to ^{235}U at the Institute of Atomic Energy, Beijing. Fig.1 shows the schematic diagram of the

Table 1. Main feactures of the absolute measurement of ^{235}U fission cross section for 14.2 MeV neutrons

Neutron source $T(d,n)^4He$ reaction
Accelerator: 600kV Cockcroft-Walton
Deuteron energy: 210 keV
Neutron target. Ti-T, 0.6-1.0 mg/cm^2
Fission detector: Fast current ionization chamber
Gas filled in chamber: 1 atm., CH4
Sample preparation: U electrodeposited on 40μ Pt backings
Areal density of layer: 271-407 $\mu g/cm^2$
Distance between fission chamber and target: 5 cm
Detector of AP: 100 μ plastic scint.+56DVP/03A
AP angle with respect to beam: 90^o
Number of AP per sec: 10^5
Corrections: Detection efficiency of fission events, Attenuation of neutrons, Fission events due to the other isotopes, etc.

Table 2. Comparison of experimental results of ^{235}U fission cross section for 14-15 MeV neutrons

Authors, ref.	Year	En,MeV	σ_f , b
Czirr et al., (7)	1975	14.6	2.075 ± 0.040
Cance et al., (8)	1978	14.0	2.062 ± 0.039
		14.6	2.063 ± 0.039
Alkhazov et al., (9)	1979	14.7	2.073 ± 0.023
Adamov et al., (10)	1979	14.0	2.084 ± 0.034
		14.5	2.101 ± 0.034
		14.7	2.096 ± 0.031
Arlt et al., (11)	1981	14.7	2.085 ± 0.023
Wasson et al., (12)	1981	14.1	2.080 ± 0.030
Mahdavi et al., (13)	1983	14.63	2.070 ± 0.046
Li Jingwen et al., (5)	1983	14.7	2.098 ± 0.040
Li Jingwen et al., (6)	1985	14.2	2.078 ± 0.040

TCAPM for fission cross section ratio measurement. The fission cross section ratio of ^{238}U to ^{235}U can be determined by the formula

$$ {}^{8}\sigma_f / {}^{5}\sigma_f = n_5 N^c_{f8} / n_8 N^c_{f5} $$

where n_5 and n_8 are the number of ^{235}U nuclei in ^{235}U sample and the number of ^{238}U nuclei in ^{238}U sample respectively; N^c_{f5} and N^c_{f8} are the number of coincidences for ^{235}U and ^{238}U fission events respectively.

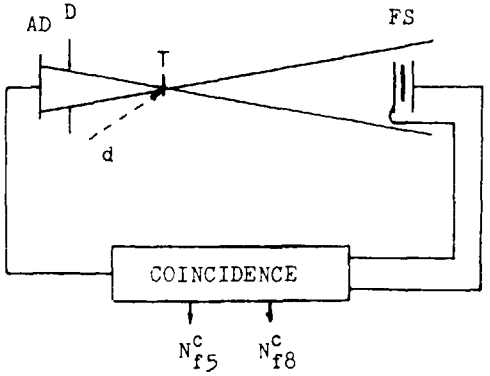

Fig.1. Schematic diagram of TCAPM for 14 MeV neutron fission cross section ratio measurement

d: deuteron beam, T: T-Ti target,
D. diaphragm, AD: alpha particle detector,
FS: ^{235}U and ^{238}U samples.

The preliminary experiment was carrying out using the 600kV Cockcroft-Walton accelerator. The energy of incident deuterons was 220 keV. The alpha particle angle with respect to deuteron beam was selected as 135^o and the 14.7 MeV correlated neutrons were obtained in the direction of 40^o with respect to the incident deuteron beam. The fission chamber of fast current type was placed 20 cm away from the T-Ti target at the correlated direction. This distance enabled that all the fissionable samples fixed in the chamber were situated inside the correlated neutron beam. The chamber was filled with methane gas of about 1.3 atm.

In order to raise the counting rate of the fission events, two pairs of ^{238}U and ^{235}U samples were used. They were placed "back to back" respectively in the fission chamber. The quantities of the samples were determined by direct weighting, alpha counting technique and by titration. A thin film scintillation counter consisted of a 100 μ thick plastic scintillation film and a fast photomultiplier of 56DVP/03A type was used as the alpha particle detector whereas the ORTEC electronic plug-in units were used as the main electronic circuits. The experimental arrangement for fission cross section ratio measurement is shown in Fig.2.

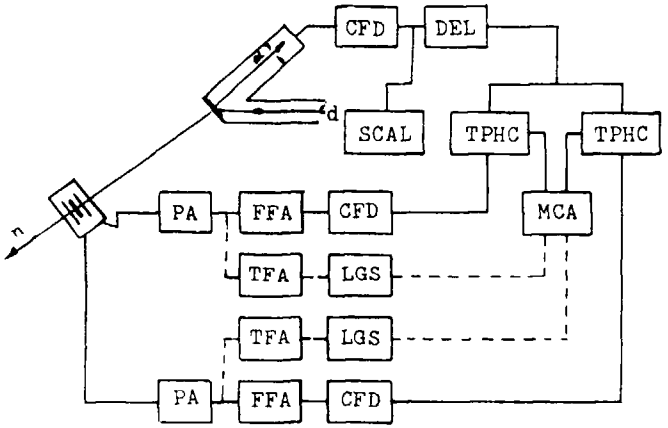

Fig.2. Experimental arrangement for fission cross section ratio measurement
dashed line shows the electronic circuits for fission spectrum measurement.
PA: pre-amplifier
FFA: fast filter amplifier
CFD: constant fraction discriminator
TPHC: time to pulse height converter
MCA: multichannel pulse analyzer
TFA: timing filter amplifier
LGS: linear gate stretcher
DEL: delay circuit
SCAL: scaler

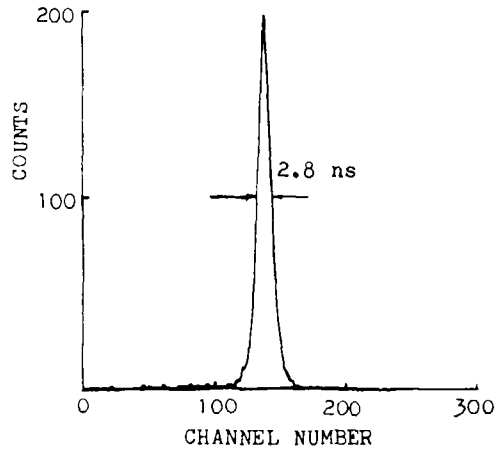

Fig.3. Time distribution of fission fragment pulses of ^{235}U

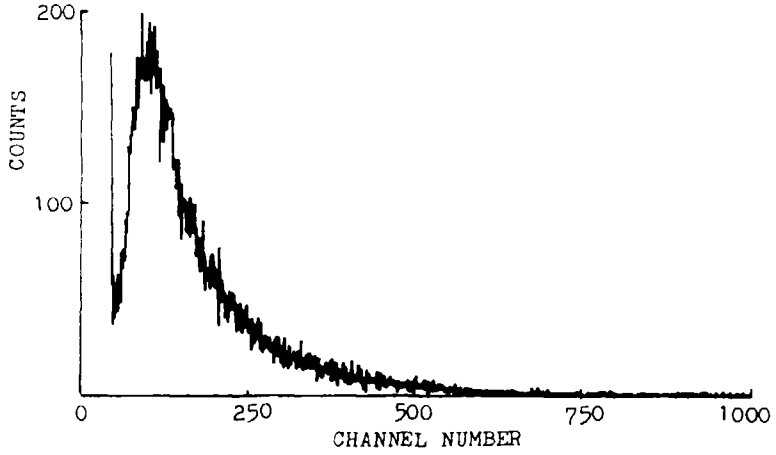

Fig.4. Amplitude distribution of fission fragment pulses of ^{235}U

Fig.3 and Fig.4 show the time distribution and amplitude distribution of fission fragment pulses of ^{235}U respectively. From these figures it can be seen that in this experiment the correlated fission events were separated very clearly from the background and the fraction of fission events which amplitudes were lower than the setting threshold of the discriminator could be obtained by extrapolating the amplitude distribution of fission fragment pulses to zero threshold with a not grave uncertainty. The experiment and calculations on determination of fission cross section ratio of ^{238}U to ^{235}U have not been finished yet. Judged by the initial experimental results, the "back to back" TCAPM with "correlated neutron beam wrapping up the samples" geometry is feasible for the fission cross section ratio measurement.

REFERENCES

1. D. Meier et al., Helv. Phys. Acta, 42, 813 (1969).
2. J. C. Alder et al., Nucl. Phys., A147, 657 (1970).
3. Bai Xixiang et al., Atomic Energy Sci. Techn., 1, 20 (1977).
4. Shen Guanren et al., Chinese J. Nucl. Phys., 3, 320 (1981).
5. Li Jinwen et al., Chinese J. Nucl. Phys., 5, 45 (1983).
6. Li Jinwen et al., unpublished.
7. J. B. Czirr et al., Nucl. Sci. Eng., 57, 18 (1975).
8. M. Cance et al., Nucl. Sci. Eng., 68, 197 (1978).
9. I. D. Alkhazov et al., Atomnaya Energiya, 47, 416 (1978).
10. V. M. Adamov et al., Proc. of the Int. Conf. on Nuclear Cross Sections for Technology, Knoxville, 1979, NBS Spec. Publ. 594, p.995, 1980.
11. R. Arlt et al., Kernenergie, 24, 48 (1981).
12. O. A. Wasson et al., Nucl. Sci. Eng., 80, 282 (1982).
13. M. Mahdavi et al., Proc. of the Int. Conf. on Nuclear Data for Science and Technology, 6-10 Sept. 1982, Antwerp, p.58, 1983.

STATUS OF THE BRATISLAVA MULTIPURPOSE NEUTRON SOURCE

J. PIVARČ, S. HLAVÁČ, V. MATOUŠEK,
R. LÓRENCZ, L. DOSTÁL
Institute of Physics,
Electro-Physical Research Centre of the
Slovak Academy of Sciences,
Bratislava, Czechoslovakia

Abstract

A multipurpose D+T neutron source, based on a 20 mA duoplasmatron ion source and a 300 kV/40 mA high voltage power supply, under construction at the Institute of Physics in Bratislava, is described. Its basic purpose is to produce intense and pulsed beams of 14 MeV neutrons. The intense section of the source is expected to produce continuously 10^{12} ns^{-1} with a rotating TiT target. The low current dc section is designed to produce continuously 10^{10} ns^{-1} and the fast pulsed section will be capable of generating a compressible D^+ ion beam of a length of 2 ns on a target spot with about 10^3 neutrons per pulse. The source components are designed to give high reliability with little maintenance in order to minimize the radiation hazard in view of the extreme concentration of radioactive tritium.

1. Introduction

At the Institute of Physics in Bratislava a multipurpose intense 14 MeV neutron source is being developed.

The intense section of the source should be capable of producing 300 keV/10 mA of a separated D^+ ion beam. With such a beam spot of 1 cm^2 and a useful target life-time of about 10 h can be expected.

The conventional dc section is designed to produce a neutron yield about 10^{10} ns^{-1} and the fast pulsed section will be capable of generating a compressible D^+ ion beam of a length of 2 ns on a target spot with 10^3 neutrons per pulse for a 1 mA D^+ ion beam. During the first step, ion pulses of a length of 46 ns will be produced in a chopper. During the second step these pulses are compressed to a length of 2 ns in a bunching system. The repetition rate of the system will be 5 MHz and the bunching frequency 10 MHz.

Recently, several components have been developed/completed and tested succesfully. i) A high voltage power supply together with a capacitor battery and all supplementary units such as water resistors, a pneumatic discharger and high voltage cable ends. ii) All high voltage transformers, i.e. an isolating transformer 300 kV/10 kVA for a high voltage terminal, an isolating transformer 50 kV/2 kVA for a duoplasmatron and 50 kV/3.75 kVA for an extraction power supply source.

Under construction are the high voltage terminal, diagnostic elements of ion beams as well as the rotating target.

The paper gives a short survey of the present status in the development of the accelerator components.

2. Description of the neutron source

The layout of the source is in Fig.1. Deuterons are extracted from the plasma of a duoplasmatron ion source by a 50 kV potential. An Einzel lens is included into the high vacuum beam line to achieve the desirable focal properties. The 50 keV deuteron beam passes then through a double focusing magnet placed directly on the high voltage terminal. The magnet is designed for the D^+ separation from molecular ions, allowing the acceleration tube and the beam transport system to be optimized for a single species of ions. The unwanted molecular ions, the energetic fraction and other unnecessary gases produced by the ion source should be removed from the high-field region of the accelerator column.

Deuterons are further conducted into an acceleration tube. After acceleration, the beam is directed either to the intense section, the dc or fast-pulse sections of the accelerator.

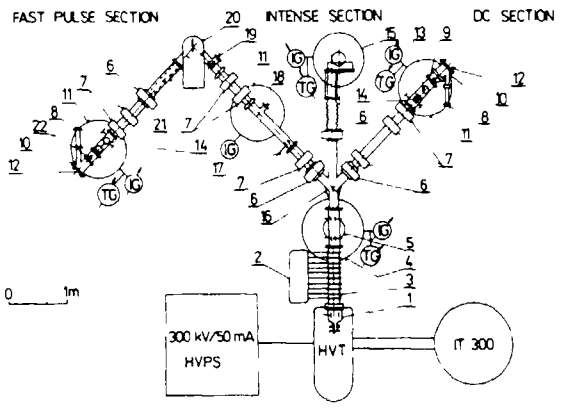

Fig.1. Layout of the neutron source. 1-ion source, 2-column resistor, 3-accelerator tube, 4-main vacuum system, 5-beam steerer, 6-gate valve, 7-quadrupole lens, 8-monitor, 9-static beam monitor, 10-target chamber, 11-auxiliary vacuum system, 12-water cooled target, 13-water cooled slit, 14-beam profile monitor, 15-rotating target, 16-analysing-switching magnet, 17-chopper, 18-slit, 19-diaphragm, 20-90° magnet, 21-bunching system, 22-pick-up system, TG-thermocouple gauge, IG-ionization gauge, IT 300-isolation transformer, HVT-high voltage terminal, HVPS-high voltage power supply.

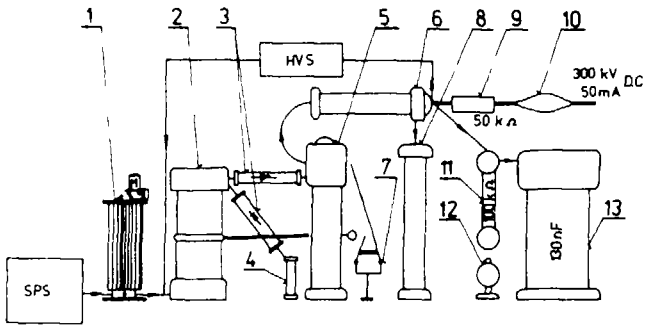

Fig.2. Scheme of the high voltage power supply. 1-regulating transformer REO gs 16/380, 2-high voltage transformer PEOI (Z) 25/300/C, 3-Se rectifier, 4-holder, 5-multiplier capacitors, 6-protective resistor, 7-electro-hydraulic discharger, 8-voltage divider, 9,11-water resistors , 10-high voltage cable end, 12-pneumatic discharger, 13-capacitor battery, SPS-stabilized power supply, HVS-high voltage stabilizer.

3. Recent developments and status

Recent developments have been centred on the completion of drawings, the assembly of a high voltage power supply, on putting the main vacuum system as well as the acceleration tube into operation on developing two isolating transformers as well as a transformer for the extraction source and on developing a Pd valve for the ion source.

The optical properties of the accelerator components have been calculated taking into account the effect of the beam space charge. Likewise, the electronics control system has also been developed[1].

3.1 High voltage power supply

The major components of the high voltage power supply were supplied by TUR Dresden (N.E.Transformer and Roentgen Plant). The scheme of the supply together with a capacitor battery, water resistors and a stabilizer are shown in Fig.2. The supply was constructed with respect to a long operation at 40 mA/20 °C or 30 mA/35 °C. The high voltage is regulated by a motor operated regulating transformer. The ripple factor of the supply is 2.5 %. The capacitor battery consisting of 12 capacitors (1.5 μF/30 kV) is added in order to obtain better parameters of the system. We are able to reduce the ripple factor to 1 % by use of such a capacitor bank.

The high voltage power supply is separated from the neutron source terminal. They are interconnected through a water resistor by a high voltage cable. Suitable cable ends were constructed to prevent a breakdown of the polyethylene isolation between the wire and the lead cable covering.

The capacitor battery is connected to the ground potential through a 100 kΩ water resistor by a pneumatic discharger. This system can quickly short circuit the capacitor battery to ground and protect the damping resistor of the high voltage power supply.

The general layout of the high voltage power supply is shown in Fig.3. It is mounted in a 6 m x 6 m cell.

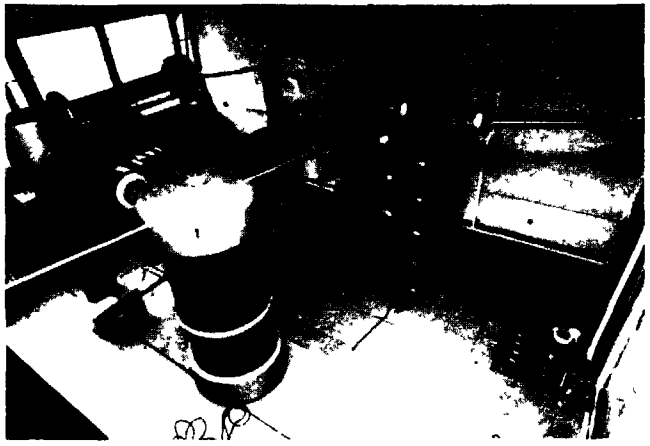

Fig.3. General view of the high voltage power supply.

3.2 Ion source and ion source electronics

The ion source is a modification of a duoplasmatron source developed at Vakutronik Dresden (N.E.Vacuum Electronic Plant). The preliminary tests of the source have been performed. It has been shown that one can achieve the expected 20 mA beam at an approximately 40 kV extraction voltage.

Ion extraction should be performed by the 50 kV potential. For this reason two transformers have been developed. One, labelled DEZ 50 provides the 50 kV dc voltage and the 3.75 kVA power for the extraction source. The other, the isolating transformer IT 50[2,3] for the 50 kV potential and the 2 kVA power, should transmit the mains for the rest of the duoplasmatron power supplies. The transformers of about 150 kg and 80 kg weight, respectively, are put into insulation cylinders made of laminated paper and filled by inhibited transformer oil.

3.3 Vacuum system

One main and 5 auxiliary vacuum pumping systems will be used to provide clean, safe pumping with pressure monitoring.

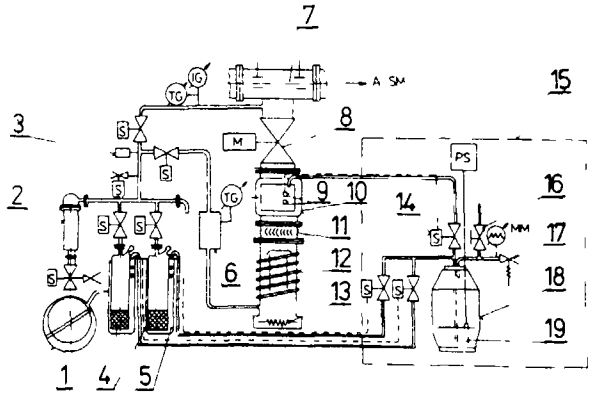

Fig.4. Scheme of the main pumping unit and LN_2 filling device. 1-rotary pump, 2-foreline trap, 3-vacuum relay, 4-desorption pumps, 5-Dewar vessel, 6-vacuum reservoir, 7-beam steerer, 8-plate valve, 9-LN_2 level sensing elements, 10 LN_2 cooled trap, 11-water cooled baffle, 12-diffusion pump, 13-heater, 14-solenoid valve, 15-LN_2 filling device, 16-valve, 17-safety valve, 18-LN_2 reservoir, 19-heater, TG-thermocouple gauge, IG-ionization gauge, A-SM-analysing-switching magnet, M-electric motor, MM-pressure sensor, PS-power supply.

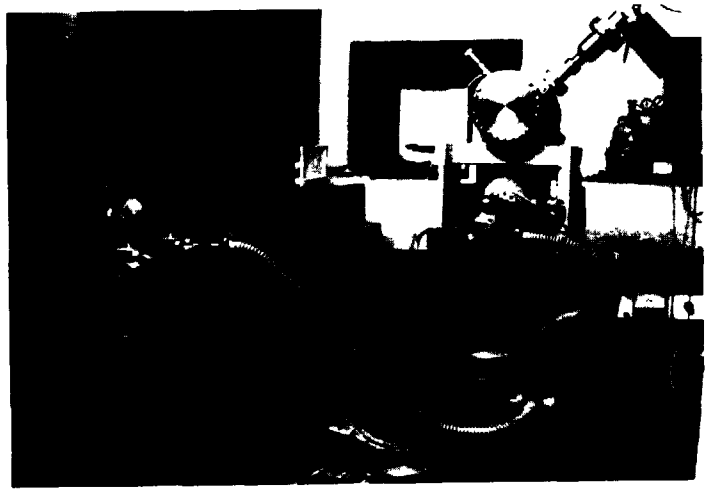

Fig.5. General view of the main vacuum pump.

Fig.6. General view of the filling device.

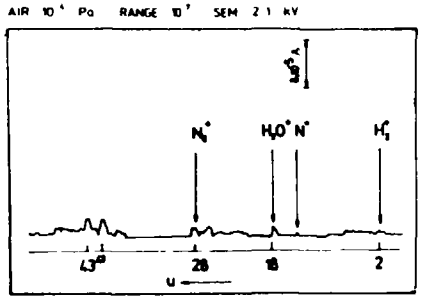

Fig.7. Rest gas spectrum of air measured inside the beam steerer of the accelerator by the QMG 112 quadrupole mass spectrometer[6] at 10^{-4} Pa.

For the main vacuum pump, a larger diffusion pump is used. The scheme of the main pumping unit is shown in Fig. 4. A 2000 ls^{-1} diffusion pump together with a baffle, and an LN_2 trap, two sorption zeolite pumps, a foreline trap and a rotation pump are used. The diffusion pump usually pumps either with the sorption pump or the rotary pump depending on the pumping efficiency of the molecular sieves used at the LN_2 temperature for hydrogen gases. As soon as a vacuum of 10 Pa is reached, the sorption pump is automatically connected to the diffusion pump while the rotary pump is connected to it when the fore vacuum increases to 20 Pa. Two sorption pumps are provided (EGS 500 [4]). The pumpdown time of the pump operating with a 40 l volume from 0.1 MPa to 4 Pa is about 1 h.

The general layout of the main vacuum pump is shown in Fig.5. The LN_2 filling device is designed for three cold Dewar vessels. The LN_2 is forcing through the riser tube extending to the bottom of the main reservoir of the LN_2. The coolant flows are regulated by using three LN_2 regulating solenoid valves and 6 thermistors mounted at the extremes of the desired LN_2 levels. Two thermistors are inside the one Dewar vessel.

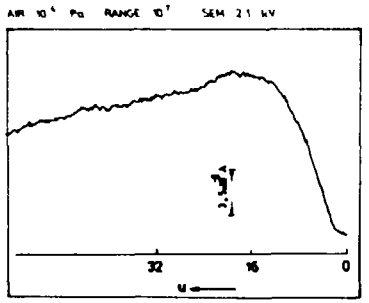

Fig.8. Total pressure measured inside the beam steerer of the accelerator by the QMG 112 quadrupole mass spectrometer[6] at 10^{-4} Pa.

The general layout of the filling device is shown in Fig.6.

The auxiliary vacuum systems have been designed to pump the ion source area, the pulse beam line and all target chambers[5].

The pressure inside the main vacuum system is measured by a thermocouple and a Bayard-Alpert ionization gauge. Also, a quadrupole type gas analyser is installed in order to permit a quick diagnosis and a residual gas analysis even with the beam on.

The rest gas spectrum of air and the total pressure measured inside the beam steerer of the accelerator by the QMG 112 quadrupole mass spectrometer[6] at 10^{-4} Pa are shown in Fig.7 and Fig. 6, respectively.

3.4 Tritium recovering system

The multipurpose neutron source will be mounted in four relatively small rooms: the power supply room, the accelerator room with the intense and the low current dc beam line the low current pulsed beam line room and the operating room[7]. A two-stage tritium recovery system (TRS) has been designed for the neutron source. A similar TRS was installed in the OKTAVIAN project[8]. The primary stage (TRS-1) is considered at the position very close to the rotating target, where high tritium quantity is absorbed into a TiT target. The recovering principle is based on the pumping of tritium by the ion sorption pump and two sorption pumps. It is assumed that about 99 % of the released tritium gas from the target will be caught at this stage.

The secondary stage (TRS-2) is based on the method of oxidation of tritium gas with a palladium catalyser doped on aluminum silicate and subsequent absorption of water with a molecular sieve No.5. The whole outlet of the vacuum system is connected with this second stage. The gas pumped out of the second stage is continuously monitored with a compensated type tritium gas monitor.

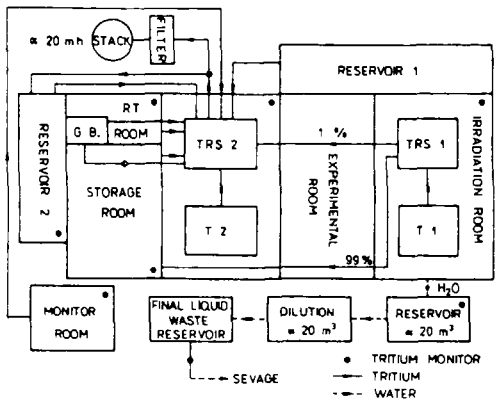

Fig.9. Tritium recovery system of the accelerator.

If the tritium concentration of the pumped out gas is higher than the value fixed by law, the gas is kept in the reservoir tank of the TRS-2 to go through the second run of the TRS-2.

A drawing representing the tritium recovery system of the accelerator is shown in Fig.9.

4. Concluding remarks

The pulse section of the multipurpose neutron source will be the main tool for the production of γ rays the coincidence in-beam experiments and the exclusive neutron spectra measurements in the next few years. The rotating target section can be utilized in the exact determination of activation cross sections of rare reactions and measurements of charge particle spectra.

The first version of the original design of the rotating target section claims a TiT target of a tritium amount of about 15 TBq (400 Ci). However, we can also use a 30 TBq target. Then, the development of more efficient rotating targets will be one of the aims of investigation in the near future.

Acknowledgements

We should like to thank Ing. Š. Luby, DrSc., the director of the IP EPRC SAS, for his support and kind interest in this work.

References

1) J.Pivarč, S.Hlaváč, P.Obložinský, I.Turzo, V.Matoušek, R. Lórencz and L.Dostál, Intense Neutron Generator Development at the Institute of Physics, Proc. of the 14 th Int. Symp.on Nucl. Phys.-Neutron Generators and Application, Gaussig, (Nov. 19-23, 1984) 16 (GDR).
2) K.Málek, J.Pivarč and B. Bajcsy, Čs Patent 237 148.
3) K.Málek, J.Pivarč and B. Bajcsy, Čs Patent 237 149.
4) Technische Dokumentation, Sorptionspumpe EGS 500, VEB Hochvakuum, Dresden (1983).
5) J.Pivarč, R.Lórencz and V.Matoušek, Vacuum System of the Multipurpose 14 MeV Neutron Source in Bratislava: Design and status, Vacuum, to be published.
6) Manual, Quadrupole Analyser QMG 112, Balzers Aktiengeselschaft, Balzers (1983).
7) J.Pivarč, S.Hlaváč, J.Král, P.Obložinský, I.Ribanský, I.Turzo and H.Helfer, Acta Phys. Slovaca 30(1980)119; see also Report INDC (CSR)-2-L^{+} Special, IAEA Nuclear Data Section, Vienna (May 1980).
8) K.Sumita, A.Takahashi, T.Iida, J.Yamamoto, S.Imoto and K. Matsuda, Osaka University 14 MeV Intense Neutron Source and its Utilizations for Fusion Studies, OKTAVIAN Report C-83-01. Osaka University, 2-1 Yamadaoka, Suita (Sept. 1982); see also Proc. of the 12 th Symp. on Fusion Techn. at Jülich, (Sept. 13-17, 1982) (Pergamon Press, 1982) Vol.I, pp 675-680.

ROTATING TARGETS FOR INTENSE 14 MeV NEUTRON SOURCES

J. PIVARČ
Institute of Physics,
Electro-Physical Research Centre of the
Slovak Academy of Sciences,
Bratislava, Czechoslovakia

Abstract

A survey of rotating target systems used for the production of 14 MeV neutrons by intense ion beam is given. Attention is paid to tritium losses from targets, their reduction and the safe operation of intense neutron sources. Also discussed are additional requirements necessary to be satisfied so that higher fluxes than 10^{12} ns^{-1} from the D-T reaction may be obtained.

1. Introduction

For the research into pure and applied nuclear physics very intense point sources of monoenergetic fast neutrons are important tools. The most suitable source reaction is the D-T reaction. The more neutrons are needed the larger is the beam power which has to be dissipated in the target so that the target and the target cooling become major problems. For the high intense neutron source used today the development of a suitable accelerator can be much easier than the development of a suitable target[1].

Three types of targets are generally used: tritium gas targets, metal tritide targets, and targets in which a mixed beam of deuterons and tritons implants the hydrogen isotopes in a metal target (drive-in targets). The tritium gas and T_2O targets give the highest source strength because of their low stopping cross sections and their high concentration of tritium atoms[2]. However, gas or T_2O targets would require the use of a barrier foil between the target and the vacuum system. Such a foil would necessarily be thin in order to pass the deuterons. Experience has shown that cooling problems connected with the use of a thin foil would limit

the beam considerably. Such foils cannot be used at beam currents much above 10 μA, and hence this type of gas target is limited to very low-intensity D-T generators[3].

That is why metal tritide targets are generally used. While numerous target materials are under investigation now-available targets include tritium occluded in either Ti, Zr, Sc or Er layers[4].

The performance and general aspects of drive-in targets have been discussed in refs[5-8]. Besides Ti, Zr, Sc and Er layers, also a Y layer with a thickness of about 1-2 mg cm^{-2} can be used[7]. One uses Cr plated Cu tubing[9]. These tubes are arranged in such a way that 280 mA of mixed D-T ions from two ion sources bombard the target from opposite directions. With this arrangement a source strength of 5 x 10^{12} ns^{-1} has been achieved within a target spot 6 cm in diameter.

The present paper gives a rather detailed survey of the rotating targets in use and designed for the production of 14 MeV neutrons by intense ion beams. Moreover, the tritium losses from the targets, their reduction and the safe operation of the intense neutron sources are also discussed. Attention is also paid to the thermal properties of the TiH, ZrH, ScH and YH systems and to the necessary requirements which are to be satisfied for higher yields than 10^{12} ns^{-1} from D-T reaction to be obtained.

2. Rotating targets

The earliest users of metal tritide targets have shown that the tritium leaves the target at temperatures above 200° C and that the targets have to be cooled by blowing air or by flowing water. Even with good cooling the beam power that could be deposited on a 1 cm spot was about 450 W[10]. It corresponds to about of 2.2 mA cm^{-2} at 200 kV. This restriction combined with the experience that the neutron output decreases to half its value with a bombardment of about 10 C cm^{-2}, limits bombarding currents to about 1 mA and neutron strength to 2 x 10^{11} ns^{-1}. This source strength would drop to half its initial value in 2-3 h.

2.1 Targets for intense neutron sources

In 1967[11] Booth and Cossuta[12] developed the first targets for intense neutron sources. The rotation of the target effectively increases the target area (without increasing the size of the neutron producing area) and also reduces the average heating of the given target area. The original desing of such target has the shape shown in Fig. 1.

2.1.1 The Lawrence Livermore RTNS I rotating target

It consists of a 4-10 mg cm^{-2} thick Ti layer vapour plated onto a 1 mm thick Cu, Cu-Zr (0.15 wt % of Zr) alloy (Amzirc) or other suitable backing material with a 15 cm outside diameter. Zr increases the mechanical strength and annealing temperature of a ductile Cu. The Ti layer is deposited in a ring of 5 cm i.d., 14 cm o.d. About 20 TBq (500 Ci) of tritium reacts with the Ti and forms a stable layer of titanium tritide. An O-ring seal holds the targets at the end of a 0.5 mm thick cylinder wall attached to the accelerator vacuum system by a rotating seal. In order to avoid local heating the target is rotated at 1100 rpm. The target

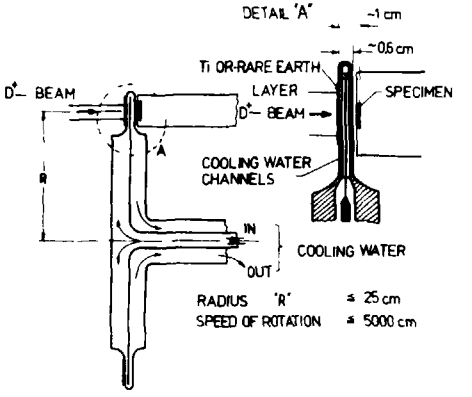

Fig. 1. Schematic representation of the rotating target.

forms the end of the accelerator vacuum system. A stationary 0.2 mm thick sheet of stainless steel is placed in parallel to the target and leaves a 0.3 mm wide gap. Water is injected at the centre of the steel sheet and causes a strong centrifugal force owing to the rotation of the target. The large velocity gradient between the rotating target and the stationary water spreader produces a turbulent water flow and efficient cooling. The axis of the rotating target can be moved with respect to the stationary deuteron beam so as to allow the use of different concentric rings on the target without moving the position of the neutron source. Design characteristics of such the rotating target are shown in Fig. 2[13].

In order to permit operation at higher source strength the 15 cm diameter rotating target was replaced by a 22 cm diameter rotating target[14]. With this target, 16 mA of 400 keV deuterons, a source strength of 4 x 10^{12} ns^{-1} is produced that decreases by 10-20 % in 50 h for a 1 cm diameter target spot.

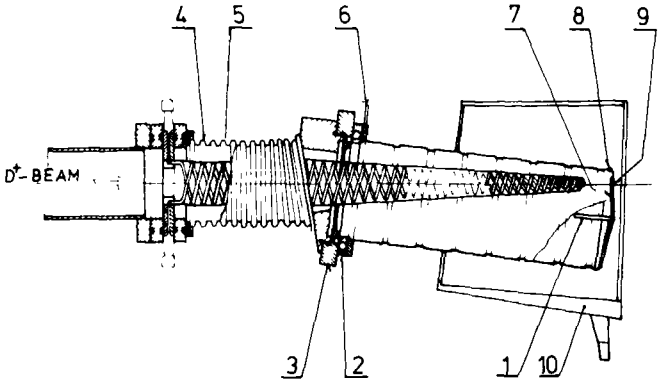

Fig. 2. The Lawrence Livermore rotating target RTNS I[13]. 1-cooling water, 2-insulator, 3-bearing and seal, 4-bellows, 5-collimator, 6-current pick-off, 7-tritium target, 8-O-ring seal, 9-water spreader, 10-water catch cage.

2.1.2 The LANCELOT rotating target

Another rotating target was constructed in de Valduc Centre, France[15]. The scheme of the target is shown in Fig. 3. The target consists of a 1 mm thick cold-beaten Cu baseplate in the shape of a portion of a sphere-1, the rotation of which is driven by the frustrum of a cone-2 within which the beam is propagated. The ring-shaped target (R_{int}=29.5 cm, R_{ext}=34.5 cm) is covered by a tritiated titanium deposit of a 0.4 mg cm^{-2} thickness and contains about 40 TBq (1000 Ci) of tritium. Two high-precision roller bearings-3 allow a vibration free, 1500 rpm rotation. The tightness is ensured through two plane seals-4 the fixed part of which is pushed by a jack-5 using the pressure of the seal cooling water. The cavity-6 between the seals is pumped by a differential pumping system. A cooled electrically insulated tube-7 prevents any heating of the lateral walls of the cone-2 and is used for beam losses measurement.

The cooling water comes through pipes-9 and is centrifuged between 2 and 8. The cooling thus obtained is sufficient because of the high circulation speed of the water on the target. With this target, 80 mA of a 200 keV deuterons, a source strength of 3 x 10^{12} ns^{-1} is produced. A half-life time of the target is 3 h for a 13 cm diameter beam spot size on the target.

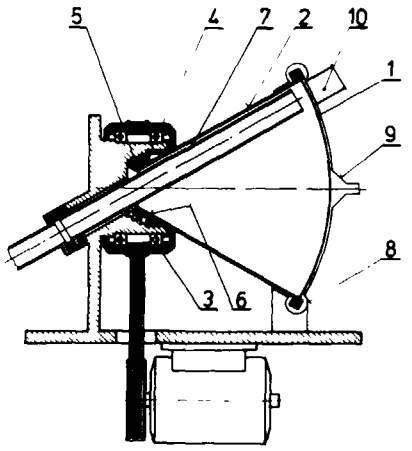

Fig. 3. LANCELOT rotating target[15]. 1-sphere, 2-conical frost-room, 3-rollerbearings, 4-two plane seals, 5-jack, 6-cavity, 7-insulated tube, 8-water cooled gap. 9-pipe, 10-sample.

2.1.3 The Osaka University rotating target

In the OKTAVIAN project[16] of the intense neutron source a commercially available rotating target system is used which includes a titanium tritide layer on a Cu backing metal disk. The same target is prepared for experiments in Dresden[17]. A drawing of the rotating target is shown in Fig. 4. The ring-shaped target (R_{int}=5,65 cm, R_{ext}=9,325 cm) is covered by a tritiated titanium deposit of 6 mg cm^{-2} thickness and contains about 30 TBq (800 Ci) of tritium. The operation speed of the rotating target has been chosen to be 800 rpm in order to keep the target surface temperature well below 120° C.

The hollow shaft carries the coolant to the central region of the target disk which has a large number of narrow slots. There is a single seal on the side of the water, and the other on the side of the vacuum. The attractive features of this design are that the two ball bearings are in air, the shaft and seal diameter are comparatively small, which makes their life-time longer and, if any of the seals fail, the water will not enter into the vacuum system. The vacuum enclosure has a disc shape with connections to the beam tube, the water and the flexible drive shaft.

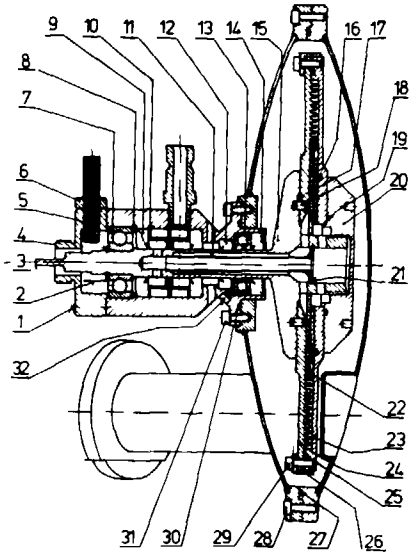

Fig.4.OKTAVIAN rotating target[16]. 1,28-29,31-hexagon socked screws, 2-rotation trigger, 3-motor coupler, 4-stopper ring, 5-sensor for rotation, 6-holder, 7,13-ball bearings, 8,10-inserts, 9-packing ring, 11-inner cooling water pipe, 12,14-packing rings, 15-target shaft (SS 304), 16-flat head screw, 17,19,25,27,30-O ring seals, 18-straight pin, 20-sealing plate (SS 304), 21-Seger circlip ring, 22-water cooled plate, 23-bottom of target insert (SS 304), 24-target disk (Cu), 26-centring ring, 32-oil feed cup.

The rotating target was manufactured by NUKEM Co.Ltd, Hanau (FRG). With this target, 20 mA of 300 keV deuterons a source strength of 3 x 10^{12} ns^{-1} was obtained. A half-life time of the target is about 100 h for a 1.5 cm diameter beam spot size.

2.1.4 The NIIEFA rotating target

The intense neutron source in Leningrad[18] uses a rotating target system (Fig. 5) which enables to use tritium targets on a 10 (20) cm diameter Cu backing metal disk. The titanium ring-shaped target (R_{int}= 3 cm, R_{ext}= 5 cm) contains about 2.5 TBq (65 Ci) of tritium. The operating speed of the rotating target is 1200 rpm and the life-time of the vacuum seal is 1000 h.

The rotating seal consists of a loaded PTFE ring sliding on

stainless steel. There are two sealing surfaces the central part of which is differentially pumped out to a vacuum of 1 Pa.

The titanium tritide target is of USSR[19] make. With this target, 20 mA of 150 keV deuterons, a source strength of 10^{12} ns^{-1} is produced.

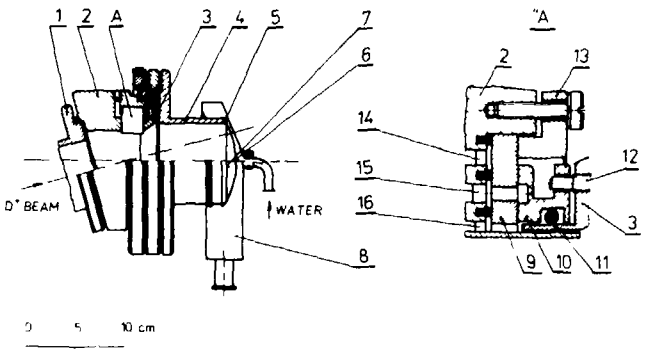

Fig. 5. Scheme of the Leningrad rotating target[18]. 1-beam tube, 2-stator, 3,13-flanges, 4-holder, 5-O-ring seal, 6-target, 7-diaphragm, 8-water catch, A-rotating block of the target, 9-insert, 10-PTFE seal, 11-O-ring seal, 12-screw, 14-water cooled channel, 15-forevacuum channel, 16-high vacuum channel.

2.2 The Bratislava and Debrecen rotating targets

Intense D+T neutron sources based on duoplasmatron ion sources and low energy deuteron accelerators (10 mA/300 keV dc) are under construction also in Bratislava[20], Debrecen[21] and Dresden[17], where recent developments have centred on the completion of rotating target designs or on obtaining suitable targets from industry.

2.2.1 The Bratislava rotating target

The scheme of the rotating target is shown in Fig. 6[22]. The target consists of subtargets located on a rotation disk. It has been designed so as to use the 16 MoTiT or CuTiT subtargets manufactured in the USSR[19]. The ring-shaped target (R_{int}=9.5 cm, R_{ext}=14 cm) contains totally 15 TBq (400 Ci) of tritium. The thickness of the subtarget backing and the titanium tritide layer are 0.3 mm and 2-5 μm, respectively. The concentration of tritium is about 60 GBq cm^{-2} (1.6 Ci cm^{-2}). The layout of the subtargets on the disk periphery is seen in Fig. 7.

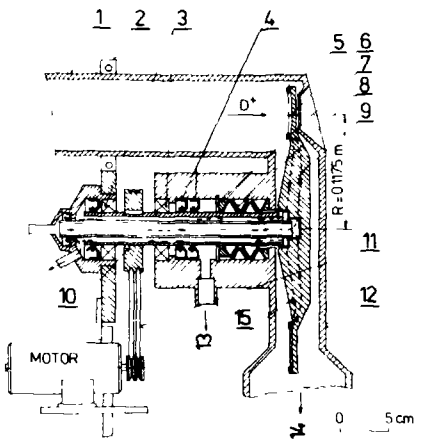

Fig. 6. Scheme of the Bratislava rotating target system, 1-beam tube, 2-isolation support, 3-bearings, 4-simmerings, 5-ring, 6-target, 7-support, 8-sealing rings, 9-rotor, 10-pulley, 11-"V" belt, 12-stator, 13-differential pump, 14-ion sorption pump, 15-water channels.

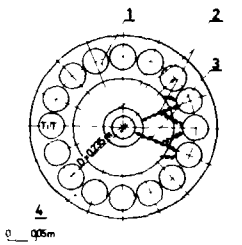

Fig. 7. Layout of the 4.5 cm diameter subtargets through the rotation disc periphery. 1-subtarget, 2-water outlet, 3-water inlet, 4-clamping ring.

The rotating target will be cooled by water driven through the centre of the rotating target assembly to a cavity from where it is further delivered to eight 0.5 cm diameter channels. Two sub-

targets are connected with one channel. To cool the target to a suitable temperature with respect to the tritium desorption rate it is necessary to supply the channels by a sufficient amount of cooling water. Our design assumes that water consumption would not be higher than 1.2 l s^{-1}. It corresponds to the minimum water velocity in channels of 1.5 m s^{-1}.

The rotor of the rotating target is moved in a vacuum of 10^{-3} Pa. It is separated from the high vacuum by three special O-ringe seals fixed by a support. Two simmerings separate the vacuum chamber from the outside. The cavity placed between the rings and the simmerings is pumped by a differential pumping system. It involves a mechanical rotary pump and a foreline trap. The rotor is further carried in two high precision ball bearings which allow only a small vibration. We expect that the bearings will be suitable for targetoperations at any spead up to 1100 rpm, although the necessary target revolution rate for the heat dissipation of 1.5 kW cm^{-2} is about 35 rpm[23].

With this target, 10 mA of 300 keV deuterons, a source strength of 10^{12} ns^{-1} and a useful target life-time of about 10 h for a 1 cm diameter beam spot size are expected.

The detailed scheme of the neutron source target chamber with the rotating target are shown in Fig. 8.

2.2.2 The Debrecen rotating target

In the project of the intense neutron source in Debrecen the use of a rotating target shown in Fig. 9 is considered[21]. A thick Cu disc of about 20 cm diameter is similar to the targets of the Multivolt Limited of the Crawley series RTH. It has been proved that the 3-8 kW cm^{-2} beam power can be dissipated on a tritium target. The ring-shaped target contains about 19 TBq (500 Ci) of tritium. The operation speed of the rotating target has been chosen to be 30 rpm. The atractive feature of the design is that the magnetic ferrofluid seals are used in order to separate high vacuum parts of the target from atmospheric pressure.

A similar rotating target has been developed by the Multivolt Limited, Crawley, Sussex (England)[24]. With this target, 10-20 mA of 220 keV deuterons, a source strength of 10^{12} ns^{-1} is obtained.

2.2.3 Other rotating targets

There are several other rotating targets which are used in intense neutron sources. The first of these was built by Broerse et al.[25] at the Radiobiological Institute in Rijswijk, The Netherlands. It uses 6 mA of 270 keV deuterons and produces a source strength of 6 x 10^{11} ns^{-1} with a 15 h half life-time. Another rotating target is in operation at the Eppendorf Hospital in Hamburg, (FRG). This unit has been manufactured by Radiation Dynamics (Westbury, Long Island, New York) and uses 12 mA of 500 keV deuterium ions. It produces[26] 2.5 x 10^{12} ns^{-1} with a half life-time of less that 10 h. A rotating target is also in operation at the Institute of Nuclear Research at Lanzhou University, China[27]. A 20 cm diameter target, which rotates at 1100 rpm is used for production of neutrons. When the target is bombarded with 20 mA of 300 keV deuterons a source strength of 2 x 10^{12} ns^{-1} can be obtained. Their home-made ring shaped thick tritium target[28] (R_{int}=7 cm, R_{ext}=9 cm) contains totally about 13 TBq (350 Ci). A thick Ti layer of about 2.5 mg cm^{-2} is vapour plated onto a 3 mm thick Cu backing.

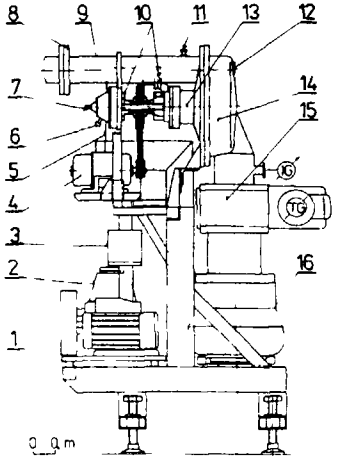

Fig. 8. Detailed scheme of the neutron source target chamber with the rotating target. 1-holder, 2-rotary pump, 3,15-solenoid valves, 4-motor, 5-foreline trap, 6-water out, 7-water in, 8-flange in, 9-beam tube, 10-bearings, 11-feedthrough, 12-sample, 13-stator, 14-target chamber, 16-ion sorption pump.

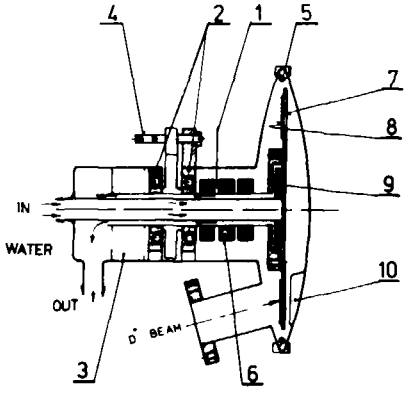

Fig. 9. Scheme of the Debrecen rotating target assembly[21]. 1-magnetic fluid seal, 2-bearings,3-PTFE insert, 4-remote drive, 5-O-ring seal, 6-annular magnets, 7-OFHC Cu disc, 8-TiT coating, 9-radiator shaped cooling system, 10-place for samples.

2.3 Target for a high intensity neutron source

In order to increase the source strength further the beam current, the rotation speed and the diameter of the target have to be increased. A new rotating target system had to be designed which involved a different type of rotating seal and a different target cooling system. The seal[29] is designed to rotate at 5000 rpm and has been tested up to 10^4 rpm. Fig. 10 is a drawing of the air bearing rotating seal and the target system. An air cushion prevents the rotating part from touching the stationary accelerator vacuum system. Two stages of differential pumping maintain the pressure gradient between the air cushion and the accelerator vacuum. A matched pair of ball bearings holds the load of the rotating target. The rotor is driven by an air jet that hits the blades of a turbine wheel.

With larger targets and a higher rotation speed the power requirement to overcome the viscous drag caused by external cooling would be excessive. This difficulty has been overcome by placing the cooling water inside a sandwich target backing that contains convoluted channels to produce a turbulent flow. The channels are etched onto a 1 mm thick Cu alloy sheet which is then bonded to a second sheet of the same alloy using two techniques: diffusion bonding and electroforming. The sandwich is coldformed to the desired curvature. Cooling water enters and leaves the target through a rotating hub at the centre of the target. Chilled water flows through the target at a rate of 10 l min^{-1}.

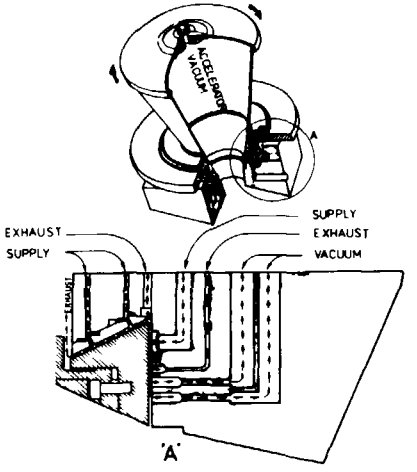

Fig. 10. Schematic diagram of air bearing and rotating target assembly RTNS II. The bearing provides a vacuum seal and permits target rotation at 5000 rpm[30].

3. Conclusion

The rotating targets must be capable of resisting a relatively high heat load. The heat loads of the systems TiH, ZrH, ScH, ErH and YH were investigated in refs[4,31]. It was shown that the YH system is thermally the most stable. After heating to a temperature of 426° C in a vacuum of about 10^{-1} mPa there is practically no desorption of hydrogen. The equilibrium temperatures corresponding to the dissociation pressure of 100 Pa are given in Tab.1.

The front-surface temperature history calculations for an element moving across the beam centre were done by Logan[30]. It was shown that the front-surface temperatu-

re rise can be limited to about 300° C by moving the target at a velocity of 10^4 cm s^{-1} (50 cm diameter of the target and 5000 rpm). Similar results were shown also in our refs[20,23].

In order to reduce further losses from the target it is necessary to prevent the sputtering of atoms, the displacement of tritium by deuterium, surface degassing and the creation of the carbon layer on the target surface. A considerable limitation of sputtering and surface degassing of the target can be achieved by evaporation of thin Al or Cr protective layers on the target surface (0.05 mg cm^{-2} thickness). The energy loss in such coatings is about 15 keV. To prevent the formation of the carbon layer on the target surface it is necessary to construct neutron generators with ion sorption pumps or ion-sublimation titanium pumps. It is also important to use a clean D^+ ion beam. The molecular ions are accumulated near the surface of the target where only a small quantity of tritium is present so they contribute only minimally to the neutron source strength.

Tab. 1. Thermal properties of the TiH, ZrH, ScH, ErH and YH systems.

Hydride		TiH	ZrH	ScH	ErH	YH
Dissociation	temperature (° C)	390	590	700	790	810
	pressure (Pa)	100				

In order to increase the source strength to about 10^{14} ns^{-1} some additional requirements must be fulfilled. The following is required:

(i) Tritium should be absorbed in the Sc or Ti layers,
(ii) the energy of the D^+ ion beam should be adequate to the target thickness (400 keV for the 0.6 μm thick TiT target),
(iii) the target should have a thin Al or Cr protective layer (0.1 μm thickness),
(iv) the target should have a thin Pd "blocking" layer placed between the sorption layer of the target and the backing of the target (0.5 μm thickness) and
(v) the substrate of the target should be conveniently constructed in order to dissipate and conduct the heat to a coolant fluid for removal.

Such a target has been designed by Davis[32].

Acknowledgements

I should like to thank Ing. Š. Luby, DrSc., the director of the IP EPRC SAS, for his support and kind interest in this work, as well as Dr. P. Obložinsky and Dr. S. Hlaváč for useful discussions.

References

1) H.H. Barschall, Ann. Rev. Nucl. Part Sci 28(1978)222.
2) T.G. Provenzano, E.J. Story, F.F. Haywood, H.T. Miller, Feasibility study: Intense 14 MeV Neutron Source for Operation HENRE, Report ORNL-CEX-65-0.1, Oak Ridge, Tennessee (Sept. 1965).
3) H.H. Barschall, 14 MeV D-T Sources, Report UWFDM-331, University of Wisconsin, Madison (1979).
4) J. Pivarč, ATOMKI közlemények 18(1976)463.
5) M. Hillier, P.D. Lomer, D.S. Stark, J.D. Wood, Performere of targets in sealed-off neutron tubes, Proc. of the Acc. Targets Designed for the Production of Neutrons, Euratom Report EUR 3895-d-f-e, Liege (Sept. 18-19, 1967).
6) J. Kim, Nucl. Instr. and Meth. 145(1977)9.

7) P. Cloth, J. Darvas, D. Filges, H.B. Haubold, J. Hemmerich, H.R. Ihle, N. Kirch, P. Kupschus, C. Meixner, ATOMKI közlemények 18(1976)439.

8) G.I. Primenko, T. Sztaricskai, V.I. Strižak, J. Csikai, 14 MeV nejtrony-puti uveličenja vychoda nejtronov i stabilnosti ego vo vremeni, Pribory Technika Experimenta, to be published.

9) J.T. Brennan, G.O. Hendry, P. Block, J.L. Hilton, J. Kim, W.M. Quam, Br. J. Radiol. 47(1974)912; see also Br. J. Radiol. 46 (1973)233.

10) Z. Hůlek, Čs. Čas. Fyz. 14(1964)467.

11) R. Booth, IEEE Trans. Nucl. Sci. NS14(1967)938.

12) D. Cossuta, A. Rotating Target Assembly for 10^{12} ns^{-1}, Proc. of the 3 rd Conf. on Acc. Targets Designed for the Production of Neutrons, Liege (Sept. 18-19, 1967)191 (Belgium).

13) R. Booth, J.C. Davis, C.L. Hanson, J.L. Held, C.M. Logan, J.E. Osher, R.A. Nickerson, B.A. Pohl, B.J. Schumacher, Rotating Target Neutron Generators, Preprint UCRL-78805, Lawrence Livermore Lab., California (Nov. 1976).

14) R. Booth, Nucl. Instr. and Meth. 120(1974)353.

15) J.B. Hourst, M. Roche, Acta Phys. Slovaca 30(1980)137; see also Proc. of the Int. Conf.on Radiation Test Facility for the CTR Surface and Materials Program, ANL-CTR-75-4, Argonne National Lab. (1975).

16) K. Sumita, A. Takahashi, T. Iida, J. Jamamoto, S. Imoto, K. Matsuda, Intense 14 MeV Neutron Source Facility, OKTAVIAN Report C-83-01, Osaka University, 2-1 Yamadaoka, Suita (Sept. 1982).

17) D. Schmidt, U. Jahn, E. Paffrath, Intense Neutron Generator Development at the Technical University Dresden, Proc. of the 14th Int. Symp. on Nuclear Physics-Neutron Gen. and Application, Gaussig (Nov. 19-23, 1984)24 (GDR).

18) G.G. Voronin, A.M. Morozov, A.I. Solnyškov, G.V. Tarvid, Uskoriteĭ ionov s mišennym ustrojstvom dlja polučenija intensivnogo potoka 14 MeV nejtronov, Report NIIEFA P-O-0443, Naučno-issledovateĭskij institut elektrofizičeskoj apparatury imeni D.V. Efremova, Leningrad (1979).

19) Mišani tritievje (deuterievje) Techničeskije uslovja), Institut jadernych issledovanij Ukrainskoj Akademii Nauk, Kiev (1979).

20) J. Pivarč, S. Hlaváč, J. Král, P. Obložinsky, I. Ribansky, I. Turzo, H. Helfer, Acta Phys. Slovaca 30(1980)119; see also Report INDC (CSR) - 2 - L^+ Special, IAEA Nuclear Data Section, Vienna (May 1980).

21) T. Sztaricskai, ATOMKI közlemények 22(1980)47; see also J. Csikai, T. Sztaricskai, I. Berkes, S. Szegedi, E. Koltay, G. Morik, G. Szabó, S. Bohatka, The Intense Generator Concept in Debrecen, private communication (1984).

22) J. Pivarč, J. Král, Rotating Target for a 300 keV Neutron Source: Design, Proc. of the 10th Int. Symp. on Selected Topics of the Interaction of Fast Neutrons and Heavy Ions with Atomic Nuclei-Fission-Heavy Ion Reactions, Gaussig (Nov. 17-21, 1980), 185 (GDR).

23) J. Pivarč, Heat Diagnostic of a Rotating Target for a 300 keV Neutron Generator, IP SAS Report, Bratislava (1979), in Slovak.

24) D.D. Cossuta, Target Technology for Medium and High-Power Applications, Proc. of the 2nd Oak Ridge Conf. on the Use of Small Acc. for Teaching and Research, CONF-700 322, Oak Ridge, Tennessee (March 23-25, 1970)431.

25) J.J. Broerse, J.E. Broers-Challiss, B.J.Mijnheer, Strahlentherapie 149(1975)585.

26) M.R. Cleland, B.P. Offermann, Nucl. Instr and Meth. 145(1977) 41.

27) Sun Biehe, Design of a 10^{12} ns^{-1} Compact Neutron Generator, Proc. of the 14th Int. Symp. on Nuclear Physics-Neutron Gen. and Applications, Gaussig (Nov. 19-23, 1984)40 (GDR).

28) Tong-Tai-Xin, Specification of the large size targets, Beijing, P.O. Box 2102, China Corp. (Nov. 1985), private communication.

29) R. Booth, C.M. Logan, Nucl. Instr. and Meth. 142(1977)471.

30) C.M. Logan, D.W. Heikkinen, Nucl. Instr. and Meth. 200(1982) 105.

31) V.V. Sofina, N.G. Pavlovskaja, Žurnal fiz. chimii 34(1960) 1104.

32) J.C. Davis, Rotating Target Neutron Source II: Facility and Exp. Program, Lecture given on the 14th Int. Symp. on Nuclear Physics-Neutron Gen. and Applications, Gaussig (Nov. 19-23, 1984) (GDR), private communication, see also in the Proc. of the IAEA Advisory Group Meeting on "Properties of Neutron Sources", Leningrad (June 9-13,1986), to be published.

INTENSE 14 MeV NEUTRON GENERATOR

M.I DEKHTYAR, V.K. MAYDANYUK,
V.M. NEPLYUEV, G.I. PRIMENKO,
Yu.A. SEDOV, V.I. STRIZHAK, V.K. TARAKANOV
Institute of Nuclear Physics,
Ukrainian Academy of Sciences,
Kiev, Union of Soviet Socialist Republics

Abstract

An experimental generator of fast neutrons via $T(d, n)^4He$ reaction is described, Neutron yield of $5 \cdot 10^{11}$ neutron.s^{-1} is achieved.

Fast neutron fluxes generated by controlled radiators on the basis of direct acceleration of deuterium ions to tritium targets are widely used for carrying out investigations in the field of neutron physics as well as for solution of a number of applied tasks like engineering problems of thermonuclear fusion, activation analysis, radiation therapy ets. In order to solve the majority of these tasks neutron fields with an average flux over 4 solid angle exceeding or equal to $5 \cdot 10^{11}$ neutr. s^{-1} are necessary.

To create a controlled neutron source with a total flux of 10^{12} neutr.$\cdot s^{-1}$, a number of investigations has been carried out. As a result of those the task of obtaining and shaping of deuterium ion beams with 10 mA current and 200 kev energy in a continuous mode has been solved and a target device was designed. The principal view of the neutron generator is shown in Fig. 1.

The ion source, a duoplasmatron, cooled with transformer oil, is divided from eath potential by means of a china accele-

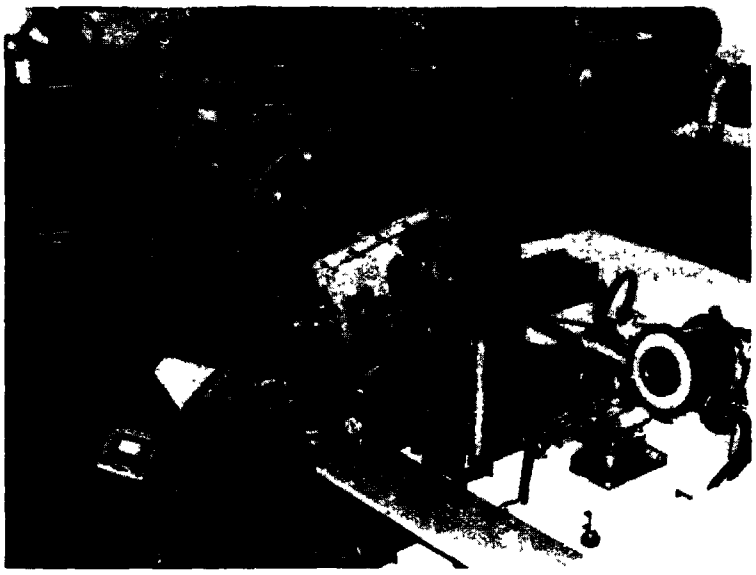

FIG. 1.

ration tube. The ion source is supplied from a motor-generator with a power of 5 kw. The ion source makes it possible to obtain a deuteron beam of up to 15 mA with discharge current of about 3A. The atomic component in the beam exceeds 50 %. A duration of continuous ion source operation is determined by enlargement of the emission opening in the molybdenum anode insertion within the process of operation, as well as by the direct-filament cathode life-time, and is normally several dozens of hours. The ions are selected from the surface of plasma penetrating into a conical expander. A preliminary focusing of the ion beam is made by means of electrical field between the extractor and the main source anode.

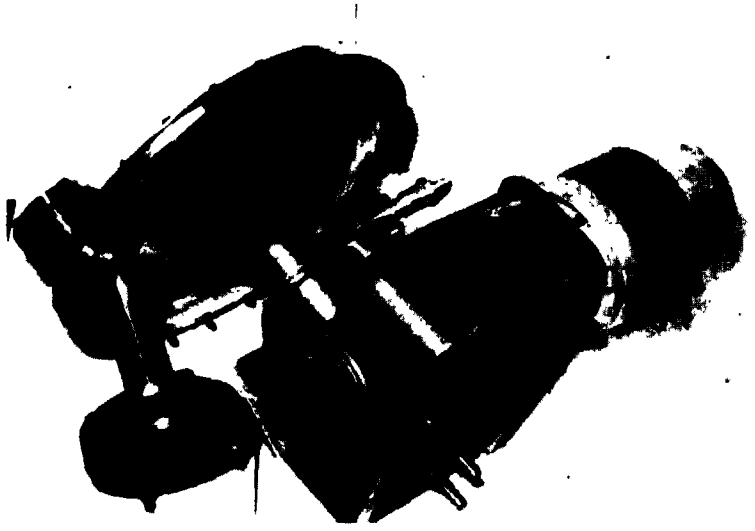

FIG. 2.

The acceleration tube is made of china rings glued together. To increase electric strength, it is put into an isolation sheath. The space between the tube and the sheath is filled with liquid dielectric. The length of the acceleration tube is 25 cm. Average gradient of electric field in gaps between the three electrodes of the acceleration tube is 40 $kv \cdot cm^{-1}$.

High-voltage supply of the acceleration tube is provided by two series rectifiers constituting a voltage-doubling circuit. From each stage, voltage is directed through a limiting resistor to a corresponding acceleration tube gap. Automatic protection from overvoltage and current overloads is provided.

In order to provide normal thermal mode of neutron generator target operation at ion beam power of several kW, a rotating target with a large surface of active layer is designed (Fig. 2). The inner surface of the target is cooled with water, going into the gap between the target substrate and the screen, rotating together with it. Vacuum-tight joint of rotating parts is achieved by means of a system of rings made of teflon. The gaps between the sealing surface of these rings are addionally pumped. The target active layer is a ring with the outside diameter of 280 mm and inner diameter of 220 mm; the layer thickness is I,5 $mg \cdot cm^{-2}$. Also the possibility to install fixed targets of varios diameters is envisaged, both immediately behind the acceleration tube and behind the mass-separator.

When the target is placed directly behind the tube both atomic and molecular components are present in the deutron beam. Simultaneouse target bombardment with ions of different component composition (D_1^+, D_2^+, D_3^+) decreases its life-time. That is why it is advisable to bombard the target with the analized beam - only atomic or only molecular species. In order to achieve this a magnet is installed in the area of ionic conductor between the acceleration tube and the target of neutron generator. The same magnet fulfils one more function - it decreases the load of high-voltage rectifier with electrones, knocked-out by deutrons from the tagret surface.

In neutron sources, based on lowvoltage accelerators, the electrostatic locking of electrons in the area adjacent to the target is more widely used on comparison with the method of placing an antidinatron grid-like electrode at a certain distance from the target. However, electrostatic systems suppressing electron component become not very much effective, being used in high-current accelerators, since at high currents the antidinatron elec-

trode itself starts to emit a large number of electrons into the acceleration gap. It seems that in high-current accelerators the method of magnetic electron locking now widely used at creation of powerful ion diods is to be considered as a preferred one.

The accelerator vacuum pumping is carried out via magnetodischarge and zeolite sorption pumps, that provides for a closed pumping system. Additionally near the target one more magnetodischarge pump is installed, which mainly pumps out the gases desorbed from the target.

The absolute value of neutron yield is determined by the method of activation of gold and aluminium foils with relative error about 5 %. The neutron flux into the whole solid angle was $5 \cdot 10^{11}$ neutron$\cdot s^{-1}$.

The decrease of neutron yield depending on the duration of deutron bombardment was controlled by means of a santillation detector and a fission chamber. On the fixed target at target current of 5 mA decrease neutron flux density 2 times took place during 2 hours, accordingly the total charge was about 40 Coulomb and the charge density was about 7 Coulomb$\cdot cm^{-2}$.

PULSED 14 MeV NEUTRON SOURCE

V.V. BOBYR, A.P. BORDULYA
Kiev State University,
Kiev, Union of Soviet Socialist Republics

Abstract

This paper deals with pulsed 14 MeV neutron sources. Time length is within 2 mks to 10 min.

In nuclear-phisical experiments pulsed fast neutron sources find wide application, in particular, while measuring isomeric nuclear states, delay nuclear fission, when working in neutron-activation analysis.

The authors worked out the pulsed neutron source with time-length pulsed and intervals between them changing within the range of 2 mks up to some minutes. The average neutron yield reaches 10^{10} neutrons per second.

The principal of source operation differs from the above mentioned [1] by expanded time range and additional functional possibilities. The reliable current suppression on the generator target within the intervals between neutron pulses is obtained by the counter-phase changing voltage - 4 + + 2 KV and + 2 + - 1 KV input on the focusing and extraction intervals of ions accelerator. For improving the time stability of a neutron generator the key control of focusing and extraction voltage is exercised by the control block (CB) (see Fig. 1a), the reference frequency of which being given by the quartz resonator. The impulses of the reference generator M1-1, M1-2, the frequency being 1 MHz, flow to invertors M6-1 and M6-2 and further on binary counters M2, M3, M4, where reference frequency is counted with the needed coefficient, which makes it possible to get pulses with periods from 4 mks up to the required largest possible time multiple of 2. The pulse period is formed by the switch /M1/. From the selected output of the recal-

culation decade through ПП1-б the signal goes to the counter trigger input M5-1, the trigger being converted into the state of "1" while the first negative drop voltage appears. From output M5-1 the state "1" is transferred to the transmitting circuit M6-3. On the other input of the transmitting circuit M6-3 the signal is sent from ПП1-а.

Switches ПП1-а and ПП1-б operate synchronously (ПП1-б gives period of neutron pulse and ПП1-а gives on-off time ratio). As indicated in the scheme ПП1 with the help of switch ПП2 on-off time ratio of neutron pulses can be chosen 2, 4, 8.

Output signal from M5-1 through the invertors M1-4 and M1-3 goes to the CB output keys T2 and T3, as well as to the pulse formers M8-1 and M8-2, invertor M7 and key T1, which determine the neutron pulse start or end time.

As CB is under voltage of 200 KV, this mark of time is given for the control of the registration electronic equipment through the system of light-emitting diode - of light guide - photomultiplier.

From the keys T2 and T3 the signals appear at the input of a stabilizer of constant voltage (SCV) extraction and focusing output keys (in Fig. 1б a scheme and a stress sheet diagram of SCV of focusing key are shown). The application of SCV between CB and the keys of the focusing and extraction voltage Л1 and Л2 is required, on the one hand, by the capacitance between high-voltage grid keys and low voltage CB, on the other hand, by the necessity of halvanic control of keys Л1 and Л2, because the on-off time ratio is not equal to 2 in all cases.

The SCV of the focusing and extraction keys are similar. Counterphase operation of SCV is provided by cross switch to CB.

The metal ceramic triodes ГИ-7Б with the forced air cooling are applied in output switches Л1 and Л2.

The application of SCV under modulation of the focusing and extraction voltages made it possible to obtain neutron pulses with the frount 0,2 mks, and the ratio of the number of neutrons background between the pulses to the number of neutrons in the pulse equal to the order of 10^{-5}.

1. Bobyr V.V., Bordulya A.P., Mitrochin O.E., Mikhnitsky I.B., Moiseev A.N. Pulse neutron source in millisecond band // Вестник Киевского университета. - 1980. - № 2I.

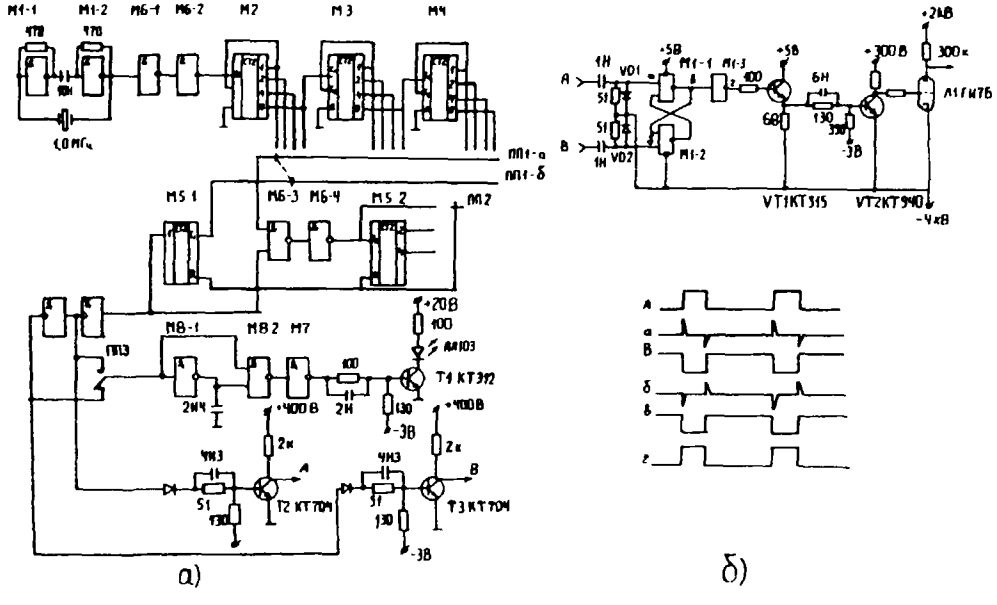

INTENSE NEUTRON GENERATOR DEVELOPMENT AT THE TECHNICAL UNIVERSITY DRESDEN

P. ECKSTEIN, U. JAHN, E. PAFFRATH,
D. SCHMIDT, D. SEELIGER
Technical University of Dresden,
Dresden, German Democratic Republic

Abstract

A Cockroft-Walton type accelerator producing low-energy intense hydrogen ion beams is presented.This accelerator is aimed for the production of monoenergetic neutron beams by the DD- and DT-reactions So far,ion currents up to 25 mA at a maximum of 24o keV energy have been obtained.

1. Introduction

General requirements in the field of accelerator development are the enhancement of the projectile energy as well as the increase of the ion beam current.At acceleration energies below 5oo keV ion beam currents of more than 1oo mA at the target have been obtained.The field of application of such accelerators is mainly the production of intense 14 MeV neutron beams using the DT-reaction.Intense 14MeV neutron sources commonly are used for cancer therapy,nuclear data measurements,material damage studies,fusion neutronics,shielding tests and other applications/1/. Further more,intense ion beam accelerators can be applied as pre-injectors for LINACs [2]) and other accelerators.They could be used also for the investigation of fusion reactions and technical applications of ion beams.

At present,there are in operation several neutron generators. Recently a review was presented elsewhere [3]).These machines differ between each other in many technical detail,as in the ion sources used,the accelerationtubes,ion optical elements,targets, control equipment and others.Although intense neutron generators in the range of $1o^{12}$ neutrons per second are available commercially, most of the research institutes have constructed their own accelerator, because in this way an optimal adaption of the parameters of the machine can be realized.It is of high interest both for users and designers of intense neutron generators to exchange information concerning experimental problems and results connected with the development of the high current accelerators,such as beam handling, beam diagnostic, working regimes, secondary electron suppression, vacuum conditions, heating of beam pipe elements and other experimental details. Therefore, the aim of this paper is the description of an accelerator for intense ion beams. Its single components are desribed in detail as well as some ionoptical calculations. Furthermore, technical parameters obtained for the components and experimental investigation methods and results concerning formation of the ion beam are reported.

2. The accelerator and its components

The main parts of the accelerator are shown schematically in fig.1. Inside a high-voltage (h.v.) screening fence the h.v. terminal, the h.v. power supply, the insulating transformer and the acceleration tube are situated. The latter is connected with the accelerator part on ground potential.

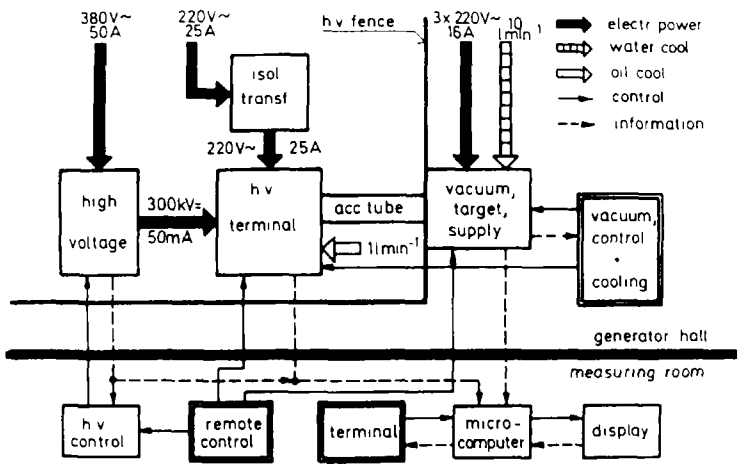

Fig.1 Arrangement of the main parts of the intense ion beam accelerator drawn schematically.

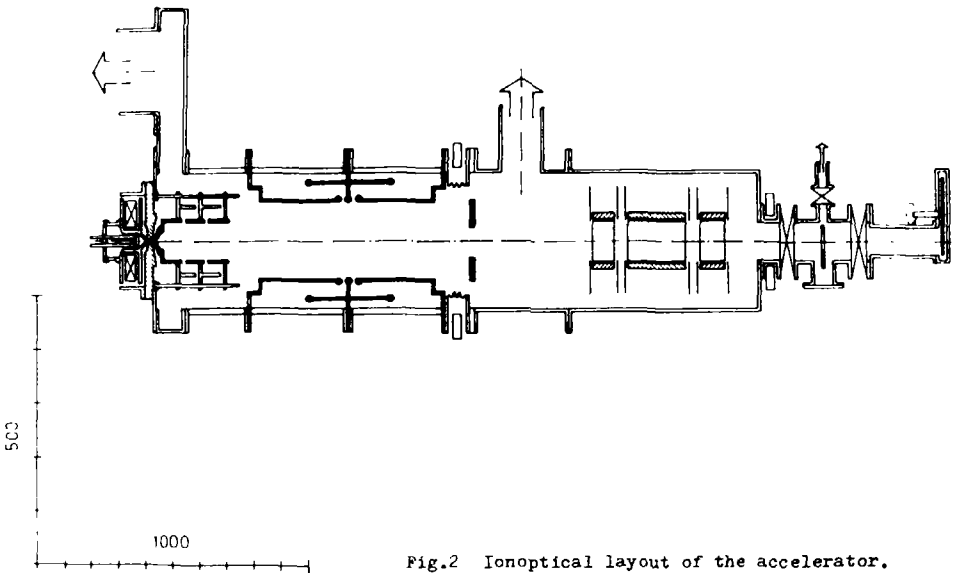

Fig.2 Ionoptical layout of the accelerator.

All devices for data acquisition and control of the accelerator, except the vacuum system control, are located in a separate control room. The h.v. terminal contains the ion source with its electrical supply, a special ion getter pump and the supply unit for the einzel lens after extraction. The ground potential part of the accelerator includes a quadrupole triplet, the vacuum system, the target, measuring sensors and control and supply units. The different components of the accelerator are described in the following in detail. For illustration fig.2 shows the ionoptical layout of the accelerator.

The ion source is one of the well known duoplasmatron type [4], its electrical supply can be seen in fig.3. Typical opera-

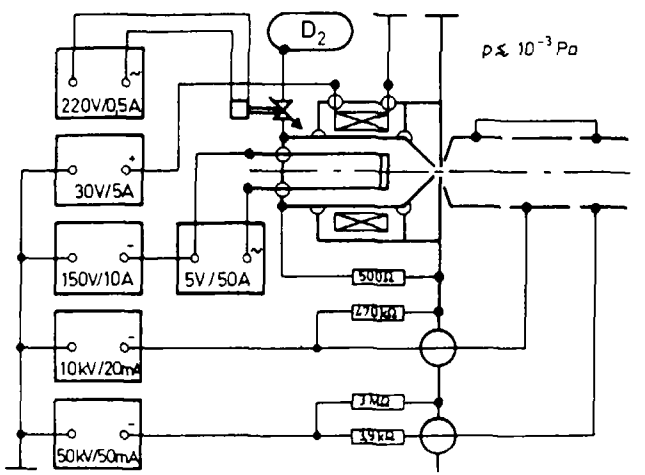

Fig.3 Electrical supply of the duoplasmatron ion source and the einzel lens; for typical operation values see text.

tion values of our duoplasmatron are: cathode current 20 A, arc current 3 ÷ 5 A, magnet current 3 ÷ 4 A and gas pressure 2 ÷ 10 Pa. The cathode consists of a directly heated pure nickel grid covered with an oxide layer of barium, calcium and strontium. The extraction region of the anode was specially designed as shown in fig.4. The expansion cup is combined with a Pierce geometry, the distance of the extraction electrode from the anode is nearly 5 mm. The extraction voltage has a typical value of 30 kV.

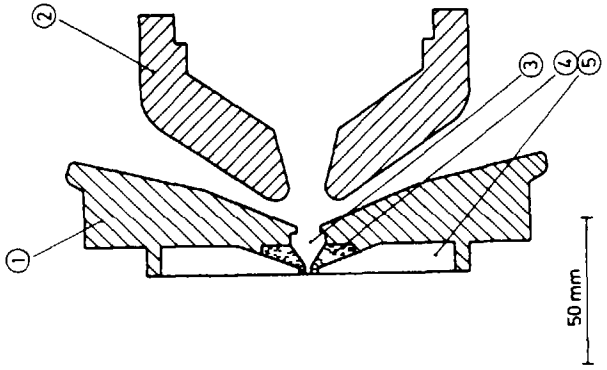

Fig.4 Geometry and materials used in the extraction region of the ion source (1 - anode, 2 - extraction electrode, 3 - expansion cup, 4 - tungsten insert, 5 - septum).

The einzel lens (see also figs.2 and 3) is connected with the extraction electrode and consists of three tubes, which are hold concentrically by ceramic rods. The ceramic material is screened against particle striking by rings arround the gaps between the electrodes. All metal used for the einzel lens is stainless steel. The inner diameter of the electrodes is 80 mm. The two outer electrodes have the same potential with respect to the anode as the extraction electrode, i.e. nearly -30 kV. The central electrode is fixed at a potential of about -4 kV, where the exact value is chosen to maximize the ion current at the target, see also sect.4.

The acceleration tube is a two-gap version (see fig.2) described in detail in ref. [5]). The gap widths between each of the two tube-like electrodes and the middle electrode can be chosen individually between 15 and 35 mm. Up to now the acceleration tube was investigated experimentally with a gap width of 25 mm symmetrically only. The wall near the gaps is screened against scattered charged particles and x-rays by a broad ring which is connected with the middle electrode. The aperture of the tube electrodes is 144 mm. The acceleration tube is constructed from ceramic and stainless steel elements which are glued together.

The ceramic tube wall consists of 7 segments separated by potential rings for potential linearization. These are connected with a voltage divider which has a total resistance of 7 G Ohm. For good h.v. reliability of the tube a h.v. training is necessary, especially after opening of the machine, i.e. a very slow increasing of the high voltage over the time. In this way h.v. values of 280 kV without beam and 240 kV with full ion beam have been obtained. For stabilization against breakdowns two potential rings were arranged ar ound the acceleration tube, seen in fig.7.

After acceleration the ion beam is focused by means of a electrostatic quadrupole triplet. The need of an additional lens follows from ionoptical calculations (see sect.3) taking into account the requirement of a distance between acceleration tube and target more than 1 m, which came from some application possibilities. The lens consists of two symmetrical quadrupole pairs which are connected to a triplet, i.e. the inner electrodes have the double length of the outer ones. The shape of the electrodes perpendicular to the beam axis is circular forming an aperture circle with radius 80 mm. The stainless steel electrodes are arranged inside aluminium rings using Teflon insulators, the rings are hold by steel rods. All electrodes are screened from both sides against direct striking of the ion beam and scattered charged particles by tantalum diaphragms with diameter of 70 mm. Both the outer quadrupoles are connected electrically and provided symmetrically by supply units $\pm$10 kV/20 mA. The voltage of the inner quadrupole can be controlled independently in the same manner. The operation voltage of the triplet is typically 2 + 4 kV.

For beam analysing (current and profile) different targets have to be used. Beside the beam current which is measured in each cases, the maximum power and possibility for obtaining of informations about beam distribution are important characteristics [6]. Fig.5 shows a target version for beam profile measurement, whereby an infrared camera detects the temperature distribution on the metallic target plate [7].

The material and thickness of the target plate limits the maximum beam power, because the maximum temperature should lie in the region below 1100 K. For example, using iron with a thickness 3 mm, the ion beam power may amount up to 1 kW, also slightly depending on the actual current density, i.e. focusing conditions. An other target version consists simply of two water-cooled thick copper diaphragms (diameter 30 and 15 mm, resp.) in front of a cooled thick copper plate (fig.5). In this way a maximum beam power of 5 kW could be converted and a rough information about beam distribution can be derived also. A further target investigated was a rotating target of the NUKEM type (U = 300 rpm, N_{max} = 5 kW, diam. 15 cm). In this case the beam spot and diameter are fixed by a diaphragm in front of the target with a given diameter.

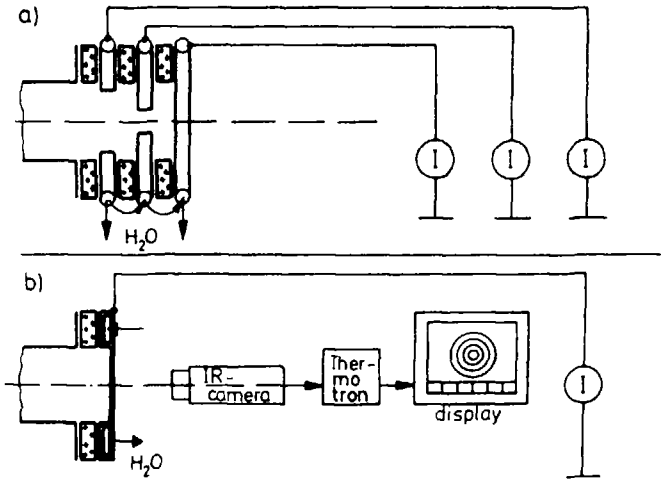

Fig.5 Targets for beam current and profile measurements.

The vacuum system includes three types of high vacuum pumps. A commercial magnetic getter pump holds the vacuum in the accelerator in the order of 10^{-4} Pa without source operation. A so called orbitron pump was developed and located near the ion source inside the h.v. terminal [8]. The advantages of this pump type are small mass and dimensions and nearly constant pumping speed in the pressure region 10^{-4} to 10^{-1} Pa. During source and low beam power operation the two ion getter pumps are sufficient for maintaining a reliable vacuum. In order to compensate the gas production by ion bombardment, during intense beam operation a 2000 l/s diffusion pump with lN_2-trap has to be used additionally.
The pressure in the accelerator holds normally at 10^{-4} Pa, it doesn't increase after the start of the ion source due to the effect of the orbitron pump near the source. During beam operation the pressure was obtained in the range between 10^{-4} and 10^{-2} Pa, depending on intensity and focusing conditions of the beam as well as on quality of secondary electron suppression. Higher pressure values should be avoided for maintaining h.v. stability. The high voltage and also all high vacuum pumps permanently were controlled by safety feed-back loops.
The h.v. supply is a commercial device with nominal parameters 300 kV/50 mA, the ripple factor is below 10%. As h.v. circuit a ground potential-free double rectification is used, in this way the half output voltage can be taken to supply the middle electrode of the acceleration tube.

The electrical energy is transferred to the h.v. terminal by a 25 kW/50 Hz transformer for an insulating voltage at maximum 300 kV. The h.v. supply can be controlled remotely.

The electrical supply of the ion source, orbitron pump and quadrupole triplet is designed by the use of supply units which are operating for output powers below 500 W in switching mode [9]. In this way small mass and dimensions and a high efficiency could be achieved. Furthermore, each supply unit can be controlled remotely by a microprocessor and gives a standardized signal for check-up. The power supplies above 500 W (150 V/10 A and 50 kV/50 mA, see fig.3) are of conventional type using thyristors and a regulating transformer, respectively. Other information signals were taken from developed sensors [10], as for temperatures and flow rates in the different cooling circuits, or converted into standardized signals, as the pressure inside the source and in the accelerator or beam current magnitudes from diaphragms and targets. Thus, all analogue informations are represented by signals between 0 and +5 V corresponding to the maximum value of the magnitude examined.
The control and reference signals are transferred by opto-electronical blocks in connection with glass fibres using analogue-to-frequency and frequency-to-analogue converters. The electrical potential of the glass fibres have to be terminated definitely on h.v. and ground potential in order to avoid discharges and destruction of the glass fibres. All

informations arriving from the accelerator are accumulated in a microcomputer. By a display different pictures can be chosen which represent a selected part of information ("accelerator with target", "ion source", "vacuum system", "ion optics", "list of all parameters"). At a head line in each picture the most important accelerator paremeters are shown. Into the head line is also implemented the alarm function indicating that one parameter has exceeded certain limits which can be given into the list before operating. If two or more parameters are outside the limits, the alarm order is fixed by priorities. Fig.6 shows the display picture "ion source" as example. All supply units of the accelerator (and in this way the gas inlet into the ion source also) are controlled by hand, the control desk is arranged near the microcomputer in the control room (see also fig.1).

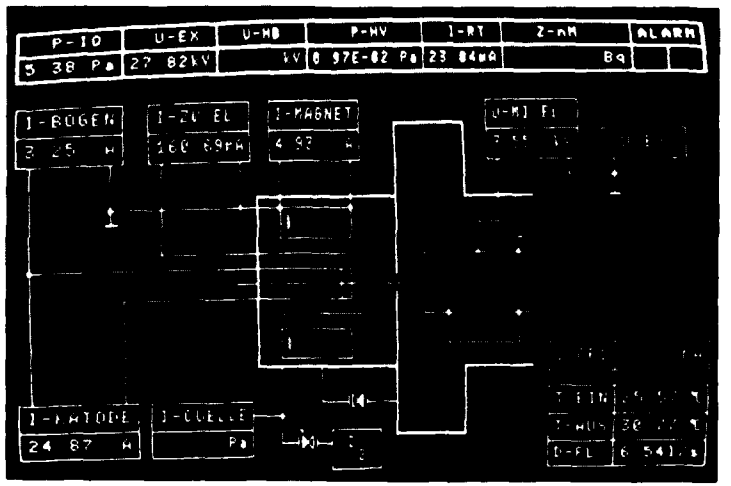

Fig.6 Display picture "ion source"; the head line shows from the left: ion source pressure, extraction voltage, acceleration voltage, pressure in the accelerator, target current, monitor counting rate, alarm function

The complete accelerator is shown in fig.7. From the left -hand side the following details can be seen: the h.v. terminal -- the two potential rings (upper part) -- the terminated glass fibres (lower part) -- the low-energy section of the acceleration tube with resistors of the divider -- the magnetic ion getter pump (upper part) and quadrupole triplet (lower part) -- valves and a water-cooled diaphragm -- rotating target. Below the triplet one can see the vacuum system control (left side) and the four supply units 10 kV/20 mA (right side).

3. Ionoptical calculations

The aim of the ionoptical calculations was to find the best configuration of ionoptical elements with respect to their geometry and operation parameters. Uncertainties of such calculations arise from the uncertainties of initial conditions as well as approximations in the models and computer codes used. Nevertheless, the results of ionoptical calculations show some tendencies in the behaviour of the ionoptical system investigated in dependence on the variation of parameters and enable, therefore, the designer to find the best arrangement in a short time.

It is known that space charge effects plays an important role in the ion beam current region investigated here. In order to estimate its influence the beam divergence of a parallel beam on a field-free drift path was calculated [6]).

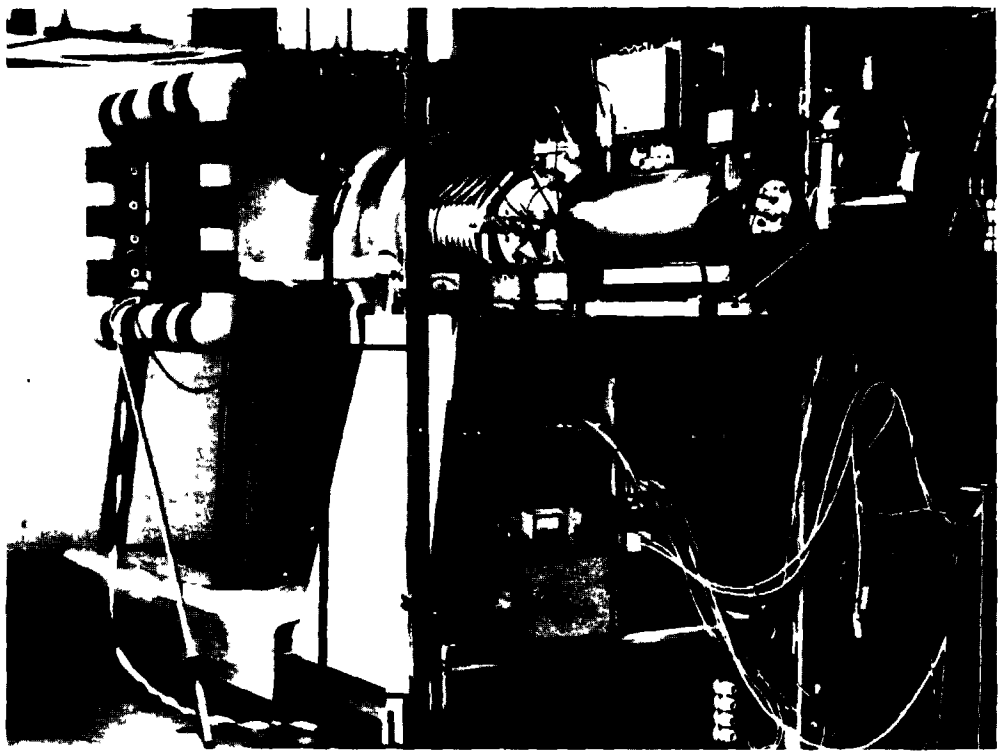

Fig.7 The intense neutron Generator INGE - 1

It follows that this effect must be taken into account, especially at lower ion energies. In opposite to it the residual gas in the accelerator causes a partial compensation of the spacecharge divergence, this effect can be evaluated also in the order of magnitude. And a further important question with respect to calculation performance are the initial conditions. This point was taken into consideration by the assumption of a plane and curved surface of the emitting plasma area in the expansion cup of the ion source.

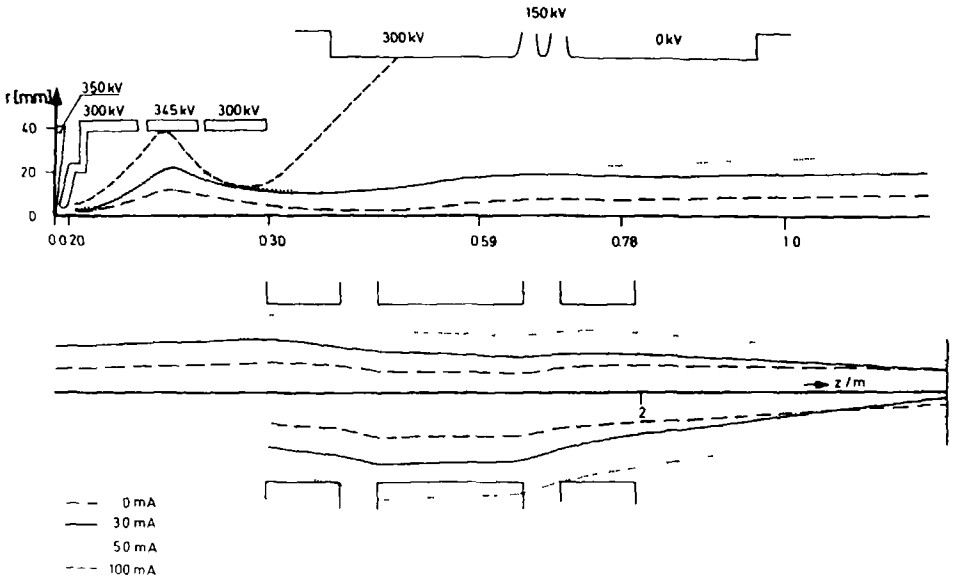

Fig.8 Deuteron beam envelopes for a plane plasma emitter surface (in the triplet region results for two perpendicular planes are drawn).

A lot of calculations have been carried out for different parameter sets and conditions. For the ion path between the source and the acceleration tube exit the space charge was taken into account (code ELENS [11]). After tube up to the target the code SYSFIT [12] without space charge effects was used. An example of such calculations is shown in fig.8. It could be demonstrated that an ion beam transport with currents up to 30 mA should be possible, i.e. a beam power on the target of 5 to 6 kW could be obtained.

Concerning the residual gas, a compromise must be found: high pressure causes a good space charge neutralization, but diminishes on the other hand the h.v. stability against breakdowns.

4. Experimental methods and results

The duoplasmatron ion source has been investigated extensively using a special test stand. The emittance was determined from traces on thermopaper which was located behind a screen with parallel slits (width 0.5 mm, distance 5 mm). This method is from the technical point of view very simple and effective, but the gas production deteriorates the vacuum conditions. The emittance value of nearly 10π mm·mrad $\sqrt{\text{MeV}}$ [13]) was reproduced by calculations quite well [14]) allowing conclusions concerning the ion beam initial conditions. The improved extraction geometry was shown in fig.4. The cooling of the duoplasmatron is realized by means of an oil circulation from ground potential. The ion beam current was measured as a function of arc current, extraction voltage and magnet current. In this way could be shown that a current of 35 mA from the source is possible without problems (for the accelerator a current of 25 mA is sufficient).

Before acceleration of intense ion beams a careful suppression of secondary electrons must be required. The electrons are accelerated in direction to the ion source heating the striked material. In this way gas production occurs and the vacuum deteriorates drastically. Furthermore, the accelerated electrons produce bremsstrahlung which can diminish the h.v. stability. Electron suppression was investigated using permanent magnets and water-cooled diaphragms in connection with an electrical field. In fig.2 the magnets are shown as squares (outside the accelerator, near the exit of the acceleration tube and of the triplet) and the diaphragms as black slits (inside the beam line near the magnets). The most attention in this sense must be spent to the region ar ound the acceleration tube exit. The efficiency of the secondary electron suppression was measured indirectly by use of a dosimeter with an energy threshold near 25 keV. The dosimeter was arranged near the ion source inside the h.v. terminal as well as in the accelerator hall outside the h.v. fence. In order to minimize the bremsstrahlung, positions and orientation of the magnets as well as magnitude and sign of the voltages on diaphragms, respectively, were varied.

An important point is the connection of all electrodes which can be striked by particles, with ground or h.v. terminal potential by power resistors. In the other case the

striking particle beam causes a certain potential which cannot be changed by the voltage supply unit, i.e. the electrode potential cannot be controlled to zero. The resistor R should have a value which is determined by the maximum voltage U_m of the supply unit and the possible current I_i of striking particles. Two of such power resistors coupled parallel to the corresponding supply unit are shown also in fig.3 (470 k Ohm at 10 kV/20 mA and 3 M Ohm at 50 kV/ 50 mA).

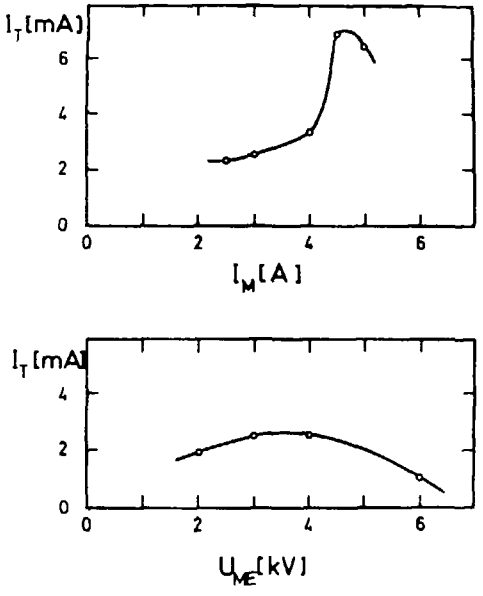

Fig.9 Target current versus magnet current I_M as well as potential U_{ME} of the zwischen electrode of the einzel lens (I_{arc} = 1.2 A, U_{extr} = 25 kV, $U_{h.v.}$ = 200 kV); upper part: U_{ME} = 3 kV; lower part: I_M = 3 A.

At first the ion beam was studied without quadrupole triplet. The focusing effect of the einzel lens is shown in fig.9, the curve has a flat maximum. The magnitude of the integral beam current on the target can be changed in certain limits by operating the magnet current of the duoplasmatron. The beam current change in larger steps is possible by changing the arc current. In this case the operating pressure inside the ion source must be regulated also.

If the high voltage is changed during constant ion source operation, the integral current decreases due to the changed focusing, indicating that the acceleration tube acts as a focusing lens. The changed focusing behaviour of the tube can be compensated slightly by changing the zwischen electrode potential of the einzel lens. The focus diameter (fwhm) of the beam on the target can be obtained within 10 ÷ 15 mm at beam currents up to 10 mA without triplet. For higher beam currents below 30 mA the focus diameter is estimated to be lower than 30 mm at the best focusing conditions. The focusing properties of the quadrupole triplet has been proved also, see fig.10. The real parameters depend upon the requirements following from the intended application.

The measuring method for beam profile determination was characterized in sect.2. This method is relatively simple but effective. Fig.10 shows two examples obtained. From them it can be concluded that the temperature spread is probably smaller than the dimensions of the beam current gradient, i.e. the temperature distribution reflects quite correctly the beam current profile.

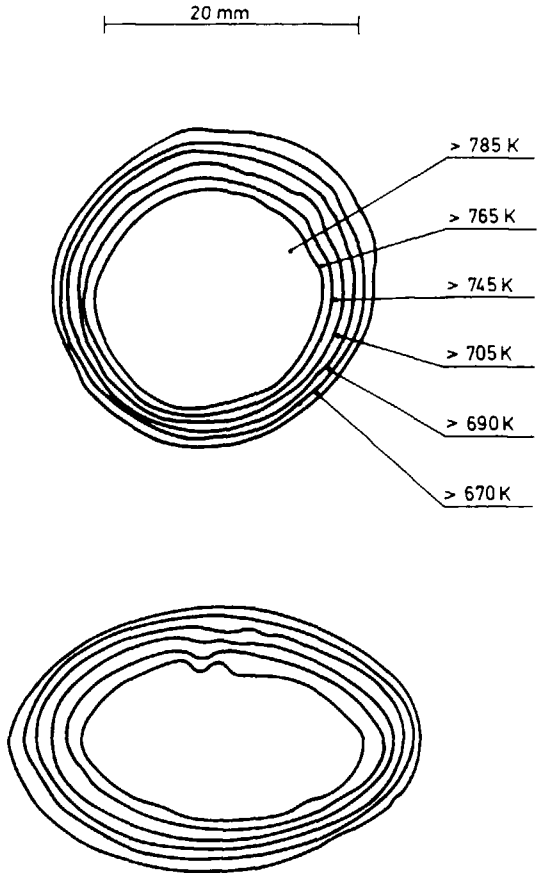

Fig.10 Temperature distributions reflecting the beam profile; a) without triplet; b) focusing effect of the triplet for one plane.

As a résumé all beam current investigations can be summarized to the following data: the beam current on the target can result into 25 mA or more, the high voltage during beam operation was at maximum 240 kV. A power on the target up to 5 kW can be converted. The focus diameter is smaller than 30 mm at all these machine parameters. A long time stability of the operating accelerator over hours is possible without remarkable correction of source and other parameters. The number of breakdowns in that time was smaller than one per hour.

5. Summary

An accelerator for high-intense ion beams was developed. A compact construction of the accelerator was achieved concerning the h.v. terminal as well as the whole machine. An important role in this sense plays the developed supply units in switching mode.
There have been reported some methods for experimental investigation of the beam current and distribution and also problems which are related to it. Beam currents on the target up to 25 mA and also a beam power of 5 kW are possible, whereby the focus diameter doesn't exceed 30 mm.
The use of a microcomputer for data acquisition of all standardized parameter values enables a comfortable control of the accelerator and effective safety and alarm system.

References

[1]) H.H.Barschall, 14 MeV DT-sources, Chap.IV in Neutron Sources for Basic Physics and Applications, Vol.2 of Series Neutron Physics and Nuclear Data in Science and Technology, Pergamon Press (1983)

[2]) P.M.Lapostolle & A.L.Septier, Linear Accelerators, North-Holland Publishing Company Amsterdam (1970)

[3]) U.Jahn, E.Paffrath, D.Schmidt and D.Seeliger, Kernenergie, in print

[4]) C.Leyjeune, Nucl.Instr.and Meth. 116 (1974) 417

[5]) U.Jahn, D.Schmidt, D.Seeliger, A.I.Glotov and V.A. Romanov, submitted to Prib.Tekh.Eksp.

[6]) U.Jahn and J.Dietrich, Proc.XIV.Int.Symp.on Interaction of Neutrons with Nuclei, Gaußig 1984

[7]) H.Buttig, report ZfK-453, ZfK Rossendorf (1981)

[8]) E.Paffrath, U.Jahn and D.Schmidt, see ref. [6])

[9]) F.Gleisberg and H.-J.Esche, report ZfK-503, ZfK Rossendorf (1983) 135

[10]) P.Eckstein, F.Gleisberg, R.Krause, R.Schwierz, D.Schmidt, E.Paffrath, D.Seeliger, A.I.Glotov and V.A.Romanov, see ref. [6])

[11]) J.S.Hornsby, CERN 6600 Computer Program Library (1965)

[12]) M.Friedrich, ZfK Rossendorf, to be published

[13]) A.Tunia, U.Jahn and E.Paffrath, see ref. [6])

[14]) J.Dietrich and U.Jahn, see ref, [6])

SESSION VI

SELECTED SPECIAL APPLICATION

MEDICAL APPLICATIONS OF NEUTRON SOURCES

J J BROERSE*
Radiobiological Institute TNO,
Rijswijk, Netherlands

Abstract

The degree of biological damage produced by ionizing radiation depends on the energy deposition at a macroscopic and a microscopic level. For this purpose the quantities absorbed dose and linear energy transfer (LET) are introduced. Due to the steepness of the dose-effect relations the absorbed dose should be determined with an accuracy of better than ±5 per cent. The uncertainties in the assessment of the absorbed dose are discussed and the results of neutron dosimetry intercomparisons are summarized.

Fundamental radiobiological findings have initiated the renewed application of fast neutrons in clinical radiotherapy. At present more than 10.000 patients have been treated with external beams of fast neutrons. Interstitial neutron therapy with californium-252 has been performed at a limited number of centers. For teletherapy with neutron beams with energies below 20 MeV, clinical trials have only shown an advantage for neutrons in comparison with photons for a limited number of tumours. Most of the neutron beams applied for radiotherapy have been less than optimal because of inadequate physical and technical conditions. It is expected that these defects can to a large extent be overcome with neutron beams produced by cyclotrons accelerating protons or deuterons to energies in the range of 40 to 60 MeV.

A special aspect of neutron radiotherapy is the installation of low energy filtered reactor beams to be used for boron capture therapy. The large cross section for the ^{10}B (n, α) ^{7}Li reaction in the thermal and epithermal energy region could provide a high local energy deposition. The problem of attaching the boron isotope to tumour cells in the human body is under continuous investigation.

* And Department of Clinical Oncology, Academic Hospital Leiden, Netherlands

1 Introduction

Radiotherapy is an important means for the treatment of malignant diseases. In the Netherlands approximately 50-60 per cent of all cancer patients are subjected to radiation alone or as part of combined treatments e.g. in conjunction with surgery or chemotherapy (1). Although radiotherapy with ^{60}Co gamma-rays and megavolt X-rays has been successful for a number of cancers e.g. 90 per cent cure (10-year survival) for Hodgkin's disease, the results for tumours of other types have been very disappointing, e.g. 5 per cent cure for lung carcinoma (5-year survival) and 10 per cent cure (10-year survival) for brain tumours. Due to the limitations of photon radiotherapy, considerable effort has been invested over the past 20 years in biomedical research with nuclear particles with advantageous physical and/or biological properties.

Neutron teletherapy started already within a few years after the discovery of the neutron when patients were treated with these indirectly ionizing particles produced by the reaction of 8 MeV deuterons on a beryllium target with the 37 inch cyclotron at Berkeley (2). A historical survey of the radiobiological and radiotherapuetic experiences with fast neutrons can be found elsewhere (3). The initial tumour regression was quite impressive, but the clinical results showed large variations. This was to be expected since the dose per fraction and the number of fractions varied considerably due to unreliable operation of the cyclotron. In addition, the patients treated were generally in an advanced stage of the disease. Another conclusion of the first clinical applications was that late effects in different normal tissues were more serious than anticipated. In later analyses of the data, a number of complications could be attributed to differences in the effects of fractionation of neutrons as compared to photons. However, the mechanism of repair of sublethal damage for different types of radiation had not yet been investigated. Only at the end of the fifties new radiobiological data became available which provided a stimulus to renew the application of fast neutrons for clinical radiotherapy.

To predict tumour response and to restrict normal tissue complications after radiotherapy, the absorbed dose at the position of the tumour should be determined with a sufficient degree of precision and accuracy. To allow a direct comparison of clinical results obtained at different centers, intercomparison of neutron dosimetry are imperative. The basic concepts of neutron dosimetry are described and the results of neutron dosimetry intercomparisons are summarized. When a biological system is irradiated with neutrons, the energy is for the major part dissipated by fast protons, alpha particles, and heavy recoils which are produced in the tissue through interactions of the neutrons with the tissue constituents. The secondary particles produced by the neutrons have a higher ionization density than electrons produced by X- or gamma radiation; consequently, neutrons can be described as high LET radiation.

The biological effects of high LET radiation, including fast neutrons, are different from those obtained with X-rays in several respects. As will be discussed in the section on current radiobiological knowledge, wide variations have been observed in relative biological effectiveness (RBE) for different tumours and normal tissues. From studies on the response of pulmonary metastases in patients it has been concluded that the RBE for slowly growing tumours which are generally well-differentiated is higher than for tumours with much smaller doubling times. Results of clinical trials with fast neutrons performed in Europe and in the United States have only shown some advantages compared to conventional photon therapy in a relatively small group of tumours. It is now recognized that most neutron radiotherapy applications have been inadequate to a variety of reasons. Patients were treated with cyclotrons constructed for other purposes, essentially unsuitable for clinical work or with d+T neutron generators which technically fell far short of modern megavoltage X-ray machines due to relatively low dose rate, relatively poor depth dose, large penumbra and limited target or tube lifetimes. High energy cyclotrons constructed for medical applications will be the first step to improve the beam characteristics and to make comparisons with megavoltage photon beams feasible.

Appreciable efforts have been made to employ thermal or epithermal neutron beams in combination with borated compounds for treatment of malignant diseases, such as brain tumours. The on-going pre-clinical studies will be summarized. Another medical application of neutron beams will be discussed notably the detection of insufficiencies in the normal distribution of specific elements in certain organs. Deviations in elemental composition in a living person can be investigated by in vivo neutron activation analysis.

2. Neutron dosimetry for biomedical applications

The most elementary description of a radiation field is one in terms of the type, energy, direction and number of particles. For this purpose radiometric quantities have been introduced such as fluence, fluence rate and energy fluence (4). A second category of quantities deals with the interaction of radiation and biological material. In the third category dosimetric quantities are devised to provide a physical measure to be correlated with actual or potential effects. In essence these dosimetric quantities are products of the quantities mentioned in the first two categories.

Biological effects are the consequence of energy deposition by ionizing radiations in tissue. In the case of indirectly ionizing radiation such as photons or neutrons, charged particles are produced through secondary processes. The objectives of dosimetry and dose specification concern the description of the temporal and spatial distribution of the energy deposition at a macroscopic and microscopic level.

The absorbed dose, D, is defined (4) as the quotient of $d\bar{\varepsilon}$ by dm, where $d\bar{\varepsilon}$ is the mean energy imparted by ionizing radiation to matter of mass dm:

$$D = \frac{d\bar{\varepsilon}}{dm} \quad (\text{SI unit: J kg}^{-1})$$

The special name for the unit of absorbed dose is gray (Gy). The special unit of absorbed dose, rad, has been abandoned but can still be found in older literature (1 rad = 10^{-2} J.kg^{-1}). The absorbed dose rate is defined as the increment of absorbed dose in the time interval dt.

When the amount of mass is reduced, the stochastic aspects of the energy deposition process will become evident. This has led to the introduction of stochastic dosimetric quantities such as:

The specific energy (imparted), z, defined as the quotient of ε by m, where ε is the energy imparted by ionizing radiation to matter of mass m:

$$z = \frac{\varepsilon}{m} \quad (\text{SI unit: J.kg}^{-1})$$

The special name for the unit of specific energy is gray (Gy). The specific energy, z, is a stochastic quantity.

The specific energy may be due to one or more energy deposition events, i.e. traversals of charged particles through a volume element considered. The statistical fluctuations will be less apparent when the mass of the irradiated material is increased (5), as shown in figure 1. The solid line covers the region in which the absorbed dose can be

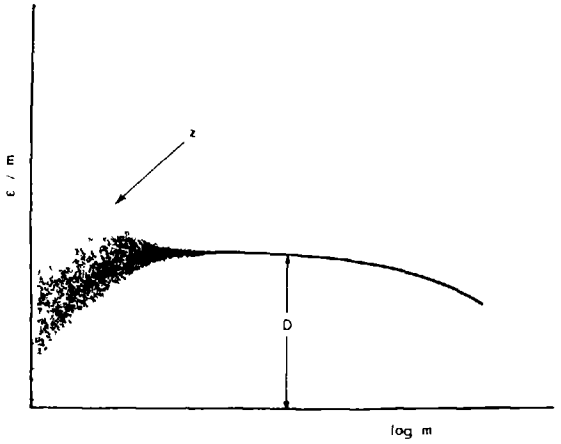

Figure 1. Energy density as a function of mass showing the statistical fluctuations which become apparent at small masses (5).

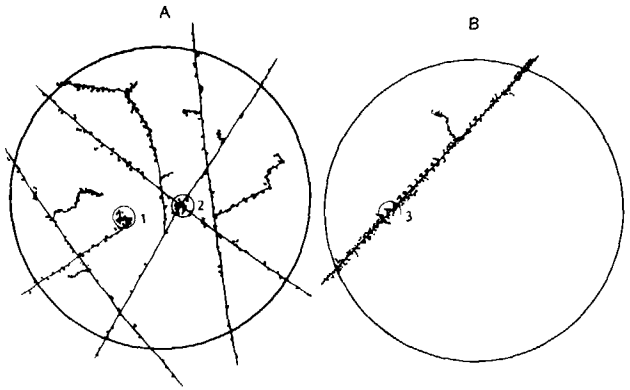

Figure 2. Schematic representation of energy dissipation patterns in small volumes in cells irradiated with equal doses of X-rays (A) or high-LET α-particles (B). High concentrations of energy events occur for both types of radiation (small circles 1, 2 and 3), but they are per unit of dose less frequent for low-LET radiation.

established in a single measurement. At large masses the energy density is reduced due to attenuation of the indirectly ionizing particles. The shaded portion represents the range where statistical fluctuations are important.

On the microscopic level the energy dissipation patterns of various types of radiation are considerably different as shown schematically in figure 2 for sparsely ionizing electrons produced by X-rays and a densely ionizing alpha-particle. The differences in biological effects produced by equal doses of different radiations have to be attributed to these differences in the spatial distribution of the energy deposition. To quantify the local energy transfer, the following quantity has been introduced:

The linear energy transfer or restricted linear collission stopping power L_Δ, of a material for charged particles is defined (4) as the quotient of dE by dl, where dE is the energy lost by a charged particle in traversing a distance dl due to those collisions with electrons in which the energy loss is less than Δ:

$$L_\Delta = \left(\frac{dE}{dl}\right)_\Delta \quad \text{(SI unit: } J.m^{-1}\text{)}$$

The energy may also be expressed in eV (1 eV = $1{,}6.10^{-19}$) and hence, L_Δ may be expressed in $eV.m^{-1}$ or some conventient submultiple or multiple, such as $keV.\mu m^{-1}$ (1 keV μm^{-1} = $1{,}6.10^{-10} Jm^{-1}$). In order to simplify the notation, Δ may be expressed in eV. Thus, L_{100} is understood to be the linear energy transfer for an energy cut off of 100 eV.

An example of LET spectra for different types of radiation is shown in figure 3 (6). For ^{60}Co photons, neutrons from the d(50)+Be reaction, heavy ions and pions a wide range of LET values is observed. When a relatively high proportion of the absorbed dose is delivered in the LET interval between 30 and 300 keV μm^{-1} the biological effects can deviate appreciably from those observed after exposure to sparsely ionizing radiation.

As a measure of differences in effectiveness of various radiations, the term relative biological effectiveness (RBE) has been introduced (7), which is defined as the ratio of the absorbed dose of a reference radiation to the absorbed dose of a test radiation required to produce the same level of biological effect, other conditions being equal. Orthovoltage X-rays (250-300 kV) are generally taken as the reference radiation. For any given type of radiation, environmental factors such as the oxygen concentration can modify the radiation response. In this connection the term oxygen enhancement ratio (OER) has been introduced, which is defined as the ratio of absorbed dose required under conditions of hypoxia to that under conditions in air, to produce the same level of effect.

In practical situations a neutron fluence is always accompanied by a fluence of photons. In view of the differences in effectiveness of the two types of radiation the absorbed doses of neutrons and photons should be evaluated separately. This is generally performed by using two dosimeters with different sensitivities. One instrument (T) is usually

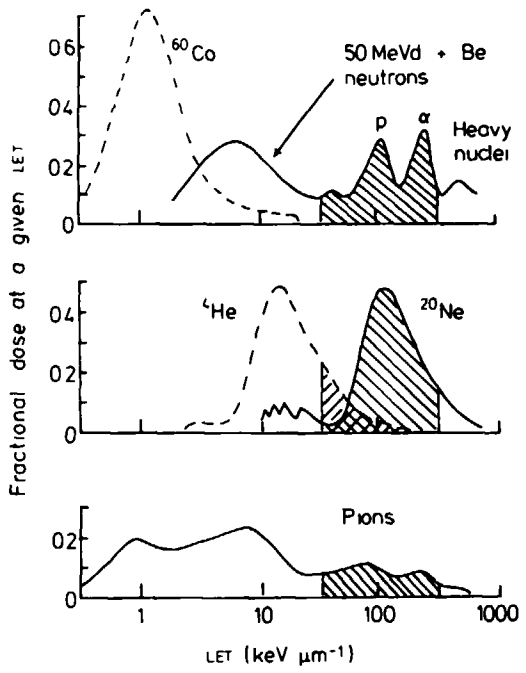

Figure 3. Distribution of absorbed dose as a function of LET for ^{60}Co gamma-rays, d(50)+Be neutrons, charged helium and neon particles and negative pi mesons (6).

constructed to have approximately the same sensitivity to neutrons and to photons, whereas the construction of the second instrument (U) results in a lower sensitivity to neutrons than to photons (8). Thus, for the same mixed field, the quotients of the responses of dosimeters by their sensitivities to the gamma rays used for calibration, R_T and R_U, respectively, are given by

$$R_T = k_T D_N + h_T D_G$$

$$R_U = k_U D_N + h_U D_G$$

where D_N and D_G are the absorbed doses in tissue of neutrons and of photons in the mixed field, k_T and k_U are the ratios of the sensitivities of each dosimeter to neutrons to its sensitivity to the gamma rays used for calibration, and h_T and h_U are the ratios of the sensitivities of each dosimeter to the photons in the mixed field to its sensitivity to the gamma rays used for calibration, respectively.

The charge produced within the cavity of an ionization chamber is derived from the reading, R, of the chamber multiplied by several correction factors, k_R, including those for incomplete charge collection, leakage current and density and composition of the gas in the cavity (9). For measurements inside a phantom, a displacement factor k_d has to be introduced which is defined as the ratio of the absorbed dose for an infinitesimally small cavity to the absorbed dose actually measured. The absorbed dose in the tissue adjacent to the cavity of the chamber, D_t, can be derived from the reading of a tissue equivalent (TE) ionization chamber:

$$D_t = R.\Pi k_R.k_d.\frac{1}{e.m} W.r_{m,g} \frac{(\mu_{en}/\rho)_t}{(\mu_{en}/\rho)_m}$$

where e is the charge of the electron, m the mass of the gas in the cavity, W the average energy required to produce an ion pair in the gas and $r_{m,g}$ the gas-to-wall absorbed dose conversion factor. For the neutron component, the ratio of the mass energy absorption coefficients, μ_{en}/ρ, can be replaced by the ratio of kerma in tissue and in wall material, K_t/K_m. Detailed information on the actual values of the basic physical parameters can be found elsewhere (9). The mass of the gas in the cavity can be derived from a calibration of the chamber in a reference photon field. For the calibration of the chamber and for measurements of neutron kerma in air complementary corrections have to be applied, including those for wall thickness, stem scatter and angular dependence of response.

The uncertainties in the determination of the total absorbed dose for radiobiology and radiotherapy applications in mixed neutron-gamma-ray field using TE ionization chambers are summarized in table 1 (9).

Table 1

UNCERTAINTIES (IN %) IN THE DETERMINATION OF THE TOTAL ABSORBED DOSE IN TISSUE IN A NEUTRON FIELD

Parameter	Uncertainty
R_T	0 2
$(\pi k_R)_T$	0 3
$(k_d)_T$	0 5
$N_c (\pi k_A)_c (f_t)_c$	1 2
W_N/W_c	4 0
$r_N/(s_{m,g})_c$	2 0
$(K_t/K_m)_N$	2 6 to 9 7*
$\left[(\mu_{en}/\rho)_t/(\mu_{en}/\rho)_m\right]_c$	0 1
	Overall 5 4 to 10 8*

*According to Bewley (1980) The lower value is valid for a d(16)+Be beam the higher for a p(66)+Be beam

It can be concluded that the largest uncertainties are due to the variations in the values for the basic physical parameters W and kerma. Radiotherapeutical and radiobiological studies have shown that the probability of tumour control and incidence of normal tissue complications are steep functions of the absorbed dose. This has led to the requirements of a reproducibility of ±2% of the delivery of the absorbed dose and an overall uncertainty of ±5% in the determination of the dose in the region of interest. It can be concluded from the table that the overall uncertainty for dose determinations with TE ionization chambers does not completely fulfil this requirement, especially at the higher neutron energies. When the different groups involved in fast neutron therapy adhere to the same dosimetry protocol a number of discrepancies can be avoided as shown in recent neutron dosimetry intercomparisons.

3. Results of neutron dosimetry intercomparisons

The most important motive for the performance of dosimetry intercomparisons is to allow for an adequate evaluation and comparison of biological and clinical results obtained by different groups. Additional aims of dosimetry intercomparisons are to provide a basis for uniformity in dosimetry for patients and biological specimens and to obtain information on the advantages, disadvantages, corrections and systematic errors involved in various methods.

The dosimetry intercomparison programs can be subdivided into two classes. Intercomparisons of dosimetry systems at specific locations under standardized conditions and intercomparisons at the beams actually used for biomedical applications. In the first type of intercomparisons such as the International Neutron Dosimetry Intercomparison, INDI (10) and the first European Dosimetry Intercomparison Project, ENDIP-1 (11), all participants brought their systems to central locations. In the second type of intercomparisons, including those carried out under the auspices of Task Group 18 of the American Association of Physicists in Medicine, AAPM (12), by European institutes involved in clinical trials (13) and the second European Neutron Dosimetry Intercomparison Project, ENDIP-2 (14) the dosimetry systems were taken to each institution and, where possible, reciprocal visits among institutes were made.

The results of INDI performed in 1973 and ENDIP-1 carried out during 1975 were rather discouraging. The neutron absorbed dose values showed standard deviations in the order of ±7 to 8 per cent for measurements in a phantom. For a few specific situations maximum differences of up to 20 per cent were observed in the assessment of the neutron absorbed dose. The values reported for the gamma-ray absorbed dose showed large variations of up to 100 per cent from the mean value. These deviations are not acceptable for the measurements in-phantom where relatively large photon contributions can be expected (up to 25 per cent of the total absorbed dose). Analysis of the results showed that for the same experimental conditions, the various groups employed divergent basic physical parameters. In addition it appeared that there were also great systematic differences in measurement procedures.

The early intercomparisons have stimulated the collection of new dosimetry data, studies on the characteristics of tissue equivalent ionization chambers (15) and the drafting of protocols for neutron dosimetry for external beam therapy (9,16). Information on the recommended physical parameters and the similarities and dissimilarities of the various protocols can be found elsewhere (13). A further consequence of the initial intercomparisons was the introduction of a common ionization chamber for clinical neutron dosimetry. The European groups adopted the Exradin T-2 0.5 cm^3 thimble TE ionization chamber and the American centers the spherical FWT IC-17 1 cm^3 spherical TE ionization chamber.

Since 1977 multicenter clinical trials were performed in Europe by the EORTC (European Organization for Research on the Treatment of Cancer) High LET Therapy Group. The results of three small scale neutron dosimetry intercomparisons between institutes participating in these trials are shown in table 2 for the total absorbed dose at 10 cm depth in a phantom. The greatest variations are observed in the intercomparison performed by the German groups. However, it should be noted that these groups use different types of TE ionization chambers and applied diverging physical parameters. The discrepancies in the intercomparison between Amsterdam, Edinburgh and Essen were mainly a result of differences in the photon calibration. The good agreement between the Dutch and Belgian groups results from the application of the ECNEU protocol (9) by all participants.

Table 2

NEUTRON DOSIMETRY INTERCOMPARISONS BETWEEN EUROPEAN INSTITUTES INVOLVED IN CLINICAL TRIALS

	Hesz et al 1981			Williams et al 1981	Octave-Prignot et al 1982
Amsterdam				0 985	1 005
Edinburgh				0 967	
Essen	1 023	0 956	1 000	1 000	
Hamburg	1 000	1 009	1 073		
Heidelberg	1 070	1 000	1 036		
Louvain					1 000
Rijswijk					0 990

Within the framework of the radiation protection programme of the Commission of the European Communities, CEC, an on-site neutron dosimetry intercomparison was performed, ENDIP-2 (14). In four sessions eighteen participating groups in six countries were visited. The dosimetry instrumentation of the ENDIP-2 group included two Exradin tissue-equivalent chambers, a Geiger-Muller counter, gasflow systems and Keithley 616 electrometers. The preliminary conclusion of ENDIP-2 is that the instrument responses of the participants deviate less than 3 per cent from those of the measurement team. This indicates a great improvement compared to ENDIP-1 which can be attributed to the efforts made in TE ionization chamber dosimetry techniques within the CEC and to the adherence to the same neutron dosimetry protocol.

Despite these improvements, it should be realized that some of the conversion factors still have appreciable uncertainties such as the kerma ratios for kerma in wall-material versus that in soft tissue. In this connection, there is a need for more reliable kerma values, for the neutron energy range between 15 and 80 MeV. In addition, more information is required on reaction cross-sections and total cross-sections for oxygen and carbon. Further experimental and theoretical investigations are indicated for the gas-to-wall absorbed dose conversion factor, and the corrections for the effective point of measurement.

4. Current radiobiological knowledge

Interest in the use of fast neutrons for cancer radiotherapy was stimulated by three radiobiological findings concerned with the oxygen enhancement ratio, the sensitivity of cells at different phases of the cell cycle, and the contribution of sublethal damage to cell reproductive death. It appeared that the cellular responses after irradiation with high LET radiation were different from those obtained with low LET radiation.

For a number of cell systems, it has been demonstrated that, in the absence of oxygen, cells have a much higher resistance to irradiation than when in the presence of oxygen. The quantitative factor derived to described this effect, the oxygen enhancement ratio (OER), is in the

range of 2.5 to 3.5 for conventional X-rays. Studies performed in the early sixties have shown that the OER for neutron beams of different energies is considerably smaller: about 1.5 to 1.8 (17,18). This reduced oxygen enhancement ratio could represent a clinical advantage, especially for those types of tumours which contain a certain fraction of anoxic cells. Subsequent studies with Chinese hamster cells (19) have shown that the OER is rather independent of neutron energy and remains fairly constant up to high neutron energies produced by the p(100)+Be reaction (see figure 4).

Secondly, investigations on the radiosensitivity of cells in different cell cycle stages performed with X-rays have demonstrated that cells in S phase have the lowest radiosensitivity. Radiosensitivity as a function of cell cycle phase is less variable with neutrons than with X-rays (20). The findings of different radiosensitivities in different phases of the cell cycle could be of clinical significance. In the situation where the tumour contains a higher percentage of cells in S phase than do the dose-limiting normal tissues, a higher RBE for tumour response and preferential killing of tumour cells can be expected. The response to neutrons will be less affected by cyclic fluctuations in radiosensitivity; consequently, variations in response from tumour to tumour will be less than observed after irradiation with X-rays.

Thirdly, studies on the survival of a number of normal tissue and tumour cells have shown a large variation in the intrinsic radiosensitivity of these different cell types, which is demonstrated by differences in the slopes of the survival curves, the D_0, and the extrapolation numbers, N, or by the linear and quadratic components, α and β, of the exponential survival curves (7). The survival curves for effects on normal tissues (21) show that there is a great variation in the intrinsic cellular radiosensitivity (see figure 5). Parallel with the investigations on the radiosensitivity of normal tissues, the sensitivity of a number of experimental animal tumour systems has been investigated. Information is now available on the in vitro survival characteristics of a number of animal tumours. Studies on cell cultures derived from an osteosarcoma, a lymphosarcoma, and an ureter carcinoma (22) have shown that these tumours have distinctly different radiosensitivities (see figure 6). For neutrons, the recovery from sublethal

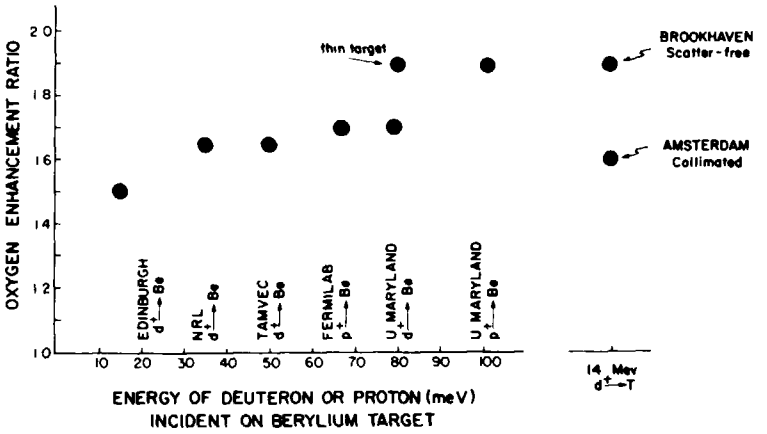

Figure 4. Values of the oxygen enhancement ratio (OER) for various neutron beams produced by the p+Be, d+Be and d+T reactions (19).

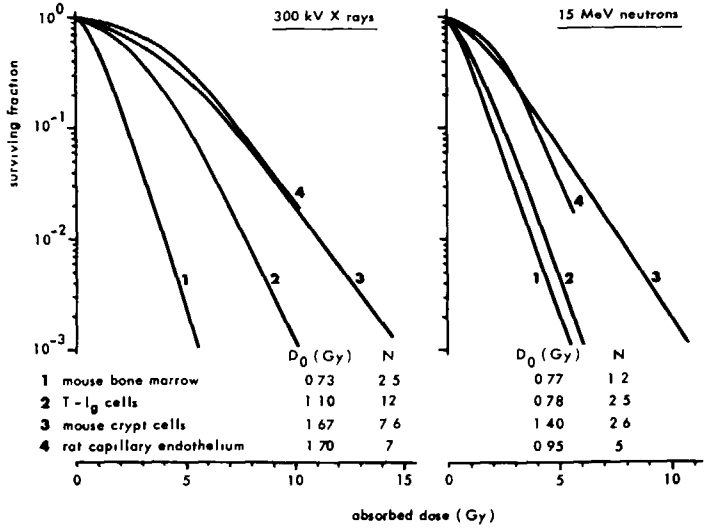

Figure 5. Survival curves of clonogenic cells in different types of normal tissues (21).

damage is reduced and this could have clinical advantages, especially for those combinations of tumours and dose-limiting normal tissues where the survival curve for the tumour cells treated by conventional X-rays shows a larger shoulder.

Theoretical survival curves for normal and tumour cells after X- and neutron irradiation, are shown in figure 7 (23). In the first hypothetical clinical situation where cancer cells are more radiosensitive to X-rays than the cells of the dose-limiting normal tissues, there is no indication to use neutrons. On the contrary there is an advantage for neutrons when cancer cells are more radioresistant to X-rays than the critical normal cell population.

The final assessment of the possible advantages of the use of fast neutrons for radiotherapy has to be based on a comparison of the RBE values for effects on tumours with those for effects on normal tissues. For neutron beams of different energies, extensive information is currently available on the RBE as a function of the neutron dose for

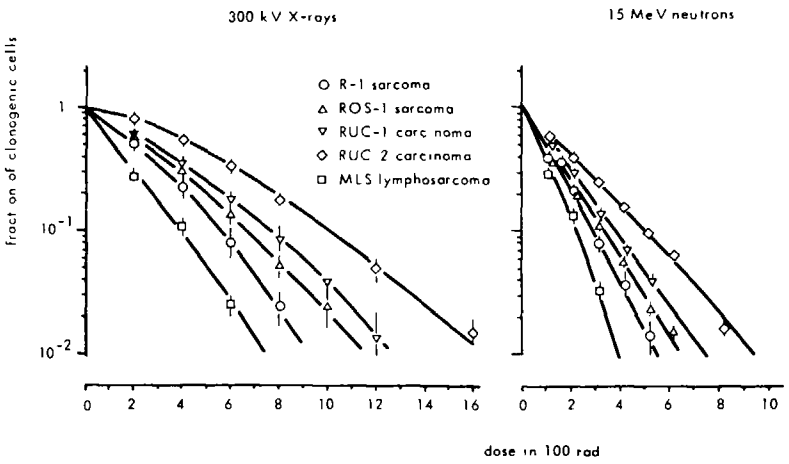

Figure 6. Survival curves of cells in culture derived from different types of animal tumours (22).

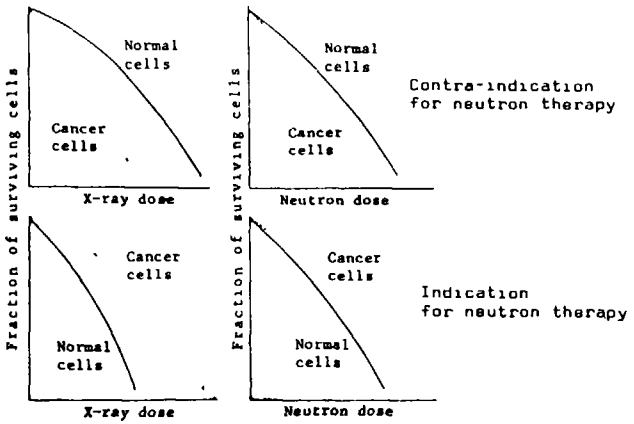

Figure 7. Theoretical survival curves for normal and cancer cells after X- and neutron-irradiation. The only hypothesis is that neutrons reduce the difference in radiosensitivity between cell lines (23).

both normal tissues and experimental tumours. From studies performed with both in vitro and in vivo irradiations of a rhabdomyosarcoma in the rat and an osteosarcoma in the mouse, it was concluded that, for these types of tumours, the RBE values are generally higher than those for effects on normal tissues (see figure 8). Studies by Field and Hornsey (24) have also shown differences between tumour and normal tissue response after irradiation with d(16)+Be neutrons. The fundamental radiobiological findings have stimulated the renewed application of fast neutrons for clinical radiotherapy.

In the preclinical studies, special attention was devoted to the probable occurrence of late tissue reactions. Studies on response of pig skin (25) showed that the RBE of neutrons is continuously increasing with the increasing number of fractions. This increase in RBE means that the neutron doses chosen by Stone et al. (2) on the basis of single-dose effects for X-rays, were too large. Since observations up to five years after neutron treatment did not show any sign of increased late reactions in pig skin, sufficient confidence was gained to try fast

neutrons again in the treatment of cancer. In 1966 new radiotherapeutical irradiations with fast neutrons were started at the Hammersmith Hospital in London. In the years following neutron machines were installed in a number of countries, including Belgium, France, Germany, Japan, the Netherlands, the UK and the USA.

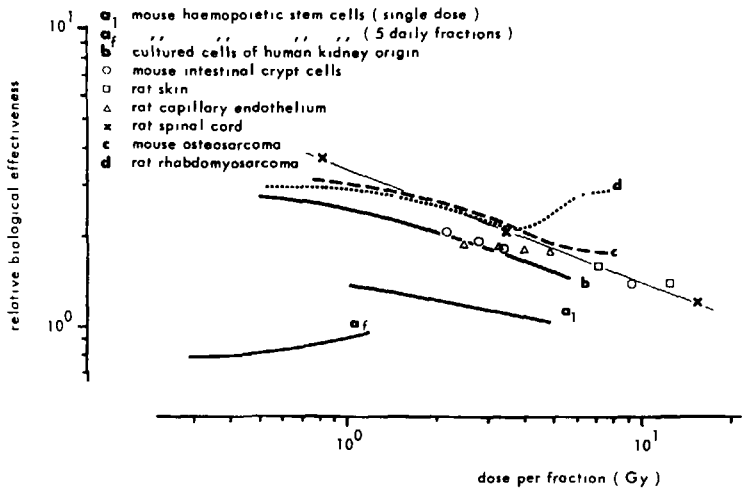

Figure 8. Relation between the relative biological effectiveness (RBE) of 15 MeV neutrons and the neutron dose or daily dose per fraction (21).

5 Clinical results of fast neutron teletherapy

With the aim of investigating the radiation response of different types of tumours, studies were carried out at Rijswijk and Amsterdam on volume changes of pulmonary metastases. A substantial number of patients develop distant metastases in the lungs which are visible and measurable on routine chest X-rays. Observations of the diameter of these lesions show an exponential growth for many of these tumours. Since the introduction of this lung metastases model by Breur (26) data accumulated from 200 patients with a variety of primary tumours show large differences in growth rate. If two or more metastatic foci in the same patient could be treated separately, the effectiveness of different types of radiation could be compared by irradiation of one metastasis with fast neutrons and another with X- or gamma rays (27,28).

From the growth curves, the growth delay and the extrapolated residual volume can be derived and this allows a quantitative evaluation of the effect of the irradiation (see figure 9). For 34 patients, the results of single dose irradiations with d+T neutrons and ^{60}Co gamma rays have been compared and RBE values for volume reduction of pulmonary metastases have been assessed. As shown in figure 10, a wide range of RBE values is derived, with a significant increase in RBE with longer doubling times. For patients with multiple metastases the volume reduction after neutron and photon irradiation allowed a direct assessment of the RBE (closed circles). When only one metastasis was present and the condition of the patient did not allow a second irradiation, an approximate RBE value was derived by assuming that the response to photons would have been similar to that of the group with corresponding volume doubling times (open circles). Radiobiological data and some clinical observations suggest normal tissue RBE values of about three at these dose levels for 14 MeV d+T neutrons relative to gamma rays. This implies that only for a proportion of patients can a therapeutic gain be expected from neutron treatment. It can be concluded from figure 10 that tumours with volume doubling times in excess of 100 days may benefit from high LET radiation. Battermann et al. (28) concluded that the RBE for slowly growing tumours which are generally welldifferentiated will be higher than that for poorly differentiated lesions. More radiobiological and clinical investigations will be required to decide which tumours will benefit most from high LET radiation; the lung metastases model may be helpful in this selection.

Neutron radiotherapy with curative intent started in 1969 in London with the MRC cyclotron. Due to the poor physical characteristics of he 6.7 MeV fast neutron beam at Hammersmith Hospital, the first neutron treatments were focused on rather superficial lesions, such as head and neck tumours, brain tumours, breast tumours, and skin lesions. The first report on results of a randomized clinical trial of fast neutrons in comparison with X- or gamma-rays in the treatment of advanced tumours of the head and neck indicated an appreciable advantage for the neutron

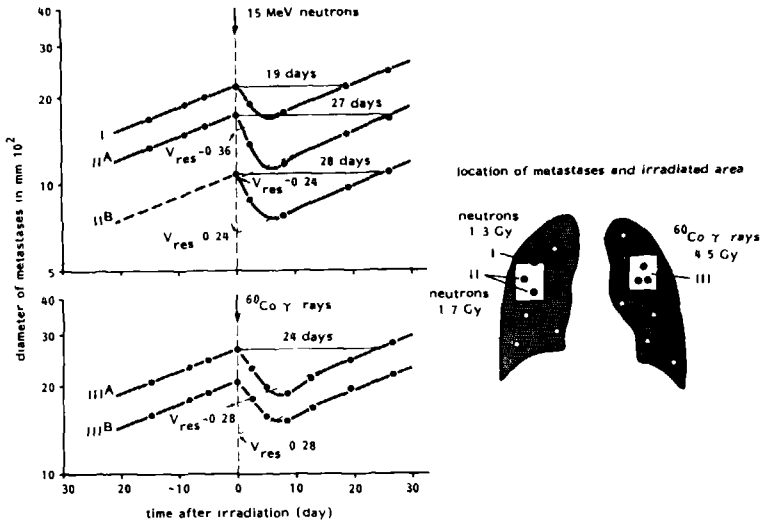

Figure 9. Variation of the diameters of metastases in a patient with an embryonal carcinoma of the testicle after irradiation with 15 MeV neutrons or gamma-rays from ^{60}Co. The values of the residual volume, V_{res}, and the growth delay are indicated (27).

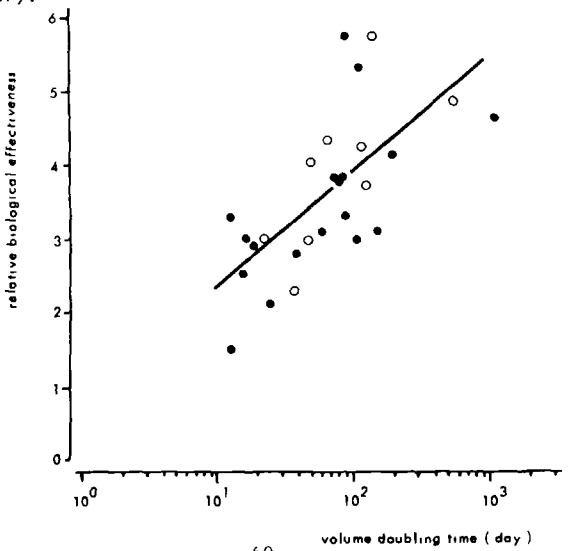

Figure 10. RBE values relative to ^{60}Co gamma-rays for volume changes of pulmonary metastases as a function of the volume doubling time (28).

irradiated groups (29). These good results in the treatment of head and neck made malignant lesions in this, region of the body of particular.

The clinical results of fast neutron therapy, which have been reviewed regularly (30-32), vary according to the method of application and the type of cancer involved. A randomized trial on locally advanced head and neck tumours performed at Houston (33) with d(50)+Be neutrons shows a slight superiority for mixed-beam irradiation (twice weekly with neutrons and three times weekly with photons). The local control and survival rates for patients treated with the mixed beam irradiation were greater than those achieved with photons (see figure 11) although the difference in local control rates was not statistically significant. Employing a d+T neutron beam Batterman and Breur (34) could not demonstrate an advantage for locally advanced head and neck cancer with reference to photons (see figure 12).

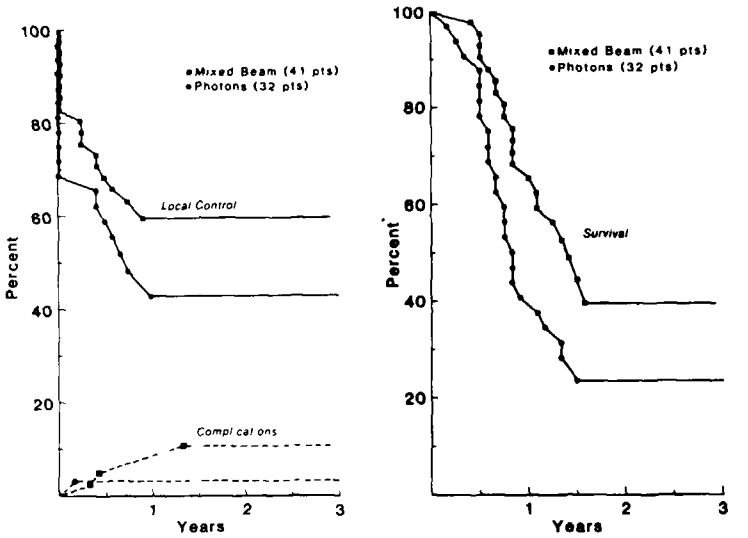

Figure 11. Actuarial local control and complication rates (left panel) and survival curves (right panel) for patients with head and neck cancer in a randomized trial at Houston (33).

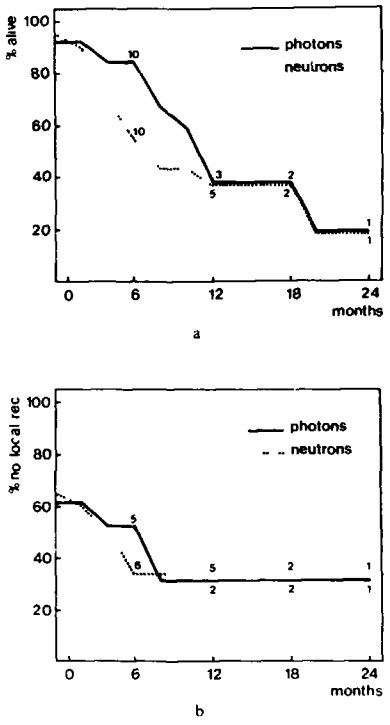

Figure 12. Actuarial curves for patient survival (panel 1) and local tumour control (panel b) for locally advanced head and neck tumours treated with 15 MeV neutrons or photons (34).

An interim analysis of a clinical trial of certain cancers of the oral cavity, pharynx and larynx performed at Edinburgh with d(15)+Be neutrons has failed to demonstrate differences in tumour control following neutron therapy compared with X-ray therapy (35). This is in contradiction with the earlier Hammersmith results (29) where a highly significant improvement in local tumour control was observed after irradiation with cyclotron neutrons with a neutron beam of closely similar quality. Because of these apparent inconsistencies the two trials have been subjected to a comparative review (36). Important aspects in which the clinical applications have differed include the stage of the disease, radiation dosage, and differences in treatment techniques. Another difference is that the 'photon arm' of the Edinburgh trial was performed on site whereas that at Hammersmith was carried out at various hospitals in the London area.

Multicenter neutron therapy trials have been organized in Europe through the EORTC High LET Therapy Group (37) and in the United States through the Radiation Therapy Oncology Group (38). After the initial great expectations, the prospectives for the usefulness of fast neutron radiotherapy are now more modest. Concerning the applicability of neutrons for the treatment of different tumour types a number of conclusions (39) can be formulated:

1) for salivary gland tumours, neutrons are the treatment of choice.
2) for soft tissue sarcomas (especially when they are slowly growing and well-differentiated) and prostatic carcinomas, advantages have been demonstrated in the majority of trials.
3) As far as head and neck tumours, rectal and cervix carcinomas are concerned neutrons have shown advantages in some trials but not in others.

It should be realized that most neutron radiotherapy studies have been handicapped by a number of factors, including suboptimal dose distribution due to the low neutron energy or the large penumbra; suboptimal fractionation resulting from lack of cyclotron availability; and suboptimal positioning of patients due to fixed horizontal beams and too low dose rates. Despite these difficulties, a number of interesting clinical data have become available and it has to be stressed that, because of these handicaps, the possible advantages of fast neutron therapy are probably underestimated for many tumour sites. Improvement in the dose distributions will be indispensable for making the best use of high LET radiation therapy. As indicated in figure 13 only with cyclotrons accelerating protons or deuterons to energies in excess of 50 MeV, the neutron beams have depth dose characteristics comparable to those of megavoltage X-rays (40). A number of high energy cyclotrons and linear accelerators constructed for specific medical purposes have recently been put into operation or are near completion. Some of the most important characteristics of these cyclotrons are summarized in table 3. The notation p(42)+Be(15) describes the reaction of 42 MeV protons bombarding a beryllium target in which the protons lose only 15 MeV.

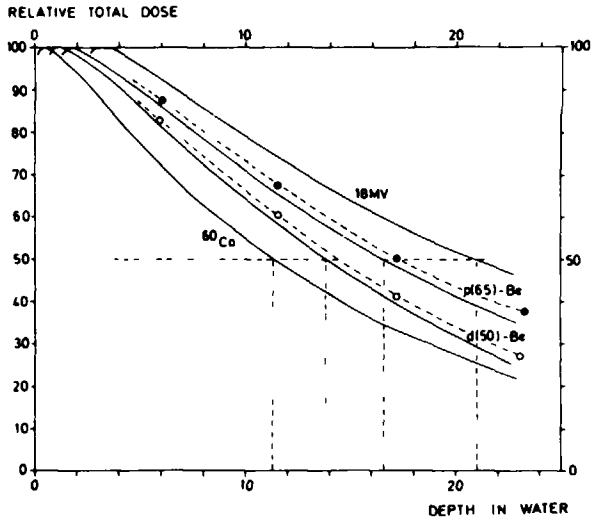

Figure 13. Depth dose curves for different beam qualities for a 10 cm x 10 cm field. The relative total dose is given in per cent for measurements in water (solid lines) and TE liquid (broken lines), and the depth in cm (40).

Table 3

CHARACTERISTICS OF SOME HIGH ENERGY ACCELERATORS EMPLOYED FOR FAST NEUTRON THERAPY

site	reaction employed	dose rate ($mGy\ min^{-1}$) at 2 m distance	gamma contamination (%) free-in-air	gamma contamination (%) at 20 cm depth	depth (cm) for 50% of maximum dose for 20 cm x 20 cm field
Batavia	p(66)+Be(49)	400	5	-	16
Houston	p(42)+Be(15)	120	5	20	16
Liverpool	p(62)+Be(36)	276	2	5	19
Los Angeles	p(46)+Be(26)	460	5	-	15
Louvain	p(65)+Be	149	-	6	17.5
Seattle	p(50)+Be(25)	225	-	8	15

6. Neutron brachytherapy and boron capture therapy

A compact source of fission neutrons which can be implanted into tissues for brachytherapy in a similar way as done with gamma-emitting sources is ^{252}Cf (half-life of 2,65 years). An assortment of californium sources is available either in applicator tubes intended for intracavitary treatments whereas needles, cells and seeds are designed for interstitial implantation (8). For an adequately encapsulated ^{252}Cf source (0.7 mm Pt) the ratio of neutron to gamma-ray absorbed dose at 1 meter from the source in free air is approximately equal to 2. When the source is embedded in tissue, the gamma-ray component will account for an increasingly significant part of the absorbed dose at larger distances.

Brachytherapy with ^{252}Cf sources has mainly been applied for treatment of tumours of the oral cavity and gynaecological tumours (41). For these types of cancers a rapid regression has been observed at Obninsk, significantly faster than after photon therapy. At Lexington promising results with a low complication rate were reported for patients with advanced cervix carcinoma. Treatment of tumours of the oral cavity with high intensity Cf sources at Tokyo have shown survival rates which are not clearly different from those expected after external irradiation. Biological considerations (42, 43) suggest caution in the clinical application of ^{252}Cf. For a number of radiobiological endpoints the RBE values for Cf show wide variations e.g. between 3 and 10. In the low dose region outside the treatment volume in interstitial implants with californium, an increase in relative biological effectiveness is to be expected. It can not be predicted in how far this effect will increase the risks for normal tissue complications.

The potentialities of neutron capture therapy have been recognized since long time (44, 45). The underlying principle is that stable nuclides with large cross sections for the absorption of slow neutrons have to be located in the tumour. The products of the neutron capture reaction should have a short range in tissue to provide a high local energy deposition. In view of the high cross section for the $^{10}B(n,\alpha)^{7}Li$ reaction most interest has centered on the use of this stable isotope. Clinical trials of neutron capture therapy performed at

Brookhaven National Laboratory and Massachusetts General Hospital, Boston, were terminated in the early sixties since the average survival of patients was not prolonged in comparison with conventional therapy. The adverse results were attributed to the poor penetration of the thermal beams used and the fact that the water-soluble boron compounds were not selectively localized in the tumour. Intense beams of intermediate energy neutrons can now be produced by using interchangeable filters in the beam tubes of high flux reactors (46). In the search for suitable methods of concentrating the boron in the tumour (47) including the development of tumour-specific monoclonal antibodies (48), significant improvements have been accomplished. Clinical applications at Tokyo with new boron compounds have shown evidence (49) that slowly growing brain tumours may benefit from boron neutron capture therapy (BNCT). Additional studies on the pharmacology of these compounds and the effective dose distribution of neutron beams of various energies have to be performed before initiation of clinical trials on the therapeutic efficacy of BNCT.

7. Conclusions

Neutron beams of different energies offer specific features for biomedical applications. This is due to their high-LET characteristics including their capacity of activating the irradiated material. In vivo neutron analysis can be employed for the detection of insufficiencies in the normal distribution of selected elements in certain organs or of undesirable accumulation of toxic agents in the human body during industrial occupation. The subjects are exposed to relatively low absorbed doses of neutrons and the induced radioactivity is measured either subsequently or immediately by analysis of prompt gamma radiation. A number of elements, e.g. cadmium, calcium, phosphorus, sodium, chlorine, oxygen and nitrogen can be determined employing total and partial body irradiations (50, 51). However, the number of reports on this application is strongly diminishing which might be attributed to the increased concern about the potential hazard from exposure to low doses of fast neutrons (52, 53).

Under the conditions of delivering a prescribed dose of neutrons (neutron teletherapy with high energy cyclotrons) or of charged secondaries (boron neutron capture therapy) to the tumour volume with significant damage to critical normal tissues, beneficial effects can be expected. Considering the shortcomings of conventional radiations for the cure of certain malignant lesions, high-LET neutrons could provide an effective additional utensil for cancer treatment.

Acknowledgement

The cooperation of Dr. D. Bonnett (London), Dr. J. Eenmaa (Seattle), Dr. J.C. Horton (Houston), Dr. A.J. Lennox (Batavia), Dr. J.B. Smathers (Los Angeles and Dr. S. Vynckier (Louvain) in kindly providing the information on the characteristics of the high energy neutron sources and the assistance of Mrs. J.E. Legué-Smit in the preparation of the manuscript are gratefully acknowledged.

References

1. Broerse, J.J., Lyman, J.T. and Zoetelief, J. In: The Dosimetry of Ionizing Radiation. Vol. I. Kase, K.R., Bjarngard, B.E. and Attix, F.H. (eds). Academic Press, Orlando, 229-291 (1985).
2. Stone, R.S., Lawrence, J.H. and Aebersold, P.C. Radiology 35, 322, (1940).
3. Field, S.B., Curr. Top. Rad. Res. Quart. 11, 1 (1976).
4. ICRU Report 33. Radiation Quantities and Units. ICRU, Washington (1980).
5. Rossi, H.H. In: Radiation Dosimetry. Attix, F.H. and Roesch, W.C. (eds). Academic Press, New York, 43-92 (1968).
6. Fowler, J.F. Nuclear Particles in Cancer Treatment. Adam Hilger Ltd, Bristol (1981).
7. ICRU Report 30. Quantitative Concepts and Dosimetry in Radiobiology. ICRU, Washington (1979).
8. ICRU Report 26. Neutron Dosimetry for Biology and Medicine. ICRU, Washington (1977).

9. Broerse, J.J., Mijnheer, B.J. and Williams, J.R., Brit. J. Radiol. 54, 882 (1981).
10. IRCU Report 27. An International Neutron Dosimetry Intercomparison. ICRU, Washington (1978).
11. Broerse, J.J., Burger, G. and Coppola, M., A European Neutron Dosimetry Intercomparison Project (ENDIP), Results and Evaluation, Commission of the European Communities, EUR 6004, Luxembourg (1978).
12. Almond, P.R. and Smathers, J.B. Int. J. Radiat. Oncol. Biol. Phys. 3, 169 (1977).
13. Broerse, J.J. and Mijnheer, B.J. Int. J. Radiat. Oncol. Biol. Phys. 8 2049 (1982).
14. Zoetelief, J. and Schraube, H. Proc. Fifth Symposium on Neutron Dosimetry, EUR 9762, CEC, Luxembourg, 1179-1190 (1985).
15. Broerse, J.J. (ed.) Ion Chambers for Neutron Dosimetry. EUR 6782, Harwood Academic Publishers, London (1980).
16. AAPM. Protocol for Neutron Beam Dosimetry. Task Group no. 18, AAPM Report no. 7, American Association of Physicists in Medicine (1980).
17. Broerse, J.J. and Barendsen, G.W., Nature 206, 208 (1963).
18. Fowler, J.F., Curr. Top. Rad. Res. 2, 303 (1966).
19. Hall, E.J. and Kellerer, A. Eur. J. Cancer Suppl., 171 (1979).
20. Withers, H.R., Strahlentherapie 161, 739 (1985).
21. Broerse, J.J., Barendsen, G.W., Gaiser, J.F. and Zoetelief, J. In: Radiobiological Research and Radiotherapy, Vol. II (International Atomic Energy Agency, Vienna), 19 (1977).
22. Barendsen, G.W. and Broerse, J.J., Int. J. Radiat. Oncol. Biol. Phys. 3, 211 (1977).
23. Wambersie, A, Barendsen, G.W. and Breteau, N. J., Eur. Radiother. 5, 248 (1984).
24. Field, S.B. and Hornsey, S., Eur. J. Cancer 7, 161 (1971).
25. Bewley, D.K., Field, S.B., Morgan, R.L., Page, B.C. and Parnell, C.J., Brit. J. Radiol. 40, 765 (1967).
26. Breur, K., Eur. J. Cancer 2, 157 (1966).
27. Peperzeel, H.A. van, Breur, K., Broerse, J.J. and Barendsen, G.W., Eur. J. Cancer 10, 349 (1974).,
28. Battermann, J.J., Breur, K., Hart, A.A.M. and Peperzeel, H.A. van., Eur. J. Cancer 17, 539 (1981).
29. Catterall, M., Sutherland, I. and Bewley, D.K., Br. Med. J. 2, 653 (1975).
30. Barendsen, G.W., Broerse, J.J. and Breur, K. (eds.). High-LET Radiations in Clinical Radiotherapy. Pergamon Press, Oxford (1979).
31. Broerse, J.J. and Battermann, J.J., Med. Phys. 8, 751 (1981).
32. Hall, E.J., Graves, R.G., Phillips, T.L. and Suit, H.D. (eds), Particle Accelerators in Radiation Therapy, Pergamon Press, New York (1982).
33. Maor, M.H., Hussey, D.H., Fletcher, G.H. and Jesse, R.H., Int. J. Radiat. Oncol. Biol. Phys. 7, 155 (1981).
34. Battermann, J.J. and Breur, K., J. Eur. Radiother. 2, 27 (1981).
35. Duncan, W., Arnott, S.J., Orr, J.A. and Kerr, G.R., Int. J. of Radiat. Oncol. Biol. Phys. 8, 2155 (1982).
36. MRC Neutron Therapy Working Group. British Journal of Radiology, 59, 429 (1986).
37. Wambersie, A. and Battermann, J.J., Strahlentherapie 161, 746 (1985).
38. Peters, L.J., Maor, M.H., Laramore, G.E., Griffin, Th.W. and Hendrickson, F.R., Strahlentherapie 161, 731 (1985).
39. Fowler, J.F., Strahlentherapie 161, 804 (1985).
40. Vynckier, S., Pihet, P., Octave-Prignot, M., Meulders, J.P. and Wambersie, A., Acta Radiologica Oncology 21, 281 (1982).
41. Kal, H.B., Nuclear Science Applications, (1986) in press
42. Fairchild, R.G., Atkins, H.L., Drew, R.M. and Robertson, J.S., Europ. J. Cancer 10, 305 (1974).
43. Nias, A.H.W., Europ. J. Cancer 10, 301 (1974).
44. Sweet, W.H., Soloway, A.H. and Wright, R.L., J. Pharmacol. Exp. Ther. 137, 263 (1962).
45. Archambeau, J.O., Alcober, V., Calvo, W.G. and Brenneis, H. In: Biological Effects of Neutron and Proton Irradiatons, Vol. II. 55, IAEA, Vienna (1964).

46. Harvey, J.R. and Mill, A.J. In: Proc. of the Fourth Symposium on Neutron Dosimetry. EUR 7448, CEC, Luxembourg, 431 (1981).
47. Larsson, B., Gabel, D. and Borner, H.G., Phys. Med. Biol. 29, 361 (1984).
48. Soloway, A.H., Alam, F. and Barth, R.F. In: Proc. Workshop on Neutron Capture Therapy, Brookhaven National Laboratory, 162 (1986).
49. Sweet, W.H. In: Proc. Workshop on Neutron Capture Therapy, Brookhaven National Laboratory, 3 (1986).
50. IAEA. Neutron Activation Analysis, IAEA, Vienna (1973).
51. IAEA. Nuclear Activation Techniques in the Life Sciences. IAEA, Vienna (1979).
52. ICRU Report 40. The Quality Factor in Radiation Protection. ICRU, Washington (1986).
53. Broerse, J.J., Hennen, L.A. and Zwieten, M.J. van, Int. J. Radiat. Biol. 48, 2, 167 (1985).

SESSION VII

GENERAL INTEREST SESSION

SPALLATION SOURCES FOR NEUTRON NUCLEAR PHYSICS

C D BOWMAN
Los Alamos National Laboratory,
Los Alamos, New Mexico,
United States of America

Abstract

New intense pulsed spallation neutron sources have come on line within the past few years at the Argonne National Laboratory the KEK Laboratory the Rutherford Appleton Laboratory and the Los Alamos National Laboratory While the construction of new spallation sources is driven primarily by condensed matter physics studies using thermal and epithermal neutrons these sources also may provide excellent opportunities for neutron nuclear physics research Essentially all spallation sources produce microsecond wide bursts for work in the keV region and below and offer the potential to produce intense sources of nanosecond wide neutron bursts for the MeV range The useful spectrum runs potentially from 10^{7} to 10^{+9} eV if full advantage is taken of spallation source technology The properties of the source configuration used throughout this energy range are discussed and illustrated using the Los Alamos Proton Storage Ring (PSR) Facility as an example The primary impact of the spallation neutron source is an intensity gain often several orders of magnitude over existing neutron source technology The new neutron physics possible is discussed in some depth and illustrated with the first examples of measurements over much of the energy range Finally future prospects are described promising for the foreseeable future increases in intensity of perhaps an order of magnitude beyond present technology

---

I INTRODUCTION

The past several years have seen major increases in neutron intensity through improvements in spallation neutron source technology These intensity advances are driven primarily by the extraordinary promise of intense pulsed neutrons for study of condensed matter physics The primary purpose of this paper is to draw attention to the opportunities for neutron nuclear physics using the new sources For some energy regions effective neutron intensities have increased by several orders of magnitude over that available a decade ago

Thus experiments which then were unquestionably impractical may now be feasible

Neutron nuclear physics and neutron scattering for condensed matter at the same facility have not always been good bed partners usually for reasons which are more cultural than scientific However if the two disciplines can work together a broader research base is established for making the next advance in source intensity Although this conference emphasizes modest neutron sources the field should be aware of prospects for neutron physics at the major central neutron facilities Advances in neutron physics with the most intense sources almost certainly will open up new vistas for research and instrumentation or technique development using more modest sources It may well be true that the future of research at the smaller facilities is directly tied to the health of neutron physics at the larger facilities In this report we will review opportunities for neutron nuclear physics at spallation sources with the purpose of encouraging the growth of such research and the resulting enhancement of neutron physics wherever it can be done

II SPALLATION NEUTRON SOURCES

Condensed matter physics using pulsed neutrons requires a spallation source with proton energy of several hundred MeV and a pulse width of a few tenths of a microsecond The proton burst is produced in two stages First protons are accelerated in an r f linac to an energy of at least 100 MeV This beam is accumulated in a ring possibly accelerated to considerably higher energy and then dumped in one circuit of the ring Inside the ring the beam may be in a continuous ribbon or it may be bunched into several pulses In the latter case the individual pulses can be ejected one at a time and pulse widths of a few nanoseconds or less are practical Presently the maximum average current which can be ejected from such a ring is about 100 microamperes of protons and the maximum energy is about 800 MeV The pulse rate is generally 50 Hz or less

Such a system also can provide intense subnanosecond bursts of protons from the linac used to inject protons into the ring[1] The linac ordinarily produces a string of subnanosecond wide bursts spaced by about 5 nanoseconds If only one in 200 of these bursts were injected into the accelerator then these bursts would be produced with a spacing of about 1 microsecond which is a useful spacing for higher MeV range neutron physics experiments Since an r f linac can simultaneously accelerate both negative and positive ions on opposite phases of the r f wave the linear accelerator can supply H beam to the storage/accelerator ring and simultaneously subnanosecond wide proton bursts spaced by about one microsecond to a target providing a white neutron spectrum for MeV neutron nuclear physics

Presently this approach is only being implemented at the new neutron facilities associated with LAMPF at Los Alamos which are illustrated in Fig 1

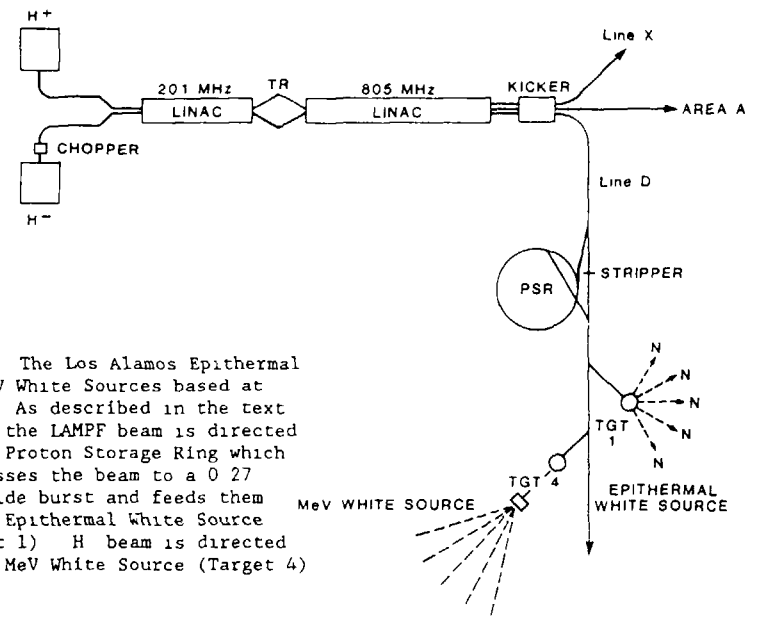

Fig. 1 The Los Alamos Epithermal and MeV White Sources based at LAMPF As described in the text 10% of the LAMPF beam is directed to the Proton Storage Ring which compresses the beam to a 0 27 μsec wide burst and feeds them to the Epithermal White Source (Target 1) H beam is directed to the MeV White Source (Target 4)

Two injectors are shown injecting oppositely charged beams into one linac The two injectors operating at 200 MHz produce strings of r f bursts spaced by 5 nanoseconds and lasting for about 850 microseconds at a rate of 120 strings per second Ten percent of these strings consists of H beam injected into the accelerator and accelerated to 800 MeV before injection into the Proton Storage Ring Approximately 60% of these strings consist of ^{+}H beam accelerated to 800 MeV for pion physics studies However chopped H beam of low current also can be accelerated simultaneously with the ^{+}H beam and magnetically separated at the output of the accelerator This sequence of H bursts with widths as short as 150 picoseconds bypasses the storage ring and strikes a several centimeters

thick tungsten target to produce a white source of neutrons. For a one microsecond wide spacing, the average current is about 3 microamperes. This current might be doubled by bunching twice as many protons into each r.f. burst. The neutron production target and drift tube arrangement has undergone a rapid evolution since this approach was first recognized[1]; the final geometry being implemented is close to that reported by Lisowski[2] *et al.* and is shown in Figs 2 and 3.

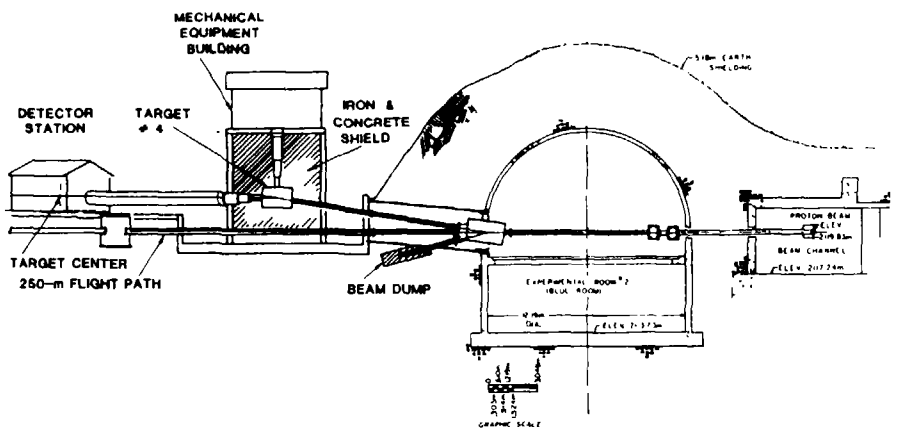

Fig. 2 Side View of Beam Transport and Target 4. Microbursts of 800 MeV protons may be directed at targets located at the center of Target 2 which is viewed by reversed neutron drift tubes. Alternatively it can be bent upward to Target 4 which is the new MeV White Source viewed by additional drift tubes. The two sets of drift tubes are at different elevations so that they do not intersect. The proton beam will usually be directed at Target 4.

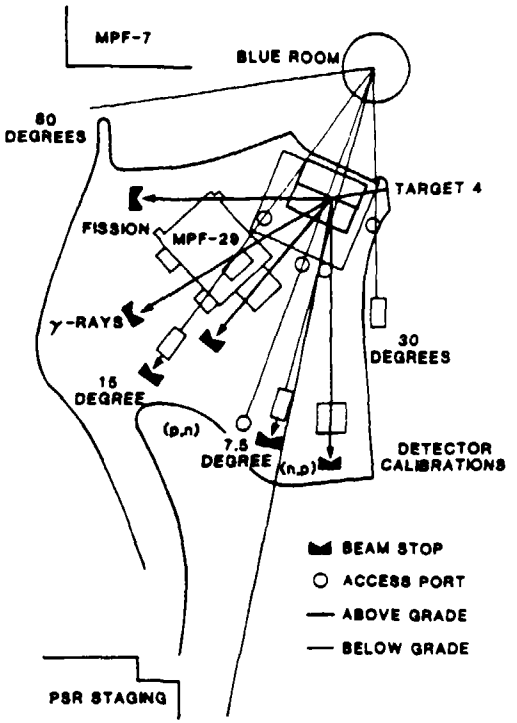

Fig. 3 Neutron Drift Tubes for MeV Neutrons. Four drift tubes are now in planning for use with Target 2 (Blue Room) Five additional drift tubes are under construction for viewing Target 4. An unevacuated neutron beam line extends to 250 meters for (p,n) measurements on neutrons with energies near 800 MeV.

Although constructed parasitically to the PSR and operating parasitically on the primary pion production mode of LAMPF, this white source will be the most intense in the world for neutron physics in the 3 to 500 MeV range. Some of the science which will be conducted with this facility will be presented later in this report. Neutron physics in the MeV range could be very substantially boosted at low cost by the introduction of this concept early in the design phase of new accelerators for neutron scattering studies in condensed matter physics.

The production of pulsed neutrons for condensed scatter physics studies is well developed[3] and will not be discussed in detail. We only mention that the current generation of pulsed neutron sources, while competitive with the world's best reactor sources for some thermal experiments, is clearly superior for the production of epithermal neutrons[4]. The presence of moderators tailored for epithermal neutrons at such sources offers extraordinary intensity gains over electron linacs in the region below 100 eV and competitive intensities up to several tens of keV. The combination of the pulsed source with doppler shifted energy reduction[5] for producing ultracold neutrons is highly effective. The spallation source is useful over much of the 10^{-7} to 10^{+9} eV energy range.

Electron linacs are competitive in the 10 keV to 10 MeV range and monoenergetic beams from lower energy accelerators also remain competitive in the same energy range The reactor will probably maintain its role in the thermal neutron region for the foreseeable future Nevertheless, where spallation sources excel, they excel markedly over the competition

A summary of early, existing, and proposed spallation sources are listed in Table I along with source characteristics of interest for the energy region from 10^{-2} to 10^{4} ev. The average intensity of the early and existing spallation sources is shown in Fig. 4. It is intriguing to note the exponential growth in

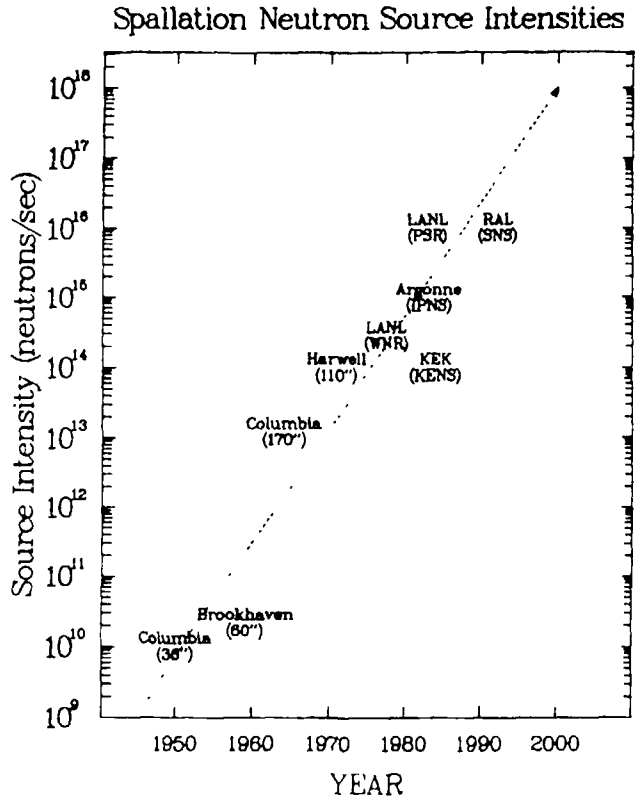

Fig. 4 Spallation Neutron Source Intensities The advance in intensity of spallation neutron sources for the production of epithermal neutrons is shown for the past 30 years The intensity is the total neutron production averaged over one second

Table I

Spallation Sources for Slow Neutron Spectroscopy

Facility	Proton Energy (MeV)	Proton Pulse Width (nsec)	Repetition Rate (Hz)	Average Neutron Rate (neutron/sec)	Reference
			Early		
Columbia 36" Cyclotron	8	2000	60	7.2×10^{9}	Havens & Rainwater[6]
Brookhaven 60" Cyclotron	21	1000	60	1.8×10^{10}	Havens[7]
Columbia 170" synchrocyclotron	385	20	60	$1\ 9 \times 10^{13}$	Havens[8]
Harwell 110" Synchrocyclotron	150	4	800	$9\ 6 \times 10^{13}$	Rae & Good[9]
Los Alamos WNR	800	5000	120	3×10^{14}	Woods[10]
			Existing		
Kek Kens	500	50	16	2×10^{14}	Sasaki[11]
Argonne IPNS	500	250	30	1.2×10^{15}	Lander[12]
Los Alamos PSR	800	270	12	1×10^{16}	Bowman[13]
Rutherford-Appleton, SNS	800	500	50	1×10^{16}	Manning[14]
			In Planning or Construction		
Argonne Aspun	1100	500	50	2×10^{17}	Khoe[15]
KeK Gemini	800	500	50	5×10^{16}	Sasaki[16]
Oak Ridge Liric	250	5	5000	1×10^{15}	Olsen[17]
NBS Induction linac	100	100	1000	7.5×10^{14}	Johnson[18]
Meson Factory USSR, Accumulator Ring	600	200	100	3.5×10^{16}	Lobashev[19]

intensity with time particularly the implications of extrapolation to the future Among the facilities under consideration for the future, four contain high power r f linacs operating as follows Aspun (200 MeV) Gemini (80 MeV) Liric (250 MeV) and the USSR Meson Factory (600 MeV) Each of these therefore could provide excellent capability for MeV neutron physics as well as the high intensity epithermal beams which presently are a primary objective

The induction linac under consideration by the NBS is a substantially different concept The accelerator consists of a string of induction modules which each add 0 25 MeV to the beam energy The phase relationship among them can be individually controlled so that any particle can be accelerated The impedance of each unit is small so that high currents can be accelerated The present plan includes peak currents of 250 A of electrons space charge effects limit the proton current to about 2 5 A Power efficiency is lower them the r f linac and the gradient is lower at about 1 25 meters/MeV As a white neutron source the facility can operate with either electrons or protons producing about equal neutron intensity Any proton beam energy can be obtained by accelerating to that energy and drifting the beam through the remaining sections Therefore the accelerator can serve as both a white source and a variable monoenergetic source of neutrons via the (p n) reaction The technology is new and unproven in the high repetition rate mode and a few MeV prototype for technology demonstration is required

III NEUTRON PHYSICS

Progress in neutron physics has been influenced strongly by the availability of adequate neutron intensity for challenging experiments for different energy ranges For many years the field has been dominated by ion beam facilities and electron linacs which have produced effective neutron intensity for the keV and lower MeV range While exciting work will continue to be done with these established sources, the spallation source provides intensity which should allow major research advances in other energy ranges Los Alamos has established new facilities for this work which should become fully operational this year Hopefully the description of some of the research either under way or under consideration at Los Alamos will serve as at least an introduction to the new science which the spallation sources makes possible Current problems in both basic and applied science will be included

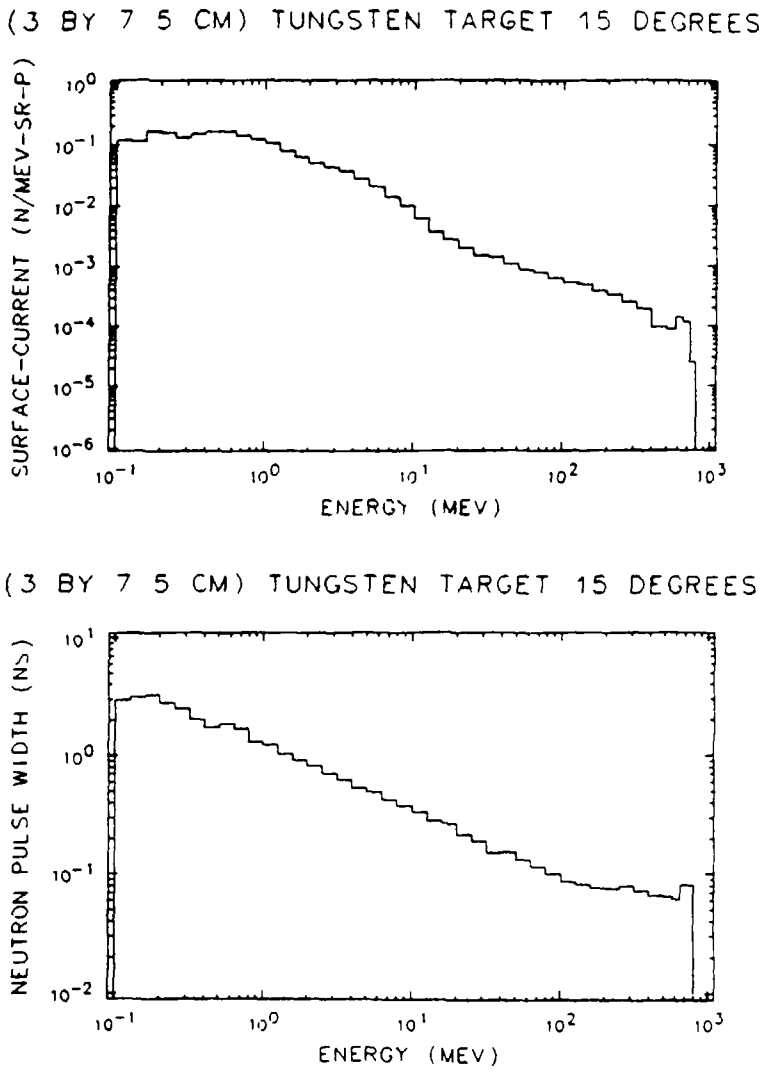

Fig. 5 Properties of the MeV White Neutron Source
a) The surface current is given as neutrons/MeV sr proton as a function of neutron energy
b) The standard deviation of the gaussian neutron pulse width in nanoseconds is given assuming the best micropulse width measured of 150 picoseconds (FWHM) To obtain the full width at half maximum multiply the ordinate by 2 35

A. 3-500 MeV Range

The spectrum of neutrons at forward angles[20] produced by 800 MeV protons as calculated by an intra-nuclear cascade code is shown in Fig 5a; the standard deviation of the timing uncertainty is given in Fig 5b. An important point to note is the shelf which extends to about 500 MeV. Fig 6 shows the flux comparison[2] with ORELA when the flight path is adjusted for any energy to give a resolution of about $\Delta E/E = 10^{-2}$ A five-ns pulse is assumed for ORELA and a one-ns pulse for Los Alamos Clearly Los Alamos should concentrate its program above 3 MeV where the neutron intensity advantage over ORELA is very large

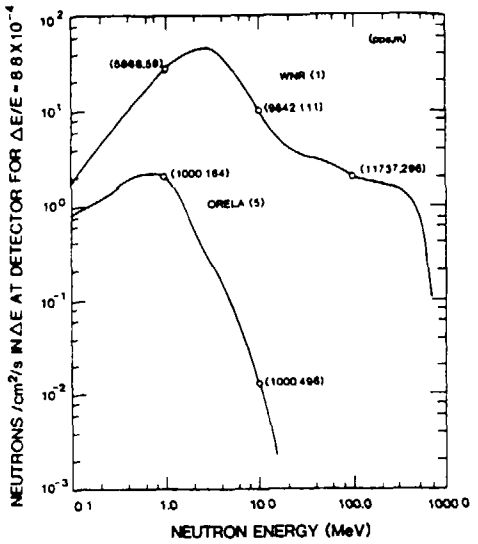

Fig. 6 Comparison of neutron flux at the WNR MeV White Source with ORELA. The burst widths assumed are one nanosecond for the WNR and five nanoseconds for ORELA. The first number is parenthesis is the pulse rate assumed and the second is the flight path length in meters

1 (n,γ) and (n,γγ)

The high intensity, high repetition rate and low γ-flash make this a powerful facility for neutron capture and neutron induced gamma ray production studies. As an example, we show in Fig. 7 data on $^{40}Ca(n,\gamma_0)$ which clearly exhibits the E-1 giant dipole resonance This spectrum was measured[21] using spallation neutrons at our earlier source associated with the WNR in about twelve hours. The intensity of the new source will be about 100 times that used for the $^{40}Ca(n,\gamma_0)$ experiment Using bismuth germanate detectors, which provide sufficient resolution to resolve particular final states in many cases, it should be possible to explore giant resonance phenomena in great detail by this technique

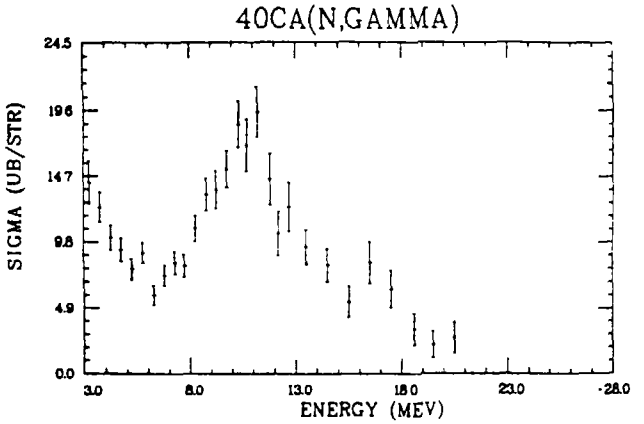

Fig 7 The Cross Section for the $^{40}Ca(n,\gamma_0)$ reaction. This data was measured in about 12 hours by Wender[21] *et al.* using the earlier white source facilities at the WNR. The peak at MeV is the E-1 giant dipole resonance. With the new white source data rates will be higher by a factor of more than 100.

2 (n,p) Reactions

The study of (p n) reactions has been a major program at the Indiana University Cyclotron again directed at the study of a variety of excitation modes of the nucleus The white source is sufficiently intense to allow study of the complementary (n,p) reactions Time of flight can be used to define the incoming neutron energy and trajectory analysis and total energy deposition used to determine the energy and angular distribution of the protons The detector to be used for these experiments[22] is similar to that shown in Fig 8 The neutron intensity at WNR Target 4 should allow a quality of data comparable with that obtainable for (p,n) reactions

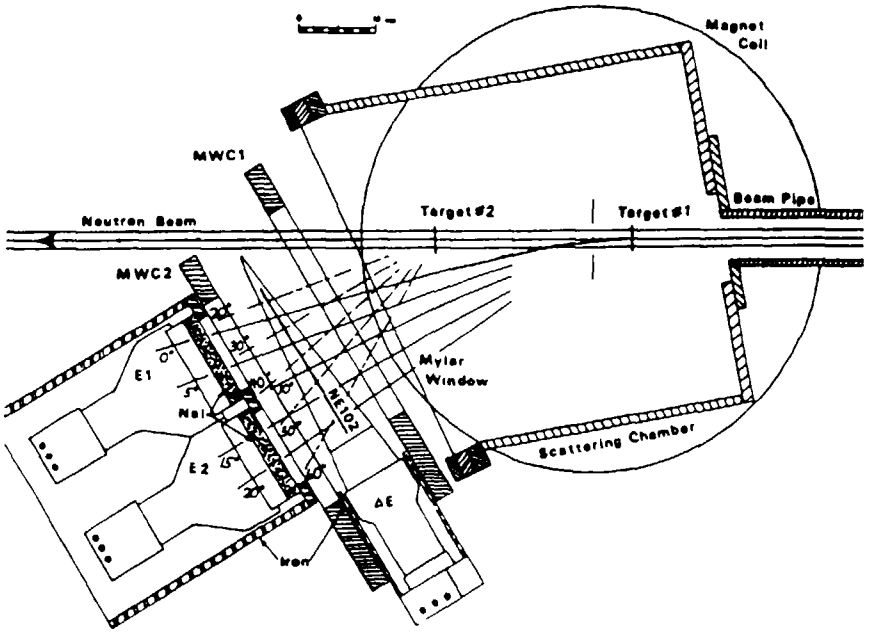

Fig. 8 The detector for MeV (n,p) experiments using a white neutron source will be similar to that shown here Using magnetic field multiwire position sensitive detectors, and the ΔE detector trajectory analysis allows the proton energy and angular distribution to be determined The neutron energy is determined by time-of flight

3 (n,f) Reactions

Accurate neutron fission cross section measurements in the 3 to 20 MeV region have been difficult to obtain using the best of the electron linac white sources owing to insufficient intensity and the strong energy dependence of the flux The National Bureau of Standards will begin a high accuracy measurement on the $^{235}U(n\ f)$ standard cross section at Los Alamos in 1986

4 Total Cross Sections

This source also will probably be used for some high resolution and high accuracy total cross sections The pulse width of 0 25 nsec will be preserved in a 2-cm thick target, with a flight path of 250 meters the resolution might be better than 0 5 MeV at 500 MeV Although no source of fine structure is known at these high energies a high resolution and high statistical accuracy measurement on several samples at these energies clearly would be of interest

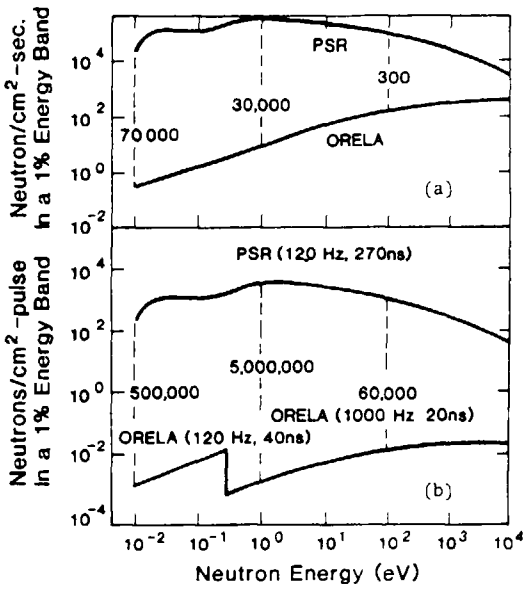

Fig. 9 Comparison of PSR and ORELA Neutron Intensities
a) The average neutron intensity per second in a 1% energy band is shown with flight path and repetition rate adjusted for greatest intensity and no frame overlap The figure gives the ratio of intensities
b) The neutron intensity per pulse is given to emphasize the advantage for experiments requiring a low duty cycle Practical repetition rates and burst widths are included The curve demonstrates the advantage of the PSR for the epithermal range, ORELA is competitive in the higher kilovolt and lower MeV range

B eV-keV Range

The average intensity in the 10^{-2} to 10^{4} eV range is shown in Fig 9a for the PSR and for ORELA A marked advantage is evident for the PSR in the lower energy portion of this range The advantage in neutron intensity per pulse achievable with the lower pulse rate of the PSR is even more evident in Fig 9b This intensity is clearly an advantage when background is an issue as in studies on radioactive targets or when work requiring long flight paths might introduce overlap

problems The low repetition rate might be disadvantageous for experiments where high duty cycle is required such as in measurements of resonance neutron capture γ-ray spectra We mention below some of the experiments under consideration at Los Alamos using the PSR

1 (n,p) Reactions on Unstable Nuclei

Most unstable neutron deficient nuclei exhibit a positive Q for the (n p) reaction Our first measurement[23] using the PSR was the (n p) reaction on ^{7}Be which has a half life of 53 3 days The experimental apparatus is shown in Fig 10 The neutron beam from the PSR was collimated into a 4 mm diameter umbra at a distance of 5 5 meters from the source About 90 nanograms of ^{7}Be was deposited in a 2 mm diameter spot on a thin aluminum foil A small amount of ^{6}LiF also was included for flux measurement Protons from the (n p) neutron were detected using a surface barrier detector placed outside of the reaction beam Reaction products from neutrons on ^{6}Li also were detected in the same detector for a measurement period of about 10 hours with average PSR proton current of 30 microamperes The cross section normalized at thermal energies is shown in Fig 11 The measurements will be extended to several keV this summer using an improved proton detector arrangement This cross section and a number of others on targets with mass less than that of nickel are of significant interest for nucleosynthesis studies

2 (n,γ) Reactions on Unstable Nuclei

The intensity of the PSR is sufficient to overpower the decay γ-ray background encountered in capture cross section measurements on many unstable targets A 4π high efficiency capture γ ray detector is being designed by Koehler and Bowman at Los Alamos for measurements at the PSR in the thermal to 30 keV range Fast timing features of the detector and a high level bias set to separate the γ-ray cascade following neutron capture from the decay γ-rays will be used to detect neutron capture It appears that measurements of eV resonance capture will be practical on samples with half lives as short as 5 days and capture at 30 keV will be practical for half lives as short as 100 days Neutron capture measurements on radioactive targets will be valuable for better understanding of the nucleosynthesis of the heavy elements by the s- and r process and the intermediate n process

3 Parity Violation

It has been demonstrated by measurements on a few nuclei[24] that slow neutron resonances are not states of pure parity and that parity violation can be readily detected The parity violation arises from the admixture of amplitude from an s wave resonance into a nearby p-wave resonance The

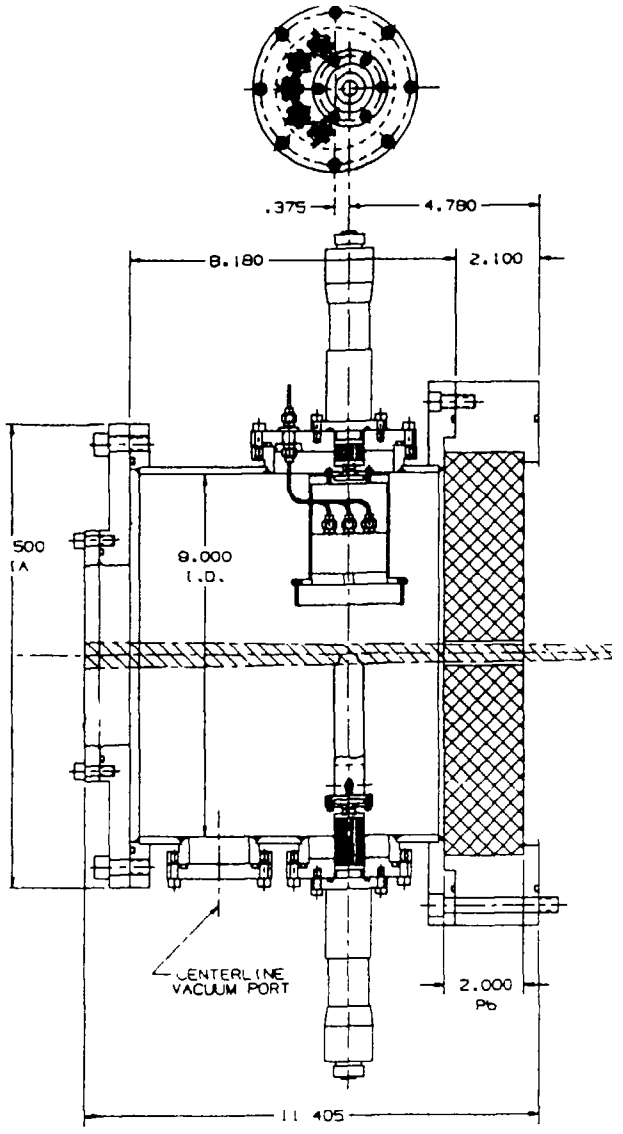

Fig. 10 Apparatus for low energy (n,p) measurements A collimated neutron beam emerges from the right and strikes a sample mounted on a thin aluminum foil adjusted in position from the bottom A surface barrier detector adjusted from above detects the charged particles

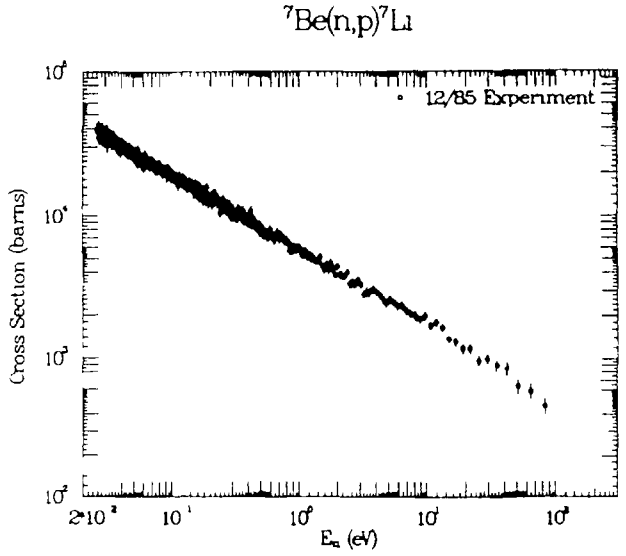

Fig. 11 Measurements at the PSR of the ^{7}Be(n p) Cross Section Preliminary results as a function of neutron energy

observable p wave amplitude is much more strongly attenuated by the angular momentum barrier than the s wave parity violating admixture Therefore the effect is easiest to see in p wave resonances The experimental effect actually measured is the difference in transmission of a neutron beam polarized parallel and antiparallel to the neutron momentum The sensitivity practical with the PSR is about 10^3 times greater than that previously brought to bear in these experiments[25] It is therefore practical to conduct measurements on many resonances in the same nucleus and to study many targets in a short time Since the parity admixture is a manifestation of the parity non conserving weak force such studies would allow a general study of the role of the weak force in the compound nucleus for heavy nuclei The largest P violation amplitude detected to date is 7% of the total resonance reaction cross section[24]

4 Time Reversal Invariance Violation

Although CP violation was detected long ago in neutral kaon decay[26] the implied T violation property of the weak force has never been directly detected experimentally The most sensitive and most extensive search has been for a detection of an electric dipole moment of the neutron which would be an unambiguous signature for T violation in the neutron The presence of substantial P violation is a signature for a substantial amplitude arising from the weak force Such resonances are therefore candidates for a sensitive search for T violation The T violation will be manifested in an amplitude containing a term of the form $(\sigma \cdot k \times I)$ where σ is the neutron spin I the spin of the target nucleus and k the neutron momentum vector The experiment requires the polarization of the neutron beam and the target nucleus normal to one another and also both normal to k T violation would be manifested as a change in the transmission at resonance when the neutron spin direction is changed by 180° The sensitivity of the proposed experiment[25] at Los Alamos appears to be in a class with the forefront of attempts to detect T violation by measurement of the neutron electron dipole moment This measurement allows the search for the force exhibiting simultaneous P and T violation According to Kabir[27] similar experiments using a polarized beam on an aligned target through the amplitude $\sigma \cdot (k \times I)(k \cdot I)$ would allow a search for a T violation in the absence of P violation a sensitive search for a T violating component in the strong force

5 (n,γ) Spectra

Although the low repetition rate and the associated low duty cycle of the PSR is not conducive to neutron capture γ ray spectral measurements the spallation source has some substantial advantages for this work The low gamma flash intensity is, of course an advantage for such measurements The high intensity also allows one to overpower the radioactivity of unstable targets and the high intensity allows measurements on very small amounts of sample The duty cycle problem can be substantially ameliorated by measurements at long flight paths but under these conditions the electron linac using shorter flight paths may be competitive

6 Resonance Neutron Optics

The wave properties of the neutron give rise to optical properties of the neutron which are well established for thermal neutrons These properties are usually expressed through an index of refraction $n = 1 - \lambda^2 p a_{coh}/2\pi$ where λ is the wavelength of the neutron p is the density of nuclei and a_{coh} is the real component of the neutron coherent scattering length For higher energy neutrons the strong wavelength dependence results in a value for n very close to unity except at resonances where the scattering length can become quite large compared to that at thermal energies thereby compensating

for the shorter wave length At resonance it is probably possible to observe resonance total reflection and perhaps even neutron focusing with long focal length lenses The large resonance scattering length also should allow enhanced diffraction effects at resonances which should be observable in powder and single crystal diffraction studies While these effects are now primarily of academic interest some application might be made of them for neutron beam handling and in spectroscopy of low energy neutrons without resorting to time of flight techniques

7 Neutron Induced Electronic Excitation

Neutron induced electronic excitation via neutron induced reactions can occur by three distinct mechanisms The first is the much discussed interaction of the magnetic moments of the neutron and electron[28] One is interested in eV incoming neutron energies and in electron excitations of a few eV with small momentum transfer and in excellent energy resolution (~1/1000) The second is excitation arising from recoil of the nucleus under the electron cloud when the nucleus is struck by a neutron in a high momentum transfer interaction[29] The third is another high momentum transfer excitation arising from non adiabatic coupling (NAC) between the nuclei in a diatomic or more complex molecule[29] None of these neutron interactions have been observed However the intensity of the new spallation sources is probably sufficient to detect and exploit all of them The signature for such neutron inelastic scattering would be the change in energy of the neutron in the collision Background could be significantly reduced by detecting the decay photon following electronic excitation in coincidence with the scattered neutron For the NAC interaction the selection rules are substantially different from electromagnetic selection rules and more restrictive so that the spectrum might be less complex and, therefore, more easily resolved and interpreted The potential for advances in atomic molecular and condensed matter physics through neutron interactions of this type is very substantial

8 Physics of Neutron Dosimetry

In contrast to biological damage arising from γ rays which is primarily dependent on the deposited ionization energy density the damage from neutrons is probably more nearly dependent on the density of nuclear displacements produced by neutron nucleus collisions There are four damage regimes for low energy neutrons which can be postulated

a The neutron energy is so low that not even hydrogen atoms can be displaced from their sites by neutron nucleus collisions This implies a threshold neutron energy around 10 eV for damage by neutrons below which no damage is possible other than that produced by neutron capture on hydrogen and nitrogen

b The neutron energy is not large enough to displace a heavy nucleus such as C N or P from its site In this case damage also might be small since displacement of a hydrogen atom might not give rise to serious radiological damage This threshold is probably about 150 eV

c The neutron energy is large enough to displace a heavy nucleus but the energy of the displaced nucleus is insufficient to simultaneously displace its partner nucleus in the DNA double helix In this case the damage is substantial but the undamaged strand provides the key to repair This energy might be around 1 KeV

d The neutron energy is large enough to displace a heavy nucleus which carries away enough energy to displace its partner in the DNA strand In this case the key to repair is also damaged and the damage might be irreparable

Thus it appears that there might be several different biological damage thresholds for neutrons between thermal and 1 KeV energy However within this window of about 5 decades of energy 10^2 10^3 eV there might be no significant damage produced by neutrons to biological tissue except by neutron capture on hydrogen and nitrogen The disassociation of an atom from a molecule might be evident from a measure of the inelastic neutron spectra in this energy range An intense spallation neutron source in the epithermal range would undoubtedly be useful for such studies

9 Lead Slowing Down Spectrometer

The lead slowing down spectrometer[30] is a means of creating a very high intensity source of neutrons which can be used as a spectrometer with poor resolution using the time energy correlation of the neutrons in a 1 m^3 lead assembly The PSR spallation source could inject 10^{15} n/burst into the assembly which is probably at least four orders of magnitude more neutrons than have been used previously Since the sensitivity gain of this instrument is about 10^4 times that of a comparable neutron time of flight experiment the sensitivity for cross section measurements would be extraordinary for experiments where high resolution is not important

C Thermal Neutron Range

Even for the new generation of spallation sources the reactor is a formidable competitor in the thermal neutron range While the peak thermal flux

for the spallation source might exceed that in the reactor by an order of magnitude the average thermal neutron intensity of the reactor is higher than that of the spallation source Nevertheless the pulsed source can be an advantage for some experiments as we illustrate next

The neutron neutron scattering length has never been directly measured and its value to an accuracy of a few percent is of great interest Experiments on the edge of practicality have been proposed[31] for steady state thermal neutron sources A cavity is created containing a gas of thermal neutrons which is viewed by a detector through a collimated path which does not allow the detector to see the walls of the cavity Only neutrons which scatter from other neutrons can strike the detector Since the n n scattering depends on the square of the neutron flux, the spallation pulsed source has an advantage over the steady state reactor If the scattering volume is filled with a low density of hydrogen gas, the n p scattering will be proportional to the first power of the flux Therefore by measuring the scattering rate as a function of peak flux in the cavity, the n-n scattering rate can be separated from the n-p rate and the n-n scattering length measured relative to the n p scattering length Although a calculation has not been done for a spallation source, it has been done for a pulsed reactor[32] For a flux of 10^{17} n/cm^2 sec a cavity 10 cm long and 10 cm in radius, a detector distance of 12 meters, a detector radius of 10 cm, and a pulse width of 6 milliseconds the detected rate is 30 neutrons per pulse

D Ultracold Neutrons

The pulsed spallation source is potentially a very powerful source for production of a high density of ultracold neutrons A rotating mechanical doppler shifting device viewing a cold source can be operated synchronously with the accelerator pulse to reduce cold neutrons to ultracold velocity of < 8 m/sec The expected density[33] possible with the current generation of spallation sources is substantially greater than that which has been achieved at reactors Several interesting experiments have been proposed[34] taking advantage of the special properties of ultracold neutrons but the search for a neutron electric dipole moment continues to be the experiment receiving greatest attention

IV FUTURE DEVELOPMENTS

Fig 4 suggests that substantial increases in spallation neutron source intensity can be expected in the next decade It appears unlikely that greater neutron intensity will come as a result of further increases in proton energy since increases in energy beyond about 1 GeV may not increase source brightness owing to the increasing range of protons with increasing energy and the mismatch between proton range and neutron moderation distance Without increasing proton current or energy the neutron intensity can be increased by a factor of two using a depleted uranium target instead of a lower Z material such as tungsten Uranium targets are generally either planned or in use now for most facilities A further increase in intensity without increasing current is practical with a subcritical fission booster[35] These targets allow an increase of about a factor of five in neutrons produced per proton with the disadvantages of some pulse broadening substantially greater heat deposition in the target, and a delayed neutron background Owing to greater complexity in the target arising from handling the extra heat, the effective neutron intensity is increased by only a factor of three when the total neutron gain is a factor of five

As an extreme in fission boosters, King[36] long ago proposed a concept in which a liquid fuel is vaporized but, nevertheless, contained in an expansion volume producing 1 4 x 10^{20} n/pulse in a 35 μsec wide pulse The system was not driven by a spallation source The repetition rate for such a system is necessarily low and, therefore might not be useful for condensed matter physics studies However, for some nuclear physics studies such a source might be of interest

The ultimate in high average intensity with substantial repetition rate for epithermal neutrons is achievable by spallation on a rotating depleted uranium target since the energy deposited per neutron produced of 20 MeV per neutron is lowest for this concept The most ambitious pulsed spallation epithermal proposal to date is the Aspun concept[15] under development at the Argonne National Laboratory The most effective MeV source using the linac microstructure for MeV neutron physics would be the facility nearing completion at LAMPF with 800 MeV energy a current of about 3 microamps and a pulse rate (larger duty factor) of about 50 000 Hz The meson factory of the USSR could operate with similar characteristics

Summary

We summarize this paper with the following comments and recommendations regarding the application of spallation neutrons in advancing the field of neutron nuclear physics

Completion of spallation sources now under construction will allow very substantial advances in intensities for neutron physics in the energy range below 1 KeV

- The r f linac component of essentially all existing and new spallation sources can be used parasitically as a very high intensity subnanosecond pulsed white neutron source
- Neutron physicists should plan and establish experiments on the epithermal spallation sources
- Neutron physicists should urge introduction of the MeV capability into existing spallation neutron sources or into plans for new spallation sources
- The current rapid developments in accelerator technology should be closely watched for opportunities for enhancement of neutron source intensity
- Monoenergetic and variable energy neutrons from ion beam accelerators and electron linac white sources will continue to be competitive sources in the high keV and lower MeV range
- For neutron research in the thermal range reactors will be pushed but probably not supplanted by the next generation of spallation sources
- Substantial neutron physics programs at the major neutron sources should strengthen the research program at more modest facilities by increasing the spectrum of problems and depth of investigation in neutron nuclear physics research

Acknowledgements

Discussions with P W Lisowski, S A Wender, and G J Russell of the Los Alamos National Laboratory were helpful and much appreciated

References

(1) C D Bowman, S A Wender, and G F Auchampaugh, "Nuclear Physics in the 10-300 MeV Energy Range Using a Pulsed White Neutron Source," Proceedings at a Conference on Neutron-Nucleus Collisions A Probe of Nuclear Structure, American Inst of Phys , Conference Proceedings No 124 p 259 (1985)

(2) P W Lisowski, S A Wender and G F Auchampaugh, Proceedings of the International Conference on Nuclear Data for Basic and Applied Science Santa Fe, Gordon and Breach New York, Paper 8 2 (1985)

(3) C W Windsor, "Pulsed Neutron Scattering" Halsted Press New York (1981)

(4) "Scientific Opportunities with Advanced Facilities for Neutron Scattering' Workshop held at Shelter Island, New York, Edited by G A Lander and V J Emery (1984)

(5) J W Lynn, W A Miller, T W Dombeck, G R Ringo, V E Krohn, and M S Freedman, Physica 120B, 114 (1983)

(6) W W Havens, Jr , and L J Rainwater, Phys Rev 83, 1123 (1951)

(7) W W Havens, Jr Proc Intl Conf on Peaceful Uses of Atomic Energy 4, 74 (1955)

(8) W W Havens, Jr , "Intense Neutron Sources," USAEC CONF-660925 p 565 (1966)

(9) E R Rae and W M Good, "Experimental Neutron Resonance Spectroscopy," Academic Press, New York, p 2 (1970)

(10) R Woods, Proceedings of the 5th Meeting of the International Collaboration on Advanced Neutron Sources, Vernforschungsanlage Julich Report ISSN-0344-5789, p 1 (1981)

(11) H Sasaki, Proceedings of the Seventh Meeting of the International Collaboration on Advanced Neutron Sources, Chalk River Nuclear Laboratories Report AECL-8488, p 15 (1984)

(12) G Lander, J M Carpenter, R L Kustom and T K Khoe, Ibid, p 40

(13) C D Bowman, Ibid, p 9

(14) G Manning, Ibid, p 34

(15) T K Khoe and R L Kustom, Ibid, p 46

(16) H Sasaki, Ibid, p 50

(17) D K Olsen, J A Martin, D J Horen, "Possible ORELA Replacement Option," Report ORNL/TM-8669 (1984)

(18) R G Johnson, "Conceptual Design of an Induction Linac for Neutron Research," Proceedings of the International Conference on Nuclear Data for Basic and Applied Science, Santa Fe, Gordon and Breach New York, Paper 8 7 (1985)

(19) V M Lobashev and A N Tavkelidze, Vest ANSSR 2, 115 (1983)

(20) M M Meier, D Holtkamp, G L Morgan, H Robinson, G Russell, R Whitaker, W Amian and N Paul, International Conference on Nuclear Data for Basic and Applied Science Santa Fe, 1985

(21) S Wender and G F Auchampaugh, "Fast Neutron Capture With a White Source," Capture Gamma-Ray Spectroscopy and Related Topics, Conference Proceedings, p 483, American Institute of Physics, New York (1984)

(22) F P Brady, "Facilities for Neutron Induced Reactions," AIP Conf Proc No 124, p 382, Neutron-Nucleus Collisions, Burr Oak State Park, Ohio (1984)

(23) P E Koehler, C D Bowman, F J Steinkruger, D C Moody, S A Wender, R C Haight, P W Lisowski and W L Talbert, BAPS 31, 854 (1986)

(24) V P Alfimenkov, S B Borzakov, Vo Van Thuan, Yu D Mareev, L B Pikelner, A S Khrykin and E I Sharapov Conf Proc Nuclear Data for Science and Technology, Antwerp, p 773, D Reidel Publishing Co , Boston, Mass (1982)

(25) C D Bowman and J D Bowman, "A Proposed High Sensitivity Search for T-Violation in eV Neutron Resonances," International Symposium on Weak and Electromagnetic Interactions in Nuclei, Heidelburg, (July 1986)

(26) J H Christenson, J W Cronin, V L Fitch and R Turlay, Phys Rev Lett. 13, 138 (1964)

(27) P K Kabir, "Tests of T-Invariance with Slow Neutrons," National Bureau of Standards Special Publication 711, Edited by G L Green (1986)

(28) J F Cooke, J A Blackman, and T Morgan "Band Structure Effects in the Electronic Properties of Solids Accessible in Neutron Scattering Studies,' in Condensed Matter Research Using Neutrons Today and Tomorrow, p 63, Plenum Press, New York, (1984)

(29) S W Lovesey, C D Bowman, and R G Johnson, Zeitschrift fur Physik B 47 137 (1982)

(30) R C Block, R W Hockenbury, D S Cramer, E Bean, and R E Slovacek, National Bureau of Standards Special Publication 425, Nuclear Cross Sections and Technology p 93 (1975)

(31) C O Muehlhouse, "Proposed Experiment to Observe n-n Scattering," International Conference on Nuclear Physics with Reactor Neutrons, ANL Report 6797, p 21 (1963)

(32) W C Dickinson, E M. Lent, and C D Bowman, "An Analysis of a Proposed n-n Scattering Experiment," UCRL Report 50848 (1970)

(33) J W Lynn, W A Miller, T W Dombeck, G R Ringo, V E Krohn and M S Freedman, Physica 120B 114 (1983)

(34) K A Steinhauser, "Production and Use of Ultra-Cold Neutrons," IAEA Conference Proceedings, Neutron Scattering in the Nineties, Julich p 99 (1985)

(35) G Fraysse, "Pulsed Neutrons and their Utilization," Joint Meeting Euratom - Japan Atomic Energy Society Ispra (1971)

(36) L D P King, "Disposable-Core Fast Burst Reactors," Proceeding of the National Topical Meeting on Fast Burst Reactors, Albuquerque, N M CONF-690102 (1969)

ELECTRON LINACS AND BEYOND

K.H. BÖCKHOFF
Central Bureau for Nuclear Measurements,
Joint Research Centre,
Commission of the European Communities,
Geel

This paper has been combined with the paper by the same author in Session I.

RESEARCH HIGH FLUX REACTOR PIK

K.A. KONOPLEV
Leningrad Institute of Nuclear Physics,
Gatchina, Leningrad,
Union of Soviet Socialist Republics

Abstract

The research reactor is now under construction at the Leningrad Institute of Nuclear Physics, 45 km away from the city. The projected power of the reactor is 100 Mwt. The reactor will be used for physical investigations with external neutron beams.

The thermal neutron flux in the reflector is higher than 10^{15} neutrons/cm^2 sec and the flux in the usual water trap in the centre of the core is 4.10^{15} neutrons/cm^2 sec.

Sources of cold and fast neutronsare designed in the reactor. Most of the experiments will be conducted on stationary neutron guides.

High Neutron Flux Research Reactor PIK

1. RR as a neutron source

There are at present about 300 nuclear research reactors (RR) in operation all over the world [1]. With the exception of a few of them constructed specifically to study reactor technology or for training purposes, all these reactors are used as neutron sources. The time-averaged power of these sources may reach in special cases several hundred MW, the mean fluxes of fast and thermal neutrons being a few times 10^{15} cm^{-2}s^{-1}. The areas of RR application may be conventionally divided into several broad classes, among them materials science, production of nuclides and physical research. The PIK reactor [7] dealt with in the present report belongs to physical research reactors thus making it necessary to consider this class of reactors in more detail.

Rather than discussing the advantages of pulsed sources in neutron scattering experiments , we will restrict ourselves to continous operation reactors to which the PIK belongs. From the view-point of the design of the core, reflector, beam tubes and other reactor assemblies the most essential factor is the character of the experiments being planned, namely, whether they should be performed inside a tube or on an external neutron beam Physical research reactors intended for experiments on external beams are called beam reactors.

In-tube devices are needed primarily for nuclear physics studies. As examples may serve parity violation studies in nucleon-nucleon interactions [2], measurement of spectra in the (n, γ) reaction on nuclei carried out on the WWR-M reactor in Gatchina [3], fission fragment studies [4] on the ILL reactor in Grenoble, or measurement of the light fragment parameters in triple fission [5]. In all these cases the target was mounted in a high neutron flux within the tube while the radiation was led out to the instrumentation which was located in the experiment hall outside the reactor This scheme requires ready access to the tube, a possibility to introduce samples and, quite frequenty, facilities for cooling. In some experiments the tube has to be evacuated, and a gate has to be provided to intercept radiation From this view-point, such experiments are most suited for vertical tubes in pool reactors, since the size and location of the tubes can be varied here within a broad range. An obvious draw-back is that the vertical arrangement of the instrument complicates its design.

Progress in shaping the external neutron beam spectra changed the requirements also to beam reactors Restricting the in-tube assemblies to beam collimators or neutron filters only became insufficient. The use of cold (CN) and hot (HN) neutron sources and of neutron guide techniques required easier access to the reflector region and even to the core proper Probably the most remarkable illustration of neutron beam shaping is the universal beam tube (Fig 1) for the production of cold

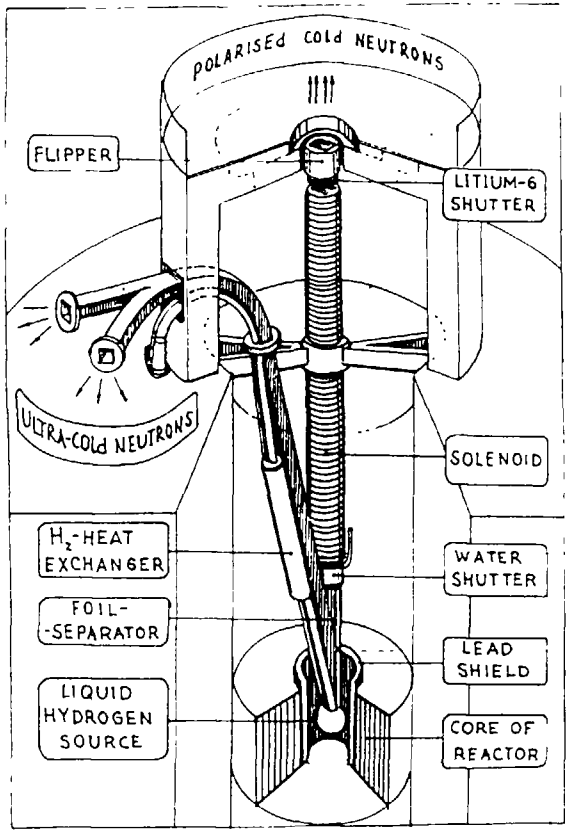

Fig.1. Schematic of the polarized cold and ultracold neutron source in the WWR-M reactor.

and ultracold neutron in the WWR-M reactor in Gatchina representing a further development of an earlier scheme /6/. Easy access to the reactor core was used to advantage by placing at its center a liquid hydrogen source of cold and ultracold neutrons. A polarizing neutron guide is mounted inside the tube for cold neutrons, while at the outlet the ultracold neutron beam is led out to several instruments Such an arrangement permitted one to obtain record-high fluxes at the instruments starting with a moderate reactor neutron flux of 10^{14} cm^{-2} s^{-1}, namely, 5×10^5 ultracold neutrons/s, and 3×10^{10} polarized cold neutron/s.

After these introductory remarks a description of the PIK reactor is in order.

The reactor is intended for a broad range of fundamental search covering nuclear physics, weak interactions, condensed state, and biology. The high neutron flux provided (in excess of $10^{15} cm^{-2} s^{-1}$) offers possibilities for research at a qualitatively new level compared with that reached on any other in our country.

The reactor power is set at 100MW which exceeds by about a factor 5-10 the power level of other reactors in our country used for these purposes. The reactor is going to be provided with experimental halls, neutron research hall and various experimental facilities. This gives us grounds to consider PIK reactor as a neutron beam research center. During the first years major emphasis will be placed on neutron scattering studies The center is expected to be operational for many years to come which requires the reactor design to be flexible enough, particularly in what concerns the core, reflector, and the beam tubes. The principal requirements to the reactor as a neutron source are that it should provide a small volume with a record-high thermal neutron flux (at a level of 5×10^{15} $cm^{-2} s^{-1}$) for target irradiation, and a large volume with a flux of $10^{15} cm^{-2} s^{-1}$ to accommodate beam tubes and neutron spectrum shapers. Experiments inside the core are considered as exclusive, since the core of such a reactor should obviously be at a high pressure, and the energy released there should be prohibitively high.

2 Physical Criteria for Selection of the Core

Basing on the above requirements, the general scheme of the reactor is as follows There is a compact core of 100MW power The core accommodates a neutron trap with a record-high neutron flux The core is surrounded by a good reflector of a sufficient volume to arrange many beam tubes, preferrably of a large diameter, with at least part of them located in a thermal neutron flux on the order of $10^{15} cm^{-2} s^{-1}$

To reduce the design work, the PIK reactor uses fuel elements of the SM-2 reactor [8] which have a good record of operation The SM-2 operates at 100MW with a 50 liter core, light water at 50 atm being used for cooling

The thermal neutron flux in the reflector grows with decreasing core volume at a constant power Obviously enough, placing a trap at core center increases the core volume and reduces the flux in the reflector, however providing a beam tube at core center with a flux about three times that in the reflector compensates this loss[9]

While reducing the core volume to below 50 l in order to increase the neutron flux in the trap and reflector is possible, this would increase fuel consumption because of reduced burnout A 50 l core is far from being a point source of fast neutrons slowing down in the reflector Different fuel elements provide different contributions to the overall flux in the reflector This is illustrated by Fig 2 [10].

Fig 3 displays the radial distribution of the sources in the PIK reactor. It is readily seen that it is the fuel elements providing the largest contribution to the thermal neutron flux that bear the heaviest load The fast neutrons are produced in the core and leak into the reflector On slowing down they form a flux of thermal neutrons which, in their turn, propogate to the core (Fig 4[7]) The reason for such a nonuniform distribution of energy release is that the thermal neutrons transferring from the reflector into the core are absorbed in a comparatively thin layer. If no special precautions are made, the coefficient of nonuniformity of the energy release along the core radius may

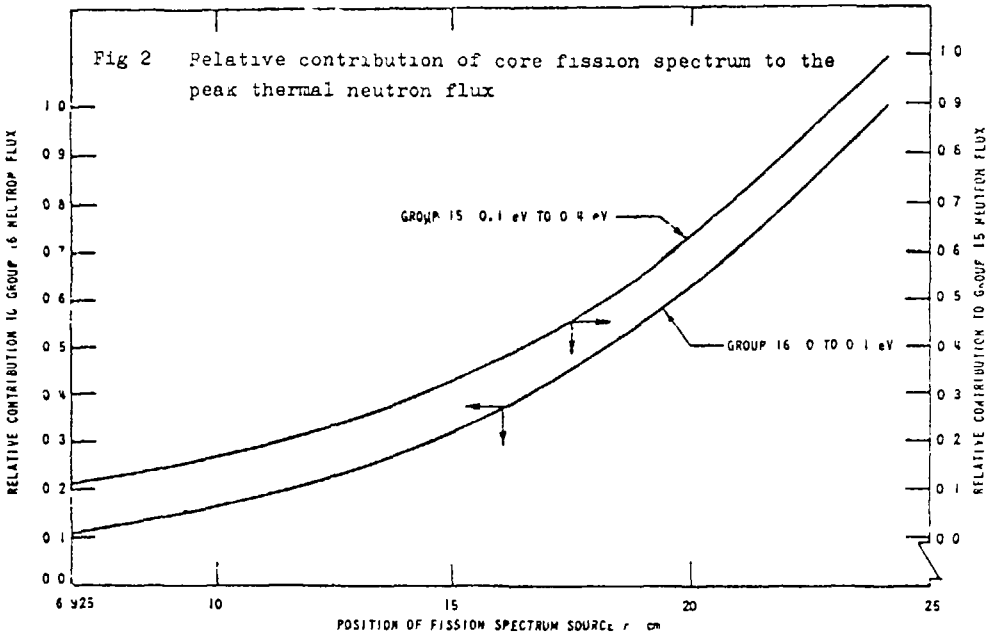

Fig 2 Relative contribution of core fission spectrum to the peak thermal neutron flux

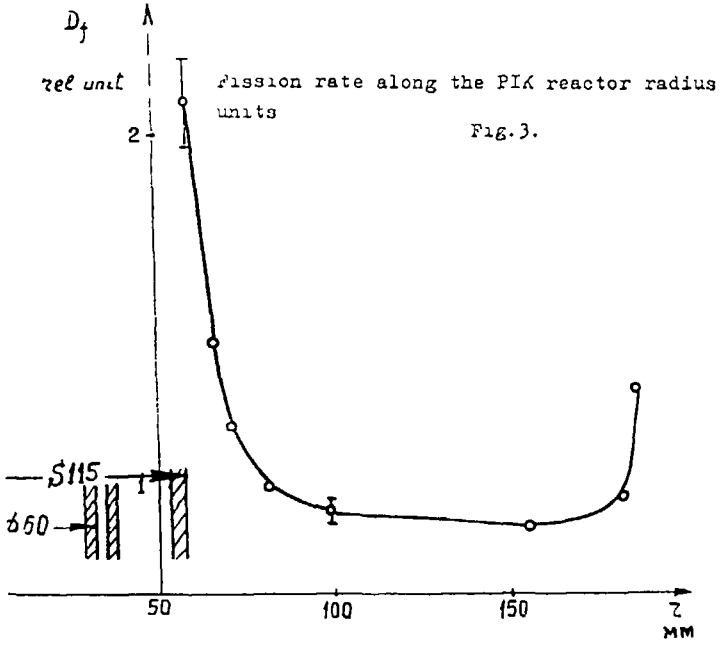

Fission rate along the PIK reactor radius in arbitrary units

Fig.3.

reach a factor 5 to 6 or even more. Although the ratio of the reflector (or trap) flux to power (Φ/W) grows, one has to level off the energy release because of limitations on the specific power. The levelling off in the PIK reactor is achieved by placing a semi-transparent shield at the core boundary. While being practically transparent to the fast neutrons leaving the core, this shield limits the thermal neutron flux incident on the core and thus reduces the coefficient of nonuniformity down to $\simeq 2.5$.

Heavy water was chosen as reflector. The heavy water reflector used to slow down the fast neutrons provides the best ratio of thermal neutron flux to power compared with other moderators[9]. Due to the large diffusion length in heavy water (L=1m for 0.2%H_2O) and considerable reflector thickness ($\simeq$ 1m), the thermal neutron flux is sufficiently high far from the core, where the background of fast and slowing down neutrons, as well as γ -photons, is low (Fig.4).

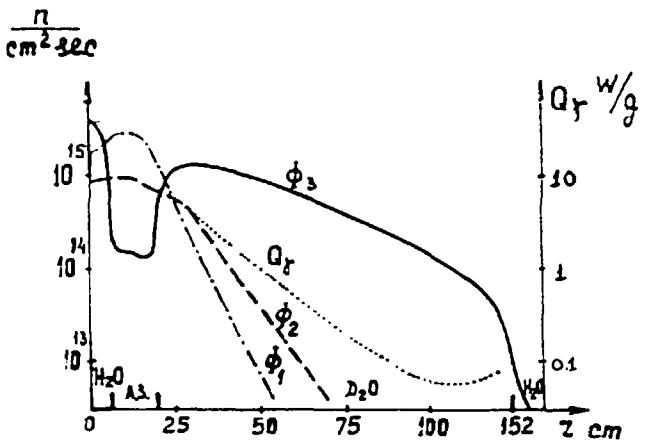

Fig.4. Radial distribution of neutron flux Φ_i and energy release Q_γ for reactor operating at 100 MW.
Φ_1 : fast neutron flux, E > 5keV
Φ_2 : epithermal neutron flux, 5keV > E > 0,5eV
Φ_3 : thermal neutron flux, E < 0.6 eV

3. Reactor Design and Parameters

The evaluation and top view of the reactor is presented in Figs.5 and 6 . The 50l-core is in a pressure vessel and cooled by light water. The vessel representing a long double-walled pipe passes through the heavy water reflector tank. The tank is 2.5m in diameter and 2m high. The beam tubes are located in the heavy water tank. The low pressure (2 atm) in the tank simplifies its use in experiments. Horizontal, inclined and vertical beam tubes are provided. The latter are intended for sample irradiation, and the horizontal and inclined tubes, for leading the radiation out. The neutron trap at core center accommodates a vertical tube with an independent cooling loop

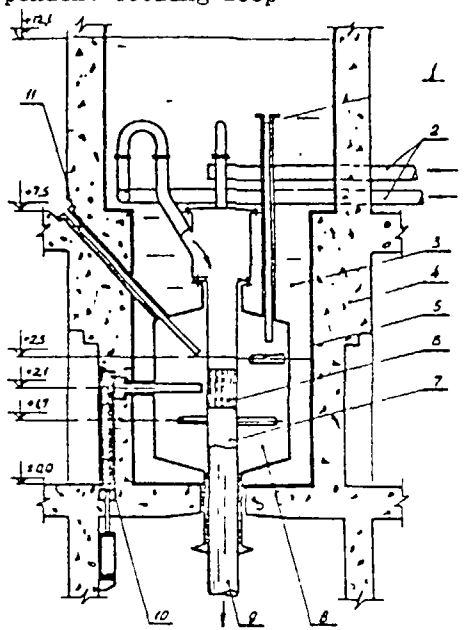

Fig.5. Elevation of PIK reactor (schematic)
1- vertical tube; 2- coolant inlet; 3- well with water; 4- biological shielding; 5- horizontal beam tube; 6-core; 7- replaceable vessel; 8- heavy water reflector; 9- coolant outlet; 10- gate; 11- inclined beam tube. Given on the left are distances from experiment hall in meters.

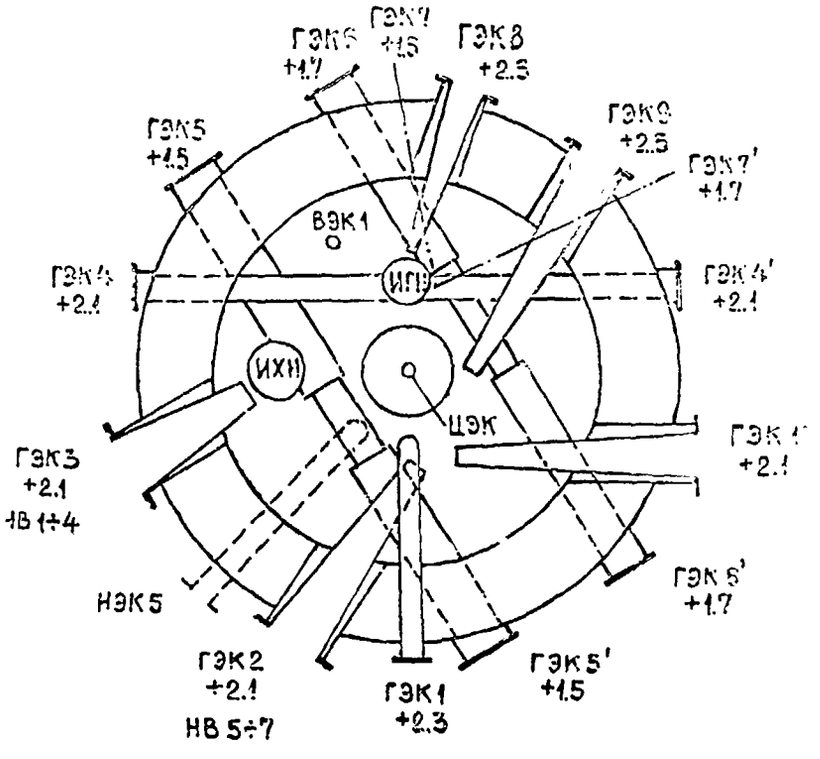

Fig.6. Layout of beam tubes in the PIK reactor reflector [7].

ГЭК - HBT - horizontal beam tube;
НЭК - IBT - inclined beam tube;
ВЭК - VBT - vertical beam tube;
ЦЭК - CBT - central beam tube;
ИХН - CNS- cold neutron source;
ИГН - HNS - hot neutron source;

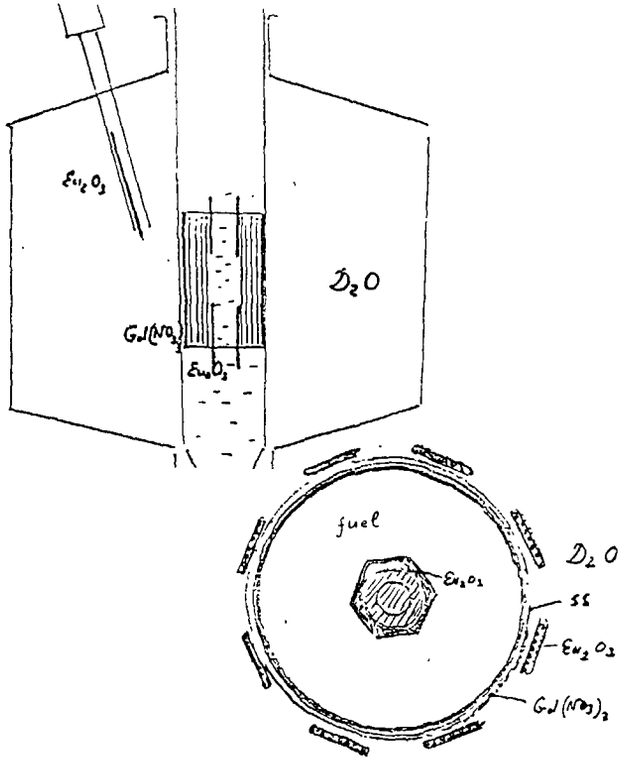

Fig 7. Layout of controls and alarm "rods"

The controles (Fig.7) are arranged in such a way as, on the one hand, not to increase the core volume and to exclude local pertubations and, on the other, to minimize any effect on the fluxes in the beam tubes. Smooth control of the reactor is effected by varying the concentration of the water solution of gadolinium nitrate. The solution flows through a gap between the two shells of the vessel. Fast control and emergency protection are realized by means of two absorbing rings enclosing the trap and shifting aside simultaneously to avoid asymmetry of the neutron flux. Additional emergency protection is provided by the absorbing rods dropping into the heavy water reflector. In this case the rods affect strongly the fluxes in the reflector, however they are led in and out only when shutting or starting up the reactor.

An essential aspect of the reactor design is the possibility of replacing all the units in the reflector tank. This replacing stems from the need of periodic replacement of the damaged material (the fast neutron flux on the reactor wall is $5 \times 10^4 cm^{-2} s^{-1}$) and of having sufficiently flexible and mobile design for mounting new experiments. The vessel can be replaced by either a new one of the same design, or another one of a different diameter. Facilities are provided for increasing the vessel diameter up to 520mm. In the first version incorporating a 501-core with a trap at the center the vessel diameter is 380 mm. This offers a possibility for carrying out in-core experiments and for shifting the maximum of the thermal neutron flux in the reflector to a somewhat larger radius. At the same time it becomes possible to replace the fuel elements with another type which usually meets with difficulties in conventional reactors. The replacement of the vessel and core is facilitated by moving the liquid control circuit to the outer diameter of the vessel.

The same principle of interchangeability was applied also to the beam tubes in the reflector tank. The rated diameter for the horizontal tubes is 100 mm, for the inclined ones 80 mm, and for the vertical tubes 50 mm, however the parts in the reflector tank and the flanges bearing the tubes permit increasing these sizes. In particular, almost for any horizontal tube this diameter can be increased to 250 mm. Obviously enough, bringing several adjacent tubes to their maximum size may fail to increase statistics in experiments. The perturbing effect of a tube on the flux and the interference between too closely located beam tubes may reach tens of percent.[11]

Fig.8 displays a realistic selection of the first horizontal tube set. One readily sees that the largest diameter here is 200 mm, and it is used only for one beam tube (HBT 4). It is intended to accommodate the ultracold and polarized cold neutron source similar to the one employed in the WWR-M but made horizontal. For beam collimation one uses not circular tubes with a collimator insert, but rather tubes of appropriate shape, mainly 120mm x 250mm

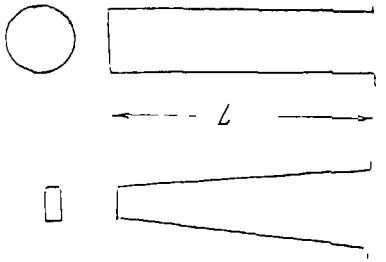

Fig.8. Dimensions of the PIK horizontal beam tubes (1 set).
HBT 1: circular, dia.82, length 820 mm
HBT 2: rectangular, tapered, 120x250 at inlet and 320x250 at outlet, length 1600 mm.
HBT 3: rectangular, tapered, 120x250 at inlet, 320x250 at outlet, length 1000 mm.
HBT 4: through, circular, dia.200, length 2210 mm
HBT 5: through, circular, dia.150, length 2210 mm
HBT 6: through, circular, dia.120, length 2210 mm

HBT 7: V-shape, circular, dia 190 length 1450 mm
HBT 8: rectangular, tapered, 190x60 at inlet and 190x190 at outlet, length 1100 mm
HBT 9: rectangular, tapered, 190x60 at inlet and 190x190 at outlet, length 1710 mm.
HBT 10: rectangular, tapered, 190x60 at inlet and 190x190 at outlet, length 1470 mm

and 190mm x 60 mm Such tubes displace a smaller amount of heavy water from the reflector Calculation of the effect of beam tube shape and relative tube arrangement on the reactor operation and external fluxes appears difficult however the reactor is provided with a full-scale physical mock-up intended for modeling the optimal size and arrangement of the beam tubes when planning new experiments.

The approach to designing biological shielding appears to be original (This does not mean, naturally, changing the allowable irradiation dose of the personnel which is set by the law to be not higher than 5 rem/yr while being, as a rule, below 0 5 rem/yr). In many cases it may be practical to move a sample (say, the first scattering crystal) in the tube closer to the source with a corresponding increase of the incident flux Special wide recesses were sometimes provided for this purpose in the biological shielding (Fig 9). Such a recess can be made in cases where there are few beam tubes passing through the shielding With many tubes these recesses would overlap Another aspect of the problem is that when a beam is lead out the instrument should be enclosed in a separate shielding irrespective of the thickness of the main biological shielding This additional shielding should meet not only purely biological but more stringent requirements as well, since it is necessary to reduce the background in the given experimental system and at the same time to avoid any enhancement of background on the nearby instrument Thus practically on each beam led out from a high power reactor one has to construct biological shielding around the instrument The shape and the thickness of this shielding vary in each particular case.

These two factors were used to advantage in the PIK reactor to reduce the shielding thickness to the level permitting close operation only with the shutdown reactor and closed gate With the reactor in operation and the gate open, biological shielding should be installed at the instrumentation This approach allowed us to make the biological shielding thinner by about 1 meter and to increase accordingly to neutron flux at the beam tube outlet by approximately a factor two As a result, the side shielding

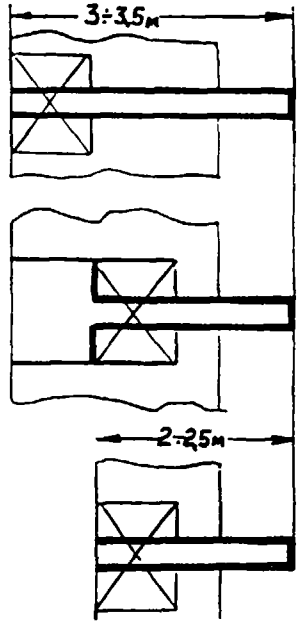

Fig.9. Schematic of biological shielding.
1: beam tube, 2- biological shielding; 3: gate,
4: recess for experimental instrumentation

consists of iron and water combination (0 5 m) and heavy concrete (0.9 m, γ =3 6.g/cm^3). This shielding called physical reduces the radiation to the level permitting one to operate the instrumentation with the shutdown reactor. The physical shielding is complemented by a 1 m thick dismountable biological shielding The latter represents an integral part of the research instrumentation and is moved directly to the physical shielding only when no experiments are in progress. These two layers of shielding bring the radiation from a running reactor down to 0 4 μrem.s^{-1}, i e to one half the standard regulations

4. Characteristics of Experimental Facilities

The PIK reactor is provided with experimental facilities for carrying out physical research. They include a light water trap, cold (CN) and hot (HN) neutron sources, neutron guides,

horizontal and inclined tubes for leading out the neutron beams, vertical tubes for sample irradiation, and other devices Some of these devices have already been discussed Consider now in more detail the principal experimental facilities

4.1. Trap

The cylindrical light water trap with an optimum diameter of about 10 cm is located at core center. In the central tube the unperturbed flux of thermal neutrons reaches approximately $4x10^{15}cm^{-2}s^{-1}$, and that of fast (E > 5keV) neutrons $2x10^{15}cm^{-2}s^{-1}$ Only two reactors specially designed for operation with a trap have close values of neutron fluxes, namely, the Soviet materials testing reactor SM-2[8] and the american HFIR [12] for the production of transuranium elements The PIK combines the advantages of the trap and beam reactors Although the presence of a trap leads to a loss in reactivity, nevertheless it is useful since the neutron flux in it is three times that in any reflector beam tube The PIK is particularly effective when studying neutron characteristics of short lived isotopes produced in the trap, since the number of events obtained in this case is proportional to the product of neutron fluxes in the two devices, i e to the reactor flux squared The central beam tube in the trap of i d. 6 cm is cooled by an independent 400kW water loop with a pressure of 1 to 50 atm, depending on the energy released in the sample under irradiation This tube can be conveniently used to irradiate targets for high specific activity neutrino sources. When the energy released in the sample is sufficiently small to permit operation at a tube pressure of 1 atm, samples can be led in and out without shutting down the reactor.

4.2 CN Source

Some areas of condensed state and biological research require high fluxes of neutrons with wavelength $\lambda \geqslant 4$Å (E≤0 005 eV). The long wavelength neutron flux intensity can be raised tens of times by reducing considerably the neutron gas temperature The reactor reflector houses a cold neutron source representing a dia 19 cm sphere contains about 25 l of liquid deuterium at a pressure of 1 5 atm (Figs 10 and 11) A 10 kW cryogenic helium installation maintains the deuterium temperature near 25 K via a piping

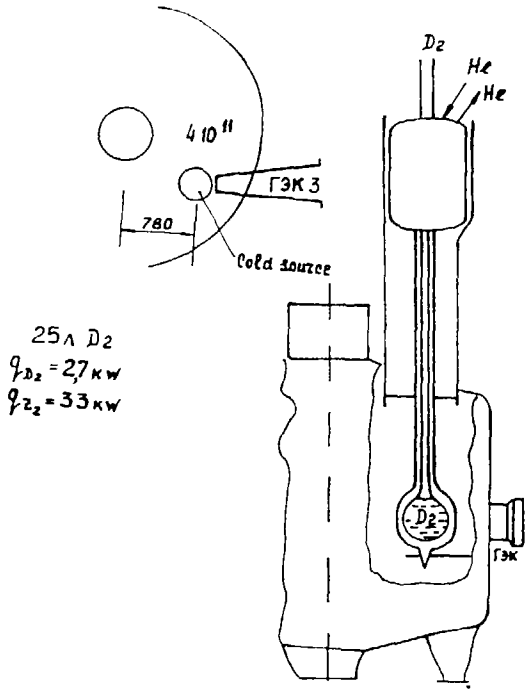

Fig 10 Schematic of the PIK cold neutron source

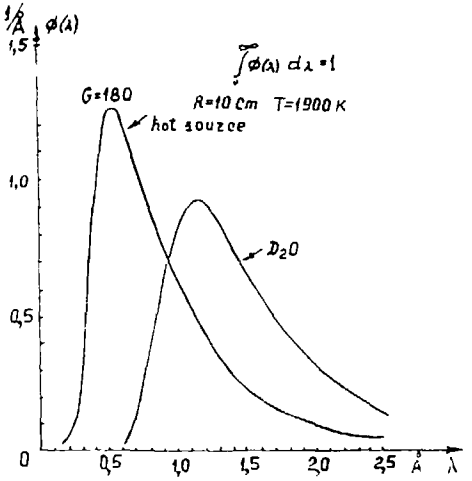

Fig. 11. Neutron spectrum in D_2O and HNS

passing through the vertical beam tube. The center of the source lies at a distance of 78 cm from the core center, with the unperturbed thermal neutron flux here being, on the average, 3.5×10^{14} $cm^{-2}s^{-1}$. The horizontal beam tube HBT 3 from which the neutron guides originate connects with the CN source.

4.3. HN Source

Precise localization of atoms needed in the investigation of biological, crystalline and magnetic structures, as well as studying high energy excitations in solids and liquids require the use of short wavelength ($\lambda < 1$ Å) neutrons To produce them, the PIK reactor is equipped with a hot neutron source The HN source represents a sylindrical graphite block 30 cm high and 20 cm in diameter separated by a double zirconium shell from the main reflector. The graphite is isolated from the inner shell with helium-filled graphite wool. The graphite is heated by core γ - rays to about 2000 K The center of the HN source lies at 65 cm from core center and 40 cm above the midplane (Fig. 12). The unperturbed thermal neutron flux at the HN source is, on the average, about 3×10^{14} $cm^{-2}s^{-1}$. The HN source piping is led out up through the vertical tube The hot neutrons are directed into the experimental hall through the horizontal beam tube HBT8

4.4. Beam Tubes

The reflector tank houses three tangential through, one radial, one V-shaped tubes and three tangential thimbles. Apart from this, one horizontal beam tube connects to the HN source, and another, to the CN source (Fig 6). Each tangential through tube can be replaced by two thimbles. To reduce interference between the horizontal tubes they are mounted at different levels.

The reflector accommodates also six inclined tubes with an inner diameter of 8 to 14 cm which supply neutron beams to the inclined tube hall located under the horizontal tube hall Apart from this, one can mount in the reflector tank seven vertical tubes with an inner diameter of 5 cm for irradiation of containers with samples.

The unperturbed thermal neutron flux Φ_0 at the sites where the tubes are mounted is given in Table 1 The flux Φ_0 is

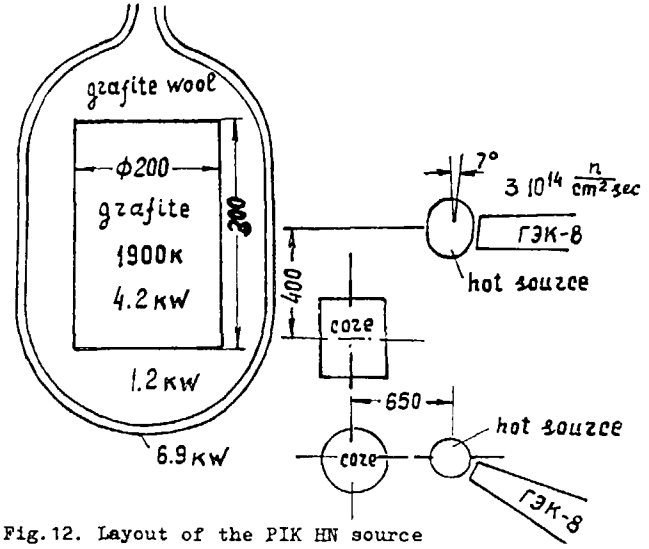

Fig. 12. Layout of the PIK HN source

TABLE 1 Experimental beam tubes at the PIK reactor [7]

	Beam tubes	Φ_0 10^{15}n/cm²sec	q_γ Watt/g	h m	l m	Φ_c 10^{10}n/cm²sec
CEK	central	4	25÷30	-	-	-
	horizontal					
GEK 1	radial	1	2	+0.2	2.3	10
GEK 2	tangential (1)	1.2	2	0	2.4	30
GEK 3	tangential (2) (cold source)	0.4 (3)	1	0	1.7	9 (4)
GEK 4	going through tube	1	4	0	2.5 (5)	9
GEK 5	going through tube	0.2	0.2	-0.6	2.5 (5)	2
GEK 6	going through tube	0.4	0.4	-0.4	2.5 (5)	4
GEK 7	V-shaped	0.1	0.1	-0.8	2.1	2
GEK 8	tangential (hot source)	0.3 (3)	0.1	+0.4	1.8	-
GEK 9	tangential	0.5	0.5	0	2.3	5
GEK 10	tangential	1	2	+0.05	2.3	9
NEK 1÷6	inclined	0.2÷1	0.2÷4	0 ÷ +0.5	5.7	0.4÷2
VEK 1÷7	vertical	0.1÷0.3	0.06÷0.2			

(1) Tapering beam tube of the initial rectangular cross section 9.5 x 23 cm; (2) Tapering beam tube of the initial rectangular cross section 12 x 25 cm; (3) Mean value for cold source or hot source; (4) Only cold neutrons; (5) Distance from the center of the beam tube. CEK - Central experimental beam tube; GEK - Horizontal experimental beam tube; NEK - Inclined experimental beam tube; VEK - Vertical experimental beam tube.

averaged over the tube cross sectional area Also presented are the length of the tube and the distance from its center to core midplane, h (the direction upward is taken positive) The table specifies the outlet fluxes Φ_k from the bottom of the dia 10 cm horizontal tube. Because of the small solid angle the fluxes are reduced by about a factor 10^4 A correction for the pertubation of the neutron flux by the tube proper which is roughly evaluated as 15-20% was also introduced. Since the flux at the outlet of the tangential through channel depends on the scatterer installed in it, the table gives data for an equivalent thimble mounted in the same place. The table specifies also the energy released in the tube material by γ - rays from the core for the hottest point It can reach a few W per gram. Therefore the tube parts which are closest to the core and thus suffer the highest thermal stress are cooled by heavy water For the same reason a closed 200 kW water loop is provided for the cooling of collimators or large experimental devices. A gas loop is designed to cool small samples

4.5. Neutron Guides

To reduce the fast neutron and γ- ray background, it is desirable to lead slow neutrons out of direct visibility of the emitting tube to a large distance from the reactor without substantial loss. For this purpose the PIK is equipped with a system of mirror-type neutron guides [13]. The inner surface of the neutron guide tubes is coated by the nickel isotope ^{58}N, having a total internal reflection cut off wavelength λ_c of about 500 Å ($v_c \approx 8.2$ m/s). The neutron guides bent to a radius of curvature ρ capture the neutrons within a characteristic small angle $\vartheta^* = (2a/\rho)^{1/2}$ (a is the width of a rectangular neutron guide) with wavelengths up to $\lambda^* = \vartheta^* \lambda$ and transport them over an arc of length L.

The neutron guides are installed in two adjacent tubes, the 2.4 m long horizontal HBT 2 and 1 7 m long HBT 3 which houses the CN source. Both tubes are of rectangular cross section tapering off toward the bottom. The neutron guide system is designed for the installation of 10 guides (5 for the thermal, and the other five for the cold neutrons, Fig.13). The neutron guides are enclosed in a common shielding. The six neutron guides specified

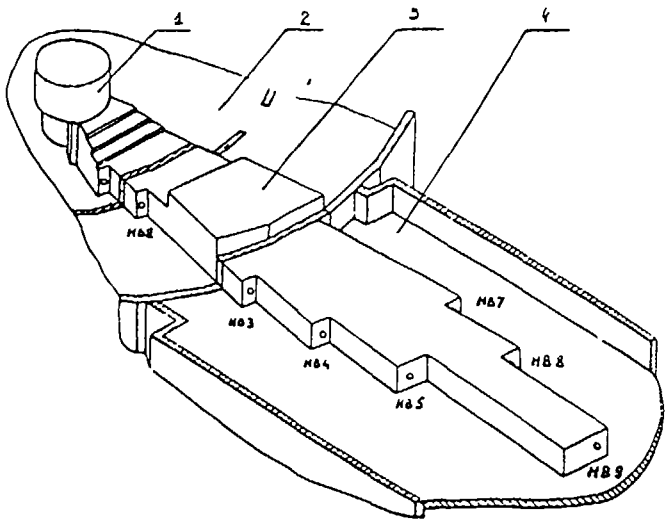

Fig.13. Layout of the neutron guide system [7].
1: reactor; 2: ring-shaped experiment hall;
3: neutron guide shielding; 4: neutron guide hall,
N6 - neutron guides.

in Table 2 will be first to be installed Each neutron guide is of rectangular cross section, 3 x 20 cm^2 The original calculated thermal neutron flux at the site of the HBT 2 is 1.2 x $10^{15} cm^{-2} s^{-1}$ The cold neutron flux at the bottom of the HBT 3 is estimated to be approximately 10^{14} $cm^{-2} s^{-1}$ The geometrical characteristics of the PIK neutron guides being similar to those of the GHFR reactor in Grenoble [14], both systems should have close order-of-magnitude fluxes at the outlet For the long wavelength and thermal neutrons these fluxes at a considerable distance from the reactor and under conditions with a particularly low background are in excess of $10^9 cm^{-2} s^{-1}$

TABLE 2. Parameters of the neutron guides.

Beam Tube	Neutron Guide	λ^*	S	L	Flux at Exit of neutron guide
		Å	. m	m	n/cm^2 sec
GEK 3 (Cold Neutrons)	NV3	2.7	2000	27.1	$1.4 \cdot 10^9$
	NV4	2.5	2400	36.7	$1.2 \cdot 10^9$
	NV5	2.5	2400	46.3	$1.1 \cdot 10^9$
GEK 2 (Thermal Neutrons)	NV7	1.7	5200	41.5	$1.1 \cdot 10^9$
	NV8	1.3	8500	51	$1.2 \cdot 10^9$
	NV9	1.0	15000	65.5	$1.2 \cdot 10^9$

It should be pointed out that the above calculated characteristics of the neutron beams are preliminary.

The reactor has three halls for operation with the external beams and experimental equipment (Figs. 14 and 15), namely, the horizontal and inclined beam and the neutron guide halls. The physical laboratories of the horizontal beam hall are arranged circularly adjoining it and can in principle be used to extend the horizontal neutron beams beyond the confines of the hall.

An essential feature of the horizontal beam hall is its vibration-proof design. The high intensity neutron beams provided make possible fast accumulation of the statistics required in high precision measurements. Accordingly, the systematic errors, in particular, the effect of the building vibrations on the physical instrumentation become a primary concern. Therefore paritcular emphasis in designing the PIK reactor was placed on the suppression of vibrations, primarily in the horizontal beam hall. The pumping station representing a major source of vibrations was removed to a separate unit. Only a minimum of equipment is left close to the horizontal beam hall, it is a part of the heavy water system. The ring-shaped experiment hall proper rests upon a special vibration-damping cushion (Fig 16). These precautionary measures permit cutting down the amplitude of vibrations in different parts of the spectrum tens and hundred of times.

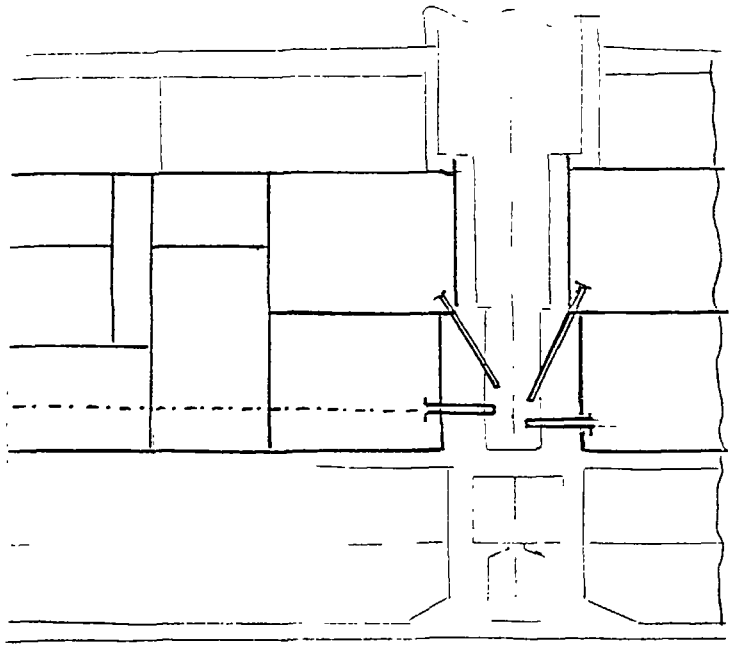

Fig. 14. Schematic elevation of reactor building.

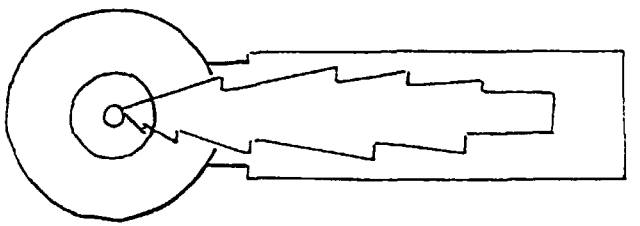

Fig. 15. Top view of the horizontal beam tube and neutron guide halls.

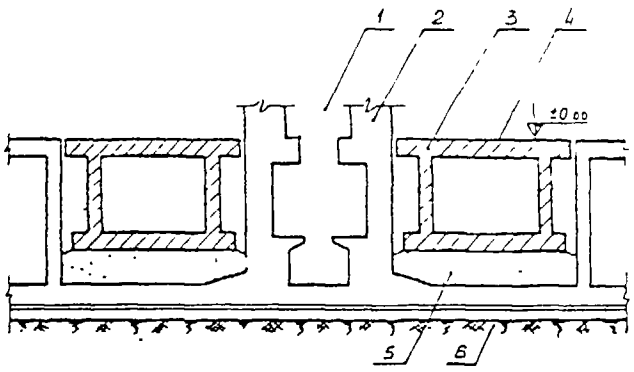

Fig.16. Schematic of vibration damping of the PIK horizontal beam tube hall.
1: reactor pit; 2: biological shielding; 3: concrete foundation; 4: experiment hall floor; 5: vibration damping cushion; 6: rocky ground.

A general view of the PIK complex is shown in Fig.17 Only three of the units making up the complex, 100A, 104 and 105, are intended for the accommodation of physical instrumentation. Unit 105 houses electronics and working rooms of the experimenters and thus has no provisions for external neutron beams The other units contain reactor servicing equipment The volume of these three units is about one half of the total volume, and that of the core, one ten millionth.

The present communication is based on the few papers specified in the references list, primarily, on ref.[9] . The reactor is in the stage of erection and assembly, it is constructed at the Leningrad Nuclear Physics Instituted located near Gatchina, 45 km to the south of Leningrad. The reactor project was developed under general scientific direction of LNPI by the Research and Design Institute for Power Engineering and other institutes under the auspices of the USSR State Committee on Atomic Energy

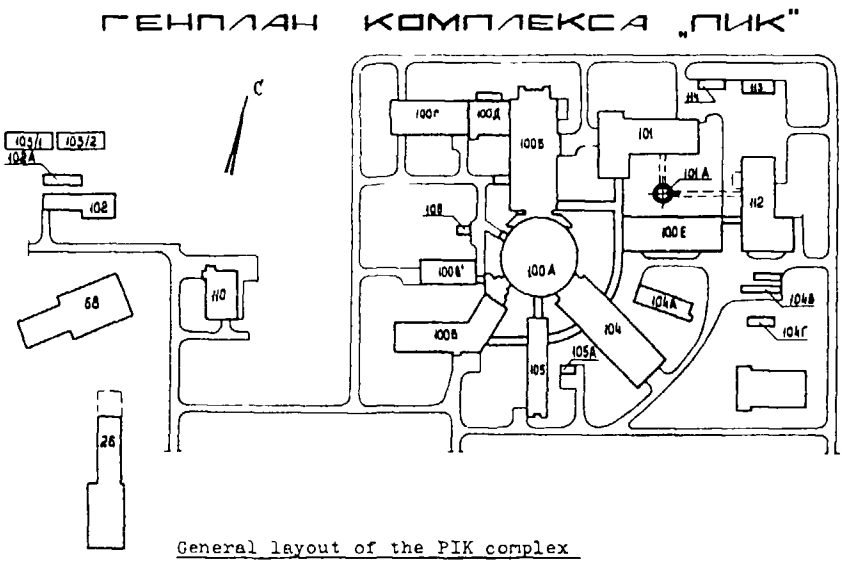

General layout of the PIK complex

100A - reactor and physical laboratories;
100J - 1st loop pumphouse, cooling pond, hot chambers etc
100B - sanitary facilities and plenum ventilation chambers;
100Г - intermediate circuit pumping station,
100D - power supply;
101 - cryogenics (CN source and cryogenics for physical research);
101A - ventilation stack;
102 - water supply pumphouse;
102A - cold water chamber;
103/1- cooling tower;
103/2- cooling tower;
104 - neutron guide hall and laboratories
104A - technical unit;
104B - water supply pumphouse;
104Г - cooling tower;
105 - multicomputer complex;
105A - storehouse,
108 - carbon dioxide facilities,
110 - high pressure compressor house,
113 - liquid nitrogen facilities;
114 - containers storehouse,
21 - chemical water purification;
88 - emergency tanks.

Список литературы

I. [illegible] reactor in member states. 1980 edition IAEA. Vienna, 1980.

2. В.М.Лобашов ЯФ 1965, 2, 957

3. А.И.Смирнов, В.А.Шабуров, Д.М.Каминкер, В.Л.Алексеев, А.С.Рыльников, О.И.Сумбаев Nucl. Instr. and Methods 1968, 60, 103.

4. Moll et al. Nucl. Instr. and Methods 1975, 123, 615

5. А.А.Воробьев, В.Г.Грачев, А.П.Комар, А.М.Никитин, Д.М.Седиверстов
Атомная энергия, 1969, 27, 31

6. I.S.Altarev, Yu.V.Borisov, A.B.Brandin, V.F.Ezhov, S.I.Ivanc G.K.Kunstman, V.M.Lobashev, V.A.Nazarenko, V.L.Ryabov, A.P.Serebrov, R.R.Taldaev. Physics Letters 1980, 80A, 413.

7. А.Н.Ерыкалов, И.А.Кондуров, К.А.Коноплев, З.К.Красоцкий, Ю.В.Петров, О.И.Сумбаев, В.А.Трунов
"Экспериментальные возможности реактора ПИК" Препринт ЛИЯФ - 852, Л, 1983 г

8. В.А.Цыканов, П.Г.Аверьянов, В.П.Бурукин, В.А.Зверев, Е.П.Клочков, Ю.П.Кормушкин, А.С.Кусовников, Н.П.Матвеев
Симпозиум "Опыт эксплуатации и использования исследовательских реакторов". Предеал, 1974, с.236.

9. А.Н.Ерыкалов, Д.М.Каминкер, К.А.Коноплев. Ю.В.Петров
Выбор основных параметров реактора для физических исследований ПИК. Изд.ФТИ им.А.Ф.Иоффе АН СССР, Ленинград, 1968

10. D.H.Shaftman. 1966 ANL - 7211, p.95.

11. C.Golinelli, H.Tellier. Rapport CEA - R3318, 1967.

12. C.E.Winters "Nucl.Sci. and Eng." 1963, 17, 443.

13. В.А.Кудряшов, А.П.Булкин, В.Я.Кезерашвили, Г.К.Кунстман, В.А.Трунов, А.Ф.Щебетов, В.Б.Щебетова, В.А.Ковалев
"Нейтроноводная система реактора ПИК". Препринт ЛИЯФ №421 Ленинград, 1978г.

14. Grenoble High Flux Reactor. Directory of Nuclear Reactors. v.10, 335. IAEA, Vienna, 1976.

Invited Paper

A NEW INTENSE SOURCE OF VERY-COLD AND ULTRA-COLD NEUTRONS

A MICHAUDON
Institut Max von Laue — Paul Langevin,
Grenoble, France

Abstract

This paper presents a new source of very cold and ultra-cold neutrons recently put into operation at the High-Flux Reactor of the Institut Laue-Langevin in Grenoble (France). This source consists in a primary source of liquid deuterium, a set of metallic nickel vertical and curved guides and a neutron turbine Results about the flux and density of very low energy neutrons are given both at the exit of the curved guide and after the neutron turbine. A preliminary list of experiments that will be carried out with this new source is also presented.

I. INTRODUCTION

Intense beams of thermal neutrons having a wavelength λ of about 1 Å are available at high-flux reactors and spallation neutron sources. These neutrons are widely used for basic research in many disciplines ranging from nuclear physics to condensed matter. The neutron intensity at wavelengths longer or smaller than 1 Å can still be increased by moderating the neutrons in cold or hot moderators, with temperatures ranging from 25°K (liquid H^2 or D^2) to about 2000°K (hot graphite) respectively. Neutrons thermalised at room temperature are traditionally called thermal neutrons whereas those moderated in cold or hot sources are called cold or hot neutrons respectively. A recent review of these special sources is given in /1/.

An example of a facility providing many beams of thermal as well as cold and hot neutrons is the Institut Laue-Langevin (ILL). Its High-Flux Reactor, with a thermal flux of about

10^{15} n/cm2.s. is equipped with a vertical cold source recently upgraded to give 70% more cold neutrons and with a hot source. A second cold source will be installed in 1987.

There is also a need for neutrons of still longer wavelengths than those for cold neutrons (i.e. above 15 to 20 Å), the so-called very-cold neutrons (VCN) with 20 Å $\lesssim \lambda \lesssim$ 600 Å and ultra-cold neutrons (UCN) with $\lambda \gtrsim$ 600 Å. The UCN's have the unique property of being totally reflected by some materials. First observed by Fermi and Zinn [2], total reflection proved to be very useful for transporting neutrons with neutron guides as was first demonstrated by Maier-Leibnitz and Springer [3]. For example eight neutron guides transporting thermal or cold neutrons up to about 100 meters are installed at the Institut Laue-Langevin. The use of total reflection to trap and store UCN's in bottles was first considered in print by Zeldovich [4] and the first observation of the storage of UCN's was reported by Luschikov et al. [5]. The maximum energy of UCN's depends on the material used for storage but is typically about 0.18 μeV (corresponding to v = 6m/s and λ = 670 Å). These neutrons are ideal for experiments in fundamental physics needing a long observation time such as those for the measurement of the electric dipole moment (EDM) or life time τ_n of the neutron. The domain of VCN's, in between those of cold neutrons and UCN's is very promising in particular for some diffraction and surface studies with very high resolution (10^{-6} eV to 10^{-9} eV). Also VCN's can be an intermediate step towards the production of UCN's. Both UCN's and VCN's are of great importance for neutron optics. Illustrations of the use of VCN's and UCN's are given later in this paper.

Very low energy neutrons can be extracted from thermal neutron sources, but the fraction f of the flux of neutrons with energy below E_{Max} in a Maxwellian spectrum of temperature T is only :

$$f = \frac{1}{2}\left(\frac{E_{Max}}{kT}\right)^2 \quad \text{for} \quad E_{Max} << kT \qquad (1)$$

For UCN's, the value of f is as low as $2.5.10^{-11}$ for a Maxwellian spectrum at room temperature but reaches $f = 3.3\ 10^{-9}$ for a cold source at T = 25°K. To produce UCN's in reasonable number despite the very low value of f, it is therefore necessary to dispose of a primary neutron source with a high flux and a low temperature. This is especially true because, from Liouville's theorem and phase space considerations, it is well known that the UCN flux or density given by the primary source cannot be increased by spectral transformations obtained by external forces acting collectively on the neutrons.

Reviews of the properties, the production and the use of very low energy neutrons (VCN's and UCN's) have been made several times (see for example [6], [7], [8], [9]).

II. DESCRIPTION OF THE NEW ILL SOURCE OF VERY LOW ENERGY NEUTRONS

The purpose of this paper is to describe briefly the new source of VCN's and UCN's recently put into operation at the ILL, already presented in more detail elsewhere ([9], [10], [11]) and to give its latest status.

This source is obtained by combining three elements: a) an intense primary source of cold neutrons, b) a set of vertical and curved neutron guides of excellent reflectivity and c) a neutron turbine. It should be said, at the outset, that this source is the result of a joint undertaking of the Garching Group (FRG) and the ILL (see general lay-out in Fig. 1).

The primary neutron source is the liquid deuterium cold source installed in the ILL High-Flux Reactor. The unperturbed flux in that source is 4.5×10^{14} n/cm^2.s. Supposing that the neutrons are completely thermalised in that vessel, an Al sphere of 38 cm diameter and 1.5 mm wall thickness filled with liquid D_2 at T = 25°K, the UCN flux in that source is $\phi_{UCN} = 1.6 \cdot .10^6$ n/cm^2.s.

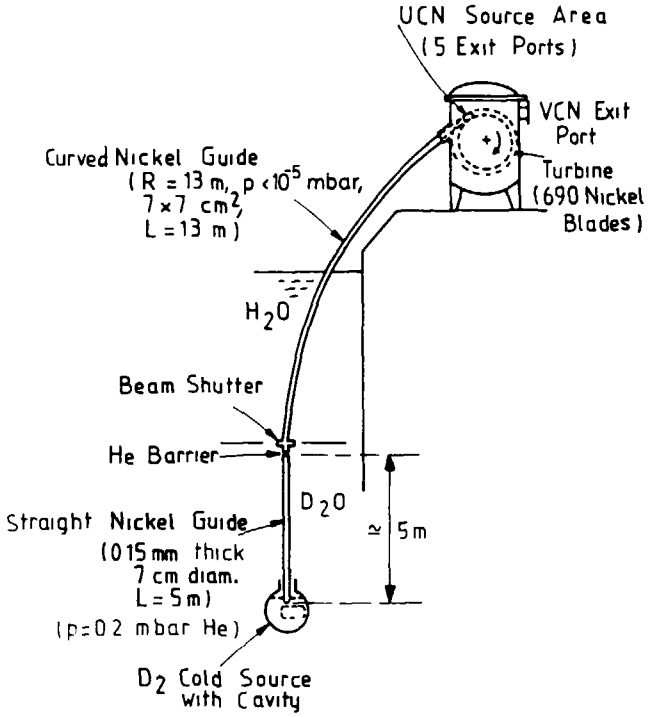

Fig. 1 General lay-out of the ILL source of very cold and ultra-cold neutrons (After A.Steyerl et al /9/).

For being used outside the reactor, the neutrons must be extracted from the primary source with a pipe (or a guide). This guide can have any inclination but needs to be closed by a wall at the end where it dips into the cold source. The UCN's in the cold source cannot cross this wall. Therefore, if the guide is horizontal, no UCN's are available unless a converter is placed next to the wall on the opposite side of the primary source. The best arrangement is a vertical guide in which neutrons are decelerated by gravity (1neV/cm). UCN's do not exist at the bottom of the guide but are produced higher up from more energetic neutrons wich have crossed the wall at the lower end of the guide and have then been decelerated to UCN energies when moving up. UCN's at the upper end of the guide of height h(cm) have initially energies between h and (h + 180)neV at the bottom of the guide. Therefore no converter is needed, in contrast to the case of a horizontal guide, provided that h is greater than 180 cm. Another advantage of the vertical guide is that neutrons are reflected less often than in a horizontal guide during their transportation away from the primary source simply because of their greater velocity.
For being reflected, and consequently transported, neutrons must have a velocity component in the horizontal plane lower than v_{lim}, *the velocity for total reflection. Therefore the* solid angle to be considered is not constant for all neutrons but rather varies as $(v_{lim}/v)^2$. This shows that the neutron flux at the exit of the neutron guide is no longer Maxwellian but varies as v, at least for very low energy neutrons.

The above considerations explain why a vertical guide was chosen at the ILL to extract very low energy neutrons. This guide is made of two sections of metallic nickel. The first one is cylindrical (Ø 7 cm and 0.15 mm thick) with a length of 5 m. It is housed in an Al guide located itself inside the pile and filled with helium at low pressure (p = 0.2 mbar) for heat conduction without degrading the neutron beam. The second section is curved (with R = 13 m) with a square cross-section of 7 x 7 cm^2 and a length of 13 m. It is located above the first straight section, outside the pile and evacuated for there is no need of heat removal at this location. These two sections are separated by two 0.1 mm thick zircalloy membranes with helium in between (this is the He barrier) and a neutron shutter is installed just above. An important factor is the good reflectivity of the nickel guide obtained by using a new replication process. This method is described in more detail in a patent /12/. Neutron metallic guides obtained in this manner have a mean reflectivity superior to that of nickel coated on glass. The neutrons coming from the curved guide have a broad spectrum (20 to 400 Å) centered to about 80 Å.

This guide is connected to a neutron turbine inside which the beam is split into two parts:

a) one half by-passes the turbine, with the help of a lamellated bender and is available outside the turbine, thus providing an intense source of VCN's,

b) the other half is fed to the entrance of the turbine where the neutrons are Doppler decelerated by the rotating blades down to UCN energies. They are then available as separate beams outside the turbine at 5 exit ports.

The principle of operation of a neutron turbine for decelerating VCN's down to the UCN energy region is well known [13] and is illustrated in Fig. 2. The angle of incidence of the incoming neutrons relative to the entrance edge of the blades is small

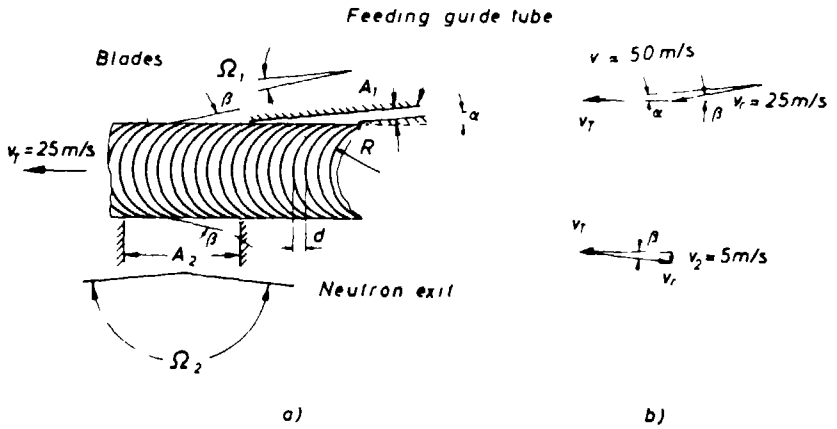

Fig. 2 Principe of neutron deceleration in a turbine. Incoming neutrons, with velocity v_1 and solid angle Ω_1, come out from the feeding guide inclined at an angle α. These neutrons enter the turbine at an angle β in the reference frame of the moving blades. After several reflections from the moving blades the neutrons come out with a relative exit velocity V_r, equal in magnitude but almost reversed compared to the entrance relative velocity. This phenomenon brings the exit velocity v_2, in the laboratory frame, in the UCN velocity range. The exit solid angle becomes Ω_2, much larger than Ω_1 (after A.Steyerl [13]).

enough for total reflection to occur. After several reflections between the moving blades the neutrons emerge with an exit velocity, equal in magnitude but almost completely reversed compared to the entrance velocity in the frame of the moving blades. Then if the radial velocity v_T of the blades is half the velocity v_1 of the incoming neutrons, the velocity v_2 of the outgoing neutrons is close to zero in the laboratory frame. For incoming neutrons having $\lambda \simeq 80$ Å, (i.e. $v_1 \simeq 50$ m/s) the blade velocity should be $v_T \simeq 25$ m/s, well within technological capabilities. The neutron turbine installed at the ILL by the Garching group is essentially the same as the initial Garching turbine with a few modifications only which increase its gain by a factor of 2.

III. PROPERTIES OF THE NEW ILL SOURCE OF VERY LOW ENERGY NEUTRONS

The properties of this facility, as obtained since it started to be operated in Autumn 1985, are briefly summarised below.

At the exit of the curved guide, the neutron density and the neutron flux were measured by different methods:

a) Storage of the UCN's in a 6000 cm^3 bottle made of electro-polished stainless steel. A density of 41 UCN/cm^3 (extra-polated to zero storage time) was measured. Taking into account the efficiency of the whole system, this corresponds to a UCN density (with $v < 6.2$ cm/s) of 68 UCN/cm^3 at the exit of the curved guide.

b) Time of flight of VCN's by chopping the beam collimated by a vertical slit at the end of the curved guide. The neutrons are detected at a flight distance of 1.5 m and the beam profile is scanned there with a movable horizontal slit. The results for various positions of the horizontal slit are displayed in Fig. 3 where they are compared to the intensity which would be obtained in the absence of losses by reflections in the neutron guides.

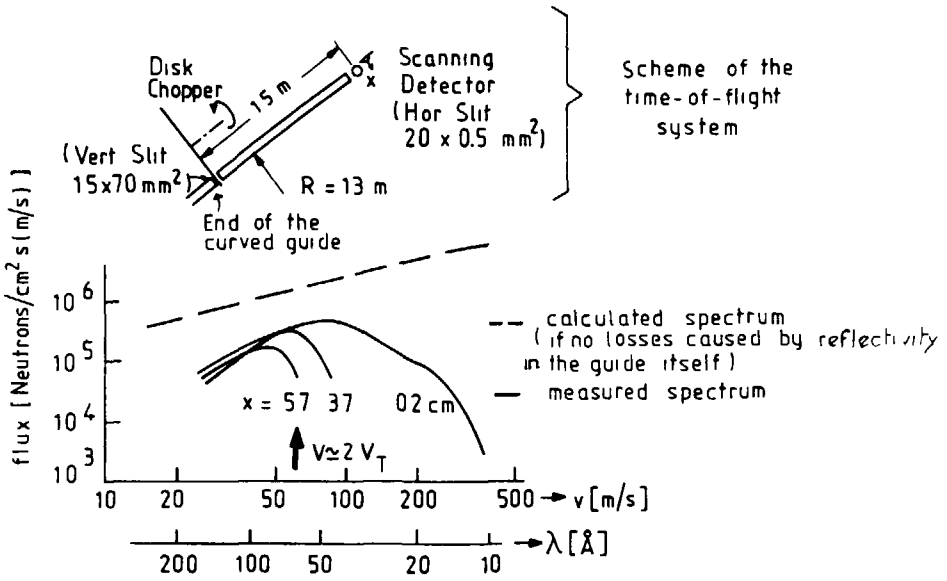

Fig. 3 Measurement by the time-of-flight method of the flux of very cold neutrons at the exit of the curved guide (After A.Steyerl et al /11/).

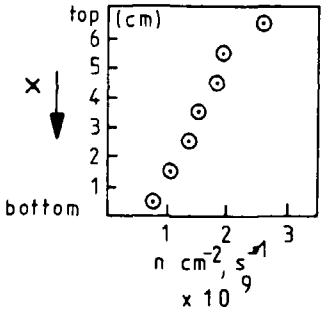

Fig. 4 Measurement of the very low energy neutron flux profile, by the gold foil activation technique, as a function of height across the beam at the exit of the curved guide. The abcissa is the flux of 2200 m/s neutrons which would give the same observed activation (After P.Ageron et al /10/).

c) Activation of gold foils. The results of this measurement are plotted in Fig. 4.

These three types of measurements are consistent with a mean phase-space density of 0.25 cm^{-3} $(m/s)^{-3}$ at v = 50 m/s. This represents an improvement of about 75 compared to the previous ILL facility (called PN5) using a primary neutron source at room temperature, a converter and an inclined tube.

At the exit of the turbine, the flux and density of the UCN's were also measured using two methods:

a) By time of flight, the neutron beam being chopped by a set of blades of the turbine itself. The measurements were carried out to explore both the flux profile across the source (about 16 x 8 cm^2) and the angular distribution of the outgoing neutrons. The results are displayed in Fig. 5. Analysis of these results yields the following figures for the flux ϕ_{UCN}, the intensity I_{UCN} and the density n_{UCN} of the UCN's, depending on the maximum value of v_z which is used (v_z is the neutron velocity component perpendicular to the plane of the turbine). For $v_z < 6.2$ m/s, we have : $\phi_{UCN} = 2.6.10^4$ $n/cm^2.s$, $I_{UCN} = 3.3.10^6$ n/s and $n_{UCN} = 87$ n/cm^{-3} whereas for $v_z < 7$ m/s, these figures become: $\phi_{UCN} = 3.3.10^4$ $n/cm^2.s$, $I_{UCN} = 4.2.10^4$ n/s and $n_{UCN} = 110$ n/cm^3.

b) By neutron storage using the same bottle as for the measurement at the exit of the curved guide. A density of 46 n_{UCN}/cm^3 was actually observed, a result consistent with the above figure if an overall efficiency of 41% is assumed for this experiment.

The flux of UCN at the exit of the turbine is comparable to that at the exit of the curved guide. This is an illustration of the excellent quality of the neutron guide reflectivity. The advantage of the turbine however is to provide UCN's over a much larger area than that of the curved guide.

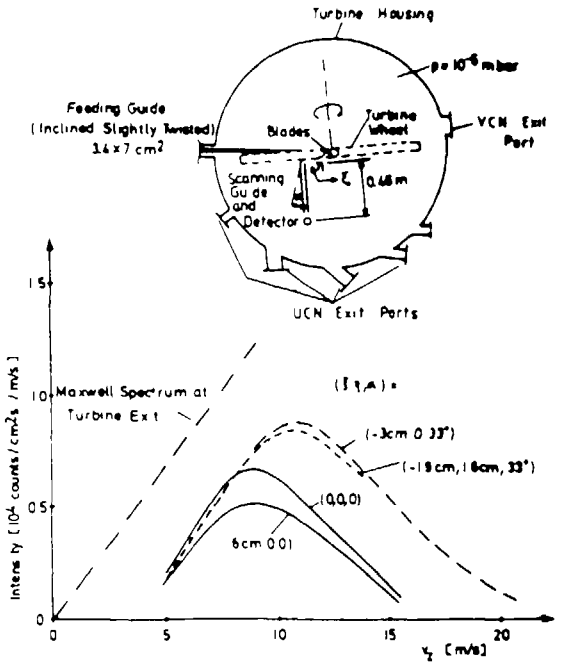

Fig. 5 Measurement of the properties of the UCN source at the exit of the turbine for several values of the parameters ξ, η and α. The parameters η and ξ are the cartesian coordinates in the turbine plane. The parameter α is the angle of inclination. The abscissa v_z is the neutron velocity component along the normal to the turbine plane (After A.Steyerl et al /11/).

IV. SCIENTIFIC PROGRAMME WITH VERY-COLD AND ULTRA-COLD NEUTRONS

Several experiments are already planned or envisaged for the use of this intense source of very low energy neutrons. Among them, let us cite:

- Measurement of the neutron electric dipole moment. With the previous PN5 set-up, on accuracy of 3.10^{-25} e.cm was achieved /14/. An increase of 100 in the UCN density should improve the accuracy down to the 10^{-26} e.cm level.

- Magnetic storage of UCN's (called NESTOR) for the measurement of the life-time τ_n of the free neutron /15/. Many τ_n measurements have already been made but with discrepancies of about 10% in the results. An increase of 100 in the UCN density should permit measurement by this method with 1% accuracy.

- Neutron microscope using UCN's. This instrument has already been tested at PN5 with a slit in a cadmium sheet used as the object /9/. A magnification of about 50 has been obtained and, after being moved to the new facility, a resolution of 60 µm has been measured /16/.

- High-resolution neutron spectroscopy with UCN's using a neutron gravity spectrometer. Such a system called NESSIE /17/, based on the analysis of the maximum reach of UCN's in their parabolic trajectory, is already in operation at Garching. Present performances of momentum transfer $Q \leq 0.03$ Å^{-1} and resolution $\Delta E \simeq 200$ neV already present a great interest in such fields as polymers, biology etc.

- Neutron optics with VCN's since such neutrons i) have a wavelength long enough for standard optical diffraction elements to be used and ii) have an energy for which the refractive index differs significantly from 1. It has been proposed to install a granite optical bench, as free of vibrations as possible, to study a wide range of applications.

- The VCN source, associated with a chopper, could be used also for some cross section measurements at very low energy. An example is the ^{235}U fission cross-section which needs to be known at very low energy for reactor physics applications as well as for a basic physics standpoint /18/.

V. CONCLUSION

To conclude, an intense source of very cold and ultra-cold neutrons has recently been put in operation at the ILL. The characteristics of this source represent probably the ultimate of what can be obtained with a steady-state reactor. The presentation of these results is particularly relevant in a country where the study of ultra-cold neutrons has been pioneered and especially at the Leningrad Institute of Nuclear Physics where excellent results for the production and the use of ultra-cold neutrons have been obtained. Further improvements can be envisaged with intense pulsed spallation neutron sources provided one can take advantage of the peak flux /197. This new ILL source of very cold and ultra-cold neutrons is opening and expanding a rich field of basic physics of which the examples given above provide only an illustration.

ACKNOWLEDGEMENTS

The author is very much indebted to P. AGERON, W. MAMPE and A. STEYERL for many fruitful discussions about their work and for supplying him with their most recent results before publication.

References

/1/ P. AGERON "Special Neutron Sources" Paper IAEA-CN-46/38 in "Neutron Scattering in the Nineties", Conference Proceedings, Julich 14-18 January 1985, p. 135

/2/ E. FERMI and W.N. ZINN. Phys.Rev. 70(1946)103

/3/ H. MAIER-LEIBNITZ and T. SPRINGER, J.Nucl.Energy A/B 17(1963)217.

/4/ Yu.B. ZELDOVICH, Sov.Phys. JETP 9(1959)1389

/5/ V.I. LUSCHIKOV, Y.N. POKOTILOVSKY, A.v. STRELKOV and F.L. SHAPIRO, JINR Dubna Preprint P3-4127(1968) Sov.Phys.-JETP Lett. 9(1969)23.

/6/ R. GOLUB and J.M. PENDLEBURY, Rep.Prog.Phys. 42(1979)439.

/7/ R. GOLUB, W. MAMPE, J.P. PENDLEBURY and P. AGERON Sc.Am. 240 Nb (1979)134.

/8/ L. KOESTER and A. STEYERL, Neutron Physics (1977) Springer-Verlag.

/9/ A. STEYERL and S.S. MALIK, Physica 137 B(1986)270.

/10/ P. AGERON and W. MAMPE, Proceedings Workshop on Investigation of Fundamental Interactions with Neutrons, Washington D.C.(1985) in press.

/11/ A. STEYERL, H. NAGEL, F.Y. SCHREIBER, K.A. STEINHAUSER, R. GÄHLER, W. GLÄSER, P. AGERON, J.M. ASTRUC, W. DREXEL, R. GERVAIS and W. MAMPE, to be published.

/12/ French patent n° 85.01650 dated Feb., 1985.

/13/ A. STEYERL, Nucl.Inst. and Meth. 125(1975)461.

/14/ J.M. PENDLEBURY, K.F. SMITH, R. GOLUB, J. BYRNE, T.J.L. McCOMB. T.J. SUMNER, S.M. BURNETT, A.R. TAYLOR, B. HECKEL, N.F. RAMSEY, K. GREEN, J. MORSE, A.I. KILVINGTON, C.A. BAKER, S.A. CLARK, W. MAMPE, P. AGERON, and P.C. MIRANDA, Phys. Lett. 136B, (1984) 327.

/15/ - K.J. KÜGLER, W. PAUL, U. FRINKS, Phys.lett. 72B (1978) 422
- K.J. KÜGLER, K. MORITZ, W. PAUL and U. FRINKS, Nucl.Inst. and Meth. 228(1985)240.

/16/ A. STEYERL, Private communication (1986).

/17/ A. STEYERL, Z.Physics, B.30(1978)231.

/18/ A. MICHAUDON, Nuclear Data for Science and Technology - Proceedings of the International Conference (6-10 Sept 1982, Antwerp) p. 1013.

/19/ K.A. STEINHAUSER, "Production and Use of Ultra-Cold Neutrons" in "Neutron Scattering in the Nineties". Conference Proceedings. Jülich 14-18 January 1985, p. 99.

LIST OF USSR PARTICIPANTS

RADIEVYJ INSTITUT V G KHLOPINA
Ul Rentgena 1
Leningrad 197022

S S Kovalenko
M V Blinov
N P Kocherov
(Local Organizer)
L A Pleskachevsky
K A Petrzhak
L V Drapchinsky
V A Rubchenya
V I Shpakov
O V Lozhkin
A I Obukhov
I A Baranov
E A Ganza
S V Khlebnikov
E M Kozulin
E V Korolyov
O I Batenkov
V P Mayorov

FIZIKO ENERGETICHESKIJ INSTITUT
Ploshchad Bondarenko
249 020 Obninsk, Kaluga Region

B D Kuzminov
N V Kornilov
O A Salnikov
A A Goverdovsky
S P Simakov

INSTITUTE OF ATOMIC ENERGY
Ploshchad Kurchatova
Moscow D 182, 123182
G V Muradyan
A I Frank

INSTITUTE OF PHYSICS AND TECHNOLOGY OF THE UKRAINIAN ACADEMY OF SCIENCES, Kharkov
V Ya Golovnya

VNIIET, Leningrad
N P Dergachyov
V I Anpilogov

JOINT INSTITUTE OF NUCLEAR RESEARCH
Dubna, Moscow Region
V I Lushchikov

LENINGRAD INSTITUTE OF NUCLEAR PHYSICS
Gatchina, Leningrad Region
K A Konoplev

INSTITUTE OF NUCLEAR PHYSICS of the Ukrainian Academy of Sciences, Kiev
M V Passechnik
V P Vertebny

KIEV STATE UNIVERSITY
Kiev
G M Primenko

LATVIAN STATE UNIVERSITY
Raina Blvd, Riga
Kh Ya. Bondars

STATE COMMITTEE ON ATOMIC ENERGY
Staromonetny per 26
Moscow
N N Zvonov
Yu G Klimov

LIST OF PARTICIPANTS

AUSTRIA

A. Chalupka
Institut fuer Radiumforschung
und Kernphysik
Boltzmanngasse 3
A-1090 Vienna

M. Drosg
Institut fuer Experimentalphysik
der Universitaet Wien
Strudlhofgasse 4
A-1090 Vienna

H.K. Vonach
Institut fuer Radiumforschung
und Kernphysik
Boltzmanngasse 3
A-1090 Vienna

AUSTRALIA

J.W. Boldeman
AAEC Research Establishment
Private Mail Bag
Sutherland, N.S.W. 2232

PEOPLE'S REPUBLIC OF CHINA

Yuan Hanrong
Chinese Nuclear Data Center (CNDC)
Beijing Atomic Energy Institute
P.O. Box 275
Beijing

CZECHOSLOVAKIA

J. Pivarc
Institute of Physics of the
Slovak Academy of Sciences
Dubravska Cesta
CS-899 30 Bratislava

FRANCE

A. Michaudon
Institut Max von Laue
- Paul Langevin
B.P. No. 156 X
F-38042 Grenoble Cédex

GERMAN DEMOCRATIC REPUBLIC

H. Maerten
Sektion Physik
Technische Universitaet Dresden
Mommsenstrasse 13
DDR-8027 Dresden

D. Seeliger
Sektion Physik
Technische Universitaet Dresden
Mommsenstrasse 13
DDR-8027 Dresden

GERMANY, FEDERAL REPUBLIC

R. Boettger
Physikalisch Technische
Bundesanstalt
Abteilung 6
Bundesallee 100
D-3300 Braunschweig

W. Mannhart
Physikalisch Technische
Bundesanstalt
Abteilung 6
Bundesallee 100
D-3300 Braunschweig

S.M. Qaim
Institut fuer Chemie 1
(Nuklearchemie)
Kernforschungsanlage Juelich
G.m.b.H.
Postfach 1913
D-5170 Juelich 1

HUNGARY

G. Petoe
Institute of Experimental Physics
of Kossuth Lajos University
P.O. Box 105
H-4001 Debrecen

A. Lajtai
Central Research Institute for
Physics of the Hungarian
Academy of Sciences
P.O. Box 49
H-1525 Budapest

ITALY

C. Coceva
Divisione Fisica
Centro di Calcolo del E.N.E.A.
Via Mazzini 2
I-40138 Bologna

E. Menapace
Centro di Calcolo del E.N.E.A.
Via Mazzini 2
I-40138 Bologna

JAPAN

S. Iwai
Ohmiya Technical Institute
Radiation Control & Analysis Team
Mitsubishi Atomic Power
Industries Inc. (MAPI)
1-297, Kitabukuro, Ohmiya
Saitama 330

I. Kimura
Research Reactor Institute
Kyoto University
Kumatori-Cho
Sennan-Gun, Osaka-Fu 590-04

T. Nakamura
Institute for Nuclear Study
University of Tokyo
Midori-cho 3-2-1, Tanashi
Tokyo 188

N. Shikazono
Division of Physics
Japan Atomic Energy Research
Institute (JAERI)
Tokai-Mura, Naka-Gun
Ibaraki-Ken 319-11

K. Sumita
Department of Nuclear Engineering
Osaka University
2-1 Yamadaoka, Suita-Shi
Osaka 565

Y. Yamanouti
Division of Physics
Japan Atomic Energy Research
Institute (JAERI)
Tokai-Mura, Naka-Gun
Ibaraki-Ken 319-11

NETHERLANDS

J.J. Broerse
Radiobiological Institute TNO
P.O. Box 5815
151 Lange Kleiweg
NL-2280 HV Rijswijk

U.S.S.R. (See separate list)

UNITED KINGDOM

A.G. Bardell
Division of Radiation Science
and Acoustics
National Physics Laboratory
Teddington, Middlesex TW11 OLW

U.S.A.

C.D. Bowman
Los Alamos National Laboratory
Mail Stop D-443, P.O. Box 1663
Los Alamos, New Mexico 87545

J.C. Davis
E-Division
Lawrence Livermore National
Laboratory
P.O. Box L-405
Livermore, CA 94550

R.G. Johnson
National Bureau of Standards
Gaithersburg, MD 20899

A.B. Smith
Applied Physics Division-316
(Bldg. 314)
Argonne National Laboratory
9700 South Cass Avenue
Argonne, IL 60439

INTERNATIONAL ORGANIZATIONS

K.H. Boeckhoff
Central Bureau of Nuclear
Measurements
Steenweg Naar Retie
B-2440 Geel

R. Dierckx
Physics Division B44
Euratom CCR
C.C.E. - Commission of the
European Communities
Joint Research Centre
Ispra Establishment
I-21020 Ispra (Varese)

INTERNATIONAL ATOMIC ENERGY AGENCY

K. Okamoto
Scientific Secretary
IAEA Nuclear Data Section
P.O. Box 100
Wagramerstrasse 5
A-1400 Vienna

LIST OF USSR PARTICIPANTS

RADIEVYJ INSTITUT V G KHLOPINA
Ul Rentgena 1
Leningrad 197022

S S Kovalenko
M V Blinov
N P Kocherov
(Local Organizer)
L A Pleskachevsky
K A Petrzhak
L V Drapchinsky
V A Rubchenya
V I Shpakov
O V Lozhkin
A I Obukhov
I A Baranov
E A Ganza
S V Khlebnikov
E M Kozulin
E V Korolyov
O I Batenkov
V P Mayorov

FIZIKO ENERGETICHESKIJ INSTITUT
Ploshchad Bondarenko
249 020 Obninsk, Kaluga Region

B D Kuzminov
N V Kornilov
O A Salnikov
A A Goverdovsky
S P Simakov

INSTITUTE OF ATOMIC ENERGY
Ploshchad Kurchatova
Moscow D 182, 123182
G V Muradyan
A I Frank

INSTITUTE OF PHYSICS AND TECHNOLOGY OF THE UKRAINIAN ACADEMY OF SCIENCES, Kharkov
V Ya Golovnya

VNIIET, Leningrad
N P Dergachyov
V I Anpilogov

JOINT INSTITUTE OF NUCLEAR RESEARCH
Dubna, Moscow Region
V I Lushchikov

LENINGRAD INSTITUTE OF NUCLEAR PHYSICS
Gatchina, Leningrad Region
K A Konoplev

INSTITUTE OF NUCLEAR PHYSICS of the Ukrainian Academy of Sciences, Kiev
M V Passechnik
V P Vertebny

KIEV STATE UNIVERSITY
Kiev
G M Primenko

LATVIAN STATE UNIVERSITY
Raina Blvd, Riga
Kh Ya. Bondars

STATE COMMITTEE ON ATOMIC ENERGY
Staromonetny per 26
Moscow
N N Zvonov
Yu G Klimov